NATIONAL ACADEMY OF SCIENCES OF UKRAINE

MINISTRY OF EDUCATION AND SCIENCE OF UKRAINE
V. N. KARAZIN KHARKIV NATIONAL UNIVERSITY

Series «Problems of Theoretical
and Mathematical Physics»

PROBLEMS OF THEORETICAL PHYSICS

Scientific works

Issue 5

Scientific editor of the release № 5 prof. V. O. Buts

Kharkiv – 2023

УДК 53; 530.1; 53.072
Р 78

Series “Problems of Theoretical and Mathematical Physics. Scientific works" under the general editorship Academician A. G. Zagorodny, Academician M. F. Shulga

Reviewers:
Corresponding member of the NAS of Ukraine O. Cheremnykh;
Prof. O. Gerasimov.

Approved for publication by the decision of the Academic Council
of V. N. Karazin Kharkiv National University
(Protocol № 10 of June 7, 2022)

Р 78 **Problems** of theoretical physics. Scientific works. Issue 5 / Yu. O. Averkov, V. O. Buts, V. I. Fesenko, I. O. Girka, V. M. Kuklin, A. V. Priymak, Yu. V. Prokopenko, O.Yu. Slyusarenko, Yu.V. Slyusarenko, D. M. Vavriv, V. M. Yakovenko, V. V. Yanovsky, A. G. Zagorodny; under the general editorship of by A. G. Zagorodny, M. F. Shulga, ed. no. 5 V. O. Buts. – Kh. : V. N.Karazin Kharkiv National University, 2023. – 488 p. (Series "Problems of Theoretical and Mathematical Physics. Scientific Works").

ISBN 978-966-285-750-4

The elementary and collective processes of interaction of charged particles in strong fields are discussed, in particular resonances, their regular and chaotic dynamics in regular and random fields. The mechanisms of excitation of electromagnetic oscillations by flows of nonrelativistic charged particles moving along dielectric and plasma-like media are discussed. Using the method of the so-called reduced description of nonequilibrium processes in nonlinear open systems of identical particles, in particular, at the kinetic stage of their evolution, a procedure for deriving kinetic equations for the cases of weak interaction between particles and a low intensity of the external field is described. Various scenarios are presented for the evolution of populations of strategies with memory interacting with each other within the framework of an iterated dilemma of prisoners in open and closed systems. The main attention is paid to collective characteristics such as memory, level of aggressiveness and complexity. The fine structure of the resonant regions for Alfvén and fast magnetosonic waves, which are used for RF heating in CTS in fusion devices, is discussed. The modification of the electrodynamic properties of media, which became possible after the advent of technologies that made it possible to create various inclusions in such media, is discussed. Metamaterials are studied, in particular, layered structures of ferrite semiconductors or thin wires embedded in a matrix. For scientists in the field of natural sciences, teachers, graduate students and senior students of physical faculties.

УДК 53; 530.1; 53.072

ISBN 978-966-285-144-1 (Issue 1)
ISBN 978-966-285-377-5 (Issue 2)
ISBN 978-966-285-594-4 (Issue 3)
ISBN 978-966-285-643-9 (Issue 4)
ISBN 978-966-285-750-4 (Issue 5)

НАЦІОНАЛЬНА АКАДЕМІЯ НАУК УКРАЇНИ

МІНІСТЕРСТВО ОСВІТИ І НАУКИ УКРАЇНИ
ХАРКІВСЬКИЙ НАЦІОНАЛЬНИЙ УНІВЕРСИТЕТ
імені В. Н. КАРАЗІНА

Серія «Проблеми теоретичної
та математичної фізики»

ПРОБЛЕМИ ТЕОРЕТИЧНОЇ ФІЗИКИ

Збірник наукових праць

Випуск 5

Науковий редактор випуску № 5 проф. В. О. Буц

Харків – 2023

УДК 53; 530.1; 53.072
П 78

Серія «Проблеми теоретичної та математичної фізики. Наукові праці» за загальною редакцією академіка А. Г. Загороднього, академіка М. Ф. Шульги

Рецензенти:
член-кореспондент НАН України О. Черемних;
проф. О. Герасимов.

Затверджено до друку рішенням Вченої ради
Харківського національного університету імені В. Н. Каразіна
(протокол № 10 від 7 червня 2022 року)

П 78 **Проблеми** теоретичної фізики. Збірник наукових праць. Випуск 5 / Ю. О. Аверков, В. О. Буц, В. І. Фесенко, І. О. Гірка, В. М. Куклін, О. В. Приймак, Ю. В. Прокопенко, О. Ю. Слюсаренко, Ю. В. Слюсаренко, Д. М. Ваврів, В. М. Яковенко, В. В. Яновський, А. Г. Загородній; за загальною редакцією А. Г. Загороднього, М. Ф. Шульги, наук. ред. вип. № 5 В. О. Буц. – Харків : ХНУ імені В. Н. Каразіна, 2023. – 488 с. (Сер. «Проблеми теоретичної та математичної фізики», за заг. ред. А. Г. Загороднього, М. Ф. Шульги).

ISBN 978-966-285-750-4

Обговорюються елементарні та колективні процеси взаємодії заряджених частинок у сильних полях, зокрема резонанси, їх регулярна та хаотична динаміка у регулярних та випадкових полях. Обговорюються механізми збудження електромагнітних коливань потоками нерелятивістських заряджених частинок, що рухаються вздовж діелектричних та плазмоподібних середовищ. Методом так званого скороченого опису нерівноважних процесів у нелінійних відкритих системах тотожних частинок, зокрема на кінетичному етапі їх еволюції, описано процедуру виведення кінетичних рівнянь для випадків слабкої взаємодії між частинками та малої інтенсивності зовнішнього поля. Представлені різні сценарії еволюції популяцій стратегій з пам'яттю, що взаємодіють один з одним у рамках ітерованої дилеми ув'язнених у відкритих та замкнутих системах. Основну увагу приділено колективним характеристикам, таким як пам'ять, рівень агресивності та складність. Обговорюється тонка структура резонансних областей для альфвенових і швидких магнітозвукових хвиль, що використовуються для ВЧ нагрівання в установках КТС. Обговорюється модифікація електродинамічних властивостей середовищ, що стала можливою після появи технологій, що дозволили створювати різні включення в такі середовища. Вивчаються метаматеріали, зокрема шаруваті структури з напівпровідників фериту або тонкі дроти, впроваджені в матрицю. Для вчених у галузі природознавства, викладачів, аспірантів та студентів старших курсів фізичних факультетів.

УДК 53; 530.1; 53.072

ISBN 978-966-285-144-1 (вип. 1)

ISBN 978-966-285-377-5 (вип. 2)

ISBN 978-966-285-594-4 (вип. 3)

ISBN 978-966-285-643-9 (вип. 4)

ISBN 978-966-285-750-4 (вип. 5)

CONTENTS

FOREWORD
(history reference)

Readers are invited to the fifth issue of scientific papers "Problems of Theoretical Physics". This project began to be implemented at the beginning of the second decade of this century by professors of V. N. Karazin's Kharkiv National University V. A. Buts, V. V. Yanovsky, V. I. Karas and V. M. Kuklin, which was the initiator of this project. The formation of this series of scientific works was supported by the directors of the two largest institutes of theoretical physics in Ukraine, academicians A. G. Zagorodny and N. F. Shulga, who took on the work of the general editorial of this series of issues. The first issue of scientific papers was presented to the scientific community in 2014 and was dedicated to the two hundredth anniversary of the establishment of the Kharkov Classical University of Eastern Europe. The second issue was published in 2017, the editor of these two issues was V. M. Kuklin, the third issue was published in 2019, V. V. Yanovsky took over the editing and compilation of the issue. The fourth issue was presented in 2020, the editor of this issue was V.I. Karas, who, unfortunately, did not manage to see it during his lifetime. A special feature of the fifth issue, which was edited by V. A. Buts, is the fact that it is published in English. Since many scientists in Ukraine and the countries of the former USSR are not in the English-speaking environment, at the end of each collection, annotations and extended abstracts of review papers are traditionally presented in three languages: English, Ukrainian and Russian. Therefore, each interested reader can first get acquainted with the content of the abstract in a language convenient for the reader. All issues of scientific papers of the series "Problems of Theoretical and Mathematical Physics" under the general editorship of A. G. Zagorodny, N. F. Shulga are placed in the collection of the Scientific Library of V. N. Karazin Kharkiv National University and are placed in researchgate. For example:

Problems of theoretical physics. Scientific works / V. A. Buts, A. G. Zagorodniy, V. E. Zakharov, V. I. Karas, V. M. Kuklin, A. V. Tur, S. P. Fomin, N. F. Shulga , V. V. Yanovsky; ed. issue V. M. Kuklin. – Kh. : V. N. Karazin KhNU, 2014. – Issue. 1. – 532 p. http://dspace.univer.kharkov.ua/handle/123456789/13728; https://www.researchgate.net/publication/345804085_Problems_of_theoretical_physicsScientific_works_issue_1

Problems of theoretical physics. Scientific works. Issue 2 / V. A. Buts, A. G. Zagorodniy, A. V. Kirichok, V. M. Kontorovich, V. M. Kuklin, A. A. Rukhadze, V. P. Silin, A. V. Tur , V. V. Yanovsky;, ed. issue V. M. Kuklin. – Kh. : V. N. Karazin KhNU, 2017. – Issue. 2. – 376 p. http://dspace.univer.kharkov.ua/handle/123456789/13729; https://www.researchgate.net/publication/345171947_Problems_of_theoretical_physicsScientific_works_issue 2

Problems of theoretical physics. Scientific works. Issue 3 / Yu. L. Bolotin, V. E. Zakharov, V. I. Karas, V. M. Kuklin, E. A. Pashitsky, V. I. Pentegov, V. I. Sokolenko, A. V. Tur , A. A. Turkin, V. V. Yanovsky; ed. issue V. V. Yanovsky. – Kh. : V. N. Karazin KhNU, 2019. – Issue. 3. – 398 p. http://dspace.univer.kharkov.ua/handle/123456789/15830 ; https://www.researchgate.net/publication/345172058_Problems_of_theoretical_physicsScientific_works_issue_3

Problems of theoretical physics. Scientific works. Issue 4 / N. A. Azarenkov, S.S. Apostolov, V.G. Baryakhtar, V.A. Buts, A. A. Golovanov, A.G. Danilevich, V.I. Karas, M.I. Kopp, I.Yu. Kostyukov, Z.A. Mayzelis, A.M. Pukhov, T.N. Rokhmanova, P.S. Strelkov, J. Thomas, A.V. Tur, V.A. Yampolsky, V.V. Yanovsky; under the general editorship of A.G. Zagorodny, N.F. Shulgi, ed. issue IN AND. Carp. – Kharkiv: KhNU named after V.N. Karazin, 2020. – Issue. 4. – 548 p. http://dspace.univer.kharkov.ua/handle/123456789/17608;http://dspace.univer.kharkov.ua/handle/123456789/17608_Problems_of_theoretical_physicsScientific_works_issue_4

FROM THE SERIES EDITORS

The issues of scientific papers publish reviews of scientific results in the field of theoretical and mathematical physics, which were obtained by Ukrainian scientists and their foreign colleagues. It should be said that by now the number of works in the field of theoretical and mathematical physics is growing almost exponentially. It's not bad. The scientific community largely lives under the slogan - "There is nothing more practical than a good theory." Indeed, theoretical and mathematical physics create the base, the foundation on which our understanding of the world around us is built. On this basis, on this foundation, new technologies are being created, the building of the Science of Nature is being built. Over time, it is difficult to capture the entire volume of rapidly growing information. Therefore, review papers are very useful, which are largely based on experiments that stimulate and confirm theoretical developments. These review papers cover a large amount of information, focusing on the most interesting results and the most important directions in the development of physics. Such reviews are a generalization and quintessence of our understanding of the world around us. They are well thought out, conclusions and generalizations have been formulated for many years, and are the result of numerous publications, reports and discussions at conferences and seminars. Undoubtedly, these collections of scientific works pave the way for all those who want to understand any direction of physical research.

The issue contains six reviews. The collection opens with a review by Buts V.A. and Zagorodny A.G. 'Features of the dynamics of charged particles in electromagnetic fields'. This review is devoted to the features of the interaction of electromagnetic waves with charged particles. Both elementary processes of such interaction and collective ones are considered. Particular attention is paid to the analysis of resonances, the analysis of the regular and chaotic dynamics of charged particles both in regular fields and in random fields. In particular, it

is shown that multiplicative fluctuations that act on charged particles lead to fluctuation instability. The development of this instability is characterized by the fact that the higher moments grow faster than the lower moments. Moreover, it turned out that such a feature is also characteristic of regimes with dynamic chaos at cyclotron resonances. This means that the usual Fokker-Planck type equations cannot be used to describe such processes. An equation is given that is a generalization of such equations (higher moments are taken into account). The review gives a description of the new resonances. These new resonances take into account the essential role of the wave field strength in the interaction of charged particles with regular electromagnetic waves. The mechanism of practically unlimited acceleration of charged particles in a vacuum without a magnetic field is described. A new mechanism for the emergence of chaotic dynamics is also described. This mechanism allows chaotic dynamics to exist in systems with one degree of freedom or even in fully integrable systems.

Review O. Averkov, Yu. V. Prokopenko, and V. M Yakovenko 'Excitation of electromagnetic radiation during the interaction of charged particles with dielectric and plasma-like solid media' describes the mechanisms of excitation of electromagnetic oscillations both by individual particles and by streams of nonrelativistic charged particles that move along dielectric and plasma-like (including artificial) environments. The mechanisms of nonlinear stabilization of emerging instabilities are also described. In the electrostatic approximation, the electron energy losses due to the excitation of surface magnetoplasmons are calculated. The interaction between a tubular beam of charged particles and a dispersive metamaterial of cylindrical configuration has been investigated theoretically. Of particular interest is the case when the metamaterial is characterized by negative permittivity and magnetic permeability. This interest is due to the possibility of absolute instability. In this case, the metamaterial can be used as a delaying medium in electromagnetic radiation oscillators without the need to provide an additional feedback in the system, as is required, for example, in a backward-wave tube.

Review by O. Yu. Slyusarenko, Yu.V. Slyusarenko, A.G. Zagorodny 'The reduced description method in the kinetic theory of complex systems of identical particles' is based on the approaches proposed by M. M. Bogolyubov in 1946 in his famous book 'Problems of Dynamical Theory in Statistical Physics'. For quantum systems of many particles, the method required significant generalizations and modifications, the main of which were proposed by S.V. Peletminsky and set out in the book (also very famous) 'Methods of Statistical Physics' in collaboration with A.I. Akhiezer. The material presented in this review demonstrates the effectiveness of the reduced description method, which is modified to consider nonequilibrium processes in complex systems of identical particles, in particular, at the kinetic stage of evolution. In the review, the term "complex" unites some selected systems of many identical compound particles with a complex internal structure. Such systems are non-linear, open. They demonstrate new properties of dynamics. In particular, they demonstrate the properties of self-organization. As an example of such systems,

dissipative media are considered, which are under the influence of an external random field. In particular, low-temperature gases of hydrogen-like atoms in an external electromagnetic field. The systems are specially selected in such a way as to cover the cases of both classical and quantum complex systems. For systems of this kind, recipes for constructing microscopic approaches to describing their evolution, in particular, its kinetic stages, are proposed. The approaches are constructed in such a way that the noted internal construction of the structural units of the system does not affect the possibilities of considering these composite particles as point objects. It is observed that microscopic approaches to the description of evolutionary processes in enzymes are being developed in the future, either completely or insufficiently developed. Within the scope of the approaches, a procedure for revealing kinetic features for all mentioned systems is described in the case of a weak interaction between particles and a small pronounced external field. A number of revenues received, in particular, for the purpose of application development, are analyzed.

In the review Kuklin V. M., Priymak A. V., Yanovsky V. V. 'A world of strategies with memory' discusses the evolution of the strategy population with memory. It should be noted that consistent microscopic approaches to the description an iterated prisoner's dilemma, gaining evolutionary advantage points according to the payoff matrix. The review focuses on collective characteristics such as memory, the level of aggressiveness (the proportion of non-cooperation), the complexity of strategies. Different scenarios of evolution appear when using different selection rules for strategies intended for removal in the corresponding generation. The cases of resetting points of evolutionary advantages after each cycle (or generation) and summation (inheritance) of points of previous cycles are considered. At the first (primitive) stage of evolution, all simple strategies exist, aggressiveness grows at the second stage of the developed community, as a result of increased competition, complex strategies with a large memory depth win. If successful strategies are artificially removed, only aggressive counterparts remain. It has been empirically found that in the process of population evolution, a universal relationship between general aggressiveness and evolutionary advantages is preserved. In open societies that are injected with complex strategies with large memory (replacing the remote losers), complex strategies with large memory depth and less aggressive ones dominate. Penetration in this way of primitive strategies leads to their dominance, while complex strategies with a greater depth of memory in the population is preserved. The case of interaction of 50 thousand objects, each of which uses 50 strategies, is considered. In interaction, the losing strategy is replaced by the winning strategy. On average, subjects retain a third of the strategies, and complex ones dominate, with a large memory depth.

The review by I. O. Girka Fine structure of the local Alfven resonances in cylindrical plasmas with axial periodic inhomogeneity describes the structure of Alfven resonances (AR). In particular, the fine structure of these resonances has been studied. Low-frequency waves in a magnetoactive plasma are Alfvén (A), fast magnetosonic (FMSV) have great potential for use in applications.

First of all, we have in mind the use of these waves for high-frequency heating in CTS installations. These waves can also be used to create drag currents. Alfvén resonances (ARs) are interesting in that a significant part of the high-frequency power is absorbed in the vicinity of local ARs. As the plasma density increases, the region of these resonances moves towards the plasma boundary. This is undesirable. The review describes these features, and also describes the methods of combating this withdrawal of the AR to the border. In particular, it is shown that as the frequency and longitudinal wave vector decrease, the local AR region moves deep into the plasma. The results described in the review can be useful in planning experiments on plasma heating, as well as in geophysical experiments.

Review Fesenko V.I., Vavriv D.M. 'Electromagnetic waves in artificial composite media' is devoted to the study of the influence of the molecular structure of materials on their dispersion properties. It is noted that some particular cases of modification of the electrodynamic properties of natural media have been studied for a very long time. However, explosive interest in such media appeared after the advent of new technologies that allowed the creation of inclusions (in natural environments), in particular, it is possible to create an IC in which both the permittivity and magnetic permeability are negative. This review describes the simplest and most interesting properties of such artificial media. Surfaces of isofrequency are described (the surface of wave vectors at a fixed frequency). The properties of hyperbolic metamaterials are also discussed. These are materials that are layered structures of ferrite semiconductors in an external magnetic field or thin wires embedded in a natural environment (matrix). The name hyperbolic media comes from the fact that the isofrequency surface of such materials is a hyperboloid of revolution. Thus, this review can be called a review of the electrodynamics of metamaterials.

Academician **A. G. Zagorodny**
Academician **M. F. Shulga**

CHAPTER I

FEATURES OF THE DYNAMICS OF CHARGED PARTICLES IN ELECTROMAGNETIC FIELDS

V.A. Buts[1,2], A.G. Zagorodny[3]

[1].National Scientific Center "Kharkov Institute of Physics and Technology," National Academy of Sciences of Ukraine, 61108 Kharkov, Ukraine.
[2].Radio Astronomy Institute, National Academy of Sciences of Ukraine, 61002, Kharkov, Ukraine
[3]. Bogolyubov Institute for Theoretical Physics, 14B Metrolohichna Street, Kyiv 03143, Ukraine

This review describes some important features of the interaction of charged particles with electromagnetic waves. Both regular regimes and chaotic regimes of such interaction are described. The mechanisms of the transition of the regular motion of particles (and waves) to stochastic regimes are described. The role of additive and multiplicative fluctuations on the dynamics of individual particles and on their collective dynamics is described. It is shown that in many regimes the chaotic dynamics is such that the highest moments turn out to be much larger than the lowest moments. Such regimes must be described by kinetic equations, in which the role of higher moments is significantly reflected. Note that the Einstein-Fokker-Planck equations contain only the first two moments. The equations that take into account the higher moments are formulated in the review. Particular attention in this review is paid to resonances. In particular, the review describes new cyclotron resonances. The conditions of these new resonances differ from the known ones in that they substantially take into account the influence of the field strength of the wave with which the particles interact. The dynamics of particles under the conditions of these new resonances is described. New resonances in the interaction of charged particles with waves in vacuum are also described. The presence of such resonances leads to practically unlimited acceleration of charged particles by fields of electromagnetic waves (lasers) in a vacuum. The review also discusses and describes new mechanisms for the emergence of regimes with dynamic chaos. In particular, when waves are excited by an electron beam in a constant magnetic field, regimes with dynamic chaos arise as a result of a rapid, qualitative and periodic change in the form of the phase portrait. Regimes with dynamic chaos under the conditions of new cyclotron resonances arise as a result of the passage of phase trajectories through regions in which the uniqueness

theorem is violated. Such regimes can arise even in systems with one degree of freedom.

Keywords*: Cyclotron resonances, new cyclotron resonances, dynamic chaos, additive and multiplicative fluctuations, beam-plasma interaction, acceleration, synchronization.*

PACS numbers*: 05.45.Ac ; 05.45.Xt; 41.75.Jv; 52.25.Gj; 52.35.Mw; 52.50.Sw*

INTRODUCTION

The processes that take place in plasma, as well as in beam systems, are traditionally divided into two classes of processes. The first class is processes of the wave-particle interaction, the second class is the interaction of the wave-wave. This division is rather arbitrary. However useful. In the first class, the emphasis is on the dynamics of particles in external or even in self-consistent electromagnetic fields. Wave-to-wave processes describe the dynamics of waves in parametric and nonlinear processes [1,2].

In this review, we consider processes of the wave-particle type. Special attention is paid to the emergence of various instabilities, as well as the emergence of complex chaotic particle dynamics. The features of particle dynamics in the presence of random fields are also described. In particular, the conditions for the appearance of superdiffusion at cyclotron resonances are determined. New resonance conditions for wave-particle interactions are described.

These new resonances are generalizations of known cyclotron resonances. This generalization consists in the fact that the resonance conditions include the intensity of the electromagnetic wave with which the particles interact. Note that the conditions of known cyclotron resonances include only the dispersion characteristics of the wave (frequency and wave vector of the wave), as well as the strength of the external magnetic field. The magnitude of the electric field of the wave is not included in these conditions.

Regimes with dynamic chaos play an important role in the dynamics of particles and waves. This review describes some new mechanisms with complex chaotic dynamics, i.e. modes with dynamic chaos. New modes are also described, which are called modes with piecewise deterministic dynamics. The appearance of such regimes is due to the presence of either specific regions or specific points in the phase space in which the uniqueness theorem is not satisfied.

The appearance of chaotic dynamics of plasma particles or particles of beams of charged particles leads, in turn, to the appearance of chaotic (random) fields. The influence of such fields on the dynamics of individual particles and on the dynamics of some collective processes is also described in the review. Note that a special role in determining the conditions for the appearance of regimes with dynamic chaos is played by the criteria for the appearance of such regimes.

The most famous of them are the Melnikov criterion [3-5], the criterion for overlapping homoclinic trajectories in the phase space, and the

Chirikov criterion [6]. Note that the Melnikov criterion is the most stringent criterion. But it is difficult in specific applications. On the contrary, Chirikov's criterion is a phenomenological criterion. It is extremely useful when considering a huge number of physical processes. The review indicates situations when the Chirikov criterion can lead to incorrect conclusions.

The overview is divided into seven sections. **In the first section**, a fairly general formulation of the problem is formulated and the basic equations are written out that describe the dynamics of charged particles at cyclotron resonances. Various special cases are considered. Among the new ones, we note - obtaining a general analytical solution to the problem of the dynamics of charged particles for the case when the external electromagnetic wave propagates strictly along the direction of the external magnetic field. In this solution, only one cyclotron resonance is clearly visible, which corresponds to the autoresonant acceleration of particles. The disadvantage of this solution is its implicit time dependence. In the considered case, the width of the nonlinear cyclotron resonance tends to infinity. Therefore, there is no overlap of nonlinear cyclotron resonances. The dynamics are regular. In the second subsection, the situation is considered when an external electromagnetic wave propagates strictly perpendicular to the external magnetic field. This configuration of the field is typical for some high-frequency devices of the gyrotron type. In this case, there are a large number of cyclotron resonances. They can overlap. This gives rise to a regime with dynamic chaos. Further (in the third subsection) these and other special cases are generalized. For this, new variables were used, which made it possible to explicitly distinguish single cyclotron resonances. The widths of nonlinear cyclotron resonances and the distances between these resonances are determined. Under the condition when nonlinear resonances overlap (homoclinic trajectories intersect) regimes with dynamic chaos arise. These conditions correspond to the Melnikov-Chirikov criterion for the emergence of chaotic dynamics.

In the last subsection of this section, attention is drawn to the fact that the criteria obtained for the onset of dynamic chaos may turn out to be untenable. Note that the criterion for the emergence of dynamic chaos is an expression for the amplitude of the external electromagnetic wave, which must be greater than a certain expression. This expression depends both on the characteristics of the wave itself (frequency, wave vector) and on the characteristics of particles that are accelerated (from longitudinal and transverse impulses).

The peculiarity of the obtained inequality lies in the fact that the strength of the external field of the wave must be greater than the expression, in the denominator of which is the Bessel function. The argument of the Bessel function includes the transverse momentum of the particle. As soon as the momentum of the particle acquires a value that corresponds to the root of the Bessel function, then the amplitude of the external wave, which is necessary for the development of dynamic chaos, tends to infinity.

Therefore, one might expect that in this case the particle would cease to acquire energy from the wave. Numerical calculations show that such stabilization of energy gain does not occur. The reasons for this, at first glance, discrepancy are discussed. It turns out that only the fact that the Chirikov criterion must be used with caution is clear.

In the second section, we analyze the effect of additive and multiplicative fluctuations on the particle dynamics at cyclotron resonances. The most important result of this section is the result that, under conditions close to those of autoresonance, additive fluctuations have an anomalously large effect on particle dynamics. This anomaly is expressed in the fact that in the equation for the phase of the particle, the numerator contains the magnitude of the additive fluctuation, and the denominator contains an expression that tends to zero with parameters that tend to autoresonance.

If the autoresonance condition is strictly fulfilled, this expression cannot be used. However, in this case it is possible to obtain a rigorous analytical expression for the mean square of the particle energy. This expression indicates that the dynamics of particles is characterized by a superdiffusion process. The influence of multiplicative fluctuations turns out to be even more destructive for regular particle dynamics. It turns out that in this case the moments, starting from the second moment, grow exponentially. The so-called stochastic instability develops.

An important feature of this instability is the fact that the higher moments grow faster than the previous moments. This feature of the behavior of the moments indicates that the well-known kinetic equations such as the Einstein-Fokker-Planck equation cannot be used to describe such processes. Indeed, such equations are obtained taking into account only the second moments. Higher moments were not taken into account. The general form of the kinetic equation is given, in which all higher moments are taken into account.

The third section describes new cyclotron resonances. This section is the most interesting. All results in this section are new. The main feature of this section is that it is shown that it is necessary to take into account the amplitude of the external electromagnetic wave in the known cyclotron resonances. Note that the known cyclotron resonances contain only the dispersion characteristics of the wave (frequency and wave vector) and the strength of only the external magnetic field. The intensity of the external electromagnetic wave is not included in these conditions. Such a limitation can be justified only in the case of low intensities of the external wave.

Considering the advances in laser and high-frequency technologies, this is far from the case. These tensions can be significant. In addition, as it turned out, taking into account the strength of the external electromagnetic wave can be essential even in the case of low fields. We note two significant features of the particle dynamics under the conditions of these new resonances.

The first feature is that the dynamics of particles is stepwise in the dependence of momenta on time. On the steps themselves, the dynamics

turns out to be regular. Only the transitions from step to step are irregular. The steps themselves correspond to the conditions of the new resonances. Moreover, the neighborhood of the new resonances is described by the Adler equation. Note that Adler's equation is an ordinary differential equation of the first order. It is much simpler than the equation of a mathematical pendulum, which describes the dynamics of particles in the vicinity of the known cyclotron resonances

The second feature is that the dynamics of particles in a cross section is described by trajectories, which can be topologically represented as circles with different radii. The most important thing is that all these circles have one common point. Thus, in its dynamics, a particle falls into the vicinity of this common point and can accidentally jump from one circle to another. Note that the uniqueness theorem is violated at this common point. A mathematical model has been built that describes such dynamics. As a result, the mechanism of occurrence of randomness in particle dynamics resembles throwing a die with an unlimited number of faces. This dynamics was called piecewise deterministic dynamics.

The previous sections was devoted the dynamics of individual particles. In particular, the dynamics of individual particles in the presence of fluctuations. ***In the fourth section***, the role of spatial and temporal fluctuations on the dynamics of a collective of particles is considered. As an example, the influence of fluctuations on the well-studied regular dynamics of plasma-beam interaction is considered. If a beam of charged particles propagates in plasma with a random spatial inhomogeneity, then, as a result, not only the regular component of the wave grows, but also the random one. Using the methods of functional analysis (variational (functional) derivatives), it was possible to obtain an explicit expression for any moments of particle dynamics. It turned out that, both in the presence of spatially inhomogeneous fluctuations and fluctuations that depend on time, the higher moments grow faster than the lower moments. This means that the regular excitation of oscillations by a beam of charged particles in plasma can develop only during a limited time interval or in a limited spatial interval. Analytical expressions for these intervals are obtained.

The fifth section also examines the role of collective processes in the excitation of chaotic oscillations. In this case, a model of an electron beam was chosen, which is under conditions close to those of autoresonance. In this case, as noted in the first section, the width of the nonlinear cyclotron resonance in this case tends to infinity. There is no overlap of nonlinear cyclotron resonances. It could be assumed that the dynamics of excited oscillations by a flow of charged particles in a magnetic field, as well as the dynamics of particles, will be regular. Numerical studies show that the dynamics at the initial stage of instability development turns out to be really regular. However, when a certain value of the intensity of the excited wave is reached, this dynamics becomes chaotic. The mechanism of occurrence of chaotic dynamics does not fit into the known mechanisms. It is shown that the reason for the appearance of complex chaotic dynamics is a periodic, qualitative change in the form of the phase

portrait of particle motion. The appearance of this portrait resembles the phase portrait of the Duffing oscillator.

The dynamics of individual particles in the field of one regular electromagnetic wave and some features of the collective dynamics of particles were considered above. However, real electromagnetic waves are a packet of waves. The question arises: What is the difference between the dynamics of particles in the field of one regular wave from the dynamics of particles in a packet of waves? When can be used the approximation of one regular wave and when the dynamics of particles in a wave packet is qualitatively different from the dynamics in the field of one regular wave?

These questions are answered in ***section six***. It is shown that if the phase velocity is close to the group velocity of the wave packet, then the dynamics of particles in such wave packet practically does not differ from the dynamics of particles in one regular wave. If the phase and group velocities differ significantly from each other, then the dynamics of particles in the wave packet becomes chaotic. In this case, it is impossible to describe the wave packet by one regular wave.

The seventh section is devoted to the description of the discovered new resonances in the interaction of transverse electromagnetic waves with charged particles in vacuum. The conditions and mechanisms for the emergence of these new resonances are described. These resonances allow practically unlimited acceleration of electrons by fields of transverse electromagnetic waves in a vacuum. For example, by fields of laser radiation. It is shown that there is an analogy regarding the appearance of these new resonances with the appearance of cyclotron resonances. Indeed, these new resonances and cyclotron resonances arise only when the waves have nonzero transverse components of the wave vector.

SECTION 1. FEATURES OF PARTICLE DYNAMICS AT CYCLOTRON RESONANCES

This section was written based on materials from [7-10]

1.1. Problem statement and basic equations

Consider a charged particle that moves in an external constant magnetic field directed along the axis Z and in the field of a plane electromagnetic wave, which in generally has the following components:

$$\boldsymbol{\varepsilon} = \mathrm{Re}(\mathbf{E}\exp(i\omega t - i\mathbf{kr})), \quad \mathbf{H} = \mathrm{Re}\left(\frac{c}{\omega}[\mathbf{kE}]\exp(i\omega t - i\mathbf{kr})\right),$$

where $\mathbf{E} = E_0\boldsymbol{\alpha}$, $\boldsymbol{\alpha} = \{\alpha_x, i\alpha_y, \alpha_z\}$ - is the wave polarization vector.

Equation motion charged particles:

$$\frac{d\mathbf{p}}{dt} = e\boldsymbol{\varepsilon} + \frac{e}{c}\left[\frac{\mathbf{p}}{\gamma}\left(\mathbf{H}_0 + \mathbf{H}\right)\right]. \tag{1.1}$$

Without loss of generality, one can choose a coordinate system in which the wave vector of the wave has only two components k_x and k_z. It is also convenient to use the following dimensionless dependent and independent variables: $\mathbf{p} \to \mathbf{p}/mc$, $\tau \to \omega t$, $\mathbf{r} \to \frac{\omega}{c}\mathbf{r}$. Also it's usefully to take into account such formula: $\left[\mathbf{p}\left[\mathbf{k}\boldsymbol{\varepsilon}\right]\right] = \mathbf{k}\left(\mathbf{p}\cdot\boldsymbol{\varepsilon}\right) - \boldsymbol{\varepsilon}\left(\mathbf{k}\cdot\mathbf{p}\right)$.

The equations of motion in these variables will be as follows:

$$\begin{gathered}\frac{d\mathbf{p}}{d\tau} = \left(1 - \frac{\mathbf{kp}}{\gamma}\right)\mathrm{Re}\left(\boldsymbol{\varepsilon}e^{i\psi}\right) + \frac{\omega_H}{\gamma}\left[\mathbf{ph}\right] + \frac{\mathbf{k}}{\gamma}\mathrm{Re}\left[\left(\boldsymbol{\varepsilon}\cdot\mathbf{p}\right)e^{i\psi}\right], \\ \mathbf{v} = \frac{d\mathbf{r}}{d\tau} = \frac{\mathbf{p}}{\gamma},\ \dot{\psi} = \frac{d\psi}{d\tau} = 1 - \frac{\mathbf{kp}}{\gamma},\end{gathered} \tag{1.2}$$

where $\mathbf{h} = \mathbf{H}/H_0$, $\omega_H = eH_0/mc\omega$, $\boldsymbol{\varepsilon} = \varepsilon_0\boldsymbol{\alpha}$, $\varepsilon_0 = (eE_0/mc\omega)$, $\psi = \tau - \mathbf{kr}$, $\mathbf{k}$ - unit vector in the direction of the wave vector, $\gamma = (1 + \vec{p}^{\,2})^{1/2}$ dimensionless particle energy (measured in units mc^2), $\mathbf{p}$ - particle momentum. Multiplying the first equation of system (1.2) by $\vec{p}$, we obtain a useful equation that describes the change in the energy of a particle:

$$\frac{d\gamma}{d\tau} = \mathrm{Re}\left(\mathbf{v}\boldsymbol{\varepsilon}e^{i\psi}\right). \tag{1.3}$$

The system of equations (1.2) and (1.3) have well-known integrals:

$$\mathbf{p} + \mathrm{Re}\left(i\boldsymbol{\varepsilon}e^{i\psi}\right) - \omega_H\left[\mathbf{rh}\right] - \mathbf{k}\gamma = \mathbf{p}_0 - \mathbf{k}\gamma_0 + \mathrm{Re}\left(i\boldsymbol{\varepsilon}e^{i\psi_0}\right) - \omega_H\left[\mathbf{r}_0\mathbf{h}\right] = \mathrm{const} \tag{1.4}$$

Index "0" denotes the values of the initial variables.

Note that the system of equations (1.1) – (1.4) practically coincides with the system of equations, which was studied in [7-10].

1.2. Common solution of the system of equations (1.1) - (1.3). (Implicit form of decisions)

We firstly consider the case of wave propagation along an external magnetic field $\vec{k} = \{0, 0, k_z\}; \vec{H}_0 \| z$. Then the vector equation (1.2) and equation (1.3) can be conveniently rewritten in the following form:

$$\begin{aligned} \dot{p}_x &= \dot{\psi}\varepsilon_x \cos\psi + \omega_H (p_y/\gamma), \\ \dot{p}_y &= -\dot{\psi}\varepsilon_y \sin\psi - \omega_H (p_x/\gamma), \\ \dot{\gamma} &= \frac{1}{\gamma}\left(p_x\varepsilon_x \cos\psi - p_y\varepsilon_y \sin\psi \right), \end{aligned} \tag{1.5}$$

where $\varepsilon_x = \alpha_x\varepsilon_0$, $\varepsilon_y = \alpha_y\varepsilon_0$.

Note that the value $\gamma\dot{\psi} = C$ is an integral. Then the equations for the transverse components of the particle pulse can be issued separately in closed form:

$$\begin{aligned} p_x' &= \varepsilon_x \cos\psi + \Omega p_y \\ p_y' &= -\varepsilon_y \sin\psi - \Omega p_x \end{aligned} \tag{1.6}$$

here $p' = \dfrac{dp}{d\psi}$; $\Omega = \left(\omega_H / \gamma\dot{\psi}\right)$.

Solution of the system of equations (1.6) provided that $\Omega = const$ it can be found in analytical form. For this, it is convenient to represent the system of equations in the form of a system of oscillators:

$$p_x'' + \Omega^2 p_x = -\varepsilon_1 \sin\psi \; ; \qquad p_y'' + \Omega^2 p_y = -\varepsilon_2 \cos\psi \, , \tag{1.7}$$

where $\varepsilon_1 = \varepsilon_x + \Omega\varepsilon_y$; $\varepsilon_2 = \varepsilon_y + \Omega\varepsilon_x$.

It is easy to see that the system of equations (1.7) has resonances when the condition $\Omega = 1$ is fulfilled. This condition is an autoresonance condition. In the general case, it is convenient to represent solutions of the system of equations (1.7) in the form:

$$\begin{aligned} p_x &= A\sin\Omega\psi + B\cos\Omega\psi + \frac{\varepsilon_1}{\left(1-\Omega^2\right)}\sin\psi, \\ p_y &= C\sin\Omega\psi + D\cos\Omega\psi + \frac{\varepsilon_2}{\left(1-\Omega^2\right)}\cos\psi \end{aligned} \, , \tag{1.8}$$

where

$$A = p_{x0}\sin\Omega\psi_0 + p_{y0}\cos\Omega\psi_0 + \sin\Omega\psi_0\sin\psi_0\frac{\varepsilon_1}{\Omega^2-1} + \cos\Omega\psi_0\cos\psi_0\frac{\varepsilon_2}{\Omega^2-1}$$

$$B = p_{x0}\cos\Omega\psi_0 - p_{y0}\sin\Omega\psi_0 + \cos\Omega\psi_0\sin\psi_0\frac{\varepsilon_1}{\Omega^2-1} - \sin\Omega\psi_0\cos\psi_0\frac{\varepsilon_2}{\Omega^2-1}$$

$C = -B$, $D = A$; $\varepsilon_1 = \varepsilon_x + \Omega\varepsilon_y$; $\varepsilon_2 = \varepsilon_y + \Omega\varepsilon_x$

Using equation (1.2) and (1.5), as well as solution (1.8), as well as the fact that the expression $\gamma\dot{\psi} = C$ is an integral, it is easy to find analytical expressions for the longitudinal momentum and for the particle energy:

$$p_z = \frac{1}{2\gamma\dot{\psi}}\left[p_x^2 + p_y^2 - \left(p_{x0}^2 + p_{y0}^2\right)\right] + p_{z0} \tag{1.9}$$

$$\gamma = \frac{1}{2\gamma\dot{\psi}}\left[p_x^2 + p_y^2 - \left(p_{x0}^2 + p_{y0}^2\right)\right] + \gamma_0 \tag{1.10}$$

1.3. Autoresonance

Of particular interest is the form of the solution in the case of autoresonance ($\Omega = 1$). To solve the problem in this case, it is convenient to use a slightly different way of solving system (1.5). Namely, it is convenient to rewrite system (1.5) using complex functions:

$$\Phi' + i\Phi = f(\psi) \tag{1.11}$$

where $\Phi = p_x + ip_y$; $f(\psi) = \left(\varepsilon_x\cos\psi - i\varepsilon_y\sin\psi\right)$

Using the solution of equation (1.11), it is easy to find expressions for the transverse momenta (for p_x and for p_y). General formulas are rather cumbersome. Therefore, as an example, we give expressions for the case when the wave has circular polarization:

$$p_x = \varepsilon\left(\psi - \psi_0\right)\cos\psi + p_x(0); \qquad p_y = -\varepsilon\left(\psi - \psi_0\right)\sin\psi + p_y(0) \tag{1.12}$$

Solution (1.12) is presented in an implicit form, therefore, from this form of the solution it is difficult to see the laws of change in momenta and energy from time (or from coordinate). However, it is easy to estimate such temporal dynamics at large values of time, and, accordingly, at large values of energy. For such estimation, we will be use expression for integral $\gamma\dot{\psi} = \gamma - p_{\|} = C$. As result one can get such expression for transverse momenta:

$$p_\perp = \sqrt{2\gamma C} \tag{1.13}$$

Let's use the equation for energy. For simplicity, consider a wave with linear polarization ($\varepsilon_x = \varepsilon;\ \varepsilon_y = 0$). Then:

$$\frac{d\gamma}{d\tau} = \varepsilon^2 \frac{p_\perp}{\gamma}\left(\cos\psi\right)^2. \tag{1.14}$$

We substitute the expressions for the transverse momentum into these equations, carry out averaging over the phases, and integrate this equation. As a result, we obtain the following asymptotic estimate for the particle energy:

$$\gamma \approx \varepsilon^{4/3} \cdot \left(\tau\right)^{2/3}. \tag{1.15}$$

Thus, we have obtained a general solution to the dynamics of particles in the wave field and in a constant magnetic field (1.8) - (1.10), (1.12). Pay attention to the fact that the solution is presented implicitly. It's very simple. Seeming simplicity. ... In this case, only one resonance is clearly (analytically) visible - autoresonance. Other (cyclotron) resonances in this form of the solution cannot be seen. These resonances are hidden in the implicit form of decisions. We also note that in the form of the solutions obtained, there are no explicit modes with dynamic chaos.

1.4. The emergence of chaotic dynamics

In this subsection, we will show that despite the simple expressions of the equations (1.5) themselves, as well as their solutions at $k_z = 1$, the dynamics of particles can be of a complex chaotic nature. To prove this fact, it is most simple to use numerical methods for solving the system of equations (1.5). ***The appearance of chaotic dynamics is associated with the appearance of a nonzero transverse component of the wave vector of the wave***. Below, for definiteness, we will consider the case when the wave vector of the wave has only one transverse component ($\vec{k} = \{1,0,0\}$). This case is interesting not only because regimes with dynamic chaos will appear, but this case is also a model of particle dynamics in such a well-known device as a gyrotron [11]. Below are the results of numerical calculations of the system of equations (1.5) at $\vec{k} = \{1,0,0\}$.

The equations of motion for this case have the form:

$$\begin{aligned} &\dot{x} = p_x/\gamma\,,\quad \dot{y} = p_y/\gamma \\ &\dot{p}_x = \left(p_y/\gamma\right)\left(-\varepsilon_0 \sin(\psi) + \omega_H\right) \\ &\dot{p}_y = -\varepsilon_0 \sin(\psi) + \left(p_x/\gamma\right)\left(\varepsilon_0 \sin(\psi) - \omega_H\right). \end{aligned} \tag{1.16}$$

Figure 1.1 shows solutions to the system of equations (1.16) at $\varepsilon_0 = 5 \cdot 10^{-4}$, $p_\perp(0) = 0$, $p_\parallel(0) = 0$ Figure 1.1a shows a pulse p_x, Figure 1.1b shows its spectral density of power and Figure 1.1c shows its correlation function. It can be seen from these figures that for the given values of the parameters, the dynamics of particles is regular. In this case, the dynamics of particles is regular for all initial phases of particles in the interval $0 \le (x_0, y_0) < 2\pi$.

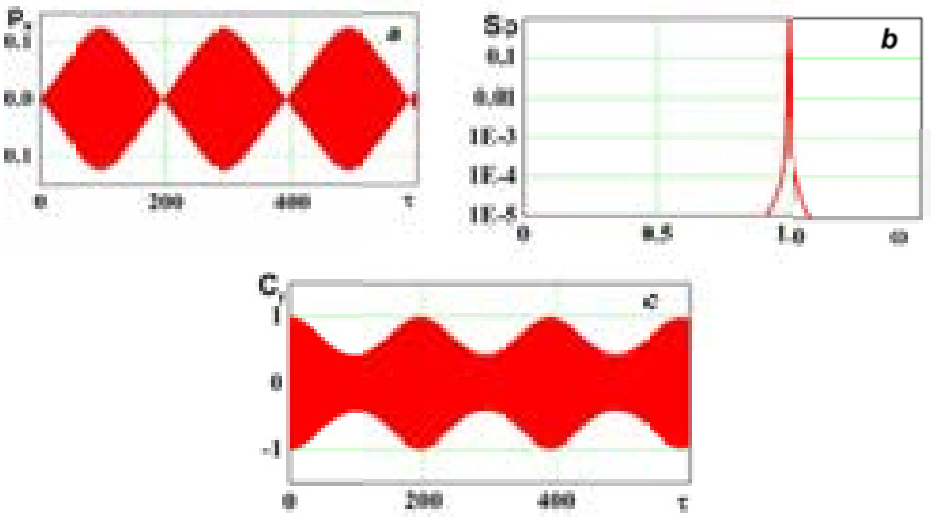

Fig.1.1. Particle momentum p_x (a), its spectral density of power (b) and correlation function (c) at $\varepsilon_0 = 5 \cdot 10^{-4}$, $p_{x,y} = 0$, $p_z = 0$, $x_0 = 0$, $y_0 = 0$

As the field strength increases to values of the order of magnitude $\varepsilon_0 = 0.1$, more intense beatings of the momentum amplitudes occur. However, the particle dynamics remains regular. The spectrum consists of narrow peaks, the correlation function does not decrease (see Figure 1.2).

In this case, the dynamics of particles also remains regular over the entire range of the initial phases of particles $0 \le \{x_0, y_0\} < 2\pi$.

With an increase in the field strength higher $\varepsilon_0 = 0.15$, $p_{x,y}(0) = 0$, $p_z(0) = 0$ a qualitative change in dynamics occurs (see Figures 1.3). It should be noted that this field strength is lower than that required to satisfy the resonance overlap condition (see next section).

The overlap criterion of nonlinear cyclotron resonances (1.34) is not met (at zero pulse values). The obtained result can be explained as follows. At the beginning, and during a certain period of time, the dynamics of particles is really regular, the particles are in cyclotron resonance, and gain energy.

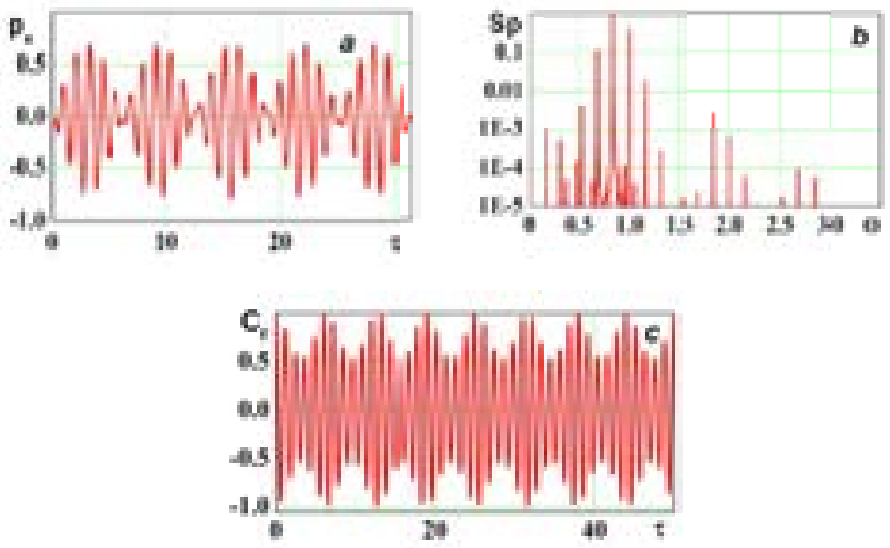

Fig. 1.2. Particle momentum (a), its spectral density of the power (b) and correlation function (c) at $\varepsilon_0 = 0.1$, $p_{x,y} = 0$, $p_z = 0$, $x_0 = 0$, $y_0 = 0$

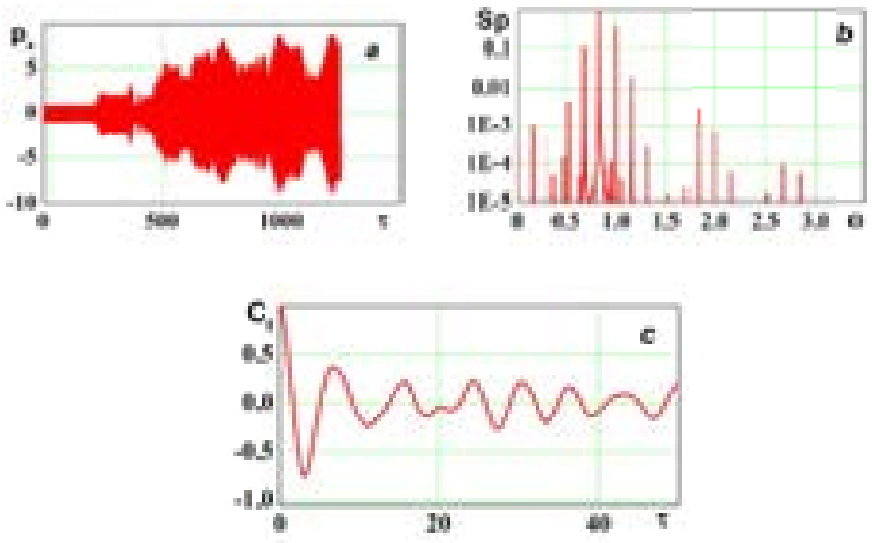

Fig. 1.3. Momentum p_x *of a particle (a), its spectral density of the power (b) and correlation function (c) at* $\varepsilon_0 = 0.19$, $p_{x,y}(0) = 0$, $p_z(0) = 0$, $x_0 = 0$, $y_0 = 0$

In this time interval, in accordance with criterion (1.34), the dynamics of particles is regular. Upon reaching a certain value of the transverse

momentum, the overlap criterion (1.34) begins to be met. The dynamics are becoming chaotic. Figure 1.3 shows solutions to the system of equations (1.5). Figure 1.3a shows the pulse, Figure 1.3b - its spectral density of the power, and Figure 1.3c - the correlation function. It can be seen from these figures that, for the given values of the parameters, the dynamics of particles becomes irregular. Note that insignificant changes in the initial coordinates of a particle, its dynamics change significantly. This means that there is local instability.

In the next section, we will point out a way that will allow us to explicitly detect cyclotron resonances and also detect regimes with dynamic chaos.

1.5. New variables. Cyclotron resonances

To see other features (besides autoresonance at $\vec{k}=\{0,0,1\}$) and to understand the reasons for the appearance of regimes with dynamic chaos at $\vec{k}=\{1,0,0\}$, it is convenient to go to new dimensionless variables: $p_\perp, p_z, \theta, \xi$ and η These variables will make it possible to explicitly detect cyclotron resonances, and also allow to explicitly describe the dynamics of particles in the vicinity of nonlinear cyclotron resonances, and also make it possible to find the conditions for the occurrence of local instability (overlap of nonlinear cyclotron resonances). These conditions make it possible to determine the parameters of the system under which a regime with dynamic chaos arises. Let's define these new variables using the following expressions:

$$p_x = p_\perp \cos\theta;\ \ p_y = p_\perp \sin\theta;\ \ p_\perp = \sqrt{p_x^2 + p_y^2};\ \ p_z = p_\parallel;$$
$$x = \xi - \frac{p_\perp}{\omega_H}\sin\theta;\ \ y = \eta + \frac{p_\perp}{\omega_H}\cos\theta \quad . \tag{1.17}$$

Let us substitute these variables into the vector equation (1.2). Let us expand the right-hand sides of the equations in a series in Bessel functions. As a result, we obtain the following equation, which describes the dynamics of the transverse momentum of particles:

$$\frac{dp_\perp}{d\tau} = \varepsilon_0\left[\left(1-k_z v_z\right)\sum_{n=-\infty}^{+\infty}\left(\alpha_x\frac{n}{\mu}J_n + \alpha_y J_n'\right)\cos(\theta_n) + \alpha_z k_x v_z \sum_{n=-\infty}^{+\infty}\frac{n}{\mu}J_n\cos(\theta_n)\right], \tag{1.18}$$

where $\mu = k_x p_\perp/\omega_H$, $\theta_n = k_z z + k_x\xi - \tau - n\theta$, $J_n = J_n(\mu)$, $J_n' = dJ_n(\mu)/d\mu$, .

Similarly, we obtain the equation for the remaining dependent variables, i.e. for $\dot{p}_z$, $\dot{\gamma}$, $\dot{\theta}$, $\dot{\xi}$, $\dot{\eta}$, $\dot{\theta}_n$:

$$\frac{dp_z}{d\tau} = \varepsilon_0 \alpha_z \sum_{n=-\infty}^{\infty} \left(1 - \frac{n\omega_H}{\gamma}\right) J_n \cos\theta_n + \varepsilon_0 k_z v_\perp \sum_{n=-\infty}^{\infty} \left(\alpha_x \frac{n}{\mu} J_n + \alpha_y J_n'\right) \cos\theta_n \quad , \tag{1.19}$$

$$\frac{d\gamma}{d\tau} = \varepsilon_0 \sum_{n=-\infty}^{\infty} \left(\alpha_x v_\perp \frac{n}{\mu} J_n + \alpha_y v_\perp J_n' + \alpha_z v_z J_n\right) \cos\theta_n \,, \tag{1.20}$$

$$\frac{d\theta}{d\tau} = \frac{\varepsilon_0 \left(1 - k_z v_z\right)}{p_\perp} \sum_{n=-\infty}^{+\infty} \left(\alpha_x J_n' + \alpha_y \frac{n}{\mu} J_n\right) \sin(\theta_n) + \\ + \frac{k_x \varepsilon_0}{p_\perp} \sum_{n=-\infty}^{+\infty} \left(\alpha_z v_z J_n' - \alpha_y v_\perp J_n\right) \sin(\theta_n) - \frac{\omega_H}{\gamma} \tag{1.21}$$

$$\frac{d\xi}{dt} = \frac{\boldsymbol{\varepsilon}_0}{\omega_H} \sum_{n=-\infty}^{\infty} \left(\alpha_y \left(1 - k_z v_\parallel\right) + \alpha_y k_x v_\perp \frac{n}{\mu}\right) J_n \sin\theta_n \,, \tag{1.22}$$

$$\frac{d\eta}{dt} = -\frac{\boldsymbol{\varepsilon}_0}{\omega_H} \sum_{n=-\infty}^{\infty} \left(\alpha_x \left(1 - k_z v_\parallel\right) J_n + k_x (\alpha_y v_\perp J_n' + \alpha_z v_\parallel J_n)\right) \cos\theta_n \,, \tag{1.23}$$

$$\frac{dx}{dt} = \frac{p_\perp \cos(\theta)}{\gamma}, \quad \frac{dy}{dt} = \frac{p_\perp \sin(\theta)}{\gamma}, \quad \frac{dz}{dt} = \frac{p_z}{\gamma}. \tag{1.24}$$

When obtaining formulas (1.18) - (1.24), they were used to expand functions in a series in terms of Bessel functions (see, for example, [8-10, 22]):

$$\exp(\pm i\mu \sin\theta) = \sum_{n=-\infty}^{\infty} J_n(\mu) \exp(\pm in\theta),$$

here $J_n = J_n(\mu)$ Bessel functions first kind , $\mu = k_x p_\perp / \omega_H$, $J_n' = dJ_n(\mu)/d\mu$, $\theta_n = \tau - k_z z - k_x \xi + n\theta$

Formulas (1.17) - (1.23) are difficult to analyze. Therefore, in what follows, we will leave on the right-hand side only those terms whose phases practically do not change. This condition for the stationarity of the phases will be the condition for cyclotron resonances:

$$\theta = const \qquad \dot{\theta}_n = \Delta_n \equiv k_z v_z + n\frac{\omega_H}{\gamma} - 1 = 0 \qquad \omega = \vec{k}\vec{v} + \frac{n\omega_H}{\gamma}. \tag{1.25}$$

1.6. Conditions for overlapping nonlinear cyclotron resonances. Caution at using the Chirikov test

Let us find the conditions for the overlap of nonlinear cyclotron resonances. For this, we will assume that the particle energy changes little as a result of interaction with the electromagnetic wave $\left(\gamma = \gamma_0 + \tilde{\gamma}\right)$, $\tilde{\gamma} << \gamma_0$, and resonance condition (1.25) is exactly satisfied for a particle with energy γ_0 :

$$\Delta_s\left(\gamma_o\right) \equiv k_z v_{z0} + s\frac{\omega_H}{\gamma_0} - 1 = 0. \tag{1.26}$$

Then, performing the expansion $\Delta_s\left(\gamma\right)$ near γ_0, from the system of equations (1.18) - (1.24) we obtain the following shortened system of equations:

$$\begin{aligned}
\dot{p}_\perp &= \frac{1}{p_\perp}\left(1 - k_z v_z\right) W_s \cdot \varepsilon_0 \cos\theta_s; \\
\dot{p}_z &= \frac{1}{\gamma} k_z W_s \varepsilon_0 \cos\theta_s; \\
\dot{\theta}_s &= \Delta_s \equiv k_z v_z + s\frac{\omega_H}{\gamma} - 1; \\
\dot{\gamma} &= \frac{\varepsilon_0}{\gamma} W_s \cdot \cos\theta_s;
\end{aligned} \tag{1.27}$$

here $W_s \equiv \alpha_x p_\perp \frac{s}{\mu} J_s - \alpha_y p_\perp J_s' + \alpha_z p_z J_s$, $\mu \equiv k_x p_\perp / \omega_H$.

The last two equations of system (1.27) make it possible to obtain a closed system of two equations for determining θ_s and γ :

$$\frac{d\tilde{\gamma}}{d\tau} = \frac{\varepsilon_0}{\gamma_0} W_s \cos\theta_s, \quad \frac{d\theta_s}{d\tau} = \frac{k_z^2 - 1}{\gamma_0}\tilde{\gamma}\ . \tag{1.28}$$

Equations (1.28) represent the equations of a mathematical pendulum. From them we find the width of the nonlinear resonance:

$$\Delta\dot{\theta}_s = 4\sqrt{\left(k_z^2 - 1\right)\varepsilon_0 \cdot W_s / \gamma_0^2}\ . \tag{1.29}$$

It is convenient to express the width of the nonlinear resonance in energy units

$$\Delta\tilde{\gamma}_s = 4\sqrt{\varepsilon_0 W_s / \left(k_z^2 - 1\right)}. \tag{1.30}$$

To find the distance between resonances, we write down resonance conditions (1.26) and averaged conservation law (1.4) for two adjacent resonances

$$k_z p_{s+1} + \left(s+1\right)\omega_H - \gamma_{s+1} = 0, \qquad \gamma_{s+1} - p_{s+1}/k_z = C. \tag{1.31}$$

$$k_z p_s + s\omega_H - \gamma_s = 0, \qquad \gamma_s - p_s / k_z = C. \tag{1.32}$$

Note that the constant C in integral (1.31) and in integral (1.32) is the same. From these conditions, we find the following value of the distance between resonances:

$$\delta\gamma = \omega_H / \left(1 - k_z^2\right). \tag{1.33}$$

From expressions (1.30) and (1.33) it follows that when there is inequality

$$\varepsilon_0 > \omega_H^2 / 4\left[\sqrt{W_s} + \sqrt{W_{s+1}}\right]^2 \left(1 - k_z^2\right), \tag{1.34}$$

then the sum of the half-widths of nonlinear resonances is greater than the distance between the resonances and their overlap occurs. In fig. 1.4 for the case $\beta_f < 1$ shows the direct resonances and one of the straight lines of the averaged integral of motion, along which the particle moves within the isolated resonance and according to which the distance between the resonances is calculated.

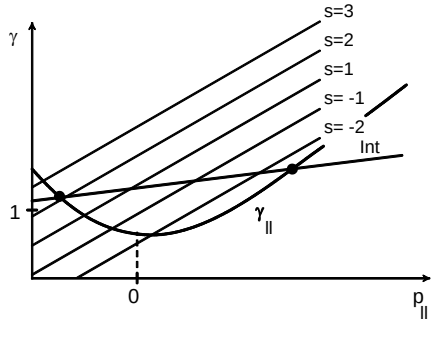

Fig. 1.4. Projection onto the plane $\left(\gamma, p_{\|}\right)$ *of resonance conditions (1.26) and integral (1.4) for the case* $k_z > 1$. *Depicted resonances:* $s = \pm 1; \pm 2; \pm 3$

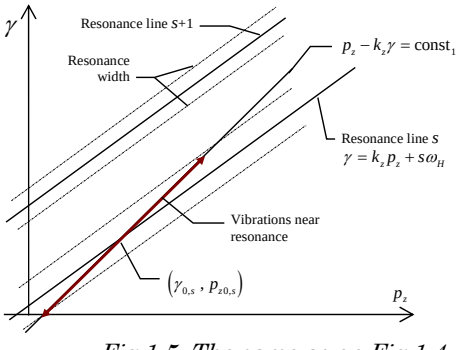

Fig.1.5. The same as on Fig.1.4. Only $k_z < 1$. *Additionally one can see width of nonlinear resonance*

Expression (1.30) for the width of nonlinear resonance and condition (1.34), under which a stochastic instability of particle motion arises, are rather general and describe the most important cases of resonant interaction of particles with electromagnetic waves.

Indeed, expression (1.30) gives the width of the nonlinear resonance for the Cherenkov interaction of a particle with the field $(s=0)$, for cyclotron resonances $(k_z=0)$, for nonlinear resonances on the normal $(s>0)$ and anomalous $(s<0)$ Doppler effects.

Accordingly, expression (1.34) gives the condition for the onset of stochastic instability caused by the overlap of the corresponding nonlinear resonances. Accordingly, expression (34) gives the condition for the onset of stochastic instability caused by the overlap of the corresponding nonlinear resonances.

Let us discuss some specific cases of the overlap condition for nonlinear resonances (1.34).

1. Consider the interaction of a particle with a longitudinal wave in a constant magnetic field. The criterion for the appearance of chaotic motion of a charged particle under these conditions for a nonrelativistic particle was obtained in [12, 13]. In [14], these results were generalized to the relativistic motion of a particle. Formula (1.34) contains these results. Indeed, for a longitudinal wave $(\alpha_x=\frac{k_x}{k},\ \alpha_y=0,\ \alpha_z=k_z/k)$ with taking in account resonant conditions $(s\omega_H+k_z p_z=\gamma)$ we have $W_s=\gamma\cdot J_s(\mu)/k$. Assuming $\mu>>1$, from (1.34), we find the following condition for the occurrence of stochastic instability due to the overlap of Cherenkovsky $(s=0)$ and neighboring resonances on the normal ($s=1$) and anomalous ($s=-1$) Doppler effects:

$$\varepsilon>\frac{\omega_H^2\sqrt{\mu}}{\gamma\left(1-k_z^2\right)}\frac{1}{16}\sqrt{\frac{\pi}{2}}. \qquad (1.35)$$

This expression, up to a numerical factor $\frac{1}{16}\sqrt{\frac{\pi}{2}}$, coincides with the criterion obtained in [14]. The difference in the numerical coefficient is due to the fact that in [14] is only an estimation of the width of the nonlinear resonance was given.

2. Let a transverse electromagnetic wave propagate perpendicular to the external magnetic field. This case simulates the dynamics of particles in gyrotrons . In this case, the overlap of resonances is due only to relativistic effects. For the E-wave (polarization = (0, i, 0), the criterion for resonance overlap is:

$$\varepsilon > \omega_H^2 / 16 p_{\perp 0} J_s^{'}(\mu) \tag{1.36}$$

and does not depend on the longitudinal velocity.

For the H-wave $\vec{\alpha} = (0,0,1)$, formula (1.34) becomes

$$\varepsilon > \omega_H^2 / 16 p_{z0} J_s(\mu) . \tag{1.37}$$

In contrast to the case of the E-wave, the amplitude of the H-wave, required for the development of stochastic instability, depends significantly on the value of the initial longitudinal impulse.

3. Consider condition (1.34) for the case of motion of a particle in the field of a plane polarized electromagnetic wave propagating at an angle ϕ to the external magnetic field in a medium with a refractive index $n > 1$. To overlap the Cherenkov $(s = 0)$ and adjacent cyclotron resonances in the E-wave field $\vec{\alpha} = (\cos\phi, 0, \sin\phi)$, condition (1.34) is transformed to the form

$$\varepsilon > \omega_H v_{zo} / 16 J_o(\mu) \gamma_o (1 - v_{zo}^2) \sin\phi . \tag{1.38}$$

In the field of the H-wave, this expression takes the form

$$\varepsilon > \omega_H v_{zo}^2 / 16 J_1(\mu) p_{\perp o} (1 - v_{zo}^2) . \tag{1.39}$$

From expressions (1.38) and (1.39) it follows that with an increase in the longitudinal velocity of the particle, the value of the wave amplitude required to overlap the resonances increases.

4. The case of longitudinal propagation of an electromagnetic wave in vacuum $(k_z = 1)$ should be especially noted. In this case, stochastic instability does not develop $(\varepsilon \to \infty)$. In the case under consideration, the resonance condition coincides with the integral of motion (see formulas (1.31) and (1.32)) and the change in the particle energy does not remove it from resonance. This condition is condition for autoresonance, which was first studied in [15,16], are satisfied. Thus, it can be claimed that the stochastic instability of particle motion does not develop under autoresonance conditions.

5. For the purposes of stochastic acceleration, it is of interest to consider the case of high energies of a particle $(\gamma >> 1)$ that interacts with a plane electromagnetic E-wave $(\vec{\alpha} = (0, i, 0))$ propagating perpendicular to the external magnetic field $(k_z = 0)$. For simplicity, we will assume that the particle has no longitudinal velocity $(p_z = 0)$, and the interaction with the wave occurs at high cyclotron resonances $(s >> 1)$. The last condition corresponds to the case of stochastic acceleration of a particle in the field of a wave whose frequency is

much higher than the cyclotron frequency $(\omega >> \omega_H)$. The resonance condition in the considered case has the form $\omega_H = \frac{s}{\gamma}$. Since $p_{\perp s} \sim \gamma$, then $\mu \cong s >> 1$ and you can use the asymptotics of the Bessel functions $J_s(\mu) \sim 0,44/(s)^{1/3}$. Substituting these estimates into formula (1.34), we obtain

$$\varepsilon > 0,28 \cdot \omega_H \cdot s^{1/3}. \qquad (1.40)$$

From formula (1.40) it follows that with an increase in the resonance number, the wave amplitude required to overlap the resonance increases.

1.7. Caution at using the Chirikov test

The formula (1.34) obtained above indicates the value of those parameters at which the dynamics of charged particles is in a regime with dynamic chaos. This formula is a consequence of the Chirikov criterion [6]. We saw above that it can be used over a very wide range of parameters. At first glance, one gets the impression that criterion (1.34) is satisfied in all the parameters specified in this formula. In most cases, this turns out to be true. However, as we will see below, in some cases formula (1.34) gives incorrect results. Let's consider this case in more detail. We will consider the particle dynamics for the values of the wave parameters that were used in Section 4. Using formula (1.34), we define the parameter regions for which there are regimes with dynamic chaos and the regions where the dynamics should be regular. It is enough to consider the region of parameters on the plane ($p_\perp$, ε_0).

Figure 1.6 shows the space of two main parameters ε_0 and $p_\perp$. In addition, this figure shows a curve that divides this space in two. The space above the curve corresponds to the parameters for which condition (1.34) is satisfied.

The region below this curve is the region where the conditions for overlapping resonances are not fulfilled and chaotic dynamics should not arise.

From criterion (1.34), in particular, it follows that when the condition $W_s \to 0$ is fulfilled, the wave amplitude necessary for the occurrence of a regime with dynamic chaos tends to infinity. Physically, this condition means that the width of one of the nonlinear cyclotron resonances tends to zero. In particular, the width of the first nonlinear cyclotron resonance tends to zero when $J_1' \to 0$. This condition is easily attained at a certain value of the transverse momentum $p_\perp$. In this case, it can be expected that the particle, getting energy from the wave as a result of resonant cyclotron interaction with the wave, ceases to effectively take energy from the wave.

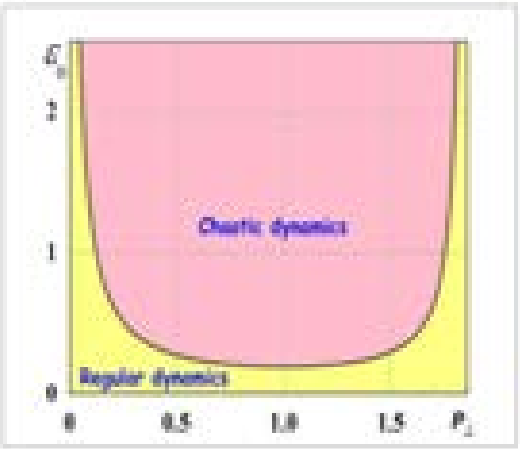

Fig. 1.6. Parameter space ε_0 *and* $p_\perp$ *. The region above the curve corresponds to the regime with dynamic chaos*

Our preliminary numerical studies of the particle dynamics under these conditions show that such a breakdown of the chaotic particle dynamics does not occur. Therefore, more thorough analytical and numerical studies of this apparent contradiction have been undertaken.

As follows from works [7-11,17], when nonlinear cyclotron resonances are overlapped (at sufficient field strength), particles continuously gain energy (according to the diffusion law). In this case, they must fall into the region with a transverse momentum of the order of $p_\perp = 1.8$. In accordance with criterion (1.34), the field strength required for the occurrence of a regime with dynamic chaos increases sharply in this case. One would expect that at these values of transverse momenta, the energy level that the particles can get will stabilize. However, numerical calculations show that there is no stabilization. The particles continue to gain energy (see Fig. 1.3a).

... This result can be explained by the fact that for these values of the parameters, the cyclotron resonances that remained unaccounted for in criterion (1.34) begin to play a decisive role. Thus, the results obtained above indicate that, under the conditions considered above, cyclotron resonances not taken into account in criterion (1.34) can play an essential role. Recall that criterion (1.34) was obtained as a condition for the overlap of two adjacent nonlinear cyclotron resonances (Chirikov's criterion). Note that the effect of a large number of nonlinear cyclotron resonances with which the particle interacts weakly can be simulated by the presence of an external noise effect. Indeed, as we will see in the next section, the role of even small external fluctuations can radically change the dynamics of charged particles at cyclotron resonances. These results can qualitatively explain the contradictions that have arisen.

1.8. Conclusion

Here, we formulate and briefly discuss the most important results of this section:

1. Analytical criteria for the appearance of dynamic chaos are found both for the general case and for the most physically interesting particular cases.

2. Criterion (1.34) for the appearance of chaotic dynamical regimes in the systems with cyclotron resonances should be used with caution. It has been shown that the formal application of this criterion can lead to incorrect results for the dynamics of particles. The analysis has shown that discrepancy between analytical and numerical results appear because criterion (1.34) was obtained under the assumption that two neighboring cyclotron resonances that can be synchronous with particles play the main role in the dynamics of particles. This assumption is well justified in most cases. However, this assumption is no longer valid if one of the chosen synchronous resonances ceases to efficiently interact with particles under certain conditions. One of these conditions is the case where the width of one of these resonances tends to zero. The role of other cyclotron resonances disregarded in the analysis becomes decisive under these conditions. Such an analysis of criterion (1.34) is novel. However, from the general methodological point of view, it is more instructive than novel. There is the problem: how can the effect of these resonances on the dynamics of particles be taken into account? The simplest way is to describe their effect as the effect of external noise.

3. In addition, as will be seen in the third section, as well as in the fifth section, other mechanisms can play a significant influence on the emergence of such regimes.

SECTION 2. EFFECT OF FLUCTUATIONS ON THE DYNAMICS OF PARTICLES AT CYCLOTRON RESONANCES

2.1. Introduction

An important feature of cyclotron resonances is that the long-term (up to infinity) effective energy exchange between particles and waves can be expected under nearly self-resonance conditions because the integrals of motion of particles under autoresonance conditions coincide with cyclotron resonance conditions. Such a feature of the dynamics of interaction of particles with electromagnetic fields is promising for its implementation in generators and accelerators.

However, attempts to use this fact for the efficient excitation of oscillations were unsuccessful [18]. The authors of [19] believe that the

efficiency of interaction is low because of a large number of additional nonresonance electromagnetic modes (and even improper) that are disregarded in analytical and numerical studies and always accompany the excitation of intense electromagnetic waves. In many cases, the effect of a large number of disregarded modes can be simulated by external noise. Furthermore, noise components always exist in the processes of interaction of intense electromagnetic radiation with particles. For this reason, the effect of external fluctuations on the dynamics of particles is often necessary. As will be found in this section, the inclusion of this effect is necessary under nearly self-resonance conditions. Indeed, as was shown in [17, 19-21], the dynamics of particles under nearly autoresonance conditions can be anomalously sensitive to external fluctuations. Below, we consider this problem in more detail for the simplest structure of the field of an electromagnetic wave propagating along the direction of the field

$$\vec{H}_0 \parallel z\,,\ \vec{E} = \mathrm{Re}\{E_x, 0, 0\}\,,\ \ \vec{H} = \{0, H_y, 0\}\,,\ \vec{k} = \{0, 0, k_z = 1\} \tag{2.1}$$

We analyze the effect of additive and multiplicative fluctuations in the most interesting case, i.e., under nearly self-resonance conditions:

$$R_s = k_z \upsilon_z + (s\omega_H / \gamma) - 1 \to 0 \tag{2.2}$$

2.2. Influence of additive fluctuations on particle dynamics. Superdiffusion.

We first consider the role of additive fluctuations. Since the field amplitude is small, $\varepsilon_0 << 1$, the system of equations (1.26) and (1.27) from first section can be linearized [14]:

$$\frac{d\tilde{\gamma}}{d\tau} = -B\tilde{\theta},\quad \frac{d\tilde{\theta}}{d\tau} = \alpha\tilde{\gamma} + f\,, \tag{2.3}$$

where $B \equiv (\varepsilon_0 W_1 / 2\gamma_0)\sin\theta_0$, $\theta_1 = \theta + \tilde{\theta}, \tilde{\theta} << 1$, $\tilde{\gamma} << 1$, $\alpha = (\partial R_{n0} / \partial\gamma)_{\gamma_0}$, $\gamma << \tilde{\gamma}$, $f = \tilde{\omega}_H$, is the additive fluctuation force. In the analytical study, we assume that $f(\tau)$ is a Gaussian delta-correlated random process with zero mean:

$$\langle f(\tau) f(\tau') \rangle = 2D\delta(\tau - \tau')\,,\ \langle f \rangle = 0\,. \tag{2.4}$$

where D is the diffusion coefficient. The parameter α determines the closeness of conditions to the self-resonance conditions. This parameter is zero if autoresonance conditions are exactly satisfied. Under these

conditions, the system of equations (2.3) with relations (2.4) is solved analytically:

$$\left\langle \gamma^2 \right\rangle = \frac{2}{3} DB\tau^3 \tag{2.5}$$

Such a time dependence of the average energy squared indicates that the diffusion of particles in the energy space in this case has a character of superdiffusion.

We will use the method moments and the method of variational derivatives to solve system (2.3) in the general case for an arbitrary value $\alpha = \left(\partial R_{n0} / \partial \gamma\right)_{\gamma_0}$.

From equations (2.3) it is easy obtain the system of equations for the first moments

$$\frac{d\left\langle \tilde{\gamma} \right\rangle}{d\tau} = -B\left\langle \theta \right\rangle, \quad \frac{d\left\langle \theta \right\rangle}{d\tau} = d\left\langle \tilde{\gamma} \right\rangle \tag{2.6}$$

For the second moments we will have:

$$\begin{gathered} \frac{d\left\langle \tilde{\gamma}^2 \right\rangle}{d\tau} = -2B\left\langle \tilde{\gamma}\theta \right\rangle, \\ \frac{d}{d\tau}\left\langle \tilde{\gamma}\theta \right\rangle = -B\left\langle \theta^2 \right\rangle + d\left\langle \tilde{\gamma}^2 \right\rangle + \left\langle f\tilde{\gamma} \right\rangle, \\ \frac{d\left\langle \theta^2 \right\rangle}{d\tau} = 2d\left\langle \tilde{\gamma}\theta \right\rangle + 2\left\langle f\theta \right\rangle. \end{gathered} \tag{2.7}$$

To split the correlations $\left\langle f\tilde{\gamma} \right\rangle$ and $\left\langle f\theta \right\rangle$ we use the method of variational derivatives (see, for example, [23]). The formula is important for us:

$$\left\langle f(t)R\left[f(t)\right] \right\rangle = \int_t \left\langle f(t)f(\tau) \right\rangle \left\langle \frac{\delta R\left[f(\tau)\right]}{\delta f(\tau)} \right\rangle d\tau \tag{2.8}$$

Here $R\left[z\right]$ is an arbitrary functional of z. Using (2.8), we find that $\left\langle f\tilde{\gamma} \right\rangle = 0$ and $\left\langle f\theta \right\rangle = D$. Here D is diffusion coefficient, which is defined in formula (2.4). Taking into account the obtained relations, the system of equations (2.7) can be rewritten in the form:

$$\frac{d^2\left\langle \tilde{\gamma}\theta \right\rangle}{d\tau^2} + 4dB\left\langle \tilde{\gamma}\theta \right\rangle = -2BD \tag{2.9}$$

The particular solution of equation (2.9), which are interested for us, is equal to $\langle \tilde{\gamma}\theta \rangle = -D/4d$. The average square of the energy in this case will be determined by the formula:

$$\left\langle \tilde{\gamma}^2 \right\rangle = \frac{\varepsilon_0 W_1 D}{2\gamma_0 \alpha}\tau \tag{2.10}$$

According to this expression, particles acquire the energy by a normal diffusion law. However, the diffusion coefficient becomes anomalously large when approaching the autoresonance conditions.

It is of interest to find the conditions under which the normal diffusion law (2.10) changes to the superdiffusion law (2.5). Formula (2.10) is valid for arbitrary $\alpha \neq 0$. To determine the dynamics of particles at $\alpha = 0$, it is necessary to return to the system of equations (2.3) and put in it $\alpha = 0$.

Then, it is easy to find the mean square of energy as a function of time under the exact autoresonance condition ($\alpha = 0$),

$$\left\langle \tilde{\gamma}^2 \right\rangle = \frac{B^2 D\tau^3}{3} = \frac{\varepsilon_0^2 p_\perp^2 D}{12\gamma_0^2}\left(\cos\theta_0\right)^2 \tau^3 \tag{2.11}$$

In terms of its main characteristics, formula (2.11) coincides with formula (2.5). It follows from these formulas that, under autoresonance conditions, additive fluctuations lead to particle dynamics, which is described by a law much faster than the usual quasilinear diffusion law. This law (2.11) is called superdiffusion.

2.3. Numerical analysis of the transition of particle dynamics with ordinary diffusion to superdiffusion

It is of interest to clarify the law of transformation of ordinary diffusion (2.10) to superdiffusion (2.11). To answer this question we will use numericall methods. We numerically study the time dynamics of charged particles in the cases close to self-resonance. The numerical calculations were performed with the parameter $B \approx 0.033$. The parameters α and B can be obtained under the corresponding initial conditions for particles and at the external field parameter $\varepsilon_0 = 0.1$. The parameter α was varied in the range of $10^{-7} \leq \alpha \leq 10^{-1}$. Fluctuations were described by a random variable uniformly distributed in the interval $(-\Delta\omega_H, \Delta\omega_H)$ $\Delta\omega_H = 0.1$ The initial conditions for addition of the energy and phase were taken in the form $\tilde{\gamma}(0) = 0,\ and\ \tilde{\theta}(0) = \pi/60$, respectively.

The average energy gain squared $\langle \gamma^2 \rangle$ was calculated by averaging over an ensemble of 40 realizations. In each realization, a random number generator generated a sequence of random numbers in the interval $(-\Delta\omega_H, \Delta\omega_H)$. The dimensionless time $\tau = t/T$ was measured in units of the period. The results of the numerical analysis of the time dependence of the average energy squared of the particle for various parameters α are presented in Fig. 2.1, where the solid lines show the numerical results for the average energy squared over the ensemble of 40 realizations and the points present their least squares approximations by a power-law function $F(\tau) = D \cdot \tau^{\mu}$ (D is a constant). The parameters for fields and particles, as well as initial conditions for the time addition to the energy and phase, did not change.

Fig. 2.1. Dependence of the mean square particle energy on time for a) a=0.01, b) a=.0001

As is seen in Fig. 2.1a, the time dependence of the average energy squared is almost linear, $\langle \gamma^2 \rangle \approx D \cdot \tau$. This corresponds to the well-known diffusion law $\langle \gamma \rangle \approx D \cdot \tau^{1/2}$. When the parameter α is reduced to $\alpha = 5 \times 10^{-4}$, the time dependence of the average energy square changes insignificantly: $\langle \gamma^2 \rangle \approx D \cdot \tau^{1.3}$ (Fig. 2.1b), and the diffusion coefficient increases. This variation of the average energy squared is in qualitative agreement with Eq. (2.10). A further decrease in the parameter α to $\alpha = 10^{-5}$ results in a qualitative change in the time dependence of the average energy squared. The parameter ν increases significantly ($\nu \approx 2.4$):.

The average square of the energy is proportional $\langle \gamma^2 \rangle \approx D \cdot \tau^{2.4}$. An illustration of such a change in energy is shown in the graph in Fig. 2.2a.

When the parameter α is reduced from 10^{-5} to 10^{-7}, the diffusion coefficient increases insignificantly and the exponent increases to $\nu \approx 3$. The data for $\alpha = 10^{-7}$ are shown in Fig. 2.2b. As follows from this figure, there is a fairly good agreement between the numerical calculation and the approximation using a power function $D \cdot \tau^3$.

. These results show that the presence of additive fluctuations even with very small amplitudes indeed leads to the appearance of superdiffusion. However, as is seen in Figs. 2.2a–2.2b, this occurs only in an

extremely small vicinity of the exact autoresonance conditions. In real experiments (in almost all experiments), the autoresonance conditions cannot be satisfied with the required accuracy. Consequently, Eq. (2.10) rather than Eq. (2.5) or Eq. (2.11) should be used.

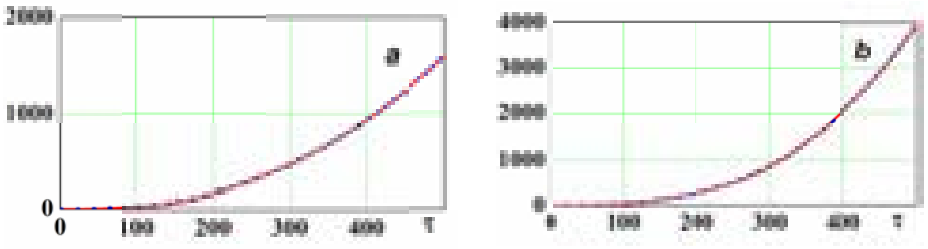

Fig. 2.2. Time dependence of the average square of the particle energy for a) $\alpha = 10^{-5}$ *, b)* $\alpha = 10^{-7}$

2.4. Influence of multiplicative fluctuations on particle dynamics

We now consider consequences of the presence of multiplicative fluctuations. Such fluctuations appear, e.g., in the presence of fluctuations of the wave amplitude in which the particle moves. The dynamics of the particle located near a "center-type" singular point, rather than near a "saddle" point is of the most interest because the distance between particles near the saddle point increases exponentially even under the action of regular forces. The equations for the time dynamics of particles near the center-type points of a mathematical pendulum can be represented in this case in the convenient form [21]

$$\frac{du}{d\tau} = -(1 + f(\tau))\theta, \quad \frac{d\theta}{d\tau} = u. \tag{2.12}$$

Here, $\tau \equiv \omega \cdot t \cdot \sqrt{|\alpha \cdot B|}$ is the new dimensionless time and the relation between the energy of the particle and the angle $\tilde{\gamma} = \dot{\theta} \cdot \sqrt{|B/\alpha|}$. Equations (2.12) with the initial conditions $u(0) = 0$ and $\theta(0) = \pi/60$ were numerically analyzed. Fluctuations $f(\tau)$ are also described by a random variable uniformly distributed in the interval $(-\Delta f, \Delta f)$ with the amplitude of fluctuations $\Delta f = 0.1$. The numerically calculated time dependence of the average energy squared $\langle \gamma^2 \rangle$ is shown by the solid line in Fig. 2.3 in comparison with its approximation by the function $F_{\exp}(\tau) = D \cdot \exp(\delta\tau)$, which depicted by the dots. The exponential time dependence of the average energy squared is clearly seen in Fig. 2.3.

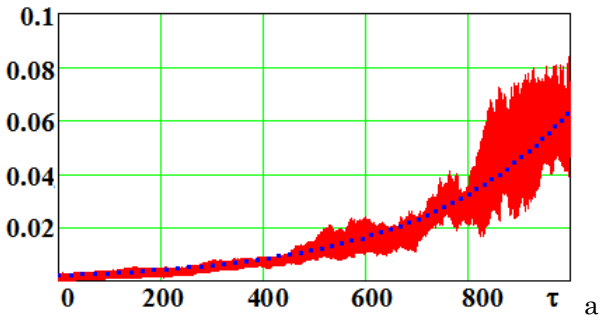

Fig.2.3. Time dependence of the average energy squared of the particle

2.5. Role of moments on the dynamics of particles

It was shown in [20] that the presence of multiplicative fluctuations under the self-resonance conditions (nonlinear cyclotron resonances do not overlap) leads to fluctuation instability. This instability results in an exponential increase in moments. It is known that an unlimited increase in the second moments corresponds to Levy flights [21, 24]. Because of such a singularity in moments, normal diffusion kinetic equations cannot be used to describe the dynamics of particles under these conditions. Either integral equations or equations with fractional derivatives should be used instead of these equations [17]. The method of moments is also a possible alternative [17]. This method was used in [21] to analyze the dynamics of particles under the cyclotron autoresonance conditions. The analysis of moments at overlapping of cyclotron resonances shows that higher moments in this case are larger than lower moments under certain conditions. It is important that such property of moments exists in the absence of fluctuations. This result is illustrated in Fig. 2.4, which shows the number dependence of the magnitude of moments divided by the factorial of their number $m!$. It is seen in Fig. 2.4 that, at a quite low strength of the external field ($\varepsilon 0 = eE/m\omega = 0.1$), moments decrease rapidly with an increase in their number (Fig. 2.4a). However, at high strengths (at $\varepsilon_0 = 0.19$), higher moments are larger than lower moments. It is seen in Fig. 2.4b that moments increase with the number up to $m = 6$.

Since even moments are much larger than odd moments, the distribution of the momentum px in the momentum space is symmetric. However, since the quantities shown in Fig. 2.4 are moments divided by the factorial of their number, which is a rapidly increasing function, these quantities corresponding to moments higher than sixth moment decrease rapidly. This property of moments also requires the modification of equations for the description of the kinetics of particles.

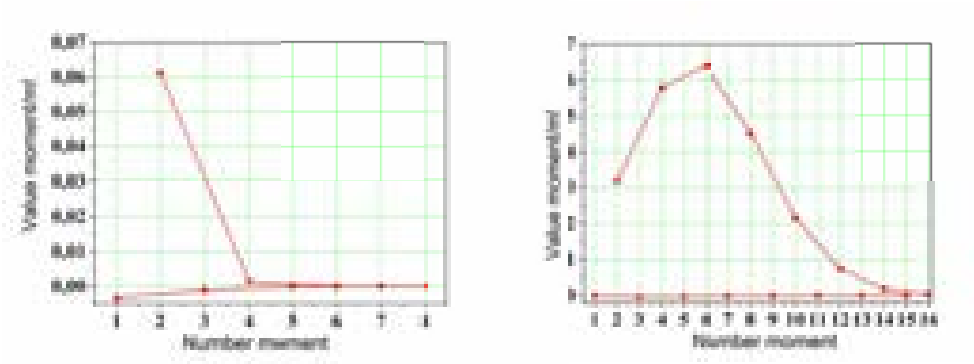

(a) (b)

Fig. 2.4. Time dependences of the moments p_x *divided by the factorial of their number m! for the field amplitudes (a)* $\varepsilon_0 = 0.10$ *0.10 and (b)* $\varepsilon_0 = 0.19$

2.6. Kinetic equations that take into account the role of higher moments

For such modification, we write the relation of the density of particles at the time $\tau + \Delta\tau$ to the density of particles at the time τ:

$$n(p,\tau+\Delta\tau) = \int_{-\infty}^{\infty} \left[n(p-p',\tau)\right] \mathrm{f}(p')dp' \tag{2.13}$$

Relation (2.13) mathematically means that the density of particles having the momentum p at the time $\tau + \Delta\tau$ is determined by all other particles (with different energies), which acquire the momentum p' with the probability $f(p')$ in the time interval $\Delta\tau$. It is convenient to rewrite Eq. (2.13) in the form

$$n(p,\tau+\Delta\tau) - n(p,\tau) = \int_{-\infty}^{\infty} \left[n(v-p',\tau) - n(p,\tau)\right] \mathrm{f}(p')dp' \tag{2.14}$$

If the moments are finite, retaining the terms up to the second moments in the expansion of the integrands in Eq. (2.14) in small displacements, we obtain the normal diffusion equation for the density of particles with the diffusion coefficient $D = \left\langle p^2 \right\rangle / 2$:

$$\frac{\partial n}{\partial \tau} = D \frac{\partial^2 n}{\partial p^2} \tag{2.15}$$

If the moments do not decrease, it is necessary to use the more general equation

$$\frac{\partial n}{\partial \tau} = \sum_m \frac{\left\langle (p)^m \right\rangle}{m!} \frac{\partial^m n}{\partial p^m} \; ; \quad m = 2j; \; j = \{1,2,3...\} \tag{2.16}$$

For the case shown in Fig. 8b, it is necessary to take into account four or five terms in the sum in Eq. (2.16). It is noteworthy that diffusion kinetic equations are often used to describe the dynamics of particles at cyclotron resonances (see, e.g., [47,48] and references therein).

Note that the equation (2.16) describes the dynamics of particles in one-dimensional momentum space. It is easy to generalize it to a three-dimensional case. In many important cases, it is sufficient to consider the diffusion of particles in a scalar energy space. In this case, the evolution of particles in the energy space will not differ from the equation (2.16).In it, it is only necessary to replace the impulse with energy.

2.7. Conclusion

Here, we formulate and briefly discuss the most important results:

1. For the study of cyclotron resonances, conditions under which the integrals of motion of particles coincide with resonance lines are of particular interest. These are the autoresonance conditions. When conditions approach the autoresonance conditions, the distance between cyclotron resonances increases rapidly. These resonances do not overlap in this limit. Conventional chaotic dynamical regimes (caused by the overlapping of resonances) do not occur. However, as was shown in [20, 21,17], the dynamics of particles under the autoresonance conditions is anomalously sensitive to external fluctuations. In this case, the analysis of conditions under which the diffusion dynamics of particles in the presence of fluctuations becomes superdiffusion is of particular interest. This analysis can be performed only numerically. This numerical analysis has been performed and the results have been presented abowe. It appeared that the autoresonance conditions in the presence of additive fluctuations should be satisfied with an accuracy of 10^{-7} for the transition of normal diffusion to superdiffusion. This means that, in the presence of additive fluctuations, the superdiffusion regime cannot be really reached. These results supplement the results reported in [20,21,17].

2. The presence of multiplicative fluctuations leads to the development of stochastic instability. A feature of this instability is the fact that the higher moments grow faster than the lower moments. In this case, the moments increase exponentially with the time. The dispersion becomes asymptotically unlimited. As is known, this is the condition for the appearance of Levy flights or “strange” kinetics [24]. Such kinetics has been numerically studied in this work. This study has indicated that the average energy squared of particles increases exponentially (see Fig. 2.2).

3. When the higher moments turn out to be larger than the previous moments, the well-known kinetic equations of the Einstein-Foker-Planck type

are already insufficient to describe the processes. New kinetic equations are needed that take into account the influence not only of the first and second moments, but also the influence of higher moments. Such equations have been obtained.

SECTION 3. NEW CYCLOTRON RESONANCES

3.1. Introduction

The acceleration of charged particles in a vacuum is a tempting prospect. There are a large number of works (both theoretical and experimental) devoted to this problem (see, for example, [10, 18, 25]). See also [56]. These works indicate the advantages of such acceleration and the problems that one has to face when solving such problems.

In the presence of a constant magnetic field, the situation changes qualitatively. Cyclotron resonances ($\omega = \vec{k}\vec{v} + \omega_H / \gamma$) appear. When using them, effective interaction of waves and particles is possible. The autoresonan acceleration scheme is especially attractive. However, to implement this scheme when using laser radiation fields, anomalously large external magnetic fields are required.

It should be noted that only the strength of the external magnetic field (ω_H) is included in the conditions of cyclotron resonances. There is no wave field strength under these conditions. This is due to the fact that the theory of cyclotron resonances was developed when the parameter of the wave strength ($\varepsilon = eE / mc\omega$) was almost always small.

Therefore, there was no need to take it into account. The wave intensity appeared only when studying nonlinear cyclotron resonances. With the advent of lasers, the situation could change. As indicated above, the use of cyclotron resonances seemed simply impossible.

In addition to lasers, sources of intense electromagnetic radiation, such as MCR, have appeared. However, all the same, only the usual conditions of cyclotron resonances were used (see above). It is clear that when the force parameter becomes significant, the usual conditions of cyclotron resonance must be modernized.

In this condition, both the strength of the external magnetic field and the strength of the fields with which the particles interact must be present.

This is especially true in the case of laser fields, when the cyclotron frequency turns out to be significantly lower than the laser radiation frequency ($\omega_H / \omega << 1$). This section is devoted to the analysis of the use of both the usual conditions of cyclotron resonance and new modernized conditions.

3.2. Formulation of conditions for new resonances

The initial equations for finding the conditions for the emergence of new resonances will be equations (1.18) - (1.24). The system of equations (1.27) will also be useful. One should also pay attention to formula (1.26), which is a condition for the appearance of the known cyclotron resonances. Such equations were studied in sufficient detail in [10,18, 25]. These equations are convenient for analysis when the parameter ε is small.

In this case, the averaging method was used to analyze this system. However, system (1.18) - (1.24) is strictly valid for any parameter value. Also, small parameters can be, in particular, Bessel functions for large parameter values ε . We will be interested in the dynamics of particles in laser fields. It means that in real conditions the dimensionless cyclotron frequency will also be a small parameter ($\omega_H << 1$). In addition, in most cases, we will be interested in the dynamics of relativistic particles ($\gamma >> 1$). In general case, the resonance conditions are conditions:

$$\dot{\theta}_n = k_z v_z + k_x \dot{\xi} - 1 - n\dot{\theta} = 0 . \tag{3.1}$$

Note that condition (3.1) takes into account the dynamics of the leading center, which substantially depends on the electric field strength of the laser radiation. In the special case ($\dot{\xi} = 0$), conditions (3.1) contain the well-known conditions of cyclotron resonance. We consider some particular new resonance conditions:

1. The simplest case is when the parameters of the fields and particles satisfy the following relations

$$n = 0 \quad k_z = 0,\ k_x = 1 \quad \omega_H << 1 \quad \varepsilon_x = \varepsilon_z = 0 \ . \tag{3.2}$$

Then condition (3.1) can be represented as:

$$\frac{\varepsilon_y}{\sqrt{\omega_H p_\perp}} \cos\left(\frac{p_\perp}{\omega_H} - \frac{\pi}{4} \right) \sin\theta_0 = -\sqrt{\frac{\pi}{2}} \ . \tag{3.3}$$

It can be seen that the resonance condition substantially depends on the wave strength parameter (ε_y).

2. If parameters of fields and particles satisfy relation:

$$n = 0,\ k_z \to 1,\ k_x << 1,\ \omega_H << 1,\ \varepsilon_x = \varepsilon_z = 0$$

then the expression for cyclotron resonance takes the form:

$$v_z + \frac{k_x \varepsilon_y}{\omega_H \gamma^2} \sin\theta_0 = 1. \tag{3.4}$$

Using resonance conditions (3.1), as well as equations from system (1.18) - (1.24), we can obtain the following equation for describing the phase dynamics in the vicinity of resonance:

$$\ddot{\theta}_0 + \frac{\varepsilon_y k_x v_\perp^2}{2\gamma} \cos\theta_0 = 0. \tag{3.5}$$

Equation (3.5) is the equation of a mathematical pendulum. Analysis of such equations and consequence of a similar analysis can be found in [7-10]. It should be noted that, under the condition, the known cyclotron resonances are absent. So conditions (3.3) and (3.4) are conditions for new resonances that do not go over into known resonances.

3. The interesting case is when the parameters of the wave and particles satisfy the conditions:

$$n = \mu >> 1;\ k_z \to 1,\ k_x \sim \left(1/\gamma^2\right) << 1\ ;\ \omega_H << 1;\ \varepsilon_x = \varepsilon_z = 0 \tag{3.6}$$

The importance of this case is due to the fact that it allows us to analyze the resonance at large values of number ($n >> 1$). Besides, this case corresponds to the situation when the number of the Bessel function is equal to the argument of the Bessel function. In this case, as is known, the Bessel function decreases most slowly with the growth of its number and argument ($J_n(n) \sim 1/\sqrt[3]{n}$). The resonance condition for this case has the form:

$$\dot{\theta}_n = k_x \dot{\xi} - n\dot{\theta} = \frac{n\omega_H^2 - 2\varepsilon_y k_x^2 p_\perp J_n \sin\theta_n}{\gamma\omega_H} \equiv \Delta, \qquad \Delta(\gamma_0) = 0. \tag{3.7}$$

γ_0 is value of energy at which the exact resonance condition is satisfied ($\Delta(\gamma_0) = 0$). To describe the dynamics of the phase, we can derive the equation:

$$\ddot{\theta}_n + \Omega^2 \cos\theta_n \sin\theta_n - \Omega_1^2 \cos\theta_n = 0, \tag{3.8}$$

where - $\Omega^2 = \dfrac{2v_\perp^2 \varepsilon_y^2 J_n^2}{\gamma\omega_H}$; $\Omega_1^2 = \dfrac{n\omega_H v_\perp \varepsilon_y J_n}{\gamma^2}$.

Equation (3.8) is also the equation of a nonlinear pendulum and has the integral:

$$\frac{\dot{\theta}_n^2}{2}+\frac{\Omega^2}{2}\sin^2\theta_n-\Omega_1^2\sin\theta_n=C=const \qquad (3.9)$$

Analysis of this integral shows that the maximum phase velocity can be estimated by $\dot{\theta}_{\max}\approx\Omega$. Using this estimate, it is easy to determine the value of addition to the particle energy that they obtain when interacting with the wave under resonance conditions:

$$\dot{\theta}_n=\Delta(\gamma_0)+\left(\frac{\partial\Delta}{\partial\gamma}\right)_{\gamma_0}\delta\gamma\ ; \qquad (\delta\gamma)_{\max}=\left(\dot{\theta}_{\max}\right)/\left(\partial\Delta/\partial\gamma\right)\approx\varepsilon_y J_n\sqrt{\omega_H\gamma^3} \qquad (3.10)$$

Comparing this additive with those obtained under conditions of known cyclotron resonances, we can see that it can be more significant.

3.3. Numerical analysis

Above, in Section 1, we found analytical solutions of equations (1.5, 1.6) for the momenta and coordinates of a particle in implicit form as a function of phase. These solutions were found for a wave propagating strictly along the direction of the external magnetic field. When the wave propagates at an angle to the external magnetic field $(k_\perp=k_x\neq 0)$, the integral $\gamma\dot{\psi}=C$ is destroyed. In this case, the analysis is difficult

Therefore, a numerical analysis of equations (1.2) was carried out to investigate the dynamics of charged particles in the field of the plane electromagnetic wave and in the external constant magnetic field H_0 directed along the axis Z. The cases of linear and circular polarization of the wave field are considered. Since we are mainly interested in particle acceleration, we consider this process at sufficiently large initial values of the longitudinal momentum of the particles and small values of the transverse momentum (for small values of the transverse momentum, the parameter $\mu<<1$).

The analysis was carried out at the initial values of the longitudinal momentum $p_{z0}=10$; the transverse momenta were chosen equal to $p_{x0}=p_{y0}=0.1$. The initial values of the transverse coordinates are selected in accordance with the values of the transverse momenta and the external constant magnetic field, the initial coordinate $z_0=z(t=0)=0$. The accuracy of the calculations was controlled using the integral (1.4). In all the numerical studies, the value of the integral was preserved with a sufficient degree of accuracy: the value of deviation from the integral did not exceed the values $10^{-7}-10^{-6}$ for the coordinates and momenta of charged particles of the order 10^3.

As follows from the above formulas, the value of the longitudinal momentum $p_z >> p_\perp$ therefore the value p_z practically coincides with the energy value γ .

If the initial values of the momenta of the charged particles are such that the condition is satisfied $C = \gamma - p_z$, where $C = \gamma\dot{\psi} = const$ is the integral of particle motion, a scheme of autoresonant interaction of particles with laser fields at $\omega_H = \gamma\dot{\psi}$ can be realized.

Figure 3.1, 3.2 shows graphs of the dependence of the longitudinal and transverse pulses, as well as the longitudinal and transverse coordinates of the particles on time under conditions of autoresonance for a wave with circular polarization $\varepsilon_x = \varepsilon_y = \varepsilon_0,\ \varepsilon_z = 0$ for the field amplitude $\varepsilon_0 = 0.75$ and $\omega_H = \gamma_0\dot{\psi}_0 = 0.5087$.

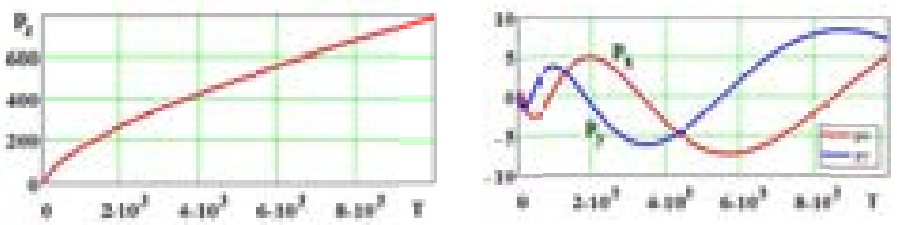

Fig. 3.1. Dependences of the longitudinal p_z *and transverse momenta on time* $T = \tau / 2\pi$ *. Circular polarization*

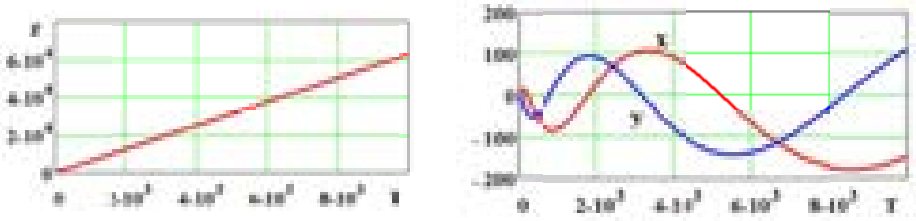

Fig.3.2 Dependences of the longitudinal z *and transverse coordinates* x, y *on time* $T = \tau / 2\pi$ *. Circular polarization*

In the case of linear polarization $\varepsilon_x = \varepsilon_z = 0,\ \varepsilon_y = \varepsilon_0$, the graphs of the dependence of the longitudinal and transverse pulses, as well as the longitudinal and transverse coordinates of the particles on time under conditions of autoresonance are shown in Fig. 3.4.

As can be seen from these graphs, the maximum values of the longitudinal and transverse momenta with circular polarization are approximately two times higher than their values with linear polarization. The dependence of the longitudinal coordinate on time, as expected ($\beta_z \approx c$), has not

practically changed. The oscillation period of the transverse coordinates and momenta is approximately two times large than in the case of linear polarization.

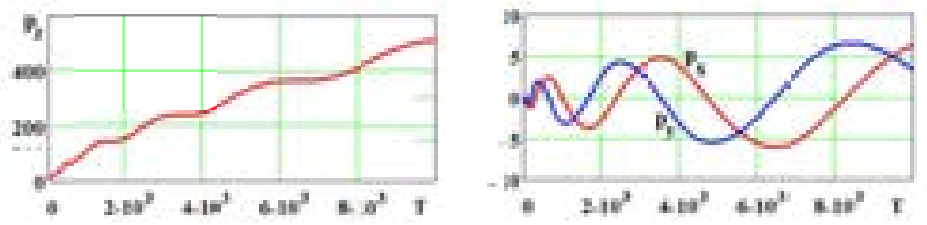

Fig. 3.3. Dependences of the longitudinal p_z *and transverse momenta on time* $T = \tau / 2\pi$ *. Linear polarization*

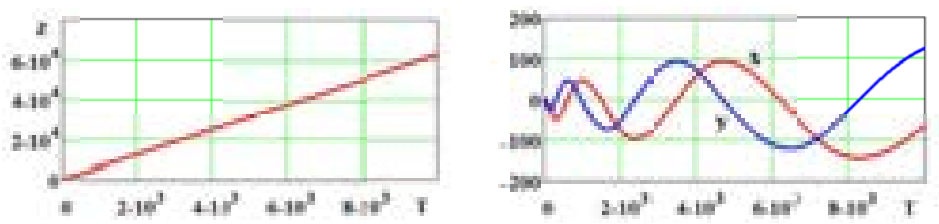

Fig.3.4. Dependences of the longitudinal Z *and transverse coordinates* x, y *on time* $T = \tau / 2\pi$ *. Linear polarization*

In the case of oblique propagation $(k_x = 0.075)$ of the linearly polarized wave $\varepsilon_x = \varepsilon_z = 0$, $\varepsilon_y = \varepsilon_0$, the dependences of the longitudinal and transverse coordinates and momenta of the particle for cyclotron frequency $\omega_H = \gamma_0 \dot{\psi}_0$ and parameter values are shown in Fig.3.5, 3.6.

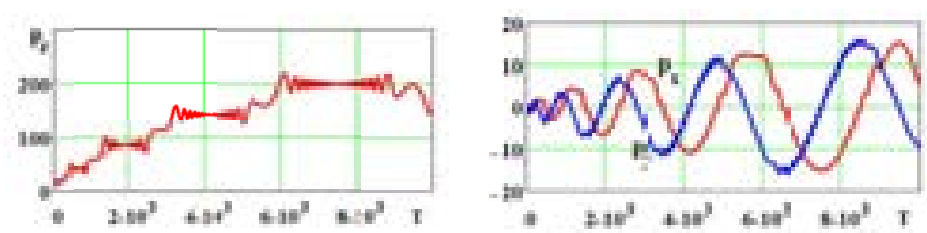

Fig. 3.5. Dependences of the longitudinal p_z *and transverse momenta on time* $T = \tau / 2\pi$ *. Linear polarization*

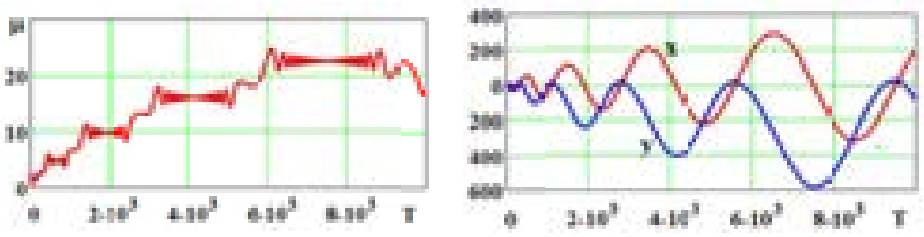

Fig.3.6. Dependences of the parameter μ *and transverse coordinates* x, y *on time* $T = \tau / 2\pi$ *. Linear polarization*

From the graphs in Fig. 3.5, 3.6 it is seen that the interaction of a charged particle with a field is resonant character. The time intervals at which the parameter μ oscillates around a certain average value are clearly distinguished. In accordance with the change in the parameter μ, the average energy of the oscillations of the energy of the charged particle also changes. At the same time, contribution to the energy increment gives not only one harmonic with a fixed number n, but also adjacent harmonics $n-1,\ n+1$:

$$\Delta\gamma(n) \approx \varepsilon_y \sum_{k=n-1}^{n+1} J_n(\mu)\sqrt{\omega_H \gamma^3}\,. \tag{3.11}$$

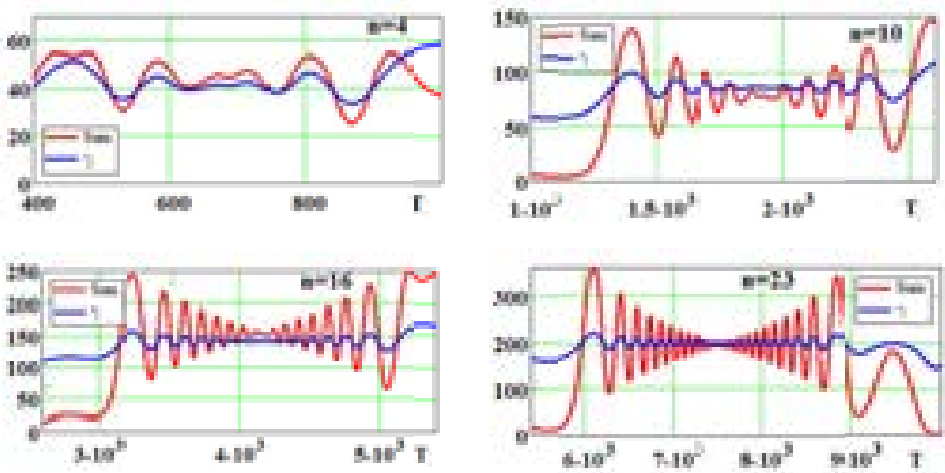

Fig. 3.7. Dependences of particle energy on time $T = \tau / 2\pi$ *for different regions change of parameter* $\mu = n$ *. The curves in each of these figures that have a large amplitude were obtained using formula (3.11). Curves with smaller amplitudes were obtained as a result of solving the original system of equations (1.2)*

As can be seen from the graphs in Fig. 3.7, we can speak of a sufficiently good qualitative agreement between the results of the numerical calculation of the system of equations (1.2) and the results of evaluation by formula (3.11)

Some Conclusion

Let's state the most important results of this subsection.

1. It is shown that the well-known conditions of cyclotron resonance should be generalized. The generalization is that these conditions include both the strength of the external magnetic fields and the field strength of the electromagnetic waves with which the particles interact. The use of these new resonant conditions makes possible to implement a scheme of resonant interaction of particles even with laser radiation fields in vacuum.

2. If the initial parameters of charged particles are such that the condition $C = \gamma - p_z = \omega_H$, where $C = \gamma\dot{\psi} = const$ is satisfied, then a scheme of autoresonant interaction of particles with laser fields in vacuum can be implemented.

3. Conducted numerical studies confirm qualitatively and quantitatively the key results of analytical studies within the framework of this model.

3.4. Stepped structure of the dynamics of energy exchange between a wave and particles

Figure 3.5 shows the characteristic time dependence of the longitudinal pulse. One of the most characteristic new features of particle dynamics is visible, namely, its "stepwise" character of the dependence of momenta and energy on time. Note that such a feature of the particle dynamics is already visible in Figures 3.5 and 3.6. With an increase in the field amplitude, this feature of the dynamics is manifested most clearly. Below we will try to give a qualitative explanation of this dependence.

Let us recall the characteristic dynamics of charged particles at low values of the wave intensity ($\varepsilon << 1$) under conditions of cyclotron resonances. Under these conditions, as is known (see, for example [8, 9]), the dynamics of particles can be described by the equation of a mathematical pendulum. In this case, the width of the nonlinear resonance turns out to be directly proportional to the square root of the wave force parameter and inversely proportional to the square root of the deviation of the longitudinal wave number from unity:

$$\Delta\gamma \sim \sqrt{\varepsilon / \left|1 - k_z^2\right|}. \tag{3.12}$$

The distance between nonlinear cyclotron resonances is determined by the formula:

$$\delta\gamma \sim \left\{\omega_H / \left|1 - k_z^2\right|\right\} \tag{3.13}$$

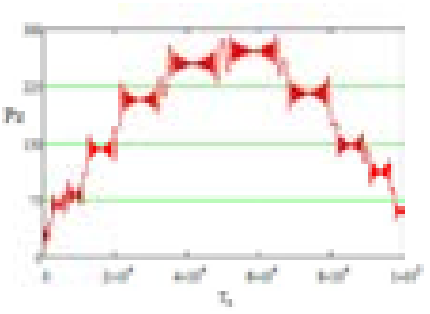

Fig.3.8. Time dependence of the longitudinal momentum of a particle in the presence of the influence on its dynamics of both the wave field and the external magnetic field. The parameter values are far from the values that correspond to autoresonance:

$$\varepsilon = 1.23;\ p_y(0) = 1.4;\ p_x(0) = 0\ \omega_H = 0.1$$

$$p_z(0) = 10 \quad k_z = 0.99 \quad z(0) = 0.9$$

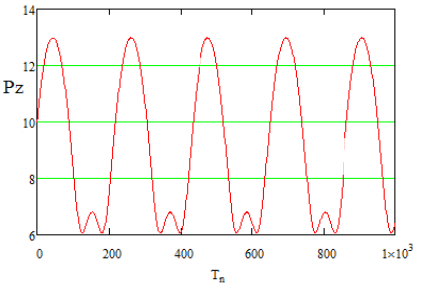

Fig.3.9. The same dependence of the longitudinal particle momentum from time, as in Figure 3.8. Only in the absence of an external magnetic field:

$$\varepsilon = 1.23; \quad p_y(0) = 1.4;\ p_x(0) = 0$$

$$\omega_H = 0; \quad p_z(0) = 10; \quad k_z = 0.99;$$

$$z(0) = 0.9$$

In this case, the phase dynamics is determined by the equation:

$$\dot{\theta}_n = \Delta = \left[\left(1 - k_z v_z\right) - n\frac{\omega_H}{\gamma} \right]. \tag{3.14}$$

In this equation, the dependence on the wave field strength is implicitly contained only in the particle energy (γ). Therefore, to describe the dynamics of particles, it is necessary to add to Eq. (3.14) an equation that describes the dependence of the particle energy on time:

$$\frac{d\gamma}{d\tau} = \varepsilon_0 v_\perp J_n' \cos\theta_n . \tag{3.15}$$

The system of equations (3.14) and (3.15) with small changes in energy (its change is proportional to a small parameter of the wave force) is equivalent to the equation of a mathematical pendulum. The regular and chaotic dynamics of particles at cyclotron resonances within the framework of these models was studied (see, for example, [9,17]). If the field strength turns out to be large enough, then the particle dynamics can change qualitatively. Indeed, taking into account the wave force parameter, equation (3.14) for the phase acquires an additional term:

$$\dot{\theta}_n = \Delta - 2\varepsilon_0 \frac{nk_x}{\gamma} J_n \sin\theta_n . \tag{3.16}$$

In this equation, the explicit dependence of the phase on the wave force parameter is already visible.

Therefore, when this additional term turns out to be greater than the addition that associated with the change in energy, then namely Eq. (3.16) will describe the phase dynamics. It is important to note that in Eq. (3.16) (with a sufficiently large parameter of the wave force) the values of the impulses and energy can be considered as slowly varying functions. Under these conditions, equation (3.16) practically coincides with the Adler equation. This equation is widely known in synchronization theory. To see that in equation (3.16) the value of energy and momenta can be considered as slow functions, let us return to system equations (1.27), which describe the dynamics of these variables. For definiteness, we will study the dynamics of additional acceleration of particles under conditions close to autoresonance ($k_x << 1,\ \gamma \approx p_z >> 1$). Under these conditions, the system of equations (1.27) can be simplified:

$$\frac{dp_\perp}{d\tau} = \varepsilon_0 \left(1 - k_z v_z\right)\left(J_n'\right)\cos(\theta_n) \tag{3.17}$$

$$\frac{dp_z}{d\tau} = \varepsilon_0 k_z v_\perp J_n' \cos\theta_n \tag{3.18}$$

$$\frac{d\gamma}{d\tau} = \varepsilon_0 v_\perp J_n' \cos\theta_n . \tag{3.19}$$

It can be seen from these equations that at a stationary value of the phase ($\dot{\theta}_n = 0$), each of them has stationary points, which are determined by the condition:

$$J_n'(\mu) = 0 . \tag{3.20}$$

It is seen that when condition (3.20) is satisfied, both the energy and the longitudinal momentum do not change. Thus, equation (3.16) really can be considered as the well-known Adler equation (see, for example, [26, 27]). In this case, the synchronization condition (the condition for the phase stationarity) will be presented as:

$$2\varepsilon_0 \frac{nk_x}{\gamma} J_n > \Delta . \tag{3.21}$$

Thus, for sufficiently high field strengths, the dynamics of charged particles will be described not by the equation of a mathematical pendulum,

but by the Adler equation. The steps in the dependence of momenta and energy on time are determined by the zeros of the derivative of the Bessel function (formula (3.20)). Of course, this is a rather crude picture of dynamics. There does not reflect the oscillatory nature of the dependence of the impulses on the "steps" themselves. Note that condition (3.21) corresponds to the "capture" of particles in the main Arnold tongue. Such tongues have been studied in detail in the theory of synchronization (see, for example, [27]).

3.5. Mechanism of occurrence of local instability and regimes with dynamic chaos

Regimes with dynamic chaos when the conditions of the usual cyclotron resonances are realized are due to the overlap of nonlinear cyclotron resonances (Chirikov's criterion). This is due to the fact that the dynamics of particles at isolated cyclotron resonances is described by the equation of a mathematical pendulum. It is well-known that a mathematical pendulum, in addition to singular points of the "saddle" type, also has a homoclinic trajectory (separatrix). These singular points (saddles) and this particular trajectory (separatrix) have the property that small deviations from these points or from this trajectory lead to qualitatively different particle dynamics.

It was seen above that the phase which characterizing the interaction of particles with a wave at sufficiently high wave field strengths obeys not the usual conditions of cyclotron resonances, but the Adler equation (3.16). Moreover, this equation already contains the parameter of the wave force in an explicit form, and the moments and energy of the particle in this equation can be considered as constants. Thus, it is enough for us to analyze not the equation of the mathematical pendulum, but the equation of Adler. Formally, this equation is much simpler (first order nonlinear equation) compared to the mathematical pendulum equation (second order nonlinear equation). It does not contain saddle singular points and singular trajectories (separatrices) like the equation of a mathematical pendulum. Its dynamics should be simpler and more regular. In general, it turns out to be so. However, despite this simplicity, it can be seen that in many cases (see, for example, Figure 3.10), the overall dynamics, with taking into account the transitions between the steps, may be irregular. In this case, the usual mechanisms for the appearance of dynamic chaos do not work, since there are no homoclinic trajectories and saddle points. The mechanism for the emergence of dynamic chaos should be different. To understand this mechanism, one should look at the figure 3.11, which shows the projection of the particle dynamics onto the coordinates (x, y). This figure shows that topologically all trajectories are circles. An important feature of these circles is that they all pass near the zero point. Therefore, small perturbations (regular or random) can lead to a trajectory jump from one circle to another. This process can be random. We will show below that it can indeed be

random. Thus, the chaos that occurs in the particle dynamics we are studying is analogous to the chaos that occurs when throwing dice with a large number of edges. The element of probability appear when trajectory passing the area of the point (x = y = 0). Any trajectory can jump (randomly) to another trajectory (circle). This mechanism of occurrence of randomness is very similar to the mechanism described in works [28-30]. In these works, the modes in which such a mechanism is implemented are called modes with piecewise deterministic dynamics. It seems that such a name is more in line with the dynamics that are being implemented. Therefore, below we will call such regimes modes with piecewise deterministic dynamics

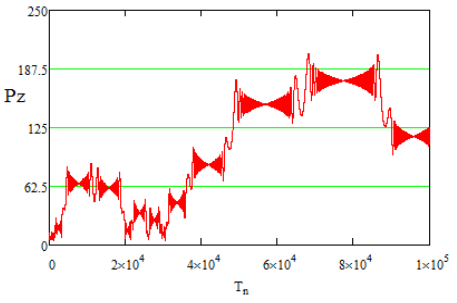

Fig. 3.10. Dependence of the longitudinal momentum of a particle on time in the presence of the influence on its dynamics of both the wave field and the external magnetic field. Conditions are the same as on the figure 8

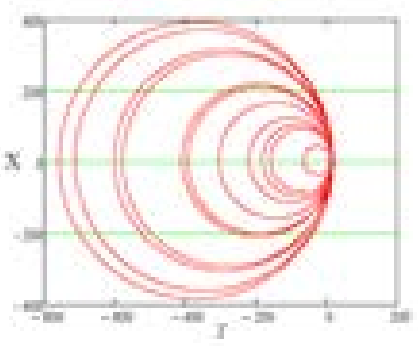

Fig. 3.11. A typical view of the projection of the trajectory of particles on the plane (x, y). Conditions close to autoresonance

$$\omega_H = \gamma - p_z$$

$$\varepsilon = 1.23;\ p_y(0) = 1.4;\ p_x(0) = 0$$

$$\omega_H = 1/20 \quad p_z(0) = 10\ ;\quad k_z = 0.99\ ;$$

$$z(0) = 0.9$$

To confirm the possibility of such a mechanism for the occurrence of randomness and a regime with piecewise deterministic dynamics, we construct a simple model of the system, the dynamics of which corresponds to figure 3.8. This system describes the dynamics of the representing point, which moves in a circle with a certain radius. Moreover, as in Figure 3.8, all circles have a common point. For example, point (x = y = 0). It is easy to see that the equation that describes such circles can be written in the following form:

$$\varphi = (x - R)^2 + y^2 - R^2 = 0. \tag{3.22}$$

Equation (3.22) describes circles whose centers are located on the y = 0 axis, and the radius of each of these circles can be arbitrary. All these circles have a common point. It is necessary to find a differential equation

that would describe the dynamics of the representing point along these circles. Moreover, the parameters of this equation should not contain the radius of these circles. Assuming that expression (3.22) is integral, then using the well-known algorithm of inverse problems of mechanics (see, for example, [28]), one can write a system of ordinary differential equations that describes the dynamics of particles along such circles. In particular, such a system of equations will be the system:

$$\begin{aligned} \dot{x} &= y \\ \dot{y} &= \left(\frac{y^2}{2x}\right) - 0.5 \cdot x \ . \end{aligned} \tag{3.23}$$

System (3.23) is equivalent to the equation of an oscillator with nonlinear friction:

$$\ddot{x} - \left(\frac{\dot{x}}{2x}\right)\dot{x} + 0.5 \cdot x = 0. \tag{3.24}$$

Moreover, the parameter R (radius of circles) is excluded from these equations. It can take arbitrary values. The phase portrait of system (3.23) is shown in figure 3.9. The integral curves in this case are circles. Moreover, the centers of the circles are located on the axis $y = 0$, and the radii of these circles are equal to the distance of these centers to the zero point ($x = 0; y = 0$). This point is common to all circles. Moreover, this point is a special solution to system (3.23) (see below). Looking at the integral of equation (3.24), it is difficult to imagine that the dynamics of system (3.23) or (3.24) can be irregular. Really, this system has only one degree of freedom. However, numerical calculations show that it is irregular. Indeed, figure 3.13 shows the time dependence of the variable. It is seen that the phase trajectory after passing the point of the singular solution ($x = 0; y = 0$) can jump from one circle to another circle. Moreover, these jumps are random. Almost any change in the counting accuracy changes the temporal dynamics of the system. In addition, the spectral analysis of the dynamics of system (3.23) shows that the spectra of this dynamics are wide, and the correlation function decreases rather quickly (see Fig. 3.14). The irregularity is due to the fact that all trajectories of system (3.23) pass through the zero point, at which the uniqueness theorem is violated. This point is a singular solution to system (3.23). Note that in the numerical analysis of the dynamics of a pendulum with nonlinear friction (3.24), the value of nonlinear friction (the second term in Eq. (3.24)) should be reduced. If this is not done, then very quickly the dynamics of the nonlinear pendulum will be going up on a circle, the radius of which significantly exceeds the radius of all other circles. Such dynamics are difficult to represent graphically. In particular, Figures 3.13 and 3.14 were obtained for the case when the

nonlinear friction in equation (3.24) was reduced by a factor of 10. Let us now show that the zero point is a singular solution to system (3.23). In this case, by a singular solution we mean those solutions at the points of which the uniqueness theorem is violated. Point $x=0; y=0$ belongs to the family of circles (3.22). The same circles are integral curves of system (3.23). It is convenient to rewrite these integral curves in the form: $y^2/x+x=2R$. It follows from these integral curves that the Lipschitz conditions for system (3.23) are violated in the vicinity of the zero point. Indeed, the Lipschitz condition for system (3.23) can be written in the form:

$$\left|\frac{\tilde{y}^2}{\tilde{x}}-\frac{y^2}{x}\right|\le L\left(|\tilde{x}-x|+|\tilde{y}-y|\right) \qquad (3.25)$$

where L - is a positive constant.

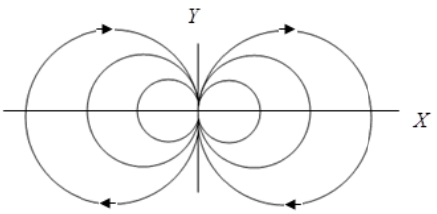

Fig. 3.12. Phase portrait of the system (3.24)

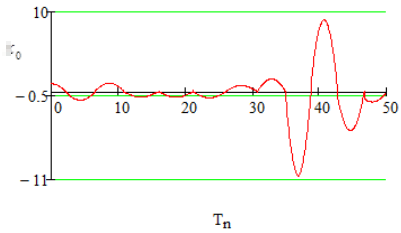

Fig. 3.13. Time dependence of a variable $x=x_0$. The transitions of the representing point from one circle to another are visible

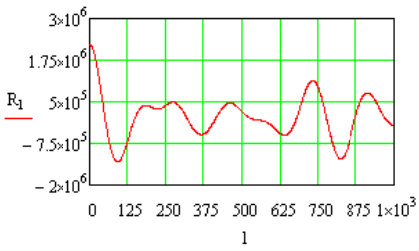

Fig. 3.14. Correlation function of variable X

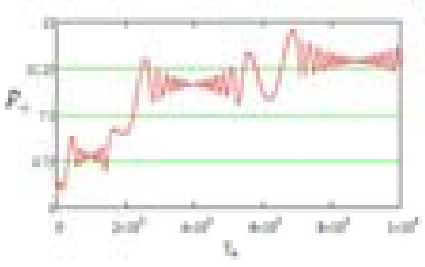

Fig. 3.15. Dependence of the transverse momentum on time. The same steps are visible as for the longitudinal impulse (see figures 3.6 - 3.10)

In a neighborhood of zero, the left-hand side of inequality (3.25) can be estimated by the quantity $\left(\left|\tilde{R}-R\right|\right)$, where $\tilde{R}$ and R are the radii of two arbitrary circles. In general, the difference between these radii can be arbitrary big. Thus, the Lipschitz condition is not satisfied at the zero point, i.e. the conditions of the uniqueness theorem for system (3.25) are violated.

3.6. Discussion and conclusion

Thus, the results obtained above show that the dynamics of particles, undertaking into account the high intensity of the wave field, has significant features. Let's note the most important of them:

1. If the field strength of the wave is large enough, so that inequality (3.21) is satisfied, then the conditions for the stationary of the phase (conditions for resonance interaction) and the nature of the energy exchange between the particles and the wave change qualitative. In particular, the dynamics of particles in the vicinity of the stationary phase (in the vicinity of resonances) changes. Indeed, at ordinary cyclotron resonances, this dynamics is described by the equation of a mathematical pendulum. This is a second-order nonlinear equation that has singular points of the "saddle" type, as well as a special homoclinic trajectory - a separatrix. The presence of these singular points and a special trajectory essentially determines the dynamics of particles in the vicinity of resonances. It was seen above that taking into account the wave field strength when inequality (3.21) is satisfied leads to a description of the particle dynamics in the vicinity of resonances not to the equation of a mathematical pendulum, but to the Adler equation. This is an ordinary first order differential equation. It is nonlinear, but much simpler than the equation of a mathematical pendulum. It has no singular points of the saddle type and no homoclinic trajectories. It has only alternating stable and unstable points. As a result, the trajectory of the particle is quickly grouped in the vicinity of stable points. Under these conditions, the energy and momenta of the particles do not change. Note that the Adler equation is used to analyze synchronization processes [26, 27]. Using the analogy with the synchronization process, we can say that when condition (3.21) is satisfied, the particles are captured by the main tongue of Arnold [27]. The result of such dynamics of particles in the vicinity of resonances is the stepwise nature of the energy exchange of particles with the wave.

2. As follows from the previous point, the dynamics of particles with accounting strength of the wave field can become more regular than it is under conditions of ordinary cyclotron resonances. In most cases, it is so. However, as it can be seen in Figure 3.10, the processes of transition from one step to another step can be random. The reason for this random particle dynamics is the fact that, all particle trajectories pass near the zero point (as it follows from Figures 3.11, 3.12). This point is a common point for all trajectories of the particles. The particle, getting in the vicinity of this point,

under the influence of arbitrarily small fluctuations (perturbations), can randomly cross over to other trajectories. Such a mechanism for the emergence of chaotic dynamics is described, for example, in [32, 33, 54].

It is also similar to the mechanism that has been studied in a series of works, which can be defined as Continuous 'chaotic' dynamics in two dimensions, or Piecewise deterministic dynamics (see, for example [29-31] and the literature cited there). It should be said that, strictly mathematically, there are significant differences in the systems studied in these works and in the one considered in our work. We will only point out the main difference. In the models considered in these works, the singular point is the singular point of the "saddle" type. The trajectories can never reach this point (the time of reaching tends to infinity). In the models that we have considered, the singular point is not a saddle point. In it, as in the saddle point, the uniqueness theorem is violated. However, trajectories (all trajectories) can ***pass*** through this point. The travel time of the vicinity of this point and the point itself is quite finite. Note also that the singularities of such points, as well as similar trajectories (envelopes of trajectories), in which the uniqueness theorem is violated, were studied by V.A. Steklov in 1927 [34]. However, Steklov himself, analyzing such solutions, pointed out that, apparently, such solutions do not describe the dynamics of real physical systems ... ..

3. An important result obtained above (see Figure 3.5) is the fact that the joint accounting of the wave field under resonant conditions can significantly increase the efficiency of energy exchange between particles and the wave.

4. It should be noted that the above model of analysis of particle dynamics is rather limited. It allowed revealing some important features of particle dynamics. However, analytical consideration within the framework of this model does not allow convincing answers to many questions that appear in numerical analysis. As an example, we can cite the difficulties that arise when analyzing jumps from one step to another step. It seems that in the general case, these transitions are also random. In particular, using equations (3.17)-- (3.19), it is easy to find (asymptotically for large μ) that the distance between adjacent stable steps is order of $\pi / 2$. However, as can be seen from Figure 3.12 and similar figures, this distance varies randomly. Some steps are skipped. Perhaps these and other questions that arise can be answered if we take as a basis not cyclotron resonances (as was done in this work), but the dynamics of particles in the field of an intense wave without a magnetic field.

5. It is obvious that with an increasing wave force parameter (with an increase in the wave field strength) its influence on the particle dynamics will increase. The following question arises. Are the above-described features of the particle dynamics preserved at lower values of this parameter? The answer to this question is to some extent contained in Figures 3.13, 3.14. These figures show the dependence of the longitudinal momentum of particles on time for a sufficiently small parameter of the wave force ($\varepsilon = 0.1$).

Figure 3.13 shows this dependence under conditions close to autoresonance, and Figure 3.14 - under conditions far from autoresonance. These figures show the "rudiments" of the stepwise structure of particle dynamics.

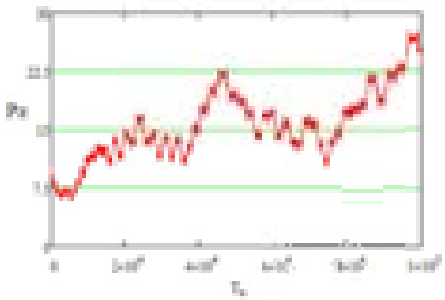

Fig. 3.13. Conditions close to autoresonance:

$$\omega_H = \gamma - p_z$$

$$p_y(0) = 1.4;\ p_x(0) = 0\ \omega_H = 1/20$$

$$\varepsilon = 0.1 \quad p_z(0) = 10 \quad k_z = 0.99$$

$$z(0) = 0.9$$

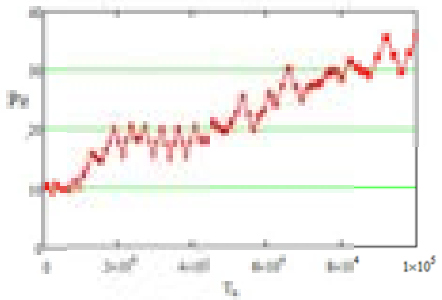

Fig. 3.14. Conditions far from autoresonance:

$$p_y(0) = 1.4;\ p_x(0) = 0\ \omega_H = 1/10$$

$$\varepsilon = 0.1 \quad p_z(0) = 10 \quad k_z = 0.99$$

$$z(0) = 0.9$$

6. The results obtained above correspond to the parameters that are convenient to choose for the purpose of additional acceleration of relativistic charged particles. A situation where the wave vector of an external electromagnetic wave is directed perpendicular to the external magnetic field may have a considerable interest too. Such a configuration corresponds, for example, to the configuration of fields in gyrotrons. The analysis of the dynamics of particles in this case is in many respects similar to the dynamics considered above: there is a rather efficient transfer of wave energy into the energy of particles, a similar stepped structure of energy collection by particles appears; the mechanism of the appearance of piecewise deterministic dynamic is similar too.

SECTION 4. INFLUENCE OF PLASMA DENSITY FLUCTUATIONS ON PLASMA - BEAM INTERACTION

4.1. Introduction

The interaction of a beam of charged particles with plasma has now been studied in sufficient detail. A theory has been developed for the interaction of a beam with both homogeneous and regularly inhomogeneous plasma (see, for

example, [35]). When the beam interacts with the plasma, instabilities arise, which can lead to signal amplification. Along with this, there is an increase in the fluctuations that are always present in the plasma. Using the plasma-beam instability to amplify signals or to heat the plasma, it is necessary to know the relationship between the growth rates of the regular signal component and fluctuations. In [36, 37], the plasma-beam interaction was studied when the plasma density varied along the coordinate according to a random law. In them, the analysis was limited to the correlation theory of stability, i.e. the dynamics of changes in the first and second moments was investigated.

In this section, the instability of a beam moving in plasma is investigated, the density of which varies according to a random law in space or time. When changing the plasma density in space, in contrast to [37], a system of equations for moments of arbitrary order was obtained and investigated. It is shown that each subsequent moment grows faster than the previous one.

The result of this dependence of the increment on the moment number is the intermittent nature of the development of instability [38], as well as the appearance of a certain critical length of the interaction region, where the amplification of the regular signal is still possible. The last conclusion is related to the fact that the growth rate of the second moments is more than twice the growth rate of the regular part of the signal.

For plasma, the density of which randomly depends on time, equations are obtained that determine the dynamics of the behavior of the first and second moments, the growth rates of their growth are found, and the maximum time for which the signal is destroyed by fluctuations is calculated.

4.2. Basic Equations

Let a compensated electron beam with a density n_b move in the plasma in the direction of the x axis with velocit υ_b. The perturbations of the densit $\tilde{n}_b$ and velocity $\tilde{\upsilon}_b$ of the beam satisfy the equation of motion

$$\frac{\partial}{\partial t}\tilde{\upsilon}_b+\upsilon_b\frac{\partial}{\partial x}\tilde{\upsilon}_b=-\frac{e}{m}E(x,t), \tag{1}$$

where $E(x,t)$ is the electric field strength,
and the continuity equation

$$\tilde{n}_b+\frac{\partial}{\partial x}\left(n_b\tilde{\upsilon}_b+\tilde{n}_b\upsilon_b\right)=0. \tag{4.2}$$

The perturbations of the plasma velocity $\tilde{\upsilon}_p$ and density $\tilde{n}_p$ satisfy the equations

$$\frac{\partial}{\partial t}\tilde{n}_p + \frac{\partial}{\partial x}\left(n_p \upsilon_p\right) = 0, \tag{4.3}$$

$$\frac{\partial}{\partial t}\tilde{\upsilon}_p = -\frac{e}{m}E(x,t), \tag{4.4}$$

Where n_p is the unperturbed plasma density, which is a random function of time or coordinates. The statistical characteristics of this function are specified. The electric field strength is connected with changes in the plasma and beam density by Maxwell's equation:

$$\frac{\partial}{\partial x}E(x,t) = -4\pi e\left(\tilde{n}_p + \tilde{n}_b\right). \tag{4.5}$$

4.3. Spatially – inhomogeneous plasma

Let the dependence of all unknown quantities on time have the form $\exp(-i\omega t)$, and the plasma will be considered spatially inhomogeneous: $n_p = n_p(x)$. Having made the necessary transformations and choosing the boundary conditions so that the integration constant vanishes, we obtain from (4.1) - (4.5) the equation for the frequency Fourier components of the electric field:

$$\left(i\omega + \upsilon_b \frac{\partial}{\partial x}\right)^2 \varepsilon(x) E_\omega + \omega_b^2 E_\omega = 0, \tag{4.6}$$

$$\varepsilon(x) = 1 - \frac{\omega_p^2}{\omega^2},\ \omega_p^2 = \frac{4\pi e^2 n_p(x)}{m},\ \omega_b^2 = \frac{4\pi e^2 n_b}{m}.$$

Substituting $E(x)$ from $D(\omega,x) \equiv \varepsilon(\omega,x)\,\mathrm{E}_\omega(x)\exp\left(i\omega_x/\upsilon_b\right)$ into (4.6), we obtain an equation for a spatial oscillator with a randomly varying frequency $\omega_b^2/\upsilon_b^2\,\varepsilon(x)$, similar to (4.3):

$$\frac{d^2 D}{dx^2} + \frac{\omega_b^2}{\upsilon_b^2\,\varepsilon(x)} D = 0. \tag{4.7}$$

Let's take a case, for the sake of clarity, $\varepsilon < 0$. Let us assume that the plasma density fluctuations have the form $n_p = n_{p0}(1 + z_1(x))$ and z_1 is a stationary Gaussian random process with zero mean. Assuming the

amplitude of fluctuations to be small $z \equiv z_1(x)\omega_{p0}^2 \big/ (\omega^2 \varepsilon_p) \langle\langle 1$; introduce $\varepsilon_{p0} = 1 - \omega_{p0}^2 \big/ \omega^2$, $\omega_{p0}^2 \equiv \langle \omega_p^2 \rangle$; changing variables $\tau \equiv \omega_b x \big/ \upsilon_b \sqrt{|\varepsilon_{p0}|}$, $\dot{D} = -u$, we obtain a system of equations of the first order:

$$\begin{aligned} \dot{D} &= -u, \\ \dot{u} &= -(1 + z(\tau))D. \end{aligned} \tag{4.8}$$

From equations (4.8), one can obtain a system of equations for the moments of any order (m). For this, multiplying the left and right sides of the first equation of system (4.8) by $u^{m-n} D^{n-1}$, and the second by $D^n u^{m-n-1}$, adding these equations and averaging over the ensemble of realizations, we obtain for the finding moments of the nth order following system:

$$\langle u^{m-n} D^n \rangle'_\tau = -n \langle u^{m-n+1} D^{n-1} \rangle - (m-n) \langle (1+z) D^{n+1} u^{m-n-1} \rangle \tag{4.9}$$

To decouple the correlations $\langle z D^{n+1} u^{m-n-1} \rangle$, we use the method of variational derivatives [23] and the following from this method the relation:

$$\langle z(t) R[z(t)] \rangle = \int_t \langle z(t) z(\tau) \rangle \left\langle \frac{\delta R[z(\tau)]}{\delta z(\tau)} \right\rangle d\tau, \tag{4.10}$$

where $R[z]$ is an arbitrary functional of z. z – is a Gaussian random process with zero mean. Using (4.10) in (4.9) and calculating the corresponding variational derivatives, we find:

$$\begin{aligned} &\langle u^{m-n} D^n \rangle'_\tau = -n \langle u^{m-n+1} D^{n+1} \rangle - (m-n) \langle (1+z) D^{n+1} u^{m-n-1} \rangle + \\ &+ \frac{B}{2} (m-n-1)(m-n) \langle u^{m-n-2} D^{n+2} \rangle \\ &B \cdot \langle u^{m-n-2} D^{n+2} \rangle \equiv \int_t^\infty d\tau \langle z(t) z(\tau) \rangle \langle u^{m-n-2} D^{n+2} \rangle \approx \sigma_0^2 r_0 \left\langle u^{m-n-2} D^{n+2} \right\rangle \end{aligned} \tag{4.11}$$

Where σ_0^2 – variance; r_0 – dimensionless correlation radius of a random process.

To analyze stability (4.11), we choose all moments proportional to $\exp(\lambda t)$. The determinant of the resulting system, calculated using the Routh algorithm, gives the following recurrence relation for the coefficients of the characteristic equation:

$$Det_m(\lambda) \equiv A_m^n(\lambda) = 0$$
$$A_n^m = \frac{\lambda}{n} A_{n-1}^m - \left(\frac{m}{n-1} - 1\right) A_{n-2}^m - \left(\frac{m}{n-2} - 1\right)(m-n+1)\frac{B}{2} A_{n-3}^m, \tag{4.12}$$
$$A_0^m = \lambda, A_1^m = \lambda^2 - m, A_2^m = \frac{\lambda}{2}\left(\lambda^2 - m\right) - \lambda(m-1) - m(m-1)\frac{B}{2}, \; A_n^m \neq 0, \; \forall n < m.$$

In particular, for m = 1 (first moments), the characteristic equation takes the form:

$$\lambda^2 - 1 = 0, \tag{4.13}$$

And for $m = 2$ (second moments):

$$\lambda^3 - 4\lambda - 2B = 0. \tag{4.14}$$

Obviously, the increment of the second moments is more than twice the increment of the first. Similarly to [37], we introduce the dimensionless variance:

$$\Delta = \frac{\langle D^2 \rangle - \langle D \rangle^2}{\langle D \rangle^2} \tag{4.15}$$

To amplify the signal, it is necessary that this value must be much less than unity; otherwise the signal is diffused by fluctuations. Substituting into (4.15) the growth rates of the first and second moments found from (4.13) and (4.14), and returning to dimensional variables, we obtain from the condition the following expression for the critical length at which amplification of the regular signal is still possible:

$$x << x_m = \frac{4\omega^4 \upsilon_b^2}{\omega_{p0}^2 \omega_b^2 \left|\varepsilon_{p0}\right| \sigma_1^2 r_1}, \tag{4.16}$$

σ_1^2, r_1 – variance and correlation radius of a random process z(x).

Setting the amplitude of the fluctuations equal to zero (B = 0) and using the recurrence relations for the coefficients, one can make sure that and $Det_m(m) = 0$ and $\lambda = m$ is the maximum root of equation (4.12) (see Appendix). Therefore, even if the amplitude of fluctuations can be neglected, the difference between the increments of the next and previous moments is equal to unity.

Subsequent moments grow faster than the previous ones, but the dimensionless variance does not increase in this case. The presence of a nonzero amplitude of fluctuations leads to an additional increase in the

difference between the increments and, consequently, to an increase in variance (see Attachment). As shown in [38], such a feature of the growth of the moments indicates the intermittent nature of the oscillator motion. Note that the advanced growth of the higher moments is also characteristic of systems described by the first-order Langevin equations [23,39]; therefore, in accordance with [38], such systems should also have intermittency.

4.4.Plasma with a density which is fluctuating in time

Let us consider the case when the plasma density is a random function of time $n_p = n_{p0}\left(1+z(t)\right)$, where $z(t)$ is a random Gaussian process with zero mean. Due to the fact that the resulting expressions are very cumbersome, we restrict ourselves to the study by the correlation approximation. Assuming all unknown quantities are depend on the coordinate x as e^{-ikx}; passing to dimensionless variables $\tau \equiv k\upsilon_b t$, $\alpha \equiv \frac{\omega_{p0}}{k\upsilon_b}$, $\beta \equiv \frac{\omega_b}{k\upsilon_b}$; and eliminating the variable E using (4.5), we obtain from (4.1) - (4.5) the system of equations for the spatial Fourier components of the density and velocity perturbations of the beam and plasma:

$$\frac{\partial \tilde{n}_b}{\partial \tau} + i\tilde{n}_b + i\tilde{\upsilon}_b = 0 \tag{4.17}$$

$$\frac{\partial \tilde{\upsilon}_b}{\partial \tau} + i\tilde{\upsilon}_b + i\beta\,\tilde{n}_b + i\alpha^2\tilde{n}_p = 0 \tag{4.18}$$

$$\frac{\partial \tilde{n}_p}{\partial \tau} + i\tilde{\upsilon}_p\,(1+z(\tau)) = 0 \tag{4.19}$$

$$\frac{\partial \tilde{\upsilon}_p}{\partial \tau} + i\alpha^2\tilde{n}_p + i\beta^2\tilde{n}_b = 0 \tag{4.20}$$

After averaging (4.17)-(4.20) over the ensemble of realizations, splitting the correlation using (4.10) and choosing all variables proportional to $e^{-i\lambda\tau}$ analyze the stability of the obtained expressions, we obtain for the first moments of density and velocity perturbations a system of fourth-order algebraic equations, the determinant of which gives the classical dispersion equation of the system beam-plasma:

$$\begin{aligned} &\Delta_p\Delta_b = \alpha^2\beta^2, \\ &\Delta_p \equiv \lambda^2 - \alpha^2, \\ &\Delta_b \equiv (\lambda-1)^2 - \beta^2, \end{aligned} \tag{4.21}$$

having an unstable solution near the points of intersection of the resonances of the plasma ($\Delta_p = 0$) and beam ($\Delta_b = 0$) oscillators ($\lambda = 1+\delta, \alpha = 1$) with the maximum increment $\gamma_1 = \left(\frac{1}{2}\beta^2\right)^{\frac{1}{3}}$. (under natural assumption $\omega_{p0} \rangle\rangle \omega_b$).

Having obtained from (4.17) - (4.20) the system of equations for the second moments and use the operations described above, we obtain two matrix equations of the third order:

$$\begin{pmatrix} -\frac{\lambda}{2}+1 & 1 & 0 \\ \beta^2 & -\lambda+2 & 1 \\ 0 & \beta^2 & -\frac{\lambda}{2}+1 \end{pmatrix} \begin{pmatrix} \langle n_b^2 \rangle \\ \langle n_b \upsilon_b \rangle \\ \langle \upsilon_b^2 \rangle \end{pmatrix} = \alpha^2 \begin{pmatrix} 0 \\ \langle n_p n_b \rangle \\ \langle n_p \upsilon_b \rangle \end{pmatrix} \tag{4.22}$$

$$\begin{pmatrix} -\frac{\lambda}{2} & 1 & \beta \\ \alpha^2 & -\lambda & 1 \\ 0 & \alpha^2 & -\frac{\lambda}{2} \end{pmatrix} \begin{pmatrix} \langle n_p^2 \rangle \\ \langle n_p \upsilon_p \rangle \\ \langle \upsilon_p{}^2 \rangle \end{pmatrix} = -\beta^2 \begin{pmatrix} 0 \\ \langle n_p n_b \rangle \\ \langle n_b \upsilon_p \rangle \end{pmatrix} \tag{4.23}$$

for the second moments of density and velocity perturbations of the plasma and beam oscillators ($B \equiv -ik\upsilon_b \sigma_0^2 r_0/2; \sigma_0^2, r_0$ variance and dimensionless correlation radius of a random process), and a matrix equation of the fourth order for their mutual correlations:

$$\begin{pmatrix} -\lambda+1 & 1 & 1 & 0 \\ \beta^2 & -\lambda+1 & 0 & 1 \\ \alpha^2 & 0 & -\lambda+1 & 1 \\ 0 & \alpha^2 & \beta^2 & -\lambda+1 \end{pmatrix} \begin{pmatrix} \langle n_p n_b \rangle \\ \langle n_p \upsilon_b \rangle \\ \langle n_b \upsilon_p \rangle \\ \langle \upsilon_p \upsilon_b \rangle \end{pmatrix} = \begin{pmatrix} 0 \\ \alpha^2 \langle n_p^2 \rangle \\ \beta^2 \langle n_b^2 \rangle \\ \alpha^2 \langle n_p \upsilon_p \rangle + \beta^2 \langle n_b \upsilon_b \rangle \end{pmatrix} \tag{4.24}$$

Systems (4.22) - (4.24) correspond to the characteristic equation of the tenth degree

$$Det_2(\lambda) = 0.$$

$$Det_2(\lambda) \equiv \Delta_s + \lambda^{*2}(2\Delta_{b1} + 2\Delta_{p1} - \Delta_{p2}\Delta_{b2}) + 2\lambda^*(\Delta_x + \Delta_{p2}(\alpha^2 - \Delta_{b1}) + \Delta_{b2}(\beta^2 - \Delta_{p1})) +$$
$$+ 2(\alpha^2 - \beta^2)(\Delta_{p1} - \Delta_{b1}) + (\Delta_{p1} - \Delta_{b1})^2 - \Delta_x(\Delta_{p2} - \Delta_{b2}), \tag{4.25}$$

where $\lambda^* = \lambda - 1$, Δ_s - determinant of system (4.24),

$$\Delta_s \equiv (\lambda^{*2} - (\alpha^2 - \beta^2))^2,\ \Delta_{p1} \equiv \frac{\alpha^2\beta^2}{\Delta_p}\left(\frac{\lambda}{2} + \alpha^2 B\right),$$

$$\Delta_{p2} \equiv \frac{\alpha^2\beta^2}{\Delta_p}(1 + \lambda B),\ \Delta_{b1} \equiv \frac{\alpha^2\beta^2}{\Delta_p}\left(\frac{\lambda}{2} - 1\right),$$

$$\Delta_{b2} \equiv \frac{\alpha^2\beta^2}{\Delta_b},\ \Delta_x \equiv \alpha^2\beta^2\left(\left(\frac{\lambda}{2}\right)^2 \frac{1}{\Delta_p} + \left(\frac{\lambda}{2} - 1\right)^2 \frac{1}{\Delta_b}\right). \qquad (4.26)$$

Δ_p и Δ_b – determinants of the systems (4.23) и (4.24) respectively:

$$\Delta_p \equiv -\lambda\left(\frac{\lambda^2}{4} - \alpha^2\right) + \alpha^4 B, \qquad \Delta_b \equiv -(\lambda - 2)\left(\left(\frac{\lambda}{2} - 1\right)^2 - \beta^2\right). \qquad (4.27)$$

To analyze (4.25), we choose the field structure at which the instability of the first moments ($k\upsilon_b = \omega_p$) is observed. In this case, the maximum increment of the second moments is localized in the region close to $\lambda = 2$. Expanding (4.25) in small parameters δ ($\lambda = 2 + \delta$) and β, we obtain the following expression for the increment of the second moments:

$$\tau\langle\tau_m \equiv \frac{9(2\beta)^{-1/3}}{\omega_b k \upsilon_b \sigma_0^2 \tau_R}, \qquad (4.28)$$

where σ_0 —variance , τ_R — correlation time random processes $z(\tau)$.

ATTACHMENT

Let us denote S_n^m - the maximum root of the polynomial A_n^m defined by (4.12). Let us prove that $\lambda = S_m^m = m$ - the maximum root of the equation $Det_m(\lambda) = 0$ at $B = 0$ and the addition $B \rangle 0$ S_m^m increases.

Let's suppose that

$$A_m^m(m) = A_{m-n}^m(m) - \left(\frac{m}{m-n} - 1\right) A_{m-n-1}^m(m) \qquad (A1)$$

At $n = 1$, relation (A1) turns into (4.12). Let it be valid for any certain n. Then, using (4.12) one have

$$A_{m-n}^{m}=\frac{m}{m-n}A_{m-n-1}^{m}-\left(\frac{m}{m-n-1}-1\right)A_{m-n-2}^{m} \tag{A2}$$

Substituting (A2) into (A1), we obtain

$$A_{m}^{m}=A_{m-n-1}^{m}-\left(\frac{m}{m-n-1}-1\right)A_{m-n-2}^{m} \tag{A3}$$

Those (A1) is also true for $n+1$. For $n=m+1$ is checked directly by substitution $A_0(m)$ and $A_1(m)$ in (A1). The presence $B\rangle 0$ leads to an increase in this root. Indeed, recurrence relation (4.12) can be rewritten as

$$\frac{\lambda}{m}A_{m-1}^{m}(\lambda)=\left(\frac{m}{m-1}-1\right)A_{m-2}^{m}+\frac{2B}{m-2}(m-1)A_{m-3}^{m} \tag{A4}$$

At $B=0$ relation (A4) was performed at $\lambda = m$. If the condition

$$S_n^m > S_{n-1}^m > S_{n-2}^m \tag{A5}$$

is satisfied, then the coefficient at on the right-hand side of B equality (A4) is positive. Then for fulfill (A4) it is necessary to increase λ. (When $\lambda\rangle m$ the left side (A4) grows faster than the right one, since the maximum degree λ on the left is $\frac{\lambda^{m+1}}{(m+1)!}$, and on the right $\frac{\lambda^{m-1}}{(m-1)!(m-1)}$ -).

Proof of (A5) is carried out by induction. For $n = 0,1,2$ value S_n^m is, respectively, 0, $\sqrt{m}$, $\sqrt{4m-1}+\delta(B)$ ($\delta(B)$ is a positive addition associated with the influence of noise). If (A5) holds for n $(S_n^m\rangle S_{n-1}^m\rangle S_{n-2}^m)$, then at $\lambda\to+\infty$ and $\lambda\rangle S_{n-1}^m$ the second and third terms on the right-hand side of (4.12) tend to $-\infty$ proportionally λ^{n-1} and λ^{n-2} accordingly. But as soon as $\lambda\rangle S_n^m$ the first term tends to $+\infty$ and grows faster (proportionally λ^{n+1}).

When these terms are equal, the polynomial A_{n+1}^m has one more (maximum) root, which is larger S_n^m. Relation (A5) is proved.

Let us prove that m is the maximal root of (4.12) for B = 0. Let $S_m^m=m+\delta$, where δ is a positive addition. Then

$$A_m^m(S_m^m)=0=\frac{m+\delta}{m}A_{m-1}^{m}-\left(\frac{m}{m-1}-1\right)A_{m-2}^{m} \tag{A6}$$

Successively applying relations (4.12) to (A6), we finally obtain:

$$\delta\left[1+\sum_{n=0}^{m-1}A_n^m(S_m^m)\frac{1}{n+1}\right]=0. \qquad \text{(A7)}$$

Due to the fact that $S_m^m \rangle S_n^m$ for any $n \le m-1$, all terms in (A7) are positive and the equality holds only for $\delta = 0$. Expand (4.12) in a series in powers of B and limit ourselves to the linear term of the expansion. Then using (A7) we obtain an addition to the increment due to the nonzero noise amplitude:

$$\delta = \frac{B}{2}\frac{m(m-1)+\sum_{n=2}^{m-1}(m-n)\left(\frac{m}{n-1}-1\right)A_{n-2}^m}{1+\sum_{n=0}^{m-1}A_n^m\frac{1}{n+1}}. \qquad \text{(A8)}$$

This addition is always positive and, apparently, grows with increasing m.

4.5. Conclusion

The main point of this section is the conclusion that one should pay attention to the presence of fluctuations (spatial or temporal). Such fluctuations can significantly disrupt the regular dynamics of the processes under study.

SECTION 5. SELF-CONSISTENT THEORY OF EXCITATION OF WAVES BY BEAMS OF OSCILLATORS UNDER THE CONDITIONS OF ISOLATED CYCLOTRON RESONANCE

5.1. Introduction

We have considered above the criterion of appearance of chaotic dynamical regimes in the case of overlapping of nonlinear cyclotron resonances and have analyzed the effect of additive and multiplicative fluctuations under nearly self-resonance conditions (cyclotron resonances do not overlap). If the amplitudes of excited waves are not too large and criterion (1.34) for the appearance of local instability is not satisfied, and the dynamics of particles and fields can be simulated by the dynamics in a single isolated nonlinear cyclotron resonance. Our preliminary studies indicate that chaotic dynamical regimes

also appear. In addition, the development of stochastic instability stabilizes the level of excited fields as in the case of the overlapping of cyclotron resonances. Below, we analyze this problem and reveal a mechanism responsible for the development of stochastic instability. We consider the simplest model that allows answering these questions.

5.2. Problem statement and basic equations

We consider the problem of excitation of the electromagnetic field by a monoenergetic beam of oscillators with the distribution function:

$$f_0 = \frac{N_b}{2\pi p_\perp}\delta(p_\perp - p_{\perp 0})\delta(p_\parallel), \tag{5.1}$$

where $p_\perp$ and $p_\parallel$ are the momentum components perpendicular and parallel to the z axis, respectively, and N_b is the equilibrium density of the beam. We consider the excitation of a wave propagating in the direction perpendicular to the external magnetic field. The complete nonlinear self-consistent system of equations that describes the dynamics of particles and fields consists of Maxwell's equations and equations of motion of particles. This system was presented in [40,41]. We write the truncated system of equations describing the dynamics of particles and fields in the s-th isolated cyclotron resonance:

$$\begin{aligned}
\frac{dp_\perp}{d\tau} &= iJ_s'(\mu)e^{i\theta_s}\varepsilon\ , \\
\frac{d\theta_s}{d\tau} &= \frac{s\omega_H}{\gamma} - 1 + \frac{1}{\omega_H}\left(1 - \frac{s^2}{\mu^2}\right)\mathrm{Re}\left(J_s(\mu)e^{i\theta_s}\varepsilon\right)\ , \\
\frac{d\varepsilon}{d\tau} &= i\frac{\omega_b^{\,2}}{2\pi}\int_0^{2\pi} d\theta_{s0}\frac{p_\perp}{\gamma}J_s'(\mu)e^{-i\theta_s}
\end{aligned} \tag{5.2}$$

where: $p_\perp = p_\perp / mc$, $\mu = p_\perp / \omega_H$, $\gamma = \sqrt{1+\mu^2\omega_H{}^2}$, $\omega_H = eH_o / mc\omega$, $\omega_b^2 = 4\pi e^2 n_b / m_e\omega^2$, $\varepsilon = eE / mc\omega$.

5.3. Analysis of the system of equations (5.2)

Note that the problem we are considering is a Hamiltonian problem. Due to this, in the expression under the integral in the last equation of system (5.2) it was possible to use the fact of conservation of the phase volume and to perform integration only over the initial phases (index 0).

It can be expected that the last term on the right hand side of the equation for the phase is mainly responsible for the appearance of stochasticity.

Indeed, if the field amplitude is fixed, the system of equations (5.2) is similar to the equation of mathematical pendulum subjected to an external periodic force. The development of stochastic instability in this model was studied in [43], where, in particular, the criterion for the appearance of local instability was obtained. However, it will be shown below that ***fields excited by the beam of oscillators cannot satisfy this criterion***. There is an additional mechanism. To reveal it and to answer the questions formulated above, we numerically solve the system of equations (5.2). The results of the numerical calculation are shown in Fig. 5.1 – 5.6, which demonstrates the following features of the dynamics of the interaction between particles and fields at cyclotron resonances. First, it is seen that the level of the excited field increases with the density of active particles. The dynamics of particles and excited field is regular up to $\omega_b^2 = 0.04$ (Fig. 5.1). This is the convenient dynamics of an increase in the field. The chaotic component appears in the dynamics of the excited field at a higher beam density, $\omega_b^2 > 0.04$ 0.04 (Fig. 5.2.). The dynamics of the field at small times is regular and similar to dynamics at low beam densities. In this case, the field amplitude first increases to values corresponding to the capture of particles by the field of the excited wave. Then, the field amplitude decreases chaotically.

Beginning with a beam density of 0.5, the asymptotic value of the field does not exceed 0.15.

Thus, similar to the case of overlapping of cyclotron resonances (see, for example, [40]), the appearance of local instability limits the level of the beam-excited field (Fig. 5.3.). It is noteworthy that the same process of stabilization is also characteristic of the beam–plasma instability [40 - 42]. Such a dynamics of the field with an increase in the density of particles remains quite convenient until the density of particles satisfy the inequality $\omega_b^2 < 1$. With a further increase in the density of particles, when $\omega_b^2 > 1$, it could be expected that oscillations at the chosen frequencies ($\omega \approx \omega_H$) are not excited.

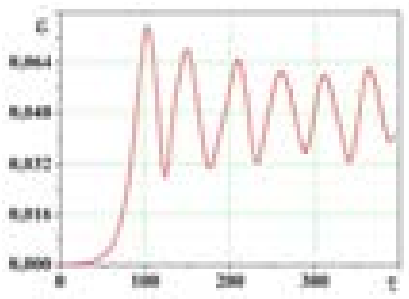

Fig. 5.1. Field amplitude versus time at low beam density: ω_b^2 =0.04

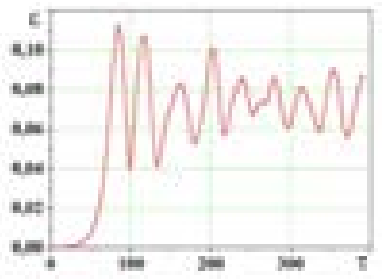

Fig. 5.2. Field amplitude versus time at a beam density: ω_b^2 =0.1

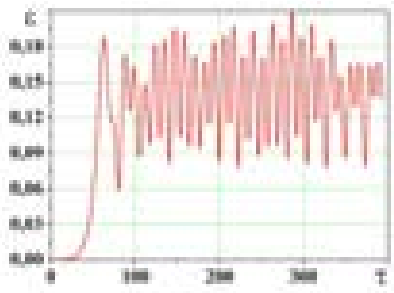

Fig. 5.3. Field amplitude versus time at a beam density: $\omega_b^2 = 0.5$

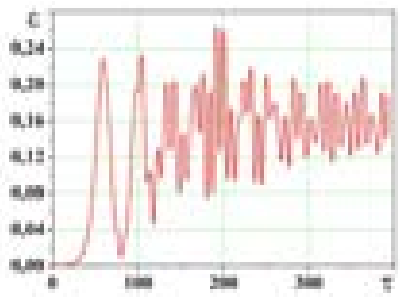

Fig.5.4. Field amplitude versus time at a beam density: $\omega_b^2 = 1.5$

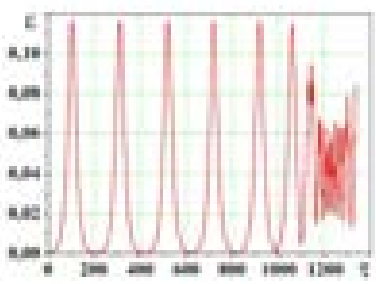

Fig. 5.5. Field amplitude versus time at a beam density: $\omega_b^2 = 4$

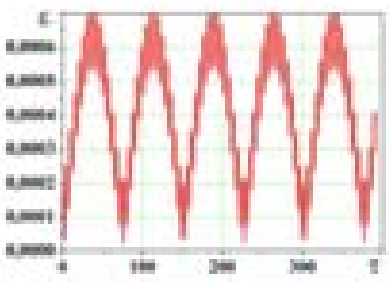

Fig.5.6. Field amplitude versus time at a beam density: $\omega_b^2 = 4.6$

Indeed, oscillations at the frequencies $\omega \approx \omega_H$ under the condition $\omega_b^2 > 1$ are not natural in such medium. Being excited, they decay. As is seen in Figs. 5.4 – 5.6, oscillations are excited because the beam system is nonequilibrium at the frequencies $\omega \approx \omega_H$. However, these oscillations decay quite rapidly. The regime of relaxation oscillations appears. It exists in a fairly wide time interval; further, this regime is transformed to the regime of chaotic oscillations and the excitation of oscillations at these frequencies ceases. In this case, the amplitude of excited oscillations decreases with increase in the density of particles. As far as we know, the excitation of such relaxation oscillations has not yet been described. Such oscillations can apparently appear in the ionospheric plasma.

5.4. The origin of local instability

In the above model (see Eqs. (5.2)), the dynamics of the interaction between particles with the field of an isolated cyclotron resonance is studied.

In this case, the mechanism of overlapping of cyclotron resonances is absent. The analysis of the behavior of the field amplitude in Fig. 5.1 – 5.4 shows that the mechanism of stabilization is qualitatively the same as at development of local instability. However, the reason for such instability should be different. It could be assumed that this mechanism is similar to the mechanism of appearance of the local instability of the dynamics of motion of the mathematical pendulum subjected to the external periodic force. Such a mechanism of appearance of chaotic dynamical regimes was described in [8].

One – particle approximation

The analysis of the conditions for the appearance of dynamic chaos through this mechanism shows that forces acting on the particle are insufficiently strong for the development of dynamic chaos. For this reason, we additionally analyzed the dynamics of particles in isolated cyclotron resonance. The simplest model for this case is the model of motion of the charged particle in the field of the external electromagnetic wave under the conditions of isolated cyclotron resonance. The wave amplitude can be assumed as constant. In this case, the system of equations describing the dynamics of the particle coincides with the system of equations (5.2), where the third equation can be omitted. As a result, the dynamics of particles is described by the first two equations. Such a system corresponds to the Hamiltonian

$$H(\theta_s, I) = \frac{s}{\omega_H}\gamma - I + \frac{\varepsilon}{\omega_H} 2I \frac{d}{dI}\left(J_s(\sqrt{2I})\right)\cos(\theta_s) \qquad (5.3)$$

where $I = \mu^2 / 2$

The phase portrait of the system with Hamiltonian (5.3) is topologically similar to the phase portrait of the Duffing oscillator. Indeed, the ($p_\perp$, θ_s) phase plane generally contains three singular points: ($\theta_s = 0$, $p_{\perp 1} = G$) ($\theta_s = 0$, $p_{\perp 2} = 1 - G/2$) ($\theta_s = \pi$, $p_{\perp 3} = 1 + G/2$) where $G = \varepsilon / p_{\perp,0}^3$, $p_{\perp,0}$ is the initial momentum of the particle. The first point is a saddle point, whereas two other points are «center» - type points. The phase space has such a form at small amplitude of the external wave ($G \ll 1$). If the amplitude is fairly large ($G \gg 1$), the first two singular points (saddle point and «center» - type point) merge and disappear. Only one center-type point remains. All these features of the phase space are similar to the features of the phase space of the Duffing oscillator. However, it is remarkable that oscillations of the Duffing oscillator are potential, whereas a potential for our equations cannot be found. The topology of the phase space of the system under consideration has an important feature: closed trajectories near a «center» - type point can be attributed to trapped particles, whereas

open trajectories that enclose closed trajectories can be attributed to flying particles. The characteristic forms of the phase portrait at low ($G \ll 1$) and high ($G > 1$) field strengths of the external wave are shown in Fig. 5.7 and 5.8. Trapped and flying particles are usually separated by separatrices, i.e. homoclinic or heteroclinic trajectories.

In this case, at $G > 1$ (Fig. 5.8), it is difficult to find such trajectories. Only regions for trapped and flying particles are pronounced. As is seen in Fig. 5.7, the phase plane contains, in complete agreement with the above results, three singular points: two "center" - type points and one saddle point. With an increase in the wave amplitude, the saddle point and center-type point at $\theta_s = 0$ approach each other and disappear (Fig. 5.8). Thus, an increase in the wave amplitude qualitatively changes the form of the phase portrait describing the dynamics of motion of particles. Such qualitative change in dynamics can be responsible for the appearance of the chaotic dynamical regime. In addition, it is seen that even quantitative characteristics of the appearance of such qualitative change in dynamics shown in Fig. 5.8 confirm such a possibility. Indeed, it is seen in this figure that the dynamics of particles becomes irregular when the amplitude of the excited wave becomes larger than 0.105. With a further increase in the density of particles and, correspondingly, the strength of the excited wave, this irregularity becomes more noticeable. Already at the strength of the excited field at small times, it can exceed 0.2. However, the dynamics of the particle is such that the field amplitude irregularly oscillating approaches a value of about 0.15. This field strength is in qualitatively good agreement with the field strength of the wave at which the phase dynamics of particles changes qualitatively. Just this mechanism of bifurcation of the form of the phase portrait is responsible for the chaotic dynamical regime (see also [43]–[46]). Thus, in the case under consideration (in the case of the interaction of charged particles with electromagnetic fields under the conditions of isolated cyclotron resonance), the stabilization of the level of the excited field is determined by the appearance of dynamic chaos. In contrast to the case of overlapping of nonlinear cyclotron resonances, the main reason for the appearance of dynamic chaos in our case is a qualitative change in the phase portrait at the variation of the field amplitude of excited oscillations.

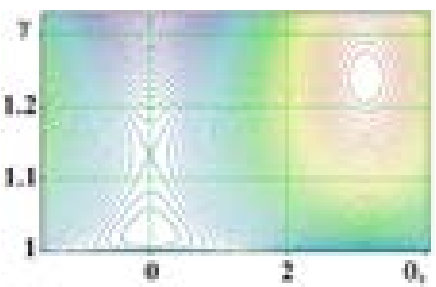

Рис.5.7.. Phase trajectories at ε = 0.08

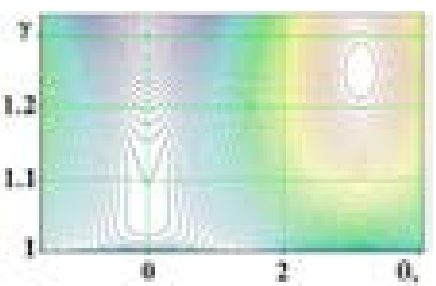

Рис.5.8.. Phase trajectories at ε =0.105

5.5. Conclusion

The main result of this section is the fact that in many cases, even under conditions of isolated resonances, when there are no intersections of homoclinic or heteroclinic trajectories, when the Melnikov and Chirikov criteria are not met, regimes with dynamic chaos can appear. In this case, they appeared as a result of a qualitative quasiperiodic change in the form of the phase portrait.

SECTION 6. PARTICLE ACCELERATION BY THE WAVE PACKET FIELD

The dynamics of particles in the field of a wave packet excited in plasma is considered in this section. The conditions are found under which such dynamics is regular, and when it becomes chaotic. It was found that the well-known (phenomenological) criterion for the emergence of dynamic chaos – the criterion for overlapping Chirikov nonlinear resonances – requires careful use.

6.1. Introduction

When charged particles are accelerated by electro-magnetic waves, in particular, when accelerated by laser radiation, electromagnetic fields are mainly modeled by a coherent electromagnetic wave field. In real conditions, the fields are limited both in space and in time (for example, long electromagnetic pulses). Under these conditions, sometimes it is necessary to model such fields with an electromagnetic packet. The question arises: "What features of the dynamics of charged particles can arise in this case and under what conditions is it justified to simulate such a packet by a coherent electromagnetic wave?"

There are answers on these questions. The motion of particles in a plasma in the general case obeys random dynamics. This fact is noted when describing the results of numerous theoretical and experimental works (see, for example [47 - 52]). A rigorous proof of this fact and the criteria for the emergence of regimes with dynamic chaos were obtained for cyclotron resonances (see [53 - 55]). The dynamics of particles in the fields of numerous waves that are excited in plasma should also be chaotic (in the absence of cyclotron resonances). Intuitively, this fact is not in doubt. However, there is apparently no rigorous proof of this fact and the conditions for the occurrence of such dynamics. Below, using simple examples, the conditions have been obtained when this statement is true, as well as the conditions when the particle dynamics left regular.

6.2. Non – relativistic dynamics of particles in the fields of wave package

It is known that plasma, especially plasma in a magnetic field, has a rich spectrum of natural wave oscillations. Let us show that plasma particles in these even regular fields move randomly. To prove this, consider the movement of charged particles in the field of a wave packet:

$$\ddot{z} = \frac{e}{m}\sum E_i \sin(k_i z - \omega_i t) \tag{6.1}$$

Let us first consider the dynamics in the field of a single wave. For such dynamics, from equation (6.1) we can obtain the well-known integral. To do this, we first transform equation (6.1) (with one wave) into the equation of the mathematical pendulum:

$$k\ddot{z} = \frac{d}{dt}(k\dot{z}) = \frac{d}{dt}(k\dot{z} - \omega) = \frac{d^2}{dt^2}(kz - \omega t) = \ddot{\varphi};\ \ddot{\varphi} + \Omega^2 \sin\varphi = 0 \tag{6.1a}$$

The mathematical pendulum equation (6.1a) has a well-known integral:

$$\frac{\dot{\varphi}^2}{2} - \Omega^2 \cos\varphi = H = const \tag{6.2}$$

Here $\varphi = kz - \omega t$, $\Omega^2 = |e|Ek / m\omega^2$, $\dot{\varphi} = d\varphi / d\tau$, $\tau = \omega t$, $H = \frac{\dot{\varphi}(0)^2}{2} - \Omega^2 \cos[\varphi(0)]$

Using the integral (6.2), we find the width of the non-linear resonance:

$$\delta\dot{\varphi} = \dot{\varphi}_{\max} - \dot{\varphi}_{\min};\quad \dot{\varphi}_{\max} = +2\Omega;\quad \dot{\varphi}_{\min} = -2\Omega;\quad \delta\dot{\varphi} = 4\Omega \tag{6.3}.$$

To determine the distance between resonances, we note that the effective interaction of particles with pack-et waves occurs under Cherenkov resonance conditions $(\omega_k = kv)$. In this case, it is easy to determine the distance between the resonances:

$$\Delta\dot{\varphi} = \dot{\varphi}_{k+\Delta k} - \dot{\varphi}_k = \dot{\varphi}_k + \frac{\partial\dot{\varphi}_k}{\partial k}\Delta k + \ldots - \dot{\varphi}_k = \frac{\partial\dot{\varphi}_k}{\partial k}\Delta k = \Delta k\left[\dot{z} - \frac{\partial\omega_k}{\partial k}\right] \tag{6.4}$$

Upon receipt of (6.4), it was taken into account that $v = v_{ph} = \omega / k$

Using expressions (6.3) and (6.4), we find the conditions for the occurrence of local instability:

$$K = \frac{4\Omega}{\Delta\dot{\varphi}} = N\frac{4\Omega}{\left(1 - v_g / v_{ph}\right)}, \quad K > 1 \tag{6.5}$$

where v_g – group speed; $N = \omega / \Delta\omega$ – the number of waves in the package.

By analyzing formulas (6.4) and (6.5), several important conclusions can be drawn. The first one shows (from formula (6.4)) that if the group velocity tends to the phase velocity of the wave, then the distance between the resonances tends to zero. This means that all the waves of the packet are located in a rectilinear dispersion region. In the phase space, the resonances of such waves all coincide. For particles, such resonances are almost indistinguishable. Dynamics should be regular. Second, if the group wave velocity tends to zero (for example, Langmuir waves in a plasma), then, as can be seen from formula (6.5) $1 < K << N;\ \Omega << 1$. In this case, as it was the first, apparently, it was noted in [6], the particle dynamics should be chaotic. We note that the dynamics of particles in a plasma almost always corresponds to the case $\Omega << 1$. Indeed, the maximum electric field strength of a longitudinal wave in a plasma (with complete separation of charges) is described by the expression: $E_{\max} = \sqrt{4\pi n m c^2 \gamma}$

$$\Omega^2 = A = \frac{eE_{\max}}{m\gamma c\omega_p} = 1 \qquad \omega = \omega_p\ , \quad k = \omega_p / c\ , \quad m \to m\gamma$$

If, $K > N$ then the dynamics should be regular. In this case, the particle does not distinguish the resonances of the individual waves of the packet. We are used to the fact that as soon as the inequality $K > 1$ is fulfilled, the particle dynamics becomes chaotic. It can be seen that this simple, convenient, and very common criterion requires careful use when it comes to particle dynamics in wave packets.

6.3. Relativistic dynamics of particles in the fields of wave packages

In the relativistic case, the system of equations (6.1) should be rewritten:

$$\dot{p} = \sum_{n=1}^{N} A_n \sin\psi_n \tag{6.6}$$

The following dimensionless dependent and independent variables are introduced here:

$$p = \frac{p}{mc}, \quad A_n = \frac{eE_n}{mc\omega}, \quad \psi_n = \omega_n \tau - k_n z, \quad \tau = \omega t, \quad z = \omega z / c,$$
$$k_n = k_n c / \omega = k_n / k, \quad k = \omega / c, \quad \dot{p} = dp / d\tau, \quad \omega_n \equiv \omega_n / \omega$$

Here ω – maximum frequency of the spectrum of the wave packet.

Multiply the left and right sides of equation (6.6) by p, we obtain a useful equation for the dimensionless particle energy:

$$\dot{\gamma} = v \cdot \sum_{n=1}^{N} A_n \sin \psi_n \tag{6.7},$$

where $v = v / c, \quad \gamma = \sqrt{1 + p^2}$

Below we assume that the momentum of the particle is large ($p >> 1$). In this case, using equations (6.6) and (6.7), we can obtain the equation of the mathematical pendulum for the phase of the separately allocated wave of the wave packet:

$$\ddot{\psi}_n + \Omega_n^2(\tau)\psi_n = 0 \tag{6.8}$$

where $\Omega_n^2(\tau) = \left[A_n / 2p^3 \right]$

Note that the frequency of the mathematical pendulum, which describes the capture vibrations of particles in the wave field, is a function of time. In addition, it is seen that the frequency of these capture vibrations de-creases with increasing particle momentum. This dependence is quite obvious, since with increasing momentum the particles become heavier. In full accordance with the algorithm described in the previous section, we can determine the condition for the emergence of a regime with dynamic chaos. This condition can be rep-resented as:

$$K = \frac{4\Omega_n}{\Delta \dot{\psi}_n} \tag{6.9}$$

We note that in both the relativistic and nonrelativistic cases we are talking about Cherenkov resonances. Therefore, the distance between resonances in the relativistic case does not differ from the distance between resonances in the nonrelativistic case ($\Delta \dot{\psi}_n = \Delta \dot{\varphi}_n$).

Finally, the expression for the conditions for the emergence of dynamic chaos takes the form:

$$K = \frac{4\Omega_n}{\Delta \dot{\psi}_n} = N \frac{4\Omega_n}{\left(1 - v_g / v_{ph}\right)} \tag{6.10}$$

Formula (6.10) practically does not differ from formula (6.5). The difference lies only in the physical content of the numerator. From formula (6.10), one can see the important result that, with an increase in the energy of accelerated particles, the particle dynamics is regularized (parameter K decreases). This result is quite obvious, since with increasing energy the particles become heavier.

6.4. Numerical analysis of particle dynamics in the field of a wave package

Numerical modeling can show a number of features of particle dynamics in the fields of wave packets. Using the example of the relativistic case, we show the dependence of particle dynamics on the ratio of the phase and group velocities of packet waves. To do this, we rewrite the system of equations (6.6) in the form:

$$\dot{x}_0 = \frac{x_1}{\sqrt{1+x_1^2}}$$
$$\dot{x}_1 = -A\sum_{i=0}^{N}\sin\left[\left(k1+i\frac{\Delta k}{N}\right)x_0-\left(\omega 1+i\frac{\Delta\omega}{N}\right)t\right] \qquad (6.11)$$

where $x_0 = z$, $x_1 = p$, A – amplitude of the waves in the packet; $k1$, ω1 – wave vector and frequency of the initial wave; Δk, $\Delta\omega$ – difference between the wave vectors and the frequencies of the extreme waves of the packet; N – number of waves in the packet.

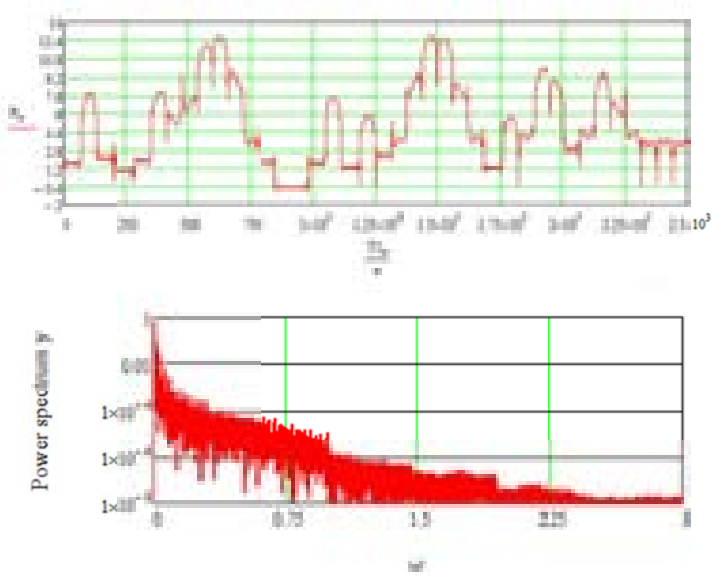

Fig. 6.1. Particle momentum and its spectrum in the packet field at $v_g = 0$, N=30, A=0,03

The initial conditions were chosen so that the particle was in the center of the resonance. $x_0 = 0$, $x_1 = \omega 1/k1$. The wavenumbers of the extreme waves of the packet are K1 = 2, Kn = 1, and the frequency of the first wave is also fixed ω1 =1. The waves of the packet were evenly distributed between two fixed waves.

In the case when the group velocity tends to 0, (in this case it is possible when the frequencies of all waves become the same), then the particle dynamics in the field of such a packet turns out to be chaotic Fig. 6.1.

In the case when the group velocity tends to the phase velocity, the particle dynamics in the field of such a packet becomes regular see Fig. 6.2.

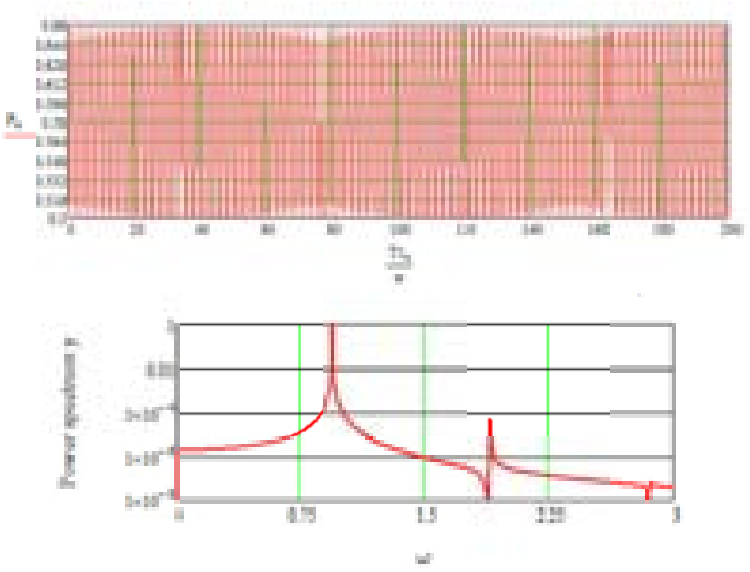

Fig 6.2. Particle momentum and its spectrum in the packet field at $v_g = v_{ph}$, N=30, A=0,03.

It is worth noting that a similar dynamics is observed in the nonrelativistic case.

6.5. Some conclusion

Let's list the most significant results of the work:

1. The well-known wave strength parameter for waves excited in a plasma ($A = eE / mc\omega\gamma$) does not exceed unity ($A \leq 1$).

2. If the group velocity of the wave packet in the plasma tends to zero, then the particle dynamics in the field of such a packet is chaotic.

3. If the group velocity of the wave packet tends to the phase velocity of the wave packet, then the dynamics of the particles in the wave packet is regular.

4. Analysis of numerical results is in good agreement with analytical results.

SECTION 7. NEW RESONANCES IN THE INTERACTION OF CHARGED PARTICLES WITH WAVES IN VACUUM

The conditions for the emergence of new resonances in the interaction of charged particles with waves in vacuum are described. Some features of this resonant interaction are also described. In practice, these conditions mean that charged particles are captured by the field of a transverse electromagnetic wave and their unlimited acceleration by the field of this wave in vacuum. The position of new resonances in the general physical picture of the interaction of waves with particles in a vacuum is also described. The discovered resonances can play a special role for laser acceleration of charged particles in vacuum.

7.1. Introduction

Accelerating charged particles in a vacuum is an attractive option. This is especially true for laser acceleration schemes. There are many attempts to find such acceleration schemes. There is a large number of works that describe various scenarios for such acceleration. One of the last works in this direction is the work [56] (see also the literature cited therein). The main difficulty in constructing such schemes, which is noted by almost all authors, is the transverse (relative to the wave vector of the wave) dynamics of particles in the field of laser radiation. Therefore, the most common acceleration schemes contain a complex field structure, in which it is possible to distinguish the longitudinal (relative to the wave vector of the wave) component of the wave field with a phase velocity less than the speed of light. Such structures are created by external material elements (lenses, lattices, their combinations, and others). Already the presence of such elements limits the intensity of the laser radiation. As a result, the efficiency of such acceleration schemes is not high.

Special attention should be paid to the existence of rigorous solutions of particle dynamics in the field of a transverse electromagnetic wave. After Volkov D.M. [57] such solutions were obtained and analyzed in works [58-61]. Based on the solutions obtained, several new acceleration schemes were proposed. Note that in these rigorous solutions, the particle momentum components were described by periodic functions of the wave phase. Therefore, the acceleration process was replaced by the deceleration process (see below the formulas of system (7)). The impression was that particles in the field of a transverse electromagnetic wave in a vacuum can be effectively accelerated only in a limited region of space. The fact of the

existence of rigorous solutions in which there are no resonances was, in a sense, a brake for finding such solutions. Our researches have shown that strict solutions do not contain all solutions. There are other solutions that contain resonances. Such solutions are described in this section.

In this section, it is shown that the existing exact solutions describing the dynamics of particles in the field of a transverse electromagnetic wave and presented in [58-61] do not exhaust all the features of the dynamics of particles in such fields. There are other solutions as well. These solutions contain new resonances. When the conditions of these resonances are met, effective and unlimited acceleration of charged particles by the fields of transverse waves in vacuum is possible. This section is devoted to the description of the features of these resonances. It is shown that there is some analogy with the appearance of new resonances and with the appearance of cyclotron resonances. Below, in the second subsection, the statement of the problem is formulated and the basic equations are written out. In the third subsection, it is shown how rigorous solutions appear to describe the dynamics of particles in the field of a transverse electromagnetic wave, both without an external magnetic field and in the presence of an external magnetic field. As a result, the constraints under which these decisions are valid become visible. In the same section, it is recalled how, in the presence of an external magnetic field, these restrictions are removed, and how cyclotron resonances appear. In the fourth subsection, it is shown how the problem of the motion of particles when the strength of the external magnetic field tends to zero can be solved, in the general case. This section is the most important. There are formulates conditions under which charged particles in the field of a transverse electromagnetic wave can be effectively (resonantly) accelerated in a vacuum. In the fifth subsection, the results of a numerical study of the considered processes are presented. Good qualitative agreement of the obtained numerical results with analytical results is shown. In the conclusion, the main results are formulated and some of them are discussed.

7.2. Statement of the problem and basic equations

Consider a charged particle that moves in an external constant magnetic field directed along the axis z and in the field of a plane electromagnetic wave, which in the general case has the following components:

$$\mathbf{E} = \mathrm{Re}(\mathbf{E}_0 \exp(i\omega t - i\mathbf{kr})), \quad \mathbf{H} = \mathrm{Re}\left(\frac{c}{\omega}\left[\mathbf{kE}\right] \exp(i\omega t - i\mathbf{kr}) \right)$$

Where $\mathbf{E}_0 = E_0 \cdot \boldsymbol{\alpha}$, $\boldsymbol{\alpha} = \left\{ \alpha_x, i\alpha_y, \alpha_z \right\}$ - polarization vector of the wave.

Vector equation of motion of charged particles:

$$\frac{d\mathbf{p}}{dt} = e\mathbf{E} + \frac{e}{c}\left[\frac{\mathbf{p}}{\gamma}\left(\mathbf{H}_0 + \mathbf{H} \right) \right]. \tag{7.1}$$

Without loss of generality, one can choose a coordinate system in which the wave vector of the wave has only two components k_x and k_z. For follows, it is convenient to use the following dimensionless dependent and independent variables:, $\mathbf{p} \to \mathbf{p}/mc$, $\tau \to \omega t$, $\mathbf{r} \to \omega \mathbf{r}/c$. It is also convenient to use the expression for the double cross product: $\left[\mathbf{p}\left[\mathbf{k}\boldsymbol{\varepsilon}\right]\right] = \mathbf{k}\left(\mathbf{p}\cdot\boldsymbol{\varepsilon}\right) - \boldsymbol{\varepsilon}\left(\mathbf{k}\cdot\mathbf{p}\right)$.

The equations of motion in these variables will be as follows:

$$\frac{d\mathbf{p}}{d\tau} = \left(1 - \frac{\mathbf{kp}}{\gamma}\right)\mathrm{Re}\left(\boldsymbol{\varepsilon} e^{i\psi}\right) + \frac{\omega_H}{\gamma}\left[\mathbf{ph}\right] + \frac{\mathbf{k}}{\gamma}\mathrm{Re}\left[\left(\boldsymbol{\varepsilon}\cdot\mathbf{p}\right)e^{i\psi}\right],$$

$$\mathbf{v} = \frac{d\mathbf{r}}{d\tau} = \frac{\mathbf{p}}{\gamma},\ \dot{\psi} = \frac{d\psi}{d\tau} = 1 - \frac{\mathbf{kp}}{\gamma} \tag{7.2}$$

where, $\mathbf{h} = \mathbf{H}/H_0$, $\omega_H = eH/mc\omega$, $\boldsymbol{\varepsilon} = \varepsilon\cdot\boldsymbol{\alpha}$, $\varepsilon = (eE_0/mc\omega)$, $\psi = \tau - \mathbf{kr}$, $\mathbf{k}$ - is the unit vector in the direction of the wave vector, $\gamma = (1+\vec{p}^{\,2})^{1/2}$ is the dimensionless energy of the particle (measured in units mc^2), $\mathbf{p}$ -is the momentum of the particle.

Multiplying the first equation of system (7.2) by $\mathbf{p}$, we obtain a useful equation that describes the change in the energy of a particle:

$$\frac{d\gamma}{d\tau} = \mathrm{Re}\left(\mathbf{v}\boldsymbol{\varepsilon} e^{i\psi}\right) \tag{7.3}$$

Equations (7.2) and (7.3) have well-known integrals:

$$\mathbf{p} + \mathrm{Re}\left(i\boldsymbol{\varepsilon} e^{i\psi}\right) - \omega_H\left[\mathbf{rh}\right] - \mathbf{k}\gamma = \mathbf{p}_0 - \mathbf{k}\gamma_0 + \mathrm{Re}\left(i\boldsymbol{\varepsilon} e^{i\psi_0}\right) - \omega_H\left[\mathbf{r}_0\mathbf{h}\right] = \text{const} \tag{7.4}$$

Index "0" denotes the values of the initial variables.

7.3. Precise solutions without external magnetic field

Looking at equation (7.2) at $\omega_H = 0$, it is easy to see that without loss of generality in this case it is convenient to choose such components of the particle momentum $\mathbf{p} = \left\{p_{\|}, \mathbf{p}_{\perp}\right\}$, $p_{\|} \| \mathbf{k}$.

Let's take into account that $\left(\mathbf{k}\cdot\boldsymbol{\varepsilon}\right) = 0$; $\left(\boldsymbol{\varepsilon}\cdot\mathbf{p}\right) = \left(\varepsilon_{\|}\cdot p_{\|} + \boldsymbol{\varepsilon}_{\perp}\cdot\mathbf{p}_{\perp}\right) = \left(\boldsymbol{\varepsilon}_{\perp}\cdot\mathbf{p}_{\perp}\right)$; $\mathbf{k} = \left\{0, 0, k_{\|} = 1\right\}$ ... Then the system of equations (7.2) takes the form:

$$\frac{dp_{\|}}{d\tau} = \frac{1}{\gamma}\mathrm{Re}\left[\left(\boldsymbol{\varepsilon}\cdot\mathbf{p}\right)e^{i\psi}\right]$$
$$\frac{d\mathbf{p}_{\perp}}{d\tau} = \left(1-\frac{\mathbf{kp}}{\gamma}\right)\mathrm{Re}\left(\boldsymbol{\varepsilon}_{\perp}e^{i\psi}\right) = \dot{\psi}\cdot\boldsymbol{\varepsilon}_{\perp}\cdot\cos\psi \qquad (7.5)$$

After dividing the left and right sides by the derivative of the wave phase ($\dot{\psi} = d\psi / d\tau$), system (7.5) can be rewritten:

$$\frac{dp_{\|}}{d\psi} = \frac{1}{\left(\gamma\cdot\dot{\psi}\right)}\mathrm{Re}\left[\left(\boldsymbol{\varepsilon}_{\perp}\cdot\mathbf{p}_{\perp}\right)e^{i\psi}\right]$$
$$\frac{d\mathbf{p}_{\perp}}{d\psi} = \boldsymbol{\varepsilon}_{\perp}\cdot\cos\psi \qquad (7.6)$$

Taking into account that in the case under consideration $\left(\gamma\cdot\dot{\psi}\right) = const \equiv C$, we easily find the following solutions for the momentum components:

$$\mathbf{p}_{\perp} = \mathbf{p}_{\perp}(\psi_0) + \boldsymbol{\varepsilon}_{\perp}\left(\sin\psi - \sin\psi_0\right) \qquad (7.7)$$
$$\frac{dp_{\|}}{d\psi} = \frac{1}{C}p_{\perp}\frac{dp_{\perp}}{d\psi},\quad p_{\|}(\psi) = p_{\|}(\psi_0) + \frac{1}{2C}\left[p_{\perp}^2 - p_{\perp}^2(0)\right] \sim \left(\boldsymbol{\varepsilon}_{\perp}\right)^2\frac{1}{C}$$

Such solutions come from the work of D.M. Volkov [57] and V.I. Ritus [58]. Within the framework of classical electrodynamics, they are presented in [59-61]. Such solutions are often referred as exact solutions. It can be shown that these solutions do not exhaust all solutions of the problem.

There are other solutions. To see this, and to see an analogy between the emergence of these new solutions and the appearance of cyclotron resonances, let us take into account the presence of an external magnetic field and go over to the Cartesian coordinate system. In this system, the vector equation (7.2) takes the form:

$$\dot{p}_x = \varepsilon_x\left(1-k_xv_x-k_zv_z\right)\cos\psi +$$
$$+\frac{k_x}{\gamma}\left[\left(\varepsilon_xp_x+\varepsilon_zp_z\right)\cos\psi - \varepsilon_yp_y\sin\psi\right] + \omega_Hp_y$$
$$\dot{p}_y = -\varepsilon_y\left(1-k_xv_x-k_zv_z\right)\sin\psi - \omega_Hp_x \qquad (7.8)$$

$$\dot{p}_z = \varepsilon_z\left(1-k_x v_x - k_z v_z\right)\cos\psi +$$
$$+\frac{k_z}{\gamma}\left[\left(\varepsilon_x p_x + \varepsilon_z p_z\right)\cos\psi - \varepsilon_y p_y \sin\psi\right]$$
$$\dot{\gamma} = \frac{1}{\gamma}\left[\left(\varepsilon_x p_x + \varepsilon_z p_z\right)\cos\psi - \varepsilon_y p_y \sin\psi\right].$$

Here $\dot{p} \equiv dp/d\tau$

System of equations (7.8) also has rigorous solutions (7.7). To obtain these solutions, we remove the external magnetic field ($\omega_H = 0$). Then it easily to see that if the wave vector of the wave is directed along one of the axes of the Cartesian coordinate system, then the solutions of this system will be solutions that coincide with the exact solutions (7.7). Indeed, let as an example the wave vector of an electromagnetic wave is directed along the z-axis.

The wave vector has no transverse component ($k_x = 0;\ k_z = 1;\ \boldsymbol{\varepsilon}_z = 0$). Then the system of equations (7.8) turns into the system of equations, which was considered above (7.5). Thus, the exact solution is accurate only if the wave vector of the wave coincides with one of the components of the momentum of the particle and one of the axes of the coordinate system can be associated with this component. In the general case, such a choice cannot be made, and there is no simple rigorous solution. It can be seen from the system of equations (7.8) that the presence of the transverse wave number of the wave does not allow one to obtain such simple solutions. This is due to the fact that in the presence of a transverse wave number, the expression $\gamma\dot{\psi}$ is no longer an integral.

7.4. Dynamics of particles in a wave field with circular polarization in the presence of an external magnetic field

We will assume that the wave vector of the electromagnetic wave is located in the plane $\{x,z\}$, that is $\mathbf{k} = \{k_x, 0, k_z\}$. The system of equations (7.8) at $\omega_H \neq 0$ describes the dynamics of particles in the field of a wave with arbitrary polarization. For our purposes, it is useful first to consider the case when the wave propagates strictly along the external magnetic field. In this case $k_x = 0;\ k_z = 1;\ \boldsymbol{\varepsilon}_z = 0$.

In this case, all the features (first of all, integrals) can be used in the same way as was done above for the case of the absence of a magnetic field. So, for a wave with circular polarization ($\varepsilon_x = \varepsilon_y$), equations (7.8) can be rewritten as:

$$\begin{aligned} p_x' &= \varepsilon\cos\psi + \Omega p_y \\ p_y' &= -\varepsilon\sin\psi - \Omega p_x \\ p_z' &= \varepsilon\left[\, p_x\cos\psi - p_y\sin\psi \,\right]/\left(\gamma\dot{\psi}\right), \end{aligned} \tag{7.9}$$

Where $p_i' = dp_i / d\psi$, $\Omega = \omega_H / \left(\gamma\dot{\psi}\right)$, the condition $\Omega = 1$ corresponds to the autoresonance condition. Note that in the case under consideration, the expression $\gamma\dot{\psi} = C = const$ is an integral. The system of equations (7.9) has a rigorous analytical solution:

$$\begin{aligned} p_x &= -\frac{\varepsilon}{\left(\Omega-1\right)}\left\{\sin\psi + \sin\left[\psi_0\left(\Omega-1\right) - \Omega\psi\right]\right\} \\ p_y &= -\frac{\varepsilon}{\left(\Omega-1\right)}\left\{\cos\psi - \cos\left[\psi_0\left(\Omega-1\right) - \Omega\psi\right]\right\} \\ p_z &= p_z(\psi_0) + \frac{\varepsilon^2}{C\left(\Omega^2-1\right)}\left\{\cos\left[\psi\left(\Omega+1\right) - \psi_0\left(\Omega-1\right)\right] - \cos\left(2\psi_0\right)\right\}. \end{aligned}$$

(7.10)

Here $p_x(\psi_0) = p_y(\psi_0) = 0$.

From formula (7.10) in the considered case ($k_x = 0$) it can be seen that, firstly, there is an exact analytical solution, and secondly, there is only one cyclotron resonance $\Omega = 1$ - this is autoresonance. There are no other cyclotron resonances.

The question arises under what conditions do many other cyclotron resonances arise? The answer is known - the transverse wavenumber must differ from zero ($k_x \neq 0$). Next, the question arises: how can the features of these cyclotron resonances be investigated analytically? The answer is also known. It is contained in many works (see, for example, [7]-[10], [62]). It turns out that for an analytical description of these cyclotron resonances, it is convenient to introduce new variables:

$$\begin{aligned} &p_x = p_\perp\cos\theta; \quad p_y = p_\perp\sin\theta; \quad p_z = p_\parallel; \quad x = \xi - \frac{p_\perp}{\omega_H}\sin\theta; \\ &y = \eta + \frac{p_\perp}{\omega_H}\cos\theta. \end{aligned} \tag{7.11}$$

Using these new variables, a large number of important properties of cyclotron resonances have been discovered. Moreover, new cyclotron resonances were discovered [10]. In addition to the strength of the external magnetic field, the conditions of new cyclotron resonances include the

strength of the wave field. The work [10] is devoted to the study of the features of new cyclotron resonances.

However, for further purposes, of interest is the case when the external magnetic field tends to zero ($\omega_H \to 0$). At the same time, it is incorrect to use new variables (7.11). Therefore, below we will introduce other new variables:

$$p_x = p_\perp \cos\theta,\ p_y = p_\perp \sin\theta,\ p_z = p_\parallel,\ p_\perp = \sqrt{p_x^2 + p_y^2},$$
$$x = \xi - \frac{p_\perp}{\gamma\dot{\psi}}\sin\theta,\ y = \eta + \frac{p_\perp}{\gamma\dot{\psi}}\cos\theta\ . \qquad (7.12)$$

These new variables explicitly take into account the oscillatory dynamics of particles in the transverse direction. Transverse dynamics and phase dynamics in these new variables are described by the equations

$$\dot{p}_\perp = \dot{p}_x\cos\theta + \dot{p}_y\sin\theta$$
$$\dot{\theta} = \left(\dot{p}_y\cos\theta - \dot{p}_x\sin\theta\right)/\ p_\perp$$
$$\psi = \left(\tau - k_z z - k_x\xi\right) - \mu\sin\theta \equiv a - \mu\sin\theta, \qquad (7.13)$$

Where $\mu = \left(k_x p_\perp\right)/\left(\gamma\cdot\dot{\psi}\right)$.

For what follows, it is convenient to use the expansion formulas (see, for example, [22])

$$\cos\psi = \cos\left(a - \mu\sin\theta\right) = \sum_{n=-\infty}^{\infty} J_n(\mu)\cos\left(a - n\theta\right)$$
$$\sin\psi = \sin\left(a - \mu\sin\theta\right) = \sum_{n=-\infty}^{\infty} J_n(\mu)\sin\left(a - n\theta\right).$$

A fairly simple analysis of the dynamics of particles can be carried out at small values of the transverse component of the wave vector of the wave ($k_x << 1;\ \left(k_z - 1\right) << 1$). It turns out that new results can be obtained by taking into account the value only in the expressions for the phases. Then the second equation (the equation for the phases) of the system (7.13) takes the form:

$$\dot{\theta} = -\varepsilon\frac{\left(1 - v_z\right)}{p_\perp}\sum_{n=-\infty}^{\infty} J_n(\mu)\sin\left[\left(\tau - z\right) + \theta - n\theta\right]. \qquad (7.14)$$

Here $\mu << 1$, $\gamma\dot{\psi} \simeq \gamma - p_z = const$.

The main role in the total sum will be played by those members in which the phase will not change. The conditions for the stationarity of the phases will be the conditions for resonances. Let the term with $n = 0$ be the stationary member. Then the equation for phase (7.14) can be replaced by the equation:

$$\dot{\Phi} = \left(1 - v_z\right)\left[1 - \frac{\varepsilon}{p_\perp}\sin\Phi\right], \tag{7.15}$$

where $\Phi = \left(\tau - z\right) + \theta$.

The first bracket on the right side of equation (7.15) is positive. We will consider the relativistic case. In this case, it is small and only decreases with acceleration. If the transverse energy of the particles does not change, then Eq. (7.15) resembles the Adler equation in the theory of synchronization (see, for example, [27]).

At $\varepsilon > p_\perp$ there is a stationary state ($\dot{\Phi}_m = 0$). If $\cos\Phi_m > 0$, then this stationary state will be stable. However, the dynamics of particles is described not only by Eq. (7.15), but also by equations for transverse and longitudinal momentum. They must be taken into account.

So the equation for the longitudinal impulse is:

$$\dot{p}_z = \varepsilon\frac{p_\perp}{\gamma}\sum_{n=-\infty}^{\infty} J_n(\mu)\cos\left[\left(\tau - z\right) + \theta - n\theta\right] \tag{7.16}$$

We leave only the stationary term in the sum of the right-hand side. We will assume that the phase is stationary at $n = 0$. Then equation (7.16) is simplified:

$$\dot{p}_z = \varepsilon\frac{p_\perp}{\gamma}J_0(\mu)\cos\Phi_m. \tag{7.17}$$

Taking into account that in the considered approximation $\mu \sim k_x << 1$, we find that the value of the longitudinal impulse depends on time according to the law, which is characteristic of resonances:

$$p_z \approx p_z(0) + \left(\varepsilon\cdot\cos\Phi_n\right)\tau. \tag{7.18}$$

The magnitude of the transverse momentum is determined by the equation

$$\dot{p}_\perp = \varepsilon\left(1 - v_z\right)\sum_{n=-\infty}^{\infty} J_n(\mu)\cos\left[\left(\tau - z\right) + \theta - n\theta\right]. \tag{7.19}$$

Similar considerations that were used for the definition p_z give:

$$\dot{p}_\perp = \varepsilon\left(1-v_z\right) J_0(\mu)\cos\Phi_m \approx \approx \left(\frac{1}{2}\varepsilon\cdot k_x\cdot\cos\Phi_m\right) . \tag{7.20}$$

The magnitude of the transverse momentum also grows linearly with time. However, the slope of this linear function has a small factor, which is proportional to the transverse wave number ($k_x << 1$):

$$p_\perp \approx p_\perp(0)+\left(\varepsilon\cdot\frac{k_x}{2}\cos\Phi_m\right)\tau . \tag{7.21}$$

When obtaining (7.21), we took into account what $\left(1-v_z\right)\approx\left(1-k_z v_z - k_x v_x\right)>0$ and what can be estimated the value of this bracket by the value k_x. Note that the numerical calculations are in good agreement with this estimate (see below).

Thus, asymptotically there are such time dependences

$$\gamma \approx p_z \approx \varepsilon\cdot\tau;\quad p_\perp \approx k_x\varepsilon\cdot\tau . \tag{7.22}$$

Let us now return to the phase equation (7.15). Taking asymptotics (7.22) into account, this equation can be rewritten:

$$\dot{\Phi} \approx -\left(1-v_z\right) \approx \frac{1}{2\gamma^2} \sim \frac{1}{\tau^2} . \tag{7.23}$$

Thus, asymptotically $\Phi_m = const$. The set of results obtained from the analysis of equations (7.13) - (7.23) indicate that, within the framework of the formulated conditions, the resonant acceleration of charged particles (electrons) by the field of a regular transverse wave in vacuum is realized.

7.5. Numerical analysis of the initial system of equations (2)

The analytical results obtained above are largely of an evaluative and asymptotic nature. To clarify the conditions under which the resonant acceleration of particles by the field of a transverse electromagnetic wave in vacuum is realized, a series of numerical calculations of the system of equations (7.2) was carried out. We note right away that good qualitative agreement was obtained between the numerical and analytical results. Typical results of

numerical calculations are presented in Figures 7.1 – 7.11. The main feature of the obtained resonance conditions is that the greater the field strength of the electromagnetic wave and the greater the initial longitudinal velocity of the particles, the easier the charged particles are captured into resonance. Figures 7.1 – 7.2 show the results of numerical analysis for the values of the initial conditions and wave parameters that correspond to the onset of particle capture into resonant acceleration. Unlimited acceleration of charged particles is seen. The value of the longitudinal impulse grows linearly during the entire counting time (Figure 7.1). Moreover, the growth rate of the transverse impulse (Figure 7.2) is in accordance with formula (7.21), that is, it is 10 times less than the velocity of the longitudinal impulse. This corresponds to the fact that the transverse wavenumber is 10 times less than the longitudinal wavenumber $k_x \sim 0.1 \cdot k_z$. Comparing formulas (7.18) - (7.22) with the results of numerical calculation, it can be argued that there is a good qualitative agreement between them.

The saturation process is not visible in Figures 7.1 – 7.2. To see the process of transition from unlimited acceleration to a mode in which the acceleration process is limited, it is sufficient to reduce the value of the longitudinal initial impulse to 1.07. This process is shown in Figure 7.3. It can be seen in this figure that the law of variation in the value of the longitudinal impulse becomes already nonlinear. Some saturation of the particle acceleration process is observed. Thus, if the parameter of the wave force is of the order of 2, then at the value of the initial longitudinal impulse slightly larger than unity, complete capture of particles in unlimited resonant acceleration does not occur.

The saturation process develops even faster when the value of the transverse wave vector is reduced by another 10 times ($k_x \sim 0.01 \cdot k_z$). The dynamics of particles at these values of the parameters is shown in Figure 7.4. Disruption of the capture of particles into an unlimited resonant acceleration will also occur when its transverse momentum is greater than the wave force parameter $\left(p_x > \varepsilon\right)$. This situation corresponds to the case when the synchronization process, which is described by the Adler equation (7.15), does not have stationary stable points. In this case, the synchronization process, which help to the capture of particles in an unlimited resonant acceleration, stops working, and if the second mechanism of particle capture does not come into play, then the process of resonant unlimited acceleration breaks down (see Figure 7.5).

A twofold increase in the wave force parameter lead to more than doubles the maximum value of the longitudinal impulse. This result is illustrated in Figure 7.6. This figure shows the longitudinal momentum versus time. All parameters of this case coincide with the parameters of the case, which is shown in Figure 1, with the exception of the wave strength parameter, which was doubled ($\varepsilon = 4$).

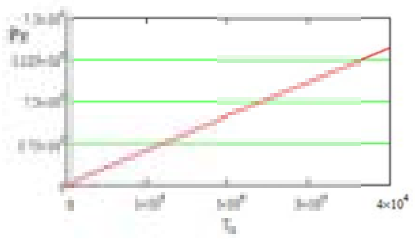

Fig. 7.1. Dependence of the transverse momentum on time at: $\varepsilon = 2$ *; Pz=2; Px=0.5;* $\varphi = 0.1$

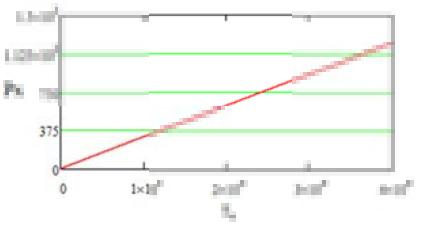

Fig. 7.2. Dependence of the transverse momentum on time at: $\varepsilon = 2$ *; Pz=2; Px=0.5;* $\varphi = 0.1$

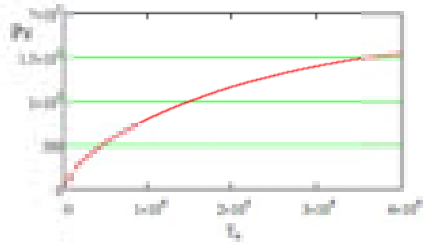

Fig. 7.3. Dependence of the longitudinal impulse on time at : $\varepsilon = 2$ *; Pz=1.07; Px=0.0;* $\varphi = 0.1$ *The growth rate of the longitudinal impulse decreases*

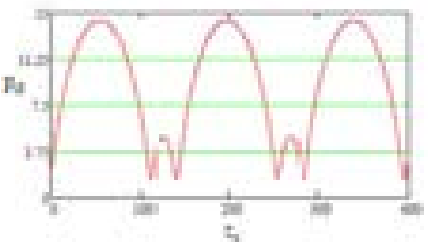

Fig. 7.4. Dependence of the longitudinal impulse on time at : $\varepsilon = 2$; Pz=2; Px=0.5; $\varphi = 0.01$

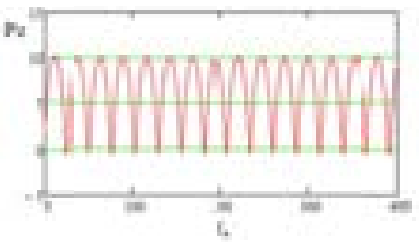

Fig. 7.5. Dependence of the longitudinal impulse on time at: $\varepsilon = 2$; Pz=2; Px=3; $\varphi = 0.1$

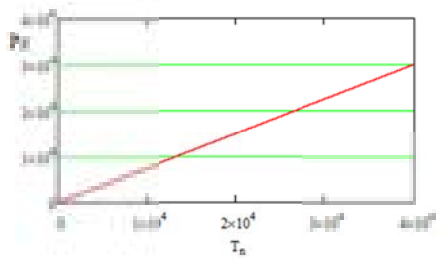

Fig. 7.6. Dependence of the longitudinal impulse on time at: $\varepsilon = 4$ *; Pz=2; Px=0.5;* $\varphi = 0.1$

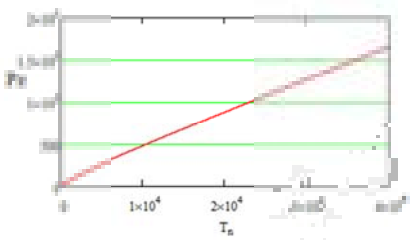

Fig. 7.7. Dependence of the longitudinal impulse on time at: $\varepsilon = 0.45$ *; Pz=20; Px=0.5;* $\varphi = 0.1$

If the transverse wavenumber is not too small, then the analytical results cannot be considered correct. However, there are no restrictions for obtaining numerical results. In particular, it turns out that an increase in the angle from 0.1 to 0.6 increases the maximum value of the longitudinal impulse almost sixfold. A further increase in the angle leads to a decrease in the value of the longitudinal impulse. This result applies only to particles whose initial values correspond to Figure 7.1.

One more remark should be made. The capture of a particle in the conditions of resonant acceleration is the easier to carry out, the greater the parameter of the wave force and the greater the longitudinal momentum of the particle. Moreover, looking at the expression for the longitudinal momentum (the third expression in system (7.10)), one might think that only when the wave force parameter is greater than unity it is possible to capture particles in the condition of resonant acceleration.

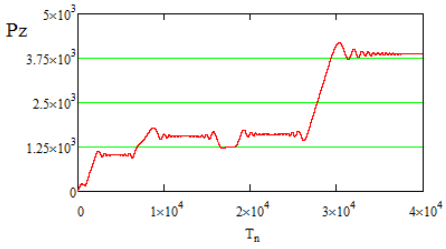

Fig. 7.8. Dependence of the longitudinal impulse on time at: $\varepsilon = 4$ *; Pz=10; Px=0;* $p_y = 1$; $\varphi = 0.1$ *;* $\omega_H = 1$

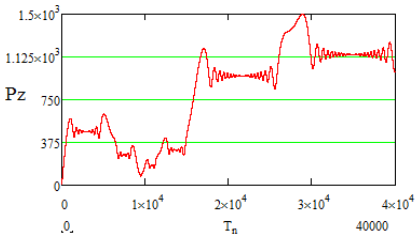

Fig. 7.9. Dependence of the longitudinal impulse on time at: $\varepsilon = 4$ *; Pz=10; Px=0;* $p_y = 1$; $\varphi = 0.1$ $\omega_H = 0.5$

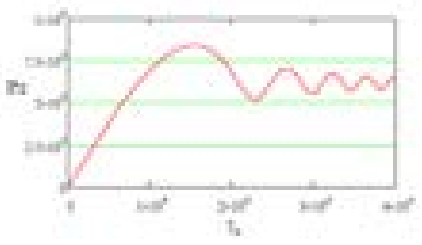

Fig. 7.10. Dependence of the longitudinal impulse on time at: $\varepsilon = 4$ *; Pz=10; Px=0;* $p_y = 1$; $\varphi = 0.1$ *;* $\omega_H = 0.1$

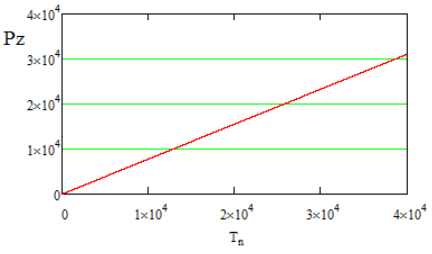

Fig. 7.11. Dependence of the longitudinal impulse on time at: $\varepsilon = 4$ *; Pz=10; Px=0;* $p_y = 1$; $\varphi = 0.1$ $\omega_H = 0.01$

However, in the general case, this is not the case. In particular, if the longitudinal momentum of the particle is large enough, then capture into the resonant acceleration is possible even when the wave force parameter is

less than unity. This fact is illustrated in Fig. 7.7. Note that a decrease in the wave force parameter by five hundredths ($\varepsilon = 0.4$) disrupts the capture of particles into resonance.

The question arises about the influence of the finite value of the external magnetic field on the above-described particle dynamics. The results of numerical calculations of particle dynamics in the presence of an external magnetic field are presented in Figures 7.8-7.11.

It can be seen from Figures 7.8-7.11 that the presence of an external magnetic field in the general case reduces the acceleration efficiency. In addition, the dynamics of particles changes qualitatively. It becomes piecewise deterministic. This dynamics is described in detail in [9]. It is seen that already at $\omega_H = 0.01$, the influence of the external magnetic field is practically absent throughout the entire counting time. Let us pay attention to Figure 7.9. It can be seen that in the general case the stepped structure of particle dynamics can be irregular. A so-called periodically deterministic mode arises. It is also described in [10].

7.6. Dynamics of particles in a wave field with linear polarization

The dynamics of particles in the field of a wave with linear polarization will be described by the system of equations (7.2), in which it is sufficient to set the strength of the field component ε_y equal to zero ($\varepsilon_y = 0$). All the features of the dynamics of particles in the field of a wave with linear polarization are qualitatively similar to the features of the dynamics of particles in the field of a wave with circular polarization. For this reason, we will not dwell on this dynamic.

7.7. Conclusion

Let us note the most important results obtained in this section:

1. The most important of the result obtained is the result that in a vacuum a transverse electromagnetic wave can effectively (resonantly) accelerate charged particles. New resonances have been discovered. Moreover, the acceleration is performed by both a circularly polarized wave and a linearly polarized wave.

2. Note that rigorous solutions to particle dynamics exist both in the presence of an external magnetic field and in its absence. They can be found only when the expression is an integral. This occurs when only one longitudinal component of the wave vector can be preserved for the wave (in the considered case).

3. Note the importance of rigorous solutions. The form of these solutions shows the existence of qualitatively different particle dynamics. If $\varepsilon << 1$, then the dynamics of particles in the field of a transverse wave is the usual transverse dynamics. If $\varepsilon >> 1$, then, the dynamics changes

qualitatively. It becomes longitudinal. It should also be noted that the longitudinal dynamics arises as a result of the action of the Lorentz magnetic force on the particles. And when $\varepsilon > 1$ this longitudinal dynamics will prevail over the transverse dynamics.

4. Attention should be paid to the analogy between the appearance of cyclotron resonances (not cyclotron autoresonance) and the appearance of new solutions that differ from rigorous solutions. Both cyclotron resonances and new solutions appear only when the role of the transverse components of the wave vector of the wave ($k_x \neq 0$) in the particle dynamics is taken into account, when the expression $\gamma\dot{\psi}$ ceases to be an integral.

5. The condition for the capture of charged particles in the resonant acceleration mode is the presence of a wave, the force parameter of which is large enough, as well as the presence of a sufficiently large initial longitudinal momentum of the charged particle ($p_z > 1$). The larger these parameters are, the easier it is to capture particles in the resonant acceleration mode.

6. Let us note two features that determine the capture of particles in the resonant acceleration mode. The first feature is related to the fact that the phase dynamics of particles at the initial stage of the acceleration process is described by an equation that resembles the Adler equation in synchronization theory. However, Adler's equation contains functions that are independent of time. Equation (7.15), which resembles Adler's equation, contains functions that change over time. For this reason, the usual synchronization process can be carried out only for a limited time interval. The second feature is related to the first factor on the right-hand side of equation (7.15). In the relativistic case, this factor is small. He's positive. In addition, it decreases rather quickly. It is easy to see that it is inversely proportional to the square of the particle's energy. Considering that the energy grows linearly with time, the phase derivative quickly tends to zero (as $1/\tau^2$). The phase itself tends to a constant value rather quickly. Moreover, an analysis of the numerical results shows that the stationary phase itself tends to zero.

CONCLUSION

First of all, we note that the authors tried to present the material in such a way that each part (section) of the review is, if possible, independent. Therefore, at the end of each part, the main results were formulated, which were described in this section. Therefore, below we will only very briefly, if possible without repeating ourselves, describe the main results of this review.

In the first section, the characteristics of nonlinear resonances (widths of nonlinear resonances, distances between them, etc.) are determined for practically all resonant interactions of waves with charged particles.

Criteria for the emergence of regimes with dynamic chaos when the main resonances are overlapped are obtained. Such resonances are Cherenkov resonances, cyclotron resonances based on normal and anomalous Doppler effects (see formula (1.34). It is shown that when the longitudinal component of the wave vector tends to unity ($k_z \to 1$), the distance between nonlinear resonances grows faster than the width of the nonlinear resonance. This feature is the fact that, with autoresonance ($k_z = 1$), regimes with dynamic chaos do not arise. In the same section, attention is drawn to the fact that the use of the Chirikov criterion for the emergence of regimes with dynamic chaos may not always give the correct result. The reasons for this discrepancy are discussed, in particular, in numerical and analytical studies.

In the second section, the dynamics of particles is investigated in the presence of additive and multiplicative fluctuations. As indicated above, in the first section it was shown that regimes with dynamic chaos do not arise during autoresonance. However, it turned out that it is under conditions of autoresonances that the dynamics of particles is anomalously sensitive to additive fluctuations. Superdiffusion mode may occur. In the presence of multiplicative fluctuations, fluctuation instability arises, in which the increments of the higher moments turn out to be larger than the increments of the lower moments (see, for example, Figure 2.2.). In such regimes, the Einstein-Fokker-Planck (EPP) equation, which is widely used to describe the dynamics of particles, cannot be used. Note that the EPP equation takes into account only the first two moments. In this section, a generalization of the EPP equation for the case of taking into account higher moments is obtained (see equation (2.16).

The third section describes new cyclotron resonances. The novelty of these new cyclotron resonances lies in the fact that the conditions of their occurrence include the value of the field strength of the wave with which the particles interact (see equation (3.16)). Note that only the strength of the external magnetic field is included in the conditions of the known cyclotron resonances. Note that the dynamics of particles under the conditions of new cyclotron resonances also significantly differs from the dynamics of particles in known cyclotron resonances. The main difference is that the dynamics in a known resonance is described by the equation of a mathematical pendulum, while the dynamics in new resonances is described by the Adler equation. Recall that the equation of a mathematical pendulum is a second-order nonlinear equation. It has special points such as "centers", "saddles", and is also characterized by a special trajectory - the separatrix. Adler's equation is an ordinary differential equation of the first order. The dynamics described by such an equation is much simpler. In particular, regimes with dynamic chaos are piecewise deterministic. The spectra of such regimes are much more regular than those in regimes with known cyclotron resonances. This section describes the characteristics of the particle dynamics under the conditions of new resonances.

The fourth section describes the process of plasma-beam instability in the presence of fluctuations (in time or in space) of the plasma density. It is shown that the presence of such fluctuations destroys the regular process of excitation of plasma oscillations. The distances at which the plasma-beam interaction can still be regular are determined.

In the fifth section, the dynamics of excitation of oscillations by an electron beam under conditions of isolated cyclotron resonance is considered. One might expect that, within the framework of an isolated cyclotron resonance, the dynamics of excitation of oscillations would be regular. It turned out that the dynamics may be irregular. The reasons for the emergence of regimes with dynamic chaos have been clarified. It turned out that the reason for the irregularity is a quasiperiodic qualitative change in the form of the phase portrait of the beam particles. Thus, the process of periodic or quasiperiodic qualitative change in the form of the phase portrait should also be referred to the known mechanisms of the emergence of regimes with dynamic chaos.

The models of waves used in theoretical considerations as purely monochromatic waves is an idealization. Real waves are always packets of waves, that is, they are more or less sets of regular monochromatic waves. The characteristics of these waves are very close to each other. This means that the distance between these individual resonances is small. The question arises: What dynamics (chaotic or regular) describes the dynamics of particles in a wave packet? The answer to this question is contained in the sixth section of the review. It is shown that if the group and phase velocities of waves in a packet are close to each other, then the dynamics of particles in such a packet will be regular. This means that the model of a regular monochromatic wave for such a packet is quite justified. If the phase and group velocities are different, then in most cases the chaotic dynamics of particles is realized. Such a packet cannot be modeled as an isolated regular wave. In this section, in addition to these results, it is shown that the parameter of the wave strength (the most important parameter for us $A = eE / mc\omega\gamma$) in plasma is always less than unity ($A < 1$).

The seventh section describes the discovered new resonances in the interaction of transverse electromagnetic waves with charged particles in a vacuum. Under the conditions of these new resonances, practically unlimited acceleration of electrons by the field of transverse electromagnetic waves is possible. In particular, by the field of laser radiation. It is shown that these resonances arise only when the electromagnetic waves have a transverse component of the wave vector (in this case, some integrals cease to be integrals). Note that ordinary cyclotron resonances (not autoresonance) also arise only when the waves have a nonzero transverse component of the wave vector ($k_\perp \neq 0$).

Let's formulate some considerations (thoughts) regarding the possibility of resonances between particles and waves in a vacuum.

1. It is known that the trajectories of particles in the fields of electromagnetic waves in vacuum have a rather complex configuration. For example, it can be a well-known figure eight or, for example, a circle in the field of a circularly polarized wave. In general, these are rather complex shapes (see, for example figures 1 and 2). Of course such trajectory appears only for certain wave parameters and certain characteristics of the particles. Another thing is important - the trajectory in the general case has a complex trajectory. In the expansion of such particle trajectories in series, one can expect that some terms of the series will be in resonance with field of the wave. In particular, it can be noted that the structure of the particle trajectory under conditions of cyclotron autoresonance is such that the usual cyclotron resonances are absent. This is because the structure of the trajectory is very simple in this case. The cyclotron resonances (not autoresonances) appear only when there is transversal component of the wave vector of the wave ($k_{\perp} \neq 0$).

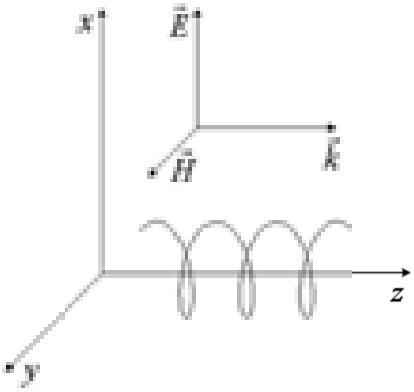

Fig.1. Possible form of the particle trajectory in the field of a transverse electromagnetic wave

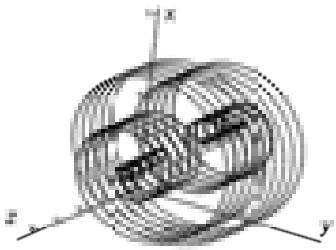

Fig.2. Particle trajectory in the field of a transverse electromagnetic wave pulse

2. Let's pay attention to the relationship between the magnetic and electric Lorentz forces. Little attention has been paid to magnetic force. This is due to the fact that in the original equations, where both the electric Lorentz force and the Lorentz magnetic force appear

$$\frac{d\mathbf{p}}{dt} = e\mathbf{E} + \frac{e}{c}[\mathbf{vH}] \tag{1}$$

Looking at this formula, in some cases it is possible to draw an incorrect conclusion that the magnitude of the Lorentz magnetic force becomes comparable to the Lorentz electric force only asymptotically at $v \to c$. In some cases, this conclusion is erroneous. In particular, the

efficiency of the interaction of charged particles with a wave in a vacuum can be determined mainly by the Lorentz magnetic force. This is due to the fact that the efficiency of the interaction of particles with the wave is determined only by the phase dynamics of the particles in the wave. This equation has the form

$$\frac{d\mathbf{p}}{d\tau}=\left(1-\frac{\mathbf{kp}}{\gamma}\right)\mathrm{Re}\left(\boldsymbol{\varepsilon}e^{i\psi}\right)+\frac{\mathbf{k}}{\gamma}\mathrm{Re}\left[\left(\boldsymbol{\varepsilon}\cdot\mathbf{p}\right)e^{i\psi}\right] \tag{2}$$

Note that the first multiplier in the first term on the right-hand side is the time derivative of the wave phase

$$\left(1-\frac{\mathbf{kp}}{\gamma}\right)=\dot{\psi}$$

Note also that the expression $\dot{\psi}\gamma=const$ is the integral. Then equation (2) transforms into

$$\frac{d\mathbf{p}}{d\psi}=\mathrm{Re}\left(\boldsymbol{\varepsilon}e^{i\psi}\right)+\frac{\mathbf{k}}{(\gamma\dot{\psi})}\mathrm{Re}\left[\left(\boldsymbol{\varepsilon}\cdot\mathbf{p}\right)e^{i\psi}\right];\qquad \frac{d\mathbf{p}}{d\psi}\sim\boldsymbol{\varepsilon}+\boldsymbol{\varepsilon}^2 \tag{3}$$

It follows from these formulas that for a large parameter of the wave force ($\varepsilon>>1$), the main role in the phase dynamics of particles will be played by the Lorentz magnetic force. Note that this force is directed along the wave vector of the wave. Thus, at large values of the wave force parameter, the dynamics of particles ***from the familiar transverse dynamics turns into longitudinal dynamics*** ***($\varepsilon>1$ then $F_H>F_E$).***

3. Analogy with the occurrence of cyclotron resonances.

Attention should be paid to the analogy between the appearance of known cyclotron resonances (with the exception of autoresonance) and the appearance of our resonances. Both those and other resonances appear only when the structure of the electromagnetic wave with which the particles interact has a nonzero transverse component of the wave vector $k_\perp\neq 0$.

4. Above, in Section 7.2, it was shown that charged particles by the field of a plane electromagnetic wave in a vacuum can be captured in an almost unlimited acceleration. The conditions for such capture were written out. Let us pay attention to only one of these conditions - the need for a wave to have a transverse component of the wave vector. The question arises about the possibility of the capture of particles by the field of waves that have a different configuration. Our preliminary analysis shows that the field of a wave that propagates in a circular waveguide with components

$$E_r = E_0 \frac{m}{k_\perp r} J_m(k_\perp r)\sin(m\varphi)\sin(k_z z - \omega t);\quad E_\varphi = E_0 J'_m(k_\perp r)\cos m\varphi \sin(k_z z - \omega t)$$

;

$$H_z = E_0 \frac{k_\perp}{k} J_m(k_\perp r)\cos(m\varphi)\cos(k_z z - \omega t)$$

can also capture charged particles. It can be expected that laser fluxes with a Gaussian field structure will have the same trapping property.

REFERENCES

1. Plasma Electrodynamics, Edited by A.I. Akhiezer, "Science", Moscow, 1974, 720 pages.
2. Fundamentals of Plasma Physics, Edited by R.Z. Sagdeev and M.N. Rozesenblut Vol. 1 and Vol. 2, Moscow Energoatomizdat 1984, 632 pp.
3. Emil Simu Chotic Transitions In Deterministic And Stochastic Dynamical Systems (Application Of Melnikov Processes) Prinston University Press Prinston And Oxford 2002, pp. 208.
4. A.J. Lichtenberg, M.A. Lieberman Regular and Stochastic Motion, Springer-Verlag New York Heidelberg Berlin 1983 pp. 500.
5. J.S. Allen, R.M. Samelson and P.A. Newberger, Chaos in a model of forced quasi-geostrophic flowover topography : an application of Melnikov's method // Journalof Fluid Mechanics. 1991 V.226 pp. 511-547.
6. G.M. Zaslavsky, B.V. Chirikov. Stochastic instability of nonlinear oscillations // *Phys. Usp*. 1971, v. 105, p. 1-42.
7. V.A. Buts, V.V. Kuzmin, A.P. Tolstoluzhsky, Peculiarity of the charged particles dynamics at the cyclotron resonances // Problems of atomic science and technology. 2016, № 6. Series: Plasma Physics (22), pp. 152-155.
8. V. A. Balakirev, V. A. Buts, A. P. Tolstoluzhskii, and Yu. A. Turkin, "Randomization of motion of a beam of phased oscillators, // ZhETF 84(4), 1279 (1983) (in Russian) [Sov. Phys. JETP 57, 741 (1983) (in English).
9. V. A. Balakirev, V. A. Buts, A. P. Tolstoluzhskii, and Yu. A. Turkin, "Charged-particle dynamics in the field of two electromagnetic waves," ZhETF 95(4), 1231 (1989) (in Russian) [Sov. Phys. JETP 68(4), 710 (1989) (in English)].
10. V. A. Buts and A. G. Zagorodny "New cyclotron resonances and features of charged-particle dynamics in the presence of an intense electromagnetic wave" Phys. Pasmas 28, 022311 (2021); https://doi.org/10.1063/5.0037808
11. *Gyrotrons, Collection of Articles* (Inst. Prikl. Fiz. AN SSSR, Gorkii, 1989) [in Russian]
12. Gary R. Smith. Allan N. Kaufman. Stochastic acceleration by an obliquely propagating wave. An example of overlapping resonances // Phys. Fluids, 1978, v. 21, №12, - P. 2230-2241.
13. Gell Y. Nanach R. Stochastic ion heating by electrostatic wave in sheared magnetic field // Phys. Fluids, 1980, v.23 , №8, -pp. 1646-1655.
14. Shklyar D.R. Stochastic motion of relativistic particles in the field of a monochromatic wave // Sov. Phys. JETP , 1981, v. 80, No. 6, - pp. 2272-2282. (in Russian)
15. A. A. Kolomensky and A. N. Lebedev, "Autoresonant motion of a particle in a plane electromagnetic wave," Dokl. Akad. Nauk SSSR 145(6), 1259 (1962); Sov. Phys. Dokl. 7, 745 (1963)
16. V. Ya. Davydovskii, "On the possibility of resonant acceleration of charged particles by electromagnetic waves in a constant magnetic field," [Sov. Phys. JETP 16, 629 (1963) (in English)].
17. V. A. Buts, V. V. Kuz'min, and A. P. Tolstoluzhsky*a, Features of the Dynamics of Particles and Fields at Cyclotron Resonances //* Sov. Phys. JETP *2017, Vol. 125, No. 4, pp. 651–662.*
18. V. P. Milant'ev, "Cyclotron autoresonance (on the occasion of the 50th anniversary of the discovery)," UFN 183(8), 875–884 (2013).
19. Kravchenko V. F., Kuraev A. A., Sinitsyn A. K. Nonsynchronous interactions *//Phys. Usp. 2007,vol. 50, № 5, p. 489–511. (UFN, vol.177, № 5, p. 511–534).*
20. Buts V. A. Stabilization of classic and quantum systems // Problems of atomik science and technology, 2012, N 6(82), – P. 146–148.
21. S.S. Moiseev, V.A. Buts, N.S. Erokhin, Peculiarities of Charged Particle Dynamics under Cyclotron Resonance Conditions // Plasma Physics Reports, 2016, Vol. 42, No. 8, pp. 761–768.

22. G. Korn and T. Korn, Handbook of Mathematics (Science, Moscow, 1968).

23. Klyatskin V.I. Statistical description of dynamical systems with fluctuating parameters - "Nauka", 1975, - 240 p.

24. G. M. Zaslavsky, Chaos, fractional kinetics, and anomalous transport Phys. Rep. **371**, 461-580 (2002).

25. V. A. Buts and A. V. Buts, "Dynamics of charged particles in the field of an intense transverse electromagnetic wave // ZhETF 110(3), 818–831 (1996) (in Russian) [Sov. Phys. JETP 83(3), 449 (1969) (in English)].

26. R. Adler, Proc. I.R.E. Waves Electrons 34(6), 351 (1946).

27. A. Pikovsky, M. Rosenblum, and J. Kurths, Synchronization. Fundamental Nonlinear Phenomenon (Tekhnosfera, Moscow, 2003) (in Russian).

28. A. S. Galiullin, "Inverse problems and problems of motion control of material systems," Differ. Uravn. 8(9), 1535–1541 (1972).

29. D. D. Dixon, F. W. Cummings, and P. E. Kaus, "Continuous 'chaotic'dynamics in two dimensions," Physica D 65, 109–116 (1993).

30. D. D. Dixon, "Piecewise deterministic dynamics from thea pplication of noise to singular equations of motion," J. Phys. A 28, 5539–5554 (1995).

31. J. Alvarez-Ramirez, J. Delgado-Fernandez, and G. Espinosa-Parades, "The origin of a continuous two-dimentional 'chaotic' dynamics," Int. J. Bifurcation Chaos 15(9), 3023–3029 (2005).

32. V. A. Buts, "Chaotic motion of dynamic systems with 'one' degree of freedom," Probl. At. Sci. Technol., Ser. 57(1), 328–332 (2012).

33. V. A. Buts, "Regular and chaotic dynamics of charged particles in wave-particle interactions," Probl. Theor. Phys..Issue 2, 122–241 (2017).

34. V. A. Steklov, Foundations of the Theory of Integration of Ordinary Differential Equations (Gostekhizdat,Moscow, Leningrad, 1927) (in Russian).

35. Mikhailovsky A.B. The theory of plasma instabilities. T. 1. Instabilities of a homogeneous plasma. - M.: Atomizdat, 1975, 272 p. T. 2. Instabilities of an inhomogeneous plasma. - M .: Atomizdat, 1977, 360 p.

36. Begiashvili G.A., Monin Yu.S. On the stability of a beam of charged particles in statistically inhomogeneous media. Message AN SSSR.-1969.-55, No. 3.-S. 557-560.

37. Virchenko Yu.P., Polovin R.V. On stochastic destruction of a growing wave in a randomly inhomogeneous medium. UFZh.-1988.-33, No. 12.- S. 1863-1868.

38. Molchanov S.A., Ruzmaikin A.A., Sokolov D.D. Kinematic dynamo in a random stream. UFN. - 1985, 145, no. 4. -C. 593-628.

39. Polovin R.V. Applied theory of stochastic processes. Kharkov: Vishcha school, 1982, 102 p.

40. V. A. Buts, A. N. Lebedev, and V. I. Kurilko, *The Theory of Coherent Radiation by Intense Electron Beams* (Springer, Berlin, 2006).

41. V. A. Buts, O. V. Manuilenko, and A. P. Tolstoluzhskii, Stochasticization of oscillations in a plasma-beam system under the action of an external monochromatic field Ukr. Fiz. Zh. 39, 429 (1994).

42 . V. A. Buts and A. P. Tolstoluzhsky, Nonrelativistic dynamics of the charged particles at cyclotron resonanses. Problems of atomic science and technology, Series "Plasma Physics" **14** (5), 117 (2008).

43. A.N.Antonov, V.A.Buts, O.F.Kovpik, E.A.Kornilov, O.V.Manuilenko, V.G.Svichenskii, K.N.Stepanov. Stochastic heating of plasma at electron cyclotron resonance. JETP LETTERS, v. 69, N 11, 10 June 1999, p. 851-857.

44. V.A.Buts, A.P.Tolstoluzhsky. Nonrelativistic dynamics of the charged particles at cyclotron resonanses. Problems of atomic science and technology, Series: "Plasma Physics" Issue 14, 2008, N 5, p. 117-119.

45. V.A.Buts, E.S. Voitsenya, A.P. Tolstoluzhsky. The initial stage of stochastic acceleration of charged particles in a constant magnetic field and in the field of an electromagnetic wave. VANT, No. 3 (67), 2010, p. 80-84.

46. V. A. Buts, E. A. Voitsenya, and A. P. Tolstoluzhskii, Unrelativistic dynamics of charged particles at cyclotron resonances. Usp. Sovrem. Radioelektron., No. 8, 44 (2009).

47. E.G. Shustin, N.V. Isaev, M.P. Temiryazeva, V.P. Tarakanov, Yu.V. Fedorov. Beam-Plasma Dis-charge in a Weak Magnetic Field as a Source of Plasma for a Plasma-Chemical Reactor // *Problems of Atomic Science and Technology*. 2008, № 4, p. 169.

48. I.N. Meshkov, S.S. Nagaitsev, I.A. Seleznev, E.M. Syresin. *Beam – Plasma Discharge at Electron Beam Injection Into Rare Gas*: Preprint 90-12. Novosibirsk Institute of Nuclear Physics. 1990, 630090, 15.

49. S.S. Moiseev, V.A. Buts, N.S. Erokhin. Peculiarities of Charged Particle Dynamics under Cyclotron Res-onance Conditions // *Plasma Physics Reports*. 2016, v. 42, № 8, p. 761-768.

50. V.A. Buts, V.V. Kuzmin, A.P. Tolstoluzhsky. Features of the dynamics of particles and fields at cyclotron resonances // *ZhETF*. 2017, v. 152, № 4 (10), p. 767-780.

51. V.A. Buts, A.N. Lebedev, V.I. Kurilko. *The Theory of Coherent Radiation by Intense Electron Beams*. Springer, Berlin, 2006.

52. V.A. Buts. Regular and chaotic dynamics of charged particles during wave-particle interactions // *Problems of Theoretical Physics. Series "Problems of Theoretical and Mathematical Physics"*. 2017, № 2, p. 122-241.

53. G.M. Zaslavsky, R.Z. Sagdeev. *Introduction to non-linear physics: from a pendulum to turbulence and chaos*. M.: "Nauka", 1988, 368 p.

54. V. A. Buts, The role of singular solutions in the analysis of the dynamics of physical systems. //Physical foundations of instrumentation. 2015, vol. 4, no. 3 (16), p. 5-32.

55. V. A. Buts and A. N. Lebedev, Coherent Radiation of Intense Electron Beams (RAS Lebedev Physical Institute (FIAN), Moscow, 2006).

56. N. N. Rozanov, N. V. Vysotina, Direct acceleration of charge in vacuum by pulses radiation with linear polarization // ZhETF, Vol.157, issu. 1, 2020 pp. 63–66.

57. D.M. Volkov, Z. Phys., 1935, **94**, S.250;

58. V.I. Ritus, Quantum effects of interaction of elementary particles with an intense electromagnetic field //Proceedings of FIAN, Vol. 111, N9, 1979, pp. 5 – 149

59. V. A. Buts and A. V. Buts, Dynamics of charged particles in the field of an intense transverse electromagnetic wave, // ZhETF 110(3), 818–831 (1996) (in Russian) [Sov. Phys. JETP; 83(3), 449 (1969) (in English)].

60. B.M. Bolotovsky A.V. Serov, Features of the motion of charged particles in an electromagnetic wave// UFN, Vol. 173, N6, 2003, pp. 667-678

61. Viktor Musakhanyan // 22nd Texas Symposium on Relativistic Astrophysics at Stanford University, Dec. 13-17, 2004

62. A. B. Kitsenko, I. M. Pankratov, and K. N. Stepanov, The nonlinear phase of monochromatic-oscillation excitation by a charged-particle beam in a plasma located in a magnetic field // Sov. Phys.-JETP, Vol. 39, No.1, July 1974

УДК 533.9
PACS numbers: 52.35.Mw, 29.27.Bd, 41.60.Bq

CHAPTER II

EXCITATION OF ELECTROMAGNETIC RADIATION DURING THE INTERACTION OF CHARGED PARTICLES WITH DIELECTRIC AND PLASMA-LIKE SOLID MEDIA

Yu. O. Averkov[a,b], Yu. V. Prokopenko[a,c], V. M. Yakovenko[a]

[a] *Usikov Institute for Radiophysics and Electronics, National Academy of Sciences of Ukraine, Kharkiv, 61085 Ukraine;*
[b] *Karazin Kharkiv National University, Kharkiv, 61022 Ukraine;*
[c] *Kharkiv National University of Radio Electronics, Kharkiv, 61166 Ukraine*

The features of the processes of interaction of charged particles and flows of charged particles with dielectric and solid-state dispersive plasma-like media are presented.

The dispersion characteristics of oblique surface magnetoplasmons in a structure with a two-dimensional plasma layer lying on the surface of a three-dimensional plasma half-space are analyzed. It is shown that from the analysis of the expression for the spectral density of the electron energy losses on the excitation of these waves, it is possible to establish the type of the dispersion law of charge carriers in a two-dimensional electron gas at the interface between the media.

The results of a theoretical study of beam instability during the motion of a nonrelativistic thin tubular electron beam over a solid cylinder made of artificial material are presented. The possibility of occurrence of absolute instability in the frequency range where the metamaterial exhibits left-handed properties is shown. The effect of nonlinear stabilization of such a beam as it moves along the surface of a solid-state cylinder made of a dielectric as well as a plasma-like media is theoretically investigated. It is established, in particular, that in the electrostatic approximation, when the beam moves along a plasma-like cylinder, the nonlinear stabilization of the growth of the wave amplitude occurs due to the

effect of self-trapping of the beam electrons by the field of the electrostatic wave of the beam itself.

Keywords: *surface magnetoplasmons, two-dimensional plasma layer, tubular electron beam, solid-state cylinder, eigenmodes, dispersive metamaterial, left-handed media, absolute beam instability, Cherenkov resonance, anomalous Doppler effect, nonlinear stabilization, self-trapping.*

PACS numbers: *03.50.-z, 52.40.-w, 52.59.-f, 85.45.-w*

INTRODUCTION

The features of the processes of interaction of charged particles and flows of charged particles with dielectric and solid-state dispersive plasma-like media have been presented. *This chapter is divided into three sections*. The introduction to each section describes in detail the relevance of the problem under study, the object and research methods. The brief summary is provided at the end of each section. At the end of the chapter, there is the general detailed conclusion for all the considered tasks.

Section 1 is devoted to theoretical study of electron energy loss by the excitation of surface magnetoplasma oscillations by an electron moving along a static magnetic field in vacuum over a two-dimensional plasma layer on the surface of three-dimensional plasma half-space. Electron energy loss by the excitation of surface magnetoplasmons has been calculated in the electrostatic approximation. It has been shown that the type of the dispersion law of electrons in such plasma (quadratic for a two-dimensional Drude gas or linear for graphene) can be determined from the qualitative character of the dependence of the maximum of the spectral density of this loss on the electron density in the two-dimensional plasma. Consequently, the results obtained can be used, for example, as the basis for a new contactless method for testing graphite films to isolate graphene monolayers from them.

Section 2 is devoted to theoretical study of the interaction between a tubular beam of charged particles and a dispersive metamaterial of cylindrical configuration. This metamaterial may have negative permittivity and negative permeability simultaneously over a certain frequency range where it behaves like a left-handed metamaterial. The dispersion equation for the eigenmodes spectra of a metamaterial and the coupled modes spectra of the system have been derived and numerically analyzed. It has been found that the absolute beam instability of bulk-surface waves occurs because of peculiarities of the eigenmodes spectra of left-handed metamaterial. Specifically, the resonant frequency behavior of the permeability causes the emergence of the sections of dispersion curves with anomalous dispersion. It has been demonstrated that the symmetric bulk-surface mode with two field variations along the cylinder radius possesses the maximum value of instability increment. The obtained results allow us to propose the left-handed metamaterial as the delaying medium in oscillators of

electromagnetic radiation without a need to provide an additional feedback in the system just as in a backward-wave tube.

Section 3 is devoted to theoretical study of nonlinear stabilization of an electron beam moving along the solid-state cylinder. *In the first part of the section* the case of a solid-state plasma cylinder has been considered, whereas *in the second part of the section* the solid-state cylinder is supposed to be a dielectric one.

In the case of a solid-state plasma cylinder it is assumed that the electron collision frequency in the plasma cylinder is much higher than the frequency of plasma eigenmodes (oscillations). The beam is assumed to be nonrelativistic, and, thus, the problem is solved in the electrostatic approximation. It is shown that the growth of the wave amplitude is stabilized nonlinearly due to the self-trapping of the beam electrons by the field of the electrostatic wave excited in the beam itself. It is found that the saturation time of instability and the maximum amplitude of the excited wave depend on the radius of the plasma cylinder. It is established that the larger the radius of the plasma cylinder, the later the nonlinear stage of instability begins and the larger the maximum amplitude of the excited wave.

In the case of a solid-state dielectric cylinder it is assumed that the beam is non-relativistic, infinitely thin in the radial direction, and moves along the surface of the cylinder parallel to the lines of force of an external constant magnetic field, which prevents the transverse motion of the beam electrons. The mechanism of nonlinear stabilization of azimuthally symmetric E-type electromagnetic waves with different values of radial mode indices is studied by the method of slowly varying amplitudes and phases. The physical cause of excitation of such waves is the Cherenkov resonance, and the nonlinear stabilization mechanism is based on the trapping of beam particles by the field of the excited wave. It is shown that, as the radial mode index of the excited wave increases, the saturation time of instability and the maxima and the "period" of amplitude oscillations at the nonlinear stage of instability saturation decrease. It is shown that, at the nonlinear stage of instability, the waves excited by the beam have elliptical polarization. Moreover, in the vacuum region, the directions of rotation of the electric fied vectors of E_{01} and E_{02} waves turn out to be opposite.

SECTION 1. CHARGED-PARTICLE ENERGY LOSS BY THE EXCITATION OF SURFACE MAGNETOPLASMONS IN A STRUCTURE WITH TWO- AND THREE-DIMENSIONAL PLASMAS

1.1. Introduction

The properties of surface magnetoplasmons in a structure with two- and three-dimensional plasmas were studied in [1]. In particular, they can be excited by a charged particle moving over such a structure along a static magnetic field directed along the boundary of the structure. As was mentioned in [1], such an orientation of the static magnetic field is of the most interest because the frequency of a surface magnetoplasmon is an odd function of the wavevector. The Cherenkov effect [2,3] underlies the mechanism of the interaction of the charged particle with surface magnetoplasmons. Since the particle can excite only magnetoplasmons having low phase velocities (much lower than the speed of light in vacuum), the electrostatic approximation is appropriate for the description of such an interaction. The study of the so-called oblique magnetoplasma waves is of considerable interest. Many theoretical and experimental works were devoted to this issue (see, e.g., [4–12] and refs. therein).

In [4] surface oscillations in confined cold plasma with charged particle fluxes along a constant magnetic field were considered. The plasma boundary was assumed to be sharp, so that the wavelength of the oscillations was much greater than the thickness of the transition layer. General boundary conditions for matching solutions on this layer were obtained, with the help of which dispersion equations of oscillations were obtained in various special cases. It was shown that oblique surface waves were unstable in the presence of particle fluxes, which leads to the opening of the sharp plasma boundary.

In [5,6] the problem of excitation surface electromagnetic oscillations in semiconductors in strong magnetic electric and magnetic fields was theoretically investigated. The dispersion law and damping of oscillations were obtained, the possibility of amplification and generation of these oscillations was shown, and the corresponding growth rates were found. The resonant interaction of surface waves with a quasineutral flux of charged particles moving in vacuum parallel to the surface of the medium was investigated.

In [7] the propagation of potential surface waves along a flat vacuum-plasma interface was theoretically investigated. The directions of wave propagation and tension were considered arbitrary. It was shown that the field of the surface wave decays exponentially as it moves into the depth of the plasma, performing spatial oscillations. The frequencies of high-frequency and low-frequency potential surface waves were calculated. It was shown that the propagation of potential surface waves was impossible in

strong magnetic fields. The damping decrements caused by the work of the field in the plasma volume and in the plasma resonance region were found.

In [8] the non-potential surface waves propagating along the semiconductor-vacuum interface were theoretically investigated. Their spectra and attenuation were obtained in one-component (surface helicon) and compensated (surface Alfvén wave) semiconductors. The interaction of surface waves with an electron beam was investigated and the growth rates of the waves were calculated.

In [9] the theory of surface polaritons associated with the planar surface of a semi-infinite anisotropic dielectric medium with including of retardation was developed. It was shown that, in general, two attenuating components with different attenuation constants must be superposed within the medium in order to satisfy the boundary conditions, and the macroscopic electric field vector does not lie in the sagittal plane. It was demonstrated that for special cases only one attenuating component is required, and the electric vector does lie in the sagittal plane. This theory was applied to the specific case of surface magnetoplasmons in a semiconductor for magnetic field either perpendicular or parallel to the surface. In the latter case, propagation directions parallel and perpendicular to the magnetic field were considered.

In [10] the existence of electromagnetic surface waves at the boundary separating magnetized semiconductor plasma and a dielectric or metal was demonstrated. The external magnetic field was along the interface. It was shown that slow surface waves of the helicon or Alfven type can exist only with their propagation vector directed obliquely with respect to the magnetic field.

In [11-12] theoretical and experimental studies of the electromagnetic properties of the millimeter and submillimeter wavelength ranges of inhomogeneous semiconductor structures were considered in detail. The theory of wave and oscillatory processes in isotropic and magnetoactive plasma of semiconductors was developed, the interactions of surface and bulk waves with flows of charged particles were investigated, the properties of hot charge carriers and the effects accompanying their heating were described.

The dispersion properties of oblique magnetoplasma waves are very sensitive to the conductive properties of the interface. Therefore, by studying their conducting properties of such waves, it is possible, for example, to measure the conducting properties of thin surface layers. This is a very actual problem in connection with the active study of the conductive properties of thin graphene films, for example, to identify graphene monolayers among graphite films.

Graphene is known to be a two-dimensional allotropic form of carbon, the crystal lattice of which is similar to the structure of honeycomb [13]. The unit cell of this lattice is represented by a regular hexagon with carbon atoms at its vertices. Graphene can be considered as the main structural unit of other allotropic forms of carbon, namely, fullerenes (zero-dimensional

objects) [14], quantum nanotubes (one-dimensional objects) [15], and three-dimensional graphite forms (which are represented by graphene stacks bounded by weak van der Waals forces). The structure of the energy bands of graphene and its semimetal conducting properties were theoretically described in 1947 [16]. However, the first graphene films were prepared only 60 years later via multiple mechanical splitting of highly oriented pyrolitic graphite [17]. The uniqueness of work [17] also consists in the fact that it proved the possibility of existence of regular thermodynamically stable 2D crystals, which had been denied for a long time (see, e.g., [18] and refs. therein).

The main difference of the electronic properties of graphene from those of a conventional 2D electron gas (2DEG; e.g., a thin metallic or semiconductor film) is that graphene is a semimetal with a zero band overlap. The valence band and the conduction band of graphene touch each other at two points in the Brillouin zone (so-called Dirac points). Near these points, the dependence of the carrier energy on the carrier momentum is linear, and charge carriers are massless chiral Dirac fermions [19-21]. The fermion velocity in graphene is lower than the velocity of light in vacuum by a factor of 300. The Dirac character of charge carriers in graphene, e.g., makes it possible to observe a number of unique effects, such as the anomalous quantum Hall effect (at room temperature) [20], the Klein paradox [22-24], the Aharonov–Bohm effect [25], the Anderson localization [26], and the Coulomb blockage [27]. In strong magnetic fields, exciton gaps [28] and Wigner crystals [29] can form in graphene. Binary graphene layers can exhibit both ferromagnetic and antiferromagnetic properties [30].

These unusual physical properties of graphene are caused by the internal quantum mechanical features of graphene and, hence, manifest themselves at the quantum level. The quantum mechanical peculiarities of the transport properties of graphene are also reflected on its “classical” electrodynamic characteristics. For example, Rana [31] proposed a conceptual model for coherent terahertz radiation source, which is based on the inversion electron population of levels in the valence band of graphene due to the interband transitions caused by the interaction of electrons in the valence band with surface plasmons of graphene. The authors of [32] revealed a giant Purcell effect for an elementary dipole located on the surface of a metamaterial consisting of alternating graphene and dielectric layers. It was noted that this effect can be used to significantly increase the terahertz radiation source intensity. The high electron mobility in graphene (up to 10^6 $cm^2/(V\ s)$ [33]) makes it possible to create graphene-based active plasmon interferometers and photodetectors that can operate in the frequency range from terahertz to visible radiation and have an extremely high operation speed, a low control voltage, low power consumption, and very small sizes [34].

Mikhailov and Ziegler [35] predicted the ability of graphene to maintain the propagation of TE-polarized surface electromagnetic waves. The physical cause of this ability is a linear law of dispersion of conduction

electrons near a Dirac point, and a necessary condition of this ability is a negative imaginary part of the resulting conductivity of graphene.

In this section, we study the features of electron energy loss to the excitation of surface magnetoplasmons propagating at various angles to the direction of the static magnetic field. The electron with non-relativistic velocity moves in vacuum parallel to the interface between vacuum and the two-dimensional + three-dimensional plasma along an external static magnetic field. In view of non-relativistic character of the electron velocity the problem is considered in electrostatic approximation. The energy loss of an electron for the radiation of oblique surface magnetoplasmons is found as the work done by the radiation field on the electron at the point where this electron is located. In so doing, the Sokhotski theorem is used to calculate the integrals over frequency. In particular, the effect of nonreciprocity of the propagation of waves on the spectral density of electron energy loss is revealed and analyzed. In addition, it is shown that the type of the dispersion law of electrons in the two-dimensional plasma—quadratic for a Drude plasma [36] and linear for graphene (see [13] and references therein)—can be determined by analyzing the spectral density of this loss. This result can be used as a new contactless method for testing graphene films and separating graphene monolayers from them.

1.2. Statement of the Problem and Basic Equations

The coordinate system is chosen such that the y axis is directed along the normal to the interface between vacuum and the two-dimensional + three-dimensional plasma and the z axis is directed along an external static magnetic field $\mathbf{H}_0$ (Fig. 1.1).

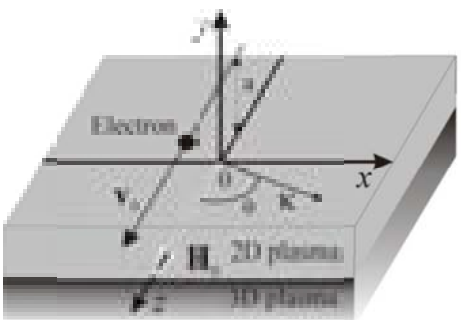

Fig. 1.1. Geometry of the problem

The two-dimensional + three-dimensional plasma is a non-magnetic medium and occupies the $y < 0$ half-space. The electron moves in vacuum at the height a from the interface along the positive direction of the z axis at the velocity $v \ll c$, where c is the speed of light in vacuum.

The field equations for the region $y > 0$ in the electrostatic approximation are written in the form

$$\mathrm{rot}\,\mathbf{E}(\mathbf{r},t) = 0\,, \tag{1.1}$$

$$\mathrm{div}\mathbf{E}(\mathbf{r},t) = 4\pi e\delta(x)\delta(y-a)\delta(z-v_0 t)\,, \tag{1.2}$$

where e is the charge of the electron and $\delta(x)$ is the Dirac delta function. The corresponding equations for the region $y < 0$ has the form

$$\mathrm{rot}\,\mathbf{E}(\mathbf{r},t) = 0\,, \tag{1.3}$$

$$\mathrm{div}\,\mathbf{D}(\mathbf{r},t) = 4\pi e n(\boldsymbol{\rho},t)\delta(y)\,, \tag{1.4}$$

where $\mathbf{D}$ and $\mathbf{E}$ are related to each other through the corresponding material equation, $\boldsymbol{\rho} = (x,z)$, $n(\boldsymbol{\rho},t)$ is the perturbed electron density in the two-dimensional plasma satisfying the continuity equation

$$e\frac{\partial n(\boldsymbol{\rho},t)}{\partial t} + \mathrm{div}\mathbf{j}(\boldsymbol{\rho},t) = 0, \tag{1.5}$$

where $\mathbf{j}(\boldsymbol{\rho},t)$ is the electron conduction current in the two-dimensional plasma, which is related to the electric field $\mathbf{E}(\boldsymbol{\rho},t)$ as

$$\mathbf{j}(\boldsymbol{\rho},t) = \int_{-\infty}^{t} \hat{\sigma}(t-t')\mathbf{E}(\boldsymbol{\rho},t')dt'\,, \tag{1.6}$$

where $\hat{\sigma}(t-t')$ is the response function. The continuity condition of the tangential components of the electric field is satisfied at the $y = 0$ interface. The normal component of the electric displacement has a break, which is determined from Eq. (1.4) by integrating along the y coordinate:

$$D_{yv}(\boldsymbol{\rho},t) - D_{yp}(\boldsymbol{\rho},t) = 4\pi e n(\boldsymbol{\rho},t)\,, \tag{1.7}$$

where the subscripts «*v*» and «*p*» refer to the vacuum and plasma regions, respectively.

We introduce the potential $\varphi(\mathbf{r},t)$ such that $\mathbf{E}(\mathbf{r},t) = -\nabla\varphi(\mathbf{r},t)$ and represent it in the form of a set of space–time harmonics:

$$\varphi(\mathbf{r},t) = \int_{-\infty}^{\infty} d\boldsymbol{\kappa}d\omega\varphi(\boldsymbol{\kappa},\omega)\exp\{i[\boldsymbol{\kappa}\boldsymbol{\rho} + k_y(\kappa,\omega)y - \omega t]\}, \tag{1.8}$$

where $\boldsymbol{\kappa} = (k_x, k_z)$. Then, the material equations can be represented in the form

$$D_i(\boldsymbol{\kappa}, \omega) = \varepsilon_{ij}(\omega) E_j(\boldsymbol{\kappa}, \omega).$$

Here, summation over the subscript " j " is implied and $\varepsilon_{ij}(\omega)$ are the elements of the tensor

$$\ddot{\varepsilon} = \begin{pmatrix} \varepsilon_\perp & i\varepsilon' & 0 \\ -i\varepsilon' & \varepsilon_\perp & 0 \\ 0 & 0 & \varepsilon_\parallel \end{pmatrix}, \tag{1.9}$$

$$\varepsilon_\perp = \varepsilon_0 \left\{ 1 - \frac{\omega_p^2 (\omega + i\nu)}{\omega \left[(\omega + i\nu)^2 - \omega_H^2 \right]} \right\}, \tag{1.10}$$

$$\varepsilon' = \frac{\varepsilon_0 \omega_p^2 \omega_H}{\omega \left[(\omega + i\nu)^2 - \omega_H^2 \right]}, \tag{1.11}$$

$$\varepsilon_\parallel = \varepsilon_0 \left[1 - \frac{\omega_p^2}{\omega(\omega + i\nu)} \right]. \tag{1.12}$$

Here, $\omega_p = \sqrt{4\pi e^2 N_0 / \varepsilon_0 m_{3D}}$ and $\omega_H = |e| H_0 / m_{3D} c$ are the plasma and cyclotron frequencies, respectively; ν is the relaxation frequency of the momentum of electrons of the three-dimensional plasma; N_0 and m_{3D} are the equilibrium density and effective mass of electrons in the three-dimensional plasma, respectively. Below, we will assume that $\omega >> \nu$. In the region $y > 0$, $\varepsilon_{ij}(\omega) = \delta_{ij}$, where δ_{ij} is the Kronecker delta.

In the absence of a charged particle, Eqs. (1.1)–(1.4) provide the following expressions for the normal components of the wavevector in the regions of vacuum, $k_{yv}(\kappa, \omega)$ and of the three-dimensional plasma, $k_{yp[}(\kappa, \omega)$:

$$k_{yv}(\kappa, \omega) = i\kappa, \tag{1.13}$$

$$k_{yp}(\kappa, \omega) = -i \sqrt{k_x^2 + \frac{\varepsilon_\parallel}{\varepsilon_\perp} k_z^2}\ . \tag{1.14}$$

It is easy to show that the Fourier components of the electron field potential have the form

$$\varphi_e(\boldsymbol{\kappa},\omega)=\frac{e}{2\pi\kappa}\exp(-\kappa a)\delta(\omega-k_z v_0). \tag{1.15}$$

To determine the field potential excited by the electron in vacuum, $\varphi_v(\boldsymbol{\kappa},\omega)$, and in the plasma, $\varphi_p(\boldsymbol{\kappa},\omega)$, we use the conditions at the $y=0$ interface. As a result, we obtain

$$\varphi_v(\boldsymbol{\kappa},\omega)+\varphi_e(\boldsymbol{\kappa},\omega)=\varphi_p(\boldsymbol{\kappa},\omega), \tag{1.16}$$

$$E_{yv}(\omega,\boldsymbol{\kappa})-D_{yp}(\omega,\boldsymbol{\kappa})=4\pi e n(\omega,\boldsymbol{\kappa}), \tag{1.17}$$

where $E_{yv}(\omega,\boldsymbol{\kappa})$ is the sum of the field of the electron and $n(\omega,\boldsymbol{\kappa})$ is the Fourier component of $n(\boldsymbol{\rho},t)$ given by the expression

$$n(\omega,\boldsymbol{\kappa})=\frac{\kappa^2\sigma(\omega)}{ie\omega}\varphi_p(\omega,\boldsymbol{\kappa}), \tag{1.18}$$

where $\sigma(\omega)=\int_0^\infty\hat{\sigma}(\tau)\exp(i\omega\tau)d\tau$ is the Fourier component of the conductivity of the two-dimensional plasma, which can be the conductivity of both the two-dimensional Drude plasma and graphene.

Conditions (1.16) and (1.17) provide the following expressions for the electron-induced field potentials:

$$\varphi_v(\boldsymbol{\kappa},\omega)=-\frac{e}{2\pi\kappa}\left[1+\frac{2\kappa}{\Delta(\boldsymbol{\kappa},\omega)}\right]\exp(-\kappa a)\delta(\omega-k_z v_0), \tag{1.19}$$

$$\varphi_p(\boldsymbol{\kappa},\omega)=-\frac{e}{\pi\Delta(\boldsymbol{\kappa},\omega)}\exp(-\kappa a)\delta(\omega-k_z v_0), \tag{1.20}$$

where

$$\Delta(\boldsymbol{\kappa},\omega)=-\frac{4\pi i\kappa^2\sigma(\omega)}{\omega}-k_x\varepsilon'-i\varepsilon_\perp k_{yp}-\kappa. \tag{1.21}$$

Charged particle energy loss per unit time to the excitation of surface magnetoplasmons is given by the known expression [37]

$$\frac{dW}{dt}=ev_0E_{zv}(x=0,y=a,z=v_0t;t), \tag{1.22}$$

where $E_{zv}\left(x=0, y=a, z=v_0 t; t\right)$ is the z component of the electric field of the magnetoplasmon at the electron location point. Taking into account Eqs. (1.8) and (1.19), we represent Eq. (1.22) in the form.

$$\frac{dW}{dt}=\frac{ie^2 v_0}{2\pi}\int\limits_{-\infty}^{\infty} d\omega dk_x dk_z \frac{k_z}{\kappa}\left[1+\frac{2\kappa}{\Delta(\boldsymbol{\kappa},\omega)}\right]\exp(-\kappa a)\delta(\omega-k_z v_0)\exp\left[i\left(k_z v_0-\omega\right)t\right]\cdot \tag{1.23}$$

The excitation of surface plasmons corresponds to the pole of the integrand in Eq. (1.23), i.e., to the condition $\Delta(\boldsymbol{\kappa},\omega)=0$. Introducing small dissipative loss in the three-dimensional plasma and using the pole bypass rule [38]

$$\frac{1}{x\pm i\gamma}=\frac{P}{x}\mp i\pi\delta(x), \tag{1.24}$$

where $\gamma\to 0$ and P/x is the principal value of the integral of function $1/x$, we arrive at the following expression for electron energy loss to the excitation of surface magnetoplasmons:

$$\begin{aligned}\frac{dW}{dt}=-\frac{2e^2}{v_0}\Bigg\{&\sum_{\ell_1}\int\limits_{-\infty}^{0} dk_x \frac{\omega_{\ell_1}(k_x)}{\Lambda^{(-)}_{\ell_1}(k_x)}\exp\left[-2\kappa(k_x)a\right]+\\ &+\sum_{\ell_2}\int\limits_{0}^{\infty} dk_x \frac{\omega_{\ell_2}(k_x)}{\Lambda^{(+)}_{\ell_2}(k_x)}\exp\left[-2\kappa(k_x)a\right]\Bigg\},\end{aligned} \tag{25}$$

where

$$\Lambda^{(\pm)}_{\ell_j}(\mathrm{k}_x)=\left|\frac{\partial\Delta(\pm k_x, k_z=\omega/v_0,\omega)}{\partial\omega}\right|_{\omega_{\ell_j}(k_x)>0}, \tag{26}$$

$\omega_{\ell_j}(k_x)$ are the positive roots of the dispersion equation $\Delta(k_x, k_z=\omega/v_0,\omega)=0$, $\kappa(k_x)=\sqrt{k_x^2+\omega(k_x)^2/v_0^2}$ and summation is performed over the roots of the dispersion equation for surface magnetoplasmons in the regions $k_x<0$ and $k_x>0$. The first integral in (1.25) describes waves propagating at negative phase velocities to the region $x<0$, whereas the second integral describes waves propagating at positive phase velocities to the region $x>0$. According to Eq. (1.25), electron energy losses at $k_x<0$ and $k_x>0$ are different from each other. This is a manifestation of the nonreciprocity of the propagation of surface magnetoplasmons.

1.3. Numerical Analysis of the Dispersion Equation For Surface Plasmons Excited By a Particle

The charged particle moving over the structure under investigation excites only those eigenmodes (surface plasmons) that satisfy the **Cherenkov resonance condition** $k_z = \omega/v_0$. We also note that the particle excites only waves traveling at acute angles with respect to the external magnetic field (in particular, along the external magnetic field). Waves propagating at a right angle to the external magnetic field are not excited because the projection of the vector $\mathbf{E}$ on the direction of particle motion is zero and, therefore, particle energy loss to the excitation of surface plasmons is absent. The dispersion equation $\Delta(\boldsymbol{\kappa}, \omega) = 0$ for surface plasmons excited by the particle has the form

$$\frac{4\pi i \kappa^2 \sigma(\omega)}{\omega} + k_x \varepsilon' + \varepsilon_\perp \sqrt{k_x^2 + \frac{\varepsilon_\parallel}{\varepsilon_\perp} k_z^2} + \kappa = 0 . \tag{1.27}$$

This equation at $k_z = 0$ describes the pure transverse propagation of surface plasmons and coincides with the corresponding dispersion equation obtained in [1].

It is convenient to numerically analyze Eq. (1.27) in the dimensionless variables

$$\bar{\omega} = \frac{\omega}{\omega_p}, \ \bar{\omega}_H = \frac{\omega_H}{\omega_p}, \tag{1.28}$$

$$\bar{k}_x = \frac{v_0 k_x}{\omega_p}, \ \bar{k}_z = \bar{\omega}, \ \bar{\kappa} = \sqrt{\bar{k}_x^2 + \bar{\omega}^2} . \tag{1.29}$$

In these dimensionless variables, dispersion equation (1.27) is represented in the form

$$\frac{4\pi i \bar{\sigma}(\bar{\omega})}{\bar{\omega}} \bar{\kappa}^2 + \bar{k}_x \varepsilon' + \varepsilon_\perp \sqrt{\bar{k}_x^2 + \frac{\varepsilon_\parallel}{\varepsilon_\perp} \bar{\omega}^2} + \bar{\kappa} = 0 . \tag{1.30}$$

where $\bar{\sigma}(\bar{\omega}) = \sigma(\omega)/v_0$.

We perform numerical estimations for the GaAs semiconductor as a three-dimensional plasma with $\varepsilon_0 = 12.53$, $m_{3D} = 0.067 m_0$ (where m_0 is the mass of the free electron), and $N_0 = 10^{14}\,\text{cm}^{-3}$ and the InSb semiconductor as a two-dimensional plasma with $m_{2D} = 0.014 m_0$ and the equilibrium electron

density $n_0 = 10^{11}\text{cm}^{-2}$ [39]. The value $v_0 = 0.1c$ is taken for the velocity of the electron. In this case, the dimensionless conductivity of electrons in the two-dimensional plasma is given by the Drude formula

$$\bar{\sigma}(\bar{\omega}) = \frac{ie^2 n_0}{m_{2D} v_0 \omega_p \bar{\omega}}. \tag{1.31}$$

Figure 1.2 shows the dispersion characteristics of surface plasmons excited by the particle at $\bar{\omega}_H = 0.6$ (solid lines 1–3). The dashed lines correspond to the frequencies $\bar{\omega} = \pm\bar{\omega}_H$ and the dash-dotted lines correspond to the hybrid frequencies $\bar{\omega} = \pm\bar{\omega}_{Hyb}$, where $\bar{\omega}_{Hyb} = \sqrt{1 + \bar{\omega}_H^2}$. For the chosen magnitude of the magnetic field, $\bar{\omega}_{Hyb} \approx 1.17$.

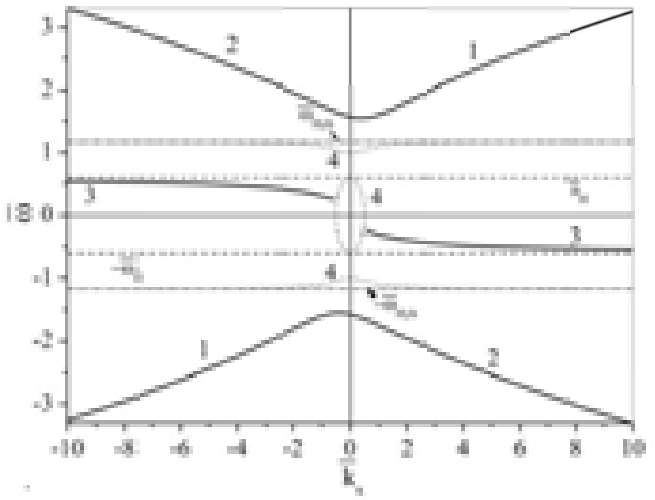

Fig. 1.2. Dependences $\bar{\omega}(\bar{k}_x)$ for surface plasmons excited by the electron over the two-dimensional + three-dimensional plasma structure at $\bar{\omega}_H = 0.6$ and $\bar{k}_z = \bar{\omega}$

At the hybrid frequency, $|\text{Im}\, k_{yp}| \to \infty$ (in the absence of dissipative loss). This physically means that the localization depth of the field of a surface plasmon vanishes; i.e., the surface plasmon disappears. Dotted lines 4 correspond to the condition $\text{Im}k_{yp} = 0$, when the surface plasmon is transformed into a homogeneous wave. Dispersion curves 3 begin on these lines. The region bounded by line 4 in the frequency range $-\bar{\omega}_H < \bar{\omega} < \bar{\omega}_H$ and regions between hybrid-frequency lines and lines 4 in the frequency ranges

$\overline{\omega}_H < \overline{\omega} < \overline{\omega}_{Hyb}$ and $-\overline{\omega}_{Hyb} < \overline{\omega} < -\overline{\omega}_H$ corresponds to the uniform electromagnetic field. The particle obviously does not excite such uniform magnetoplasma waves. It is also seen in Fig. 1.2 that dispersion curves 1 have segments with anomalous dispersion.

The number of regions where surface magnetoplasmons can propagate only in one direction with respect to the external magnetic field in the case under consideration is smaller than that in the case of the purely transverse propagation of surface magnetoplasmons with respect to the external magnetic field considered in [1]. This means that the propagation of surface magnetoplasmons at acute angles reduces the degree of asymmetry of dispersion curves. Furthermore, at the "canted" propagation of waves in the frequency range $-\overline{\omega}_H < \overline{\omega} < \overline{\omega}_H$, the points of beginning of the spectrum of the corresponding dispersion curves appear.

1.4. Numerical Analysis of Charged-Particle Energy Loss To The Excitation of Surface Plasmons

We now analyze the dependence of the integrands in Eq. (1.25) on k_x. To this end, we represent these expressions in the dimensionless form by introducing the quantity Q:

$$Q = \frac{v_0}{2e^2\omega_p^2}\frac{d^2W}{d\overline{k}_x dt}. \tag{1.32}$$

This quantity has the meaning of the dimensionless spectral density (in spatial harmonics of $\overline{k}_x$) of electron energy loss to the excitation of surface plasmons, i.e., the work produced by the field of surface plasmons on the electron.

We plot the radiation pattern of emitted canted surface magnetoplasmons in terms of the angle θ between the velocity of the electron and the two-dimensional wavevector $\boldsymbol{\kappa}$ (see Fig. 1.1):

$$\theta = \arcsin\frac{\overline{k}_x}{\overline{\kappa}}. \tag{1.33}$$

The dependences $Q(\theta)$ will be analyzed for each dispersion curve in Fig. 1.2 in the region of positive frequencies at $\theta < 0$ ($k_x < 0$) and $\theta > 0$ ($k_x > 0$).

Figure 1.3 shows $Q(\theta)$ curves for $a = 0.1v_0/\omega_p$. The curves in Fig. 1.3 are marked by the same numbers as the dispersion curves in Fig. 1.2. Line 1

(for $\bar{\omega} > 0$ and $\bar{k}_x > 0$) in Fig. 1.3 corresponds to the propagation of plasmons to the region $x > 0$, line *2* (for $\bar{\omega} > 0$ and $\bar{k}_x < 0$) corresponds to the propagation of plasmons to the region $x < 0$, and lines 3 (for $\bar{\omega} > 0$, $\bar{k}_x < 0$ and $\bar{\omega} < 0$, $\bar{k}_x > 0$) correspond to the propagation of plasmons to the region $x < 0$. Consequently, charged particle energy loss to the emission of modes 3 in Fig. 1.2 to the region $x > 0$ is absent. This clearly demonstrates the nonreciprocity principle in the excitation of surface magnetoplasmons by the electron. It is seen in Fig. 1.3 that maxima of the spectral density appear at finite values $\theta_{\max} = \arcsin \bar{k}_{x,\max} / \bar{\kappa}_{\max}$, whereas the spectral density at $\theta \to \pm \pi/2$ tends to zero. In the absence of the static magnetic field, lines 3 in Fig. 1.3 are absent and lines 1 and 2 are symmetric with respect to $\theta = 0^o$; i.e., the spectral density $Q(\theta)$ is maximal at $\theta = 0^o$ ($\bar{k}_x = 0$). Therefore, the appearance of finite angles $\theta_{\max}$ is due to the nonreciprocity effect caused by the presence of the static magnetic field.

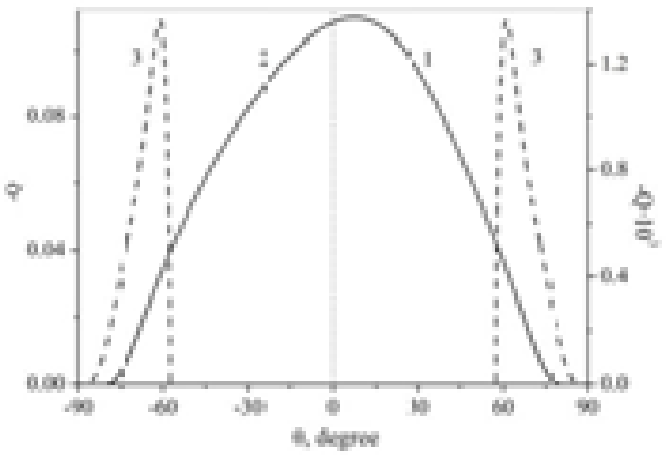

Fig. 1.3. Dimensionless spectral density Q versus the propagation angle θ for dispersion curves 1–3 in Fig. 1.2. The left vertical axis corresponds to lines 1 and 2, whereas the right ordinate axis corresponds to line 3

This is clearly demonstrated by the following asymptotic formula for $Q(\bar{k}_x)$ obtained for $|\bar{k}_x| << 1$ and $\bar{\omega}_H^2 << 1 < \bar{\omega}^2$ (i.e., at $\bar{\omega} / |\bar{k}_x| >> 1$):

$$Q(\bar{k}_x) = -\frac{\bar{\omega}^3 \exp(-2\bar{\kappa}\bar{a})}{\varepsilon_0(1+\bar{\omega}^2)+\bar{\omega}} \left[1 + \frac{3\varepsilon_0 \bar{k}_x \bar{\omega}_H}{\varepsilon_0 \bar{\omega}^2 (1+\bar{\omega}^2)+\bar{\omega}^3} + O(\bar{k}_x^2) \right], \qquad (1.34)$$

where $\bar{a} = a\omega_p / v_0$. According to Eq. (1.34), the nonreciprocity effect leads to a correction of the order $O(\bar{k}_x)$, which depends on the sign of $\bar{k}_x$ and results in the shift of the maximum of the spectral density toward positive values of $\bar{k}_x$ (positive angles θ). Corrections associated with the presence of the two-dimensional plasma are of the order $O(\bar{k}_x^2)$ and, hence, make a "symmetric contribution" to $Q(\bar{k}_x)$.

It is also seen in Fig. 1.3 that there are threshold angles $|\theta_{th}| = \arcsin|\bar{k}_{x,th}|/\bar{\kappa}_{th}$ (where $\bar{\kappa}_{th} = \sqrt{\bar{k}_{x,th}^2 + \bar{\omega}(\bar{k}_{x,th})^2}$) below which electron-energy loss is absent. These threshold angles correspond to the points of beginning of dispersion curves 3 marked by circles in Fig. 1.2. We emphasize that the points of beginning of the spectrum (at which $\mathrm{Im} k_{yp} = 0$) in Fig. 1.2 determine the threshold wavenumbers $\bar{k}_x$ at which surface magnetoplasmons appear and, correspondingly, charged particle energy loss to their emission. The asymptotic expression for the spectral density near the emission threshold has the form

$$Q(\bar{k}_x) = -\frac{|\mathrm{Im}\,\bar{k}_{yp}|(\bar{\omega}^2 - \bar{\omega}_{Hyb}^2)(\bar{\omega}^2 - \bar{\omega}_H^2)}{\varepsilon_0\left[(\bar{\omega}^2 - \bar{\omega}_{Hyb}^2)^2 - \bar{\omega}_H^2\right]}\exp(-2\bar{\kappa}\bar{a}). \qquad (1.35)$$

Expression (1.35) shows that the spectral density near the emission threshold decreases as $|\mathrm{Im}\,\bar{k}_{yp}| \to 0$. The detection of modes corresponding to lines 3 in Fig. 1.2 becomes possible if the observation angle (measured from the direction of the magnetic field) is larger than $|\theta_{th}|$. In particular, for lines 3 in Fig. 1.3, $\theta_{th} \approx \pm 57.4^o$.

It is seen in Fig. 1.3 that the maximum of the spectral density for surface modes described by dispersion curves 1 and 2 in Fig. 1.2 is approximately two orders of magnitude higher than those for surface modes described by lines 3 in Fig. 1.2. Consequently, the main contribution to electron energy loss comes from the excitation of modes 1 and 2 in Fig. 1.2.

Figure 1.4 shows the results of the numerical analysis of the dependence of the maximum of the spectral density, $Q_{\max} = Q(\theta_{\max})$, corresponding to mode 1 in Fig. 1.2 (maximum of line 1 in Fig. 1.3) on the electron density in the two-dimensional plasma at $a = 0$ (which corresponds to the condition $\kappa a << 1$) for the cases where the two-dimensional plasma is a Drude gas (with a quadratic dispersion law) and graphene monolayer (with a linear dispersion law) with the same electron density. Numerical calculations show that the qualitative form of the above dispersion curves

and $Q(\theta)$ dependences is the same as for the two-dimensional plasma in graphene. We recall that the conductivity of graphene σ_{gr} is the sum of the intraband, $\sigma_{gr}^{\text{intra}}$, and interband, $\sigma_{gr}^{\text{inter}}$, conductivities [40]. According to [40], the conductivities $\sigma_{gr}^{\text{intra}}$ and $\sigma_{gr}^{\text{inter}}$ for a degenerate electron gas, when $T << E_F$ (where T is the temperature in the energy units and E_F is the Fermi energy), are given by the expressions

$$\sigma_{gr}^{\text{intra}} = \frac{ie^2 E_F}{\pi\hbar^2\omega}, \tag{1.36}$$

$$\sigma_{gr}^{\text{inter}} = \frac{e^2}{4\hbar}\left[\theta(\hbar\omega - 2E_F) - \right.$$

$$\left. - \frac{i}{2\pi}\ln\frac{(\hbar\omega + 2E_F)^2}{(\hbar\omega - 2E_F)^2 + (2T)^2}\right], \tag{1.37}$$

$$E_F = \hbar v\sqrt{\pi n_0}, \tag{1.38}$$

where $v = 10^8$ cm/s, n_0 is the unperturbed concentration of charge carriers in graphene, and $\theta(x)$ is the Heaviside step function [41]. The above maximum of $Q(\theta)$ for line 1 (see Fig. 1.3) corresponds to the frequencies $\omega \propto \omega_P$, where $\omega_p \approx 6\cdot 10^{11}\,\text{s}^{-1}$.

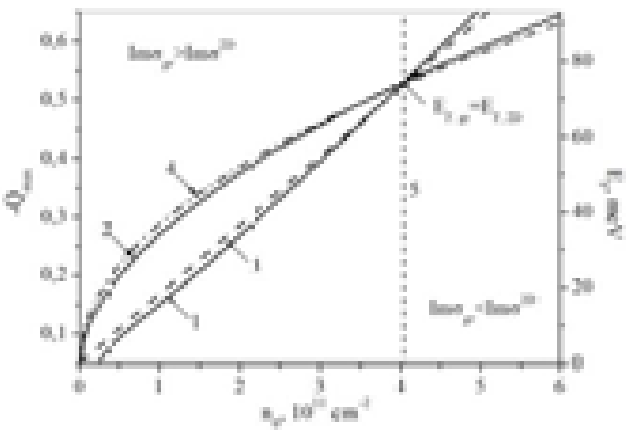

Fig. 1.4. Absolute values $Q_{\max} = Q(\theta_{\max})$ versus the electron density in (line 1) the two-dimensional Drude plasma and (line 2) graphene for surface magnetoplasmons described by dispersion curve 1 in Fig. 1.2, as well as the Fermi energies versus the electron density in (line 3) the two-dimensional Drude plasma and (line 4) graphene. Line 5 corresponds to the n_0 value at which $E_{F,gr} = E_{F,2D}$.

Since the interband conductivity makes a significant contribution to the resulting conductivity of graphene σ_{gr} at $\hbar\omega \propto E_F$ [40], the contribution $\sigma_{gr}^{\text{inter}}$ will be significant at $\omega \geq 2\cdot 10^{13}\,\text{s}^{-1}$ for $n_0 = 10^{10}\,\text{cm}^{-2}$ and at $\omega \geq 6\cdot 10^{13}\,\text{s}^{-1}$ for $n_0 = 10^{11}\,\text{cm}^{-2}$. Since ω_p is much lower than these frequencies, the intraband contribution $\sigma_{gr}^{\text{intra}}$ dominates in the conductivity of graphene. The Fermi energy for the two-dimensional Drude plasma is given by the expression $E_F = \pi\hbar^2 n_0 / m_{2D}$. The analysis of the curves in Fig. 1.4 indicates that the dependence $Q_{\max}(n_0)$ for the two-dimensional plasma with a quadratic dispersion law (line 1) is qualitatively close to the dependence $E_F(n_0) \propto n_0$ (line 3), whereas the dependence $Q_{\max}(n_0)$ for the two-dimensional plasma with a linear dispersion law (line 2) is qualitatively close to the dependence $E_F(n_0) \propto \sqrt{n_0}$ (line 4). This means that the dependence $Q_{\max}(n_0)$, more precisely, the position of the maximum in the angular distribution of the intensity of excited surface plasmons can indicate the qualitative character of the dispersion law of electrons in the two-dimensional plasma. The density n_0 can be varied by applying a gate voltage to graphene [17]. It is also seen in Fig. 1.4 that lines 1–4 intersect each other at one point corresponding to the concentration $n_{0,th} \approx 4.5\cdot 10^{11}\,\text{cm}^{-2}$, at which the Fermi energies of the two-dimensional Drude plasma and graphene are identical, $E_{F,gr} = E_{F,2D}$. We also note that the inequality $\text{Im}\sigma_{gr} > \text{Im}\sigma^{2D}$ is valid for $n_0 < n_{0,th}$, whereas the opposite inequality $\text{Im}\sigma_{gr} < \text{Im}\sigma^{2D}$ is satisfied for $n_0 > n_{0,th}$. The above analysis is also valid for coherent electron bunches, i.e., for bunches much smaller than the wavelength.

1.5. Conclusions

The excitation of surface magnetoplasmons by an electron moving along a static magnetic field in vacuum over a two-dimensional plasma layer on the surface of three-dimensional plasma has been studied theoretically. Surface magnetoplasmons are excited under the Cherenkov resonance condition. An expression for the spectral density of electron energy loss to the excitation of surface magnetoplasmons has been obtained and analyzed. The spectral characteristics of the two-dimensional plasma for the cases of the Drude electron gas and graphene with a linear dispersion law of electrons have been compared. It has been shown that the dependences of the maxima of the spectral density on the electron density in the two-dimensional plasma are in qualitative agreement with similar dependences for the Fermi energies in the two-dimensional plasma with the

corresponding dispersion law of electrons. This means that the position of the maximum of the angular distribution of the intensity of excited surface plasmons can indicate the qualitative character of the dispersion law of electrons in the two-dimensional plasma.

SECTION 2. INTERACTION BETWEEN A TUBULAR BEAM OF CHARGED PARTICLES AND A DISPERSIVE METAMATERIAL OF CYLINDRICAL CONFIGURATION

2.1. Introduction

Since the travelling-wave amplifier was created by R. Kompfner (see Ref. [42]) in the 1940s, there have been many theoretical and experimental works devoted to transform a kinetic energy of charged particle flows into an electromagnetic radiation (see, e.g., Refs. [43-47] and the references cited therein). At present time, there is a tendency towards the advancement in millimeter and submillimeter wavelength ranges in the development of electron-vacuum technology. At the same time, the use of traditional approaches to the electronic devices design is experiencing great difficulties due to the small geometric dimensions of the main elements. There is a need to use oversized (with respect to the wavelength of generated oscillations) electrodynamic structures operating in a multimode regime. The stability of the generation frequency requires excitation and selection of a high-order working mode in such structures. The possibility of excitation of the weakly decaying high-order modes (so-called "whispering gallery" modes) in cylindrical dielectric resonators (CDR) predetermines their use in the vacuum electronic devices of the short-wave range of millimeter and submillimeter wavelengths. Then, the above-mentioned structural difficulty is overcome. However, the output power of traditional sources drops down sharply with a transition to submillimeter wavelengths [48]. Hence, it becomes necessary to use high-energy oscillators excited by electron flows. It is *important to note* in this connection that with powerful new technologies many types of artificial materials can be fabricated which are endowed with unique electromagnetic properties and show promise as structural elements for the high-energy oscillators. For instance, among them there are the metal-based (see, e.g., Refs. [49-53]), all-dielectric [54-57] and graphene-based [58] metamaterials which behave like left-handed ones over a certain frequency range. *Below we dwell* on electromagnetic properties of left-handed metamaterials (LHMs) in *more detail*.

In paper [59], the results of investigations of an auto-oscillatory system based on a high-quality CDR with whispering gallery modes excited by the azimuthal-periodic current of relativistic electron beam were

presented. The possibility of using the investigated system or its modifications is shown in the millimeter wavelength range. The appearance of the detected electromagnetic radiation is associated with the excitation of CDR whispering gallery modes by a disturbed flow of charged particles. The theoretical description of the phenomena that lead to the appearance of the radiation found in Ref. [59] is rather a difficult problem. Therefore, from our viewpoint, it seems appropriate to use the simplified physical models of the electrodynamic system discussed in Ref. [59], which allow qualitative and quantitative descriptions of physical phenomena that are as close as possible to the experimental conditions. The simplest physical model is a radially thin tubular electron beam moving along an infinitely long solid-state cylinder.

An actual problem of radiophysics and electronics is the investigation of the generation mechanisms of electromagnetic waves that are excited when charged particles move in various electrodynamic systems. To create sources of electromagnetic radiation in the millimeter and submillimeter ranges, the beam instabilities occurring in electrodynamic systems of various kinds are of great interest. Particular attention is given to multiwave Cherenkov generators of surface waves [60, 61] and auto-oscillatory systems based on dielectric resonators [59,62,63]. The energy loss of one particle per unit time for eigenmodes excitation in systems is one of the fundamentally important characteristics of possible generation process [37,64-70]. Besides, the beam instabilities that occur in electrodynamic systems containing dispersive media are of special interest. In particular, the instability of tubular electron beam that interacts with a plasma-like medium was studied in Ref. [71]. In addition, an actual problem is the investigation of the electromagnetic properties of solid-state structures containing left-handed media. The technology progress of fabricating metamaterial structures stimulates studying the excitation mechanisms of their eigenmodes.

Indeed, in recent years a good deal of attention has been given to studying the electromagnetic properties of the left-handed media. We recall that these materials came to be known by this particular name because in these media the directions of electric and magnetic field vectors as well as the direction of a wave vector form a left-handed triplet. The unusual properties of the left-handed medium (LHM) electrodynamics were originally suggested in Refs. [72,73]. In Ref. [72] it was first proved the possibility of excitation of the electromagnetic waves with negative group velocity with the aid of Cherenkov radiation in a medium, which possesses negative permittivity ε and negative permeability μ simultaneously. In addition to that it was shown that if an electron moves from vacuum into the medium, the maximum of the intensity of Cherenkov radiation is in vacuum and the Cherenkov angle in this case is obtuse. The unusual properties of the LHM electrodynamics were originally classified in Ref. [73], where it was demonstrated that the LHM would exhibit unusual properties such as the negative index of refraction, antiparallel wave vector,

$\mathbf{k}$, and Poynting vector, $\mathbf{S}$, antiparallel phase and group velocities, and the time-averaged energy flux opposite to the time-averaged momentum density. Besides, as indicated in Ref. [73], opposite directions of vectors $\mathbf{S}$ and $\mathbf{k}$ in the LHM result in a reverse Doppler shift and the other phenomena of interest.

A considerably great interest in the LHM has been evoked after they had been practically implemented in Refs. [49-53] in the form of alternating layers with negative ε and positive μ and the layers with positive ε and negative μ. The permeability frequency dispersion of complex composites is provided by a periodic structure of nonmagnetic circular conducting units such as the split ring resonators, spirals, etc. The permittivity frequency dispersion is provided by a periodic grating of thin conducting wires. If a wavelength of the electromagnetic wave that propagates in such a material is much greater than the period of composite structure, the composite for this particular wave is similar to a continuous one. In Refs. [49-53] the parameters of structural elements are selected in such a way that ε and μ become negative over the GHz frequency range. Since then, a large variety of metal-based and all-dielectric LHMs with different types of unit-cell geometries has been proposed (see, e.g., Refs. [54-57]). For instance, in Ref. [56] the silver-based unit-cells were fabricated on glass substrate by using standard electron-beam lithography. The structure with lattice constant 600 nm possessed left-handedness and negative refraction at infrared frequencies. In Ref. [57] it was shown that by choosing a proper geometrical shape of the dielectric inclusions, all-dielectric LHM can be achieved by using single-sized dielectric resonators. Besides, both the left-handedness and the negative refraction phenomenon at far infrared frequencies were observed in a periodic stack of antiferromagnetic and ionic-crystal layers [74] and in graphene-sheet periodic structures [58]. A design for active LHM collaborated with microwave varactors was proposed and experimentally realized in Ref. [75].

It should be noted that a lot of work has been done on theoretical study of electromagnetic properties of LHM (see, e.g., Refs. [76-80]). Specifically, in Ref. [76], an analytical theory of low frequency electromagnetic waves in metallic photonic crystals with a small volume fraction of a metal was presented. The effective medium theory of LHM based on the transfer matrix calculations on metamaterials of finite lengths was proposed in Ref. [77]. Linear and nonlinear wave propagation in LHMs was theoretically analyzed and a number of nonlinear optical effects were predicted in Ref. [78]. In our opinion, special attention should be paid to the papers Ref. [79-82], in which the effects of Cherenkov radiation and electron-beam instability were theoretically investigated. In Ref. [79], Cherenkov radiation of bulk and surface electromagnetic waves by an electron bunch that moved in vacuum above a composite medium was theoretically investigated. It was shown that Cherenkov radiation gave rise to simultaneous excitation of bulk and surface electromagnetic waves over

one and the same frequency range. The excited surface electromagnetic waves can be of two different types: namely, the electric and magnetic ones. The instability of two electron beams passing through a slab of LHM was predicted in Ref. [80]. It was shown that this instability originates from the backward Cherenkov radiation and results in a self-modulation of the beams and radiation of electromagnetic waves. In Ref. [81] the theoretical analysis of excitation of the surface plasmon polaritons by a thin electron beam propagating in the vacuum gap separating a plasma-like medium (metal) from an artificial dielectric with negative magnetic permeability was performed. It was demonstrated that the interface-localized waves with the negative total energy flux could be excited. The case of uniform motion of the charge in infinite LHM was considered in Ref. [82]. Using complex function theory methods, the total field was decomposed into a "quasi-Coulomb" field, a wave field (Cherenkov radiation) and a "plasma trace". It was shown that the wave field in LHM lags behind the charge more so than it does in ordinary medium.

The LHMs are promising for up-to-date applications, such as amplifiers of evanescent waves [83], magnetic-optical recorders [84], directional antennas [85], and for suppression wakefields that occur during the process of particle acceleration [86,87].

In this part of the section, the interaction between a tubular beam of charged particles and eigenmodes of cylindrical dispersive medium are theoretically investigated. This medium may have negative values of ε and μ over a certain frequency range. It will be shown that the interaction gives rise to the absolute instability of the so-called bulk-surface electromagnetic waves, which are the propagating waves in the medium and, at the same time, they are evanescently confined along the normal to the lateral cylinder surface in vacuum.

For an infinitely thin nonrelativistic electron beam, the dispersion equation for coupled beam-plasma waves is obtained for arbitrary impact distances of the beam. It is shown that if the so-called effective (or reduced) plasma frequency of the beam much less than the value of the instability increment, the instability is caused by Cherenkov effect whereas in the opposite case the instability is caused by anomalous Doppler effect. For both cases of the instability incremets are derived. The qualitative analysis of the types of eigenmodes of the investigated solid-state waveguide in frequency regions with different combinations of the signs of ε and μ is carried out. The detailed analysis of the nature of the instability in a small vicinity of the so-called resonance points of the dispersion curves is performed with the use of the well-known Sturrock method. The dependences of the instability increment values of electrodynamic system with the bulk-surface modes on the azimuthal index for different values of the radial indices are analysed.

The main qualitative conclusion of this study is that LHMs can be used as the delaying media with "natural feedback" for generation of electromagnetic waves in backward-wave tubes. Besides, the possibility of

generation of weakly damped whispering-gallery waves will allow the generation electromagnetic waves in the sub-mm region of the spectrum.

2.2. Statement of the Problem and Basic Equations

Consider an infinite along the z-axis cylinder with the radius ρ_0 occupying the region $0 \le \rho \le \rho_0$, $0 \le \varphi \le 2\pi$ and $-\infty \le z \le +\infty$ (see Fig. 2.1). We suppose that the cylinder is made of a metamaterial with the frequency-dependent permittivity ε and permeability μ, which have negative values over one and the same frequency range. The frequency dependences for $\varepsilon(\omega)$ and $\mu(\omega)$ will be specified below. A tubular electron beam with the radial thickness a and density $N_0(\rho)$ moves in vacuum at a distance of ρ_b from the cylinder axis at a velocity v_0. The quasi-neutrality condition for the beam is satisfied because the charges of electrons are compensated by the background of positive charges. We assume that the thickness of the beam a is much smaller than the other spatial scales of the electrodynamic system under consideration. Hence, the undisturbed beam density can be represented as $N_0(\rho) = N_0 a\delta(\rho - \rho_b)$, where N_0 is the equilibrium beam density, $\delta(\rho - \rho_b)$ is the Dirac delta function.

Fig. 2.1. Geometry of electrodynamic system

Below we will consider the interaction between the electron beam and the cylinder eigenmodes in a linear approximation. In this case, we specify the disturbed beam current density at a point with the radius-vector $\mathbf{r}$ at a moment t as:

$$\mathbf{j}(\mathbf{r},t) = eN_0(\rho)\mathbf{v}(\mathbf{r},t) + e\mathbf{v}_0 N(\mathbf{r},t),$$

where e is the electron charge, $N(\mathbf{r},t)$ and $\mathbf{v}(\mathbf{r},t)$ are the variable components of the beam density and the electron velocity, respectively. Hereafter, we will suppose the radial component of the beam current density equal to zero because of the chosen model of the electron beam.

To describe the interaction between the electron beam and the cylinder eigenmodes, we take as a starting point the following Maxwell

equations together with the linearized continuity and motion equations for the beam electrons:

$$\mathrm{rot}\mathbf{H}(\mathbf{r},t)=\frac{1}{c}\frac{\partial}{\partial t}\mathbf{D}(\mathbf{r},t)+\frac{4\pi}{c}\mathbf{j}(\mathbf{r},t)\,; \tag{2.1}$$

$$\mathrm{rot}\mathbf{E}(\mathbf{r},t)=-\frac{1}{c}\frac{\partial}{\partial t}\mathbf{B}(\mathbf{r},t); \tag{2.2}$$

$$\mathrm{div}\,\mathbf{D}(\mathbf{r},t)=4\pi eN(\mathbf{r},t)\,; \tag{2.3}$$

$$\mathrm{div}\,\mathbf{B}(\mathbf{r},t)=0\,, \tag{2.4}$$

$$e\frac{\partial N(\mathbf{r},t)}{\partial t}+\mathrm{div}\mathbf{j}(\mathbf{r},t)=0\,; \tag{2.5}$$

$$\frac{\partial\mathbf{v}(\mathbf{r},t)}{\partial t}+v_0\frac{\partial\mathbf{v}(\mathbf{r},t)}{\partial z}=\frac{e}{m}\left(\mathbf{E}(\mathbf{r},t)+\frac{1}{c}[\mathbf{v}_0,\mathbf{B}(\mathbf{r},t)]\right), \tag{2.6}$$

where m is the electron mass, c is the velocity of light in vacuum, $\mathbf{E}(\mathbf{r},t)$ and $\mathbf{H}(\mathbf{r},t)$ are the electric and magnetic field vectors, $\mathbf{D}(\mathbf{r},t)$ and $\mathbf{B}(\mathbf{r},t)$ are the electric displacement and magnetic induction vectors that are related with the $\mathbf{E}(\mathbf{r},t)$ - and $\mathbf{H}(\mathbf{r},t)$ -vectors by the constitutive equations

$$\mathbf{D}(\mathbf{r},t)=\int_{-\infty}^{t}\tilde{\varepsilon}(t-t')\mathbf{E}(\mathbf{r},t')dt'\,, \tag{2.7}$$

$$\mathbf{B}(\mathbf{r},t)=\int_{-\infty}^{t}\tilde{\mu}(t-t')\mathbf{H}(\mathbf{r},t')dt'\,, \tag{2.8}$$

where $\tilde{\varepsilon}(t-t')$ and $\tilde{\mu}(t-t')$ are the influence functions that characterize the efficiency of the field action in time. Note that the difference nature of the kernels of the integrals is due to the homogeneity of the metamaterial properties in time.

In order to derive the dispersion equation for the electromagnetic waves in the electrodynamic system under consideration, it is necessary to satisfy certain boundary conditions at $\rho=\rho_0$ and $\rho=\rho_b$. These conditions are as follows. First, the tangential components of the electric and magnetic fields are continuous at $\rho=\rho_0$. Second, at $\rho=\rho_b$ the tangential components of the magnetic fields are discontinuous because of the beam current. Note that the normal component of the magnetic induction vector remains continuous, whereas the normal component of the electric displacement vector suffers discontinuity because of the disturbed beam charge.

We determine the discontinuities of the tangential components of the magnetic field and the normal component of the electric displacement (in vacuum $D_\rho(\mathbf{r},t) \equiv E_\rho(\mathbf{r},t)$) by integrating Eqs. (2.1) and (2.3) over the infinitesimally small beam thickness. As a result, we have

$$H_\varphi(\mathbf{r},t)\Big|_{\rho=\rho_b+0} - H_\varphi(\mathbf{r},t)\Big|_{\rho=\rho_b-0} = \frac{4\pi}{c\rho_b}\lim_{\Delta\rho\to 0}\int_{\rho_b-\Delta\rho}^{\rho_b+\Delta\rho} j_z(\mathbf{r},t)\rho d\rho\,, \tag{2.9}$$

$$H_z(\mathbf{r},t)\Big|_{\rho=\rho_b+0} - H_z(\mathbf{r},t)\Big|_{\rho=\rho_b-0} = -\frac{4\pi}{c}\lim_{\Delta\rho\to 0}\int_{\rho_b-\Delta\rho}^{\rho_b+\Delta\rho} j_\varphi(\mathbf{r},t)d\rho\,, \tag{2.10}$$

$$E_\rho(\mathbf{r},t)\Big|_{\rho=\rho_b+0} - E_\rho(\mathbf{r},t)\Big|_{\rho=\rho_b-0} = \frac{4\pi e}{\rho_b}\lim_{\Delta\rho\to 0}\int_{\rho_b-\Delta\rho}^{\rho_b+\Delta\rho} N(\mathbf{r},t)\rho d\rho\,. \tag{2.11}$$

We represent all variables in the form of the set of space-time harmonics, for instance:

$$\mathbf{E}(\mathbf{r},t) = \sum_{n=-\infty}^{\infty}\int_{-\infty}^{\infty}\int_{-\infty}^{\infty}\mathbf{E}_n(\rho,q_z,\omega)\exp[i(q_z z + n\varphi - \omega t)]dq_z d\omega\,, \tag{2.12}$$

where ω, q_z and n are the frequency, longitudinal wave number, and the number of the spatial harmonic (coinciding with the azimuthal mode index), respectively.

If we take into account Eq. (2.12), we can rewrite the original equations, Eqs. (2.1)-(2.4), for the axial spectral components of the field in the region outside the electron beam ($\rho \neq \rho_b$) in the following form:

$$\left[\frac{1}{\rho}\frac{\partial}{\partial\rho}\rho\frac{\partial}{\partial\rho} + \left(q_\nu^2 - \frac{n^2}{\rho^2}\right)\right]\begin{Bmatrix} E_{\nu,zn}(\rho,q_z,\omega) \\ H_{\nu,zn}(\rho,q_z,\omega)\end{Bmatrix} = 0\,, \tag{2.13}$$

where $\nu = 1$ for the cylinder region and $\nu = 2$ for vacuum, $q_\nu^2 = \varepsilon_\nu\mu_\nu\omega^2/c^2 - q_z^2$ is the square of the transverse wave number of electromagnetic waves. When $q_\nu^2 > 0$, the equations, Eqs. (2.13), have the form of the Bessel equations, whereas when $q_\nu^2 < 0$ they are the modified Bessel equations. Hereinafter we take the following notations: $q_1^2 = \kappa^2 = \varepsilon\mu\omega^2/c^2 - q_z^2$ in the cylinder region and $q_2^2 = q^2 = \omega^2/c^2 - q_z^2$ in vacuum.

Hereafter, we will use the frequency dependencies $\varepsilon(\omega)$ and $\mu(\omega)$ the same as in Refs. [49,51]:

$$\varepsilon(\omega) = 1 - \frac{\omega_L^2}{\omega^2}; \qquad \mu(\omega) = 1 - \frac{F\omega^2}{\omega^2 - \omega_r^2}\,, \tag{2.14}$$

where ω_L is the effective plasma frequency, ω_r is the resonance frequency, F is the fractional area of the metamaterial unit cell occupied by the interior of the split ring resonator and $F<1$. We recall that because these resonators respond to the incident magnetic field, the medium can be viewed as having an effective permeability (see Ref. [51]).

We are only interested in the waves, which are evanescently confined along the normal to the lateral cylinder surface in vacuum. For these waves the condition $q^2<0$ is satisfied. Exactly, these waves are excited by the beam of charged particles provided **the Cherenkov resonance** $\omega = q_z v_0$. ***Note that the Cherenkov resonance with the condition*** $\omega = q_z v_0$ ***means the effect of excitation of eigenmodes of the cylinder under study as a result of longitudinal bunching of electrons in the field of the excited wave and the formation of emitting electron bunches in its decelerating phases.*** Indeed, for the nonrelativistic electron velocities ($\beta<<1$, where $\beta = v_0/c$ is the dimensionless electron velocity) considered herein, we have $\omega^2/c^2 << q_z^2$ and $q^2<0$. Taking into account the aforesaid, we represent the expressions for the spectral components of the electromagnetic field $E_{zn}(\rho, q_z, \omega)$ and $H_{zn}(\rho, q_z, \omega)$ in the following form:

$$E_{zn}(\rho,q_z,\omega)=\begin{cases}\begin{cases}A_n^E J_n(\kappa\rho), & \kappa^2>0\\ A_n^E I_n(|\kappa|\rho), & \kappa^2<0\end{cases}, & \rho\le\rho_0\\ B_n^E K_n(|q|\rho)+C_n^E I_n(|q|\rho), & \rho_0<\rho<\rho_b\\ D_n^E K_n(|q|\rho), & \rho>\rho_b\end{cases}; \tag{2.15}$$

$$H_{zn}(\rho,q_z,\omega)=\begin{cases}\begin{cases}A_n^H J_n(\kappa\rho), & \kappa^2>0\\ A_n^H I_n(|\kappa|\rho), & \kappa^2<0\end{cases}, & \rho\le\rho_0\\ B_n^H K_n(|q|\rho)+C_n^H I_n(|q|\rho), & \rho_0<\rho<\rho_b\\ D_n^H K_n(|q|\rho), & \rho>\rho_b\end{cases}, \tag{2.16}$$

where $J_n(u)$ is the n-th order Bessel function of the first kind, $I_n(u)$ and $K_n(u)$ are the modified ones of the first kind (Infeld function) and the second kind (Macdonald function), respectively [41], $A_n^{E,H}$, $B_n^{E,H}$, $C_n^{E,H}$ and $D_n^{E,H}$ are the arbitrary constants. The choice of the solution is due to the fulfillment of finiteness conditions for $E_{zn}(\rho, q_z, \omega)$ and $H_{zn}(\rho, q_z, \omega)$ at $\rho\to 0$ and $\rho\to\infty$. At $\beta^2\varepsilon\mu>1$ the expressions for the components $E_{zn}(\rho, q_z, \omega)$ and $H_{zn}(\rho, q_z, \omega)$ of the fields inside the cylinder are described by Bessel functions $J_n(\kappa\rho)$, and at $\beta^2\varepsilon\mu<1$ they are described by modified Bessel functions $I_n(|\kappa|\rho)$. According

to the terminology of Ref. [47], in the first case we term the electromagnetic waves as the bulk-surface waves, whereas in the second case the electromagnetic waves are represented as the surface waves. Using the Maxwell equations, we express other Fourier components of the electromagnetic fields in the cylinder region ($\rho < \rho_0$), as well as in the annular gap ($\rho_0 < \rho < \rho_b$), and on the other side of the beam ($\rho > \rho_0$) via the components $E_{zn}(\rho, q_z, \omega)$ and $H_{zn}(\rho, q_z, \omega)$.

We note that in nonrelativistic case, when $\beta^2 << 1$ and $\varepsilon\mu\beta^2 > 1$, the discontinuities of the tangential magnetic field components $H_{\varphi n}(\rho, q_z, \omega)$ and $H_{zn}(\rho, q_z, \omega)$ at the beam surface ($\rho = \rho_b$) are small values of the order of $O(\beta)$. Therefore, in what follows, in the boundary conditions at the beam surface ($\rho = \rho_b$), we suppose these components are continuous, and take into account only the discontinuity of the electric field component $E_{\rho n}(\rho, q_z, \omega)$.

Assuming the beam is nonrelativistic, and satisfying the above-mentioned boundary conditions at the cylinder and electron beam surfaces, we obtain the following dispersion equation for the beam-cylinder coupled waves:

$$\Delta[(\omega - q_z v_0)^2 - \Gamma(q_z, n)\omega_b^2] = \alpha\omega_b^2, \tag{2.17}$$

where $\omega_b = \sqrt{4\pi e^2 N_0 / m}$ is the plasma frequency of beam electrons; $\Gamma(q_z, n)$ is the depression factor of space charge forces [43], and

$$\Gamma(q_z, n) = \frac{a}{\rho_b}(n^2 + q_z^2\rho_b^2) I_n(|q_z|\rho_b) K_n(|q_z|\rho_b)\left[1 - \frac{I_n(|q_z|\rho_0) K_n(|q_z|\rho_b)}{I_n(|q_z|\rho_b) K_n(|q_z|\rho_0)}\right]; \tag{2.18}$$

α is the coupling factor of the beam with cylinder eigenmodes that has the form

$$\alpha = \frac{a}{\rho_b}(n^2 + q_z^2\rho_b^2)\frac{K_n^2(|q_z|\rho_b)}{q_z^2\rho_0^2 K_n^2(|q_z|\rho_0)}\Delta^H; \tag{2.19}$$

$$\Delta = \Delta_0 - \Delta^E\Delta^H; \tag{2.20}$$

$$\Delta_0 = \left[\frac{nq_z\omega(\varepsilon\mu - 1)}{q^2\kappa^2\rho_0^2 c}\right]^2; \tag{2.21}$$

$$\Delta^E = \frac{1}{|q|\rho_0}\frac{K_n'(|q|\rho_0)}{K_n(|q|\rho_0)} + \frac{\varepsilon}{\kappa\rho_0}\frac{J_n'(\kappa\rho_0)}{J_n(\kappa\rho_0)}; \qquad \Delta^H = \frac{1}{|q|\rho_0}\frac{K_n'(|q|\rho_0)}{K_n(|q|\rho_0)} + \frac{\mu}{\kappa\rho_0}\frac{J_n'(\kappa\rho_0)}{J_n(\kappa\rho_0)}. \tag{2.22}$$

Note that Eq. (2.17) has the form analogous to the characteristic equation of a traveling-wave tube [43]. In our case, it describes the interaction of the beam space-charge waves (SCWs) with the cylinder

eigenmodes. Dispersion equations for the beam SCWs and the cylinder eigenmodes are described by the following equations

$$(\omega - q_z v_0)^2 - \Gamma(q_z, n)\omega_b^2 = 0 \qquad \text{and} \qquad \Delta = 0. \tag{2.23}$$

The equation $\Delta = 0$ can be interpreted as the dispersion equation of hybrid E- and H-type waves. The symmetric $(n = 0)$ cylinder E-type eigenmodes are characterized by the equation $\Delta^E = 0$, whereas the symmetric H-type waves are characterized by the equation $\Delta^H = 0$. For hybrid E- and H-type waves the conditions $|E_{zn}(\rho, q_z, \omega_p)|_{\max} / |H_{zn}(\rho, q_z, \omega_p)|_{\max} > 1$ and $|E_{zn}(\rho, q_z, \omega_p)|_{\max} / |H_{zn}(\rho, q_z, \omega_p)|_{\max} < 1$ (where the index "max" indicates the maximum value of the corresponding component) are satisfied, respectively. From these facts, it transpires that the wave type is determined by the dominant axial component of the electromagnetic field [88]. In the mode double subscript $p \equiv ns$, the radial index s represents the number of field variations along the radial coordinate and corresponds to the pair of roots order number of the equation $\Delta = 0$, whose solutions determine the frequencies ω_p of the cylinder eigenmodes with the longitudinal wave number q_z. In the case of symmetric waves, the index s corresponds to the root order number of the corresponding dispersion equation: $\Delta^E = 0$ or $\Delta^H = 0$. In the dispersion equation $\Delta = 0$ the role of the coupling factor between the E- and H-waves is played by the quantity Δ_0. If $n = 0$, the dispersion equation $\Delta = 0$ splits into two independent equations $\Delta^E = 0$ and $\Delta^H = 0$. In this case, the electromagnetic fields of symmetric waves have three components: $E_{\rho 0s}$, $H_{\varphi 0s}$ and E_{z0s} for E-waves, and $H_{\rho 0s}$, $E_{\varphi 0s}$, H_{z0s} for H-waves (here $E_{zns} \equiv E_{zn}(\rho, q_z, \omega_p)$, $H_{zns} \equiv H_{zn}(\rho, q_z, \omega_p)$, et cetera, (where $p \equiv 0s$). If $n \neq 0$, all electric and magnetic fields components of the cylinder eigenmodes are non-zero, and, therefore, they are the hybrid E- and H-type waves.

In the case of $\rho_0 \to 0$ (i.e. the cylinder is absent in the electrodynamic system), we have $\alpha/\Delta \to 0$, and the solutions of dispersion equation Eq. (2.17) determine the frequencies of the beam slow (ω_-) and fast (ω_+) beam SCWs:

$$\omega_- = q_z v_0 - R_0(q_z, n)\omega_b; \tag{2.24}$$

$$\omega_+ = q_z v_0 + R_0(q_z, n)\omega_b, \tag{2.25}$$

where $R_0(q_z, n) = \sqrt{\Gamma_0(q_z, n)}$ is the reduction factor [43], and

$$\Gamma_0(q_z, n) = \lim_{\rho_0 \to 0} \Gamma(q_z, n) = \frac{a}{\rho_b}(n^2 + q_z^2 \rho_b^2) I_n(|q_z| \rho_b) K_n(|q_z| \rho_b). \tag{2.26}$$

As follows from Eqs. (2.24) and (2.25), the phase velocities of the slow and fast SCWs are respectively less and greater than the beam velocity v_0.

Our goal is to determine the frequencies of the cylinder eigenmodes and the increments (decrements) of the beam-cylinder coupled waves. When the beam is absent in the system ($\omega_b = 0$), the dispersion equation, Eq. (2.17), is reduced to the dispersion equation for the cylinder eigenmodes $\Delta = 0$. Hence, we determine the cylinder eigenmodes ω_p. The frequencies ω_p are changed because of the interaction of the beam with the cylinder, and, as a result, small frequency corrections $|\delta\omega| << \omega_p$ are occurred. They are small because the plasma frequency of the beam electrons is less than the frequencies of the cylinder eigenmodes ($\omega_b < \omega_p$). Just this case is of interest because the cylinder eigenmodes are excited. Then Eq. (2.17) can be represented as follows:

$$\delta\omega^3 + 2(\omega_p - q_z v_0)\delta\omega^2 + [(\omega_p - q_z v_0)^2 - \Gamma(q_z, n)\omega_b^2]\delta\omega - \frac{\alpha(\omega_p)}{\Delta'_\omega(\omega_p)}\omega_b^2 = 0\,, \qquad (2.27)$$

where $\Delta'_\omega(\omega_p)$ is the frequency derivative of Δ, which is calculated at the cylinder eigenfrequency ω_p. The case of resonances is of the greatest interest. If the electron velocity v_0 satisfies the condition $\omega_p = q_z v_0$ (the Cherenkov resonance [89]) and $\Gamma(q_z, n) = 0$, then from Eq. (2.27) we obtain

$$\delta\omega^3 = \frac{\alpha(\omega_p)}{\Delta'_\omega(\omega_p)}\omega_b^2\,. \qquad (2.28)$$

This case is realized if $\rho_b = \rho_0$. If $\rho_b \neq \rho_0$, then Eq. (2.28) remains valid when the condition $R(q_z, n)\omega_b << |\delta\omega|$ is satisfied. The value $R(q_z, n)\omega_b$ makes sense of the effective (or reduced) plasma frequency of the beam [43]. Note that Eq. (2.28) has three roots, one of which is real and the other two are complex-conjugate roots. One of the complex-conjugate roots has a positive imaginary part, which leads to a wave amplitude rise with time. A root with a negative imaginary part refers to a damped wave with time. From Eq. (2.28) we determine the following expression for the instability increment:

$$\mathrm{Im}\,\delta\omega = \frac{\sqrt{3}}{2}\left|\frac{\alpha(\omega_p)}{\Delta'_\omega(\omega_p)}\right|^{1/3}\omega_b^{2/3}\,. \qquad (2.29)$$

Since, according to Eq. (2.29), the instability increment is proportional to $N_0^{1/3}$, the excitation of the cylinder eigenmodes by resonant beam particles (whose velocity satisfies the condition $\omega_p = q_z v_0$) is coherent [90]. As noted above, this instability is caused by the Cherenkov effect.

Note that if $\rho_b > \rho_0$ the resonant interaction of the electron beam with the cylinder eigenmodes is possible at frequencies

$$\omega_p^{\pm} = \omega_{\pm} = q_z v_0 \pm R(q_z, n)\omega_b .$$

If the condition $R(q_z, n)\omega_b >> |\delta\omega|$ is valid, Eq. (2.27) takes the form

$$\delta\omega^2 = \pm \frac{\alpha(\omega_p^{\pm})\omega_b}{2R(q_z, n)\Delta'_{\omega}(\omega_p^{\pm})} . \tag{2.30}$$

In Eq. (2.30) the plus sign before the fraction corresponds to the frequency ω_p^+, and the minus sign is for the frequency ω_p^-. It is evident, the condition $\delta\omega^2 < 0$ is only valid at the frequencies ω_p^-. ***This means that the instability emerges only if the slow space-charge wave interacts with the cylinder eigenmodes*** (***the anomalous Doppler effect*** [89]). The interaction of the fast space-charge wave with the cylinder eigenmodes results only in the appearance of real corrections to the frequencies ω_p^+. Thus, Eq. (2.30) has two real roots for ω_p^+ and two complex-conjugate roots for ω_p^-. The root with a positive imaginary part corresponds to an increasing with time wave. In case of the anomalous Doppler effect, from Eq. (2.30) we obtain the following expression for the instability increment:

$$\mathrm{Im}\,\delta\omega = \left[\frac{\alpha(\omega_p^-)\omega_b}{2R(q_z, n)\Delta'_{\omega}(\omega_p^-)} \right]^{1/2} . \tag{2.31}$$

It follows from Eq. (2.31), the instability increment is proportional to the $N_0^{1/4}$.

To gain a better insight into the interaction mechanism of the charged particles of tubular beam with the cylinder waves, below we present the numerical analysis results of the dispersion equation, Eq. (2.17), and the expression for the instability increment, Eq. (2.29), corresponding to Cherenkov resonance. The fact is that waves excited under the Cherenkov resonance conditions are characterized by greater instability increments (by 10 or more times) than the waves excited under the anomalous Doppler effect conditions.

2.3. Numerical Analysis of the Dispersion Equation

It is convenient to carry out a numerical analysis of the dispersion equation, Eq. (2.17), using the following dimensionless quantities: $\bar{\kappa} = \kappa\rho_0$,

$\bar{q} = q\rho_0$, $\bar{q}_z = q_z\rho_0$, $\bar{\rho}_b = \rho_b / \rho_0$, $\bar{a} = a / \rho_0$, $\bar{\omega} = \omega / \omega_0$, $\bar{\omega}_L = \omega_L / \omega_0$, $\bar{\omega}_r = \omega_r / \omega_0$, where $\omega_0 = c / \rho_0$. In calculations, we choose the following geometric and material parameters of the cylinder: $\rho_0 = 0.5$ cm; $F = 0.56$; $\bar{\omega}_L = 2$; $\bar{\omega}_r = 1$; $\bar{\omega}_{\mu=0} = \omega_{\mu=0} / \omega_0 \approx 1.51$ (it is the frequency at which $\mu = 0$). The values of the equilibrium beam electron density N_0, the radial thickness of the beam a, and the directed motion velocity the beam electrons are chosen as follows: $N_0 = 7.6\times10^{10}$ cm^{-3}, a =0.05 cm and $v_0 = 0.3c$, respectively. For the selected system parameters, we have $\omega_0 = 6\times10^{10}$ c^{-1}, and $\omega_b^2/\omega_0^2 \approx 0.07$, and the value $\bar{q}_z = 1$ refers to $q_z = 2$ cm^{-1} and the corresponding wavelength $\lambda = 2\pi / q_z = \pi$ cm.

2.3.1. The spectra of the cylinder eigenmodes

Before proceeding to the analysis of the dispersion characteristics of the cylinder eigenmodes, let us analyze the frequency dependences of ε and μ shown in Fig. 2.2. Curves 1 and 2 correspond to the dependences $\varepsilon(\bar{\omega})$ and $\mu(\bar{\omega})$, respectively. Curve 3 corresponds to the value $\mu(\bar{\omega}) = 1 - F$. Straight lines 4, 5 and 6 correspond to the frequencies $\bar{\omega} = \bar{\omega}_r$, $\bar{\omega} = \bar{\omega}_{\mu=0}$ and $\bar{\omega} = \bar{\omega}_L$, respectively. In Fig. 2.2 there are the following four frequency regions depending on the combinations of the signs of $\varepsilon(\bar{\omega})$ and $\mu(\bar{\omega})$: I) $0 < \bar{\omega} < \bar{\omega}_r$, where $\varepsilon < 0$, $\mu > 0$; II) $\bar{\omega}_r < \bar{\omega} < \bar{\omega}_{\mu=0}$, where $\varepsilon < 0$, $\mu < 0$; III) $\bar{\omega}_{\mu=0} < \bar{\omega} < \bar{\omega}_L$, where $\varepsilon < 0$, $\mu > 0$; IV) $\bar{\omega} > \bar{\omega}_L$, where $\varepsilon > 0$, $\mu > 0$. The permeability $\mu(\bar{\omega})$ tends to plus or minus infinity at $\bar{\omega} \to \bar{\omega}_r - 0$ or $\bar{\omega} \to \bar{\omega}_r + 0$, respectively.

Since in the frequency region I the conditions $\kappa^2 < 0$ and $\Delta^H < 0$ are simultaneously satisfied then E-type surface electromagnetic waves can only exist in it.

In the frequency region II, the conditions $\varepsilon < 0$ and $\mu < 0$ are simultaneously satisfied. Therefore the cylinder metamaterial behaves like the left-handed medium. In this frequency range, the conditions $\kappa^2 < 0$ and $\kappa^2 > 0$ can simultaneously be satisfied. This fact means the possibility of the simultaneous existence of bulk-surface and surface electromagnetic waves at the same frequency, but with different values of the wave number q_z. The analogous feature of the left-handed medium properties, namely, the ability to sustain the existence (at the same frequency) of bulk-surface and surface waves in case of a plane interface between a left-handed medium and a vacuum was demonstrated in Refs. [79,84,91].

In the frequency region III, just as in the frequency region I, the conditions $\kappa^2 < 0$ and $\Delta^H < 0$ are simultaneously valid. Therefore, the E-type surface electromagnetic waves can only exist.

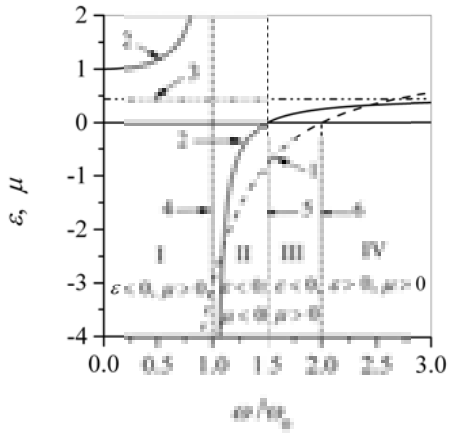

Fig. 2.2. Frequency dependences $\varepsilon(\bar{\omega})$ and $\mu(\bar{\omega})$. Curves 1 and 2 correspond to the dependences $\varepsilon(\bar{\omega})$ and $\mu(\bar{\omega})$, respectively. Curve 3 corresponds to the value $\mu(\bar{\omega}) = 1 - F$, where F = 0.56. Straight lines 4, 5 and 6 correspond to $\bar{\omega}_r$ = 1, $\bar{\omega}_{\mu=0} \approx 1.51$ and $\bar{\omega}_L$ = 2, respectively

In the region of frequencies IV, the condition $\kappa^2 > 0$ holds and, consequently, the E- and H-type bulk-surface waves can only exist. When the condition $\kappa^2 < 0$ holds we have $\Delta^E < 0$ and $\Delta^H < 0$ that indicates the absence solutions of dispersion equations $\Delta^E = 0$ and $\Delta^H = 0$. It follows that it is not possible the surface symmetric ($n = 0$) electromagnetic waves exist in this frequency range.

The region II is of the greatest interest for us because the cylinder material behaves there like a left-handed medium. Therefore, we will concentrate our attention on studying the features of the dispersion dependences of electromagnetic waves in this frequency region. Hereafter, we will evaluate the roots of corresponding dispersion equations using the simplex method for minimization a function of several variables [92].

Fig. 2.3 shows the dispersion dependences of the cylinder symmetric eigenmodes ($n = 0$). Straight lines 1, 2 and 3 correspond to $\bar{\omega} = \bar{\omega}_r$ and $\bar{\omega} = \bar{\omega}_{\mu=0}$, and the light line in vacuum $\bar{\omega} = \bar{q}_z$, respectively. Curve 4 corresponds to the solution of the equation $\bar{\kappa} = 0$. Straight lines 5 and 6 represent the frequencies at which $\varepsilon = -1$ and $\mu = -1$, respectively. Curves 7 and 8 refer to the E-type bulk-surface waves, and curves 9 and 10 are for the H-type bulk-surface waves. Curves 11 and 12 are the surface waves of E- and H-type, respectively. The empty circles show the starting (ending) points of the spectra of corresponding waves. Generally speaking, the values of $\bar{\omega}$ and $\bar{q}_z$ at these points do not satisfy the corresponding dispersion equations ($\Delta^E = 0$ or $\Delta^H = 0$).

It is seen from Fig. 2.3, the dispersion curves of bulk-surface waves (curves 7-10) are located in the region bounded by the straight lines 1 ($\bar{\omega} = \bar{\omega}_r$)

and 3 ($\bar{\omega} = \bar{q}_z$), and curve 4 ($\bar{\kappa} = 0$) where the conditions $\bar{q}^2 < 0$ and $\bar{\kappa}^2 > 0$ are satisfied. These dispersion curves originate from the light line $\bar{\omega} = \bar{q}_z$ in a vacuum. To the left of this line they convert in the dispersion curves of cylinder bulk eigenmodes, when $\bar{q}^2 > 0$, and consequently, the fields in vacuum are described by the Hankel functions of the first kind [88]. These modes cannot be excited by a beam of charged particles moving in a vacuum, since in this case $\bar{q}^2 < 0$. Therefore, they are not of interest to us. The coordinates of the starting points of the spectra of bulk-surface modes on the light line in vacuum for arbitrary values of the index n are determined from the conditions $\bar{\omega} = \bar{q}_z$ and $\Delta = 0$. Since the equation $\Delta = 0$ has infinitely many solutions, there exist infinity many starting points of the couple branches of E- and H-waves. Here, the density of such branches will increase as the frequency $\bar{\omega}$ approaches the resonance value of $\bar{\omega}_r$, when $\kappa \to \infty$. As noted above the order number of the couple branches of E- and H-waves corresponds to the mode radial index s. Consequently, in Fig. 2.3 the value $s = 1$ is for the couple curves 7 and 9, and the value $s = 2$ is for the couple curves 8 and 10. Using the classification proposed in Ref. [88], the branches 7 and 9 refer to the E_{01} and H_{01} modes, respectively. Here, the first index corresponds to the value of n, and the second one is for the value s. Similarly, the branches 8 and 10 represent the dispersion dependencies of E_{02} and H_{02} modes, respectively. Note that the dispersion curves with values $s > 2$ that are located in pairs below the curves for E_{02} and H_{02} modes are not shown in Fig. 2.3.

From Fig. 2.3, it follows that the dispersion dependences of the bulk-surface modes E_{01} and H_{01} (curves 7 and 9) have normal dispersion, and on the curve $\bar{\kappa} = 0$ they convert to the dispersion curves of the E- (curve 11) and H-type (curve 12) surface waves, respectively. The dispersion dependences of the bulk-surface modes E_{02} and H_{02} (curves 8 and 10) have parts with normal and anomalous dispersion, and if $\bar{q}_z \to \infty$ they approach the straight line $\bar{\omega} = \bar{\omega}_r$ asymptotically. Note that the dispersion dependences of the bulk-surface modes with $s > 2$ are similar to the dependences for E_{02} and H_{02} modes. Dispersion dependences of the surface E- and H-waves (curves 11 and 12) have normal dispersion. If $\bar{q}_z \to \infty$, the frequency of the surface E-wave (curve 11) approaches asymptotically the frequency at which $\varepsilon = -1$ (line 5), and the frequency of the H-wave (curve 12) approaches the frequency at which $\mu = -1$ (line 6).

Let us consider the dispersion dependences of the cylinder unsymmetrical eigenmodes ($n \neq 0$) in the frequency range where $\varepsilon < 0$ and $\mu < 0$. In Fig. 2.4, the spectra of cylinder eigenmodes with the azimuthal index $n = 1$ are shown. Note that the qualitative behavior of the dispersion dependences of cylinder eigenmodes with $n > 1$ is similar to the dependences for the modes with $n = 1$. The lines 1-6 are same as in Fig. 2.3. Curves 7 and 8

correspond to the hybrid type bulk-surface modes with the radial index $s = 1$, and curves 9 and 10 are for the bulk-surface hybrid modes with $s = 2$. The empty circles show the starting (ending) points of the spectra of corresponding waves. Note that the values of $\bar{\omega}$ and $\bar{q}_z$ at these points do not satisfy the dispersion equation $\Delta = 0$.

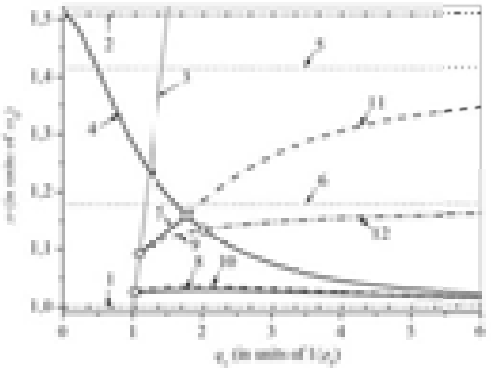

Fig. 2.3. Dispersion dependences of the cylinder symmetric eigenmodes ($n = 0$) in the frequency region where $\varepsilon < 0$ and $\mu < 0$. Lines 1, 2 and 3 represent straight lines $\bar{\omega}_r = 1$ and $\bar{\omega}_{\mu=0} \approx 1.51$, and the light line in vacuum $\bar{\omega} = \bar{q}_z$, respectively. Curve 4 is for the solution of the equation $\bar{\kappa} = 0$. Straight lines 5 and 6 are for the frequencies at which $\varepsilon = -1$ and $\mu = -1$, respectively. Curves 7 and 8 refer to the E-type bulk-surface waves, and curves 9 and 10 are for the H-type bulk-surface waves. Curves 11 and 12 are for the surface waves of E- and H-type, respectively. The empty circles show the starting (ending) points of the spectra of corresponding waves

It is seen from Fig. 2.4, the dispersion dependences of the bulk-surface waves, labeled by the numbers 8, 9 and 10, have the parts with both normal and anomalous dispersion. The dispersion dependences of the bulk-surface modes with radial indices $s > 2$ are similar. They are located below the dependences of the hybrid modes with $s = 2$, and in Fig. 2.4 they are not shown. From Fig. 2.4, it follows that only one of the dispersion branches of the bulk-surface waves (curve 7) with normal dispersion converts to the branch of the surface wave (curve 12) on the curve $\bar{\kappa} = 0$. If $\bar{q}_z \to \infty$, the frequency of this surface wave approaches asymptotically the frequency at which $\mu = -1$ (line 6). In contrast to the dispersion diagram of the cylinder symmetric waves (Fig. 2.3), in Fig. 2.4 the second branch of the surface wave (curve 11), whose frequency tends to the frequency at which $\varepsilon = -1$ (line 5) if $\bar{q}_z \to \infty$, has the starting point at the intersection of the light line $\bar{\omega} = \bar{q}_z$ in vacuum (line 3) and the curve $\bar{\kappa} = 0$ (curve 4).

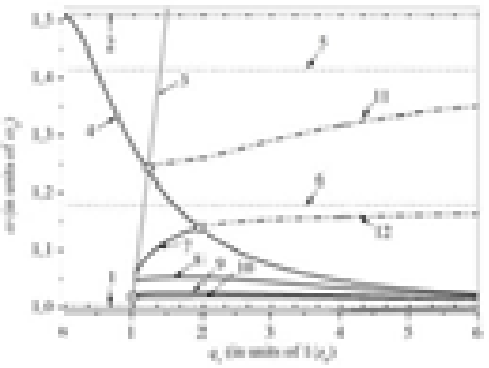

Fig. 2.4. Dispersion dependences of the cylinder unsymmetrical eigenmodes with the azimuthal index $n=1$ *in the frequency range where* $\varepsilon<0$ *and* $\mu<0$ *. Lines 1-6 are same as in Fig. 2.3. Curves 7 and 8 correspond to the hybrid type bulk-surface modes with the radial index* $s=1$*, and curves 9 and 10 are for the bulk-surface hybrid modes with* $s=2$*. The empty circles show the starting (ending) points of the spectra of corresponding waves*

2.3.2. Spectra of coupled waves. Absolute and convective instabilities

Let us ascertain the nature of instability that occurs in the Cherenkov resonant interaction between the electron beam and cylinder eigenmodes under the condition $R(q_z,n)\omega_b << |\delta\omega|$ and the condition of an extremely small distance of the beam from the cylinder. Henceforward, we will suppose that $\rho_b=\rho_0$.

It is well-known that if for real q_z we find complex ω with $\mathrm{Im}\omega>0$, a field of monochromatic wave, $\sim\exp[i(q_z z-\omega t)]$, will grow in time without bounds and the electrodynamic system will be unstable [90]. It is apparent that the increase of field amplitude without bounds is valid only in the linear approximation of the electrodynamic system under consideration. At the same time in realistic electrodynamic systems a nonlinear stage in the beam instability develops as the filed amplitude increase [91]. There are absolute and convective instabilities. Let us recall that an absolute instability implies the growth of the initial perturbation without bounds for given z as $t\to\infty$. If, however, the perturbation remains bounded for given z and $t\to\infty$, one talks about a convective instability. These instabilities find wide use in generation and amplification of electromagnetic waves (see, e.g., [42-44,90]).

Now our goal is to establish the nature of the instability in a small vicinity of the intersection points of the eigenmode dispersion curves with the beam wave $\bar{\omega}=\bar{q}_z\beta$ (the so-called resonance points). Hereafter, we use the well-known Sturrock method [90,94]. To this end, we represent the values of $\bar{\omega}$ and $\bar{q}_z$ near the resonance points $(\bar{q}_{z,res},\bar{\omega}_{res})$ in the following way:

$$\bar{\omega} = \bar{\omega}_{res} + \delta\bar{\omega}\,; \qquad \bar{q}_z = \bar{q}_{z,res} + \delta\bar{q}_z\,, \tag{32}$$

where $|\delta\bar{\omega}| << \bar{\omega}_{res}$ and $|\delta\bar{q}_z| << \bar{q}_{z,res}$.

For the sake of simplicity and without loss of physical generality, we only consider the case of symmetric modes (where $n=0$). Substituting expressions from Eq. (2.32) into Eq. (2.17) and performing the necessary expansions in terms of small variations of $\delta\bar{q}_z$ and $\delta\bar{\omega}$ about the corresponding resonance values, we obtain the following equation:

$$(\delta\bar{\omega} - \beta\delta\bar{q}_z)^2(\delta\bar{\omega} - \bar{v}_{gr}\delta\bar{q}_z) = \bar{a}\,\bar{\omega}_b^2\left(\frac{\partial\Delta^E}{\partial\bar{\omega}}\right)^{-1}_{\bar{q}_{z,res},\bar{\omega}_{res}}, \tag{2.33}$$

where $\bar{v}_{gr} = -\left(\frac{\partial\Delta^E}{\partial\bar{q}_z}\right)_{\bar{q}_{z,res},\bar{\omega}_{res}}\left(\frac{\partial\Delta^E}{\partial\bar{\omega}}\right)^{-1}_{\bar{q}_{z,res},\bar{\omega}_{res}}$ is the dimensionless group velocity (in units of the velocity of light in vacuum) of the electromagnetic wave, the values of $(\partial\Delta^E/\delta\bar{q}_z)_{\bar{q}_{z,res},\bar{\omega}_{res}}$ and $(\partial\Delta^E/\delta\bar{\omega})_{\bar{q}_{z,res},\bar{\omega}_{res}}$ are the corresponding partial derivatives of Δ^E calculated at the resonance point $(\bar{q}_{z,res},\bar{\omega}_{res})$. It is worthwhile to emphasize that only symmetric E-type eigenmodes (when $n=0$) are unstable because their electromagnetic fields have nonzero components of the electric field E_z. Note that only these components cause the interaction between the metamaterial eigenmodes and the nonrelativistic beam electrons. All further results keep valid for the excitation of unsymmetrical eigenmodes ($n\neq 0$) near the corresponding resonance points.

Let us consider the instability regions of the electrodynamic system under consideration near the points of intersection of the dispersion dependence for the beam wave ($\bar{\omega} = \bar{q}_z\beta$) with the dispersion curves of symmetric E-type bulk-surface waves and with the dispersion curve of the E-type surface wave.

Figure 2.5 presents the dispersion dependencies of the symmetric eigenmodes and the beam wave. Line 1 refers to the light line in vacuum ($\bar{\omega} = \bar{q}_z$), curve 2 is for $\bar{\kappa} = 0$, line 3 is for the beam wave ($\bar{\omega} = \bar{q}_z\beta$). Curves 4 and 5 correspond to the bulk-surface waves H_{02} and E_{02}, respectively, and curves 6 and 7 are for the surface waves of H- and E-type, respectively. Points A and B correspond to the intersection of the dispersion dependence of the beam wave with the dispersion curve of the bulk-surface wave E_{02} and with the E-type surface wave, respectively.

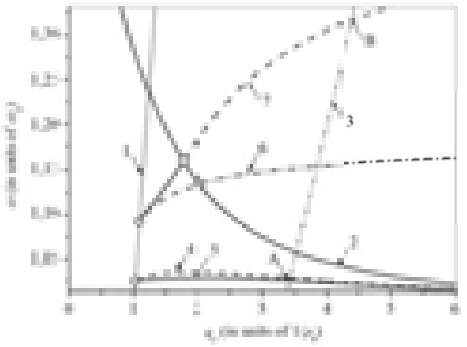

Fig. 2.5. Dispersion curves of the symmetric eigenmodes and the beam wave. Line 1 refers to the light line in vacuum, curve 2 is for $\bar{\kappa} = 0$ *, line 3 is for the beam wave (*$\bar{\omega} = \bar{q}_z \beta$ *). Curves 4 and 5 correspond to the bulk-surface waves* H_{02} *and* E_{02}*, respectively, and curves 6 and 7 are for the surface waves of H- and E-type, respectively. Points A and B correspond to the intersection of the dispersion dependence of the beam wave with the dispersion curves of the bulk-surface wave* E_{02} *and with the E-type surface wave, respectively*

Figure 2.6 presents the dispersion dependencies of the wave (which are the solutions of Eq. (2.33)) excited by the beam in small vicinity of point A with coordinates $\bar{q}_{z,res} = 1.025$ and $\bar{\omega}_{res} = 3.42$. Lines 1 and 2 refer to the values $\delta\bar{q}_z = 0$ and $\delta\bar{\omega} = 0$, line 3 is for the asymptote $\delta\bar{\omega} = \bar{v}_{gr}\delta\bar{q}_z$, line 4 is for $\delta\bar{\omega} = \beta\delta\bar{q}_z$, curves 5 and 6 are for the wave E_{02} excited by the beam.

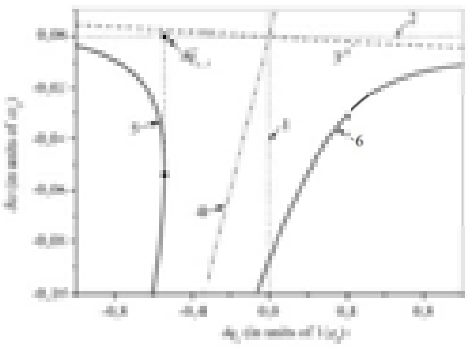

Fig. 2.6. Dispersion curves of the wave E_{02} *excited by the beam in small vicinity of point A with coordinates* $\bar{q}_{z,res} = 1.025$ *and* $\bar{\omega}_{res} = 3.42$*. Lines 1 and 2 refer to the values* $\delta\bar{q}_z = 0$ *and* $\delta\bar{\omega} = 0$*, line 3 is for the asymptote* $\delta\bar{\omega} = \bar{v}_{gr}\delta\bar{q}_z$*, line 4 is for* $\delta\bar{\omega} = \beta\delta\bar{q}_z$*, curves 5 and 6 are for the wave* E_{02} *excited by the beam. It is seen that the absolute instability occurs*

Since the dispersion equation, Eq. (2.33), is a cubic one, then, as known, it has three different real roots or one real root and two complex-conjugate roots [95]. As one of these complex roots has positive imaginary part, the instability develops. As seen from Fig. 2.6, the instability occurs at all values of δq_z that greater than $\delta q_{z,0}$. It is also seen that asymptotes 3 and 4 are inclined in different directions with respect to line 2. The negative slope of asymptote 3 is caused by the negative value of the group velocity of corresponding mode ($\bar{v}_{gr} \approx -4.2\times10^{-3}$). In accordance with the first Sturrock rule (see Ref. [90,94]) this signifies the occurrence of the absolute instability.

Fig. 2.7 shows the dispersion dependencies of the E-type surface wave excited by the beam in small vicinity of point B with coordinates $\bar{q}_{z,res} \approx 4.39$ and $\bar{\omega}_{res} \approx 1.32$. Lines 1 and 4 have the same meaning as those in Fig. 2.6. Curves 5 and 6 correspond to the dispersion curves of the E-type surface wave excited by the beam.

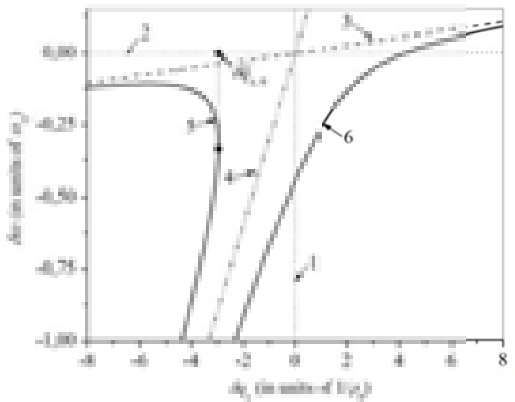

Fig. 2.7. Dispersion curves of the E-type surface wave excited by the beam in small vicinity of point B with coordinates $\bar{q}_{z,res} \approx 4.39$ and $\bar{\omega}_{res} \approx 1.32$. Lines 1 and 4 have the same meaning as those in Fig. 2.6. Curves 5 and 6 correspond to the dispersion curves of the E-type surface wave excited by the beam. It is seen that the convective instability occurs

From Fig. 2.7 it follows that the instability occurs at all values of δq_z greater than $\delta q_{z,0}$. Unlike the case shown in Fig. 2.6, asymptotes 3 and 4 are inclined in the same direction with respect to line 2. The positive slope of asymptote 3 is caused by the positive value of the group velocity of corresponding mode. In accordance with the first Sturrock rule (see Refs. [90,94]) this means the occurrence of the convective instability.

2.3.3. Analysis of instability increments

Let us dwell on the dependences of instability increments $\delta\bar{\omega}$ for bulk-surface waves on the values of azimuthal n and radial s mode indices. These increment values are calculated using the formula Eq. (2.29). Before moving on, we want to briefly remark on the type of waves excited by a beam. As noted above, if $n=0$ the beam excites the symmetric E_{0s} modes with radial indices $s\geq 2$. If $n\geq 1$ the cylinder eigenmodes have nonzero values of all electromagnetic field components and, therefore, they are the hybrid type modes. In Refs. [88,96], it was provided a method for the separation of such modes into the so-called HE_{ns} and EH_{ns} modes depending on the predominant axial component of electromagnetic field, i.e. on the ratio of the maximum values of field components $|E_{zn}(\rho,q_z,\omega_p)|_{\max}$ and $|H_{zn}(\rho,q_z,\omega_p)|_{\max}$. If the axial component of electric field dominates ($|E_{zn}(\rho,q_z,\omega_p)|_{\max}/|H_{zn}(\rho,q_z,\omega_p)|_{\max}>1$), the eigenmode is the HE_{ns} mode (E-type), otherwise it is the EH_{ns} mode (H-type). Numerical analysis of excited modes with azimuthal indices $n\geq 1$ shows that in the resonance points, in which $\bar{q}_z=\bar{q}_{z,res}$ and $\bar{\omega}_p=\bar{\omega}_{res}$, we have $|E_{zn}(\bar{\rho},\bar{q}_{z,res},\bar{\omega}_{res})|_{\max}/|H_{zn}(\bar{\rho},\bar{q}_{z,res},\bar{\omega}_{res})|_{\max}>1$. This implies that in a cylinder made of a metamaterial with $\varepsilon(\bar{\omega})<0$ and $\mu(\bar{\omega})<0$ the nonrelativistic ($\beta<<1$) electron beam excites the E-type eigenmodes.

As a matter of fact, the analytic estimations of the ratio $|E_{zn}(\bar{\rho},\bar{q}_{z,res},\bar{\omega}_{res})|_{\max}/|H_{zn}(\bar{\rho},\bar{q}_{z,res},\bar{\omega}_{res})|_{\max}$ for the modes with $n\geq 1$ and $s\geq 1$ show that if $\beta\to 0$ (that is equivalent to $\bar{q}_z\to\infty$) we have

$$\frac{|E_{zn}(\bar{\rho},\bar{q}_{z,res},\bar{\omega}_{res})|_{\max}}{|H_{zn}(\bar{\rho},\bar{q}_{z,res},\bar{\omega}_{res})|_{\max}}\propto\sqrt{\frac{\mu(\bar{\omega})}{\varepsilon(\bar{\omega})}}.$$

Since $|\mu(\bar{\omega})|\to\infty$ and $\varepsilon(\bar{\omega})$ remains finite quantity if $\bar{q}_z\to\infty$ and $\bar{\omega}(\bar{q}_z)\to\bar{\omega}_r$ (i.e. the dispersion curves of bulk-surface waves approach the straight line $\bar{\omega}=\bar{\omega}_r$ asymptotically), we have $|E_{zn}(\bar{\rho},\bar{q}_{z,res},\bar{\omega}_{res})|_{\max}/|H_{zn}(\bar{\rho},\bar{q}_{z,res},\bar{\omega}_{res})|_{\max}\to\infty$. This explains the fact that at the resonance points $(\bar{q}_{z,res},\bar{\omega}_{res})$, if $\bar{q}_{z,res}>1$, we have $|E_{zn}(\bar{\rho},\bar{q}_{z,res},\bar{\omega}_{res})|_{\max}/|H_{zn}(\bar{\rho},\bar{q}_{z,res},\bar{\omega}_{res})|_{\max}>1$.

Consequently, in electrodynamic system under study, the tubular electron beam excites coupled bulk-surface symmetric E_{0s} modes with radial indices $s\geq 2$ and hybrid $HE_{ns}^{\pm}$ modes with radial indices $s\geq 1$, where the subscripts "–" and "+" refer to the low-frequency and high-frequency branches of the pairs of dispersion dependencies for cylinder eigenmodes, respectively. In doing so, it is supposed that the cylinder is made of the metamaterial, which possesses left-handed properties in the frequency

range of interest. In this case, the absolute instability of the aforementioned modes occurs.

Fig. 2.8 shows the increment values $\mathrm{Im}\bar{\omega}$ of excited bulk-surface modes with azimuthal indices in the range $n = 0...20$. In Fig 2.8(*a*) and Fig. 2.8(*b*), these values correspond to the low-frequency and high-frequency branches of the pair of dispersion curves, respectively. Note in Fig. 2.3 and 2.4 the dispersion dependences for the modes with $n = 0$, 1 and $s = 1$, 2 are only shown. The increment values are grouped in accordance with the radial index s of cylinder eigenmodes, which is determined by the order number of the pair of dispersion curves. In Fig. 2.8(*a*), the dependences of the increment values of the E_{0s} and HE_{ns}^{-} modes with the radial indices $s = 1$, 2, 3 on the azimuthal index n are labeled by the numbers 1, 2 and 3, respectively. In Fig. 2.8(*b*), the numbers 1, 2 and 3 are for the dependences of the increment values of the HE_{ns}^{+} modes with $s = 3$, 5, 7 on the azimuthal index n, respectively.

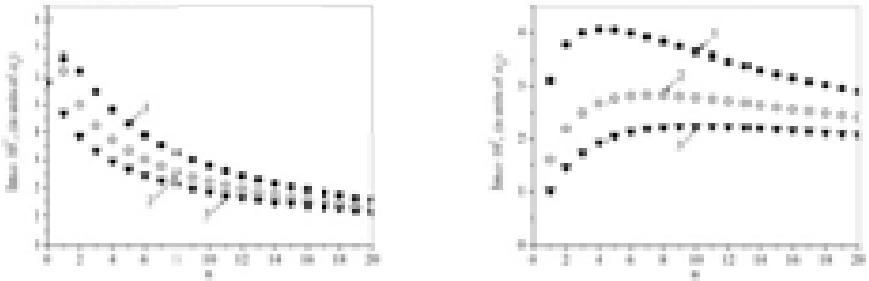

(*a*) (*b*)

Fig. 2.8. Instability increment values of electrodynamic system with the bulk-surface modes corresponding to the low-frequency (a) and high-frequency (b) branches of the pairs of dispersion dependences for cylinder eigenmodes

In Fig. 2.8(a), the dependences of the increment values of the E_{0s} and the HE_{ns}^{-} modes with the radial indices $s = 1$, 2, 3 on the azimuthal index n are labeled by the numbers 1, 2 and 3, respectively. In Fig. 2.8(b), the numbers 1, 2 and 3 are for the dependences of the increment values of the HE_{ns}^{+} modes with $s = 3$, 5, 7 on the azimuthal index n, respectively.

The analysis of the instability shows that the symmetric bulk-surface E_{02} mode has the maximum increment. In Figs. 2.8 the increments $\mathrm{Im}\bar{\omega}$ decrease with increasing n because both the value of $|\mu(\bar{\omega}_{res})|$ and its frequency derivative in the denominator of Eq. (2.29) increase with frequency. In fact, with increasing n at fixed value of s the resonant frequencies $\bar{\omega}_{res}$ tend to the frequency $\bar{\omega}_r$ at which the cylinder permeability increases indefinitely. It is seen from Fig. 2.8(b), the value of azimuthal index n that corresponds to the

maximum increment of the HE_{ns}^{+} mode increases with radial index s. Therefore, on curve 3 the $HE_{10\,7}^{+}$ mode has maximum increment. This enables the excitation of the weak decaying whispering gallery modes with large values of azimuthal index n in the electrodynamic system under study.

2.4. Conclusions

The instability of nonrelativistic tubular electron beam that moves above a dispersive metamaterial of cylindrical configuration has been theoretically examined. It has been assumed that the metamaterial possesses negative permittivity and negative permeability simultaneously over a certain frequency range where it behaves like a LHM. The dispersion equations for eigenmodes of the cylinder and for the coupled modes of the system as well as the instability increments have been derived. The instability is shown to be caused by Cherenkov or anomalous Doppler effects depending on the radial distance between the cylinder and the beam.

The numerical analysis of the dispersion curves of the eigenmodes of the cylinder and the coupled modes excited by the beam in the frequency region where the metamaterial demonstrates the left-handed behavior has been performed. It has been revealed that the parts of the dispersion curves of the bulk-surface waves with anomalous dispersion emerge. The latter implies negative group velocities of corresponding waves and results in the absolute character of the beam instability. It has been found that the resonance behavior of magnetic permeability of the metamaterial leads to the fact that all bulk-surface waves excited by the beam are the E-type waves for the resonance values of frequencies and wave vectors. The numerical analysis of the dependencies of the instability increments on azimutal and radial mode indices has been performed. We have shown that the HE_{ns}^{+} modes with large radial indices ($s >> 1$) are the whispering-gallery modes for which $n >> 1$.

Thus, this suggests applications of LHMs as delaying media for the generation of bulk-surface waves and eliminates the need for creating artificial feedbacks in slow-wave structures.

SECTION 3. NONLINEAR STABILIZATION OF INSTABILITY OF AN ELECTRON BEAM MOVING ABOVE A SOLID STATE CYLINDER

3.1. Introduction

In the last decade, much attention has been paid to the development of millimeter- and submillimeter-wave oscillators. This has been motivated by the extensive use of such radiation in biology [97] and medicine [98], for transmitting submillimeter signals in the Earth's atmosphere [99], for

implementing broadband wireless communication [100] and submillimeter wave spectroscopy [101], and in other applications of science and technology.

Search for new mechanisms of generation of electromagnetic waves within millimeter- and submillimeter- wave range by charged particle beams propagating in various electrodynamic systems is an important problem of modern radiophysics and electronics. The motion of charged particle beams in such systems is accompanied by the development of instabilities, including electrostatic ones, which leads to the generation of various types of oscillations. A stationary mode is established as a result of nonlinear interaction of charged particles with the eigenwaves of the electrodynamic system. We note that, until now, nonlinear stabilization of beam instabilities has been considered only for cases of collisionless and weakly collisional plasmas.

Nonlinear waves in plasma without allowance for thermal effects were first studied by A.I. Akhiezer, G.Ya. Lyubarskii, and R.V. Polovin more than half a century ago [102-104]. In particular, they showed that the frequency of nonlinear plasma oscillations is independent of the amplitude only in the nonrelativistic limit. It was shown in [104] that, in the relativistic case, the period of an intense plasma wave increases with increasing amplitude. Among the first studies on the nonlinear theory of beam–plasma instabilities where nonlinear stabilization of these instabilities due to the trapping of the beam electrons by a plasma wave was considered, it is worth mentioning works [105-119]. In those works, modulated and unmodulated relativistic beams interacting with plasma, which was assumed to be cold and collisionless (or weakly collisional), were considered. The density of the beam electrons was assumed to be much lower than the plasma electron density. It was shown that the efficiency of the beam-plasma interaction increases with increasing relativistic factor of the beam, in spite of a decrease in the linear growth rate.

We recall the results of some of the above-cited works, the analytical approach of which was used in this study. In [115,116], a nonlinear theory of instability of diffuse and monoenergetic electron beams in an unbounded (bulk) plasma was constructed. Thus, in [115], a system of equations describing the time evolution of the wave amplitude, as well as the coordinates and velocities of the beam electrons, in a diffuse electron beam (in which instability is kinetic) was derived using the method of slowly varying (compared to the wave period) amplitudes. It was shown that only the motion of the resonant beam particles with velocities close to the wave phase velocity is essentially nonlinear. A specific feature of the nonlinear stage of instability in the case of a diffuse beam is the damping of amplitude oscillations due to the phase mixing of the beam particles trapped by the wave field. This effect was first noted in [107, 108] and then subjected to thorough research, e.g., in [47,118,120]. For a monoenergetic beam, as was shown in [115,116], it is necessary to take into account time variations not only of the amplitude, but also of the phase of the excited wave. The nonlinear stages of instability of premodulated nonrelativistic and

relativistic monoenergetic beams in plasma were studied in [116]. In particular, it was shown that, in the relativistic case, the maximum energy of the excited wave field is comparable with the beam energy.

The nonlinear stabilization of beam–plasma instability of a nonrelativistic monoenergetic beam in a dense unbounded collisional plasma was considered in [117,118]. As in [115,116], the beam was simulated by a discrete ensemble of macroparticles (charged sheets). It was shown that, due to collisions, the beam particles do not have time to gather into a bunch by the time of trapping and have a noticeable scatter in both velocities and coordinates. Therefore, the trapping of particles by the wave does not lead to regular oscillations of the wave amplitude, as was observed, e.g., in [116].

In [119], an electrodynamic system close to that considered in the present work was studied for the case of collisionless gaseous plasma. In [119], nonlinear stabilization of instability of a finite-thickness tubular electron beam moving along a plasma cylinder in an external longitudinal magnetic field was considered. It was assumed that the beam–plasma system was placed in a metal waveguide, and the plasma was assumed to be cold and collisionless. Nonlinear stabilization of an axisymmetric surface TM wave was considered. In [121], excitation of surface electromagnetic waves propagating along a cylindrical surface of a conducting medium (metal, highly ionized plasma) by a relativistic electron beam moving along the cylinder was studied. The maximum amplitude of the excited wave was estimated from the condition of the nonlinear trap-ping of the beam electrons by the surface wave field.

The nonlinear theory of instability of a rectilinear relativistic electron beam in a bounded plasma under the Cherenkov resonance conditions was developed in [120–123]. In particular, the case of a dense plasma was considered when the unstable plasma wave excited by the beam was a potential one [122]. It was established that the nonlinear processes caused by the beam relativity prevent the system from being randomized in the stage of well-developed nonlinear instability. In contrast, in the case of a nonrelativistic beam, anomalous nonlinear chaotization of the beam is observed.

In the past decade, special attention has been paid to cylindrical systems in which a tubular electron beam [124,125] or a multijet f low of a circular cross section [56,62,63,126,127] move along a solid-state cylinder. In [63], a self-consistent nonlinear theory of the excitation of electromagnetic waves by an azimuthally periodic high-current relativistic electron beam interacting with a two-layer cylindrical dielectric resonator (CDR) was developed. Analysis of the nonlinear excitation of a CDR by an electron beam shows that the main mechanism for generation of electromagnetic oscillations in the resonator of this self-oscillatory sys-tem [56,126,127] is the so-called monotronic mechanism, when the beam particles flying through the resonator are grouped in such a phase of the excited electromagnetic field that their energy is, on the average, transferred to the resonator eigenmodes. The possibility of using such a self-oscillatory system with acceptable geometrical parameters in the submillimeter

wavelength range was noted in [63,126]. In addition, beam instabilities that arise in electrodynamic systems containing dispersive media are of particular interest. In particular, instability of a tubular electron beam interacting with a plasma-like medium was studied in [128] in the linear approximation, while that interacting with a left-handed dispersive medium of cylindrical configuration was studied in [129]. The interaction of a nonrelativistic tubular charged particle beam with a nonmagnetic anisotropic dispersive solid-state cylinder was considered in [130,131]. The possibility of excitation of absolute instability of bulk–surface waves due to specific features of an anisotropic cylinder has been discovered. The resonant character of the frequency dependence of the dielectric constant of the cylinder favors the emergence of the sections of the dispersion curves corresponding to E-type bulk–surface eigenmodes with a negative group velocity.

The debatable aspects of the theory of nonpotential surface waves excited on the boundary of a dissipative medium with frequency dispersion were considered in [132]. It was shown that, for a sufficiently strong dissipation of the energy of perturbations in the medium, surface waves the dispersion law of which differs dramatically from the conventional one may be excited. These waves are weakly damped even at a large dissipation in the medium, while their group and phase velocities exceed the speed of light in the medium.

A special place is occupied by the works devoted to beam–plasma instabilities in highly collisional solid-state plasma, when the collision frequency of charge carriers is much higher than the frequency of the excited electromagnetic (electrostatic) wave. Thus, in [133], the so-called resistive instability arising due to the absorption in the dielectric medium through which the electron beam propagates was studied. Excitation of millimeter and submillimeter plasma waves by a charged particle beam in semiconductor plasma was analyzed in [134,135].

In this part of the section, a nonlinear theory of resistive instability of a tubular electron beam moving along a solid-state plasma cylinder is constructed in an electrostatic approximation by using Poisson's equation and the equation of electron motion. The continuous tubular electron beam is represented as a set of macroparticles (charged rings). The nonlinear stabilization of the emerging instability is investigated by the method of slow varing in time amplitudes and phases of the electrostatic wave. Using the Runge–Kutta method with a variable step, the numerical analysis of a self-consistent system of equations describing the time evolution of the wave amplitude and phase, as well as the coordinates and velocities of the macroparticles, is carried out. Phase portraits of the system are constructed, from the analysis of which it follows that nonlinear stabilization of the wave amplitude occurs due to the effect of self-trapping of beam electrons by the field of the beam wave itself.

3.2. Nonlinear Stabilization of Resistive Instability of a Tubular Charged Particle Beam Moving Above a Solid-State Plasma Cylinder

3.2.1 Statement Of The Problem And Basic Equations

Let a solid-state plasma cylinder occupy the spatial region $0 \le \rho \le \rho_0$, $0 \le \varphi \le 2\pi$ and $|z| < \infty$ in cylindrical coordinates (the Z axis is aligned with the cylinder axis). A charged particle beam with equilibrium density n_0 and the velocity $v_0 << c$ (where c is the speed of light in vacuum) moves along the cylinder surface. Such an electrodynamic system is easily implemented by placing the cylinder in the drift space of a rectilinear tubular beam of radius $\rho_0 + a/2$. We assume that the beam thickness a is infinitely small and there is vacuum outside the beam ($\rho > \rho_0$).There is no direct contact between the beam and the cylinder surface.

The interaction of an electron beam with eigenmodes (oscillations) of a dielectric cylinder is described by the set of electrostatic equations supplemented with the constitutive equation and the equation of motion of plasma electrons,

$$\mathrm{rot}\mathbf{E}(\mathbf{r},t) = 0\,, \tag{3.1}$$

$$\mathrm{div}\mathbf{D}(\mathbf{r},t) = 4\pi e n(\mathbf{r},t)\,, \tag{3.2}$$

$$\mathbf{D}(\mathbf{r},t) = \varepsilon_0 \mathbf{E}(\mathbf{r},t) + 4\pi e N_0 \int_{-\infty}^{t} \mathbf{u}(\mathbf{r},t')dt'\,, \tag{3.3}$$

$$\frac{\partial \mathbf{u}(\mathbf{r},t)}{\partial t} = \frac{e}{m}\mathbf{E}(\mathbf{r},t) - \nu \mathbf{u}(\mathbf{r},t)\,, \tag{3.4}$$

where $\mathbf{E}(\mathbf{r},t)$ is the electric field at a point with the radius vector $\mathbf{r}$ at a time t, $\mathbf{D}(\mathbf{r},t)$ is the electric displacement, e is the electron charge, $n(\mathbf{r},t)$ is the electron beam density, ε_0 is the dielectric constant of the lattice, N_0 is the equilibrium electron density in the plasma cylinder, m is the electron effective mass, ν is the relaxation frequency of electron momentum in the plasma cylinder, and $\mathbf{u}(\mathbf{r},t)$ is the velocity of plasma electrons.

The beam electron density $n(\mathbf{r},t)$ is described by the expression

$$n(\mathbf{r},t) = n(z,t)\delta(\rho - \rho_0)\,,$$

where $n(z,t)$ is the electron beam surface density, $\delta(x)$ is the Dirac delta function, and

$$n(z,t) = \int f(z,t,v_z)dv_z . \tag{3.5}$$

The beam electron distribution function $f(z,t,v_z)$ in expression (3.5) satisfies the Vlasov equation

$$\frac{\partial f(z,t,v_z)}{\partial t} + v_z(t)\frac{\partial f(z,t,v_z)}{\partial z} + \frac{e}{m_0}E_z(\rho_0,z,t)\frac{\partial f(z,t,v_z)}{\partial v_z} = 0,$$

where m_0 is the mass of a free electron and $E_z(\rho_0,z,t)$ is the electric field on the beam surface $\rho = \rho_0$.

At the initial time $t = 0$, i.e., before the onset of instability, the distribution function $f(z,0,v_z)$ has the form

$$f(z,0,v_z) \equiv f_0(v_z) = n_0 a\delta(v_z - v_0),$$

where n_0 is the equilibrium bulk electron beam density. Below, we limit ourselves to considering azimuthally symmetric electrostatic waves and introduce the electric field potential $\psi(\rho,z,t)$ such that

$$\mathbf{E}(\rho,z,t) = -\nabla\psi(\rho,z,t). \tag{3.6}$$

The potential of the wave $\psi(\rho,z,t)$ and its radial derivative $\partial\psi(\rho,z,t)/\partial\rho$ satisfy the boundary conditions on the cylinder surface: the continuity of the $\psi(\rho,z,t)$ and a jump in its derivative due to the presence of the beam surface charge $en(z,t)$. We recall that these conditions are equivalent to the continuity condition for the z component of the electric field and the jump in the radial component of the electric displacement vector,

$$E_z(\rho_0 + 0,z,t) = E_z(\rho_0 - 0,z,t),$$

$$E_\rho(\rho_0 + 0,z,t) - D_\rho(\rho_0 - 0,z,t) = 4\pi en(z,t).$$

The continuity condition for the potential at the cylinder boundary has the form

$$\psi(\rho_0 - 0,z,t) = \psi(\rho_0 + 0,z,t). \tag{3.7}$$

To obtain the condition for the jump in the potential derivative $\partial\psi(\rho,z,t)/\partial\rho$, we take the time derivative of both sides of Eq. (3.2) and make use of Eqs. (3.3) and (3.4). Then, for the case of strong collisions,

$$\nu\left|\mathbf{u}(\mathbf{r},t)\right| >> \left|\frac{\partial\mathbf{u}(\mathbf{r},t)}{\partial t}\right|,$$

we obtain

$$\varepsilon_0\left[\frac{1}{\rho}\frac{\partial}{\partial\rho}\left(\rho\frac{\partial}{\partial\rho}\right)+\frac{\partial^2}{\partial z^2}\right]\frac{\partial\psi(\rho,z,t)}{\partial t}=-\frac{\omega_p^2}{\nu}\left[\frac{1}{\rho}\frac{\partial}{\partial\rho}\left(\rho\frac{\partial}{\partial\rho}\right)+\frac{\partial^2}{\partial z^2}\right]\psi(\rho,z,t)-4\pi e\frac{\partial n(\mathbf{r},t)}{\partial t}$$

,

where $\omega_p=\sqrt{4\pi e^2 N_0/m}$ is the plasma frequency of the cylinder medium. The boundary condition for the potential derivative $\partial\psi(\rho,z,t)/\partial\rho$ is obtained by calculating integrals of the form

$$\lim_{\eta\to 0}\int_{\rho_0-\eta}^{\rho_0+\eta}(...)\rho d\rho$$

on both sides of the above equality over an infinitely small beam thickness η. After integration, we obtain the following boundary condition for the radial derivative of the potential:

$$\frac{\partial}{\partial t}\frac{\partial\psi(\rho,z,t)}{\partial\rho}\bigg|_{\rho=\rho_0+0}-\varepsilon_0\frac{\partial}{\partial t}\frac{\partial\psi(\rho,z,t)}{\partial\rho}\bigg|_{\rho=\rho_0-0}=\frac{\omega_p^2}{\nu}\frac{\partial\psi(\rho,z,t)}{\partial\rho}\bigg|_{\rho=\rho_0-0}-4\pi e\frac{\partial n(z,t)}{\partial t}. \tag{3.8}$$

Following [115,116,136], the surface density $n(z,t)$ can be represented in the form

$$n(z,t)=\frac{2\pi n_0 a}{qM}\sum_{p=1}^{M}\delta[z-z_p(z_0,v_0,t)]. \tag{3.9}$$

According to expression (3.9), a continuous tubular electron beam is represented as a set of macroparticles (charged rings), with M being the number of charged rings per wavelength. The coordinate $z_p(z_0,v_0,t)$ describes the position of the p th macroparticle. We note that the coordinate $z_p(z_0,v_0,t)$ and velocity $v_{zp}(z_0,v_0,0)$ of the p th macroparticle are solutions to the system of characteristic equations

$$\begin{cases} \dfrac{dz(z_0,v_0,t)}{dt} = v_z(z_0,v_0,t) \\ \dfrac{dv_z(z_0,v_0,t)}{dt} = -\dfrac{e}{m_0}\dfrac{\partial\psi(\rho,z,t)}{\partial z} \end{cases}$$

with the initial conditions

$$z(z_0,v_0,0) = z_0,\ v_z(z_0,v_0,0) = v_0. \tag{3.10}$$

In what follows, we will analyze the time evolution of the amplitude and phase of the wave, as well as the coordinates and velocities of macroparticles, in the coordinate system associated with the beam. To this end, we make the replacement

$$z_p(z_0,v_0,t) = v_0 t + \tilde{z}_p(z_0,v_0,t), \tag{3.11}$$

$$v_{zp}(z_0,v_0,t) = v_0 + \tilde{v}_{zp}(z_0,v_0,t), \tag{3.12}$$

where $\tilde{z}_p(z_0,v_0,t)$ and $\tilde{v}_{zp}(z_0,v_0,t)$ are perturbations of the coordinate and longitudinal velocity of the p th macroparticle. Then, initial conditions (3.10) take the form

$$\tilde{z}_p(z_0,v_0,0) = \tilde{z}_{p0}, \qquad \tilde{v}_{zp}(z_0,v_0,0) = 0.$$

We represent the potential $\psi(\rho,z,t)$ as

$$\psi(\rho,z,t) = \psi_0(\rho)\psi_A(t)\exp\{i[q_z z - \omega t + \alpha(t)]\}, \tag{3.13}$$

where the wavenumber q_z and frequency ω of the electrostatic wave are related to the beam electron velocity by the Vavilov–Cherenkov resonance condition $\omega = q_z v_0$. Recall that the Cherenkov resonance with the condition $\omega = q_z v_0$ means the effect of excitation of eigenmodes of the cylinder under study as a result of longitudinal bunching of electrons in the field of the excited wave and the formation of emitting electron bunches in its decelerating phases. The quantities $\psi_A(t)$ and $\alpha(t)$ in Eq. (3.13) are the slowly varying amplitude and phase of the electrostatic wave. The relevant "slowness" conditions are

$$\frac{1}{\psi_A(t)}\frac{\partial\psi_A(t)}{\partial t} << \omega,\ \frac{1}{|\alpha(t)|}\left|\frac{\partial\alpha(t)}{\partial t}\right| << \omega.$$

Taking into account representation (3.13), we find from Eqs. (3.3) and (3.4) that, for the case of strong collisions, $\mathbf{D}(\mathbf{r},\omega)=\varepsilon(\omega)\mathbf{E}(\mathbf{r},\omega)$, where

$$\varepsilon(\omega)=\varepsilon_0+\frac{4\pi i\sigma}{\omega}, \tag{3.14}$$

$\sigma=e^2N_0/m\nu$ is the plasms cylinder conductivity. After substituting expressions (3.6) and (3.13) into Eq. (3.1), we find that the quantity $\psi_0(\rho)$ satisfies the Laplace equation

$$\frac{1}{\rho}\frac{\partial}{\partial\rho}\left(\rho\frac{\partial\psi_0(\rho)}{\partial\rho}\right)-q_z^2\psi_0(\rho)=0. \tag{3.15}$$

Taking into account that the quantity $\psi_0(\rho)$ is bounded at $\rho\to 0$ and $\rho\to\infty$ the solution to Eq. (3.15) can be represented in the form

$$\psi_0(\rho)=\begin{cases} I_0(q\rho), & \rho<\rho_0, \\ K_0(q\rho), & \rho>\rho_0, \end{cases} \tag{3.16}$$

where $q=|q_z|$, while $I_0(q\rho)$ and $K_0(q\rho)$ are zero-order modified Bessel functions of the first and second kind, respectively [41].

Our task is to study the time evolution of the quantities $\psi_A(t)$ and $\alpha(t)$. Using expressions (3.13) and (3.16), from the boundary condition (3.7) we obtain the following relations for amplitudes of the potential $\psi_A(t)$ and phase $\alpha(t)$ within the cylinder and in vacuum:

$$\psi_A(t)\big|_{\rho_0-0}=\frac{K_0(q\rho_0)}{I_0(q\rho_0)}\psi_A(t)\big|_{\rho_0+0}, \tag{3.17}$$

$$\alpha(t)\big|_{\rho_0-0}=\alpha(t)\big|_{\rho_0+0}. \tag{3.18}$$

Further, we will analyze the time evolution of the amplitude $\psi_A(t)$ and phase $\alpha(t)$ of the potential wave in the vacuum region (i.e., at $\rho>\rho_0$).

Using Eqs. (3.13), (3.15), (3.17), and (3.18), we rewrite boundary condition (3.8) in the form

$$\left[\Delta_0 \frac{\partial}{\partial t} + \frac{\omega_p^2}{\nu}\Delta_1\right]\psi_A(t)\exp\{i[q_z z - \omega t + \alpha(t)]\} = \frac{4\pi e}{qK_0(q\rho_0)}\frac{\partial n(z,t)}{\partial t}, \quad (3.19)$$

where $\Delta_0 = \varepsilon_0 \frac{I_0'(q\rho_0)}{I_0(q\rho_0)} - \frac{K_0'(q\rho_0)}{K_0(q\rho_0)}$, $\Delta_1 = \frac{I_0'(q\rho_0)}{I_0(q\rho_0)}$. Here, the prime denotes derivative of the corresponding special function with respect to its argument.

Next, following [117], we substitute Eq. (3.9) into Eq. (3.19) and perform the integration of the resulting equation over the oscillation period $2\pi/\omega$ with allowance for the Cherenkov resonance condition $\omega = q_z v_0$. Then, separating the real and imaginary parts and taking into account relations (3.11) and (3.12), we obtain the following system of equations describing the time evolution of the amplitude and phase of the wave, as well as the coordinates and velocities of the macroparticles:

$$\begin{cases} \dfrac{d\psi_A(t)}{dt} = -\dfrac{\omega_p^2}{\nu}\dfrac{\Delta_1}{\Delta_0}\psi_A(t) - \dfrac{4\pi e n_0 a\omega}{q\Delta_0 K_0(q\rho_0)M}\displaystyle\sum_{p=1}^{M}\sin[\mathrm{q}_z\tilde{z}_p(t)+\alpha(t)], \\ \dfrac{d\alpha(t)}{dt} = \omega - \dfrac{4\pi e n_0 a\omega}{q\Delta_0 K_0(q\rho_0)\psi_A(t)M}\displaystyle\sum_{p=1}^{M}\cos[\mathrm{q}_z\tilde{z}_p(t)+\alpha(t)], \\ \dfrac{d^2\tilde{z}_p(t)}{dt^2} = \dfrac{eq_z K_0(q\rho_0)}{m_0}\psi_A(t)\sin[\mathrm{q}_z\tilde{z}_p(t)+\alpha(t)]. \end{cases} \quad (3.20)$$

The last of Eqs. (3.20) describes the motion of the p macroparticle in the beam reference frame. To analyze this system, it is convenient to introduce the following dimensionless variables:

$$\phi = \frac{\psi_A(t)}{\psi_{\max}},\ \xi_p = q_z\tilde{z}_p(t),\ \eta_p = \frac{\tilde{v}_{zp}(t)}{v_0},\ \Omega = \frac{\omega}{\omega_p},\ \tau = \omega t,\ \alpha \equiv \alpha(t), \quad (3.21)$$

where $\psi_{\max}$ is the peak value of the wave potential at which the beam particles are trapped in the potential well of the wave. The expression for $\psi_{\max}$ will be given below.

To numerically analyze system of equations (3.20), we rewrite it in the form of a system of four first-order differential equations in dimensionless variables (3.21),

$$\begin{cases} \dfrac{d\phi}{d\tau} = -A\phi - \dfrac{B}{M}\sum\limits_{p=1}^{M}\sin(\xi_p + \alpha), \\ \dfrac{d\alpha}{d\tau} = 1 - \dfrac{B}{\phi M}\sum\limits_{p=1}^{M}\cos(\xi_p + \alpha), \\ \dfrac{d\xi_p}{d\tau} = \eta_p, \\ \dfrac{d\eta_p}{d\tau} = C\phi\sin(\xi_p + \alpha), \end{cases} \tag{3.22}$$

where $A = \omega_p^2\Delta_1 / v\omega$, $B = \sqrt{1 + A^2/\Delta_0^2}$, $C = aq\omega_b^2 / \omega^2\sqrt{A^2 + \Delta_0^2}$.

The quantity $\psi_{\max}$ is determined from the condition for the trapping of beam particles into the potential well of the wave [117],

$$K_0(q\rho_0)\psi_{\max} \propto \frac{m_0}{e}(v_0 - v_{ph})^2,$$

where v_{ph} is the wave phase velocity with allowance for the frequency shift caused by the interaction of the wave field with the electron beam.

Using the results of [137], the dispersion relation for the coupled waves of the beam and the plasma cylinder can be presented as

$$\Delta(\omega - q_z v_0)^2 = aq\omega_b^2. \tag{3.23}$$

Here, $\omega_b = \sqrt{4\pi e^2 n_0 / m_0}$ is the electron beam plasma frequency and

$$\Delta = \varepsilon(\omega)\frac{I_0'(q\rho_0)}{I_0(q\rho_0)} - \frac{K_0'(q\rho_0)}{K_0(q\rho_0)},$$

where $\varepsilon(\omega)$ is defined by expression (3.14). Note that the equation $\Delta = 0$ has no real solutions and describes the so-called Maxwell relaxation of the electrostatic field in collisional plasma. To find corrections to the resonance frequency $\omega_0 = q_z v_0$, the solution to Eq. (3.23) is sought in the form

$$\omega = \omega_0 + \delta\omega, \tag{3.24}$$

where $|\delta\omega| << \omega_0$. Substituting formula (3.24) into Eq. (3.23) and following the procedure of [90], we obtain

$$\delta\omega = \pm\omega_b \frac{(aq)^{1/2}}{(A^2+\Delta_0^2)^{1/4}}(\cos\varphi_0 - i\sin\varphi_0), \qquad (3.25)$$

$$\varphi_0 = \frac{1}{2}\operatorname{arctg}\frac{A}{\Delta_0}.$$

Solution (3.25) with the negative sign of the imaginary part corresponds to an increase in the amplitude of the symmetric coupled wave of the cylinder and the beam with the growth rate

$$\gamma = \omega_b \frac{(aq)^{1/2}}{(A^2+\Delta_0^2)^{1/4}}\sin\varphi_0 .$$

In this case, the phase velocity of the coupled wave is

$$v_{ph} = v_0 - \frac{\omega_b (aq)^{1/2}}{q_z (A^2+\Delta_0^2)^{1/4}}\cos\varphi_0 . \qquad (3.26)$$

According to Eq. (3.26), instability is inherent in a slow coupled wave. As a result, we obtain the following expression for $\psi_{\max}$:

$$\psi_{\max} = \frac{m_0 v_0^2 aq}{eK_0(q\rho_0)\sqrt{A^2+\Delta_0^2}}\left(\frac{\omega_b}{\omega}\right)^2 \cos^2\varphi_0 .$$

Note that, by definition, ϕ_0 does not exceed unity; therefore, we have, $\cos\varphi_0 > 0$. Note also that the use of the linear approximation for plasma electrons is justified, because, for a low-density electron beam $n_0 << N_0$, the amplitude of the excited potential wave is small and the condition $e\psi_{\max} << m_0 v_0^2$ is satisfied [136].

In the next section, we present results of numerical analysis of system of equations (3.22), as well as the phase portrait of the beam macroparticles, indicating the formation of bunches in the nonlinear stage of instability.

3.2.2 Numerical Analysis Of The System Of Nonlinear Equations

As a material of the plasma cylinder, we choose GaAs semiconductor with ε_0 = 13,2, $m = 0.063\,m_0$, $\nu = 10^{13}$ s^{-1}, and $N_0 = 10^{13}$ cm^{-3}. We analyze cylinders of radii $\rho_0 = 0.5$ cm, and 1 cm, as well as $\rho_0 \to \infty$ (limiting case of a plane interface between the media). The equilibrium electron density of the beam n_0, beam wall thickness a, and the directed velocity of the electron beam v_0 are chosen as follows: $n_0 = 10^{10}$ cm^{-3}, $a = 0.01$ cm and

$v_0 = 0.1c$, respectively. In this case, we have $\omega_b / \omega_p \approx 8 \cdot 10^{-3}$. The resonance wavelength is assumed to be $\lambda = 2$ cm, which corresponds to the resonance frequency $\omega = 1.7 \cdot 10^{10}$ s^{-1} and growth rate $\gamma \approx 10^8$ s^{-1} ($\gamma / \omega \approx 0.01$).

Figure 3.1 shows $\phi \equiv \phi(\tau)$ as a function of the dimensionless time τ for cylinders with the radii $\rho_0 = 0.5$ cm (curve 1), $\rho_0 = 1$ cm (curve 2) and $\rho_0 \to \infty$ (curve 3). We remind that curve 3 corresponds to a plane interface between the media. System of equations (3.22) was solved numerically by the Runge–Kutta method. The electron beam was simulated by individual macroparticles (charged rings) uniformly distributed at the initial time within the interval of $0 \le \xi_p \le 2\pi$. The number of macroparticles M was 500. It should be noted that the numerical code made it possible to perform integration with variable steps by specifying the relative error at each step. The initial amplitude was assumed to be $\phi_0 = 10^{-4}$. The initial values of the slow phase α and its time derivative $d\alpha / d\tau$ were assumed to be zero.

It follows from Fig. 3.1 that the larger the radius of the cylinder, the larger the maximum amplitude $\phi_{\max}$ corresponding to instability saturation. This, for $\rho_0 = 0.5$ cm, we have $\phi_{\max} \approx 0.58$, whereas for $\rho_0 = 1$ cm we have $\phi_{\max} = 0.64$. In addition, for the cylinder with a smaller radius, the slowly varying amplitude reaches its maximum value $\phi_{\max}$ earlier (at $\tau \equiv \tau_{\max} \approx 1569$, which corresponds to the time $t \equiv t_{\max} \approx 16\gamma^{-1}$, than for the cylinder with a larger radius (at $\tau \equiv \tau_{\max} \approx 1718$, which corresponds to the time $t \equiv t_{\max} \approx 17\gamma^{-1}$). Note that, as the cylinder radius increases, the dependences $\phi(\tau)$ tend to a certain common limiting time profile (curve 3), corresponding to $\Delta_0 \to \varepsilon_0 + 1$ and $\Delta_1 \to 1$. Physically, this limit corresponds to the case of a plane beam–plasma interface.

It also follows from Fig. 3.1 that at $\tau > \tau_{\max}$ the quantity ϕ oscillates around a certain average value. These oscillations are essentially irregular (chaotic) in character, because the macroparticles do not have time to gather in a bunch by the time of trapping and have an appreciable scatter in both velocities and coordinates. Qualitatively, such behavior of $\phi(\tau)$ resembles a similar dependence in [117], in which the nonlinear stage of beam–plasma instability in weakly collisionless unbounded plasma was considered. By weakly collisional plasma we mean plasma in which the collision frequency is lower than the plasma wave frequency but much higher than the instability growth rate. We note that the dependence $\phi(\tau)$ in [117] had the form of beatings associated with the presence of two characteristic times in the system: the bounce period of the particle bunch in the wave potential well and the period of variations in the potential well itself. In contrast to [117], in the solid-state plasma under consideration, the relaxation

frequency of the electron momentum satisfies the condition $\nu >> \omega >> \gamma$. As a result, by the time of trapping, the macroparticles do not form bunches and each macroparticle oscillates in the wave potential well individually.

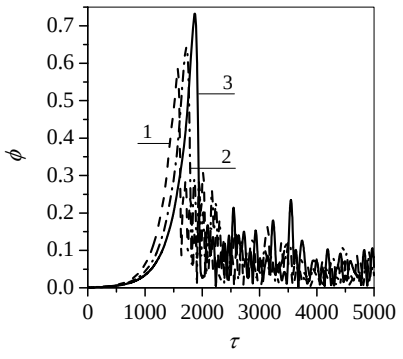

Fig. 3.1. Amplitude of the potential wave vs. dimensionless time for three values of the radius of the plasma cylinder: ρ_0 = 0.5 cm (curve 1), ρ_0 = 1 cm (curve 2), and $\rho_0 \to \infty$ (curve 3)

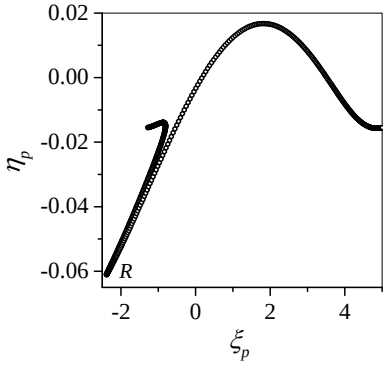

Fig. 3.2. Phase portrait of a system of M macroparticles at the time of instability saturation (τ = 1570)

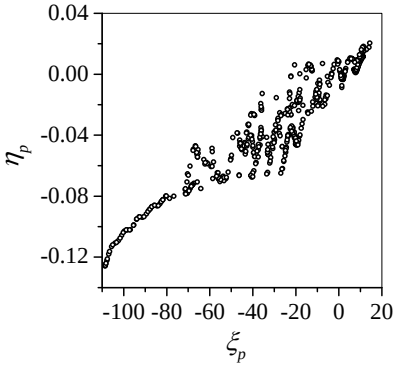

Fig. 3.3. Phase portrait of a system of M macroparticles at the time τ = 2550

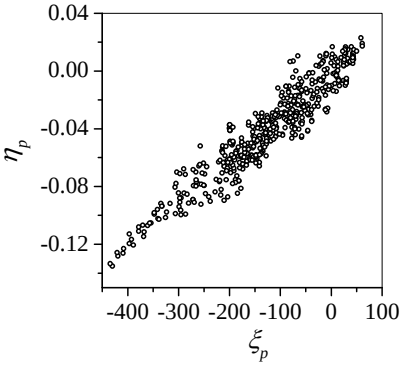

Fig. 3.4. Phase portrait of a system of M macroparticles at the time τ = 5000

Another fundamental difference between the considered case of solid-state plasma and results of [117,118] is that there are no eigenmodes in highly collisional plasma and, therefore, the beam particles are trapped by the plasma wave of the beam itself. Such a phenomenon was called self-trapping [136]. As noted in [113], it is the effect of electron self-trapping by the beam wave that leads to the chaotization of the electron beam and

disappearance of regular oscillations at the resonance frequency. Such behavior illustrated in Fig. 3.1 by the dependence $\phi(\tau)$.

The effect of self-trapping of the beam electrons and their subsequent chaotization is demonstrated by the phase portraits of macroparticles shown in Figs. 3.2–3.4 for ρ_0 = 0.5 cm. It can be seen from Fig. 3.2 that a group of reflected macroparticles (marked with the letter *R*) appears in the stage of instability saturation. The macroparticles are reflected from the humps of the beam potential wave. It is worth noting that the beam electrons are self-trapped by the beam wave in the nonlinear stage of instability of a quasi-monochromatic initial perturbation under the conditions of the collective Cherenkov effect [136].

Figures 3.3 and Fig. 3.4 show phase portraits of macroparticles for the times τ = 2550 and τ = 5000, corresponding to chaotic oscillations of the slowly varying amplitude. It can be seen that, after instability is saturated, the macroparticles occupy the progressively growing region in the phase plane and their distribution in this plane becomes more and more uniform. Physically, as noted above, this corresponds to chaotization of the beam electrons. In contrast to the weakly collisional case considered in [117], no trapped macroparticle bunches arise in this case.

3.2.3 Conclusions

The problem of nonlinear stabilization of instability of a tubular electron beam moving along the surface of a solid-state plasma cylinder has been solved. It is assumed that the beam is nonrelativistic, plasma is highly collisional, and the wave excited by the beam is electrostatic. It is shown that resistive instability is stabilized nonlinearly due to the self-trapping of the beam electrons by the beam wave. The time of instability saturation and the maximum amplitude of the wave have been analyzed as functions of the radius of the plasma cylinder. It is established that the larger the radius of the plasma cylinder, the later the nonlinear stage of instability begins and the larger the maximum value of the slowly varying amplitude. The limiting case of a plane interface between the electron beam and the solid-state plasma is considered. The results of this study expand our understanding of the physical properties of systems with plasma-like media and systematize our knowledge of the mechanisms of excitation of potential surface waves in electrodynamic systems that form the basis of microwave oscillators.

3.3. Numerical Analysis Of The Interaction Between A Tubular Beam Of Charged Particles And A Dielectric Cylinder

Here we theoretically study the nonlinear stabilization of the instability of a tubular electron beam, infinitely thin in the radial direction, when it moves along the surface of a solid dielectric cylinder. In contrast to

[63], the electromagnetic system considered is open, and the waves excited by the beam are azimuthally symmetric. In addition, unlike [63], we construct and analyze the time dependence of slowly varying amplitudes and phases of the electric and magnetic field components of the excited waves with different radial mode indices, as well as consider the question of wave polarization.

The excitation of an azimuthally sysmmetric eigenmode of the electric type of the solid cylinder under study is considered. The electron beam is presented in the form of a set of macroparticles (charged rings). We investigated the time evolution of the electromagnetic field of the excited wave by the method of amplitude and phase slowly varying in time. The self-consistent system of equations is obtained that describes both the time evolution of the wave amplitude and phase, and the coordinates and velocities of the beam. The analytical expression for the increment of the emerging instability is obtained. This system is numerically analysed with the use of the Runge–Kutta method with a variable step. The dependences of slowly varying amplitudes on time are plotted for three different values of the radial mode index. The criterion is established for the applicability of the used method of slowly varying amplitudes and phases of excited waves for the analysis of beam instability. The numerical analysis of the polarization of the excited waves is carried out.

3.3.1 Statement Of The Problem And Basic Equations

Suppose that a dielectric cylinder of radius ρ_0 occupies the region of space $0 \le \rho \le \rho_0$, $0 \le \varphi \le 2\pi$ and $|z| < \infty$ (the Z axis is directed along the cylinder axis). The cylinder is made of an isotropic nonmagnetic material with real permittivity ε. A beam of charged particles (electrons) with equilibrium density n_0 and velocity $v_0 << c$ (where c is the velocity of light in vacuum) moves along the surface of the cylinder. Such an electromagnetic system can easily be implemented if the cylinder is placed in the drift space of a rectilinearly moving tubular beam with radius $\rho_0 + a/2$. Assume that the thickness a of the beam is infinitely small and the medium outside the beam ($\rho > \rho_0$) is vacuum. There is no direct contact between the beam and the surface of the cylinder. It is assumed that the drift space is in a strong longitudinal (in the direction of the beam motion) external constant magnetic field, which prevents the transverse motion of the beam electrons. The threshold value of the external magnetic field restricting the motion of electrons along the radius and azimuth is found from the condition $\omega_H >> \omega_p$, where $\omega_H = |e| H_0 / m_0 c$ is the electron cyclotron frequency, $\omega_b = \sqrt{4\pi e^2 n_0 / m_0}$ is the plasma frequency of the beam electrons, e and m_0 are the charge and mass of a free electron, n_0 is the equilibrium bulk

density of beam electrons, and H_0 is the magnitude of the external magnetic field. For a beam with a characteristic density of $n_0 \propto 10^{10}$ cm^{-3}, we obtain $H_0 >> 336$ Oe (or $H_0 >> 26.7$ kA/m).

The system of equations describing the interaction of the electron beam with eigenwaves (oscillations) of the dielectric cylinder has the form

$$\mathrm{rot}\mathbf{H}(\mathbf{r},t) = \frac{1}{c}\frac{\partial \mathbf{D}(\mathbf{r},t)}{\partial t} + \frac{4\pi}{c}\mathbf{j}(\mathbf{r},t), \tag{3.27}$$

$$\mathrm{div}\mathbf{D}(\mathbf{r},t) = 4\pi e n(\mathbf{r},t), \tag{3.28}$$

$$\mathrm{rot}\mathbf{E}(\mathbf{r},t) = -\frac{1}{c}\frac{\partial \mathbf{H}(\mathbf{r},t)}{\partial t}, \tag{3.29}$$

$$\mathrm{div}\mathbf{H}(\mathbf{r},t) = 0, \tag{3.30}$$

where $\mathbf{H}(\mathbf{r},t)$ and $\mathbf{E}(\mathbf{r},t)$ are the magnetic and electric field strengths; $\mathbf{D}(\mathbf{r},t) = \varepsilon\mathbf{E}(\mathbf{r},t)$ is the electric field displacement vector; and $\mathbf{j}(\mathbf{r},t) = \left(0, 0, j_z(\mathbf{r},t)\right)$ and $n(\mathbf{r},t)$ are the bulk current density and the beam electron density, respectively, that satisfy the continuity equation

$$e\frac{\partial n(\mathbf{r},t)}{\partial t} + \mathrm{div}\mathbf{j}(\mathbf{r},t) = 0. \tag{3.31}$$

The quantities $j_z(\mathbf{r},t)$ $n(\mathbf{r},t)$ are determined by the expressions $j_z(\mathbf{r},t) = j_z(z,t)\delta(\rho - \rho_0)$ and $n(\mathbf{r},t) = n(z,t)\delta(\rho - \rho_0)$, where $j_z(z,t)$ and $n(z,t)$ are the surface densities of the corresponding quantities and $\delta(x)$ is the Dirac delta function. Note that, in linear theory, the surface current density $j_z(z,t)$ of the beam is specified in the linear approximation, where small perturbations of the electron velocity are related to the electric field by an appropriate equation of motion.

In what follows, we restrict the analysis to azimuthally symmetric electric-type (E-type) electromagnetic waves with the field components $E_\rho(\rho,z,t)$, $H_\varphi(\rho,z,t)$, and $E_z(\rho,z,t)$. In the absence of a beam, homogeneous wave equations describing the eigenfields in the cylinder are obtained from the corresponding system of homogeneous Maxwell equations (3.27)–(3.30) and have the form

$$\left[\frac{1}{\rho}\frac{\partial}{\partial\rho}\left(\rho\frac{\partial}{\partial\rho}\right) + \frac{\partial^2}{\partial z^2}\right]E_z(\rho,z,t) - \frac{\varepsilon}{c^2}\frac{\partial^2}{\partial t^2}E_z(\rho,z,t) = 0, \tag{3.32}$$

$$\left(\frac{\partial^2}{\partial z^2}-\frac{\varepsilon}{c^2}\frac{\partial^2}{\partial t^2}\right)E_\rho(\rho,z,t)=\frac{\partial^2}{\partial z\partial\rho}E_z(\rho,z,t), \tag{3.33}$$

$$\left(\frac{\partial^2}{\partial z^2}-\frac{\varepsilon}{c^2}\frac{\partial^2}{\partial t^2}\right)H_\varphi(\rho,z,t)=-\frac{\varepsilon}{c}\frac{\partial^2}{\partial t\partial\rho}E_z(\rho,z,t). \tag{3.34}$$

The corresponding equations for vacuum are derived from Eqs. (3.32)–(3.34) if we set $\varepsilon=1$. The solutions of Eq. (3.32) for the cylinder and vacuum regions for a bulk–surface wave with frequency ω and longitudinal wave number q_z have the form

$$E_z^{cyl}(\rho,z,t)=A_{cyl}J_0(\kappa\rho)\exp[i(q_z z-\omega t)], \tag{3.35}$$

$$E_z^{vac}(\rho,z,t)=A_{vac}K_0(q\rho)\exp[i(q_z z-\omega t)], \tag{3.36}$$

where $J_0(u)$ is the zero-order Bessel function of the first kind, $K_0(u)$ is the modified zero-order Bessel function of the second kind (the Macdonald function) [41], A_{cyl} and A_{vac} are arbitrary constants. The choice of solutions in the form of (3.35) and (3.36) is motivated by the condition that the fields remain finite as $\rho\to 0$ and $\rho\to\infty$. The quantity $\kappa^2=\varepsilon\omega^2/c^2-q_z^2$ represents the square of the transverse wave number in the, and $q^2=q_z^2-\omega^2/c^2$ is the square of the wave number in vacuum, taken with the opposite sign. It follows from the form of the solutions (3.35) and (3.36) that the fields of bulk–surface waves have an oscillatory character inside the cylinder and decrease in the direction normal to the cylinder surface – in the vacuum region.

Recall that, in the absence of a beam, the boundary conditions at $\rho=\rho_0$ for the field components are the continuity conditions for the tangential components of the electric and magnetic fields, as well as the continuity condition for the normal (radial) component of the electric displacement vector. In the presence of a beam that moves along the cylinder surface (at $\rho_b=\rho_0$), the boundary conditions at $\rho=\rho_0$ are the conditions for the continuity of the field component $E_z(\rho,z,t)$ and the jump of the component $D_\rho(\rho,z,t)$ associated with the presence of a perturbed charge of the beam:

$$E_z(\rho,z,t)\big|_{\rho=\rho_0+0}=E_z(\rho,z,t)\big|_{\rho=\rho_0-0}, \tag{3.37}$$

$$E_\rho(\rho,z,t)\Big|_{\rho=\rho_0+0}-\varepsilon E_\rho(\rho,z,t)\Big|_{\rho=\rho_0-0}=\frac{4\pi e}{\rho_0}\lim_{\Delta\rho\to 0}\int\limits_{\rho_0-\Delta\rho}^{\rho_0+\Delta\rho} n(z,t)\delta(\rho-\rho_0)\rho d\rho, \quad (3.38)$$

where integration is performed over the thickness of the beam. In what follows, we will use only the boundary conditions (3.37) and (3.38). We will determine the field components $H_\varphi(\rho,z,t)$ using Eq. (3.34). We need an equation relating the field components $E_\rho(\rho,z,t)$ and $E_z(\rho,z,t)$ to the surface electron density $n(z,t)$ of the beam at $\rho=\rho_0$. To obtain this equation, we write Eq. (3.33) for $\rho=\rho_0$, subtract a similar equation for the vacuum region from it, and apply the boundary condition (3.38) previously differentiated in time. As a result, we obtain

$$\frac{\partial^2 E_\rho(\rho,z,t)}{\partial z^2}\Big|_{\rho=\rho_0+0}-\frac{\partial^2 E_\rho(\rho,z,t)}{\partial z^2}\Big|_{\rho=\rho_0-0}=\frac{\partial^2 E_z(\rho,z,t)}{\partial z\partial\rho}\Big|_{\rho=\rho_0+0}-\frac{\partial^2 E_z(\rho,z,t)}{\partial z\partial\rho}\Big|_{\rho=\rho_0-0}+$$
$$+\frac{4\pi e}{c^2}\frac{\partial^2 n(z,t)}{\partial t^2}. \quad (3.39)$$

Following [115–120], we represent the surface density $n(z,t)$ as

$$n(z,t)=\frac{2\pi n_0 a}{q_z M}\sum_{p=1}^{M}\delta[z-z_p(z_{0p},v_{0p},t)], \quad (3.40)$$

Expression (3.40) implies that a continuous tubular flow of electrons is represented as a set of macroparticles (charged rings) whose number is M per length $2\pi/q_z$. The coordinate $z_p(z_{0p},v_{0p},t)$ describes the position of the individual p th macroparticle. Note that the coordinate $z_p(z_{0p},v_{0p},t)$ and the velocity $v_{zp}(z_{0p},v_{0p},t)$ of the p th macroparticle are solutions to the equations of motion

$$\begin{cases}\dfrac{dz_p(z_{0p},v_{0p},t)}{dt}=v_{zp}(z_{0p},v_{0p},t),\\ \dfrac{dv_{zp}(z_{0p},v_{0p},t)}{dt}=\dfrac{e}{m_0}\mathrm{Re}[E_z(\rho_0,z_p,t)],\end{cases} \quad (3.41)$$

with the initial conditions $z_p(z_{0p},v_{0p},0)=z_{0p}$ and $v_{z_p}(z_{0p},v_{0p},0)=v_{0p}$. In what follows, we will analyze the time evolution of the amplitude and phase of the wave, as well as the coordinates and velocities of the macroparticles in the coordinate system fixed to the beam. To this end, we make the change

$$z_p(z_{0p}, v_{0p}, t) = v_0 t + \tilde{z}_p(\tilde{z}_{0p}, \tilde{v}_{0p}, t),$$

$$v_{zp}(z_{0p}, v_{0p}, t) = v_0 + \tilde{v}_{zp}(\tilde{z}_{0p}, \tilde{v}_{0p}, t),$$

where $\tilde{z}_p(\tilde{z}_{0p}, \tilde{v}_{0p}, t)$ and $\tilde{v}_{zp}(\tilde{z}_{0p}, \tilde{v}_{0p}, t)$ are perturbations of the coordinate and longitudinal velocity of the p th macroparticle. Then the system of equations (3.41) and the corresponding initial conditions are rewritten as

$$\begin{cases} \dfrac{d\tilde{z}_p(\tilde{z}_{0p}, \tilde{v}_{0p}, t)}{dt} = \tilde{v}_{zp}(\tilde{z}_{0p}, \tilde{v}_{0p}, t), \\ \dfrac{d\tilde{v}_{zp}(\tilde{z}_{0p}, \tilde{v}_{0p}, t)}{dt} = \dfrac{e}{m_0} \operatorname{Re}\left\{E_z(\rho_0, \tilde{z}_p, t)\right\}, \end{cases} \tag{3.42}$$

and $\tilde{z}_p(\tilde{z}_{0p}, \tilde{v}_{0p}, 0) = \tilde{z}_{p0}$ and $\tilde{v}_{zp}(\tilde{z}_{0p}, \tilde{v}_{0p}, 0) = \tilde{v}_{0p}$. Henceforth we will assume that the beam is monovelocity at the initial moment of instability development. Therefore, we assume that, in the coordinate system fixed to the beam, the initial velocity perturbations of macroparticles are zero, i.e., $\tilde{v}_{0p} = 0$.

Equations (3.33) and (3.34), analogous equations for the vacuum region, and Eqs. (3.39) and (3.42) along with the boundary condition (3.37) represent a closed system of self-consistent nonlinear equations describing the time evolution of the fields excited by the beam. To solve this system, we assume that A_{cyl} and A_{vac} depend on time and satisfy the following conditions:

$$\left| \frac{1}{A_{cyl,vac}} \frac{\partial A_{cyl,vac}}{\partial t} \right| << \omega. \tag{3.43}$$

We represent the other field components $E_\rho(\rho, z, t)$ and $H_\varphi(\rho, z, t)$ in the cylinder and vacuum regions as

$$E_\rho^{cyl,vac}(\rho, z, t) = B_{cyl,vac}(\rho, t) \exp\left[i(q_z z - \omega t)\right], \tag{3.44}$$

$$H_\varphi^{cyl,vac}(\rho, z, t) = C_{cyl,vac}(\rho, t) \exp\left[i(q_z z - \omega t)\right], \tag{3.45}$$

where the first index “cyl” corresponds to the cylinder region and the second index “vac,” to the vacuum region, and the amplitudes $B_{cyl}(\rho, t)$, $C_{cyl}(\rho, t)$,

$B_{vac}(\rho,t)$, and $C_{vac}(\rho,t)$ satisfy conditions analogous to (3.43). Substituting expressions (3.35), (3.36), (3.44), and (3.45) into Eqs. (3.33) and (3.34) and analogous equations for the vacuum region, we obtain the following equations:

$$\frac{\partial^2 B_{cyl}(\rho,t)}{\partial t^2} - 2i\omega\frac{\partial B_{cyl}(\rho,t)}{\partial t} - \frac{c^2\kappa^2}{\varepsilon}B_{cyl}(\rho,t) = -\frac{ic^2 q_z \kappa}{\varepsilon}J_0'(\kappa\rho)A_{cyl}(t), \quad (3.46)$$

$$\frac{\partial^2 B_{vac}(\rho,t)}{\partial t^2} - 2i\omega\frac{\partial B_{vac}(\rho,t)}{\partial t} + c^2 q^2 B_{vac}(\rho,t) = -ic^2 q_z q K_0'(q\rho)A_{vac}(t), \quad (3.47)$$

$$\frac{\partial^2 C_{cyl}(\rho,t)}{\partial t^2} - 2i\omega\frac{\partial C_{cyl}(\rho,t)}{\partial t} - \frac{c^2\kappa^2}{\varepsilon}C_{cyl}(\rho,t) = c\kappa J_0'(\kappa\rho)\left(\frac{\partial A_{cyl}(t)}{\partial t} - i\omega A_{cyl}(t)\right), \quad (3.48)$$

$$\frac{\partial^2 C_{vac}(\rho,t)}{\partial t^2} - 2i\omega\frac{\partial C_{vac}(\rho,t)}{\partial t} + c^2 q^2 C_{vac}(\rho,t) = cqK_0'(q\rho)\left(\frac{\partial A_{vac}(t)}{\partial t} - i\omega A_{vac}(t)\right), \quad (3.49)$$

where the prime in the special functions denotes differentiation with respect to the argument. Substituting the expressions for the fields (3.35), (3.36) and (3.44), (3.45) into (3.39) and multiplying both sides of the equality obtained by $\exp[-i(q_z z - \omega t)]$ after averaging over the period $2\pi/\omega$, we obtain

$$B_{vac}(\rho_0,t) - B_{cyl}(\rho_0,t) = \frac{1}{iq_z}\left[qK_0'(q\rho_0)A_{vac}(t) - \kappa J_0'(\kappa\rho_0)A_{cyl}(t)\right] - \frac{4\pi e}{c^2 q_z^2}\Gamma, \quad (3.50)$$

where

$$\Gamma = \frac{\omega}{2\pi}\int_{-\pi/\omega}^{\pi/\omega}\frac{\partial^2 n(z,t)}{\partial t^2}\exp[-i(q_z z - \omega t)]dt. \quad (3.51)$$

The substitution of (3.40) into (3.51) under the Cherenkov resonance condition $\omega = q_z v_0$ yields

$$\Gamma = -\frac{\omega^2 n_0 a}{M}\sum_{p=1}^{M}\exp\left[-i\frac{\omega}{v_0}\tilde{z}_p(z_0,v_0,t)\right]. \quad (3.52)$$

Recall that just as above the Cherenkov resonance with the condition $\omega = q_z v_0$ means the effect of excitation of eigenmodes of the cylinder under

study as a result of longitudinal bunching of electrons in the field of the excited wave and the formation of emitting electron bunches in its decelerating phases. From expressions (3.35) and (3.36) and the boundary condition (3.37), we obtain the following relation between the amplitudes $A_{cyl}(t)$ and $A_{vac}(t)$:

$$A_{cyl}(t)J_0(\kappa\rho_0) = A_{vac}(t)K_0(q\rho_0). \tag{3.53}$$

Then, applying expression (3.53), from (3.50) we obtain

$$A_{cyl}(t) = \frac{iq_z\rho_0}{\Delta_0 J_0(\kappa\rho_0)}\left[B_{vac}(\rho_0,t) - B_{cyl}(\rho_0,t)\right] - \frac{4\pi ie\rho_0}{c^2 q_z \Delta_0 K_0(q\rho_0)}\Gamma \tag{3.54}$$

and $A_{vac}(t) = A_{cyl}(t)J_0(\kappa\rho_0)/K_0(q\rho_0)$, $\Delta_0 = q\rho_0 \mathrm{Y}_K - \kappa\rho_0 \mathrm{Y}_J$, where $\mathrm{Y}_K = K_0'(q\rho_0)/K_0(q\rho_0)$ and $\mathrm{Y}_J = J_0'(\kappa\rho_0)/J_0(\kappa\rho_0)$. Substituting (3.54) into Eqs. (3.46)–(3.49), we obtain a closed system of equations relating the amplitudes $B_{cyl}(\rho_0,t)$, $B_{vac}(\rho_0,t)$, $C_{cyl}(\rho_0,t)$, and $C_{vac}(\rho_0,t)$ and to the surface density $n(z,t)$ of the beam.

Let us represent the above complex amplitudes of the fields as

$$A_{cyl,vac}(t) = F_{cyl,vac}(t)\exp\left[i\alpha_{cyl,vac}(t)\right], \tag{3.55}$$

$$B_{cyl,vac}(\rho_0,t) = G_{cyl,vac}(\rho_0,t)\exp\left[i\left(\chi_{cyl,vac}(t)\right)\right], \tag{3.56}$$

$$C_{cyl,vac}(\rho_0,t) = P_{cyl,vac}(\rho_0,t)\exp\left[i\left(\psi_{cyl,vac}(t)\right)\right], \tag{3.57}$$

where $\alpha_{cyl}(t)$, $\alpha_{vac}(t)$, $\chi_{cyl}(t)$, $\chi_{vac}(t)$, $\psi_{cyl}(t)$, and $\psi_{vac}(t)$ are slowly varying (in time) phases that satisfy conditions analogous to (3.43). Substituting the representation (3.55) of complex amplitudes into the boundary condition (3.53), we obtain and $\alpha_{cyl}(t) = \alpha_{vac}(t) + 2\pi k, \forall k \in Z$. In what follows, we assume that $F_{vac}(t) = F(t)$ and $\alpha_{cyl}(t) = \alpha_{vac}(t) = \alpha(t)$ (for $k = 0$).

With regard to expressions (3.52), (3.54), (3.56), and (3.57), the system of equations (3.42) is rewritten as

$$\begin{cases} \dfrac{d\tilde{z}_p(z_0,v_0,t)}{dt} = \tilde{v}_{zp}(z_0,v_0,t), \\ \dfrac{d\tilde{v}_{zp}(z_0,v_0,t)}{dt} = \dfrac{eq_z\rho_0}{m_0\Delta_0 K_0(q\rho_0)}\Bigg[-G_{cyl}(\rho_0,t)\sin\left(\dfrac{\omega}{v_0}\tilde{z}_p(z_0,v_0,t)+\chi_{cyl}(t)\right)+ \\ +G_{vac}(\rho_0,t)\sin\left(\dfrac{\omega}{v_0}\tilde{z}_p(z_0,v_0,t)+\chi_{vac}(t)\right)- \\ -\dfrac{4\pi e v_0^2 n_0 a}{c^2 M}\left(\sigma_1(t)\cos\left(\dfrac{\omega}{v_0}\tilde{z}_p(z_0,v_0,t)\right)-\sigma_2(t)\sin\left(\dfrac{\omega}{v_0}\tilde{z}_p(z_0,v_0,t)\right)\right)\Bigg], \end{cases} \tag{3.58}$$

where

$$\sigma_1(t)=\sum_{p=1}^{M}\cos\left(\frac{\omega}{v_0}\tilde{z}_p(z_0,v_0,t)\right),\ \sigma_2(t)=\sum_{p=1}^{M}\sin\left(\frac{\omega}{v_0}\tilde{z}_p(z_0,v_0,t)\right).$$

With regard to expressions (3.52), (3.54), (3.56), and (3.57), the system of equations (3.46)–(3.49) is rewritten as

$$\frac{\partial^2 G_{cyl}(\rho_0,t)}{\partial t^2}=\left[\left(\omega-\frac{\partial\chi_{cyl}(t)}{\partial t}\right)^2+\frac{c^2\kappa\Delta_1}{\varepsilon\rho_0\Delta_0}-\omega^2\right]G_{cyl}(\rho_0,t)+$$
$$+\frac{c^2q_z^2\kappa\rho_0}{\varepsilon\Delta_0}\Upsilon_J G_{vac}(\rho_0,t)\cos\left(\chi_{vac}(t)-\chi_{cyl}(t)\right)-\frac{A_0\Upsilon_J S_{cyl}(t)}{\varepsilon M}, \tag{3.59}$$

$$\frac{\partial^2\chi_{cyl}(t)}{\partial t^2}=2\left(\omega-\frac{\partial\chi_{cyl}(t)}{\partial t}\right)\frac{1}{G_{cyl}(\rho_0,t)}\frac{\partial G_{cyl}(\rho_0,t)}{\partial t}+$$
$$+\frac{c^2q_z^2\kappa\rho_0}{\varepsilon\Delta_0}\Upsilon_J\frac{G_{vac}(\rho_0,t)}{G_{cyl}(\rho_0,t)}\sin\left(\chi_{vac}(t)-\chi_{cyl}(t)\right)+\frac{A_0\Upsilon_J U_{cyl}(t)}{\varepsilon M G_{cyl}(\rho_0,t)}, \tag{3.60}$$

$$\frac{\partial^2 G_{vac}(\rho_0,t)}{\partial t^2}=\left[\left(\omega-\frac{\partial\chi_{cyl}(t)}{\partial t}\right)^2+\frac{c^2q\Delta_2}{\rho_0\Delta_0}-\omega^2\right]G_{vac}(\rho_0,t)-$$
$$-\frac{c^2q_z^2q\rho_0}{\Delta_0}\Upsilon_K G_{cyl}(\rho_0,t)\cos\left(\chi_{vac}(t)-\chi_{cyl}(t)\right)-\frac{A_0\Upsilon_K S_{vac}(t)}{M}, \tag{3.61}$$

$$\frac{\partial^2\chi_{vac}(t)}{\partial t^2}=2\left(\omega-\frac{\partial\chi_{vac}(t)}{\partial t}\right)\frac{1}{G_{vac}(\rho_0,t)}\frac{\partial G_{vac}(\rho_0,t)}{\partial t}+$$
$$+\frac{c^2q_z^2q\rho_0}{\Delta_0}\Upsilon_K\frac{G_{cyl}(\rho_0,t)}{G_{vac}(\rho_0,t)}\sin\left(\chi_{vac}(t)-\chi_{cyl}(t)\right)+\frac{A_0\Upsilon_K U_{vac}(t)}{MG_{vac}(\rho_0,t)}, \tag{3.62}$$

where

$$A_0 = \frac{4\pi e\kappa\omega^3 n_0 a\rho_0}{\Delta_0 v_0 q_z},$$

$$\Delta_1 = q\kappa\rho_0^2 \mathrm{Y}_K - \varepsilon\rho_0^2 \frac{\omega^2}{c^2}\mathrm{Y}_J,$$

$$\Delta_2 = \rho_0^2 \frac{\omega^2}{c^2}\mathrm{Y}_K + q\kappa\rho_0^2 \mathrm{Y}_J,$$

$$S_{cyl,vac}(t) = \sum_{p=1}^{M} \cos\left(\frac{\omega}{v_0}\tilde{z}_p(z_0, v_0, t) + \chi_{cyl,vac}(t)\right),$$

$$U_{cyl,vac}(t) = \sum_{p=1}^{M} \sin\left(\frac{\omega}{v_0}\tilde{z}_p(z_0, v_0, t) + \chi_{cyl,vac}(t)\right).$$

Solving the system of equations (3.59)–(3.62) and applying relation (3.54), we can find the time dependence of the amplitude $F(t)$ of the longitudinal component of the electric field on the boundary of the cylinder. Equations (3.48) and (3.49) are expressed in the form analogous to the system of equations (3.59)–(3.62) to describe the time evolution of the amplitudes $P_{cyl}(\rho_0, t)$ and $P_{vac}(\rho_0, t)$ and the phases $\psi_{cyl}(t)$ and $\psi_{vac}(t)$ of the magnetic field of the waves. We do not present the corresponding equations in view of their awkwardness. As a result, we have a system of equations whose solution yields the slowly varying amplitudes of the fields $E_\rho^{cyl}(\rho_0, z, t)$, $E_\rho^{vac}(\rho_0, z, t)$, $H_\varphi^{vac}(\rho_0, z, t)$, $H_\varphi^{cyl}(\rho_0, z, t)$ and $E_z^{cyl}(\rho_0, z, t) = E_z^{vac}(\rho_0, z, t)$.

To solve the above system of equations numerically, it is convenient to introduce dimensionless field amplitudes. To this end, we normalize the amplitudes of all fields by a certain quantity that has the meaning of some characteristic maximum value. We determine this quantity from the condition that the period-averaged energy of the electromagnetic waves generated by the beam at the nonlinear stage of instability is on the order of the kinetic energy of the beam in the frame of reference fixed to the wave. This condition corresponds to the trapping of the beam particles by the field of the excited wave. Let us estimate the order of magnitude of the average energy of electromagnetic waves in vacuum under the condition that $\rho = \rho_0$ in the neglect of the slow dependence of the field amplitudes on time:

$$W^{vac}(\rho_0) = \frac{1}{8\pi}\mathrm{Re}\left\{\mathbf{E}^{vac}(\rho_0, z, t)\mathbf{E}^{*vac}(\rho_0, z, t) + \mathbf{H}^{vac}(\rho_0, z, t)\mathbf{H}^{*vac}(\rho_0, z, t)\right\},$$

where "*" denotes complex conjugation. According to the aforesaid, we have $W^{vac}(\rho_0) \propto m_0 n_0 (v_0 - v_{ph})^2$, where v_{ph} is the phase velocity of the wave

excited by the beam. Applying Maxwell's equations (3.33) and (3.34) for $\varepsilon = 1$ and expressions (3.35), (3.36), (3.44), (3.45), and (3.55)–(3.57) for $W^{vac}(\rho_0)$ we obtain

$$W^{vac}(\rho_0) = \frac{\kappa^2}{8\pi q^2}\left(\frac{\mathrm{Y}_K}{\mathrm{Y}_J}\right)^2\left[1+\left(\frac{\omega}{cq_z}\right)^2+\left(\frac{q}{q_z\mathrm{Y}_K}\right)^2\right](G_{cyl}^{\max})^2,$$

where $G_{cyl}^{\max}$ is an order of magnitude maximum value of the amplitude $G_{cyl}(\rho_0,t)$.

Let us find an expression for the phase velocity v_{ph} of the wave. Using the results of [138], we can represent the dispersion equation for the coupled waves of the beam and the dielectric cylinder in the case of axially symmetric waves as

$$\left(\frac{1}{q\rho_0}\mathrm{Y}_K+\frac{\varepsilon}{\kappa\rho_0}\mathrm{Y}_J\right)(\omega-q_zv_0)^2=-\frac{a}{\rho_0}\omega_b^2,$$

Notice that the expression in the first set of parentheses on the left-hand side of this equation, when set equal to zero, represents the dispersion equation of the axially symmetric *E*-type eigenwave of the dielectric cylinder. Following the methods of [90], we obtain the following expression for the increment γ of the emerging instability:

$$\gamma=\frac{\sqrt{3}}{2}\left(a\omega_R\omega_b^2\right)^{1/3}\left[\rho_0(\varepsilon-1)\left(1+\frac{\varepsilon}{\beta^2\varepsilon-1}\frac{J_1^2(\kappa\rho_0)}{J_0^2(\kappa\rho_0)}\right)\right]^{-1/3},$$

where $\beta = v_0/c$, $\kappa \equiv \kappa(q_z,\omega_R) = \omega_R\sqrt{\beta^2\varepsilon-1}/v_0$, and $\omega_R = q_zv_0$. Then, for v_{ph} we have $v_{ph} = v_0 - \gamma/\sqrt{3}q_z$, which corresponds to a slow coupled wave. As a result, we obtain the following expression for $G_{cyl}^{\max}$:

$$G_{cyl}^{\max}=\frac{2\gamma q\sqrt{2\pi m_0n_0}}{\kappa\sqrt{3}q_z}\left|\frac{\mathrm{Y}_J}{\mathrm{Y}_K}\right|\left[1+\left(\frac{\omega}{cq_z}\right)^2+\left(\frac{q}{q_z\mathrm{Y}_K}\right)^2\right]^{-1/2}. \qquad (3.63)$$

Below we give a numerical analysis of the time dependence of slowly varying amplitudes of the electromagnetic wave fields reduced to the dimensionless form with respect to (3.63) taken for fixed values of v_0 and q_z

(under the condition $\omega = q_z v_0$) and the radial mode index s corresponding to the number of variations of the field along the radial coordinate ρ.

3.3.2. Numerical Analysis Of The System Of Nonlinear Equations

We carry out a numerical analysis of the system of equations (3.58)–(3.62) and the corresponding equations for the amplitudes $P_{cyl}(\rho_0,t)$ and $P_{vac}(\rho_0,t)$ and phases $\psi_{cyl}(t),\psi_{vac}(t)$ of the magnetic field of the wave with the use of the following dimensionless quantities: $\tau = \omega_0 t$; $\overline{\omega} = \omega/\omega_0$; $\overline{\omega}_b = \omega_b/\omega_0$; $\overline{\gamma} = \gamma/\omega_0$; $\overline{q}_z = q_z\rho_0$; $\overline{\kappa} = \kappa\rho_0$; $\overline{z}_p = q_z\widetilde{z}_p$; $\overline{v}_p = q_z\widetilde{v}_{zp}/\omega$;

$$\left|\overline{E}_z^{vac}(\rho_0,\tau)\right| = \left|\overline{E}_z^{cyl}(\rho_0,\tau)\right| = \frac{F_{vac}(\rho_0,\tau)}{G_{cyl}^{\max}} K_0(q\rho_0); \tag{3.64}$$

$$\left|\overline{E}_\rho^{cyl}(\rho_0,\tau)\right| = \frac{G_{cyl}(\rho_0,\tau)}{G_{cyl}^{\max}}; \ \left|\overline{E}_\rho^{vac}(\rho_0,\tau)\right| = \frac{G_{vac}(\rho_0,\tau)}{G_{cyl}^{\max}}; \tag{3.65}$$

$$\left|\overline{H}_\varphi^{cyl}(\rho_0,\tau)\right| = \frac{P_{cyl}(\rho_0,\tau)}{G_{cyl}^{\max}}; \ \left|\overline{H}_\varphi^{vac}(\rho_0,\tau)\right| = \frac{P_{vac}(\rho_0,\tau)}{G_{cyl}^{\max}}. \tag{3.66}$$

where $\omega_0 = c/\rho_0$. As the material of the dielectric cylinder, we use polikor with $\varepsilon = 9.6$; the radius of the cylinder is $\rho_0 = 0.5$ cm. We take the following values of the equilibrium electron concentration in the beam n_0, the beam wall thickness a, and the directed velocity of the beam electrons v_0: $n_0 = 10^{10}$ cm^{-3}, $a = 10^{-3}$ cm and $v_0 = 0.48c$. For these parameters of the system, we have $\omega_0 = 6\cdot 10^{10}$ s^{-1}, $\omega_b/\omega_0 \approx 0.1$. We analyze the time dependence of the dimensionless field amplitudes (3.64)–(3.66) for three values of the radial mode index $s = 1, 2, 3$. The resonance values of q_z and ω corresponding to the intersection points of the dispersion curves of azimuthally symmetric eigenmodes of the cylinder and the dependence $\omega = q_z v_0$ are as follows (see. [138]): $\overline{q}_z \approx 3.3$; $\overline{\omega} \approx 1.6$; $\overline{\gamma} \approx 1.2\cdot 10^{-2}$ ($\omega \approx 9.56\cdot 10^{10}$ s^{-1}, $\lambda \approx 0.95$ cm) for $s = 1$; $\overline{q}_z \approx 6.15$; $\overline{\omega} \approx 2.98$; $\overline{\gamma} \approx 1.5\cdot 10^{-2}$ ($\omega \approx 1.79\cdot 10^{11}$ s^{-1}, $\lambda \approx 0.5$ cm) for $s = 2$, $\overline{q}_z \approx 8.97$; $\overline{\omega} \approx 4.35$; $\overline{\gamma} \approx 1.7\cdot 10^{-2}$ ($\omega \approx 2.6\cdot 10^{11}$ s^{-1}, $\lambda \approx 0.35$ cm) for $s = 3$, where $\lambda = 2\pi/q_z$ is the wavelength.

We calculate the quantity $G_{cyl}^{\max}$ for the values of $\bar{q}_z$ and $\bar{\omega}$ corresponding to $s=1$: $G_{cyl}^{\max} \approx 5.3\cdot 10^{-2}$ CGS (or $G_{cyl}^{\max} \approx 1.6\cdot 10^{-3}$ V/cm).

Figures 3.5–3.7 demonstrate $\left|\bar{E}_{\rho}^{cyl}(\rho_0,\tau)\right|$, $\left|\bar{E}_{\rho}^{vac}(\rho_0,\tau)\right|$, $\left|\bar{E}_{z}^{vac}(\rho_0,\tau)\right|$, $\left|\bar{H}_{\varphi}^{vac}(\rho_0,\tau)\right|$, and $\left|\bar{H}_{\varphi}^{cyl}(\rho_0,\tau)\right|$ as a function of dimensionless time τ for waves with the radial mode index $s=1$ (waves $E_{0\,1}$), $s=2$ (waves $E_{0\,2}$), and $s=3$ (waves $E_{0\,3}$), respectively. Here we use the notation adopted in [139] for the eigenmodes $E_{n\,s}$ of the cylinder. The first index n corresponds to half the number of variations of the field with respect to the azimuthal angle φ (for an azimuthally symmetric wave, $n=0$), and the second index s is the radial mode index.

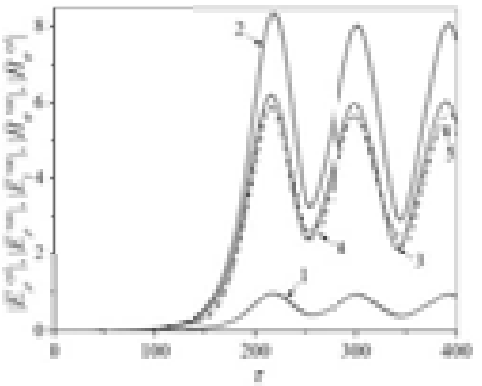

Fig. 3.5. Slow changing amplitudes of the electric and magnetic fields of the $E_{0\,1}$ wave as a function of dimensionless time

In Figs. 3.5–3.7, curves 1 correspond to the function $\left|\bar{E}_{\rho}^{cyl}(\rho_0,\tau)\right|$, curves 2, to the function $\left|\bar{E}_{\rho}^{vac}(\rho_0,\tau)\right|$, curves 3, to $\left|\bar{E}_{z}^{vac}(\rho_0,\tau)\right|$, curves 4, to $\left|\bar{H}_{\varphi}^{vac}(\rho_0,\tau)\right|$, and curves 5 to $\left|\bar{H}_{\varphi}^{cyl}(\rho_0,\tau)\right|$. We solved the system of equations for slowly varying (in time) amplitudes and phases of the fields numerically by the Runge–Kutta method. The electron beam was simulated by individual ring-shaped macroparticles that are uniformly distributed over the interval $0\le \bar{z}_p \le 2\pi$ at the initial instant of time. The number M of macroparticles was 8000. Note that the computational program used allowed us to perform integration with variable step size by defining a relative error at each step. The initial values of the dimensionless amplitudes of the fields (3.64)–(3.66) were set equal to 10^{-12}, and of their time derivatives, equal to their initial values multiplied by the dimensionless increment $\bar{\gamma}$ corresponding to each type of

waves. The initial values of the slow phases and their derivatives were assumed to be zero.

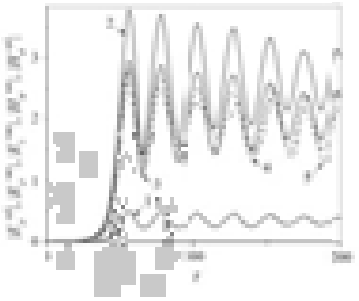

Fig. 3.6. Slow changing amplitudes of the electric and magnetic fields of the E_{02} wave as a function of dimensionless time

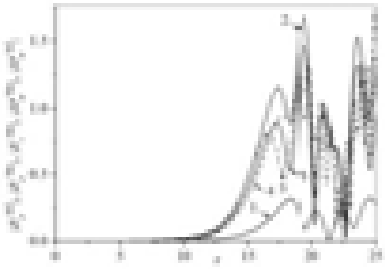

Fig. 3.7. Slow changing amplitudes of the electric and magnetic fields of the E_{03} wave as a function of dimensionless time

Figures 3.5–3.7 show that the instability saturation time for the E_{01} wave, $\tau_1 \approx 217$ (or $t_1 = \tau_1/\omega_0 \approx 3.6$ ns) is greater by a factor of about 3.8 than that for the E_{02} wave ($\tau_2 \approx 56$ or $t_2 = \tau_2/\omega_0 \approx 0.94$ ns) and by a factor of about 12.5 than that for the E_{03} wave ($\tau_3 \approx 17.3$ or $t_3 = \tau_3/\omega_0 \approx 0.07$ ns). By this time, the particles of the beam are trapped by the field of the excited wave, and a further increase in the field amplitude corresponding to the linear stage of instability development stops. The analysis of the functions presented in Figs. 3.5–3.7 shows that the instability saturation amplitudes of electric and magnetic fields for the E_{01} wave are about 2.2 times greater than the corresponding values for the E_{02} wave and about 7.3 times greater than those for the E_{03} wave. In this case, the oscillation "period" of these amplitudes at the nonlinear stage of instability saturation for the E_{01} wave is about 3.8 times greater than that for the E_{02} wave and about 40 times greater than that for the E_{03} wave. For example, for the E_{01} wave, this period is approximately equal to $T_1 \approx 1.38$ ns, for the E_{02} wave, to $T_2 \approx 0.36$ ns, and, for the E_{03} wave, to $T_3 \approx 0.033$ ns. Hence, we can conclude that, as the radial mode index s increases, the instability saturation times, the corresponding values of slow amplitudes, and the oscillation "periods" of these amplitudes at the nonlinear stage of instability saturation decrease. Note that, as the radial mode index s increases, the instability saturation time and the period of nonlinear oscillations of slow amplitudes decrease by about the same number of times.

Figures 3.5–3.7 also show that the oscillation amplitude of $\left|\overline{E}_{\rho}^{vac}(\rho_0, \tau)\right|$ (curves 2) turns out to be the greatest ones. The ratio of the maximum

instability saturation amplitudes of $\left|\overline{E}_{\rho}^{vac}(\rho_0,\tau)\right|$ and $\left|\overline{E}_{\rho}^{cyl}(\rho_0,\tau)\right|$ for the $E_{0\,1}$ wave is approximately equal to 8.7, for the $E_{0\,2}$ wave, to 7.6, and for the $E_{0\,3}$ wave, to 3.6. As applied to the boundary condition (3.38), this means that the contribution of the beam to the jump of the radial component of the electric field of the wave increases with increasing radial mode index s. The analysis of the jumps of the functions $\left|\overline{H}_{\varphi}^{vac}(\rho_0,\tau)\right|$, and $\left|\overline{H}_{\varphi}^{cyl}(\rho_0,\tau)\right|$ for the $E_{0\,1}$, $E_{0\,2}$, and E_{03} waves leads to a similar result.

Comparison of Figs. 3.5 and 3.6 with Fig. 3.7 shows that the oscillations of slow amplitudes in Fig. 3.7 exhibit an irregular behavior. A possible reason for this phenomenon is the fact that the period of nonlinear oscillations for $s = 3$ turns out to be comparable with the period of the excited wave: $\omega_0 T_3 \approx 2$ and $\omega_0(2\pi/\omega) \approx 1.44$, where the frequency ω corresponds to the $E_{0\,3}$ wave. This means the violation of condition (3.43), which actually represents the condition of slowness of the time variation of the field amplitudes. This can provide evidence for that fact that the method of slowly varying amplitudes and phases used in the present study is no longer applicable for waves with radial mode index greater than a certain "critical" value. For the chosen parameters of the cylinder and the beam, this value is $s_{cr} = 2$. Indeed, for $s = 2$, we have $\omega_0 T_2 \approx 21$, which is 7 times greater than $\omega_0(2\pi/\omega) \approx 3$, where the frequency ω corresponds to the $E_{0\,2}$ wave, while, for $s = 1$, we have $\omega_0 T_1 \approx 83$, which is almost 52 times greater than $\omega_0(2\pi/\omega) \approx 1.6$, where the frequency ω corresponds to the $E_{0\,1}$ wave. Here the quantity $\omega_0(2\pi/\omega)$ represents the dimensionless period of "fast" oscillations of the fields of the excited wave with resonance frequency ω.

Consider the question of the polarization of the waves excited by the beam. To this end, using the approach developed in [140], we write the ellipse equation for the dimensionless components of the fields $\Lambda_z = \mathrm{Re}\,E_z(\rho_0,\tau)/\Phi(\rho_0,\tau)$ and $\Lambda_\rho = \mathrm{Re}\,E_\rho(\rho_0,\tau)/\Phi(\rho_0,\tau)$:

$$\Lambda_z^2 + \Lambda_\rho^2 - 2\Lambda_z\Lambda_\rho \cos[\alpha(\tau) - \chi(\tau)] = \sin^2[\alpha(\tau) - \chi(\tau)], \tag{3.67}$$

where $\Phi(\rho_0,\tau) = F_{vac}(\rho_0,\tau)K_0(q\rho_0)$ for both the vacuum and cylinder regions (in view of the boundary condition (3.37), the same quantity $\Phi(\rho_0,\tau)$ corresponds to the cylinder region) and the component $E_\rho(\rho_0,\tau)$ and the corresponding amplitude $G(\rho_0,\tau)$ and phase $\chi(\tau)$ may refer to both the cylinder and vacuum regions. In addition, we write the equation for the polarization coefficient:

$$\Im(\tau)=\frac{E_z(\rho_0,\tau)}{E_\rho(\rho_0,\tau)}=\frac{\Phi(\rho_0,\tau)}{G(\rho_0,\tau)}\exp\{i\pi\eta(\tau)\},$$

where $\eta(\tau)=[\alpha(\tau)-\chi(\tau)]/\pi$. Recall that, in the cylinder region, $\chi(\tau)=\chi_{cyl}(\tau)$, and we consider the function $\eta_{cyl}(\tau)$; in the vacuum region, $\chi(\tau)=\chi_{vac}(\tau)$, and we consider the function $\eta_{vac}(\tau)$. Notice that, according to (3.67), the polarization of the wave may change with time. Moreover, Figs.3.5 and 3.6 show that $\Phi(\rho_0,\tau)/G(\rho_0,\tau)>1$ (i.e., $|\Im(\tau)|>1$) for the cylinder region and $\Phi(\rho_0,\tau)/G(\rho_0,\tau)<1$ (i.e., $|\Im(\tau)|<1$) for the vacuum region.

Figure 3.8 demonstrates the functions $\eta_{cyl}(\tau)$ (curve 1) and $\eta_{vac}(\tau)$ (curve 2) for the $E_{0\,1}$ wave. One can see that the phase difference $\eta_{cyl}(\tau)$ for the electric field in the cylinder oscillates with time and varies within $-1<\eta_{cyl}(\tau)\le 1.011$. This means that the polarization of the electric field in the cylinder changes with time and can be either linear for $\eta_{cyl}(\tau)=0$ and $\eta_{cyl}(\tau)=1$ or elliptic for other values of $\eta_{cyl}(\tau)$ (with regard to the fact that $|\Im(\tau)|>1$ in the cylinder). The change of sign of $\eta_{cyl}(\tau)$ implies the change of the direction of rotation of the electric field vector of the wave in the (ρ,z) plane. For example, for $\eta_{cyl}(\tau)>0$, the electric field vector of the wave rotates counter-clockwise when seen from the end of the unit vector defining the positive direction of the φ axis.

The function $\eta_{vac}(\tau)$ behaves similarly. At the instants of time when $\eta_{vac}(\tau)$ equals $0,1,2,3$, the polarization of the wave is linear, while, at other instants of time, it is elliptical. It is interesting to note that, at the nonlinear stage of instability, for $\tau>\tau_1\approx 217$, the phase difference $\eta_{vac}(\tau)$ coincides with good accuracy (with an error of about 0.1%) with a value of 3.5, while remaining an oscillating function of time. This indicates that the polarization of the wave in vacuum is elliptical ($|\Im(\tau)|<1$), and the axes of the ellipse almost coincide with the coordinate axes ρ and Z. Indeed, for $\eta_{vac}(\tau)=3.5$, Eq. (3.67) turns into the equation of an ellipse. It is also noteworthy that, at the non-linear stage of instability (for $\tau>\tau_1\approx 217$), the signs of $\eta_{cyl}(\tau)$ and $\eta_{vac}(\tau)$ are opposite. Physically, this means that, in the

$E_{0\,1}$ wave, the directions of rotation of the electric field vector in the cylinder and vacuum are opposite.

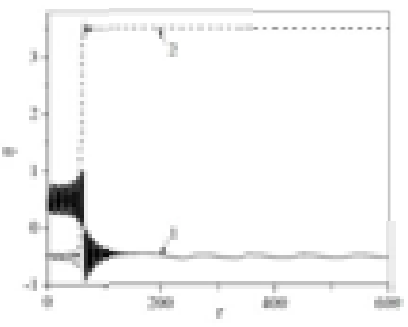

Fig. 3.8. Phase difference $\eta(\tau)$ *of the electric field components* $E_{\rho}^{cyl}(\rho_0,\tau)$ *and* $E_{z}^{vac}(\rho_0,\tau)$ *of the* $E_{0\,1}$ *wave for the cylinder (1) and vacuum (2) regions as a function of dimensionless time*

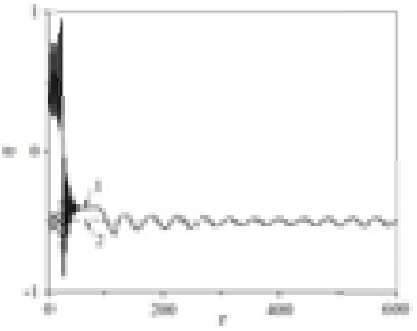

Fig. 3.9. Phase difference $\eta(\tau)$ *of the electric field components* E_{ρ}^{cyl} (ρ_0, τ) *and* E_{z}^{vac} (ρ_0, τ) *of the* $E_{0\,2}$ *wave for the cylinder (1) and vacuum (2) regions as a function of dimensionless time*

Figure 3.9 demonstrates $\eta_{cyl}(\tau)$ (curve *1*) and $\eta_{vac}(\tau)$ (curve *2*) for the $E_{0\,2}$ wave. One can see that the qualitative behavior of these functions is analogous to those for the $E_{0\,1}$ wave. Comparison of the functions $\eta_{cyl}(\tau)$ and $\eta_{vac}(\tau)$ in Figs. 3.8 and 3.9 implies that, for waves with different values of the radial mode index s at the non-linear stage of instability, the directions of rotation of the electric field vector in the cylinder region coincide ($\eta_{cyl}(\tau)<0$ for the $E_{0\,1}$ and $E_{0\,2}$ waves), while, in the vacuum region, they turn out to be opposite ($\eta_{vac}(\tau)>0$ for the $E_{0\,1}$ wave and $\eta_{vac}(\tau)<0$ for the $E_{0\,2}$ wave). Moreover, in the vacuum region, the principal axes of the polarization ellipse almost coincide with the coordinate axes ρ and z.

3.3.3 Conclusions

We have solved the problem of non-linear stabilization of the instability of a tubular electron beam as it moves along the surface of a solid dielectric cylinder. The beam was assumed to be non-relativistic, infinitely thin in the radial direction, and moving along the lines of force of an infinitely strong constant magnetic field at small (compared with the wavelength of the excited wave) impact parameters from the cylinder

surface. We have considered the excitation of azimuthally symmetric bulk–surface E- type electromagnetic waves under the *Cherenkov* resonance condition. The calculation was performed with the use of slowly varying (in time) amplitudes and phases of the electric and magnetic fields of the wave. For these quantities, we have obtained a system of differential equations from Maxwell's equations, constitutive relations, and boundary conditions, which was solved by the Runge–Kutta method with variable step size. In this case, the beam was represented as a set of macroparticles—charged rings. We have shown that the frequency of the excited electromagnetic waves decreases due to nonlinear processes. The analysis of slowly varying field amplitudes as a function of time has shown that, as the radial mode index S increases, the instability saturation time and the maximum values and the period of amplitude oscillations at the nonlinear instability saturation stage decrease. We have established that the method of slowly varying amplitudes and phases used in this work ceases to be applicable for waves with radial mode index greater than a certain "critical" value, for which the characteristic period of oscillations of the field amplitudes at the nonlinear stage of instability becomes comparable with the period of fast oscillations of the excited wave.

The analysis of the differences of slow phases of the radial and axial components of the electric field of the E_{01} and E_{02} waves as a function of dimensionless time τ has shown that, at the nonlinear instability stage, the polarization of the waves is elliptical. The directions of rotation of the electric field vectors of the E_{01} and E_{02} waves coincide in the region of the cylinder but are opposite in the vacuum region. Moreover, in the vacuum region, the principal axes of the polarization ellipse coincide with good accuracy with the coordinate axes ρ and Z.

Acknowledgments

The authors thank Professor V.I. Karas' for fruitful discussions.

General Coclusion

The following results have been derived in this Chapter.

In the first section the excitation of surface magnetoplasmons by an electron moving along a static magnetic field in vacuum over a two-dimensional plasma layer on the surface of a three-dimensional plasma has been studied theoretically. The effect of magnetoplasmons excitation has been based on the Cherenkov resonance condition. The spectra of eigenwaves of such a structure for the GaAs semiconductor as a three-dimensional plasma and the InSb semiconductor as a two-dimensional plasma has been numerically investigated. It has been shown that some of the dispersion curves of eigenmodes have segments with anomalous

dispersion. Besides, the number of frequency regions where surface magnetoplasmons can propagate only in one direction with respect to the external magnetic field in the case under consideration is smaller than that in the case of the purely transverse propagation of surface magnetoplasmons with respect to the external magnetic field. This means that the propagation of surface magnetoplasmons at acute angles reduces the degree of asymmetry of dispersion curves.

It has been denostrated that the particle excites only waves traveling at acute angles with respect to the external magnetic field (in particular, along the external magnetic field). Waves propagating at a right angle to the external magnetic field are not excited because the projection of the vector $\mathbf{E}$ on the direction of particle motion is zero and, therefore, particle energy loss to the excitation of surface plasmons is absent.

The radiation pattern of emitted canted surface magnetoplasmons in terms of the angle θ between the velocity of the electron and the two-dimensional wavevector $\mathbf{K}$ has been plotted. This clearly demonstrates the nonreciprocity principle in the excitation of surface magnetoplasmons by the electron. Indeed, the maxima of the spectral density of energy losses appear at finite values $\theta_{\max}$, which lie within the region of $0 < \theta_{\max} < \pi/2$. It has been also shown the existence of threshold angles $|\theta_{th}|$ below which electron-energy loss is absent. These angles correspond to the points of beginning of dispersion curves of the magnetoplasmons.

It is seen from the radiation pattern of emitted canted surface magnetoplasmons that the maximum of the spectral density for surface modes which have segments of dispersion curves with anomalous dispersion is approximately two orders of magnitude higher than the maxima of the spectral density for other surface modes.

The numerical analysis of the dependence of the maximum of the spectral density, corresponding to the modes which have segments of dispersion curves with anomalous dispersion, on the electron density in the two-dimensional plasma for the cases where the two-dimensional plasma is a Drude gas (with a quadratic dispersion law) and graphene monolayer (with a linear dispersion law) with the same electron density has been performed. It has been shown from the analysis of the the dependence the qualitative character of the dispersion law of electrons in the two-dimensional plasma can be established. It means that the results of the considered physical problem of excitation of surface magnetoplasmons by an electron moving along a static magnetic field in vacuum over a two-dimensional plasma layer on the surface of a three-dimensional plasma can serve as the basis for the new non-contact method for testing graphite films to identify graphite monolayers from them.

In the second section the instability of nonrelativistic tubular electron beam that moves above a dispersive metamaterial of cylindrical configuration has been theoretically examined. It has been assumed that the metamaterial possesses negative permittivity ε and negative permeability

μ simultaneously over a certain frequency range where it behaves like a left-handed material (LHM). The dispersion equations for eigenmodes of the cylinder and for the coupled modes of the system as well as the instability increments have been derived.

In order to derive the dispersion equation for the electromagnetic waves in the electrodynamic system under consideration the following boundary conditions at the cylinder surface ($\rho = \rho_0$) and at the beam surface ($\rho = \rho_b$) have to be satisfied. First, the tangential components of the electric and magnetic fields are continuous at $\rho = \rho_0$. Second, at $\rho = \rho_b$ the tangential components of the magnetic fields are discontinuous because of the beam current. Note that the normal component of the magnetic induction vector remains continuous, whereas the normal component of the electric displacement vector suffers discontinuity because of the disturbed beam charge. However, in nonrelativistic case, when $\beta^2 << 1$ (where β is the velocity of the beam devided by the velocity of light in vacuum) and $\varepsilon\mu\beta^2 > 1$, the discontinuities of the tangential magnetic field components $H_{\varphi n}(\rho, q_z, \omega)$ and $H_{zn}(\rho, q_z, \omega)$ at the beam surface ($\rho = \rho_b$) are small values of the order of $O(\beta)$. Therefore, in the boundary conditions at the beam surface ($\rho = \rho_b$) in the case where the distances of the beam from the cylinder are much less than the wavelength, we suppose these components are continuous, and take into account only the discontinuity of the radial component $E_{\rho n}(\rho, q_z, \omega)$ of electric field.

The instability is shown to be caused by Cherenkov or anomalous Doppler effects depending on the radial distance between the cylinder and the beam. Note that the Cherenkov resonance means the effect of excitation of eigenmodes of the cylinder under study as a result of longitudinal bunching of electrons in the field of the excited wave and the formation of emitting electron bunches in its decelerating phases. The anomalous Doppler effect means that the instability emerges only if the slow space-charge wave interacts with the cylinder eigenmodes.

The numerical analysis of the dispersion curves of the eigenmodes of the cylinder and the coupled modes excited by the beam in the frequency region where the metamaterial demonstrates the left-handed behavior has been performed. It has been revealed that the parts of the dispersion curves of the bulk-surface waves with anomalous dispersion emerge. The latter implies negative group velocities of corresponding waves and results in the absolute character of the beam instability. The nature of the instability in a small vicinity of the intersection points of the eigenmode dispersion curves with the beam wave $\bar{\omega} = \bar{q}_z \beta$ (the so-called resonance points) has been studied in detail with the use the well-known Sturrock method.

It has been found that the resonance behavior of magnetic permeability of the metamaterial leads to the fact that all bulk-surface waves excited by the beam are the E-type waves for the resonance values of frequencies and wave

vectors. The numerical analysis of the dependencies of the instability increments on azimutal and radial mode indices has been performed. We have shown the excitation of the weak decaying whispering gallery modes of HE-type with large values of azimuthal index n in the electrodynamic system under study is possible. Thus, this suggests applications of LHMs as delaying media for the generation of bulk-surface waves and eliminates the need for creating artificial feedbacks in slow-wave structures.

In the third section the problem of nonlinear stabilization of instability of a tubular non-relativistic electron beam moving in vacuum along the surface of a solid-state plasma cylinder has been solved. We have assumed that the beam thickness is infinitely small and there is no direct contact between the beam and the cylinder surface. The interaction of an electron beam with eigenmodes (oscillations) of a dielectric cylinder is described by the set of electrostatic equations supplemented with the constitutive equation and the equation of motion of plasma electrons. We have limited ourselves to considering azimuthally symmetric electrostatic waves and introduced the electric field potential $\psi(\rho,z,t)$ such that $\mathbf{E}(\rho,z,t)=-\nabla\psi(\rho,z,t)$. The potential of the wave $\psi(\rho,z,t)$ and its radial derivative $\partial\psi(\rho,z,t)/\partial\rho$ satisfy the following boundary conditions on the cylinder surface: the continuity of the $\psi(\rho,z,t)$ and a jump in its derivative due to the presence of the beam surface charge.

The nonlinear stabilization of the emerging instability has been investigated by the method of slow varing in time amplitudes and phases of the electrostatic wave. Using the Runge–Kutta method with a variable step, the numerical analysis of a self-consistent system of equations describing the time evolution of the wave amplitude and phase, as well as the coordinates and velocities of the macroparticles, has been carried out. It has been supposed that the frequency of the electrostatic wave are related to the beam electron velocity by the Vavilov–Cherenkov resonance condition $\omega=q_z v_0$, i.e., as has been mentioned above, the effect of excitation of eigenmodes of the cylinder under study are caused by longitudinal bunching of electrons in the field of the excited wave and the formation of emitting electron bunches in its decelerating phases.

The nonlinear stabilization of the wave amplitude due to the effect of self-trapping of the beam electrons and their subsequent chaotization has been demonstrated. It has been shown from the corresponding phase portrait of macroparticles that a group of reflected macroparticles appears in the stage of instability saturation and is reflected from the humps of the beam potential wave. Besides, it has been established that the larger the radius of the plasma cylinder, the later the nonlinear stage of instability begins and the larger the maximum value of the slowly varying amplitude. The limiting case of a plane interface between the electron beam and the solid-state plasma has been considered.

The problem of non-linear stabilization of the instability of a tubular electron beam moving along the surface of a solid dielectric cylinder has

been theoretically investigated. The beam is assumed to be non-relativistic, infinitely thin in the radial direction, and moving along the lines of force of an infinitely strong constant magnetic field at small (compared with the wavelength of the excited wave) impact parameters from the cylinder surface. We have considered the excitation of azimuthally symmetric bulk–surface E-type electromagnetic waves under the *Cherenkov* resonance condition.

The boundary conditions at the surface of the beam ($\rho = \rho_0$) are the continuity conditions for the longitudinal component of the electric field and the jump of the radial component of the electric displacement vector associated with the presence of a perturbed charge of the beam. The beam is represented as a set of macroparticles (charged rings). The homogeneous wave equations for the radial component of electric field and the azimuth component of magnetic field in vacuum as well as in the cylinder along with the above mentioned boundary condition and the equations of motion of macroparticles in the coordinate system fixed to the beam represent a closed system of self-consistent nonlinear equations describing the time evolution of the fields excited by the beam. To solve this system, we use the method of slowly varying (in time) amplitudes and phases of the excited wave.

Solving the system of equations which is consisted of equations of slowly varying amplitudes and phases of the radial component of electric field and the azimuth component of magnetic field both in vacuum and the cylinder along with the equations of motion of macroparticles we can analyse the non-linear stage of the beam instabilyty. The longitudinal component of the electric field we derive with the use of the corresponding boundary condition on the cylinder surface.

To solve the above system of selfconsistent equations numerically, we introduce dimensionless field amplitudes. To this end, we normalize the amplitudes of all fields by a certain quantity that has the meaning of some characteristic maximum value. We determine this quantity from the condition that the period-averaged energy of the electromagnetic waves generated by the beam at the nonlinear stage of instability is of the order of the kinetic energy of the beam in the coordinate system fixed to the wave. This condition corresponds to the trapping of the beam particles by the field of the excited wave. The analytical expression for the increment of the emerging instability has been derived.

The numerical analysis of the time dependence of slowly varying amplitudes of the electromagnetic wave fields reduced to the dimensionless form taken for the fixed values of beam velocity v_0 and longitudional component of the wave vector q_z (under the Cherenkov condition $\omega = q_z v_0$) and the radial mode index s corresponding to the number of variations of the field along the radial coordinate ρ has been performed. As the material of the dielectric cylinder, we use polikor.

We solved the system of equations for slowly varying (in time) amplitudes and phases of the fields along with the equation of motion of

macroparticles numerically by the Runge–Kutta method. The electron beam was simulated by individual ring-shaped macroparticles that were uniformly distributed over the interval $0 \le \bar{z}_p \le 2\pi$ (where $\bar{z}_p$ is the dimensionless longitudinal coordinate of p th macroparticle, i.e. $\bar{z}_p = q_z z_p$) at the initial instant of time. The number M of macroparticles was 8000 . Note that the computational program used allowed us to perform integration with variable step size by defining a relative error at each step. The initial values of the dimensionless amplitudes of the fields were set equal to 10^{-12}, and of their time derivatives, equal to their initial values multiplied by the dimensionless increment $\bar{\gamma}$ corresponding to each type of waves. The initial values of the slow phases and their derivatives were assumed to be zero.

From the numerical analysis we conclude that, as the radial mode index s increases, the instability saturation times, the corresponding values of slow amplitudes, and the oscillation "periods" of these amplitudes at the nonlinear stage of instability saturation decrease. Note that, as the radial mode index s increases, the instability saturation time and the period of nonlinear oscillations of slow amplitudes decrease by about the same number of times. Besides, the analysis shows that the oscillations of slow amplitudes for the radial mode index $s = 3$ exhibit an irregular behavior. A possible reason for this phenomenon is the fact that the period of nonlinear oscillations for $s = 3$ turns out to be comparable with the period of the excited wave $2\pi/\omega$, where the frequency ω corresponds to the E_{03} wave. This means the violation of condition of slowness of the time variation of the field amplitudes. This can provide evidence for that fact that the method of slowly varying amplitudes and phases used in the present study is no longer applicable for waves with radial mode index greater than a certain "critical" value.

The mumerical analysis of the polarization of the waves excited by the beam has been carried out. The analysis of the differences of slow phases of the radial and axial components of the electric field of the E_{01} and E_{02} waves as a function of dimensionless time τ has shown that, at the nonlinear instability stage, the polarization of the waves is elliptical. The directions of rotation of the electric field vectors of the E_{01} and E_{02} waves coincide in the region of the cylinder but are opposite in the vacuum region. Moreover, in the vacuum region, the principal axes of the polarization ellipse coincide with good accuracy with the coordinate axes ρ and Z .

REFERENCES

1. A. V. Chaplik, J. Exp. Theor. Phys. **117** (1), 185 (2013).
2. V. E. Pafomov, Tr. Fiz. Inst. im. P. N. Lebedeva, Akad. Nauk SSSR **16**, 94 (1961).
3. B. M. Bolotovskii, Phys.—Usp. **52** (11), 1099 (2009).

4. A. B. Mikhailovskii and E. A. Pashitskii, Sov. Phys. JETP **21**, 1197 (1965).
5. S. I. Khankina and V. M. Yakovenko, Sov. Phys. Solid State **9** (2), 443 (1967).
6. S. I. Khankina and V. M. Yakovenko, Sov. Phys. Solid State **9** (10), 2313 (1967).
7. V.I.Pakhomov, K.N.Stepanov. Zhurnal Tekhnicheskoi Fiziki. – 1967. – Vol.37, No.8. – P.1393-1400 [in Russian].
8. N.N.Beletski, A.P.Tetervov, V.M.Yakovenko. Fizika I Technika Poluprovodnikov. – 1972. – Vol.6, No.11. – P. 2129-2133. [in Russian].
9. R.F.Wallis, J.J.Brion, E.Burstaein, A.Hartstein. Physical Review B. – 1974. – Vol.9, No.8. – P. 3424-3437.
10. N.N.Beletski and V.M.Yakovenko. On the theory of electromagnetic surface waves in magnetized semiconductor plasma // Solid State Communication. – 1980. – Vol.34. – P.837-841.
11. N. N. Beletskii, V. M. Svetlichnyi, D. D. Khalameida, and V. M. Yakovenko, *Electromagnetic Phenomena in the Microwave Region in Inhomogeneous Semiconductor Structures* (Naukova Dumka, Kiev, 1991) [in Russian].
12. S. I. Khankina, V. M. Yakovenko, and I. V. Yakovenko, Izv. Vyssh. Uchebn. Zaved., Radiofiz. **47**, 562 (2004).
13. A. H. Castro Neto, F. Guinea, N. M. R. Peres, K. S. Novoselov, and A. K. Geim, Rev. Mod. Phys. **81**, 109 (2009).
14. W. Andreoni, in *Physics and Chemistry of Materials with Low-Dimensional Structures*, Ed. by F. Levy and E. Mooser (Springer, Berlin, 2000), Vol. 23, p. 448.
15. R. Saito, G. Dresselhaus, and M. S. Dresselhaus, *Phys- ical Properties of Carbon Nanotubes* (Imperial College Press, London, 1998), p. 259.
16. P. R. Wallace, Rev. Mod. Phys. **71**, 622 (1947).
17. K. S. Novoselov, A. K. Geim, S. V. Morozov, D. Jiang, Y. Zhang, S. V. Dubonos, I. V. Grigorieva, and A. A. Firsov, Science (Washington) **306**, 666 (2004).
18. J. C. Meyer, A. K. Geim, M. I. Katsnelson, K. S. Novoselov, T. J. Booth, and S. Roth, Nature (London) **446**, 60 (2007).
19. A. K. Geim and K. S. Novoselov, Nat. Mater. **6**, 183 (2007).
20. K. S. Novoselov, A. K. Geim, S. V. Morozov, D. Jiang, M. I. Katsnelson, I. V. Grigorieva, S. V. Dubonos, and A. A. Firsov, Nature (London) **438**, 197 (2005).
21. Y. Zhang, Y. W. Tan, H. L. Stormer, and P. Kim, Nature (London) **438**, 201 (2005).
22. M. I. Katsnelson, K. S. Novoselov, and A. K. Geim, Nat. Phys. **2,** 620 (2006).
23. V. V. Cheianov, V. I. Fal'ko, and B. L. Altshuler, Science (Washington) **315**, 1252 (2007).
24. C. W. J. Beenakker, Rev. Mod. Phys. **80**, 1337 (2008).
25. P. Recher, B. Trauzettel, A. Rycerz, Ya. M. Blanter, C. W. J. Beenakker, and A. F. Morpurgo, Phys. Rev. B: Condens. Matter **76**, 235404 (2007).
26. S. V. Morozov, K. S. Novoselov, M. I. Katsnelson, F. Schedin, L. A. Ponomarenko, D. Jiang, and A. K. Geim, Phys. Rev. Lett. **97**, 016801 (2006).
27. F. Sols, F. Guinea, and A. H. Castro Neto, Phys. Rev. Lett. **99**, 166803 (2007).
28. V. P. Gusynin, V. A. Miransky, S. G. Sharapov, and A. Shovkovy, Phys. Rev. B: Condens. Matter **74**, 195429 (2006).
29. C.-H. Zhang and Y. N. Joglekar, Phys. Rev. B: Con- dens. Matter **75**, 245414 (2007).
30. N. M. R. Peres, F. Guinea, and A. H. Castro Neto, Phys. Rev. B: Condens. Matter **72**, 174406 (2005).
31. F. Rana, IEEE Trans. Nanotechnol. **7**, 91 (2008).
32. I. V. Iorsh, I. S. Mukhin, I. V. Shadrivov, P. A. Belov, and Y. S. Kivshar Phys. Rev. B: Condens. Matter **87**, 075416 (2013).
33. A. S. Mayorov, D. C. Elias, M. Mucha-Kruczynski, R. V. Gorbachev, T. Tudorovskiy, A. Zhukov, S. V. Morozov, M. I. Katsnelson, V. I. Fal'ko, A. K. Geim, and K. S. Novoselov, Science (Washington) **333**, 860 (2011).
34. A. N. Grigorenko, M. Polini, and K. S. Novoselov, Nat. Photonics **6**, 749 (2012).
35. S. A. Mikhailov and K. Ziegler, Phys. Rev. Lett. **99**, 016803 (2007).
36. D. K. Ferry and S. M. Goodnick, *Transport in Nano-structures* (Cambridge University Press, Cambridge, 1997).
37. V. P. Silin and A. A. Rukhadze, *Electromagnetic Properties of Plasma and Plasma-Like Media* (Gosatomizdat, Moscow, 1961) [in Russian].
38. V. S. Vladimirov, *Generalized Functions in Mathematical Physics* (Nauka, Moscow, 1979; Mir, Moscow, 1979).
39. A. P. Babichev, N. A. Babushkina, A. M. Bratkovskii, M. E. Brodov, and M. V. Bystrov, in *Handbook of Physical Quantities*, Ed. by I. S. Grigoriev and E. Z. Meilikhov (Energoatomizdat, Moscow, 1991; CRC Press, Boca Raton, Florida, United States, 1996).

40. L. A. Falkovsky, J. Exp. Theor. Phys. **106** (3), 575 (2008).

41. M. Abramowitz and I. Stegun, *Handbook of Mathematical Functions: With Formulas, Graphs, and Mathematical Tables* (Dover, New York, 1965; Nauka, Moscow, 1979).

42. R. Kompfner, *The invention of the traveling-wave tube* (San Francisco: San Francisco Press, 1964).

43. L. A. Vainshtein, V. A. Solntsev, *Lectures on Ultrahigh-Frequency Electronics* (Moskow, Sov. Radio, 1973). [in Russian].

44. D. I. Trubetskov, A. E .Hramov, *Lectures on Ultrahigh-Frequency Electronics for Physicists* (Moscow, PhysMathLitt, 2003), Vol. 1, 496 p. [in Russian}.

45. G. V. Sotnikov, T. C. Marshall, and J. L. Hirshfield. Phys. Rev. ST Accel. Beams **12**, 051301 (2009). http://link.aps.org/doi/10.1103/PhysRevSTAB.12.061302.

46. *Encyclopedia of Low-Temperature Plasma*, edited by V. E. Fortov (Moscow, Science, 2000), Vol. 4, 507 p. [in Russian].

47. M. V. Kuzelev, A. A. Rukhadze, P. S. Strelkov, *Plasma Relativistic Microwave Electronics* (Publishing House of the N. E. Bauman Moscow State Technical University, 2002) [in Russian].

48. R. K. Parker, R. H. Abrams, B. G. Danly, B. Levush. IEEE Trans. on Microwave Theory and Techniques **50**. 835 (2002).

49. J.B. Pendry, A.J. Holden, W.J. Stewart, I. Youngs, Phys. Rev. Lett. **76**, 4773 (1996).

50. J.B. Pendry, A.J. Holden, D.J. Robbins, W.J. Stewart, J. Phys.: Condens. Matter **10**, 4785 (1998).

51. D.R. Smith, W.J. Padilla, D.C. Vier, S.C. Nemat-Nasser, and S. Schultz, Phys. Rev. Lett. **84**, 4184 (2000).

52. R.A. Shelby, D.R. Smith, S.C. Nemat-Nasser, and S. Schultz, Appl. Phys. Lett. **78**, 489 (2001).

53. R.A. Shelby, D.R. Smith, S. Schultz, Science **292**, 77 (2001).

54. J. T. Huangfu, L. X. Ran, H. S. Chen, X. M. Zhang, K. S. Chen, T. M. Grzegorczyk, and J. A. Kong, Appl. Phys. Lett. **84**, 1537 (2004).

55. H. S. Chen, L. X. Ran, J. T. Huangfu, X. M. Zhang, and K. S. Chen, Phys. Rev. E **70**, 057605 (2004).

56. G. Dolling, C. Enkrich, M. Wegener, C. M. Soukoulis, and S. Linden, Opt. Lett. **31**, 1800 (2006).

57. J.Wang, Z.Xu, B.Du, S.Xia, J.Wang. J. Appl. Phys. **111**, 044903 (2012).

58. D. Liu, Z. Xu, N. Ma, et al. Appl. Phys. A **106**, 949 (2012).

59. A. V. Dormidontov, A. Ya. Kirichenko, Yu. F. Lonin, A. G. Ponomarev, Yu. V. Prokopenko, G. V. Sotnikov, V. T. Uvarov, and Yu. F. Filippov. Tech. Phys. Lett. **38**. 85 (2012).

60. N. S. Ginzburg, V. Y. Zaslavskii, A. M. Malkin, A. S. Sergeev. Tech. Phys. **57**. 1692 (2012).

61. N. S. Ginzburg, V. Y. Zaslavskii, A. M. Malkin, A. S. Sergeev. Tech. Phys. **58**. 267 (2013).

62. K. V. Galaydych, Yu. F. Lonin, A. G. Ponomarev, Yu. V. Prokopenko, G. V. Sotnikov. Problems of Atomic Science and Technology. Series: Plasma Physics No. **6**(**16**). 123 (2010).

63. K. V. Galaydych, Yu. F. Lonin, A. G. Ponomarev, Yu. V. Prokopenko, G. V. Sotnikov. Problems of Atomic Science and Technology. Series: Plasma Physics No **6**(**82**). 158 (2012).

64. G. Bekefi, *Radiation Processes in Plasmas* (New York, Wiley, 1966).

65. L. D. Landau and E. M. Lifshits, *Electrodynamics of Continuous Media* (Moscow, Science, 1982) [in Russian].

66. A. V. Dormidontov, Yu. V. Prokopenko, S. I. Khankina, V. M. Yakovenko. Telecommunications and Radio Engineering **73**. 1165 (2014).

67. A. V. Dormidontov, Yu. V. Prokopenko, S. I. Khankina, V. M. Yakovenko. Telecommunications and Radio Engineering **75**. 507 (2016).

68. A. V. Dormidontov, Yu. V. Prokopenko, V. M. Yakovenko. Telecommunications and Radio Engineering **75**. 201 (2016).

69. A. V. Dormidontov, Yu. V. Prokopenko, S. I. Khankina, V. M. Yakovenko. Tech. Phys. **60**. 1069 (2015).

70. Yu. O. Averkov, Yu. V. Prokopenko, V. M. Yakovenko. JETP **121**. 699 (2015).

71. Yu. O. Averkov, Yu. V. Prokopenko, V. M. Yakovenko. Telecommunications and Radio Engineering **75**. 1467 (2016).

72. V.E. Pafomov. Zurn. Eksp. I Teor. Fiz. **36**, 1853 (1959) [in Russian].

73. V.G. Veselago, Usp. Fiz. Nauk **92**, 517 (1967) [Sov. Phys. Usp. **10**, 509 (1968)].

74. Y. Song, J. Ta, H. Li, and X. Zhang Wang. Journal of Applied Physics **106**, 063119 (2009).

75. D. Wang, L. Ran, H. Chen, and M. Mu. Appl. Phys. Lett. **91**, 164101 (2007).

76. A. L. Pokrovsky, A. L. Efros. Phys. Rev. Lett. **89**, 093901 (2002).

77. T. Koschny, M. Kafesaki, E.N. Economou, C.M. Soukoulis. Phys. Rev. Lett. **93**, 107402 (2004).

78. V. M. Agranovich, Y. R. Shen, R. H. Baughman, A. A. Zakhidov. Phys. Rev. B **69**, 165112 (2004).
79. Yu. O. Averkov, V. M. Yakovenko. Phys. Rev. B **72**, 205110 (2005).
80. Yu. P. Bliokh, S. Savel'ev, F. Nori. Phys. Rev. Lett. **100**, 244803 (2008).
81. Yu. O. Averkov, A. V. Kats, V. M. Yakovenko. Phys. Rev. B **79**, 193402 (2009).
82. S. N. Galyamin, A. V. Tyukhtin. Phys. Rev. B **81**, 235134 (2010).
83. X. S. Rao, C. K. Ong. Rev. B **68**, 113103 (2003).
84. Yunxia Dong, Xiangdong Zhang. J. Appl. Phys. **105**, 054105 (2009).
85. Z. Sa, Y. Poo, R. Wu et al. Appl. Phys. A **117**, 427 (2014).
86. S. Antipov, W. Liu, W. Gai, J. G. Power, L. Spentzouris. AIP Conference Proceedings **877**, 815 (2006).
87. G. V. Sotnikov, T. C. Marshall. Phys. Rev. ST Accel. Beams **14**, 031302 (2011). http://link.aps.org/doi/10.1103/PhysRevSTAB.14.031302.
88. A. Ya. Kirichenko, Yu. V. Prokopenko, Yu. F. Filippov, N. T. Cherpak, *Quasi-Optical Solid-State Resonators* (Kiev, Naukova Dumka, 2008) [in Russian].
89. M.V. Nezlin. Usp. Fiz. Nauk **120**, 481 (1976) [Sov. Phys. Usp. **19**, 946 (1976)].
90. A.I. Akhiezer, I.A. Akhiezer, R.V. Polovin, A.G. Sitenko, and K.N. Stepanov, *Plasma Electrodynamics* (Pergamonpress, New York, 1975).
91. R. Ruppin, Phys. Lett. A **277**, 61 (2000).
92. J. A. Nelder, R. Mead, Comput. J. **7**, 308 (1965)
93. Ya. B. Fineberg, V. D. Shapiro, *To the Nonlinear Theory of Interaction between Relativistic Beam and Plasma*. In book: *Interaction of Charged Particles Beams with Plasma* (Kiev, Publishing House of the Academy of Sciences of Ukrainian SSR, 1965) [in Russian].
94. P. A. Sturrock, Proc. Roy. Soc. A **242**, 277 (1957).
95. Granino A. Korn and Theresa M. Korn, *Mathematical handbook for scientists and engineers. Definitions, Theorems, and Formulas for Reference and Review* (Dover publications, Inc. Mineola, New York, 1968).
96. L. A. Vaynshteyn, *Electromagnetic waves* (Moscow, Sov. radio, 1957) [in Russian].
97. E. Pickwell, B. E. Cole, A. J. Fitzgerald, et al., Appl. Phys. Lett. **84**, 2190 (2004).
98. P. C. Ashwort, E. Pickwell-MacPherson, E. Provenzano, et al., Opt. Express **17**, 12444 (2009).
99. Y. Yang, A. Shutler, and D. Grischkowsky, Opt. Express **19**, 8830 (2011).
100. T. Nagatsuma, S. Horiguchi, Y. Minamikata, et al., Opt. Express **21**, 23736 (2013).
101. M. C. Kemp, IEEE Trans. Terahertz Sci. Technol. **1**, 282 (2011).
102. A. I. Akhiezer and G. Ya. Lyubarskii, Dokl. Akad. Nauk SSSR **80**, 193 (1951).
103. A. I. Akhiezer and R. V. Polovin, Dokl. Akad. Nauk SSSR **102**, 919 (1955).
104. A. I. Akhiezer and R. V. Polovin, Sov. Phys. JETP **3**, 696 (1956).
105. Ya. B. Fainberg and V. D. Shapiro, Sov. Phys. JETP **20**, 937 (1965).
106. Ya. B. Fainberg and V. D. Shapiro, in *Proceedings of the 4th Conference on Plasma Physics and Problems of Controlled Nuclear Fusion, Kiev, 1963,* p. 92.
107. R. K. Mazitov, Prikl. Mekh. Tekh. Fiz., No. 1, 27 (1965).
108. T. O'Neil, Phys. Fluids **8**, 2255 (1965).
109. Ya. B. Fainberg, Czech. J. Phys. **18B**, 652 (1968).
110. Ya. B. Fainberg, V. D. Shapiro, and V. I. Shevchenko, Sov. Phys. JETP **30**, 528 (1970).
111. V. I. Kurilko, JETP **30**, 484 (1970).
112. W. E. Drummond, J. H. Malmberg, T. M. O'Neil, and R. Thompson, Phys. Fluids **13**, 2422 (1970).
113. R. I. Kovtun and A. A. Rukhadze, Sov. Phys. JETP **31**, 915 (1970).
114. B. N. Breizman and D. D. Ryutov, Sov. Phys. JETP **33**, 220 (1971).
115. I. N. Onishchenko, A. R. Linetskii, N. G. Matsiborko, V.D. Shapiro, and V. I. Shevchenko, JETP Lett. **12**, 281 (1970).
116. I. N. Onishchenko and V. D. Shapiro, Plasma Phys. **14**, 591 (1972).
117. A. A. Ivanov, V. V. Parail, and T. K. Soboleva, Sov. Phys. JETP **36**, 887 (1973).
118. A. A. Ivanov, *Physics of Highly Nonequilibrium Plasmas* (Atomizdat, Moscow, 1977) [in Russian].
119.B. A. Al'terkop, S. E. Rosinskii, and V. P. Tarakanov, Sov. J. Plasma Phys. **5**, 164 (1979).
120. Yu. V. Bobylev and M. V. Kuzelev, *Nonlinear Phenomena Accompanying Electron Beam–Plasma Interaction* (Fizmatlit, Moscow, 2009) [in Russian].
121. A. V. Kukushkin and A. A. Rukhadze, Plasma Phys. Rep. **43**, 973 (2017).
122. Yu. V. Bobylev, M. V. Kuzelev, and A. A. Rukhadze, Plasma Phys. Rep. **30**, 383 (2004).
123. Yu. V. Bobylev, M. V. Kuzelev, and A. A. Rukhadze, Plasma Phys. Rep. **34**, 383 (2008).

124. A. S. Shlapakovski, S. N. Artemenko, V. A. Avgustinovich, A. I. Mashchenko, V. M. Matvienko, V. Yu. Mityushkina, I. I. Vintizenko, W. Jiang, and E. Schamilo-glu, in *Proceedings of the 14th International Symposium on High Current Electronics, Tomsk, 2006,* p. 359.

125. V. A. Avgustinovich, S. N. Artemenko, A. I. Mashchenko, A. S. Shlapakovskii, and Yu. G. Yushkov, Tech. Phys. Lett. **36**, 224 (2010).

126. A. Ya. Kirichenko, Yu. F. Lonin, V. G. Papkovich, A.G. Ponomarev, Yu. V. Prokopenko, V. T. Uvarov, and Yu. F. Filippov, Vopr. At. Nauki Tekh., Ser. Yad.-Fiz. Issl. **53** (2), 135 (2010).

127. K. V. Galaidych, Yu. F. Lonin, A. G. Ponomarev, Yu. V. Prokopenko, G. V. Sotnikov, V. L. Uvarov, Vopr. At. Nauki Tekh., Ser. Yad.-Fiz. Issl. **58** (3), 174 (2012).

128. Yu. O. Averkov, Yu. V. Prokopenko, and V. M. Yakovenko, Radiofiz. Elektron. **7** (21), 28 (2016).

129. Yu. O. Averkov, Yu. V. Prokopenko, and V. M. Yakovenko, Phys. Rev. E **96**, 013205 (2017).

130. Yu. O. Averkov, Yu. V. Prokopenko, and V. M. Yakovenko, Probl. At. Sci. Technol., Ser. Plasma Electron. New Methods Accelerat. **10** (4), 3 (2018).

131. Yu. O. Averkov, Yu. V. Prokopenko, and V. M. Yakovenko, Tech. Phys. **64**, 1 (2019).

132. I. N. Kartashov and M. V. Kuzelev, Plasma Phys. Rep. **40**, 650 (2014).

133. V. M. Lopukhin and A. A. Vedenov, Usp. Fiz. Nauk **53**, 69 (1954).

134. A. I. Borodkin, V. M. Yakovenko, G. Ya. Levin, and Yu. V. Maistrenko, Fiz. Tverd. Tela **12**, 1515 (1970).

135. E. A. Kornilov, S. A. Nekrashevich, Ya. B. Fainberg, and N. A. Shokhovtsov, JETP Lett. **11**, 185 (1970).

136. M. V. Kuzelev, O. V. Lazutchenko, and A. A. Rukhadze, Radiophys. Quant. Electron. **42**, 841 (1999).

137. Yu. O. Averkov, Yu. V. Prokopenko, and V. M. Yakovenko, Radiofiz. Electron. **7** (21), 68 (2016).

138. Yu. O. Averkov, Yu. V. Prokopenko, and V. M. Yakovenko, Telecomm. Radio Eng. **76**, 1595 (2017).

139. M. E. Il'chenko, V. F. Vzyatyshev, L. G. Gasanov, et al., *Dielectric Resonators*, Ed. by M. E. Il'chenko (Radio Svyaz', Moscow, 1989), p. 328 [in Russian].

140. M. B. Vinogradova, O. V. Rudenko, and A. V. Sukhorukov, *Wave Theory* (Nauka, Moskow, 1990), p. 432 [in Russian].

УДК 533.9
PACS numbers: 52.35.Fp, 52.35.Mw, 52.38.Kd, 52.40.Mj, 52.65.Rr

CHAPTER III

THE REDUCED DESCRIPTION METHOD IN THE KINETIC THEORY OF COMPLEX SYSTEMS OF IDENTICAL PARTICLES

O.Yu. Sliusarenko[1)], Yu.V. Slyusarenko[1,2)], A.G. Zagorodny[3)]

[1)] *Akhiezer Institute for Theoretical Physics National Science Center "Kharkiv Institute of Physics and Technology", 1 Akademichna Str., Kharkiv 61108, Ukraine,*
[2)] *Karazin National University, 4 Svobody Sq., Kharkiv 61077, Ukraine*
[3)] *Bogolyubov Institute for Theoretical Physics, 14B Metrolohichna Street, Kyiv 03143, Ukraine*

Microscopic approaches to the description of non-equilibrium processes in complex systems of identical particles, in particular, at the kinetic stage of evolution, have been developed. In this work, the term "complex" unites some selected systems of many identical constituent particles with a complex internal structure. The internal structure of particles is reflected in the peculiarities of their interaction, both among themselves and with an external field acting on the medium. Such systems are nonlinear, open (regarding the presence of an external field), demonstrating the emergence of self-organization and new properties in the process of evolution. As an example of such systems, we consider dissipative media (media with internal friction between structural units) under the influence of an external random field, active media (in this case, the dissipative media, the structural units of which are influenced by an external stochastic field, the action of which depends on the velocity of the structural unit), low-temperature gases of hydrogen-like atoms in an external electromagnetic field. The systems are specially selected in such a way as to cover the cases of both classical and quantum complex systems. For systems of this kind, recipes have been proposed for constructing microscopic approaches to describing their evolution, in particular, its kinetic stages. The approaches are constructed in such a way that the noted internal structure of the structural units of the system does not affect the possibilities of considering these composite particles as point objects. The motivation for the research is, first of all, the fact that consistent microscopic approaches to the description of evolutionary processes in these systems are

currently either completely absent or insufficiently developed.The development of microscopic approaches is based on the generalization of the Bogolyubov - Peletminsky reduced description method to the case of the listed complex systems of identical particles. The procedure for constructing microscopic approaches to describing the evolution of dissipative systems (including those with active fluctuations) demonstrates the possibility of dynamically substantiating the kinetic theory of dissipative systems of identical particles in an external stochastic field. Within the framework of the developed approaches, a procedure is proposed for deriving kinetic equations for all the systems mentioned in the case of weak interaction between particles and a low intensity of the external field. A number of particular solutions of the obtained equations are analyzed, in particular, with the aim of further applications of the developed theory.

Keywords: *complex systems, dissipative media, active fluctuations, low-temperature gases of hydrogen-like atoms, evolutionary processes, stochastic field, Furutsu-Novikov formula, chains of BBGKY equations, reduced description method, kinetic equations, self-propelled properties of dissipative systems.*

PACS numbers: *05.20.-y; 05.20.Dd; 05.10.Gg; 05.40.-a; 05.40.Jc; 45.70.-n; 47.70 Nd*

Introduction

First of all, it should be recalled that a general definition of the concept of a «complex system» does not exist at the present time. The concept itself is widely used in the scientific literature as a term that marks the presence of specific features of the objects of study in many natural and humanitarian sciences. Perhaps it is precisely because of such a comprehensiveness of the term that there is no general definition of such systems. The English-language Wikipedia, for example, characterizes such objects as follows: «Complex systems are systems whose behavior is intrinsically difficult to model due to the dependencies, competitions, relationships, or other types of interactions between their parts or between a given system and its environment. Systems that are «complex» have distinct properties that arise from these relationships, such as nonlinearity, emergence, spontaneous order, adaptation, and feedback loops, among others.»[1]. As for the physical side of the issue, the Ukrainian-language Wikipedia claims that "The physics of complex systems studies systems that consist of many interacting parts and exhibit collective behavior that is not a simple consequence of the behavior of their individual components. Examples of such systems are condensed matter, ecological and biological systems, stock markets and economic systems, and human society. The concept of a complex system applies to many traditional disciplines of science and forms a new, interdisciplinary field of knowledge. The equations used to build models of complex systems are mainly taken from statistical physics, information theory and nonlinear dynamics. Inherent features of complex systems are self-organization, the emergence of new functionalities (emergence), high sensitivity to small changes in initial conditions, obedience to power laws (distributions

[1] https://en.wikipedia.org/wiki/Complex_system

such as «thick tails»)[2]. Let us also recall that self-organization is a term used to define the processes of emergence in such a system of complex structures in the absence of order imposed by external influence, and emergence is the emergence in the process of evolution of new properties that are not reducible to the sum of the properties of the components (structural units) of the system.

In this work, the term «complex» unites some systems of many identical constituent particles with a complex internal structure. The internal structure of particles is reflected in the peculiarities of their interaction, both among themselves and with an external field acting on the environment. As will be shown in the further presentation, such systems are nonlinear, open (the presence of an external field!), Demonstrating the emergence of self-organization and new properties in the process of evolution. As an example of such systems, in this work we consider dissipative media (media with internal friction between structural units) under the influence of an external random field, active media (in this case, dissipative media, the structural units of which are exposed to an external stochastic field, the action of which depends on structural unit velocity), low-temperature gases of hydrogen-like atoms in an external electromagnetic field. It should be noted that the systems are specially selected in such a way as to cover the cases of both classical and quantum complex systems. For systems of this kind, we propose recipes for constructing microscopic approaches to describing their evolution, in particular, its kinetic stages. The approaches are constructed in such a way that the noted internal structure of the structural units of the system does not affect the possibilities of considering these composite particles as point objects. The motivation for research is, first of all, the fact that consistent microscopic approaches to the description of evolutionary processes in these systems are currently either completely absent, or insufficiently developed. We also note that in the further presentation we will omit the term «complex» in relation to the systems under study, except for those cases when it will be necessary to emphasize exactly the corresponding characteristics of the systems.

Dissipative media. In presenting the material related to the construction of the kinetics of dissipative media under an external stochastic action, we will closely adhere to the content of [1]. The research topics of this work have a fairly long history, which goes back to the problem of dynamically substantiating the Boltzmann kinetic equation. This justification was intended to link two different approaches to describing the evolution of complex systems - a dynamic theory based on Hamiltonian mechanics, and a kinetic theory, which was initiated by Boltzmann. Thus, in essence, the question of the transition from reversible equations of Hamiltonian mechanics to irreversible equations of statistical mechanics should be solved. For the first time, a consistent dynamic substantiation of statistical mechanics in the microscopic approach for the case

[2] https://uk.wikipedia.org/wiki/%D0%A4%D1%96%D0%B7%D0%B8%D0%BA%D0%B0_%D1%81%D0%BA%D0%BB%D0%B0%D0%B4%D0%BD%D0%B8%D1%85_%D1%81%D0%B8%D1%81%D1%82%D0%B5%D0%BC.

of classical (not quantum) systems of many particles was given by N.N. Bogolyubov [2]. The method proposed by Bogolyubov for a reduced description of the evolution of many-particle systems made it possible to construct a regular procedure for obtaining closed dissipative kinetic equations based on the BBGKY chain of reversible equations for many-particle distribution functions. In the case of quantum systems, such a justification was extended in the works of S.V. Peletminskii within the framework of the method of reduced description of quantum systems of many particles developed in them [3].

The approach to the construction of a kinetic theory of systems of many particles in the case of the action of an external random force on them requires significant modification. The reason lies in the need to introduce averaging of the physical characteristics of the system over the external stochastic force (see in this regard [4]). The averaging procedure itself inevitably leads to the introduction of moments of physical characteristics or related correlation functions (in the most general case, correlation functions of any order) and the derivation of evolution equations for them. Thus, the microscopic approach to the derivation of the kinetic equations of many-particle systems under an external stochastic action should be based on the method of reduced description in combination with the procedure of averaging over an external random field. In this case, the initial equations should be Newton's equations or Hamilton's equations for the coordinates and momenta of particles, taking into account the effect of an external random force on each particle.

The first steps towards the construction of such a method were taken in [5]. In this work, the foundations of the method of reduced description of classical (non-quantum) systems of many particles, subject to external stochastic action, neglecting the interaction between particles, were formulated. In the developed approach, analogs of BBGKY chains are obtained and it is shown that, in the particular case of Gaussian white noise, controlled chain termination leads to the kinetic Fokker-Planck equation. The diffusion coefficient in the momentum space in this equation is determined, as one would expect, by the pair correlation function of the external random force.

It is clear, however, that the model proposed in [5] is of interest rather from an academic point of view. Indeed, in many cases, the approximation used in this work, which neglects the interaction between particles, is simply physically unjustified. For example, when deriving the kinetic equation for Brownian particles from the Langevin equations, the interaction between these particles is usually neglected due to the low density of their number (see, for example, [3] and also [6-8]). The influence of the medium on Brownian particles, as is well known, in the Langevin equations is usually divided into the action of friction forces and the action of stochastic forces. In the case of constructing a microscopic theory of Brownian motion, the interaction between Brownian particles can be neglected due to their low density, but it is necessary to take into account the interaction of medium particles with each other and the

interaction of medium particles with Brownian particles (see in this connection [9, 10]). It should be noted that recently, articles have begun to appear on the construction of a microscopic theory of interacting Brownian particles, see, for example, [11-16]. Although, from the generally accepted point of view until recently, Brownian particles were considered non-interacting with each other.

There is also a very extensive and important class of many-particle systems under the influence of external stochastic fields, in the description of which it is impossible to avoid taking into account the interaction between particles. We are talking about systems of many particles with internal friction (the so-called dissipative systems of many particles). The concept of a «system of many particles with internal friction» is quite general. «Famous» representatives of this kind of systems are the so-called granular media (see [17]). These substances are known to often exhibit unusual or unexpected but remarkable properties. For example, if a multicomponent mixture of granular materials is shaken, then larger particles "float" to the surface (see, for example, [17, 18]). This separation of particles is called the Brazil nut effect. Several competing theories have emerged that were thought to satisfactorily explain this phenomenon. However, by the end of the last millennium, it was discovered that if the mixture of granular materials is shaken hard enough, then large particles sometimes do not «float», but rather «sink». This phenomenon was called the "reverse effect of the Brazil nut" (see in this connection, for example, [19, 20]). It was found that the direction of movement of «nuts» depends not only on their size and density, but also on the frequency and amplitude of oscillations. Consequently, the existing theories explaining, as it was believed before, the noted effect, need a significant revision.

Thus, both in the case of systems with Brownian particles and in the case of dissipative systems of many particles, the variant of constructing a microscopic theory of relaxation processes in such systems would be ideal. In accordance with the above, such a theory would have to take into account the effect on the system of external stochastic forces ("shaking") and the presence of interaction between particles. The interaction, in turn, must take into account the existence of internal friction forces in the system. In developing such a theory, the microscopic approach should be based on the reduced description method, which has proven itself so successfully in describing the evolution of simpler systems of many particles. It is clear that the construction of such a general theory at the moment seems to be more than problematic. However, it turns out that the development of a microscopic approach to constructing a fluctuation-kinetic theory for a gas with internal friction between particles that are subject to the influence of external stochastic fields is quite realistic. Demonstration of this circumstance is one of the goals of this work. Note also that such systems, in our opinion, can serve as a model of the so-called granular gases. In the case of a Gaussian external field, the systems under study can be considered prototypes of systems with interacting Brownian particles [11-16].

Active environments. Here the situation with the description of nonequilibrium processes is in many respects similar to the situation described above in the case of dissipative media. The name «active substance» or «active medium» unites systems of many particles, in which the external environment has a significant effect on the movement of structural units. Moreover, this influence depends on both the properties of the structural units themselves (their shape or internal structure), and on some of their dynamic characteristics, such as, for example, speed. Brownian motors [21,22], motile cells [23-28], macroscopic animals [29,30], artificial self-propelled particles [31, 32] are usually indicated as examples of the marked objects. The constant increase in interest in the study of such systems is associated with their demonstration of many amazing effects and properties, see in this connection the remarkable review [33] and the references therein. The study of nonequilibrium processes in systems of active particles inevitably raises the question of the correct derivation of the equations of evolution of such systems, in particular, kinetic equations. As in the case of dissipative media, an analysis of the currently existing huge number of publications related to this problem shows that in most cases the derivation of equations for the dynamics of active particles is based on phenomenological approaches of the Langevin type (see [33] and also, for example, [34, 35]). Moreover, just as in the case of systems of particles with internal friction, it must be borne in mind that the use of the Langevin equations to describe dynamic processes requires confidence in their applicability in this case. And first of all, as already noted above, such confidence is required by the circumstances associated with the need to take into account the interaction between the structural particles of the system (see in this regard [3], [9, 10], [11-16]). It should be remembered that both dissipative systems and systems of active particles can be affected by noise and of a more complex nature than Gaussian ones. We emphasize, however, that in the framework of the Langevin approach, taking into account the interaction between particles is a difficult problem, the solutions of which leave doubts about their correctness.

Here, too, the simplest way out of the situation is the development of microscopic approaches to the construction of a kinetic theory of systems of active particles. Such approaches should proceed from first principles, that is, from the idea of the object under study as a system of many identical interacting particles under external stochastic influence, in particular with active correlations. Thus, when formulating microscopic methods for constructing the kinetic theory of the noted systems, the initial equations should be Newton's equations or Hamilton's equations for the coordinates and momenta of particles, taking into account the effect of an external random force on each particle. Thus, as in the case of systems with passive fluctuations (ordinary granular gases, for example), such an approach to constructing a kinetic theory should provide a dynamic substantiation of the statistical mechanics of such systems (see in this connection [2, 3]). Consequently, the development of a microscopic approach to the construction of the kinetic theory

of the noted systems is also of purely «academic» interest from the point of view of the general theory of irreversible processes in many-particle systems. And in this case, we also proposed a microscopic approach to constructing the kinetics of such systems based on a modified method of reduced description [36].

Low-temperature weakly ionized rarefied gases of hydrogen-like atoms. In the cases described above, we are talking about the cases of classical (not quantum) systems of many identical particles with a complex internal structure. Low-temperature rarefied gases are purely quantum objects, as a result of which, to describe their evolution, it is necessary to use the methods of quantum statistical mechanics.

The first burst of interest in the topic of such studies belongs to the second half of the last century, when the classification of plasma according to its characteristics and properties was established, an understanding of the main properties of quantum plasma [37–41] and weakly ionized gases was achieved, see, for example, [42, 43] ... Note that the number of publications on plasma physics, including monographs and textbooks, is so huge that we cite here only a few references that mark (taking into account the references in these books) a certain chronology of research.

The renewed interest in the study of kinetic processes in quantum gases is due to intensive studies of systems with Bose-Einstein condensate (BEC) [44, 45]. Indeed, BEC is a vivid example of the manifestation of the quantum-mechanical nature of matter at the macrolevel. In addition, as is known, the BEC phenomenon was first realized in alkali metal vapors at temperatures on the order of hundreds of nanokelvin (quantum gases!) [46, 47]. The most powerful argument in favor of studying the kinetics of weakly ionized or excited gases is the unique effects of the interaction of such systems with electromagnetic fields and, above all, the phenomenon of strong slowing down and even «stopping» of light in gases with BEC. The possibility of observing such phenomena experimentally was demonstrated in [48, 49]. In [50-52], for a consistent theoretical description of the interaction of electromagnetic waves with gases in the presence of BEC, a microscopic approach was proposed based on a new formulation of the secondary quantization method in the presence of bound states of particles [53]. This method made it possible, in particular, to substantiate the fundamental possibility of observing strong slowing down of light in ultracold rarefied Bose gases with BEC without using artificially stimulated transparency of the medium near resonances (see in this connection [49]). In addition, other interesting effects associated with the response of ultracold gases with BEC to excitation by an electromagnetic field were predicted within the framework of this method. The possibility of slowing down microwaves in such systems to values of the group velocity of the order of 0.01 cm / s [54] was illustrated, the possibility of controlling the group speed of light using an external magnetic field [55], the possibility of filtering electromagnetic signals by such systems [56], and even «curious» the situation of acceleration of charged particles in ultracold gases with BEC [57]. We emphasize that in the above cases, systems of many identical

particles are at ultralow temperatures, which is a necessary condition for the realization of atomic or molecular BEC with modern experimental capabilities. Since, under these conditions, the densities of the charged components of quantum plasma are exponentially small (with respect to temperature, see [58] in this connection), the systems under study can be considered weakly excited ultracold gases. In other words, the contributions of the charged components of the quantum plasma to the effects listed above can be neglected altogether or taken into account in perturbation theory.

However, this situation may not be typical for all systems with BEC. Relatively recently, the observation of the BEC phenomenon of photons was announced under the conditions of a real experiment in a special dye, and at room temperature [59, 60]. Soon, a number of theoretical works devoted to the description of such a phenomenon appeared (see, for example, Refs [61–65]), in some of them the possibility of the realization of BEC photons in excited gases and even in quantum plasmas [63–65] was predicted. In the last mentioned cases, kinetic processes in the formation of BEC photons play an extremely important role [59–66]. In particular, in the noted systems they form the effective mass of a photon («rest mass») and are responsible for thermalization of photons in matter, which makes it possible to achieve a decrease in the temperature of the photonic subsystem and, as a consequence, achieve a state with BEC in it. Note that under the conditions of a real experiment, the effective photon mass can also be formed due to the establishment of a standing wave in the system along any direction due to mirrors that prevent photons from leaving the system, see [59, 60]. In addition, in the process of experimental realization of the regime with BEC of photons in a medium, it is necessary to increase the density of photons in it. Such an increase is achieved by additional pumping of photons into the medium by an external electromagnetic field (laser) [59, 60].

Thus, when describing the phenomena and effects associated with the formation of BEC photons in excited gases and weakly ionized plasma, the problem of constructing a kinetic theory of such systems comes to the fore, that is, constructing a coupled system of kinetic equations for all possible components of the system, including radiation (photons). Such a theory should be microscopic, that is, built on the first principles of quantum statistics, and take into account the possibility of an external electromagnetic field influencing the system. We also note that the microscopic approach developed and used in [50-58] to describe the effects associated with the formation of BEC photons in excited gases and weakly ionized plasma is inappropriate. The theory used in these works becomes unusable in the region of low frequencies and wave vectors and requires substantial modification. The necessary modification, in turn, requires the use of the methods of kinetic theory, taking into account the quantum nature of matter [3]. The latter circumstance brings us back to the problem of constructing a kinetic theory of such systems based on the first principles of quantum statistical mechanics.

It should be noted here that a number of chapters in monograph [67] are devoted to the construction of the kinetic theory of partially ionized

plasma within the framework of the quantum mechanical theory (see also [68]). In it, the approach to the derivation of kinetic equations for the structural units of the system in [67] consists of two stages. First, a kinetic equation is constructed for the distribution function of pairs of charged particles. Then, after analyzing the role of fluctuations of various characteristics of particles and fields, a condition for weakening correlations is introduced when particles pass from bound to free states. This allows, as a result of the application of a number of approximations (generally speaking, poorly controlled), to go from one equation for the distribution function of pairs of charged particles to a system of three kinetic equations for the distribution functions of electrons, ions and atoms. On the basis of the developed approaches, it became possible to solve a number of problems, for example, to construct a statistical theory of bremsstrahlung in plasma-molecular systems, see in this regard [68]. However, by virtue of the mentioned weakly controlled approximations used in [67], the question arises again of constructing a kinetic theory of partially ionized plasma in the framework of the first principles of quantum statistics.

It is easy to see that the «refrain» of all of the above can be the statement about the need to develop a consistent microscopic approach to describing the evolution of the systems considered above. From this point of view, in the following sections of this work, we will demonstrate the capabilities of the reduced description method for constructing a kinetic theory for each of the systems listed above.

SECTION I. THE REDUCED DESCRIPTION METHOD IN THE THEORY OF DISSIPATIVE SYSTEMS UNDER THE INFLUENCE OF AN EXTERNAL STOCHASTIC FIELD

1.1. Basic equations

In describing the evolution of dissipative media, we will closely adhere to the order of presentation of the material in [1]. So, consider a system consisting of N identical particles of mass m, each of which is characterized by a spatial coordinate $\mathbf{x}_\alpha$, $1 \le \alpha \le N$, measured from the center of mass, and momentum $\mathbf{p}_\alpha$, $1 \le \alpha \le N$. We will assume that a system of many identical particles is placed in an external stochastic field with potential $U^\omega(\mathbf{x},t)$ (with index ω we denote the belonging of the potential $U(\mathbf{x},t)$ to the space of random realizations of an external stochastic field). For definiteness, we will also assume that before the inclusion of an external random force $U^\omega(\mathbf{x},t)$ the system was in equilibrium (usually the moment of switching on the external force is extended to $t=-\infty$). The interaction between particles is assumed to consist of two parts - reversible, described

by the Hamiltonian H, and irreversible described by the dissipative function R (see in this regard [69]). We write the Hamiltonian of the system in the following form:

$$H = H_0 + V = \sum_{1\le\alpha\le N}\left(\frac{\mathbf{p}_\alpha^2}{2m} + U^\omega\left(\mathbf{x}_\alpha, t\right)\right) + \sum_{1\le\alpha<\beta\le N} V_{\alpha,\beta}, \qquad (1.1.1)$$

where $V_{\alpha,\beta}$ represents the potential of pair interaction,

$$V_{\alpha,\beta} \equiv V\left(\mathbf{x}_{\alpha\beta}\right), \quad \mathbf{x}_{\alpha\beta} \equiv \mathbf{x}_\alpha - \mathbf{x}_\beta. \qquad (1.1.2)$$

In the general case, we will also assume that the dissipative function R is determined only by the difference of coordinates $\mathbf{x}_{\alpha\beta}$ and momenta $\mathbf{p}_{\alpha\beta}$ of the particles. Due to this circumstance, the system in the absence of an external stochastic action will have Galilean invariance. Thus, we will assume that the dissipative function can be represented in the form:

$$R = \sum_{1\le\alpha<\beta\le N} R_{\alpha,\beta}, \quad R_{\alpha,\beta} \equiv R\left(\mathbf{x}_{\alpha\beta}, \mathbf{p}_{\alpha\beta}\right), \qquad \mathbf{p}_{\alpha\beta} \equiv \mathbf{p}_\alpha - \mathbf{p}_\beta. \qquad (1.1.3)$$

Since function R is considered scalar, it should only depend on the quantities $\mathbf{x}_{\alpha\beta}^2$, $\mathbf{p}_{\alpha\beta}^2$, $\mathbf{x}_{\alpha\beta}\mathbf{p}_{\alpha\beta}$.

In accordance with formulas (1.1.1) - (1.1.3), the generalized Hamilton equations can be written in the form:

$$\dot{\mathbf{p}}_\alpha = -\frac{\partial H}{\partial \mathbf{x}_\alpha} - \frac{\partial R}{\partial \mathbf{p}_\alpha}, \qquad \dot{\mathbf{x}}_\alpha = \frac{\partial H}{\partial \mathbf{p}_\alpha}. \qquad (1.1.4)$$

Thus, force $\mathbf{F}_{\alpha,\beta}$, acting on the particle α from the particle β, is defined by the expression

$$\mathbf{F}_{\alpha,\beta} \equiv \mathbf{F}\left(\mathbf{x}_{\alpha\beta}, \mathbf{p}_{\alpha\beta}\right) = -\frac{\partial V_{\alpha,\beta}}{\partial \mathbf{x}_\alpha} - \frac{\partial R_{\alpha,\beta}}{\partial \mathbf{p}_\alpha} \qquad (1.1.5)$$

Moreover, as it follows from Eq. (1.1.1), the α-th particle is under the influence of an external random force $\mathbf{Y}_\alpha^\omega$

$$\mathbf{Y}_\alpha^\omega \equiv \mathbf{Y}^\omega\left(\mathbf{x}_\alpha, t\right) = -\frac{\partial}{\partial \mathbf{x}_\alpha} U^\omega\left(\mathbf{x}_\alpha, t\right). \qquad (1.1.6)$$

The time derivative of the total energy of the system in accordance with (1.1.1), (1.1.4) is given by the expression

$$\frac{dH}{dt}=\frac{\partial'}{\partial t}\sum_{1\le\alpha\le N}U^{\omega}\left(\mathbf{x}_{\alpha},t\right)-\sum_{1\le\alpha\le N}\frac{\mathbf{p}_{\alpha}}{m}\frac{\partial R}{\partial\mathbf{p}_{\alpha}}, \tag{1.1.7}$$

where the «prime» in the partial time derivative means differentiation with respect to the explicit dependence of the potential $U^{\omega}\left(\mathbf{x}_{\alpha},t\right)$ on time. If we assume that the dissipation in the system is associated with the friction of macroscopic particles, then the dissipative function R in this case, following [21], can be chosen in the form:

$$R=\sum_{1\le\alpha<\beta\le N}R_{\alpha,\beta}\,,\quad R_{\alpha,\beta}=\frac{1}{2}\tilde{\gamma}\left(\mathbf{x}_{\alpha\beta}\right)\mathbf{p}_{\alpha\beta}^{2}\,,\qquad \tilde{\gamma}\left(\mathbf{x}_{\alpha\beta}\right)>0\,. \tag{1.1.8}$$

This implies that $\tilde{\gamma}\left(\mathbf{x}_{\alpha\beta}\right)=0$, if $\left|\mathbf{x}_{\alpha\beta}\right|\underset{\sim}{\ge}r_{0}$, where r_{0} is the characteristic radius of action of dissipative forces. Then from Eq. (1.1.7) we have

$$\frac{dH}{dt}=\frac{\partial'}{\partial t}\sum_{1\le\alpha\le N}U^{\omega}\left(\mathbf{x}_{\alpha},t\right)-\frac{2}{m}\sum_{1\le\alpha<\beta\le N}R_{\alpha,\beta}\,. \tag{1.1.9}$$

Taking into account that $\tilde{\gamma}\left(\mathbf{x}_{\alpha\beta}\right)>0$, see Eq. (1.1.8), it is easy to see that in such a system, competition is possible between dissipation due to friction and energy pumping from the side of an external stochastic field. We will return to this issue later in this article.

The next task is to obtain the Liouville equation for the system of many particles under study. For this purpose, for the convenience of further calculations, we represent equations (1.1.4) in the following form

$$\dot{x}_{\alpha}\left(t\right)=h_{\alpha}^{\omega}\left(x_{1}\left(t\right),...,x_{N}\left(t\right)\right),\qquad 1\le\alpha\le N\,, \tag{1.1.10}$$

where we introduce

$$x_{a}\left(t\right)\equiv\left(\mathbf{x}_{a}\left(t\right),\mathbf{p}_{a}\left(t\right)\right). \tag{1.1.11}$$

In other words, Eq. (1.1.10) with (1.1.11), (1.1.4) is the following system of equations

$$\dot{\mathbf{x}}_{\alpha}\left(t\right)=\mathbf{h}_{\mathbf{x}\alpha}^{\omega}\left(x\left(t\right)\right),\qquad \dot{\mathbf{p}}_{\alpha}\left(t\right)=\mathbf{h}_{\mathbf{p}\alpha}^{\omega}\left(x\left(t\right)\right), \tag{1.1.12}$$

where

$$\mathbf{h}_{\mathbf{x}\alpha}^{\omega}\left(x\left(t\right)\right)=\frac{\partial H}{\partial\mathbf{p}_{\alpha}}\,,\qquad \mathbf{h}_{\mathbf{p}\alpha}^{\omega}\left(x\left(t\right)\right)=-\frac{\partial H}{\partial\mathbf{x}_{\alpha}}-\frac{\partial R}{\partial\mathbf{p}_{\alpha}}\,. \tag{1.1.13}$$

The value of coordinates and momenta of the α-th particle in the moment of time t (see Eq. (1.1.11)), is obviously determined by the values of coordinates and momenta $x_0 \equiv \left(x_1(0),...,x_N(0)\right)$ of all particles at the initial moment of time $t=0$:

$$x_\alpha^\omega(t) = X_\alpha^\omega(t,x_0) \equiv \left(\mathbf{X}_\alpha^\omega(t,x_0), \mathbf{P}_\alpha^\omega(t,x_0)\right), \qquad (1.1.14)$$

where functions $\mathbf{X}_\alpha^\omega(t,x_0)$, $\mathbf{P}_\alpha^\omega(t,x_0)$ satisfy the generalized Hamilton equations (1.1.4) (or equations (1.1.10) - (1.1.13)). Let at $t=0$ the initial conditions $x_0 \equiv \left(x_1(0),...,x_N(0)\right)$ are distributed according to the probability density $D\left(x_1(0),...,x_N(0);0\right)$ (see in this regard [3]), while

$$\int dx_1(0)...dx_N(0)\, D\left(x_1(0),...,x_N(0);0\right) \equiv \int dx_0 D(x_0;0) = 1. \qquad (1.1.15)$$

Then at time t the probability density $D^\omega(x_1,...,x_N;t) \equiv D^\omega(x;t)$, $x \equiv (x_1,...,x_N)$, (N-particle distribution function) will obviously be determined by the expression

$$D^\omega(x_1,...,x_N;t) = \int dx_0 D(x_0;0) \prod_{1\le\alpha\le N} \delta\left(x_\alpha - X_\alpha^\omega(t,x_0)\right). \qquad (1.1.16)$$

In [5], the procedure for deriving the Liouville equation for many-particle systems in an external stochastic field is described in detail, neglecting the interaction between particles. In [69], a similar procedure is used to obtain the generalized Liouville equation for dissipative many-particle systems in the absence of an external stochastic field. A detailed adherence to the methodology outlined in these works allows one to arrive at the following evolution equation for N-particle distribution function $D^\omega(x_1,...,x_N;t)$

$$\frac{\partial D^\omega}{\partial t} + \sum_{1\le\alpha\le N} \frac{\partial}{\partial x_\alpha}\left(D^\omega h_\alpha^\omega\right) = 0, \qquad (1.1.17)$$

where function $h_\alpha^\omega\left(x(t)\right)$ is given by expressions (1.1.12), (1.1.13). This equation is the Liouville equation generalized to the case of many-particle dissipative systems under the influence of an external stochastic field. Note that this equation can be given a more familiar form (see [16]):

$$\frac{\partial D^{\omega}}{\partial t}-\left\{H,D^{\omega}\right\}=\sum_{1\le\alpha\le N}\frac{\partial}{\partial\mathbf{p}_{\alpha}}\left(D^{\omega}\frac{\partial R}{\partial\mathbf{p}_{\alpha}}\right), \qquad (1.1.18)$$

where with $\{A,B\}$ we denote N - particle Poisson brackets

$$\{A,B\}\equiv\sum_{1\le\alpha\le N}\left(\frac{\partial A}{\partial\mathbf{x}_{\alpha}}\frac{\partial B}{\partial\mathbf{p}_{\alpha}}-\frac{\partial A}{\partial\mathbf{p}_{\alpha}}\frac{\partial B}{\partial\mathbf{x}_{\alpha}}\right). \qquad (1.1.19)$$

However, in what follows, it will be more useful for us to use the Liouville equation (1.1.17), reduced, taking into account (1.1.10) - (1.1.13), (1.1.1), (1.1.5), (11.1.6), to the form:

$$\frac{\partial D^{\omega}}{\partial t}+\sum_{1\le\alpha\le N}\frac{\mathbf{p}_{\alpha}}{m}\frac{\partial D^{\omega}}{\partial\mathbf{x}_{\alpha}}+\sum_{1\le\alpha<\beta\le N}\frac{\partial}{\partial\mathbf{p}_{\alpha}}D^{\omega}\mathbf{F}_{\alpha,\beta}+\sum_{1\le\alpha\le N}\frac{\partial}{\partial\mathbf{p}_{\alpha}}D^{\omega}\mathbf{Y}_{\alpha}^{\omega}=0, \qquad (1.1.20)$$

where the values $\mathbf{F}_{\alpha,\beta}$, $\mathbf{Y}_{\alpha}^{\omega}$ are still defined by formulas (1.1.5), (1.1.6). Equation (1.1.20), as is easy to see, is a classical example of an evolution equation with multiplicative noise. In this connection, the question arises of averaging equation (1.1.20) over the external random force $\mathbf{Y}_{\alpha}^{\omega}$.

1.2. Averaging the generalized Liouville equation over a random external field

Let us introduce into consideration N-particle distribution function $D(x_1,...,x_N;t)$, which is the distribution function $D^{\omega}(x_1,...,x_N;t)$ (see Eq. (1.1.16)), averaged over a random external field $\mathbf{Y}^{\omega}(\mathbf{x},t)$ with probability density $W[\mathbf{Y}^{\omega}]$:

$$D(x_1,...,x_N;t)\equiv\left\langle D^{\omega}(x_1,...,x_N;t)\right\rangle_{\omega}, \qquad \left\langle ...\right\rangle_{\omega}\equiv\int D\mathbf{Y}^{\omega}(\mathbf{x},t)W[\mathbf{Y}^{\omega}]... \qquad (1.2.1)$$

Applying the averaging operation (1.2.1) to Eq. (1.1.20), we get:

$$\frac{\partial D}{\partial t}+\sum_{1\le\alpha\le N}\frac{\mathbf{p}_{\alpha}}{m}\frac{\partial D}{\partial\mathbf{x}_{\alpha}}+\sum_{1\le\alpha<\beta\le N}\frac{\partial}{\partial\mathbf{p}_{\alpha}}D\mathbf{F}_{\alpha,\beta}+\sum_{1\le\alpha\le N}\frac{\partial}{\partial\mathbf{p}_{\alpha}}\left\langle D^{\omega}\mathbf{Y}_{\alpha}^{\omega}\right\rangle_{\omega}=0. \qquad (1.2.2)$$

It is easy to see that in order for this equation to be a closed evolution equation for the introduced distribution function, it is necessary to express

the quantity $\left\langle D^{\omega}\mathbf{Y}_{\alpha}^{\omega}\right\rangle_{\omega}$ through $D\left(x_1,...,x_N;t\right)$. For this we use the so-called Furutsu-Novikov formula [71, 72], which was proved for the case of Gaussian distributions of an external random field. We also note that in [73] this formula was used to obtain the Kolmogorov turbulence spectra generalized to the case of a compressible fluid. The Furutsu-Novikov formula was generalized to the case of non-Gaussian distributions of an external random field in [4]. In this article, we will closely follow the methodology for this particular work. We will give the necessary calculations here in sufficient detail for the consistency of presentation and ease of reading. For this purpose, we introduce into consideration the momenta $Y_{i_1...i_n}\left(\mathbf{x}_1,...,\mathbf{x}_n;t_1,...,t_n\right)$ of the distribution of an external random field $W[\mathbf{Y}^{\omega}\left(\mathbf{x},t\right)]$ (see Eq. (2.1))

$$Y_{i_1...i_n}\left(\mathbf{x}_1,...,\mathbf{x}_n;t_1,...,t_n\right)\equiv\left\langle Y_{i_1}^{\omega}\left(\mathbf{x}_1,t_1\right)...Y_{i_n}^{\omega}\left(\mathbf{x}_n,t_n\right)\right\rangle_{\omega}, \tag{1.2.3}$$

$$Y_i^{\omega}\left(\mathbf{x},t\right)\equiv\left(\mathbf{Y}^{\omega}\left(\mathbf{x},t\right)\right)_i, \qquad i=\left(1,2,3\right).$$

Generating functional $P\left(v;Y_a\right)$ of these moments is determined by the formula (summation is assumed over twice repeated indices)

$$P\left(v;Y_a\right)\equiv\left\langle\exp\left(\int d\mathbf{x}\int_{-\infty}^{\infty}dtv_i\left(\mathbf{x},t\right)Y_i^{\omega}\left(\mathbf{x},t\right)\right)\right\rangle_{\omega}, \tag{1.2.4}$$

where $v_i\left(\mathbf{x},t\right)$ is the functional argument. With Y_a in the left-hand side of the formula (1.2.4) we denote the set of values $Y_{i_1...i_n}\left(\mathbf{x}_1,...,\mathbf{x}_n;t_1,...,t_n\right)$. Generating functional $\mathcal{P}\left(v;y_a\right)$ of the correlation functions $y_{i_1...i_S}\left(\mathbf{x}_1,...,\mathbf{x}_S;t_1,...,t_S\right)$

$$\mathcal{P}\left(v;y_a\right)\equiv\sum_{n=2}^{\infty}\frac{1}{n!}\int d\mathbf{x}_1\int_{-\infty}^{\infty}dt_1...\int d\mathbf{x}_n\int_{-\infty}^{\infty}dt_nv_{i_1}\left(\mathbf{x}_1,t_S\right)...v_{i_n}\left(\mathbf{x}_n,t_n\right)y_{i_1...i_n}\left(\mathbf{x}_1,...,\mathbf{x}_n;t_1,...,t_n\right) \tag{1.2.5}$$

is connected with the generating functional $P\left(v;Y_a\right)$ via the formula:

$$P\left(v;Y_a\right)=\exp\left(\int d\mathbf{x}\int_{-\infty}^{\infty}dtv_i\left(\mathbf{x},t\right)Y_i\left(\mathbf{x},t\right)\right)\exp\left\{\mathcal{P}\left(v;y_a\right)\right\}, \tag{1.2.6}$$

where

$$\mathbf{Y}(\mathbf{x},t) \equiv \left\langle \mathbf{Y}^{\omega}(\mathbf{x},t) \right\rangle_{\omega} \tag{1.2.7}$$

and with y_a we denote the whole set of variables $y_{i_1\ldots i_n}(\mathbf{x}_1,\ldots,\mathbf{x}_n;t_1,\ldots,t_n)$. In [4] it was shown that when averaging the generating functional $A[\mathbf{Y}^{\omega}(\mathbf{x},t)]$ over the external random field with distribution $W[\mathbf{Y}^{\omega}(\mathbf{x},t)]$ (see Eq. (1.2.1)) the result can be represented in the following way:

$$\left\langle A[\mathbf{Y}^{\omega}(\mathbf{x},t)] \right\rangle_{\omega} = \exp\left\{ \mathcal{P}\left(\frac{\delta}{\delta Y}; y_a \right) \right\} A[Y], \tag{1.2.8}$$

where $\mathcal{P}\left(\frac{\delta}{\delta Y}; y_a \right)$ is the generating functional (2.5), where the functional argument $v_i(\mathbf{x},t)$ is replaced with the operation of functional derivative over $Y_i(\mathbf{x},t)$ (see Eqs. (1.2.3), (1.2.7)):

$$v_i(\mathbf{x},t) \to \delta / \delta Y_i(\mathbf{x},t). \tag{1.2.9}$$

A consequence of formula (2.8), as it is easy to verify, is the expression:

$$\left\langle Y_i^{\omega}(\mathbf{x},t) A[\mathbf{Y}^{\omega}(\mathbf{x},t)] \right\rangle_{\omega} = \left(Y_i(\mathbf{x},t) + \frac{\delta \mathcal{P}(v; y_a)}{\delta v_i(\mathbf{x},t)} \right)_{v_i \to \delta/\delta Y_i} \exp\left\{ \mathcal{P}\left(\frac{\delta}{\delta Y}; y_a \right) \right\} A[Y].$$

Taking into account (1.2.8), the same formula can be rewritten as:

$$\left\langle Y_i^{\omega}(\mathbf{x},t) A[\mathbf{Y}^{\omega}(\mathbf{x},t)] \right\rangle_{\omega} = Y_i(\mathbf{x},t) \left\langle A[\mathbf{Y}^{\omega}(\mathbf{x},t)] \right\rangle_{\omega} + \left\langle \left. \frac{\delta \mathcal{P}(v; y_a)}{\delta v_i(\mathbf{x},t)} \right|_{v_i \to \delta/\delta Y_i} A[\mathbf{Y}^{\omega}(\mathbf{x},t)] \right\rangle_{\omega}. \tag{1.2.10}$$

Expression (1.2.10) is a generalization of the Furutsu-Novikov formula to the case of arbitrary distributions of an external random field (naturally, it is assumed that these distributions have momenta of any order). Note that for a Gaussian distribution of an external random field (1.2.10) takes the form

$$\left\langle Y_i^{\omega}(\mathbf{x},t) A[\mathbf{Y}^{\omega}] \right\rangle_{\omega} = Y_i(\mathbf{x},t) \left\langle A[\mathbf{Y}^{\omega}] \right\rangle_{\omega} + \int d\mathbf{x}' \int_{-\infty}^{\infty} dt' y_{ij}(\mathbf{x},\mathbf{x}',t-t') \left\langle \frac{\delta A[\mathbf{Y}^{\omega}]}{\delta Y_j(\mathbf{x}',t')} \right\rangle_{\omega}, \tag{1.2.11}$$

where $y_{ij}\left(\mathbf{x},\mathbf{x}',t-t'\right)$ - is a pair correlation function of the external Gaussian noise

$$y_{ij}\left(\mathbf{x},\mathbf{x}',t-t'\right)=\left\langle Y_i^{\omega}\left(\mathbf{x},t\right)Y_j^{\omega}\left(\mathbf{x}',t'\right)\right\rangle_{\omega}-\left\langle Y_i^{\omega}\left(\mathbf{x},t\right)\right\rangle_{\omega}\left\langle Y_j^{\omega}\left(\mathbf{x}',t'\right)\right\rangle_{\omega}.$$

When $Y_i\left(\mathbf{x},t\right)\equiv 0$ expression (1.2.11) exactly coincides with a similar expression obtained in [22, 23] under the assumption that the average value of the external random force acting on the system is zero.

We now use the Furutsu-Novikov formula to calculate the last term on the left-hand side of equation (1.2.2). The basis for this is the functional dependence of the distribution function $D^{\omega}\left(x_1,...,x_N;t\right)$ on the external stochastic field $Y_i^{\omega}\left(\mathbf{x},t\right)$,

$$D^{\omega}\equiv D^{\omega}[\mathbf{Y}^{\omega}],$$

as is seen from definition (1.1.16) or equation (1.1.20). In accordance with (1.2.10) the average value $\left\langle D^{\omega}\mathbf{Y}^{\omega}\right\rangle_{\omega}$ can be represented as:

$$\left\langle D^{\omega}[\mathbf{Y}^{\omega}]Y_i^{\omega}\left(\mathbf{x},t\right)\right\rangle_{\omega}=Y_i\left(\mathbf{x},t\right)D+\left\langle\left.\frac{\delta\mathcal{P}\left(v;y_a\right)}{\delta v_i\left(\mathbf{x},t\right)}\right|_{v_i\to\delta/\delta Y_i}D^{\omega}[\mathbf{Y}^{\omega}]\right\rangle_{\omega}. \qquad (1.2.12)$$

Noticing further that in accordance with (1.2.5)

$$\frac{\delta\mathcal{P}\left(v;y_a\right)}{\delta v_i\left(\mathbf{x},t\right)}=\sum_{n=1}^{\infty}\frac{1}{n!}\int d\mathbf{x}_1\int_{-\infty}^{\infty}dt_1...\int d\mathbf{x}_n\int_{-\infty}^{\infty}dt_n v_{i_1}\left(\mathbf{x}_1,t_S\right)...v_{i_n}\left(\mathbf{x}_n,t_n\right)y_{ii_1...i_n}\left(\mathbf{x},\mathbf{x}_1,...,\mathbf{x}_n;t,t_1,...,t_n\right), \qquad (1.2.13)$$

for the value $\left\langle\left.\frac{\delta\mathcal{P}\left(v;y_a\right)}{\delta v_i\left(\mathbf{x},t\right)}\right|_{v_i\to\delta/\delta Y_i}D^{\omega}[\mathbf{Y}^{\omega}]\right\rangle_{\omega}$ in Eq. (1.2.12) we get the following expression

$$\left\langle\left.\frac{\delta\mathcal{P}\left(v;y_a\right)}{\delta v_i\left(\mathbf{x},t\right)}\right|_{v_i\to\delta/\delta Y_i}D^{\omega}[\mathbf{Y}^{\omega}]\right\rangle_{\omega}= \qquad (1.2.14)$$

$$=\sum_{n=1}^{\infty}\frac{1}{n!}\int d\mathbf{x}_1\int_{-\infty}^{\infty}dt_1...\int d\mathbf{x}_n\int_{-\infty}^{\infty}dt_n y_{ii_1...i_n}\left(\mathbf{x},\mathbf{x}_1,...,\mathbf{x}_n;t,t_1,...,t_n\right)\left\langle\frac{\delta^n D^{\omega}[\mathbf{Y}^{\omega}]}{\delta Y_{i_1}^{\omega}\left(\mathbf{x}_1,t_1\right)...\delta Y_{i_n}^{\omega}\left(\mathbf{x}_n,t_n\right)}\right\rangle_{\omega}.$$

For further calculations, let us first consider the value I_i,

$$I_i\equiv\int d\mathbf{x}'\int_{-\infty}^{\infty}dt' y_{ij}\left(\mathbf{x},\mathbf{x}';t,t'\right)\left\langle\frac{\delta D^{\omega}[\mathbf{Y}^{\omega}]}{\delta Y_j^{\omega}\left(\mathbf{x}',t'\right)}\right\rangle_{\omega}. \qquad (1.2.15)$$

As is easy to see, this quantity is the first term from the sum on the right-hand side of expression (1.2.14).

We will assume that the pair correlation function $y_{ij}\left(\mathbf{x},\mathbf{x}';t,t'\right)$ differs from zero in the interval $\left|t-t'\right|\le\tau_0$ (τ_0 is random process memory). We will also assume that for $t\sim t'$ pair correlation function $y_{ij}\left(\mathbf{x},\mathbf{x}';t,t'\right)$ has a sharp maximum. Then the functional derivative $\dfrac{\delta D^{\omega}[\mathbf{Y}^{\omega}]}{\delta Y_j^{\omega}\left(\mathbf{x}',t'\right)}$ is to be calculated only at $t\approx t'$. Moreover, as shown in Refs [71, 73, 4], the exact expression for this derivative can be obtained only for $t\approx t'$ in fact, as is easy to see, the variational derivative $\dfrac{\delta D^{\omega}[\mathbf{Y}^{\omega}]}{\delta Y_j^{\omega}\left(\mathbf{x}',t'\right)}$ at $t\approx t'$ undergoes a leap:

$$\frac{\delta D^{\omega}[\mathbf{Y}^{\omega}]}{\delta Y_j^{\omega}\left(\mathbf{x}',t'\right)}\neq 0,\quad t'\le t\,,\quad \frac{\delta D^{\omega}[\mathbf{Y}^{\omega}]}{\delta Y_j^{\omega}\left(\mathbf{x}',t'\right)}=0,\quad t'>t\,. \tag{1.2.16}$$

The latter circumstance is due to the fact that according to equation (1.1.20), the quantity $D^{\omega}\left(t\right)$ cannot be field $Y_j^{\omega}\left(\mathbf{x}',t'\right)$ dependent, at later points in time than t. In accordance with (1.2.16) integration over t' in formula (1.2.15) is carried out in the range from $-\infty$ to t, not from $-\infty$ to $+\infty$.

Differentiating Eq. (1.1.20) over $Y_j^{\omega}\left(\mathbf{x}',t'\right)$ and noticing that according to (1.2.16) the derivative $\dfrac{\partial}{\partial t}\dfrac{\delta D^{\omega}[\mathbf{Y}^{\omega}]}{\delta Y_j^{\omega}\left(\mathbf{x}',t'\right)}$ need to contain a δ-like feature in time (while the value itself $\dfrac{\delta D^{\omega}[\mathbf{Y}^{\omega}]}{\delta Y_j^{\omega}\left(\mathbf{x}',t'\right)}$ does not contain them), it is not difficult to obtain the following expression for the functional derivative (see [4]):

$$\frac{\delta D^{\omega}[\mathbf{Y}^{\omega}]}{\delta Y_j^{\omega}\left(\mathbf{x}',t'\right)}=-\vartheta\left(t-t'\right)\sum_{1\le\alpha\le N}\delta\left(\mathbf{x}'-\mathbf{x}_{\alpha}\right)\frac{\partial D^{\omega}[\mathbf{Y}^{\omega}]}{\partial p_{\alpha j}}. \tag{1.2.17}$$

This formula allows one to represent the value I_i (see Eq. (1.2.15)) in the following form (see (1.2.1), (1.2.2)):

$$I_i=\int_{-\infty}^{t}dt'\sum_{1\le\alpha\le N}y_{ij}\left(\mathbf{x},\mathbf{x}_{\alpha};t,t'\right)\frac{\partial D}{\partial p_{\alpha j}}. \tag{1.2.18}$$

For Gaussian processes, expressions (1.2.12), (1.2.18) are sufficient to obtain the value (1.2.12) (and, consequently, the averaged Liouville equation generalized to the case of dissipative systems of many particles in an external stochastic field) in the final form:

$$\frac{\partial D}{\partial t}+\sum_{1\le\alpha\le N}\frac{\mathbf{p}_\alpha}{m}\frac{\partial D}{\partial \mathbf{x}_\alpha}+\sum_{1\le\alpha<\beta\le N}\frac{\partial D\mathbf{F}_{\alpha,\beta}}{\partial \mathbf{p}_\alpha}+\sum_{1\le\alpha\le N}\mathbf{Y}\left(\mathbf{x}_\alpha,t\right)\frac{\partial D}{\partial \mathbf{p}_\alpha}- \tag{1.2.19}$$

$$-\int_{-\infty}^{t}dt'\sum_{1\le\alpha\le N}y_{ij}\left(\mathbf{x}_\alpha,\mathbf{x}_\beta;t,t'\right)\frac{\partial^2 D}{\partial p_{\alpha i}\partial p_{\beta j}}=0\,.$$

In fact, the calculations performed make it possible to obtain the generalized Liouville equation in the case of non-Gaussian distributions of an external random field (naturally, it is assumed that these distributions have moments of any order). For this, according to (1.2.14), it is required to calculate the functional derivative of the n-th order. This value can be easily obtained using formula (1.2.17). Indeed, differentiating (1.2.17) with respect to $Y_l^{\omega}\left(\mathbf{x}'',t''\right)$, we get:

$$\frac{\delta^2 D^{\omega}[\mathbf{Y}^{\omega}]}{\delta Y_j^{\omega}\left(\mathbf{x}',t'\right)\delta Y_l^{\omega}\left(\mathbf{x}'',t''\right)}=-\vartheta\left(t-t'\right)\sum_{1\le\alpha\le N}\delta\left(\mathbf{x}'-\mathbf{x}_\alpha\right)\frac{\partial}{\partial p_{\alpha j}}\frac{\delta D^{\omega}[\mathbf{Y}^{\omega}]}{\delta Y_l^{\omega}\left(\mathbf{x}'',t''\right)}\,.$$

Next, we again use formula (1.2.17), as a result of which we obtain:

$$\frac{\delta^2 D^{\omega}[\mathbf{Y}^{\omega}]}{\delta Y_j^{\omega}\left(\mathbf{x}',t'\right)\delta Y_l^{\omega}\left(\mathbf{x}'',t''\right)}=\vartheta\left(t-t'\right)\vartheta\left(t-t''\right)\sum_{1\le\alpha\le N}\sum_{1\le\beta\le N}\delta\left(\mathbf{x}'-\mathbf{x}_\alpha\right)\delta\left(\mathbf{x}''-\mathbf{x}_\beta\right)\frac{\partial^2 D^{\omega}[\mathbf{Y}^{\omega}]}{\partial p_{\alpha j}\partial p_{\beta l}}\,.$$

Using this procedure as many times as necessary, one can arrive at the following expression:

$$\frac{\delta^n D^{\omega}[\mathbf{Y}^{\omega}]}{\delta Y_{i_1}^{\omega}\left(\mathbf{x}_1,t_1\right)...\delta Y_{i_n}^{\omega}\left(\mathbf{x}_n,t_n\right)}= \tag{1.2.20}$$

$$=(-1)^n\,\vartheta\left(t-t_1\right)...\vartheta\left(t-t_n\right)\left(\sum_{1\le\alpha_1\le N}\delta\left(\mathbf{x}_1-\mathbf{x}_{\alpha_1}\right)\frac{\partial}{\partial p_{\alpha_1 i_1}}\right)...\left(\sum_{1\le\alpha_n\le N}\delta\left(\mathbf{x}_n-\mathbf{x}_{\alpha_n}\right)\frac{\partial}{\partial p_{\alpha_n i_n}}\right)D^{\omega}[\mathbf{Y}^{\omega}]\,.$$

Substituting this expression into (1.2.14) using (1.2.12), the evolution equation (1.2.2) can be written in the form:

$$\frac{\partial D}{\partial t}+\sum_{1\le\alpha\le N}\frac{\mathbf{p}_\alpha}{m}\frac{\partial D}{\partial \mathbf{x}_\alpha}+\sum_{1\le\alpha<\beta\le N}\frac{\partial D\mathbf{F}_{\alpha,\beta}}{\partial \mathbf{p}_\alpha}+\sum_{1\le\alpha\le N}\mathbf{Y}\left(\mathbf{x}_\alpha,t\right)\frac{\partial D}{\partial \mathbf{p}_\alpha}- \tag{1.2.21}$$

$$+\sum_{n=2}^{\infty}\frac{(-1)^{n-1}}{(n-1)!}\int_{-\infty}^{t}dt_2...\int_{-\infty}^{t}dt_n\sum_{1\le\alpha_1\le N}...\sum_{1\le\alpha_n\le N}y_{i_1...i_n}\left(\mathbf{x}_{\alpha_1},...,\mathbf{x}_{\alpha_n};t,t_2,...,t_n\right)\frac{\partial^n D}{\partial p_{\alpha_1 i_1}...\partial p_{\alpha_n i_n}}=0\cdot$$

Equation (1.2.21) is the generalized Liouville equation for dissipative systems of many particles, averaged over an external non-Gaussian stochastic field. Note that a generalization of Liouville's theorem to the case of simple Brownian motion in the phenomenological approach based on the Langevin equations, taking into account the influence of an external force field, can be found in [74].

In the case of stationary random processes, Eq. (1.2.21) can be further simplified if we assume that the correlation functions $y_{i_1...i_n}\left(\mathbf{x}_1,...,\mathbf{x}_n;t,t_2,...,t_n\right)$ can be represented as:

$$y_{i_1...i_n}\left(\mathbf{x}_{\alpha_1},...,\mathbf{x}_{\alpha_n};t,t_2,...,t_n\right)\equiv y_{i_1...i_n}\left(\mathbf{x}_{\alpha_1},...,\mathbf{x}_{\alpha_n};\left|t_2-t\right|,...,\left|t_n-t\right|\right). \tag{1.2.22}$$

To simplify further calculations, we will also assume that the average value of the external random field is zero,

$$\mathbf{Y}\left(\mathbf{x},t\right)\equiv\left\langle\mathbf{Y}^{\omega}\left(\mathbf{x},t\right)\right\rangle_{\omega}\equiv 0\,. \tag{1.2.23}$$

In this case, the evolution equation for N- particle distribution function averaged over the external stochastic field can be written as:

$$\frac{\partial D}{\partial t}+\sum_{1\le\alpha\le N}\frac{\mathbf{p}_\alpha}{m}\frac{\partial D}{\partial \mathbf{x}_\alpha}+\sum_{1\le\alpha<\beta\le N}\frac{\partial D\mathbf{F}_{\alpha,\beta}}{\partial \mathbf{p}_\alpha}- \tag{1.2.24}$$

$$+\sum_{n=2}^{\infty}\frac{(-1)^{n-1}}{2^{n-1}(n-1)!}\sum_{1\le\alpha_1\le N}...\sum_{1\le\alpha_n\le N}y_{i_1...i_n}\left(\mathbf{x}_{\alpha_1},...,\mathbf{x}_{\alpha_n}\right)\frac{\partial^n D}{\partial p_{\alpha_1 i_1}...\partial p_{\alpha_n i_n}}=0\,,$$

where the following correlation functions are introduced $y_{i_1...i_n}\left(\mathbf{x}_{\alpha_1},...,\mathbf{x}_{\alpha_n}\right)$:

$$y_{i_1...i_n}\left(\mathbf{x}_{\alpha_1},...,\mathbf{x}_{\alpha_n}\right)\equiv\int_{-\infty}^{\infty}dt_2...\int_{-\infty}^{\infty}dt_n y_{i_1...i_n}\left(\mathbf{x}_{\alpha_1},...,\mathbf{x}_{\alpha_n};\left|t_2-t\right|,...,\left|t_n-t\right|\right). \tag{1.2.25}$$

1.3. Analogue of the BBGKY chain for dissipative systems in external stochastic fields

Along with the probability density D it is possible to introduce the probability of finding one or several particles in given elements of the phase space, regardless of where the remaining particles are located in this space (see in this connection [2, 3]). These probabilities can be obtained by integrating the function D over all variables, except for those related to the particles under consideration:

$$f_S\left(x_1,...,x_S;t\right)=\mathcal{V}^S\int dx_{S+1}...\int dx_N D\left(x_1,...,x_N;t\right),\ x_\alpha\equiv\left(\mathbf{x}_\alpha,\mathbf{p}_\alpha\right), \quad (1.3.1)$$

where $D\left(x_1,...,x_N;t\right)$ satisfies equation (1.2.21) or (1.2.24) and $\mathcal{V}$ is the volume of the system. Following the methodology [2, 3], it is easy to arrive at the following equation for S - particle distribution function $f_S\left(x_1,...,x_S;t\right)$:

$$\frac{\partial f_S}{\partial t}=-\sum_{1\le\alpha\le S}\frac{\mathbf{p}_\alpha}{m}\frac{\partial f_S}{\partial\mathbf{x}_\alpha}-\sum_{1\le\alpha<\beta\le S}\frac{\partial f_S\mathbf{F}_{\alpha,\beta}}{\partial\mathbf{p}_\alpha}-\sum_{1\le\alpha\le N}\mathbf{Y}\left(\mathbf{x}_\alpha,t\right)\frac{\partial f_S}{\partial\mathbf{p}_\alpha}- \quad (1.3.2)$$

$$-\sum_{n=2}^{\infty}\frac{\left(-1\right)^{n-1}}{\left(n-1\right)!}\int_{-\infty}^{t}dt_2...\int_{-\infty}^{t}dt_n\sum_{1\le\alpha_1\le S}...\sum_{1\le\alpha_n\le S}y_{i_1...i_n}\left(\mathbf{x}_{\alpha_1},...,\mathbf{x}_{\alpha_n};t,t_2,...,t_n\right)\frac{\partial^n f_S}{\partial p_{\alpha_1 i_1}...\partial p_{\alpha_n i_n}}-$$

$$-\frac{1}{v}\sum_{1\le\alpha\le S}\frac{\partial}{\partial\mathbf{p}_\alpha}\int dx_{S+1}f_{S+1}\mathbf{F}_{\alpha,S+1},\quad v\equiv\frac{\mathcal{V}}{N},$$

if function $D\left(x_1,...,x_N;t\right)$ satisfies Eq. (1.2.21) and

$$\frac{\partial f_S}{\partial t}=-\sum_{1\le\alpha\le S}\frac{\mathbf{p}_\alpha}{m}\frac{\partial f_S}{\partial\mathbf{x}_\alpha}-\sum_{1\le\alpha<\beta\le S}\frac{\partial f_S\mathbf{F}_{\alpha,\beta}}{\partial\mathbf{p}_\alpha}- \quad (1.3.3)$$

$$-\sum_{n=2}^{\infty}\frac{\left(-1\right)^{n-1}}{2^{n-1}\left(n-1\right)!}\sum_{1\le\alpha_1\le S}...\sum_{1\le\alpha_n\le S}y_{i_1...i_n}\left(\mathbf{x}_{\alpha_1},...,\mathbf{x}_{\alpha_n}\right)\frac{\partial^n f_S}{\partial p_{\alpha_1 i_1}...\partial p_{\alpha_n i_n}}-$$

$$-\frac{1}{v}\sum_{1\le\alpha\le S}\frac{\partial}{\partial\mathbf{p}_\alpha}\int dx_{S+1}f_{S+1}\mathbf{F}_{\alpha,S+1},\quad v\equiv\frac{\mathcal{V}}{N},$$

if function $D\left(x_1,...,x_N;t\right)$ satisfies equation (1.2.24). The quantity $\mathbf{F}_{\alpha,\beta}$ in Eqs. (1.3.2), (1.3.3) is still defined by formula (1.1.5). It is easy to see that the equation for S - particle distribution functions include $S+1$ -particle distribution function. That is, in fact, we have obtained infinite chains of kinetic equations (1.3.2), (1.3.3). These chains are a generalization of the

famous chain of Bogolyubov-Born-Green-Kirkwood-Yvon equations to the case of dissipative systems of many particles under the influence of an external stochastic field. The following remark should be made here. In accordance with definition (1.3.1), distribution functions of a higher order contain all the information contained in functions of a lower order [3]. This circumstance leads to the fact that with increasing order S the distribution functions $f_S(x_1,...,x_S;t)$ are becoming more and more complex. Since in the full description according to (1.3.3) it is necessary to take into account the distribution functions up to $S \to \infty$, we come to the conclusion that the resulting chains of equations (1.3.2), (1.3.3) are themselves equivalent to Liouville's equations (1.2.21) or (1.2.24), respectively. In other words, the most complete description of the systems under study is equally complex both in the language of the complete distribution function $D(x_1,...,x_N;t)$, and in the language of many-particle distribution functions $f_S(x_1,...,x_S;t)$.

A significant simplification in the description of the state of the system occurs in two cases: when the interaction between particles is small, or when the density of the number of particles is low, and the interaction is arbitrary, but such that does not lead to the formation of bound states [3]. This simplification in the description is a consequence of the difference in the evolutionary behavior of the many-particle and single-particle distribution functions. Indeed, at the initial stage of evolution, when the time t is small compared to the characteristic time of chaotization τ_0, multiparticle distribution functions $f_S(x_1,...,x_S;t)$ change very quickly with time, in contrast to the single-particle distribution function $f_1(x,t)$. The single-particle distribution function undergoes significant changes in time at times that are much longer than the relaxation times of the system τ_r, while $\tau_r \gg \tau_0$. Time τ_0 the order of magnitude is determined by the duration of one collision. The time τ_r the order of magnitude should coincide with the time of establishment of the state of statistical equilibrium in the system (for more details, see [3]). Such a difference in the evolutionary behavior of one-particle and many-particle distribution functions formed the basis of N.N. Bogolyubov's idea about the hierarchy of relaxation times of the system [2]. In turn, on the basis of this idea, the provisions of the now well-known method of the reduced description of Bogolyubov --Peletminskii for the study of nonequilibrium processes in systems of many particles were formulated. The basics of this method were formulated by N.N. Bogolyubov to describe the evolution of classical (not quantum) systems [2]. In the case of quantum systems, the reduced description method was generalized in the works of S.V. Peletminskii [3]. We emphasize once again that dissipative systems of many particles were

not considered in [2, 3], just as the effects of stochastic fields on these systems were not considered as well.

According to the idea of a hierarchy of relaxation times, the evolution of a system of many particles can be conditionally divided into several stages. Each subsequent stage of evolution differs from the previous one by simplification in describing the evolution of a system of many particles. The simplest scenario for the evolution of many-particle systems is as follows. At $\tau_0 \ll t \ll \tau_r$ there is a kinetic stage in the evolution of the system, when the behavior of the system can be described by a one-particle distribution function. Such a description of the evolution of the system is much simpler in comparison with the description using many-particle distribution functions. Further simplification in the description of systems of many particles occurs when $t \gg \tau_r$ (hydrodynamic stage of the evolution of the system), when the behavior of the system can be described by the hydrodynamic parameters of the description, for example, the density of the number of particles, the average velocity and temperature of the medium. This step-by-step simplification in the description of the system is used to construct the approaches of the reduced description method [2, 3].

In this work, we will use the reduced description method of nonequilibrium processes to derive kinetic equations describing the evolution of dissipative systems in an external random field (see in this connection also [3, 5]). The initial equations will be the equations of the chain (1.3.3). The mathematical formulation of the idea of the hierarchy of the relaxation times of the system lies in the functional time dependence of the many-particle distribution functions $f_S\left(x_1,...,x_S;t\right)$ only through the time dependence of the parameters of the reduced description at the corresponding stage of evolution. In particular, at the kinetic stage of the evolution of the system, the many-particle distribution functions depend on time only through the single-particle distribution function $f_1(x',t)$:

$$f_S\left(x_1,...,x_S;t\right) = f_S\left(x_1,...,x_S;\, f_1(x',t)\right). \tag{1.3.4}$$

In addition to the functional hypothesis (1.3.4), the principle of spatial weakening of correlations is also the basis of the reduced description method. In the language of many-particle distribution functions, this principle can be formulated as follows [3]. Let S particles be divided into two subgroups of particles containing S' and S'' particles, respectively, $S = S' + S''$. If distance R between these particles subgroups increases infinitely, $R \to \infty$, then, due to the weakening of the correlations between the particles S-particle distribution function splits into products of distribution functions related to each subgroup of particles:

$$f_S\left(x_1,...,x_S;t\right) \underset{R\to\infty}{\to} f_{S'}\left(x_1',...,x_S';t\right) f_{S''}\left(x_1'',...,x_S'';t\right), \tag{1.3.5}$$

In formula (1.3.5), the prime sign serves to denote the coordinates and momenta of a subgroup of particles S', and two dashes are used to denote the coordinates and momenta of the second subgroup of particles. It should be noted, however, that the principle of spatial weakening of correlations (1.3.5) refers to many-particle distribution functions in which the thermodynamic passage to the limit $\mathcal{V} \to \infty$, $\left(N / \mathcal{V}\right) = \text{const}$ [3].

According to Eq. (1.3.4), the time derivative $\frac{\partial f_S}{\partial t}$ in (1.3.3) at $S \neq 1$ should be understood as follows:

$$\frac{\partial}{\partial t} f_S\left(x_1,...,x_S; f_1(x,t)\right) = \int dx' \frac{\delta f_S\left(x_1,...,x_S; f_1(x,t)\right)}{\delta f_1(x',t)} \frac{\partial f_1(x',t)}{\partial t}, \quad (1.3.6)$$

where $\frac{\delta f_S\left(f_1(x,t)\right)}{\delta f_1(x',t)}$ is functional derivative. The single-particle distribution function $f_1(x',t)$ according to (3.3) must satisfy the equation:

$$\frac{\partial f_1}{\partial t} + \frac{\mathbf{p}_1}{m}\frac{\partial f_1}{\partial \mathbf{x}_1} + \sum_{n=2}^{\infty} \frac{(-1)^{n-1}}{2^{n-1}(n-1)!} y_{i_1...i_n}(\mathbf{x}_1,...,\mathbf{x}_1) \frac{\partial^n f_1}{\partial p_{1i_1}...\partial p_{1i_n}} = \frac{1}{v} L\left(x_1; f_1\right), \quad (1.3.7)$$

where still $v = \frac{\mathcal{V}}{N}$ and $L\left(x_1; f_1\right)$ is the generalized collision integral defined by the formula

$$L\left(x_1; f_1\right) \equiv -\frac{\partial}{\partial \mathbf{p}_1} \int dx_2 f_2\left(x_1, x_2; f_1\right) \mathbf{F}_{1,2}. \quad (1.3.8)$$

As is easy to see, in order to close equation (1.3.7), it is necessary to find the collision integral (1.3.8) as the functional of the one-particle distribution function, for which it is necessary to break the infinite chain of equations (1.3.3). It is clear that this can only be done in some approximation.

1.4. Kinetic equations for dissipative many-particle systems in external random fields in the case of weak interaction between particles

Let us demonstrate such a procedure for breaking an infinite chain of equations in the case of weak interaction between particles and a weak intensity of an external stochastic field. In other words, we will assume that the correlation functions of the external random field are small. In developing the perturbation theory in terms of the weak interaction between particles and an external field of weak intensity, we will closely adhere to

the technique proposed in [3]. Using (1.3.6), we write the chain of equations (1.3.3) in the form:

$$-\int dx \frac{\delta f_S(f_1)}{\delta f_1(x,t)} \frac{\mathbf{p}}{m} \frac{\partial f_1(x,t)}{\partial \mathbf{x}} + \sum_{1\le\alpha\le S} \frac{\mathbf{p}_\alpha}{m} \frac{\partial f_S(f_1)}{\partial \mathbf{x}_\alpha} = \frac{1}{\nu} \mathcal{K}_S(f_1), \qquad (1.4.1)$$

where

$$\mathcal{K}_S(f_1) \equiv -\nu \sum_{1\le\alpha<\beta\le S} \frac{\partial f_S \mathbf{F}_{\alpha,\beta}}{\partial \mathbf{p}_\alpha} - \sum_{1\le\alpha\le S} \frac{\partial}{\partial \mathbf{p}_\alpha} \int dx_{S+1} f_{S+1} \mathbf{F}_{\alpha,S+1} - \qquad (1.4.2)$$

$$-\int dx \frac{\delta f_S(f_1)}{\delta f_1(x,t)} \left\{ L(x; f_1) - \nu \sum_{n=2}^{\infty} \frac{(-1)^{n-1}}{2^{n-1}(n-1)!} y_{i_1\ldots i_n}(\mathbf{x},\ldots,\mathbf{x}) \frac{\partial^n f_1}{\partial p_{i_1}\ldots\partial p_{i_n}} \right\} -$$

$$-\sum_{n=2}^{\infty} \frac{(-1)^{n-1}}{2^{n-1}(n-1)!} \sum_{1\le\alpha_1\le S} \ldots \sum_{1\le\alpha_n\le S} y_{i_1\ldots i_n}(\mathbf{x}_{\alpha_1},\ldots,\mathbf{x}_{\alpha_n}) \frac{\partial^n f_S}{\partial p_{\alpha_1 i_1}\ldots\partial p_{\alpha_n i_n}}.$$

To develop the announced perturbation theory, the chain of equations (1.4.1) and (1.4.2) must be supplemented with initial conditions. To formulate these, we will use the fact that many-particle distribution functions must satisfy the principle of spatial weakening of correlations (1.3.5). For this purpose, following [2, 3], we introduce into consideration the auxiliary parameter τ having the dimension of time, but not necessarily representing physical time. Consider further the many-particle distribution function $f_S\left(\mathbf{x}_1 - \frac{\mathbf{p}_1}{m}\tau, \mathbf{p}_1, \ldots, \mathbf{x}_S - \frac{\mathbf{p}_S}{m}\tau, \mathbf{p}_S; f_1\right)$. In accordance with (3.5), this function must satisfy the asymptotic relation:

$$f_S\left(\mathbf{x}_1 - \frac{\mathbf{p}_1}{m}\tau, \mathbf{p}_1, \ldots, \mathbf{x}_S - \frac{\mathbf{p}_S}{m}\tau, \mathbf{p}_S; f_1\right) \underset{\tau\to\infty}{\to} \prod_{1\le\alpha\le S} f_1\left(\mathbf{x}_\alpha - \frac{\mathbf{p}_\alpha}{m}\tau, \mathbf{p}_\alpha\right). \qquad (1.4.3)$$

If we further define the shift operator $\hat{\Lambda}_S^0$ in coordinate space by the formula

$$i\hat{\Lambda}_S^0 \equiv \sum_{1\le\alpha\le S} \frac{\mathbf{p}_\alpha}{m} \frac{\partial}{\partial \mathbf{x}_\alpha}, \qquad (1.4.4)$$

Condition (1.4.3) can be rewritten as:

$$e^{i\tau\hat{\Lambda}_S^0} f_S(\tau) \underset{\tau\to\infty}{\to} \prod_{1\le\alpha\le S} f_1(x_\alpha), \qquad (1.4.5)$$

where $\exp\left(i\tau\hat{\Lambda}_S^0\right)$ is the so-called «free evolution operator» and

$$f_S(\tau) \equiv f_S\left(x_1,...,x_S; e^{-i\tau\hat{\Lambda}_1^0} f_1(x')\right) = f_S\left(x_1,...,x_S; f_1\left(\mathbf{x}' - \frac{\mathbf{p}'}{m}\tau, \mathbf{p}'\right)\right). \quad (1.4.6)$$

Using the introduced operators, equation (1.4.1) can be rewritten as:

$$\frac{\partial}{\partial\tau} e^{i\tau\hat{\Lambda}_S^0} f_S(\tau) = \frac{1}{\nu} e^{i\tau\hat{\Lambda}_S^0} \mathcal{K}_S(\tau), \quad (1.4.7)$$

where

$$\mathcal{K}_S(\tau) \equiv \mathcal{K}_S\left(x_1,...,x_S; e^{-i\tau\hat{\Lambda}_1^0} f_1(x')\right) = \mathcal{K}_S\left(x_1,...,x_S; f_1\left(\mathbf{x}' - \frac{\mathbf{p}'}{m}\tau, \mathbf{p}'\right)\right). \quad (1.4.8)$$

Integrating equation (1.4.7) over τ within the limits $-\infty$ to 0 and using the asymptotic conditions (1.4.5), we obtain

$$f_S\left(x_1,...,x_S; f_1(x')\right) = \prod_{1\le\alpha\le S} f_1(x_\alpha) + \frac{1}{\nu}\int_{-\infty}^{0} d\tau e^{i\tau\hat{\Lambda}_S^0} \mathcal{K}_S(\tau). \quad (1.4.9)$$

Relation (1.4.9) makes it possible to develop the theory of perturbations in weak interaction, assuming also that the intensity of the external stochastic field is low. Under these assumptions, the quantity $\mathcal{K}_S(\tau)$ (see (1.4.2)) can be considered small and, therefore, in the leading approximation we have

$$f_S\left(x_1,...,x_S; f_1(x')\right) = \prod_{1\le\alpha\le S} f_1(x_\alpha),$$

whence follows

$$f_2(x_1, x_2) = f_1(x_1) f_1(x_2). \quad (1.4.10)$$

Substituting further (1.4.10) into (1.3.8) and using (1.1.5), (1.3.7), we arrive at the following closed kinetic equation

$$\frac{\partial f_1}{\partial t} + \frac{\mathbf{p}_1}{m}\frac{\partial f_1}{\partial \mathbf{x}_1} + \sum_{n=2}^{\infty} \frac{(-1)^{n-1}}{2^{n-1}(n-1)!} y_{i_1...i_n}(\mathbf{x}_1,...,\mathbf{x}_1) \frac{\partial^n f_1}{\partial p_{1i_1}...\partial p_{1i_n}} = \quad (1.4.11)$$

$$= \frac{1}{\nu}\frac{\partial}{\partial \mathbf{p}_1} f_1(x_1)\left(\int dx_2 f_1(x_2)\frac{\partial V_{1,2}}{\partial \mathbf{x}_1} + \int dx_2 f_1(x_2)\frac{\partial R_{1,2}}{\partial \mathbf{p}_1}\right),$$

which describes the evolution (at its kinetic stage) of many-particle dissipative systems under the influence of an external stochastic field. We recall that if dissipation in the system is associated with friction of

macroscopic particles, then the quantity in this case, following [70], can be chosen in the form (1.1.8)

$$R_{1,2} = \frac{1}{2}\tilde{\gamma}(\mathbf{x}_1 - \mathbf{x}_2)(\mathbf{p}_1 - \mathbf{p}_2)^2, \qquad \tilde{\gamma}(\mathbf{x}_1 - \mathbf{x}_2) > 0. \tag{1.4.12}$$

Note that if there is no dissipation, $\tilde{\gamma}(\mathbf{x}_1 - \mathbf{x}_2) = 0$, equation (1.4.11) turns into the Vlasov equation, generalized to the case of action on the system of an external stochastic field, with a self-consistent field

$$U(\mathbf{x}_1) = \frac{1}{v}\int d\mathbf{x}_2 V(\mathbf{x}_1 - \mathbf{x}_2)\int d\mathbf{p}_2 f_1(x_2), \qquad f_1(x_2) \equiv f_1(\mathbf{x}_2, \mathbf{p}_2). \tag{1.4.13}$$

In the general case, equation (1.4.11) can be interpreted, for example, as the Fokker - Planck equation for Brownian particles, taking into account the weak interaction between these particles and generalized to the case of a non-Gaussian character of stochastic fields acting on the system, which we will demonstrate in the next section.

1.5. The case of a Gaussian stochastic field

In order to confirm the above, we will assume that the external stochastic field is Gaussian, and the one-particle distribution function $f_1(x)$ is isotropic in momentum space,

$$f_1(\mathbf{x}, \mathbf{p}) \equiv f_1(\mathbf{x}, |\mathbf{p}|). \tag{1.5.1}$$

In this case, there are only pair correlation functions of the external random field, which we will choose to simplify calculations in the form $y_{ij}(\mathbf{x}_1, \mathbf{x}_2) \equiv \delta_{ij} g(\mathbf{x}_1, \mathbf{x}_2)$. Then equation (1.4.11) takes the form:

$$\frac{\partial f_1(x,t)}{\partial t} + \frac{\mathbf{p}}{m}\frac{\partial f_1(x,t)}{\partial \mathbf{x}} - \frac{\partial U(\mathbf{x})}{\partial \mathbf{x}}\frac{\partial f_1(x,t)}{\partial \mathbf{p}} = \frac{\partial}{\partial \mathbf{p}}\left(\gamma(\mathbf{x})\mathbf{p} f_1(x,t) + \frac{1}{2} g(\mathbf{x}, \mathbf{x})\frac{\partial f_1(x,t)}{\partial \mathbf{p}}\right), \tag{1.5.2}$$

where the self-consistent field $U(\mathbf{x})$ is given by expression (1.4.13), and the quantity $\gamma(\mathbf{x})$ is defined by the formula

$$\gamma(\mathbf{x}) \equiv \frac{1}{v}\int d\mathbf{x}' \tilde{\gamma}(\mathbf{x} - \mathbf{x}')\int d\mathbf{p}' f_1(x'), \tag{1.5.3}$$

and it follows from the definition and (1.4.12) that $\gamma(\mathbf{x})>0$. It is easy to see that for $\gamma(\mathbf{x})\equiv\gamma$, $g(\mathbf{x},\mathbf{x})\equiv g$ and $V(\mathbf{x}_1-\mathbf{x}_2)\equiv 0$ (see (1.4.13)), equation (1.5.2) takes on the traditional form of the Fokker – Planck equation, which confirms the above statement. It also follows that expression (1.5.3) gives a microscopic definition of the coefficient of friction, which is customary for the Langevin equations. As is known, the Fokker – Planck equation is usually derived from the Langevin equations, see in this regard, for example, [3].

Let us analyze some more consequences from the obtained equation (1.4.11). In the spatially homogeneous case, the correlation functions $y_{i_1\ldots i_n}(\mathbf{x}_{\alpha_1},\ldots,\mathbf{x}_{\alpha_n})$ (see (1.3.3), (1.4.2)) depend only on the difference of coordinates $\mathbf{x}_{\alpha_i}-\mathbf{x}_{\alpha_j}$. For this reason, the quantities $y_{i_1\ldots i_n}(\mathbf{x}_1,\ldots,\mathbf{x}_1)$ in (1.4.11) do not depend on coordinates at all,

$$y_{i_1\ldots i_n}(\mathbf{x}_1,\ldots,\mathbf{x}_1)\equiv y_{i_1\ldots i_n}. \tag{1.5.4}$$

Thus, in the spatially homogeneous case, equation (1.4.11) in the case of validity of relation (1.4.12) takes the form:

$$\frac{\partial f_1(\mathbf{p},t)}{\partial t}+\sum_{n=2}^{\infty}\frac{(-1)^{n-1}}{2^{n-1}(n-1)!}y_{i_1\ldots i_n}\frac{\partial^n f_1(\mathbf{p},t)}{\partial p_{i_1}\ldots\partial p_{i_n}}=\frac{\tilde{\gamma}}{\nu}\frac{\partial}{\partial\mathbf{p}_1}f_1(\mathbf{p}_1)\int d\mathbf{p}_2 f_1(\mathbf{p}_2)(\mathbf{p}_1-\mathbf{p}_2),$$

$$\tilde{\gamma}\equiv\frac{1}{\nu}\int d\mathbf{x}'\tilde{\gamma}(\mathbf{x}-\mathbf{x}'). \tag{1.5.5}$$

In deriving this equation, we have not yet assumed that the system is isotropic in momentum space, see Eq. (1.5.1). We now introduce into consideration the average kinetic energy $\bar{\varepsilon}(t)$ of the studied system by the formula

$$\bar{\varepsilon}(t)\equiv\int d\mathbf{p}f_1(\mathbf{p},t)\frac{\mathbf{p}^2}{2m}. \tag{1.5.6}$$

The evolution equation for this quantity immediately follows from the kinetic equation (1.5.5):

$$\frac{\partial\bar{\varepsilon}(t)}{\partial t}=\frac{3}{2}\frac{y_{jj}n}{m}-\frac{\tilde{\gamma}}{2m\nu}\int d\mathbf{p}_1\int d\mathbf{p}_2 f_1(\mathbf{p}_2,t)\,f_1(\mathbf{p}_1,t)(\mathbf{p}_1-\mathbf{p}_2)^2, \tag{1.5.7}$$

where n is the density of the number of particles in the system,

$$n \equiv \int d\mathbf{p}\, f_1(\mathbf{p},t). \tag{1.5.8}$$

and, as is easy to verify, the following equalities are valid:

$$\frac{\partial}{\partial t}\int d\mathbf{p}\, f_1(\mathbf{p},t) = 0\,, \qquad \frac{\partial}{\partial t}\int d\mathbf{p}\, f_1(\mathbf{p},t)\mathbf{p} = 0\,, \tag{1.5.9}$$

whence it follows that the density of the number of particles in the system and the average momentum do not change with time.

From Eq. (1.5.7), we can conclude that the system under study can be both heated up and cooled down during the process of evolution. The realization of the particular case is determined by the sign of the right-hand side in (1.5.7). If we assume that at the initial time moment the average momentum of the particles in the system was equal to zero, then according to (1.5.9) it equals to zero and at all other times. In this case, Eq. (1.5.7) takes the form:

$$\frac{\partial \overline{\varepsilon}(t)}{\partial t} = -2\gamma\overline{\varepsilon}(t) + \frac{3}{2}\frac{y_{jj}n}{m}\,, \qquad \gamma \equiv n\tilde{\gamma}\,. \tag{1.5.10}$$

It is taken into account here that the density of the number of particles n determined by formula (1.5.5) does not depend on time. As a consequence, the value γ does not depend on time as well. Eq. (1.5.10) has a simple solution:

$$\overline{\varepsilon}(t) = \frac{3}{4}\frac{y_{jj}n}{m\gamma} + \left(\overline{\varepsilon}_0 - \frac{3}{4}\frac{y_{jj}n}{m\gamma}\right)\exp(-2\gamma t)\,, \tag{1.5.11}$$

where $\overline{\varepsilon}_0$ is the value of $\overline{\varepsilon}(t)$ (see (1.5.6)) at the initial time moment. From Eq. (1.5.11) we observe that the average kinetic energy of the system decreases during the evolution process (the system is cooling down) if $\overline{\varepsilon}_0 > \frac{3}{4}\frac{y_{jj}n}{m\gamma}$, and that the system heats up throughout the evolution when $\overline{\varepsilon}_0 < \frac{3}{4}\frac{y_{jj}n}{m\gamma}$. In the case of $\overline{\varepsilon}_0 = \frac{3}{4}\frac{y_{jj}n}{m\gamma}$, the average kinetic energy does not change in evolution process. We should note here that the self-cooling effect (in the sense of decreasing the average kinetic energy) of dissipative systems in the process of evolution was predicted a long time ago, we refer the reader to [75, 76] for more details. As expected, the influence on dissipative systems of external random forces can "create competition" to the cooling process, leading to their heating under certain conditions. Note also that if it is possible to establish the Maxwell distribution in the system throughout the

evolution process, then the expression for the equilibrium mean value of the kinetic energy $\bar{\varepsilon}(\infty)=\frac{3}{4}\frac{y_{jj}n}{m\gamma}$ which follows from (1.5.11) should coincide with the well-known formula $\bar{\varepsilon}(\infty)=\frac{3}{2}nT$ in the case of gaseous dissipative systems, where T is the temperature of the medium. This is possible if the pair correlation function of the external stochastic field y_{jj} is related to temperature and coefficient γ by a relationship $y_{jj}=2m\gamma T$ known from the ordinary theory of Brownian motion.

It should be recalled here that for "classical" (non-interacting) Brownian particles the concept of "temperature" has a physical meaning. In this case, we are talking about the temperature of the medium where the Brownian particles propagate. For such systems, the concepts of the equilibrium state and the Maxwell distribution have a strict meaning. In the case of dissipative systems, in particular, granular media, the kinetic energy derived above as some thermal characteristic of the system has a clear physical meaning. The temperature concept for such systems requires further explanation. For the best of our knowledge, the concept of temperature for dissipative systems of many particles has not yet been correctly defined from the point of view of statistical physics. The discussion of scientific and "philosophical" issues related to the concept of temperature for dissipative media can be found in [77, 78].

Also note that according to obtained formulas (1.5.7), (1.5.11), only pair correlation functions are responsible for the energy pumping into the system from an external stochastic field. In other words, Eqs. (1.5.7), (1.5.10) stay the same as in the case of Gaussian external noise, see Eq. (1.5.2). The reason for this is obvious and it consists in the quadratic dependence of the momentum of the kinetic energy of one particle $\varepsilon_{\mathbf{p}}=\mathbf{p}^2/2m$, see Eqs. (1.5.5) and (1.5.6). The contribution of the correlation functions of higher order will appear if we write out the evolution equation for the moments of a one-particle distribution function of higher order than the second one, see (1.5.5).

We emphasize once again that formulas (1.5.5), (1.5.7), (1.5.10) and (1.5.11) have been obtained for the special form of the dissipative function $R_{1,2}$ (see (1.4.12)) and additional assumptions (1.5.1), (1.5.4). In a more general case, as it follows from Eq. (1.4.11) and definition (1.5.6), the evolution of the average energy of the system can be more complex than predicted one by Eq. (1.5.11) or Eq. (1.5.7).

Summary and Outlook

Thus, this section we have demonstrated the way of dynamical justification of the kinetic theory of dissipative systems of identical particles in an external stochastic field. We have constructed the procedure for

deriving an infinite chain of BBGKY equations for many-particle distribution functions, which mostly uses a generalization of the Furutsu -- Novikov formula for the case of arbitrary distributions of an external random field. The theory suggests that the distributions of the stochastic external fields have the moments of any order. A generalization of the reduced description method to the case of dissipative systems of many particles under the influence of an external random force is proposed. A method for obtaining the kinetic equation for such systems in the case of weak interaction between particles and a low intensity of an external stochastic field is developed. It is shown that such a kinetic equation can be interpreted as the Fokker-Planck equation for Brownian particles, taking into account the weak interaction between these particles and generalized to the case of a non-Gaussian character of stochastic fields influencing on the system. In the case of Gaussian external noise, the derived kinetic equation transforms into the well-known Fokker-Planck equation in such form as it is usually obtained from the Langevin equations. At the same time, the theory gives a microscopic definition to the coefficient of friction, which is "usual" for the Langevin equations, expressing this coefficient in terms of the dissipative function and about the single-particle distribution function of particles. The developed perturbation theory permits one, as the matter of principle, to find the corrections to kinetic equation (1.4.11) of any order with respect to the interaction and intensity of the external stochastic field.

The possibilities of the proposed microscopic theory are not limited only to the case of weak interaction between particles. The kinetic theory of the systems under study can also be constructed in the case of a low density of particles and an arbitrary interaction between them (if only this interaction does not lead to the formation of bound states). However, the construction of such a theory is rather volumetric problem that requires an individual solution and presentation.

It should also be noted the following. According to the ideas of the reduced description method, over time, the description of the evolution of the system containing many particles should be greatly simplified. Applying to the system under study at the kinetic stage of its evolution, the possibility of further simplification in the description should be associated with the transition of the system to the hydrodynamic stage of the evolution [3]. This enables us to formulate the problem of consistent and controlled derivation of the equations of hydrodynamics of such a system based on the kinetic equations for it, i.e., from Eq. (1.4.11). The process of consistent derivation of such equations itself should answer many questions related to the relaxation of the system to a stationary state. In particular, perhaps the microscopic approach developed in this article would allow one to clarify the explicit form of the stationary distribution function of particles of a dissipative system in an external stochastic field. Recall that a generally accepted theory that gives a recipe for obtaining the form of a stationary distribution in momenta and coordinates of particles in dissipative systems (even unaffected by stochastic forces) does not currently exist (see in this regard, i.e., [17, 77-79]).

SECTION II. THE REDUCED DESCRIPTION METHOD IN THE KINETIC THEORY FOR ACTIVE PARTICLES WITH INTERACTION

The content of this section is based on paper [36]. We should note that the fundamentals of the approach to the construction of the kinetic theory for active particles from the first principles are very similar to ones presented in Section 1.1. However, there are also substantial differences. Due to this fact, let us start the following section with the introduction of the basis of evolution theory of systems with active fluctuations at its kinetic stage.

2.1. Fundamentals

Let us consider a system consisting of N identical active particles of mass m, each of which is characterized by a space coordinate $\mathbf{x}_\alpha$, $1 \le \alpha \le N$ measured from the center of mass, and momentum $\mathbf{p}_\alpha$, $1 \le \alpha \le N$. The interaction between the particles is assumed to be consisted of two parts: the "reversible" one, which is described by the Hamiltonian H, and "irreversible" one described by the function R^ω, its meaning will be explained below.

The Hamiltonian of the system can be represented as::

$$H = H_0 + V = \sum_{1\le\alpha\le N} \frac{\mathbf{p}_\alpha^2}{2m} + \sum_{1\le\alpha<\beta\le N} V_{\alpha,\beta}, \tag{2.1.1}$$

where $V_{\alpha,\beta}$ is the potential of pair interaction,

$$V_{\alpha,\beta} \equiv V\left(\mathbf{x}_{\alpha\beta}\right), \qquad \mathbf{x}_{\alpha\beta} \equiv \mathbf{x}_\alpha - \mathbf{x}_\beta. \tag{2.1.2}$$

We will also assume that the particles of the system are affected by specific forces that depend on the speed of the particles (or momentum) and are characterized by a function R. We will also suggest that the function R can be expressed in as

$$R = R^r + R^\omega, \tag{2.1.3}$$

where R^r is the regular part of this function

$$R^r \equiv \sum_{1\le\alpha<\beta\le N} R_{\alpha,\beta}, \qquad R_{\alpha,\beta} \equiv R\left(\mathbf{x}_{\alpha\beta}, \mathbf{p}_{\alpha\beta}\right), \qquad \mathbf{p}_{\alpha\beta} \equiv \mathbf{p}_\alpha - \mathbf{p}_\beta \tag{2.1.4}$$

and R^{ω} is the stochastic one R, which can be rewritten as

$$R^{\omega} \equiv \sum_{1\le\alpha\le N} R^{\omega}\left(x_{\alpha},t\right), \qquad x_{\alpha} \equiv \left\{\mathbf{x}_{\alpha},\mathbf{p}_{\alpha}\right\}.$$

The stochastic nature of the function R^{ω} is formally emphasized by the presence of an index ω in it.

Note that in the case of systems of "ordinary" (inactive) identical particles with dissipative interaction, the function is treated as a dissipative function, see Eq. (1.1.3) and also [70, 69, 1]. It is usually considered that dissipation in the system is associated with friction of macroscopic particle that results in the following representation of $R_{\alpha,\beta}$ for both this case and Eq. (1.1.3):

$$R_{\alpha,\beta} \equiv \frac{1}{2}\tilde{\gamma}\left(\mathbf{x}_{\alpha\beta}\right)\mathbf{p}_{\alpha\beta}^{2}, \qquad \tilde{\gamma}\left(\mathbf{x}_{\alpha\beta}\right) > 0, \qquad \mathbf{p}_{\alpha\beta} \equiv \mathbf{p}_{\alpha} - \mathbf{p}_{\beta}. \tag{2.1.5}$$

It is being assumed that $\tilde{\gamma}\left(\mathbf{x}_{\alpha\beta}\right) = 0$ if $\left|\mathbf{x}_{\alpha\beta}\right| \gtrsim r_0$, where r_0 is the specific radius of action of dissipative forces. In [69, 1], expressions were obtained for the friction coefficient γ entering into the Langevin equations as a functional of the value $\tilde{\gamma}^{\omega}\left(\mathbf{x}_{\alpha\beta}\right)$ and a one-particle distribution function. Moreover, the friction coefficient is always positive due to property (2.1.5).

However, as is known (see, e. g., [33]), it is not so in the case of active particles. The "friction" coefficient in equations of the Langevin type for active particles can significantly depend on the velocity and change the sign. For this reason, there is no possibility to use criteria (2.1.5) for establishing the properties of the "dissipative function" in the case of active particles. That is why the expression "dissipative function" is quoted. Later, we will use the name "dissipative function" for definiteness when referring to the function R, however, without quotes.

Following the procedure standard for classical theoretical mechanics and taking into account Eqs.(2.1.1)–(2.1.4), the generalized Hamilton equations for the system under study can be written as

$$\dot{\mathbf{p}}_{\alpha} = -\frac{\partial H}{\partial \mathbf{x}_{\alpha}} - \frac{\partial R}{\partial \mathbf{p}_{\alpha}}, \qquad \dot{\mathbf{x}}_{\alpha} = \frac{\partial H}{\partial \mathbf{p}_{\alpha}}. \tag{2.1.6}$$

Hence, the force $\mathbf{F}_{\alpha,\beta}$ acting on a particle α from the side of the particle β should be determined by the sum of two terms:

$$\mathbf{F}_{\alpha,\beta} = \mathbf{F}_{\alpha,\beta}^{p} + \mathbf{F}_{\alpha,\beta}^{r},. \tag{2.1.7}$$

the force $\mathbf{F}^{p}_{\alpha,\beta}$ related to the presence of a potential pairwise interaction between particles, and the force $\mathbf{F}^{r}_{\alpha,\beta}$ associated with the presence of a dissipative interaction between particles (in the sense mentioned above),

$$\mathbf{F}^{p}_{\alpha,\beta} \equiv -\frac{\partial V_{\alpha,\beta}}{\partial \mathbf{x}_{\alpha}}, \quad \mathbf{F}^{r}_{\alpha,\beta} \equiv -\frac{\partial R_{\alpha,\beta}}{\partial \mathbf{p}_{\alpha}}. \tag{2.1.8}$$

In addition, as it follows from Eq. (2.1.1), the α particle is under the influence of an external random force $\mathbf{Y}^{\omega}_{\alpha}$ which depends on the momentum of this particle, and:

$$-\frac{\partial R(x_{\alpha},t)}{\partial p_{i\alpha}} \equiv X^{\omega}_{\|i}(x_{\alpha},t) + X^{\omega}_{\perp i}(x_{\alpha},t), \tag{2.1.9}$$

$$X^{\omega}_{\|i}(x_{\alpha},t) \equiv X^{\omega}(\mathbf{x}_{\alpha},t)e^{h}_{\alpha i}, \quad X^{\omega}_{\perp i}(x_{\alpha},t) \equiv X^{\omega}_{j}(\mathbf{x}_{\alpha},t)\left(\delta_{ij} - e^{h}_{\alpha i}e^{h}_{\alpha j}\right), \quad e^{h}_{\alpha i} \equiv \frac{p_{\alpha i}}{|\mathbf{p}_{\alpha}|}.$$

The latter expression requires some comments. We emphasize, first of all, that the stochastic force $Y^{\omega}_{i}(x_{\alpha},t)$ in Eq. (2.1.9) is written in a form that is not related to the choice of a particular coordinate system. This notation simply reflects the fact that the stochastic force acts differently along and across the direction of a particle velocity. Figure 1 shows a schematic visualization of the assumption written in the form (2.1.9).

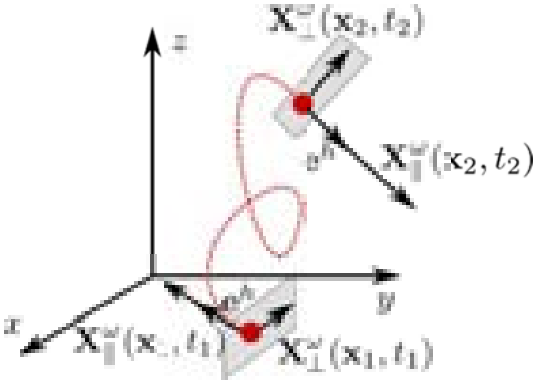

Figure 1 Schematic visualization of particle motion in the presence of stochastic effects with components $\mathbf{X}^{\omega}_{\|i}(\mathbf{x}_{\alpha},\mathbf{p}_{\alpha},t), \mathbf{X}^{\omega}_{\perp i}(\mathbf{x}_{\alpha},\mathbf{p}_{\alpha},t)$ *according to Eq. (2.1.9)*

Expression (2.1.9) looks like a natural generalization of the stochastic force $Y_i^{\omega}(\mathbf{x},t)$ typical for the Langevin equations in the case of ordinary Brownian particles:

$$\dot{\mathbf{x}} = \mathbf{v}\,, \quad \dot{v}_i = -\gamma v_i + Y_i^{\omega}(\mathbf{x},t)\,.$$

Indeed, the value $Y_i^{\omega}(\mathbf{x},t)$ in the latter equation can always be rewritten identically in the form:

$$Y_i^{\omega} = \left(\mathbf{e}^h \mathbf{Y}^{\omega}\right) e_i^h + Y_j^{\omega}\left(\delta_{ij} - e_i^h e_j^h\right),$$

where e_i^h is an arbitrary unit vector, e. g., $e_i^h = p_i / |\mathbf{p}|$. Substituting further the scalar product $\mathbf{e}^h \mathbf{Y}^{\omega}$ by $X^{\omega}(\mathbf{x}_{\alpha},t)$, Y_j^{ω} by $X_j^{\omega}(\mathbf{x}_{\alpha},t)$ and assuming that $e_{\alpha i}^h = p_{\alpha i} / |\mathbf{p}_{\alpha}|$, we get Eq. (2.1.9). We should keep in mind, however, that in Eq. (2.1.9) the values $X^{\omega}(\mathbf{x}_{\alpha},t)$ and $X_j^{\omega}(\mathbf{x}_{\alpha},t)$ in the most general case, are not related to each other. Besides, in the three-dimensional case, if necessary, the vector $X_j^{\omega}(\mathbf{x}_{\alpha},t)$ can be considered as a two-component one in the plane perpendicular to the vector $e_{\alpha j}^h$. Under no circumstances, the presence of a vector component $X_j^{\omega}(\mathbf{x}_{\alpha},t)$ along $e_{\alpha j}^h$ will not affect the description of processes and phenomena in such systems due to the factor $\left(\delta_{ij} - e_{\alpha i}^h e_{\alpha j}^h\right)$ on the right-hand side of (2.1.9).

From the foregoing, it follows that the stochastic action on the considered system in the form of Eq. (2.1.9) can be considered as a generalization of the stochastic forces used in the theory of two-dimensional systems of active particles (the case of so-called "active fluctuations") in several ways. First, in problems of the dynamics of active particles, typical random forces, as a rule, are considered as global [33]. It means that, they are acting on each particle in the same way, no matter where it is in space. But on the other hand, Eq. (2.1.9) takes into account the possibility of local action of stochastic forces on the system. Second, we can consider Eq. (2.1.9) as a generalization of typical random forces of the problems of dynamics of active particles to the case of three-dimensional systems. To make sure of this, it is sufficient considering Eq. (2.1.9) to be two-dimensional one, to get rid of its locality and assign

$$\mathbf{e}_{\alpha}^h \equiv \mathbf{e}_h\,, \; X^{\omega}(t) \equiv \sqrt{D_v}\,\xi_v(t), \quad \mathbf{X}^{\omega}(\mathbf{x}_{\alpha},t) \equiv \mathbf{e}_{\varphi}\sqrt{D_{\varphi}}\,\xi_{\varphi}(t)\,, \; \mathbf{e}_h \mathbf{e}_{\varphi} = 0\,, \quad (2.1.10)$$

where $\mathbf{e}_h$ is the unit vector along the direction of particle motion, $\mathbf{e}_\varphi$ is the unit vector along the direction of the azimuth angle φ and D_φ, D_v are intensities of angular and velocity noise, respectively (see for more details, e. g., [33]). Note that in two-dimensional systems, for the best of our knowledge, the highlighted directions in the motion of active particles can be established due to the presence of "head-tail" asymmetry properties in them. Such an advantage in the motion direction of particles is related to the existence or origin of a propulsion mechanism in the system. Thus, thanks to the "head-tail" asymmetry in the stationary state of the system of many active ones, it becomes possible to fix "naturally" the reference system by a special choice of vectors $\mathbf{e}_h$ and $\mathbf{e}_\varphi$. It is obvious that, the existence of such an asymmetry is affected on the characteristics of a many-particle system, for example, a one-particle distribution function, see below and also [33]. As will be shown later, the existence of the effects of the "thrust mechanism" is also possible in three dimensions, even though in the case of only linear friction (see Section 2.4 of this chapter). We emphasize that the source of the stochastic action can be generalized to the three-dimensional case in a different way from (2.1.9) as well. For this generalization, as in the two-dimensional case, we can use the representation of curvilinear coordinates, like spherical ones, characterized by both the above vectors $\mathbf{n}_\alpha \equiv \mathbf{e}_h$, and the unit vector $\mathbf{e}_\vartheta$ associated with the change in the polar angle. However, for solving the problems formulated in the present work, it is more convenient to use Cartesian coordinate system.

We also note the following. The time derivative of the total energy of the system according to Eq. (2.1.1) and Eq. (2.1.6) is represented by the expression

$$\frac{dH}{dt} = -\sum_{1\le\alpha\le N} \frac{\mathbf{p}_\alpha}{m}\frac{\partial R}{\partial \mathbf{p}_\alpha}. \tag{2.1.11}$$

If we assume that the system contains dissipation associated with friction of macroscopic particles and the regular part of the dissipative function R^r in this case is determined by Eq. (2.1.5), then from Eq. (2.1.11), taking into account Eq. (2.1.9), we obtain

$$\frac{dH}{dt} = -\frac{2}{m}\sum_{1\le\alpha<\beta\le N} R_{\alpha,\beta} + \sum_{1\le\alpha\le N}\frac{p_{i\alpha}}{m}\left[X^\omega(\mathbf{x}_\alpha,t)e^h_{\alpha i} + X^\omega_j(\mathbf{x}_\alpha,t)\left(\delta_{ij} - e^h_{\alpha i}e^h_{\alpha j}\right)\right], \tag{2.1.12}$$

or

$$\frac{dH}{dt} = -\frac{2}{m}\sum_{1\le\alpha<\beta\le N} R_{\alpha,\beta} + \sum_{1\le\alpha\le N}\frac{|\mathbf{p}_\alpha|}{m}X^\omega(\mathbf{x}_\alpha,t).$$

Taking into account that $\tilde{\gamma}\left(\mathbf{x}_{\alpha\beta}\right) > 0$, see Eq. (2.1.5), it is easy to note that in such a system the competition between dissipation due to friction and energy pumping from the side of the external stochastic field is possible. The situation with changing energy in systems of active particles with interaction should provide much more varied options in comparison with Eq. (2.1.12) due to the explicit form of the function $R_{\alpha,\beta}$ when calculating the expression in the right-hand side of Eq. (2.1.11), see below.

The next task is to obtain the Liouville equation for the system of many particles under study. From a formal point of view, the procedure for deriving such an equation almost completely coincides with the procedure described in Chapter 1.1. As it is done in this chapter, let us represent Eqs. (2.1.6) in the following form for the convenience of further calculations

$$\dot{x}_\alpha\left(t\right) = h_\alpha^\omega\left(x_1\left(t\right),...,x_N\left(t\right)\right), \qquad 1 \le \alpha \le N\ , \tag{2.1.13}$$

where we use the notation

$$x_a\left(t\right) \equiv \left(\mathbf{x}_a\left(t\right), \mathbf{p}_a\left(t\right)\right). \tag{2.1.14}$$

In other words, Eq. (2.1.13) in view of Eqs. (2.1.14) and (2.1.5) represents the following system of equations

$$\dot{\mathbf{x}}_\alpha\left(t\right) = \mathbf{h}_{\mathbf{x}\alpha}^\omega\left(x\left(t\right)\right), \qquad \dot{\mathbf{p}}_\alpha\left(t\right) = \mathbf{h}_{\mathbf{p}\alpha}^\omega\left(x\left(t\right)\right), \tag{2.1.15}$$

where

$$\mathbf{h}_{\mathbf{x}\alpha}^\omega\left(x\left(t\right)\right) = \frac{\partial H}{\partial \mathbf{p}_\alpha}, \qquad \mathbf{h}_{\mathbf{p}\alpha}^\omega\left(x\left(t\right)\right) = -\frac{\partial H}{\partial \mathbf{x}_\alpha} - \frac{\partial R}{\partial \mathbf{p}_\alpha}. \tag{2.1.16}$$

The value of the coordinates and momenta of α-particle at the moment of time t (see (2.1.14)), determines, obviously, by the values of the coordinates and momenta $x_0 \equiv \left(x_1\left(0\right),...,x_N\left(0\right)\right)$ of all particles at the initial moment of time:

$$x_\alpha^\omega\left(t\right) = X_\alpha^\omega\left(t, x_0\right) \equiv \left(\mathbf{X}_\alpha^\omega\left(t, x_0\right), \mathbf{P}_\alpha^\omega\left(t, x_0\right)\right), \tag{2.1.17}$$

where functions $\mathbf{X}_\alpha^\omega\left(t, x_0\right)$ and $\mathbf{P}_\alpha^\omega\left(t, x_0\right)$, satisfy to the generalized Hamilton equations (2.1.5) (or to Eqs. (2.1.13) – (2.1.16)). Assume that for $t = 0$, the initial conditions are distributed with a probability density $D\left(x_1\left(0\right),...,x_N\left(0\right);0\right)$ (see [3] in this regard), and

$$\int dx_1(0)...dx_N(0)D(x_1(0),...,x_N(0);0) \equiv \int dx_0 D(x_0;0) = 1. \qquad (2.1.18)$$

Then at the time moment t the probability density $D^{\omega}(x_1,...,x_N;t) \equiv D^{\omega}(x;t)$, $x \equiv (x_1,...,x_N)$, (N - particle distribution function) will obviously be determined by the expression

$$D^{\omega}(x_1,...,x_N;t) = \int dx_0 D(x_0;0) \prod_{1\le\alpha\le N} \delta\left(x_\alpha - X_\alpha^{\omega}(t,x_0)\right). \qquad (2.1.19)$$

In [5], it is described in detail the procedure for deriving the Liouville equation for many-particle systems in the external stochastic field neglecting the interaction between particles. In [69], a similar procedure is used to obtain the generalized Liouville equation for dissipative many-particle systems in the absence of an external stochastic field. In [1], it is shown how these techniques can be combined to derive the Liouville equation for dissipative systems (see also Chapter 1.1 of this paper). Following the methodology outlined in [1] we arrive at the evolution equation for the N-particle distribution function $D^{\omega}(x_1,...,x_N;t)$

$$\frac{\partial D^{\omega}}{\partial t} + \sum_{1\le\alpha\le N} \frac{\partial}{\partial x_\alpha}\left(D^{\omega} h_\alpha^{\omega}\right) = 0, \qquad (2.1.20)$$

where the function $h_\alpha^{\omega}(x(t))$ is given by Eqs. (2.1.16) and (2.1.17). This equation is the Liouville one generalized to the case of many solid particles with pairwise interaction under the influence of the external stochastic field which depends on the particle velocity. This equation, if we bear in mind Eqs. (2.1.13) – (2.1.16), can also be written in the form:

$$\frac{\partial D^{\omega}}{\partial t} + \sum_{1\le\alpha\le N} \frac{\partial}{\partial \mathbf{x}_\alpha}\left(D^{\omega}\frac{\partial H}{\partial \mathbf{p}_\alpha}\right) + \sum_{1\le\alpha\le N} \frac{\partial}{\partial \mathbf{p}_\alpha}\left(D^{\omega}\left(-\frac{\partial H}{\partial \mathbf{x}_\alpha} - \frac{\partial R}{\partial \mathbf{p}_\alpha}\right)\right) = 0. \qquad (2.1.21)$$

However, we will further find more useful Liouville equation (2.1.21), obtained with regard to Eqs. (2.1.13) - (2.1.16), (2.1.8), (2.1.9) as:

$$\frac{\partial D^{\omega}}{\partial t} + \sum_{1\le\alpha\le N} \frac{\mathbf{p}_\alpha}{m}\frac{\partial D^{\omega}}{\partial \mathbf{x}_\alpha} + \sum_{1\le\alpha<\beta\le N} \frac{\partial}{\partial \mathbf{p}_\alpha} D^{\omega}\mathbf{F}_{\alpha,\beta} + \sum_{1\le\alpha\le N} \frac{\partial}{\partial \mathbf{p}_\alpha} D^{\omega}\mathbf{Y}_\alpha^{\omega} = 0, \qquad (2.1.22)$$

where the values $\mathbf{F}_{\alpha,\beta}$ and $\mathbf{Y}_\alpha^{\omega}$ are determined by Eqs. (2.1.7) - (21.9), as before. Eq. (2.1.20), as is easy to see, is a classical example of the evolution equation with multiplicative noise. Consequently, as in the previous

chapter, the question arises of averaging Eq. (1.20) over the external random force $\mathbf{Y}_\alpha^\omega$. There are, however, some differences from the previous chapter. Taking this into account, as well as for ease of presentation, let us present here the main points related to such a procedure again.

2.2. Averaging the Generalized Liouville Equation in the Case of Gaussian Noise

Let us introduce into consideration N-particle distribution function $D(x_1,...,x_N;t)$, which is the distribution function $D^\omega(x_1,...,x_N;t)$ (see Eq. (2.1.19)), averaged over a random external field $\mathbf{Y}^\omega(\mathbf{x},t)$ with probability density $W[\mathbf{Y}^\omega]$:

$$D(x_1,...,x_N;t) \equiv \left\langle D^\omega(x_1,...,x_N;t)\right\rangle_\omega, \qquad \left\langle ...\right\rangle_\omega \equiv \int D\mathbf{Y}^\omega(\mathbf{x},t) W[\mathbf{Y}^\omega]... \quad (2.2.1)$$

Applying the averaging operation (2.2.1) to equation (2.1.22), we obtain:

$$\frac{\partial D}{\partial t} + \sum_{1\le\alpha\le N} \frac{\mathbf{p}_\alpha}{m}\frac{\partial D}{\partial \mathbf{x}_\alpha} + \sum_{1\le\alpha<\beta\le N} \frac{\partial}{\partial \mathbf{p}_\alpha} D\mathbf{F}_{\alpha,\beta} + \sum_{1\le\alpha\le N} \frac{\partial}{\partial \mathbf{p}_\alpha}\left\langle D^\omega \mathbf{Y}_\alpha^\omega\right\rangle_\omega = 0. \quad (2.2.2)$$

It is easy to see that in order for this equation to be a closed evolution equation for the introduced distribution function, it is necessary to express the quantity $\left\langle D^\omega \mathbf{Y}_\alpha^\omega\right\rangle_\omega$ through $D(x_1,...,x_N;t)$. As before, we will use the so-called Furutsu-Novikov formula [71, 72]. We also recall that in [73] this formula was used to obtain the Kolmogorov turbulence spectra, generalized to the case of a compressible fluid. In this section, we will not describe in detail the method of proving the Furutsu-Novikov formula, referring to the works cited above and our work [1]. Let us use the final result of such a proof from [4] in the case of a Gaussian distribution of multiplicative noise. Namely, one can make sure that in this case the quantity $\left\langle D^\omega \mathbf{Y}_\alpha^\omega\right\rangle_\omega$ is presented as:

$$\left\langle Y_i^\omega(x_\alpha,t) D^\omega[\mathbf{Y}^\omega]\right\rangle_\omega = Y_i(x_\alpha,t)\left\langle D^\omega[\mathbf{Y}^\omega]\right\rangle_\omega + \int dx' \int_{-\infty}^{\infty} dt' y_{ij}(x_\alpha,x',t-t')\left\langle \frac{\delta D^\omega[\mathbf{Y}^\omega]}{\delta Y_j(x',t')}\right\rangle_\omega, \quad (2.2.3)$$

where $Y_i(x_\alpha,t) \equiv \left\langle Y_i^\omega(x_\alpha,t)\right\rangle_\omega$, $x_\alpha \equiv \{\mathbf{x}_\alpha,\mathbf{p}_\alpha\}$ and $y_{ij}(x_\alpha,x',t-t')$ is a pair correlation function of external Gaussian noise ($x' \equiv \{\mathbf{x}',\mathbf{p}'\}$):

$$y_{ij}\left(x_\alpha, x', t-t'\right) = \left\langle Y_i^\omega\left(x_\alpha, t\right) Y_j^\omega\left(x', t'\right)\right\rangle_\omega - \left\langle Y_i^\omega\left(x_\alpha, t\right)\right\rangle_\omega \left\langle Y_j^\omega\left(x', t'\right)\right\rangle_\omega . \quad (2.2.4)$$

At $Y_i\left(x,t\right) \equiv 0$ expression (2.2.3) exactly coincides with the analogous expression obtained in [71, 72] under the assumption that the average value of the external random force acting on the system is zero. In what follows, in this paper, we will also assume that $Y_i\left(x,t\right) \equiv 0$. Such a requirement does not significantly violate the generality of consideration, since it can be considered as a redefinition of the regular force $\mathbf{F}_{\alpha,\beta}$, see Eqs. (2.1.7), (2.1.8).

For further calculations, let us first consider the value I_i,

$$I_i \equiv \int dx' \int_{-\infty}^{\infty} dt' y_{ij}\left(x_\alpha, x', t-t'\right) \left\langle \frac{\delta D^\omega[\mathbf{Y}^\omega]}{\delta Y_j^\omega\left(x', t'\right)} \right\rangle_\omega . \quad (2.2.5)$$

It is easy to see that this quantity is the first term from the sum on the right-hand side of expression (2.2.3). We will assume that the pair correlation function differs from zero in the interval $\left|t-t'\right| \le \tau_0$ (τ_0 is the random process memory). We will also assume that for $t \sim t'$ pair correlation function $y_{ij}\left(x_\alpha, x', t-t'\right)$ has a sharp maximum. Then the functional derivative $\dfrac{\delta D^\omega[\mathbf{Y}^\omega]}{\delta Y_j^\omega\left(x', t'\right)}$ it is enough to calculate at $t \approx t'$. Moreover, as shown in [1, 4, 71-73], the exact expression for this derivative can be obtained only for $t \approx t'$.

Indeed, as is easy to see, the variational derivative $\dfrac{\delta D^\omega[\mathbf{Y}^\omega]}{\delta Y_j^\omega\left(x', t'\right)}$ at $t \approx t'$ undergoes a leap:

$$\frac{\delta D^\omega[\mathbf{Y}^\omega]}{\delta \delta Y_j^\omega\left(x', t'\right)} \neq 0, \quad t' \le t, \quad \frac{\delta D^\omega[\mathbf{Y}^\omega]}{\delta Y_j^\omega\left(x', t'\right)} = 0, \quad t' > t . \quad (2.2.6)$$

The latter circumstance is due to the fact that according to equation (2.1.22), the quantity $D^\omega\left(t\right)$ cannot be dependent on field $Y_j^\omega\left(\mathbf{x}', t'\right)$, taken at later points in time than t. In accordance with (2.2.5), integration over t' in formula (2.2.5) is carried out in the range from $-\infty$ to t, not from $-\infty$ to $+\infty$.

Differentiating equation (2.1.22) with respect to $Y_j^{\omega}\left(\mathbf{x}',t'\right)$ and noticing that according to (2.2.5) the derivative $\frac{\partial}{\partial t}\frac{\delta D^{\omega}[\mathbf{Y}^{\omega}]}{\delta Y_j^{\omega}\left(x',t'\right)}$ should contain a δ-like feature in time (while the value $\frac{\delta D^{\omega}[\mathbf{Y}^{\omega}]}{\delta Y_j^{\omega}\left(x',t'\right)}$ itself does not contain these features), it is not difficult to obtain the following expression for the functional derivative (see [1, 4]):

$$\frac{\delta D^{\omega}[\mathbf{Y}^{\omega}]}{\delta Y_j^{\omega}\left(x',t'\right)} \approx -\vartheta\left(t-t'\right)\sum_{1\le\beta\le N}\delta\left(x'-x_{\beta}\right)\frac{\partial D^{\omega}[\mathbf{Y}^{\omega}]}{\partial p_{\beta j}},$$
$$\delta\left(x'-x_{\beta}\right)\equiv\delta\left(\mathbf{x}'-\mathbf{x}_{\beta}\right)\delta\left(\mathbf{p}'-\mathbf{p}_{\beta}\right), \qquad (2.2.7)$$

where $\vartheta\left(t-t'\right)$ is a unit Heaviside function. This formula allows you to represent the value I_i (see Eq. (2.5)) in the following form (see Eqs. (2.1), (2.2)):

$$I_i=\int_{-\infty}^{t}dt'\sum_{1\le\beta\le N}y_{ij}\left(x,x_{\beta};t-t'\right)\frac{\partial D}{\partial p_{\beta j}}. \qquad (2.2.8)$$

Thus, the averaged Liouville equation, generalized to the case of systems of many active particles with interaction, in its final form:

$$\frac{\partial D}{\partial t}+\sum_{1\le\alpha\le N}\frac{\mathbf{p}_{\alpha}}{m}\frac{\partial D}{\partial \mathbf{x}_{\alpha}}+\sum_{1\le\alpha<\beta\le N}\frac{\partial D\mathbf{F}_{\alpha,\beta}}{\partial \mathbf{p}_{\alpha}}+\sum_{1\le\alpha\le N}\frac{\partial D\mathbf{Y}\left(x_{\alpha},t\right)}{\partial \mathbf{p}_{\alpha}}-. \qquad (2.2.9)$$

$$-\int_{-\infty}^{t}dt'\sum_{1\le\alpha,\beta\le N}\frac{\partial}{\partial p_{\alpha i}}y_{ij}\left(x_{\alpha},x_{\beta};t-t'\right)\frac{\partial D}{\partial p_{\beta j}}=0$$

As mentioned earlier, in what follows we assume that $Y_i\left(x,t\right)\equiv 0$. If we also take into account that the pair correlation function $y_{ij}\left(x_{\alpha},x_{\beta};t-t'\right)$ has a sharp maximum at $t\approx t'$ and assume that this function is an even function of the difference $t'-t$,

$$y_{ij}\left(x_{\alpha},x_{\beta};t-t'\right)=y_{ij}\left(x_{\alpha},x_{\beta};t'-t\right), \qquad (2.2.10)$$

then equation (2.2.9) takes on an even simpler form:

$$\frac{\partial D}{\partial t}+\sum_{1\le\alpha\le N}\frac{\mathbf{p}_\alpha}{m}\frac{\partial D}{\partial \mathbf{x}_\alpha}+\sum_{1\le\alpha<\beta\le N}\frac{\partial D\mathbf{F}_{\alpha,\beta}}{\partial \mathbf{p}_\alpha}-\frac{1}{2}\sum_{1\le\alpha,\beta\le N}\frac{\partial}{\partial p_{\alpha i}}y_{ij}\left(x_\alpha,x_\beta\right)\frac{\partial D}{\partial p_{\beta j}}=0\,, \quad (2.2.11)$$

where the notation is introduced:

$$y_{ij}\left(x_\alpha,x_\beta\right)\equiv\int_{-\infty}^{\infty}d\tau y_{ij}\left(x_\alpha,x_\beta;\tau\right). \quad (2.2.12)$$

Equation (2.2.12) can be given another form that is convenient for further calculations:

$$\frac{\partial D}{\partial t}+\sum_{1\le\alpha\le N}\frac{\mathbf{p}_\alpha}{m}\frac{\partial D}{\partial \mathbf{x}_\alpha}+\sum_{1\le\alpha<\beta\le N}\frac{\partial D\mathbf{F}_{\alpha,\beta}}{\partial \mathbf{p}_\alpha}-\frac{1}{2}\sum_{1\le\alpha\le N}\frac{\partial}{\partial p_{\alpha i}}y_{ij}\left(x_\alpha,x_\alpha\right)\frac{\partial D}{\partial p_{\alpha j}}- \quad (2.2.13)$$

$$-\sum_{1\le\alpha<\beta\le N}\frac{\partial}{\partial p_{\alpha i}}y_{ij}\left(x_\alpha,x_\beta\right)\frac{\partial D}{\partial p_{\beta j}}=0$$

Note that, in fact, the developed technique allows one to obtain the generalized Liouville equation in the case of non-Gaussian distributions of a random field if these distributions have moments of any order, see in this connection [1]. In this section, however, we restrict ourselves to the Gaussian distribution for an external stochastic field.

For further calculations, we specify the explicit form of the pair correlation function $y_{ij}\left(x_\alpha,x_\beta\right)$. Using an explicit stochastic force $Y_i^\omega\left(x,t\right)$, defined by formula (2.1.9), taking into account the equality $Y_i\left(x,t\right)\equiv\left\langle Y_i^\omega\left(x,t\right)\right\rangle_\omega=0$ based on (2.2.4), it is easy to arrive at the following expression for $y_{ij}\left(x_\alpha,x_\beta\right)$:

$$y_{ij}\left(x_\alpha,x_\beta\right)=e_{i\alpha}^h e_{j\beta}^h g\left(\mathbf{x}_\alpha,\mathbf{x}_\beta\right)+\left(\delta_{il}-e_{j\alpha}^h e_{l\alpha}^h\right)\left(\delta_{jl}-e_{j\beta}^h e_{l\beta}^h\right)h\left(\mathbf{x}_\alpha,\mathbf{x}_\beta\right),$$

$$e_{i\alpha}^h=\frac{p_{i\alpha}}{\left|\mathbf{p}_\alpha\right|}, \quad (2.2.14)$$

where we introduced the notation:

$$g\left(\mathbf{x}_\alpha,\mathbf{x}_\beta\right)\equiv\int_{-\infty}^{\infty}dt\left\langle X^\omega\left(\mathbf{x}_\alpha,t\right)X^\omega\left(\mathbf{x}_\beta,t'\right)\right\rangle_\omega,$$

$$\delta_{lk}h\left(\mathbf{x}_\alpha,\mathbf{x}_\beta\right)\equiv\int_{-\infty}^{\infty}dt\left\langle X_l^\omega\left(\mathbf{x}_\alpha,t\right)X_k^\omega\left(\mathbf{x}_\beta,t'\right)\right\rangle_\omega. \quad (2.2.15)$$

When deriving expression (2.2.14), it was assumed that the stochastic force $Y_i^{\omega}(x,t)$ has the following properties:

$$\left\langle X^{\omega}(\mathbf{x}_{\alpha},t)\,X_i^{\omega}(\mathbf{x}_{\beta},t')\right\rangle = 0\,,\qquad \left\langle X^{\omega}(\mathbf{x}_{\alpha},t)\right\rangle = 0\,,$$
$$\left\langle X_i^{\omega}(\mathbf{x}_{\beta},t')\right\rangle = 0\,. \tag{2.2.16}$$

The last two formulas in (2.2.16) are a consequence of the requirement $Y_i(x,t) \equiv \left\langle Y_i^{\omega}(x,t)\right\rangle_{\omega} = 0$, see Eq. (2.1.9).

2.3. An analogue of the BBGKY chain and the kinetic equation for systems of identical active particles with interaction in external stochastic fields

As in the previous chapter (see section 1.3), along with the probability density $D(x_1,...,x_N;t)$ (D is the N-particle distribution function, N is total number of active particles in the system) you can introduce the probability of finding one or more particles in these elements of the phase space, regardless of where the rest of the particles are in this space (see in this connection also [1 - 3]). These probabilities can be obtained by integrating the function D over all variables, except for those related to the particles under consideration:

$$f_S(x_1,...,x_S;t) = \mathcal{V}^S \int dx_{S+1}...\int dx_N D(x_1,...,x_N;t)\,,\ x_{\alpha} \equiv (\mathbf{x}_{\alpha},\mathbf{p}_{\alpha})\,, \tag{2.3.1}$$

where $\mathcal{V}$ is the system volume and $D(x_1,...,x_N;t)$ satisfies equation (2.2.10). After simple calculations [36], one can arrive at the following equation for S-particle distribution function $f_S(x_1,...,x_S;t)$:

$$\frac{\partial f_S}{\partial t} + \sum_{1\le\alpha\le S}\frac{\mathbf{p}_{\alpha}}{m}\frac{\partial f_S}{\partial \mathbf{x}_{\alpha}} - \frac{1}{2}\sum_{1\le\alpha\le S}\frac{\partial}{\partial p_{\alpha i}}y_{ij}(x_{\alpha},x_{\alpha})\frac{\partial f_S}{\partial p_{\alpha j}} + \sum_{1\le\alpha<\beta\le S}\frac{\partial f_S \mathbf{F}_{\alpha,\beta}}{\partial \mathbf{p}_{\alpha}} - \sum_{1\le\alpha<\beta\le S}\frac{\partial}{\partial p_{\alpha i}}y_{ij}(x_{\alpha},x_{\beta})\frac{\partial f_S}{\partial p_{\beta j}} =$$
$$-\frac{1}{v}\sum_{1\le\alpha\le S}\frac{\partial}{\partial \mathbf{p}_{\alpha}}\int dx_{S+1} f_{S+1}\mathbf{F}_{\alpha,S+1} + \frac{1}{v}\sum_{1\le\alpha\le S}\frac{\partial}{\partial p_{\alpha i}}\int dx_{S+1} y_{ij}(x_{\alpha},x_{S+1})\frac{\partial f_{S+1}}{\partial p_{S+1\,j}}\,,$$
$$v \equiv \frac{\mathcal{V}}{N}\,, \tag{2.3.2}$$

where values $\mathbf{F}_{\alpha,\beta}$, $y_{ij}(x_{\alpha},x_{\beta})$ are still given by formulas (2.1.8), (2.2.4), (2.2.14), (2.2.15). As in the case of equations (1.3.2) or (1.3.3), equation (2.3.2) for S-particle distribution function includes an $S+1$-particle distribution function. That is, in this case, too, we are dealing with an

infinite chain of kinetic equations. These chains are a generalization of the famous chain of Bogolyubov-Born-Green-Kirkwood-Yvon equations to the case of systems of identical active interacting particles under the influence of an external stochastic field. The following remark should be made here. In accordance with definition (2.3.1), distribution functions of a higher order contain all the information contained in functions of a lower order [3]. This circumstance leads to the fact that with increasing order S of the distribution function $f_S\left(x_1,...,x_S;t\right)$ are becoming more and more complex. Since in the full description according to (2.3.2) it is necessary to take into account the distribution functions up to $S=N$, we come to the conclusion that the resulting chains of equations (2.3.2) are themselves equivalent to Liouville's equation (2.2.13). In other words, the most complete description of the systems under study is equally complex both in the language of the complete distribution function $D\left(x_1,...,x_N;t\right)$, and in the language of many-particle distribution functions $f_S\left(x_1,...,x_S;t\right)$.

We have already noted that a significant simplification in the description of the state of the system occurs in two cases: when the interaction between particles is small, or when the density of the number of particles is low, and the interaction is arbitrary, but such that does not lead to the formation of bound states. This circumstance, as in the previous chapter, allows us to use the method of reduced description of the evolution of the system under study to break the infinite chain of equations (2.3.2) and derive a closed kinetic equation for the one-particle distribution function. Here we will not set out in detail the main provisions of the reduced description method as applied to active media in order to obtain the kinetic equation. The procedure differs little from that described in the previous chapter (see Section 1.4) if we also consider the case of weak interactions (both potential and dissipative) between structural units, and assume that the intensity of the external random field is small. In this situation, in accordance with the concepts of the reduced description method, it can also be assumed that the mathematical formulation of the idea of the hierarchy of relaxation times of the system consists in the functional time dependence of the many-particle distribution functions $f_S\left(x_1,...,x_S;t\right)$ only through the time dependence of the parameters of the reduced description at the corresponding stage of evolution. In particular, at the kinetic stage of the evolution of the system, the many-particle distribution functions depend on time only through the single-particle distribution function $f_1(x',t)$:

$$f_S\left(x_1,...,x_S;t\right)=f_S\left(x_1,...,x_S;f_1(x',t)\right), \tag{2.3.3}$$

as a result, the one-particle distribution function $f_1(x',t)$ according to (2.3.2) must satisfy the equation:

$$\frac{\partial f_1}{\partial t}+\frac{\mathbf{p}_1}{m}\frac{\partial f_1}{\partial \mathbf{x}_1}-\frac{1}{2}\frac{\partial}{\partial p_{1i}}y_{ij}\left(x_1,x_1\right)\frac{\partial f_1}{\partial p_{1j}}=\frac{1}{\nu}L\left(x_1;f_1\right), \tag{2.3.4}$$

where still $\nu=\frac{\mathcal{V}}{N}$ and $L\left(x_1;f_1\right)$ is the generalized collision integral defined by the formula

$$L\left(x_1;f_1\right)\equiv-\frac{\partial}{\partial\mathbf{p}_1}\int dx_2\,f_2\left(x_1,x_2;f_1\right)\mathbf{F}_{1,2}+\frac{\partial}{\partial p_{\alpha i}}\int dx_2 y_{ij}\left(x_1,x_2\right)\frac{\partial}{\partial p_{2j}}f_2\left(x_1,x_2;f_1\right). \tag{2.3.5}$$

Here, however, a point needs to be made. Functional relation (2.3.3) does not necessarily imply an expansion of the function $f_S\left(x_1,...,x_S;f_1(x',t)\right)$ into the functional series of perturbation theory with respect to the one-particle distribution function. Such an expansion must be realized only in one of the above-mentioned cases of chain breaking - the case of a low density of the number of particles. We recall that this raises the famous question of possible divergences in higher orders of perturbation theory in the low density of the number of particles and the renormalization of such a theory (see, for example, [80-82]). In the case of perturbation theory in the weak interaction between particles, these questions do not arise, which is easy to verify from subsequent calculations (see also [3, 4]).

It is easy to see that in order to close equation (2.3.4), it is necessary to find the collision integral (2.3.5) as the functional of the one-particle distribution function, for which it is necessary to break the infinite chain of equations (2.3.2). The procedure for such an action in the case of a weak interaction between structural units and an external field of weak intensity is described in detail in [36]. Here we present only the final result, namely, the kinetic equation for the one-particle distribution function:

$$\frac{\partial f_1\left(x_1,t\right)}{\partial t}+\frac{\mathbf{p}_1}{m}\frac{\partial f_1\left(x_1,t\right)}{\partial \mathbf{x}_1}-\frac{1}{2}\frac{\partial}{\partial p_{1i}}y_{ij}\left(x_1,x_1\right)\frac{\partial f_1\left(x_1,t\right)}{\partial p_{1j}}= \tag{2.3.6a}$$

$$=\frac{1}{\nu}\frac{\partial}{\partial\mathbf{p}_1}f_1\left(x_1\right)\int dx_2\,f_1\left(x_2\right)\left(\frac{\partial V_{1,2}}{\partial\mathbf{x}_1}+\frac{\partial R_{1,2}}{\partial\mathbf{p}_1}\right)+\frac{1}{\nu}\frac{\partial}{\partial p_{1i}}f_1\left(x_1\right)\int dx_2 y_{ij}\left(x_1,x_2\right)\frac{\partial f_1\left(x_2\right)}{\partial p_{2j}},$$

where values $V_{1,2}$, $R_{1,2}$ are determined by expressions (2.1.2) - (2.1.4) and the correlation function is still given by expression (2.2.14). Equation (2.3.6a) can be given in a slightly different form:

$$\frac{\partial f_1(x_1,t)}{\partial t}+\frac{\mathbf{p}_1}{m}\frac{\partial f_1(x_1,t)}{\partial \mathbf{x}_1}-\frac{\partial U(\mathbf{x}_1,t)}{\partial \mathbf{x}_1}\frac{\partial f_1(x_1,t)}{\partial \mathbf{p}_1}= \tag{2.3.6b}$$

$$=\frac{1}{2}\frac{\partial}{\partial p_{1i}}y_{ij}(x_1,x_1)\frac{\partial f_1(x_1,t)}{\partial p_{1j}}+\frac{1}{\nu}\frac{\partial}{\partial p_{1i}}f_1(x_1,t)\int dx_2\, f_1(x_2,t)\left[\frac{\partial R_{1,2}}{\partial p_{1i}}-\frac{\partial y_{ij}(x_1,x_2)}{\partial p_{2j}}\right]$$

or

$$\frac{\partial f_1(x_1,t)}{\partial t}+\frac{\mathbf{p}_1}{m}\frac{\partial f_1(x_1,t)}{\partial \mathbf{x}_1}-\frac{\partial U(\mathbf{x}_1,t)}{\partial \mathbf{x}_1}\frac{\partial f_1(x_1,t)}{\partial \mathbf{p}_1}= \tag{2.3.6c}$$

$$=\frac{1}{2}\frac{\partial}{\partial p_{1i}}y_{ij}(x_1,x_1)\frac{\partial f_1(x_1,t)}{\partial p_{1j}}+\frac{1}{\nu}\frac{\partial}{\partial p_{1i}}f_1(x_1,t)\int dx_2\left[R_{1,2}\delta_{i,j}+y_{ij}(x_1,x_2)\right]\frac{\partial f_1(x_2,t)}{\partial p_{2j}},$$

if we introduce the mean field $U(\mathbf{x}_1,t)$, defined by the formula (see (2.1.2)):

$$U(\mathbf{x}_1,t)=\frac{1}{\nu}\int d\mathbf{x}_2 V(\mathbf{x}_1-\mathbf{x}_2)\int d\mathbf{p}_2\, f_1(x_2,t), \qquad f_1(x_2)\equiv f_1(\mathbf{x}_2,\mathbf{p}_2). \tag{2.3.7}$$

Equations (2.3.6) are kinetic equations for active particles with pair interactions between particles (potential and dissipative) under the influence of nonlocal active fluctuations. We emphasize that all equations (2.3.6) were obtained without using the explicit form of the potential interaction $V_{1,2}\equiv V(\mathbf{x}_1-\mathbf{x}_2)$, dissipative function $R_{1,2}$ (in the above sense) and the correlation function $y_{ij}(x_1,x_2)$.

We also note that the presence of a random force (2.1.9), which is characteristic of active fluctuations and has a local character of the effect on particles, leads, as is easy to see from (2.3.6b), (2.3.6c), to some additional interaction between particles, determined precisely by the pair correlation function $y_{ij}(x_1,x_2)$.

2.4. Special cases of the theory. Spatially homogeneous states

Before proceeding to the demonstration of the fact that the general kinetic equations (2.3.6) contain known particular cases of systems of active particles, we consider spatially homogeneous states of the systems described by these equations. In the spatially homogeneous case, the one-particle distribution function $f_1(\mathbf{x},\mathbf{p},t)$ should not depend on coordinates,

$$f_1(\mathbf{x},\mathbf{p},t)\equiv f_1(\mathbf{p},t). \tag{2.4.1}$$

should not depend on coordinates $y_{ij}\left(x_1, x_2\right)$ (see Eqs. (2.2.14) – (2.2.16)) and reads as follows:

$$y_{ij}\left(x_1, x_2\right) = g\left(\mathbf{x}_1 - \mathbf{x}_2\right) e^h_{1i} e^h_{2j} + h\left(\mathbf{x}_1 - \mathbf{x}_2\right)\left(\delta_{il} - e^h_{1i} e^h_{1l}\right)\left(\delta_{jl} - e^h_{2j} e^h_{2l}\right). \quad (2.4.2)$$

Recall that according to (2.1.4) all restrictions on the general properties of the function $R_{1,2}$ are contained in the expression:

$$R_{1,2} \equiv R\left(\mathbf{x}_1 - \mathbf{x}_2, \mathbf{p}_1 - \mathbf{p}_2\right), \quad (2.4.3)$$

which follows from considerations of the Galilean invariance of the system in the absence of external influences on it. Moreover, since the function $R_{1,2}$ is a scalar quantity, its dependence on the differences $\mathbf{x}_1 - \mathbf{x}_2$, $\mathbf{p}_1 - \mathbf{p}_2$ must be characterized by the expression:

$$R\left(\mathbf{x}, \mathbf{p}\right) \equiv R\left(\mathbf{x}^2, \mathbf{p}^2, \mathbf{xp}\right). \quad (2.4.4).$$

In accordance with formulas (2.4.1) - (2.4.4), equation (2.3.6a) is transformed to the form:

$$\frac{\partial f_1\left(\mathbf{p}_1, t\right)}{\partial t} - \frac{1}{2}\frac{\partial}{\partial p_{1i}}\left[g\left(0\right) e^h_{1i} e^h_{1j} + h\left(0\right)\left(\delta_{ij} - e^h_{1i} e^h_{1j}\right)\right]\frac{\partial f_1\left(\mathbf{p}_1, t\right)}{\partial p_{1j}} = \quad (2.4.5)$$

$$= \frac{\partial}{\partial p_{1i}} f_1\left(\mathbf{p}_1, t\right)\frac{\partial}{\partial p_{1i}}\int d\mathbf{p}_2\, f_1\left(\mathbf{p}_2, t\right)\bar{R}\left(\left(\mathbf{p}_1 - \mathbf{p}_2\right)^2\right) +$$

$$+ \frac{\partial}{\partial p_{1i}} f_1\left(\mathbf{p}_1, t\right)\int d\mathbf{p}_2\left[\bar{g} e^h_{1i} e^h_{2j} + \bar{h}\left(\delta_{il} - e^h_{1i} e^h_{1l}\right)\left(\delta_{jl} - e^h_{2j} e^h_{2l}\right)\right]\frac{\partial f_1\left(\mathbf{p}_2, t\right)}{\partial p_{2j}},$$

where we introduced:

$$\bar{R}\left(\left(\mathbf{p}_1 - \mathbf{p}_2\right)^2\right) \equiv \frac{1}{v}\int d\mathbf{x} R\left(\mathbf{x}^2, \left(\mathbf{p}_1 - \mathbf{p}_2\right)^2, \mathbf{x}\left(\mathbf{p}_1 - \mathbf{p}_2\right)\right), \quad \bar{g} \equiv \frac{1}{v}\int d\mathbf{x} g\left(\mathbf{x}\right),$$

$$\bar{h} \equiv \frac{1}{v}\int d\mathbf{x} h\left(\mathbf{x}\right). \quad (2.4.6)$$

Quasi-Brownian particles with active fluctuations

Let us now study possible solutions of the kinetic equation (2.4.5) isotropic in the momentum space:

$$f_1\left(\mathbf{p}, t\right) \equiv f_1\left(p, t\right). \quad (2.4.7)$$

Taking into account (5.6), (5.7), it becomes possible to reduce equation (2.4.5) to the form:

$$\frac{\partial f_1(p_1,t)}{\partial t} = \frac{\partial}{\partial p_{1i}} e_{1i}^h \left\{ f_1(p_1,t)\gamma(p_1,t)\, p_1 + \frac{1}{2} g(0) \frac{\partial f_1(p_1,t)}{\partial p_1} + \right.$$

$$\left. + \overline{g} f_1(p_1,t) \int d\mathbf{p}_2 \frac{\partial f_1(p_2,t)}{\partial p_2} \right\}, \quad (2.4.8)$$

Where

$$\gamma(p,t) \equiv 2\frac{\partial \overline{R}(p^2,t)}{\partial p^2}, \quad \overline{R}(p^2,t) \equiv \int d\mathbf{p}_2 f_1(p_2,t) \overline{R}\left((\mathbf{p}-\mathbf{p}_2)^2\right). \quad (2.4.9)$$

The resulting equation (2.4.8) is the kinetic equation for active particles with time-dependent nonlinear friction (friction coefficient $\gamma(p,t)$) in the case of a nonlocal action of an external random field on the system. This equation can be considered as a generalization of the kinetic equation for quasi-Brownian particles with active fluctuations for the case of 3D - dimension of the system, dissipative interaction, and a nonlocal external stochastic field.

The term «quasi-Brownian particles with active fluctuations» can be considered, probably, well-established by now. This term is usually understood as a system of particles in the presence of a friction force linearly dependent on momentum (or on velocity) under the influence of a «global» stochastic field of the form (2.1.9) with regard to (2.1.10), see [33, 34]. The case of linear friction in the framework of this consideration is easy to obtain: in (24.8) (and, consequently, in (2.4.9)), the friction coefficient $\gamma(p)$ must be considered independent of momentum, $\gamma(p) \equiv \gamma$, moreover, according to (2.1.5), (2.4.6), the quantity γ in this case is given by the expressions (see [1, 36]):

$$\gamma = \frac{1}{v^2} \int d\mathbf{x} \tilde{\gamma}(\mathbf{x}), \ \int d\mathbf{p} f_1(p,t) = \frac{1}{v}. \quad (2.4.10)$$

To realize the “globality” of noise in accordance with (2.1.9), (2.1.10), (2.2.14) and (2.4.2), the quantity $\overline{g}$ is to be considered equal to zero, and the value $g(0)$ is to be equal to $2D_p$ (D_p is the momentum noise intensity), $g(0) = 2D_p$. Carrying out such actions in (2.4.8), we arrive at the following kinetic equation:

$$\frac{\partial f_1(p_1,t)}{\partial t} = \frac{\partial}{\partial p_{1i}} n_{1i} \left\{ \gamma p_1 f_1(p_1,t) + D_p \frac{\partial f_1(p_1,t)}{\partial p_1} \right\}, \quad g(0) \equiv 2D_p, \qquad (2.4.11)$$

a stationary solution of which $f_\infty(p) = \lim_{t\to\infty} f_1(p,t)$ has a Boltzmann form:

$$f_\infty(p) = Ae^{-\frac{\gamma}{2D_p}p^2}, \qquad (2.4.12)$$

which differs in two-dimensional and three-dimensional cases only in the value of the normalization constant A, see (5.10):

$$A = \frac{\gamma}{2\pi D_p v} \quad \text{for} \quad 2D, \quad A = \frac{1}{v}\left(\frac{2\pi D_p}{\gamma}\right)^{-3/2} \quad \text{for} \quad 3D. \qquad (2.4.13)$$

Taking into account the normalization (2.4.10), (2.4.13) in the two-dimensional case, expression (2.4.12) for the stationary distribution function of active particles coincides with the corresponding expression, for example, in [33]. When comparing, one should only take into account that in [33] the Rayleigh distribution function $f_R(p)$ is written:

$$f_R(p) \sim pe^{-\frac{\gamma}{2D_p}p^2}.$$

Quasi-Brownian motion of particles with active «local» correlations

Consider now the stationary solutions $f_\infty(p) = \lim_{t\to\infty} f_1(p,t)$ equation (2.4.8), more general than (2.4.11). This equation is in the limit $t \to \infty$ can be written as:

$$f_\infty(p_1)\gamma(p_1)p_1 + \frac{1}{2}g(0)\frac{\partial f_\infty(p_1)}{\partial p_1} + \overline{g} f_\infty(p_1)\int d\mathbf{p}_2 \frac{\partial f_\infty(p_1)}{\partial p_2} = 0. \qquad (2.4.14)$$

It is easy to verify that the solutions of this equation are determined by the function

$$f_\infty(p) \sim \exp\left\{ -\frac{1}{D_p}\int^p dp' \left(\gamma(p')p' + \tilde{g}\right) \right\}, \qquad (2.4.15)$$

where we introduced

$$g(0) \equiv 2D_p, \qquad \tilde{g} \equiv \bar{g} \int d\mathbf{p}_2 \frac{\partial f_\infty(p_1)}{\partial p_2}, \tag{2.4.16}$$

value $\bar{g}$ is still given by expression (2.4.6) taking into account (2.3.2) and the function $\gamma(p)$

$$\gamma(p_1) = 2\lim_{t\to\infty} \frac{\partial \bar{R}(p^2,t)}{\partial p^2} = 2\frac{\partial}{\partial p^2} \int d\mathbf{p}_2 f_\infty(p_2) \bar{R}\left((\mathbf{p}-\mathbf{p}_2)^2\right) \tag{2.4.17}$$

determines the forces of nonlinear friction.

The following circumstance should be noted further. Expressions of the type (2.4.15) for the distribution function are typical for systems of particles with nonlinear friction under the influence of external active spatially homogeneous (global) fluctuations. It is the presence of nonlinear friction that is considered necessary for the emergence of self-propelled properties in the system due to the head-tail asymmetry of structural units, see, for example, [33, 34]. Indeed, in the case of nonlinear friction in one interval of momenta, dissipative forces can be negative (friction), in another interval of momenta, these forces can be positive (thrust, propulsion). If such intervals of momenta (or velocities) are somehow connected with a certain (selected) direction, then such a direction sets the direction of self-propulsion. The presence of the noted asymmetry is responsible for the appearance of two-humped stationary distribution functions of active particles [33, 34]. The position of these maxima of the distribution function is symmetric about the point $p = 0$ is set by the value of the stationary momentum p_0 of the particle head motion. Moreover, the stationary parameters of self-propelled motion (for example, the magnitude of the characteristic stationary momentum p_0) are not necessarily associated with a direct impact on the system of external forces. A typical case for systems of active particles is the situation when the average value of such an external force can be considered equal to zero, and the mentioned symmetry can be observed. Note that the case $p_0 = 0$ corresponds to the Rayleigh distribution function $f_R(p)$, see (2.4.12).

However, as will be demonstrated below, from the solution (2.4.15) of equation (2.4.14) it follows that the described situation of stationary distribution functions with two maxima (the case of self-propelled particles) can be realized even in the case of linear friction, that is, when $\gamma(p) \equiv \gamma > 0$, see Eq. (2.4.10). And responsible for such a realization in this case is the local nature of the impact on the system of stochastic forces with active

fluctuations. Indeed, the general form of the solution in the case of linear friction, as is easy to see from (2.4.15), is determined by the expression:

$$f_\infty(p) \sim \exp\left\{-\frac{\gamma}{2D_p}\left(p+\frac{\tilde{g}}{\gamma}\right)^2\right\}, \qquad \tilde{g} \equiv \bar{g}\int d\mathbf{p}_2 \frac{\partial f_\infty(p_1)}{\partial p_2}, \qquad \bar{g} \equiv \frac{1}{v}\int d\mathbf{x} g(\mathbf{x})$$

.(2.4.18)

And the existence of self-propulsion is associated with the sign of value $\tilde{g}$. Indeed, since $\gamma > 0$, then the positivity $\tilde{g} > 0$ must correspond to a purely dissipative case (real friction). When $\tilde{g} < 0$ there are momentum values for which the inequality $\gamma p + \tilde{g} < 0$. There is a propulsion for these particles. In the mixed case, the one-particle distribution function of active particles has the form (see in this connection [33, 34]):

$$f_\infty(p) = C\left\{\exp\left[-\frac{\gamma}{2D_p}(p-p_0)^2\right] + \exp\left[-\frac{\gamma}{2D_p}(p+p_0)^2\right]\right\}, \qquad (2.4.19)$$

where C is normalization constant. Momentum p_0 in (2.4.19), characterizing the location of the maxima of the distribution function, symmetric about the point $p = 0$, is defined by $\tilde{g}$:

$$p_0 = |\tilde{g}|/\gamma. \qquad (2.4.20)$$

The $\tilde{g}$ itself, according to (2.4.16), (2.4.18), depends on the derivative of the required distribution function with respect to momentum. Thus, the definition (2.4.18), taking into account the explicit form of the distribution function (2.4.19), should be considered as an equation connecting $\tilde{g}$ and the normalization constant C:

$$\tilde{g} = 8\pi\bar{g}C\int_0^\infty d\mathbf{p}\frac{\partial}{\partial p}\left\{\exp\left[-\frac{\gamma}{2D_p}(p-p_0)^2\right] + \exp\left[-\frac{\gamma}{2D_p}(p+p_0)^2\right]\right\}. \qquad (2.4.21)$$

In turn, the constant C must be determined from the normalization condition (see Eq. (2.4.10))

$$\int d\mathbf{p} f_\infty(p) = \frac{1}{v},$$

which, taking into account (2.4.19), can be written in the form:

$$\frac{1}{v} = C\int d\mathbf{p}\left\{\exp\left[-\frac{\gamma}{2D_p}(p-p_0)^2\right] + \exp\left[-\frac{\gamma}{2D_p}(p+p_0)^2\right]\right\}. \qquad (2.4.22)$$

The last expression is also an equation relating the constant C and unknown quantity $\tilde{g}$. Thus, equations (2.4.21) and (2.4.22) represent a system of two equations for determining two unknown quantities, C and $\tilde{g}$, through the parameters characterizing the system: coefficient of friction γ, particle density $1/v$ and noise parameters with active correlations - pair correlation functions $\bar{g}$ and $g(0)=2D_p$, see Eqs. (2.4.16), (2.4.18). Due to the presence of integration over the total volume in the momentum space, equations (2.4.21), (2.4.22) have a different form for the three-dimensional and two-dimensional cases.

Consider first the two-dimensional case. Then equations (2.4.21), (2.4.22) can be transformed to the form:

$$\tilde{g} = -2\pi^{3/2}\sqrt{\frac{2D_p}{\gamma}}\bar{g}C, \tag{2.4.23}$$

$$\frac{1}{v} = C\left\{4\pi\frac{D_p}{\gamma} + 2\pi^{3/2}p_0\sqrt{\frac{2D_p}{\gamma}}\,\mathrm{erf}\left(p_0\sqrt{\frac{\gamma}{2D_p}}\right)\right\},\quad p_0 \equiv \frac{|\tilde{g}|}{\gamma},$$

where function $\mathrm{erf}(x)$ is the error function:

$$\mathrm{erf}(x) \equiv \frac{2}{\sqrt{\pi}}\int_0^x dy\exp\left(-y^2\right). \tag{2.4.24}$$

In general, expressions (2.4.23) are complex transcendental equations and can be solved only numerically. However, in two limiting cases - cases of small and large values of the arguments $p_0\sqrt{\gamma/2D_p} = \sqrt{\tilde{g}^2/2\gamma D_p}$ of the error function (2.4.24) – the equations admit analytical solutions. When $p_0\sqrt{\gamma/2D_p} = \sqrt{\tilde{g}^2/2\gamma D_p} \ll 1$ these solutions are given by:

$$C \approx \frac{\gamma}{4\pi D_p v},\qquad \tilde{g} = -\pi^{1/2}\frac{\bar{g}}{v}\sqrt{\frac{\gamma}{2D_p}},\qquad p_0 \approx \pi^{1/2}\frac{1}{v}\sqrt{\frac{\bar{g}^2}{2\gamma D_p}}. \tag{2.4.25}$$

It is also easy to verify that the inequality $p_0\sqrt{\gamma/2D_p} = \sqrt{\tilde{g}^2/2\gamma D_p} \ll 1$, for which formulas (2.4.25) are valid, by using these formulas is transformed to the form:

$$\frac{|\bar{g}|}{D_p v} \ll 1. \tag{2.4.26}$$

We have already noted above that the appearance of the self-propelling property is associated with the sign of the value $\tilde{g}$. In accordance with the above analysis, from (2.4.25) we can conclude that for $\overline{g} < 0$ $\tilde{g} > 0$ and the validity of inequality (2.4.26), the considered system of active particles has no self-propelled properties. In this case, in accordance with (2.4.18), only a shift of the maximum of the distribution function by the amount p_0, defined by formula (2.4.25). If $\overline{g} > 0$, then $\tilde{g} < 0$ and then the self-propelled case is realized with a two-humped distribution function with parameters determined by formulas (2.4.25).

Let us now consider the case of large values of the parameter $p_0\sqrt{\gamma/2D_p} = \sqrt{\tilde{g}^2/2\gamma D_p}$, i.e., $p_0\sqrt{\gamma/2D_p} = \sqrt{\tilde{g}^2/2\gamma D_p} \gg 1$. Solutions of equations (2.4.23) in the principal approximation of perturbation theory in this parameter are given by the formulas:

$$C \approx \frac{1}{4\pi^{3/2}\nu}\frac{\gamma}{D_p}\sqrt{\frac{2\gamma D_p}{|\tilde{g}|^2}}, \quad \tilde{g} = -2\pi^{3/2}\sqrt{\frac{2D_p}{\gamma}}\overline{g}C, \quad p_0 = \sqrt{\frac{|\overline{g}|}{\gamma\nu}}. \qquad (2.4.27)$$

It is seen from these formulas that for $\overline{g} < 0$ the value $\tilde{g}$ is positive, $\tilde{g} > 0$. Therefore, in this case, a situation with a distribution function with a shifted maximum, such as (2.4.18), should be realized. In the opposite case $\overline{g} > 0$, $\tilde{g}$ is negative, $\tilde{g} < 0$, and the particle distribution function will be determined by expressions (2.4.19), (2.4.27). We also add that the inequality $p_0\sqrt{\gamma/2D_p} = \sqrt{\tilde{g}^2/2\gamma D_p} \gg 1$, for which formulas (2.4.27) are valid, taking them into account can be transformed into the relation

$$\frac{|\overline{g}|}{D_p\nu} \gg 1, \qquad (2.4.28)$$

opposite to relation (2.4.26).

Let us now return to equations (2.4.21), (2.4.22) and study some of their solutions in the case of a three-dimensional system of active particles with linear friction and active fluctuations of a local nature. In this case, equations (2.4.21), (2.4.22) are transformed to a form that significantly differs from (2.4.23):

$$C = \frac{1}{2\nu}\left(\frac{\pi\gamma}{2D_p}\right)^{3/2}, \qquad \tilde{g} + 2\frac{|\tilde{g}|}{\gamma}\frac{\pi^3\overline{g}}{\nu}\frac{\gamma}{D_p}\operatorname{erf}\left(\sqrt{\frac{\tilde{g}^2}{2\gamma D_p}}\right) = -8\frac{\pi\overline{g}D_p}{\gamma\nu}\left(\frac{\pi\gamma}{2D_p}\right)^{3/2},$$

$$p_0 \equiv \frac{|\tilde{g}|}{\gamma}, \qquad (2.4.29)$$

where $\mathrm{erf}(x)$ is still given by formula (2.4.24). As in the previous case of a two-dimensional system of active particles, the second of equations (2.4.29) in general form can be solved only numerically. However, in the two limiting cases studied above, this equation can also be solved analytically. Namely, in the case of small values of the parameter $p_0\sqrt{\gamma/2D_p} = \sqrt{\tilde{g}^2/2\gamma D_p} \ll 1$ the solution of equation (2.4.29) is determined by the formulas:

$$\tilde{g} \approx -4\pi^2 \frac{\bar{g}}{\nu}\left(\frac{\pi\gamma}{2D_p}\right)^{1/2}, \qquad p_0 \approx 4\pi^2 \frac{|\bar{g}|}{\nu D_p}\left(\frac{\pi D_p}{2\gamma}\right)^{1/2}, \tag{2.4.30}$$

and, as is easy to verify directly, the relations $p_0\sqrt{\gamma/2D_p} = \sqrt{\tilde{g}^2/2\gamma D_p} \ll 1$ can be reduced to the form (2.4.26), which is valid for the two-dimensional case. Note also that, similarly to the two-dimensional case, in the three-dimensional system of many active particles at $\bar{g} > 0$ the value $\tilde{g}$ is negative, $\tilde{g} < 0$, which indicates the possibility of implementing self-propelled properties in this system. When $\bar{g} < 0$ the value $\tilde{g}$ is positive, due to which the stationary state of such a system should be characterized by a distribution function with one maximum shifted to the right by the value p_0, see Eqs. (2.4.18), (2.4.20).

In case of large values of the parameter $p_0\sqrt{\gamma/2D_p} = \sqrt{\tilde{g}^2/2\gamma D_p}$, $p_0\sqrt{\gamma/2D_p} = \sqrt{\tilde{g}^2/2\gamma D_p} \gg 1$ the solution of equation (2.4.29) is given by the expressions:

$$\tilde{g} \approx -8\frac{\pi\bar{g}}{\nu}\left(\frac{\pi\gamma}{2D_p}\right)^{3/2}\frac{D_p}{\gamma}\left(1-2\pi^3\frac{\bar{g}}{\nu D_p}\right)^{-1},$$

$$p_0 \approx 4\pi^2\frac{\bar{g}}{\nu D_p}\sqrt{\frac{\pi D_p}{2\gamma}}\left|1-2\pi^3\frac{\bar{g}}{\nu D_p}\right|^{-1}. \tag{2.4.31}$$

From the analysis of formulas (24.31) it follows that for $\bar{g} > 0$ in the region of large values of the specified parameter, negative $\tilde{g}$ is possible only with $2\pi^3\frac{\bar{g}}{\nu D_p} < 1$. In this case, the expression for p_0 can be somewhat simplified:

$$p_0 \approx \sqrt{\frac{2D_p}{\pi\gamma}}\left|1-2\pi^3\frac{\bar{g}}{\nu D_p}\right|^{-1}, \tag{2.4.32}$$

and the condition $\sqrt{\tilde{g}^2/2\gamma D_p} \gg 1$ replaced by an equivalent

$$0 < \frac{\bar{g}}{\nu D_p} < \frac{1}{2\pi^3}. \tag{2.4.33}$$

Thus, we come to the conclusion that self-propelling of particles can be realized in the case of large values of the parameter $\sqrt{\tilde{g}^2/2\gamma D_p}$ also in a three-dimensional system, however, the criteria (2.4.33) of such a motion differ significantly from those in a two-dimensional case, see (2.45.28).

It should be noted that when $\bar{g} = 0$ characteristic momentum p_0 is always zero, both in two-dimensional and three-dimensional cases, see (2.4.20) and the original equation (2.4.14). This should be expected, since such a case corresponds to the degeneration of a two-humped one-particle distribution function into a distribution function symmetric with respect to $p = 0$ distribution function of Gaussian type, with parameters coinciding with those in (2.4.12), (2.4.13).

Summary and Outlook

Thus, in this chapter we present a microscopic approach to the construction of a kinetic theory of many-particle systems with dissipative and potential interactions in the presence of active fluctuations. The approach is based on a generalization of the Bogolyubov-Peletminskii reduced description method for systems of many active particles. It is shown that within the framework of the developed microscopic approach, it is possible to construct a kinetic theory of active particles both in the case of two-dimensional and three-dimensional systems, the presence of nonlinear friction (dissipative interaction), as well as the local nature of the action of an external random field with active correlations. General kinetic equations are obtained for such systems in the case of weak interactions between particles (both potential and dissipative) and a low intensity of active correlations. Some special cases are determined in which the kinetic equations we derived have solutions that coincide with the results known for systems of active particles from earlier works of other authors. It was also shown that one of the consequences of the local nature of active fluctuations is the manifestation of self-propelling properties, characteristic of systems of active particles, even in the case of linear friction (see 2.4.23) - (2.4.33)).

Let us recall in this connection that formulas (2.4.23) - (2.4.33) describe only two particular limiting cases of the existence of two-dimensional and three-dimensional systems with self-propelled particles. Outwardly, the form of the obtained expressions coincides with the form of similar expressions, see, for example, Refs. [33, 34]. However, in this chapter, the nature of the self-propelling phenomenon is associated with the local (individual) effect on

particles of an external stochastic field with active correlations, see (2.1.9). In addition, the parameters of such a self-propelled motion are self-consistently expressed through the internal characteristics of a many-particle system - the density of the number of particles in the system, the parameters of the dissipative function, and the characteristics of the external action - pair correlation functions of a stochastic field with active fluctuations. Note that the stationary direction of self-propelling within the framework of a spatially homogeneous model (see (2.4.7), (2.4.8)) cannot be determined. To define it, an interaction must be introduced into the theory, albeit arbitrarily small, but violating the spatial homogeneity of the problem. In this sense, the situation expressed in formulas (2.4.19) - (2.4.28) resembles the situation with a phase transition to magnetic ordering in ferromagnets, see, for example, Ref. [83]. As is known, the value of the total magnetic moment in a ferromagnet in the leading approximation is determined by the isotropic exchange interaction. The direction of the magnetization is specified in this case by anisotropic weak relativistic interactions.

In this regard, we note that the general kinetic equations (2.3.6) contain a description of a large set of states of systems of many particles (both two-dimensional and three-dimensional) with active local fluctuations, both spatially homogeneous and inhomogeneous, including those with numerous variations nonlinear friction. However, the study of various special cases of solutions of kinetic equations (2.3.6), in our opinion, should already lie outside the scope of this work. As emphasized above, the main task of this work was precisely the development of microscopic approaches to the derivation of general kinetic equations for active particles with nonlinear friction under the influence of active fluctuations, including with a generalization to the case of three-dimensional systems.

We also note that the microscopic approach to the construction of the kinetic theory of many-particle systems with dissipative interaction and active correlations proposed in this work allows further generalization. It can be generalized, in particular, to the case of many-particle systems with dissipative interaction and the simultaneous presence of both active and passive fluctuations in the system. In this case, the non-Gaussian nature of the external stochastic action, which generates both active and passive correlations, can be taken into account..

SECTION III. THE REDUCED DESCRIPTION METHOD AND KINETICS OF A LOW-TEMPERATURE GAS OF HYDROGEN-LIKE ATOMS IN AN EXTERNAL ELECTROMAGNETIC FIELD

In the Introduction to the current work, it was noted that when describing phenomena and effects in excited gases and weakly ionized plasmas, the problem for constructing a kinetic theory of such systems comes to the fore, that is, the problem of constructing a coupled system of

kinetic equations for all possible components of the system, including radiation (photons). Such a theory should be microscopic, i.e., it should be built on the first principles of statistical physics, and take into account the possibility of an external electromagnetic field influencing the system. Let us specially emphasize the fact that in this case, in contrast to the previous chapters, we are talking about a quantum system of many particles. As is known, the description of the evolution of quantum systems has significant specificity compared to the description of the evolution of classical systems.

For this reason, in this work, the necessary microscopic approach to construction a kinetic theory of weakly excited gases or weakly ionized plasma in an external electromagnetic field is proposed to be based on the method of reduced description for relaxation processes in multiparticle quantum systems [3]. Note that such a problem in the absence of an external electromagnetic field on these systems was solved in [84]. The content of this chapter closely related to [85].

Let us start with a reminder that the method of reduced description for quantum systems is effective when the Hamiltonian of the system can be divided into two terms $\hat{\mathcal{H}}_0$ and $\hat{V}$, $\hat{\mathcal{H}} = \hat{\mathcal{H}}_0 + \hat{V}$, where $\hat{\mathcal{H}}_0$ includes the basic interactions, and $\hat{V}$ describes relatively weak interactions and may contain interaction with an external electromagnetic field [3].

3.1. Kinetic equations for a gas of bosons and fermions in the second order of perturbation theory in the weak interaction

The approaches of the reduced description method in the formulations of [3] are based on the hypothesis that if we consider the evolution of a system with a truncated or incomplete Hamiltonian $\hat{\mathcal{H}}_0$ (as already noted, this Hamiltonian includes the main interactions), then after a sufficiently long time, its statistical operator $\rho(t)$ for long enough times $t \gg \tau_0$ (where τ_0 is the so-called time of chaotization), will have some universal form. In this case, the universal expression for the statistical operator is characterized by a certain set of operators $\hat{\gamma}_a$, which are determined by the structure of the Hamiltonian $\hat{\mathcal{H}}_0$ and the properties of its symmetry [3]. The last statement can be expressed by the relation:

$$e^{-i\hat{\mathcal{H}}_0 t}\rho e^{i\hat{\mathcal{H}}_0 t} \underset{t\to\infty}{\to} \rho^{(0)}\left(e^{iat}\,\mathrm{Sp}\,\rho\hat{\gamma}_a\right), \tag{3.1.1}$$

where ρ is the initial value of the statistical operator of the system, the statistical operator $\rho^{(0)}$ is defined by the formula:

$$\rho^{(0)}(\gamma) = \exp\left\{\Omega(\gamma) - \hat{\gamma}_a Y_a(\gamma)\right\}, \tag{3.1.2}$$

in which the thermodynamic potential $\Omega(\gamma)$ and thermodynamic forces $Y_a(\gamma)$ are found from the equations

$$\mathrm{Sp}\,\rho^{(0)} = 1, \qquad \mathrm{Sp}\,\rho^{(0)}\hat{\gamma}_a = \gamma_a. \tag{3.1.3}$$

Quantities γ_a, whose operators are present in (3.1.1) - (3.1.3) are parameters of the reduced description of the system, and the equations of motion for which will be the equations of evolution of the system at times $t \gg \tau_0$. These equations must be derived from the Liouville equation for the statistical operator. Index 'a' numbers the entire set of reduced description parameters γ_a. Operators $\hat{\gamma}_a$ depend on the symmetry properties of the Hamiltonian $\hat{\mathcal{H}}_0$, which is reflected in (3.1.1), where there is a matrix $\|a\|$, determined by the structure and symmetry of the Hamiltonian $\hat{\mathcal{H}}_0$:

$$\left[\hat{\mathcal{H}}_0, \hat{\gamma}_a\right] = a_{ab}\hat{\gamma}_b. \tag{3.1.4}$$

In formulas (3.1.2), (3.1.4) by repeating indices a, b summation is implied. Note that finding the collection of operators $\hat{\gamma}_a$ for the known Hamiltonian $\hat{\mathcal{H}}_0$ can be challenging enough. In the general formulations of the reduced description method, it is considered solved, and the main attention is paid to the procedure for deriving the evolution equations for these parameters of the reduced description.

It was shown in [3] that for quantum gases with the Hamiltonian

$$\hat{\mathcal{H}} = \hat{\mathcal{H}}_0 + \hat{V}, \tag{3.1.5}$$

where the operators $\hat{\mathcal{H}}_0$ and $\hat{V}$ are defined by expressions

$$\hat{\mathcal{H}}_0 = \sum_i \varepsilon_i \hat{a}_i^+ \hat{a}_i, \qquad \hat{V} = \frac{1}{4\mathcal{V}} \sum_{i_1 i_2 i_3 i_4} \Phi(i_1 i_2; i_3 i_4) \hat{a}_{i_1}^+ \hat{a}_{i_2}^+ \hat{a}_{i_3} \hat{a}_{i_4}, \tag{3.1.6}$$

as reduced description parameters γ_a, mentioned above, the single-particle density matrix $f_{i,i'}$, to which the following operators correspond:

$$\hat{f}_{i,i'} = \hat{a}_{i'}^+ \hat{a}_i, \tag{3.1.7}$$

where $\hat{a}_i^+$, $\hat{a}_i$ are the creation and annihilation operators of particles, respectively, and the index i numbers the set of quantum numbers characterizing the state of the particle (for example, the momentum $\mathbf{p}$, spin projection s). Note also that the quantity ε_i in Eq. (3.1.6) represents the energy of a free particle (or quasiparticle), $\Phi\left(i_1 i_2; i_3 i_4\right)$ characterizes the interaction between the structural units of the system and the letter $\mathcal{V}$ the denominator of the second of formulas (3.1.6) denotes the volume of the system.

For the one-particle density matrix $f_{i,i'}$ as a parameter of the reduced description in [3], the evolution equations were obtained in the second order of the perturbation theory in the weak interaction $\hat{V}$ (see Eqs. (3.1.5), (3.1.6)):

$$\dot{f}_{i,i'} = \mathcal{L}_{i,i'}^{(0)}(f) + L_{i,i'}^{(1)}(f) + L_{i,i'}^{(2)}(f), \tag{3.1.8}$$

$$\mathcal{L}_{i,i'}^{(0)}(f) = i\,\mathrm{Sp}\,\rho^{(0)}(f)\left[\hat{\mathcal{H}}_0, \hat{a}_{i'}^+ \hat{a}_i\right], \qquad L_{i,i'}^{(1)}(f) = i\,\mathrm{Sp}\,\rho^{(0)}(f)\left[\hat{V}, \hat{a}_{i'}^+ \hat{a}_i\right],$$

$$L_{i,i'}^{(2)}(f) = -i\int_{-\infty}^{0} d\tau e^{\eta\tau}\,\mathrm{Sp}\,\rho^{(0)}(f)\left[\hat{V}(\tau), \left[\hat{V}, \hat{a}_{i'}^+ \hat{a}_i\right] + i\sum_{i_1 i_1'} \hat{a}_{i_1'}^+ \hat{a}_{i_1} \frac{\partial L_a^{(1)}(\gamma)}{\partial f_{i_1,i_1'}}\right],$$

$$\hat{V}(\tau) \equiv e^{i\hat{\mathcal{H}}_0\tau} \hat{V} e^{-i\hat{\mathcal{H}}_0\tau},$$

and the statistical operator $\rho^{(0)}(f)$ is given by the expression:

$$\rho^{(0)}(f) = \exp\left\{\Omega(f) - \sum_{ii'} Y_{i,i'}(f)\,\hat{a}_{i'}^+ \hat{a}_i\right\}, \tag{3.1.9}$$

where $\Omega(f)$ and $Y_{i,i'}(f)$ as functionals of the one-particle density matrix in accordance with (3.1.3) should be found from the equations:

$$\mathrm{Sp}\,\rho^{(0)}(f) = 1, \quad \mathrm{Sp}\,\rho^{(0)}(f)\,\hat{a}_{i'}^+ \hat{a}_i = f_{i,i'}. \tag{3.1.10}$$

After calculating the commutators and traces in (3.1.8) taking into account formulas (3.1.5) - (3.1.7), these equations can be reduced to a closed form [3]:

$$\frac{\partial f}{\partial t} + i\left[\varepsilon, f\right] = L(f), \tag{3.1.11}$$

where matrix $\varepsilon_{i,i'}$ is defined by the formula:

$$\varepsilon_{i,i'} = \varepsilon_i \delta_{i,i'} + \frac{1}{\mathcal{V}} \sum_{i_1 i_1'} \Phi\left(i i_1; i_1' i'\right) f_{i_1',i_1}, \tag{3.1.12}$$

and the collision integral $L(f)$ for bosons is given by:

$$L_{ii'}(f)=\sum_{i_1i_2i_3i_4}\sum_{i_1'i_2'i_3'i_4'}\Phi(i_1i_2;i_3i_4)\Phi(i_1'i_2';i_3'i_4')\delta_-\left(\varepsilon_{i_1'}+\varepsilon_{i_2'}-\varepsilon_{i_3'}-\varepsilon_{i_4'}\right)\times \tag{3.1.13}$$

$$\times\left\{f_{i_4',i_2}f_{i_3',i_1}\left(\delta_{i_3,i_1'}+f_{i_3,i_1'}\right)\left(\delta_{i,i_2'}+f_{i,i_2'}\right)-f_{i_3,i_1'}f_{i,i_2'}\left(\delta_{i_1,i_3'}+f_{i_3',i_1'}\right)\left(\delta_{i_4',i_2}+f_{i_4',i_2}\right)\right\}\delta_{i_4i'}+h.c.,$$

where

$$\delta_-(x)\equiv\frac{1}{\pi}\lim_{\eta\to0}\int_{-\infty}^{0}d\tau e^{i\tau x+\eta\tau}\ . \tag{3.1.14}$$

For the case of fermions, in the lower line of expression (3.1.13) inside the parentheses, the plus sign must be replaced with a minus sign. It should also be noted that the left-hand side of equation (3.1.11) includes the quantity $\varepsilon_{i,i'}$ (see (3.1.12)) containing corrections to the energy of a free particle ε_i, related to interaction and single-particle density matrix $f_{i,i'}$ (distribution function, see below). For this reason, the value $\varepsilon_{i,i'}$ takes into account the mean field effects. Thus, equation (3.1.11), taking into account the self-consistent field (3.1.12) and the collision integral (3.1.13), (3.1.14), is, in fact, the kinetic equation for the system characterized by Hamiltonians (3.1.5), (3.1.6).

To illustrate this more clearly, one should go, as is done in [3], in the equations (3.1.11) - (3.1.13) to the momentum representation, i.e., the values characterized by a set of indices i must be considered a set of momenta $\mathbf{p}$ with the corresponding numbering. In this case, it is convenient instead of the one-particle density matrix $f_{\mathbf{p},\mathbf{p}'}\equiv\mathrm{Sp}\,\rho^{(0)}(f)\hat{a}^+_{\mathbf{p}'}\hat{a}_{\mathbf{p}}$ (see (3.1.7), (3.1.10)) introduce into consideration the Wigner distribution function $f(\mathbf{x},\mathbf{p})$:

$$f(\mathbf{x},\mathbf{p})\equiv\sum_{\mathbf{k}}e^{-i\mathbf{k}\mathbf{x}}f_{\mathbf{p}-\frac{\mathbf{k}}{2},\mathbf{p}+\frac{\mathbf{k}}{2}}=\frac{\mathcal{V}}{(2\pi)^3}\int d^3k e^{-i\mathbf{k}\mathbf{x}}f_{\mathbf{p}-\frac{\mathbf{k}}{2},\mathbf{p}+\frac{\mathbf{k}}{2}}\ . \tag{3.1.15}$$

It should be noted that in the spatially homogeneous case the quantity $f_{\mathbf{p}-\frac{\mathbf{k}}{2},\mathbf{p}+\frac{\mathbf{k}}{2}}$ is equal to $f_{\mathbf{p}}\delta_{\mathbf{k},0}$. Consequently, $f_{\mathbf{p}-\frac{\mathbf{k}}{2},\mathbf{p}+\frac{\mathbf{k}}{2}}$ should have a sharp maximum at $\mathbf{k}=0$. Based on equations (3.1.11) - (3.1.14), in perturbation theory with small spatial gradients, we obtain the following evolution equation for the Wigner distribution function $f(\mathbf{x},\mathbf{p})$ (kinetic equation) [3]:

$$\frac{\partial f(\mathbf{x},\mathbf{p})}{\partial t}+\frac{\partial\varepsilon(\mathbf{x},\mathbf{p})}{\partial\mathbf{p}}\frac{\partial f(\mathbf{x},\mathbf{p})}{\partial\mathbf{x}}-\frac{\partial\varepsilon(\mathbf{x},\mathbf{p})}{\partial\mathbf{x}}\frac{\partial f(\mathbf{x},\mathbf{p})}{\partial\mathbf{p}}=L(\mathbf{p};f), \tag{3.1.16}$$

where the particle energy $\varepsilon(\mathbf{x},\mathbf{p})$ (or quasiparticle, see [3]) and the collision integral $L(\mathbf{p};f)$ are defined by expressions:

$$\varepsilon(\mathbf{x},\mathbf{p}) \equiv \sum_{\mathbf{k}} e^{-i\mathbf{k}\mathbf{x}} \varepsilon_{\mathbf{p}-\frac{\mathbf{k}}{2},\mathbf{p}+\frac{\mathbf{k}}{2}} = \frac{\mathcal{V}}{(2\pi)^3}\int d^3k e^{-i\mathbf{k}\mathbf{x}} \varepsilon_{\mathbf{p}-\frac{\mathbf{k}}{2},\mathbf{p}+\frac{\mathbf{k}}{2}}, \tag{3.1.17}$$

$$L(\mathbf{p};f) \equiv \frac{\pi}{\mathcal{V}^2}\sum_{\mathbf{p}_1\mathbf{p}_2\mathbf{p}_3\mathbf{p}_4} \left|\Phi(\mathbf{p}_1\mathbf{p}_2;\mathbf{p}_3\mathbf{p}_4)\right|^2 \delta\left(\varepsilon(\mathbf{p}_1)+\varepsilon(\mathbf{p}_2)-\varepsilon(\mathbf{p}_3)-\varepsilon(\mathbf{p}_4)\right)\times$$

$$\times\delta_{\mathbf{p}_4,\mathbf{p}}\left\{f(\mathbf{p}_1)f(\mathbf{p}_2)\left[1+f(\mathbf{p}_3)\right]\left[1+f(\mathbf{p}_4)\right]-f(\mathbf{p}_3)f(\mathbf{p}_4)\left[1+f(\mathbf{p}_1)\right]\left[1+f(\mathbf{p}_2)\right]\right\}$$

in which $\varepsilon(\mathbf{p})$ is the energy of a free particle (or quasiparticle). Note that a similar expression for the collision integral $L(\mathbf{p};f)$ in Eq. (3.1.17) is also true for fermions if the plus sign in square brackets is replaced by a minus sign. It can be seen that the kinematic part of equation (3.1.16) looks the same as the kinematic part of the classical kinetic equation, if under the energy $\varepsilon(\mathbf{x},\mathbf{p})$ one understands the Hamiltonian of a particle $\varepsilon_{\mathbf{p}}$. The collision integral in (3.1.17) differs significantly from that in the classical case, since it reflects the influence of statistics, which the particles obey.

In the next section, the above procedure will be applied to construct a kinetic theory of weakly ionized gases of hydrogen-like atoms in an external electromagnetic field. As noted above, the construction of such a kinetic theory must begin with the concrete definition of the explicit form of the Hamiltonian of the system under study.

3.2. Hamiltonian of a low-temperature gas of hydrogen-like atoms in an external electromagnetic field

The problem of constructing the Hamiltonian of a weakly ionized plasma in an external electromagnetic field has essentially been solved. In [53], an approximate second quantization method was developed to describe many-particle systems in the presence of bound states of particles. For this, the simplest model was considered - a system composed of three different gas components: subsystems of two different oppositely charged fermions and their bound states. In [84], these Hamiltonians were used to construct a kinetic theory of weakly ionized rarefied gases of hydrogen-like atoms from the first principles of quantum statistics in the absence of an external electromagnetic field. It was also explained there that the developed method of second quantization is most correctly applied in the case of low temperatures. The reason is that the formulations of Ref. [53] are valid when the average kinetic energy of the particles in the system is small compared to the energies of bound states (atoms). In systems close to equilibrium, this condition is provided

precisely by low temperatures. It should be noted in passing that the formulations of the secondary quantization method proposed in [53] were successfully applied in [86] to describe the states of low-temperature gases of Fermi atoms of two different types in thermodynamic equilibrium with a gas of heteronuclear molecules formed by these fermions. Such circumstances make it possible to use the Hamiltonians [53] for solving the problems of the present work.

The result of the construction in [53] of an approximate (new at that time) formulation of the second quantization method in the presence of bound states is as follows. A low-temperature weakly excited and weakly ionized gas of hydrogen-like atoms in an external electromagnetic field is, first of all, a many-particle multicomponent system, the subsystems of which are oppositely charged free fermions (electrons and positively charged cores), as well as bound states of these fermions - neutral hydrogen-like atoms (bosons), which can be in excited states. Creation and annihilation operators of fermions of the first and second kind in the momentum representation

$$\hat{a}_l(\mathbf{p}), \quad \hat{a}_l^+(\mathbf{p}), \quad l = 1, 2, \tag{3.2.1}$$

satisfy the usual (Fermi) commutation relations

$$\left\{\hat{a}_l(\mathbf{p}), \hat{a}_{l'}^+(\mathbf{p}')\right\} \equiv \hat{a}_l(\mathbf{p})\hat{a}_{l'}^+(\mathbf{p}') + \hat{a}_{l'}^+(\mathbf{p}')\hat{a}_l(\mathbf{p}) = \Delta(\mathbf{p}-\mathbf{p}')\Delta(l-l'), \tag{3.2.2}$$

$$\left\{\hat{a}_l(\mathbf{p}), \hat{a}_{l'}(\mathbf{p}')\right\} = 0, \qquad \left\{\hat{a}_l^+(\mathbf{p}), \hat{a}_{l'}^+(\mathbf{p}')\right\} = 0,$$

where the quantities $\Delta(\mathbf{p}-\mathbf{p}')$ and $\Delta(l-l')$ represent the Kronecker symbols. For definiteness, in what follows we will assume that the index $l = 1$ corresponds to the electron subsystem, and $l = 2$ to the core. Note that, to simplify the calculations, Ref. [53] did not take into account the presence of spin variables as individual quantum characteristics of the particles that make up the subsystem. It will not be taken into account in this work for the same reason.

For bound states (hydrogen-like atoms) with mass $M = m_1 + m_2$ in the low-energy region, it is possible to introduce into consideration the creation $\hat{\eta}_\alpha^+(\mathbf{p})$ and annihilation $\hat{\eta}_\alpha(\mathbf{p})$ operators, which also satisfy the usual Bose commutation relations:

$$\left[\hat{\eta}_\alpha(\mathbf{p}), \hat{\eta}_\beta^+(\mathbf{p}')\right] \equiv \hat{\eta}_\alpha(\mathbf{p})\hat{\eta}_\beta^+(\mathbf{p}') - \hat{\eta}_\beta^+(\mathbf{p}')\hat{\eta}_\alpha(\mathbf{p}) = \Delta(\mathbf{p}-\mathbf{p}')\Delta(\alpha-\beta), \tag{3.2.3}$$

where the index 'α' (or 'β') denotes a set of quantum numbers characterizing the quantum mechanical state of a hydrogen-like atom.

In addition, it was assumed that the system could be influenced by an external electromagnetic field characterized by a scalar $\varphi^{(e)}(\mathbf{x},t)$ and vector $\mathbf{A}^{(e)}(\mathbf{x},t)$ potentials. The presence in the system of photons with the dispersion law was also taken into account $\omega(k)$ (ω is frequency, $\mathbf{k}$ is wave vector), by creation operators $\hat{C}_\lambda^+(\mathbf{k})$ of a photon with wave vector $\mathbf{k}$ and polarization $\lambda = 1,2$ and annihilation operators $\hat{C}_\lambda(\mathbf{k})$,

$$\omega(k) = ck, \qquad \left[\hat{C}_\lambda(\mathbf{k}), \hat{C}_{\lambda'}^+(\mathbf{k}')\right] = \Delta(\mathbf{k}-\mathbf{k}'). \tag{3.2.4}$$

In terms of the introduced particle creation and annihilation operators (3.2.1) - (3.2.4), the Hamiltonian of a low-temperature hydrogen-like plasma in accordance with [53] can be represented in the form:

$$\hat{\mathcal{H}} = \hat{\mathcal{H}}_0 + \hat{W}(t) + \hat{V}, \tag{3.2.5}$$

where $\hat{\mathcal{H}}_0$ is free particles Hamiltonian:

$$\hat{\mathcal{H}}_0 = \sum_{l=1}^{2}\sum_{\mathbf{p}} \varepsilon_l(\mathbf{p})\hat{a}_l^+(\mathbf{p})\hat{a}_l(\mathbf{p}) + \sum_{\alpha}\sum_{\mathbf{p}} \varepsilon_\alpha(\mathbf{p})\hat{\eta}_\alpha^+(\mathbf{p})\hat{\eta}_\alpha(\mathbf{p}) + \sum_{\lambda,\mathbf{k}} \omega(\mathbf{k})\hat{C}_\lambda^+(\mathbf{k})\hat{C}_\lambda(\mathbf{k}), \tag{3.2.6}$$

$$\varepsilon_l(\mathbf{p}) = \frac{\mathbf{p}^2}{2m_l}, \quad l \equiv \{1,2\}, \qquad \varepsilon_\alpha(\mathbf{p}) = \varepsilon_\alpha + \frac{\mathbf{p}^2}{2M}, \qquad M = m_1 + m_2,$$

and the value $\varepsilon_\alpha < 0$ is the energy of a bound state (hydrogen-like atom) in a state with a set of quantum numbers α. In (23) and further calculations, as is usually done, we formally set the Planck constant $\hbar$ equal to one, $\hbar \equiv 1$; if necessary, the dependence of the results on $\hbar$ may be easily restored. By repeated indexes 'α' in (3.2.6) and below, where it is not specifically stated otherwise, the summation is assumed.

Interaction Hamiltonian $\hat{W}(t)$ of a particle system with an electromagnetic field can be written as:

$$\hat{W}(t) = -\frac{1}{c}\int d\mathbf{x}\hat{\mathbf{A}}(\mathbf{x},t)\hat{\mathbf{j}}(\mathbf{x}) + \frac{1}{2c^2}\int d\mathbf{x}\hat{\mathbf{A}}^2(\mathbf{x},t)\hat{I}(\mathbf{x}) + \int d\mathbf{x}\varphi^{(e)}(\mathbf{x},t)\hat{\sigma}(\mathbf{x}), \tag{3.2.7}$$

where operator $\hat{\mathbf{A}}(\mathbf{x},t)$,

$$\hat{\mathbf{A}}(\mathbf{x},t) \equiv \mathbf{A}^{(e)}(\mathbf{x},t) + \hat{\mathbf{a}}(\mathbf{x}) \tag{3.2.8}$$

is a superposition of the vector potential of the external electromagnetic field $\mathbf{A}^{(e)}(\mathbf{x},t)$ and vector potential $\hat{\mathbf{a}}(\mathbf{x})$ of the radiation field, which in terms of the photon creation and annihilation operators has the form (see, for example, [3]):

$$\hat{\mathbf{a}}(\mathbf{x})=\left(\frac{2\pi}{\mathcal{V}}\right)^{1/2} c\sum_{\mathbf{k}}\sum_{\lambda=1}^{2}\omega^{-1/2}(k)\mathbf{e}_{\lambda}(\mathbf{k})\left\{\hat{C}_{\lambda}^{+}(\mathbf{k})e^{-i\mathbf{kx}}+\hat{C}_{\lambda}(\mathbf{k})e^{i\mathbf{kx}}\right\} \qquad (3.2.9)$$

($\mathbf{e}_{\lambda}(\mathbf{k})$ is the polarization vector of the photon in the state $\mathbf{k}$ and $\lambda=1,2$). Note that the Coulomb gauge was chosen for the radiation field.

Current density operator $\hat{\mathbf{j}}(\mathbf{x})$ in (3.2.7) is defined by the formulas:

$$\hat{\mathbf{j}}(\mathbf{x})=\sum_{a=0}^{2}\hat{\mathbf{j}}_{a}(\mathbf{x}),\quad a=\{0,l\}, \qquad (3.2.10)$$

$$\hat{\mathbf{j}}_{l}(\mathbf{x})=-\frac{ie_{l}}{2m_{l}\mathcal{V}}\sum_{\mathbf{p},\mathbf{p}'}e^{i\mathbf{x}(\mathbf{p}-\mathbf{p}')}(\mathbf{p}+\mathbf{p}')\hat{a}_{l}^{+}(\mathbf{p})\hat{a}_{l}(\mathbf{p}'),\quad e_{1}=-e_{2}=e,$$

$$\hat{\mathbf{j}}_{0}(\mathbf{x})=\frac{1}{\mathcal{V}}\sum_{\mathbf{p},\mathbf{p}'}\sum_{\alpha,\beta}e^{i\mathbf{x}(\mathbf{p}'-\mathbf{p})}\left[\frac{(\mathbf{p}+\mathbf{p}')}{2M}\sigma_{\alpha\beta}(\mathbf{p}-\mathbf{p}')+\mathbf{j}_{\alpha\beta}(\mathbf{p}-\mathbf{p}')\right]\hat{\eta}_{\alpha}^{+}(\mathbf{p})\hat{\eta}_{\beta}(\mathbf{p}'),$$

where $\mathcal{V}$ is the system volume, e is the elementary charge, m_1 and m_2 are the masses of an electron and a core, respectively, and the values $\sigma_{\alpha\beta}(\mathbf{k})$ and $\mathbf{j}_{\alpha\beta}(\mathbf{k})$ are given by the following expressions:

$$\sigma_{\alpha\beta}(\mathbf{k})\equiv e\int d\mathbf{y}\,\varphi_{\alpha}^{*}(\mathbf{y})\varphi_{\beta}(\mathbf{y})\left[\exp\left(-i\frac{m_1}{M}\mathbf{ky}\right)-\exp\left(i\frac{m_2}{M}\mathbf{ky}\right)\right],$$

$$M\equiv m_1+m_2, \qquad (3.2.11)$$

$$\mathbf{j}_{\alpha\beta}(\mathbf{k})\equiv e\frac{i}{2}\int d\mathbf{y}\left(\varphi_{\alpha}^{*}(\mathbf{y})\frac{\partial\varphi_{\beta}(\mathbf{y})}{\partial\mathbf{y}}-\frac{\partial\varphi_{\alpha}^{*}(\mathbf{y})}{\partial\mathbf{y}}\varphi_{\beta}(\mathbf{y})\right)\left[\frac{1}{m_1}\exp\left(i\frac{m_2}{M}\mathbf{ky}\right)+\frac{1}{m_2}\exp\left(-i\frac{m_1}{M}\mathbf{ky}\right)\right],$$

where M is the atom's mass and is the wave function of a hydrogen-like atom in the state α, which is assumed to be known.

Quantity $\hat{\sigma}(\mathbf{x})$, in (3.2.7) is the operator of the charge density of the system:

$$\hat{\sigma}(\mathbf{x})=\sum_{a=0}^{2}\hat{\sigma}_{a}(\mathbf{x}), \qquad (3.2.12)$$

while,

$$\hat{\sigma}_l(\mathbf{x}) = \frac{e_l}{\mathcal{V}} \sum_{\mathbf{p},\mathbf{p}'} e^{i\mathbf{x}(\mathbf{p}'-\mathbf{p})} \hat{a}_l^+(\mathbf{p}) \hat{a}_l(\mathbf{p}'),$$

$$\hat{\sigma}_0(\mathbf{x}) = \frac{1}{\mathcal{V}} \sum_{\mathbf{p},\mathbf{p}'} \sum_{\alpha,\beta} e^{i\mathbf{x}(\mathbf{p}'-\mathbf{p})} \sigma_{\alpha\beta}(\mathbf{p}-\mathbf{p}') \hat{\eta}_\alpha^+(\mathbf{p}) \hat{\eta}_\beta(\mathbf{p}'). \qquad (3.2.13)$$

Finally, operator $\hat{I}(\mathbf{x})$, contained in (24), according to [31] can be written in the form

$$\hat{I}(\mathbf{x}) = \sum_{a=0}^{2} \hat{I}_a(\mathbf{x}), \qquad (3.2.14)$$

where

$$\hat{I}_l(\mathbf{x}) \equiv \frac{e^2}{\mathcal{V} m_l} \sum_{\mathbf{p},\mathbf{p}'} e^{i\mathbf{x}(\mathbf{p}'-\mathbf{p})} \hat{a}_l^+(\mathbf{p}) \hat{a}_l(\mathbf{p}'),$$

$$\hat{I}_0(\mathbf{x}) \equiv \frac{1}{\mathcal{V}} \sum_{\mathbf{p},\mathbf{p}'} \sum_{\alpha,\beta} e^{i\mathbf{x}(\mathbf{p}'-\mathbf{p})} I_{\alpha\beta}(\mathbf{p}-\mathbf{p}') \hat{\eta}_\alpha^+(\mathbf{p}) \hat{\eta}_\beta(\mathbf{p}'), \qquad (3.2.15)$$

and tensor $I_{\alpha\beta}(\mathbf{k})$ is defined by the formula:

$$I_{\alpha\beta}(\mathbf{k}) \equiv e^2 \int d\mathbf{y} \varphi_\alpha^*(\mathbf{y}) \varphi_\beta(\mathbf{y}) \left[\frac{1}{m_1} \exp\left(i \frac{m_2}{M} \mathbf{k}\mathbf{y} \right) + \frac{1}{m_2} \exp\left(-i \frac{m_1}{M} \mathbf{k}\mathbf{y} \right) \right]. \qquad (3.2.16)$$

Thus, expressions (3.2.7) - (3.2.16) completely determine the Hamiltonian of the interaction of a hydrogen-like low-temperature plasma with an electromagnetic field.

Note that under the assumption of a weak external electromagnetic field and in the leading approximation in terms of the fine structure constant $e^2/\hbar c$ Hamiltonian $\hat{W}(t)$ of interaction of an electromagnetic field with matter is reduced to a simple sum of Hamiltonians $\hat{W}_{ext}(t)$ and $\hat{W}_{int}(t)$:

$$\hat{W}(t) = \hat{W}_{ext}(t) + \hat{W}_{int}, \qquad (3.3.17)$$

in which the Hamiltonian of the interaction of matter with an external electromagnetic field $\hat{W}_{ext}(t)$ is defined by formulas:

$$\hat{W}_{ext}(t) = \hat{W}_{ext}^{(1)}(t) + \hat{W}_{ext}^{(2)}(t) + \hat{W}_{ext}^{(0)}(t), \qquad (3.2.18)$$

$$\hat{W}_{ext}^{(1)}(t) = \frac{e}{\mathcal{V}} \sum_{\mathbf{p}_1\mathbf{p}_2} \left\{ \frac{i}{2m_1 c} \mathbf{A}^{(e)}(\mathbf{p}_1 - \mathbf{p}_2, t)(\mathbf{p}_1 + \mathbf{p}_2) + \varphi^{(e)}(\mathbf{p}_1 - \mathbf{p}_2, t) \right\} \hat{a}_1^+(\mathbf{p}_1) \hat{a}_1(\mathbf{p}_2),$$

$$\hat{W}_{ext}^{(2)}(t)=\frac{e}{\mathcal{V}}\sum_{\mathbf{p}_1\mathbf{p}_2}\left\{\frac{i}{2m_2c}\mathbf{A}^{(e)}(\mathbf{p}_1-\mathbf{p}_2,t)(\mathbf{p}_1+\mathbf{p}_2)+\varphi^{(e)}(\mathbf{p}_1-\mathbf{p}_2,t)\right\}\hat{a}_2^{+}(\mathbf{p}_1)\hat{a}_2(\mathbf{p}_2)$$

$$\hat{W}_{ext}^{(0)}(t)=-\frac{1}{\mathcal{V}c}\sum_{\alpha,\beta}\sum_{\mathbf{p}_1\mathbf{p}_2}\mathbf{A}^{(e)}(\mathbf{p}_1-\mathbf{p}_2,t)\left[\frac{(\mathbf{p}_1+\mathbf{p}_2)}{2M}\sigma_{\alpha\beta}(\mathbf{p}_1-\mathbf{p}_2)+\right.$$

$$\left.+\mathbf{j}_{\alpha\beta}(\mathbf{p}_1-\mathbf{p}_2)\right]\hat{\eta}_\alpha^{+}(\mathbf{p}_1)\hat{\eta}_\beta(\mathbf{p}_2)+$$

$$+\frac{1}{\mathcal{V}}\sum_{\mathbf{p}_1,\mathbf{p}_2}\sum_{\alpha,\beta}\varphi^{(e)}(\mathbf{p}_1-\mathbf{p}_2,t)\sigma_{\alpha\beta}(\mathbf{p}_1-\mathbf{p}_2)\hat{\eta}_\alpha^{+}(\mathbf{p}_1)\hat{\eta}_\beta(\mathbf{p}_2),$$

in which the functions $\mathbf{A}^{(e)}(\mathbf{p},t)$, $\varphi^{(e)}(\mathbf{p},t)$ are Fourier - images of potentials $\mathbf{A}^{(e)}(\mathbf{x},t)$ and $\varphi^{(e)}(\mathbf{x},t)$ of external electromagnetic field:

$$\mathbf{A}^{(e)}(\mathbf{p},t)=\int d\mathbf{x}e^{-i\mathbf{p}\mathbf{x}}\mathbf{A}^{(e)}(\mathbf{x},t),\ \varphi^{(e)}(\mathbf{p},t)=\int d\mathbf{x}e^{-i\mathbf{p}\mathbf{x}}\varphi^{(e)}(\mathbf{x},t). \qquad (3.2.19)$$

The Hamiltonian of the interaction of matter with radiation is given by the expressions:

$$\hat{W}_{\text{int}}=\hat{W}_{int}^{(1)}+\hat{W}_{\text{int}}^{(2)}+\hat{W}_{int}^{(0)}, \qquad (3.2.20)$$

$$\hat{W}_{int}^{(0)}\equiv-\sum_{\lambda=1}^{2}\sum_{\mathbf{k},\mathbf{p}}\mathbf{e}_\lambda(\mathbf{k})\left(\frac{2\pi}{\mathcal{V}\omega_{\mathbf{k}}}\right)^{1/2}\sum_{\alpha,\beta}\left[\frac{(2\mathbf{p}-\mathbf{k})}{2M}\sigma_{\alpha\beta}(-\mathbf{k})+\mathbf{j}_{\alpha\beta}(-\mathbf{k})\right]\hat{\eta}_{\alpha\mathbf{p}}^{+}\hat{\eta}_{\beta\mathbf{p}-\mathbf{k}}\hat{C}_{\mathbf{k}\lambda}-$$

$$-\sum_{\lambda=1}^{2}\sum_{\mathbf{k},\mathbf{p}}\mathbf{e}_\lambda(\mathbf{k})\left(\frac{2\pi}{\mathcal{V}\omega_{\mathbf{k}}}\right)^{1/2}\sum_{\alpha,\beta}\left[\frac{(2\mathbf{p}+\mathbf{k})}{2M}\sigma_{\alpha\beta}(\mathbf{k})+\mathbf{j}_{\alpha\beta}(\mathbf{k})\right]\hat{\eta}_{\alpha\mathbf{p}}^{+}\hat{\eta}_{\beta\mathbf{p}+\mathbf{k}}\hat{C}_{\mathbf{k}\lambda}^{+},$$

$$\hat{W}_{int}^{(1)}=\frac{e}{2m_1}\sum_{\mathbf{p},\mathbf{p}',\mathbf{k}}\sum_{\lambda=1}^{2}\left(\frac{2\pi}{\mathcal{V}\omega_{\mathbf{k}}}\right)^{1/2}\mathbf{e}_\lambda(\mathbf{k})(\mathbf{p}'+\mathbf{p})\hat{a}_1^{+}(\mathbf{p})\hat{a}_1(\mathbf{p}')\left(\Delta(\mathbf{p}'-\mathbf{p}+\mathbf{k})\hat{C}_{\mathbf{k}\lambda}+\Delta(\mathbf{p}'-\mathbf{p}-\mathbf{k})\hat{C}_{\mathbf{k}\lambda}^{+}\right)$$

$$\hat{W}_{\text{int}}^{(2)}=-\frac{e}{2m_2}\sum_{\mathbf{p},\mathbf{p}',\mathbf{k}}\sum_{\lambda=1}^{2}\left(\frac{2\pi}{\mathcal{V}\omega_{\mathbf{k}}}\right)^{1/2}\mathbf{e}_\lambda(\mathbf{k})(\mathbf{p}'+\mathbf{p})\hat{a}_2^{+}(\mathbf{p})\hat{a}_2(\mathbf{p}')\left[\Delta(\mathbf{p}'-\mathbf{p}+\mathbf{k})\hat{C}_{\mathbf{k}\lambda}+\Delta(\mathbf{p}'-\mathbf{p}-\mathbf{k})\hat{C}_{\mathbf{k}\lambda}^{+}\right]$$

.

Note that Hamiltonian (3.2.18) plays the main role in describing the processes of the system's response to an external disturbance by a weak electromagnetic field (see [50-58]). Hamiltonian (3.2.20) determines relaxation processes in the photonic subsystem. In fact, this Hamiltonian accurately takes into account the processes of emission and absorption of photons, but leaves the processes of scattering of photons by atoms outside the scope of the description. For these processes of scattering of photons by atoms are responsible for those unaccounted for in the Hamiltonians (3.2.17) - (3.2.20) (they are contained in the complete Hamiltonian (3.2.17)). However, the same contribution to the relaxation processes in the system (for example, to the collision integral) is made by the quadratic approximation in $\hat{W}_{\text{int}}$, see Ref. [3].

It remains to give an explicit form of the last term in formula (3.2.5), that is, the Hamiltonian of the interaction between particles of all components of the system $\hat{V}$, which, according to [53], can be represented in the form of three terms:

$$\hat{V} = \hat{V}^{(1)} + \hat{V}^{(2)} + \hat{V}^{(3)}, \tag{3.2.21}$$

where $\hat{V}^{(1)}$ is the Hamiltonian of the interaction of free fermions of both types with hydrogen-like atoms:

$$\hat{V}^{(1)} = \frac{e}{\mathcal{V}} \sum_{\mathbf{p}_1\mathbf{p}_2\mathbf{p}_3\mathbf{p}_4} \Phi_{\alpha\beta}(\mathbf{p}_1,\mathbf{p}_2;\mathbf{p}_3,\mathbf{p}_4)\hat{\eta}_\alpha^+(\mathbf{p}_3)\hat{\eta}_\beta(\mathbf{p}_4)\left\{a_2^+(\mathbf{p}_1)a_2(\mathbf{p}_2) - a_1^+(\mathbf{p}_1)a_1(\mathbf{p}_2)\right\}, \tag{3.2.22}$$

$$\Phi_{\alpha\beta}(\mathbf{p}_1,\mathbf{p}_2;\mathbf{p}_3,\mathbf{p}_4) \equiv \Delta(\mathbf{p}_4 - \mathbf{p}_3 - \mathbf{p}_1 + \mathbf{p}_2)\nu(\mathbf{p}_1 - \mathbf{p}_2)\sigma_{\alpha\beta}(\mathbf{p}_2 - \mathbf{p}_1).$$

Hamiltonian $\hat{V}^{(2)}$ in (3.2.21) describes the interaction between atoms in different quantum-mechanical states:

$$\hat{V}^{(2)} = \frac{1}{4\mathcal{V}} \sum_{\mathbf{p}_1\mathbf{p}_2\mathbf{p}_3\mathbf{p}_4} \Phi_{\alpha_1\alpha_2;\alpha_3\alpha_4}(\mathbf{p}_1,\mathbf{p}_2;\mathbf{p}_3,\mathbf{p}_4)\hat{\eta}_{\alpha_1}^+(\mathbf{p}_1)\hat{\eta}_{\alpha_2}^+(\mathbf{p}_2)\hat{\eta}_{\alpha_3}(\mathbf{p}_3)\hat{\eta}_{\alpha_4}(\mathbf{p}_4), \tag{3.2.23}$$

$$\Phi_{\alpha_1\alpha_2;\alpha_3\alpha_4}(\mathbf{p}_1,\mathbf{p}_2;\mathbf{p}_3,\mathbf{p}_4) \equiv \frac{1}{2\mathcal{V}}\Delta(\mathbf{p}_4 + \mathbf{p}_3 - \mathbf{p}_1 - \mathbf{p}_2)\times$$

$$\times\left\{\nu(\mathbf{p}_3 - \mathbf{p}_2)\sigma_{\alpha_1\alpha_4}(\mathbf{p}_3 - \mathbf{p}_2)\sigma_{\alpha_2\alpha_3}(\mathbf{p}_2 - \mathbf{p}_3) + \nu(\mathbf{p}_3 - \mathbf{p}_1)\sigma_{\alpha_2\alpha_4}(\mathbf{p}_3 - \mathbf{p}_1)\sigma_{\alpha_1\alpha_3}(\mathbf{p}_1 - \mathbf{p}_3) + \right.$$

$$\left. + \nu(\mathbf{p}_4 - \mathbf{p}_2)\sigma_{\alpha_1\alpha_3}(\mathbf{p}_4 - \mathbf{p}_2)\sigma_{\alpha_2\alpha_4}(\mathbf{p}_2 - \mathbf{p}_4) + \nu(\mathbf{p}_4 - \mathbf{p}_1)\sigma_{\alpha_2\alpha_3}(\mathbf{p}_4 - \mathbf{p}_1)\sigma_{\alpha_1\alpha_4}(\mathbf{p}_1 - \mathbf{p}_4)\right\},$$

and Hamiltonian $\hat{V}^{(3)}$ determines the interaction of free fermions with each other:

$$\hat{\mathcal{H}}_{\text{int}}^{(3)} = -\frac{e^2}{\mathcal{V}} \sum_{\mathbf{p}_1\mathbf{p}_2\mathbf{p}_3\mathbf{p}_4} \Phi_1^{(3)}(\mathbf{p}_1,\mathbf{p}_2;\mathbf{p}_3,\mathbf{p}_4)\hat{a}_1^+(\mathbf{p}_2)\hat{a}_1(\mathbf{p}_3)\hat{a}_2^+(\mathbf{p}_1)\hat{a}_2(\mathbf{p}_4) + \tag{3.2.24}$$

$$+\frac{1}{4} \sum_{\mathbf{p}_1\mathbf{p}_2\mathbf{p}_3\mathbf{p}_4} \Phi_2^{(3)}(\mathbf{p}_1,\mathbf{p}_2;\mathbf{p}_3,\mathbf{p}_4)\left[\hat{a}_{1\mathbf{p}_1}^+\hat{a}_{1\mathbf{p}_2}^+\hat{a}_{1\mathbf{p}_3}\hat{a}_{1\mathbf{p}_4} + \hat{a}_{2\mathbf{p}_1}^+\hat{a}_{2\mathbf{p}_2}^+\hat{a}_{2\mathbf{p}_3}\hat{a}_{2\mathbf{p}_4}\right],$$

$$\Phi_1^{(3)}(\mathbf{p}_1,\mathbf{p}_2;\mathbf{p}_3,\mathbf{p}_4) \equiv \Delta(\mathbf{p}_4 - \mathbf{p}_1 + \mathbf{p}_3 - \mathbf{p}_2)\nu(\mathbf{p}_2 - \mathbf{p}_3)$$

$$\Phi_2^{(3)}(\mathbf{p}_1,\mathbf{p}_2;\mathbf{p}_3,\mathbf{p}_4) \equiv \frac{e^2}{2\mathcal{V}}\Delta(\mathbf{p}_4 - \mathbf{p}_1 + \mathbf{p}_3 - \mathbf{p}_2)\times$$

$$\times\left(\nu(\mathbf{p}_2 - \mathbf{p}_3) + \nu(\mathbf{p}_1 - \mathbf{p}_4) - \nu(\mathbf{p}_1 - \mathbf{p}_3) - \nu(\mathbf{p}_2 - \mathbf{p}_4)\right).$$

The quantity $\nu(\mathbf{p})$ in formulas (3.2.22) - (3.2.24) is the Fourier transform of the Coulomb potential divided by e^2, an elementary charge squared:

$$\nu(\mathbf{p}) = \frac{4\pi}{\mathbf{p}^2}. \qquad (3.2.25)$$

Thus, expressions (3.2.2) - (3.2.25) determine all types of interactions between the components of a weakly ionized gas of hydrogen-like gases at low temperatures and the interaction of the system with an external electromagnetic field. Thus, the Hamiltonian of the system in the form (3.2.5) will be used by us in the description of the system within the framework of the method of reduced description modified for this case, with some reservations, which will be reported as necessary.

3.3. Parameters of the reduced description of a low-temperature gas of hydrogen-like atoms in an external electromagnetic field

To construct the kinetic theory of the system under study, it is necessary to slightly modify the approach outlined in Section 3.2, first of all taking into account the fact that in the case of weakly ionized gases of hydrogen-like atoms, we are talking about a multicomponent system. This description, as already mentioned, is based on the Hamiltonians of the system defined above by formulas (3.2.5) - (3.2.25) (see also [53]). Here, however, the following remark should be made. Hamiltonian (3.2.5) differs from Hamiltonian (3.1.5) by the presence of an additional term $\hat{W}(t)$, describing the interaction of system components with an external field and radiation (photons), see (3.2.5) - (3.2.20). Let's make a reservation right away that in order to simplify the calculations and more clearly present the results in further consideration in $\hat{W}(t)$ we will neglect the interaction of the components of the system with photons, that is, ignore the presence of the term $\hat{W}_{int}$, see (3.2.17), (3.2.20). Note that neglecting the term $\hat{W}_{int}$ is not necessary for any reasons of principle. Indeed, we could include among the parameters of the reduced description the one-particle photon density matrix $f_{\lambda\mathbf{k},\lambda'\mathbf{k}'}$, defining it by formulas (see (3.1.10), (3.1.15)):

$$f_{\lambda\mathbf{k},\lambda'\mathbf{k}'} \equiv \mathrm{Sp}\,\rho^{(0)}(f)\,\hat{f}_{\lambda\mathbf{k},\lambda'\mathbf{k}'}, \qquad \hat{f}_{\lambda\mathbf{k},\lambda'\mathbf{k}'} = \hat{C}^{+}_{\mathbf{k}'\lambda'}\hat{C}_{\mathbf{k}\lambda}. \qquad (3.3.1)$$

This would add the Hamiltonian $\hat{W}_{\mathrm{int}}$ (see (3.2.20)) to the number of interaction Hamiltonians (3.2.21) and as a result, following the method of [3], the kinetic equation for the Wigner photon distribution function. As it

will be easy to see below, such a procedure would greatly clutter up the calculations and the visibility of the results. Taking into account also that photons have little effect on relaxation processes in the medium, we can also neglect the term $\hat{W}_{\text{int}}$ in the Hamiltonian $\hat{W}(t)$. For the same reason, we exclude from further consideration the term $\sum_{\lambda,\mathbf{k}} \omega(\mathbf{k}) \hat{C}_{\lambda}^{+}(\mathbf{k}) \hat{C}_{\lambda}(\mathbf{k})$, which determines in (3.2.6) the kinetic energy of free photons. However, if one is interested in the processes of relaxation of photons in a medium, then it is necessary, as noted above, to write out the kinetic equation for the distribution function (3.31) of photons and to take into account the presence of the term $\sum_{\lambda,\mathbf{k}} \omega(\mathbf{k}) \hat{C}_{\lambda}^{+}(\mathbf{k}) \hat{C}_{\lambda}(\mathbf{k})$, and the Hamiltonian $\hat{W}_{\text{int}}$. It is the terms contained in $\hat{W}_{\text{int}}$ that determine the relaxation of the photonic subsystem, see in this regard Ref. [3].

As for the Hamiltonian $\hat{W}_{ext}(t)$ (see Eq. (3.2.18)) in $\hat{W}(t)$, associated with the interaction of matter with an external electromagnetic field, then its influence on the evolution of the system in the framework of the method of reduced description in certain cases can also be taken into account. In particular, in [3], the procedure for modifying the reduced description method for the case of the action on the system of an external force of weak intensity and slowly varying with time is described in detail. The essence of the modification is that in deriving the kinetic equation taking into account the effect of an external random force on the system, an additional perturbation theory with respect to the time derivatives of the field characteristics is used (along with the perturbation theory with respect to the weak interaction between particles, for example). If the goal is to obtain kinetic equations in the leading approximation in additional small parameters (time derivatives of the field characteristics), then the noted modification becomes minimal and practically obvious [3].

As applied to the system under study, this means that one-particle density matrices of the type (3.1.3), (3.1.7) for each of the components of the system can be chosen as the parameters of its reduced description. It is the entire set of such density matrices that will serve as parameters for the reduced description of the system at its kinetic stage. The evolution equations for them can be considered as a system of kinetic equations for the system (see in this connection also Ref. [84]). Taking into account the proposal made above to neglect the contribution of photons to relaxation processes in the system, we introduce into consideration the single-particle density matrices $\tilde{f}_{\mathbf{p},\mathbf{p}'}^{(1)}$, $\tilde{f}_{\mathbf{p},\mathbf{p}'}^{(2)}$ of free (unbound) fermions of the 1st and 2nd kind by the formulas, see (3.2.1) - (3.23), (3.1.9), (3.1.10), (3.3.1) (recall that we agreed above to number the physical characteristics of the electronic subsystem with the index «1», and the characteristics of the cores with the index «2»):

$$\tilde{f}^{(1)}_{\mathbf{p},\mathbf{p}'} \equiv \mathrm{Sp}\,\rho^{(0)}\left(\tilde{f}\right)\hat{f}^{(1)}_{\mathbf{p},\mathbf{p}'}, \qquad \hat{f}^{(1)}_{\mathbf{p},\mathbf{p}'} \equiv \hat{a}^{+}_{1}(\mathbf{p}')\hat{a}_{1}(\mathbf{p}), \tag{3.3.2}$$
$$\tilde{f}^{(2)}_{\mathbf{p},\mathbf{p}'} \equiv \mathrm{Sp}\,\rho^{(0)}\left(\tilde{f}\right)\hat{f}^{(2)}_{\mathbf{p},\mathbf{p}'}, \qquad \hat{f}^{(2)}_{\mathbf{p},\mathbf{p}'} \equiv \hat{a}^{+}_{2}(\mathbf{p}')\hat{a}_{2}(\mathbf{p}),$$

as well as single-particle density matrices of atoms in various quantum-mechanical states $\tilde{f}^{(0)}_{\alpha\mathbf{p},\beta\mathbf{p}'}$ (See Eq. (20)):

$$\tilde{f}^{(0)}_{\alpha\mathbf{p},\beta\mathbf{p}'} \equiv \mathrm{Sp}\,\rho^{(0)}\left(\tilde{f}\right)\hat{f}^{(0)}_{\alpha\mathbf{p},\beta\mathbf{p}'}, \qquad \hat{f}^{(0)}_{\alpha\mathbf{p},\beta\mathbf{p}'} \equiv \hat{\eta}^{+}_{\beta}(\mathbf{p}')\hat{\eta}_{\alpha}(\mathbf{p}), \quad \mathrm{Sp}\,\rho^{(0)}\left(\tilde{f}\right)=1, \tag{3.3.3}$$

where the statistical operator $\rho^{(0)}\left(\tilde{f}\right)$ in accordance with (3.1.9) should be determined by the formula:

$$\rho^{(0)}\left(\tilde{f}\right) = \exp\left\{\Omega\left(\tilde{f}\right) - \sum_{\mathbf{p}\mathbf{p}'} Y^{(1)}_{\mathbf{p}',\mathbf{p}}\left(\tilde{f}\right)\hat{f}^{(1)}_{\mathbf{p},\mathbf{p}'} - \sum_{\mathbf{p}\mathbf{p}'} Y^{(2)}_{\mathbf{p}',\mathbf{p}}\left(\tilde{f}\right)\hat{f}^{(2)}_{\mathbf{p},\mathbf{p}'} - \sum_{\mathbf{p}\mathbf{p}'} Y^{(0)}_{\beta\mathbf{p}',\alpha\mathbf{p}}\left(\tilde{f}\right)\hat{f}^{(0)}_{\alpha\mathbf{p},\beta\mathbf{p}'}\right\}, \tag{3.3.4}$$

in which the thermodynamic potential $\Omega\left(\tilde{f}\right)$ and the relationship of quantities $Y^{(1)}_{\mathbf{p}',\mathbf{p}}\left(\tilde{f}\right)$, $Y^{(2)}_{\mathbf{p}',\mathbf{p}}\left(\tilde{f}\right)$, $Y^{(0)}_{\beta\mathbf{p}',\alpha\mathbf{p}}\left(\tilde{f}\right)$ with the introduced one-particle density matrices is determined by expressions (3.3.2), (3.3.3).

Further, for each of the one-particle density matrices introduced by expressions (3.3.2), (3.3.3), one can write down the evolution equations, adhering to the technique used in [3] (see also [84], [85]) to obtain formulas (3.1.8) - (3.1.12). In this work, for the system under study, we will obtain kinetic equations with an accuracy of the first order in the weak interaction between particles, which corresponds to the approximation of the mean (or self-consistent) field. In addition, as already mentioned above, we will restrict ourselves to the main approximation in time derivatives of the field characteristics and ignore the cross-terms, that is, those that are proportional to the products of the quantities characterizing the external field by the amplitudes of the weak interaction between particles. By neglecting the second order in the interaction, we avoid the problem of constructing collision integrals, see (3.1.13), (3.1.14), (3.117). There is no fundamental need for the approximations mentioned above. As it is easy to see from (3.1.13), (3.2.21) - (3.2.25), expressions for the collision integrals can be obtained, although due to the cumbersome calculations, this problem, in our opinion, should be taken out of the scope of this work.

Taking into account the specified approximations and in accordance with formulas (3.1.8), the evolution equations for one-particle density matrices $\tilde{f}^{(1)}_{\mathbf{p},\mathbf{p}'}$, $\tilde{f}^{(2)}_{\mathbf{p},\mathbf{p}'}$ free fermions of both kinds are written in the following form (see also (3.3.2)):

$$\dot{\tilde{f}}^{(1)}_{\mathbf{p},\mathbf{p}'} = \mathcal{L}^{(1,0)}_{\mathbf{p},\mathbf{p}'}\left(\tilde{f}\right) + L^{(1,1)}_{\mathbf{p},\mathbf{p}'}\left(\tilde{f}\right), \tag{3.3.5}$$

$$\mathcal{L}^{(1,0)}_{\mathbf{p},\mathbf{p}'}\left(\tilde{f}\right) = i\,\mathrm{Sp}\,\rho^{(0)}\left(\tilde{f}\right)\left[\hat{\mathcal{H}}_0,\, \hat{f}^{(1)}_{\mathbf{p},\mathbf{p}'}\right],$$

$$L^{(1,1)}_{\mathbf{p},\mathbf{p}'}\left(\tilde{f}\right) = i\,\mathrm{Sp}\,\rho^{(0)}\left(\tilde{f}\right)\left[\hat{V} + \hat{W}_{ext}(t),\, \hat{f}^{(1)}_{\mathbf{p},\mathbf{p}'}\right];$$

$$\dot{\tilde{f}}^{(2)}_{\mathbf{p},\mathbf{p}'} = \mathcal{L}^{(2,0)}_{\mathbf{p},\mathbf{p}'}\left(\tilde{f}\right) + L^{(2,1)}_{\mathbf{p},\mathbf{p}'}\left(\tilde{f}\right),$$

$$\mathcal{L}^{(2,0)}_{\mathbf{p},\mathbf{p}'}\left(\tilde{f}\right) = i\,\mathrm{Sp}\,\rho^{(0)}\left(\tilde{f}\right)\left[\hat{\mathcal{H}}_0,\, \hat{f}^{(2)}_{\mathbf{p},\mathbf{p}'}\right],$$

$$L^{(1,1)}_{\mathbf{p},\mathbf{p}'}\left(\tilde{f}\right) = i\,\mathrm{Sp}\,\rho^{(0)}\left(\tilde{f}\right)\left[\hat{V} + \hat{W}_{ext}(t),\, \hat{f}^{(1)}_{\mathbf{p},\mathbf{p}'}\right],$$

where the Hamiltonians $\hat{\mathcal{H}}_0$, $\hat{V}$ и $\hat{W}_{ext}(t)$ are determined by expressions (3.2.18) and (3.2.21) - (3.2.25). A similar equation can be written for the one-particle density matrix of bound states of these fermions - hydrogen-like atoms in different quantum states (see (3.3.3)):

$$\dot{\tilde{f}}^{(0)}_{\alpha\mathbf{p},\beta\mathbf{p}'} = \mathcal{L}^{(0,0)}_{\alpha\mathbf{p},\beta\mathbf{p}'}\left(\tilde{f}\right) + L^{(0,1)}_{\alpha\mathbf{p},\beta\mathbf{p}'}\left(\tilde{f}\right), \tag{3.3.6}$$

$$\mathcal{L}^{(0,0)}_{\alpha\mathbf{p},\beta\mathbf{p}'}\left(\tilde{f}\right) = i\,\mathrm{Sp}\,\rho^{(0)}\left(\tilde{f}\right)\left[\hat{\mathcal{H}}_0,\, \hat{f}^{(0)}_{\alpha\mathbf{p},\beta\mathbf{p}'}\right],$$

$$L^{(0,1)}_{\alpha\mathbf{p},\beta\mathbf{p}'}\left(\tilde{f}\right) = i\,\mathrm{Sp}\,\rho^{(0)}\left(\tilde{f}\right)\left[\hat{V} + \hat{W}_{ext}(t),\, \hat{f}^{(1)}_{\mathbf{p},\mathbf{p}'}\right].$$

Introducing further the Wigner distribution functions $\tilde{f}^{(1)}(\mathbf{x},\mathbf{p})$, $\tilde{f}^{(2)}(\mathbf{x},\mathbf{p})$, $\tilde{f}^{(0)}_{\alpha_1,\alpha_2}(\mathbf{x},\mathbf{p})$, as was done in [84], [85] (see also (3.1.15)):

$$\tilde{f}^{(1)}(\mathbf{x},\mathbf{p}) \equiv \sum_{\mathbf{k}} e^{-i\mathbf{k}\mathbf{x}}\, \tilde{f}^{(1)}_{\mathbf{p}-\frac{\mathbf{k}}{2},\mathbf{p}+\frac{\mathbf{k}}{2}} = \frac{\mathcal{V}}{(2\pi)^3}\int d^3k e^{-i\mathbf{k}\mathbf{x}}\, \tilde{f}^{(1)}_{\mathbf{p}-\frac{\mathbf{k}}{2},\mathbf{p}+\frac{\mathbf{k}}{2}}, \tag{3.3.7}$$

$$\tilde{f}^{(2)}(\mathbf{x},\mathbf{p}) \equiv \sum_{\mathbf{k}} e^{-i\mathbf{k}\mathbf{x}}\, \tilde{f}^{(2)}_{\mathbf{p}-\frac{\mathbf{k}}{2},\mathbf{p}+\frac{\mathbf{k}}{2}} = \frac{\mathcal{V}}{(2\pi)^3}\int d^3k e^{-i\mathbf{k}\mathbf{x}}\, \tilde{f}^{(2)}_{\mathbf{p}-\frac{\mathbf{k}}{2},\mathbf{p}+\frac{\mathbf{k}}{2}},$$

$$\tilde{f}^{(0)}_{\alpha_1,\alpha_2}(\mathbf{x},\mathbf{p}) \equiv \sum_{\mathbf{k}} e^{-i\mathbf{k}\mathbf{x}}\, \tilde{f}^{(1)}_{\alpha_1\mathbf{p}-\frac{\mathbf{k}}{2},\alpha_2\mathbf{p}+\frac{\mathbf{k}}{2}} = \frac{\mathcal{V}}{(2\pi)^3}\int d^3k e^{-i\mathbf{k}\mathbf{x}}\, \tilde{f}^{(1)}_{\alpha_1\mathbf{p}-\frac{\mathbf{k}}{2},\alpha_2\mathbf{p}+\frac{\mathbf{k}}{2}},$$

and following the methodology [3, 84, 85], proceeding from (3.3.5), (3.3.6), one can come to kinetic equations for quantities (3.3.7), the form of which is similar to the form of equation (3.1.16), if in the latter ignore the collision integral. The most consistent procedure is described in Ref. [84]. The above procedure, however, requires a certain modification to take into account the

effect of an external electromagnetic field on the system [85]. In accordance with this, the derived system of kinetic equations will take into account the effect of an external electromagnetic field on the system, including on the subsystem of neutral hydrogen-like atoms. In the explicit form of these kinetic equations, however, there is a rather «unpleasant» circumstance associated with the method of introducing the Wigner distribution functions (3.3.7), which we will consider in the next section.

3.4. Gauge invariance conditions for a low-temperature gas of hydrogen-like atoms in an external electromagnetic field

The point is that in the mentioned kinetic equations the potentials of the external electromagnetic field $\mathbf{A}^{(e)}(\mathbf{x},t)$ и $\varphi^{(e)}(\mathbf{x},t)$ (see Eqs. (3.2.18), (3.2.19)) are not included in the form of combinations corresponding to the strengths of the electrical $\mathbf{E}^{(e)}(\mathbf{x},t)$ and the magnetic $\mathbf{H}^{(e)}(\mathbf{x},t)$ fields:

$$\mathbf{E}^{(e)}(\mathbf{x},t)=\frac{1}{c}\frac{\partial}{\partial t}\mathbf{A}^{(e)}(\mathbf{x},t)-\frac{\partial}{\partial \mathbf{x}}\varphi^{(e)}(\mathbf{x},t),$$
$$\mathbf{H}^{(e)}(\mathbf{x},t)=\mathrm{rot}\,\mathbf{A}^{(e)}(\mathbf{x},t). \qquad (3.4.1)$$

This is due to the fact that the Wigner distribution functions (3.3.7) are not gauge-invariant: indeed, in the classical limit, they determine the distribution of particles over the coordinates and projections of the generalized momentum, which are gauge-non-invariant (see in this connection [3] and also [87]). It is possible, however, to introduce gauge-invariant distribution functions, the kinetic equations for which will already contain the characteristics of the external electromagnetic field in combinations (3.4.1), that is, will already be gauge-invariant. For this purpose, we draw attention, first of all, to the fact that the gauge-non-invariant Wigner distribution functions (3.3.7) can be introduced in another, equivalent way (see also (3.3.2)):

$$\tilde{f}^{(1)}(\mathbf{x},\mathbf{p})=\int d\mathbf{y}e^{i\mathbf{y}\mathbf{p}}\tilde{f}^{(1)}\left(\mathbf{x}+\frac{1}{2}\mathbf{y},\mathbf{x}-\frac{1}{2}\mathbf{y}\right), \qquad (3.4.2)$$
$$\tilde{f}^{(2)}(\mathbf{x},\mathbf{p})=\int d\mathbf{y}e^{i\mathbf{y}\mathbf{p}}\tilde{f}^{(2)}\left(\mathbf{x}+\frac{1}{2}\mathbf{y},\mathbf{x}-\frac{1}{2}\mathbf{y}\right),$$
$$\tilde{f}^{(0)}_{\alpha_1,\alpha_2}(\mathbf{x},\mathbf{p})=\int d\mathbf{y}e^{i\mathbf{y}\mathbf{p}}\tilde{f}^{(0)}_{\alpha_1,\alpha_2}\left(\mathbf{x}+\frac{1}{2}\mathbf{y},\mathbf{x}-\frac{1}{2}\mathbf{y}\right),$$

where single-particle density matrices are determined by the expressions:

$$\tilde{f}^{(1)}(\mathbf{x}_1,\mathbf{x}_2) \equiv \mathrm{Sp}\,\rho\hat{\chi}_1^+(\mathbf{x}_2)\hat{\chi}_1(\mathbf{x}_1), \qquad (3.4.3)$$
$$\tilde{f}^{(2)}(\mathbf{x}_1,\mathbf{x}_2) \equiv \mathrm{Sp}\,\rho\hat{\chi}_2^+(\mathbf{x}_2)\hat{\chi}_2(\mathbf{x}_1),$$
$$\tilde{f}^{(0)}_{\alpha_1,\alpha_2}(\mathbf{x}_1,\mathbf{x}_2) \equiv \mathrm{Sp}\,\rho\hat{\eta}^+_{\alpha_2}(\mathbf{x}_2)\hat{\eta}_{\alpha_1}(\mathbf{x}_1).$$

In Eq. (3.4.3) field operators $\hat{\chi}_1^+(\mathbf{x}), \hat{\chi}_1(\mathbf{x}), \hat{\chi}_2^+(\mathbf{x}), \hat{\chi}_2(\mathbf{x})$ and $\hat{\eta}^+_{\alpha_2}(\mathbf{x}), \hat{\eta}_{\alpha_1}(\mathbf{x})$ are related to the creation and annihilation operators of particles of the subsystem in momentum space (3.2.1) - (3.2.3) by the formulas

$$\hat{\chi}_1^+(\mathbf{x}) = \frac{1}{\sqrt{\mathcal{V}}}\sum_{\mathbf{p}} a_1^+(\mathbf{p})e^{-i\mathbf{px}}, \qquad \hat{\chi}_1(\mathbf{x}_1) = \frac{1}{\sqrt{\mathcal{V}}}\sum_{\mathbf{p}} a_1(\mathbf{p})e^{i\mathbf{px}}, \qquad (3.4.4)$$
$$\hat{\chi}_2^+(\mathbf{x}) = \frac{1}{\sqrt{\mathcal{V}}}\sum_{\mathbf{p}} a_2^+(\mathbf{p})e^{-i\mathbf{px}}, \qquad \hat{\chi}_2(\mathbf{x}_1) = \frac{1}{\sqrt{\mathcal{V}}}\sum_{\mathbf{p}} a_2(\mathbf{p})e^{i\mathbf{px}},$$
$$\hat{\eta}_\alpha^+(\mathbf{x}) = \frac{1}{\sqrt{\mathcal{V}}}\sum_{\mathbf{p}} e^{-i\mathbf{px}}\hat{\eta}_\alpha^+(\mathbf{p}), \qquad \hat{\eta}_\alpha(\mathbf{x}) = \frac{1}{\sqrt{\mathcal{V}}}\sum_{\mathbf{p}} \hat{\eta}_\alpha(\mathbf{p})e^{i\mathbf{px}}.$$

The equations of motion for operators (3.4.4) will be gauge-invariant if these operators satisfy transformations (see [53]):

$$\hat{\chi}_1(\mathbf{x}_1) \to \hat{\chi}_1'(\mathbf{x}_1) = e^{ie_1a(\mathbf{x}_1,t)}\hat{\chi}_1(\mathbf{x}_1),$$
$$\hat{\chi}_1^+(\mathbf{x}_2) \to \hat{\chi}_1'^+(\mathbf{x}_2,t) = e^{-ie_1a(\mathbf{x}_2,t)}\hat{\chi}_1^+(\mathbf{x}_2), \qquad (3.4.5)$$
$$\hat{\chi}_2(\mathbf{x}_1) \to \hat{\chi}_2'(\mathbf{x}_1) = e^{ie_2a(\mathbf{x}_1,t)}\hat{\chi}_2(\mathbf{x}_1),$$
$$\hat{\chi}_2^+(\mathbf{x}_2) \to \hat{\chi}_2'^+(\mathbf{x}_2,t) = e^{-ie_2a(\mathbf{x}_2,t)}\hat{\chi}_2^+(\mathbf{x}_2),$$
$$\hat{\eta}_{\alpha_1}(\mathbf{X}) \to \hat{\eta}'_{\alpha_1}(\mathbf{X},t) = K_{\alpha_1\beta_1}(\mathbf{X},t)\hat{\eta}_{\beta_1}(\mathbf{X}),$$
$$\hat{\eta}^+_{\alpha_2}(\mathbf{X}) \to \hat{\eta}'^+_{\alpha_2}(\mathbf{X},t) = \hat{\eta}^+_{\beta_2}(\mathbf{X})K^+_{\alpha_2\beta_2}(\mathbf{X},t),$$

where the matrix elements $K_{\alpha\beta}(\mathbf{X},t)$ are defined by expressions:

$$K_{\alpha_1\beta_1}(\mathbf{X},t) \equiv \int d\mathbf{x}\varphi^*_{\alpha_1}(\mathbf{x})\exp\left\{i\left[e_1a\left(\mathbf{X}+\frac{m_2}{M}\mathbf{x},t\right)+e_2a\left(\mathbf{X}-\frac{m_1}{M}\mathbf{x},t\right)\right]\right\}\varphi_{\beta_1}(\mathbf{x}), \qquad (3.4.6)$$
$$K^+_{\alpha_2\beta_2}(\mathbf{X},t) \equiv \int d\mathbf{x}\varphi_{\alpha_2}(\mathbf{x})\exp\left\{-i\left[e_1a\left(\mathbf{X}+\frac{m_2}{M}\mathbf{x},t\right)+e_2a\left(\mathbf{X}-\frac{m_1}{M}\mathbf{x},t\right)\right]\right\}\varphi^*_{\beta_2}(\mathbf{x}),$$

and the potentials of the electromagnetic field are converted in accordance with the expressions:

$$\mathbf{A}^{(e)}(\mathbf{x},t) \to \mathbf{A}^{(e)\prime}(\mathbf{x},t) = \mathbf{A}^{(e)}(\mathbf{x},t) - \frac{\partial}{\partial \mathbf{x}} a(\mathbf{x},t), \tag{3.4.7}$$

$$\varphi^{(e)}(\mathbf{x},t) \to \varphi^{(e)\prime}(\mathbf{x},t) = \varphi^{(e)}(\mathbf{x},t) - \frac{\partial}{\partial t} a(\mathbf{x},t).$$

In expressions (3.4.5) - (3.4.7) the quantity $a(\mathbf{x},t)$ is a certain gauge function on which no restrictions have been imposed yet [53]. Note that the matrices (3.4.6) satisfy the equality

$$K^{+}_{\alpha_2\beta_2}(\mathbf{X},t) K_{\beta_2\alpha_1}(\mathbf{X},t) = \delta_{\alpha_1\alpha_2}, \tag{3.4.8}$$

which is easy to see if we assume that the wave functions of a hydrogen-like atom $\varphi_\alpha(\mathbf{x})$ satisfy the equality:

$$\varphi^{*}_{\beta}(\mathbf{x})\varphi_{\beta}(\mathbf{y}) = \delta(\mathbf{x}-\mathbf{y}), \tag{3.4.9}$$

that is, to refer the wave functions of the atom to the region of the discrete spectrum (summation is implied by the repeated indices in (3.4.9), as in the formulas above). In fact, condition (3.4.9) was already considered fulfilled at the stage of formulating the method of second quantization in the presence of bound states of particles. The rationale for this circumstance and the area of its applicability are detailed in [53]. Note also that for $e_1 = -e = -e_2$ matrices (3.4.6) take the form

$$K_{\alpha_1\beta_1}(\mathbf{X},t) \equiv \int d\mathbf{x}\varphi^{*}_{\alpha_1}(\mathbf{x}) \exp\left\{ie\left[a\left(\mathbf{X}-\frac{m_1}{M}\mathbf{x},t\right) - a\left(\mathbf{X}+\frac{m_2}{M}\mathbf{x},t\right)\right]\right\}\varphi_{\beta_1}(\mathbf{x}), \tag{3.4.10}$$

$$K^{+}_{\alpha_2\beta_2}(\mathbf{X},t) \equiv \int d\mathbf{x}\varphi_{\alpha_2}(\mathbf{x}) \exp\left\{-ie\left[a\left(\mathbf{X}-\frac{m_1}{M}\mathbf{x},t\right) - a\left(\mathbf{X}+\frac{m_2}{M}\mathbf{x},t\right)\right]\right\}\varphi^{*}_{\beta_2}(\mathbf{x}).$$

Thus, in accordance with (3.4.2) - (3.4.10), the gauge-invariant one-particle density matrices should be determined by the following expressions:

$$f^{(1)}(\mathbf{x}_1,\mathbf{x}_2) \equiv \mathrm{Sp}\,\rho\hat{\chi}^{\prime+}_1(\mathbf{x}_2)\hat{\chi}^{\prime}_1(\mathbf{x}_1) = e^{-ie\{a(\mathbf{x}_1,t)-a(\mathbf{x}_2,t)\}}\tilde{f}^{(1)}(\mathbf{x}_1,\mathbf{x}_2), \tag{3.4.11}$$

$$f^{(2)}(\mathbf{x}_1,\mathbf{x}_2) \equiv \mathrm{Sp}\,\rho\hat{\chi}^{\prime+}_2(\mathbf{x}_2)\hat{\chi}^{\prime}_2(\mathbf{x}_1) = e^{ie\{a(\mathbf{x}_1,t)-a(\mathbf{x}_2,t)\}}\tilde{f}^{(2)}(\mathbf{x}_1,\mathbf{x}_2),$$

$$f^{(0)}_{\alpha_1,\alpha_2}(\mathbf{x}_1,\mathbf{x}_2) = \mathrm{Sp}\,\rho\hat{\eta}^{\prime+}_{\alpha_2}(\mathbf{x}_2,t)\hat{\eta}^{\prime}_{\alpha_1}(\mathbf{x}_1,t) = K^{+}_{\alpha_2\beta_2}(\mathbf{x}_2,t)K_{\alpha_1\beta_1}(\mathbf{x}_1,t)\tilde{f}^{(0)}_{\beta_1,\beta_2}(\mathbf{x}_1,\mathbf{x}_2;t),$$

moreover, due to properties (3.4.8), the relation:

$$\tilde{f}^{(0)}_{\gamma_1,\gamma_2}\left(\mathbf{x}_1,\mathbf{x}_2;t\right)=K^{+}_{\gamma_1\alpha_1}\left(\mathbf{x}_1,t\right)K_{\gamma_2\alpha_2}\left(\mathbf{x}_2,t\right)f^{(0)}_{\alpha_1,\alpha_2}\left(\mathbf{x}_1,\mathbf{x}_2\right). \qquad (3.4.12)$$

Further, proceeding from the definitions of the Wigner distribution functions (3.4.2), (3.4.3), we have:

$$f^{(1)}\left(\mathbf{x},\mathbf{p}\right)=\int d\mathbf{y}e^{i\mathbf{y}\mathbf{p}}e^{-ie\left\{a\left(\mathbf{x}+\frac{1}{2}\mathbf{y},t\right)-a\left(\mathbf{x}-\frac{1}{2}\mathbf{y},t\right)\right\}}\tilde{f}^{(1)}\left(\mathbf{x}+\frac{1}{2}\mathbf{y},\mathbf{x}-\frac{1}{2}\mathbf{y}\right), \qquad (3.4.13)$$

$$f^{(2)}\left(\mathbf{x},\mathbf{p}\right)=\int d\mathbf{y}e^{i\mathbf{y}\mathbf{p}}e^{ie\left\{a\left(\mathbf{x}+\frac{1}{2}\mathbf{y},t\right)-a\left(\mathbf{x}-\frac{1}{2}\mathbf{y},t\right)\right\}}\tilde{f}^{(2)}\left(\mathbf{x}+\frac{1}{2}\mathbf{y},\mathbf{x}-\frac{1}{2}\mathbf{y}\right),$$

$$f^{(0)}_{\alpha_1,\alpha_2}\left(\mathbf{x},\mathbf{p}\right)=\int d\mathbf{y}e^{i\mathbf{y}\mathbf{p}}K^{+}_{\alpha_2\beta_2}\left(\mathbf{x}-\frac{1}{2}\mathbf{y},t\right)K_{\alpha_1\beta_1}\left(\mathbf{x}+\frac{1}{2}\mathbf{y},t\right)\tilde{f}^{(0)}_{\beta_1,\beta_2}\left(\mathbf{x}+\frac{1}{2}\mathbf{y},\mathbf{x}-\frac{1}{2}\mathbf{y};t\right).$$

On the other hand, for any one-particle density matrix, for example, $\tilde{f}^{(1)}\left(\mathbf{x}+\frac{1}{2}\mathbf{y},\mathbf{x}-\frac{1}{2}\mathbf{y}\right)$, the representation in terms of the Wigner distribution function is valid:

$$\tilde{f}^{(1)}\left(\mathbf{x}+\frac{1}{2}\mathbf{y},\mathbf{x}-\frac{1}{2}\mathbf{y}\right)=\frac{1}{\left(2\pi\right)^3}\int d\mathbf{p}'e^{-i\mathbf{y}\mathbf{p}'}\tilde{f}^{(1)}\left(\mathbf{x},\mathbf{p}'\right), \qquad (3.4.14)$$

as a result, expressions (3.4.13) for gauge-invariant Wigner distribution functions can be written in the form:

$$f^{(1)}\left(\mathbf{x},\mathbf{p};t\right)=\frac{1}{\left(2\pi\right)^3}\int d\mathbf{p}'\tilde{f}^{(1)}\left(\mathbf{x},\mathbf{p}';t\right)\int d\mathbf{y}e^{i\mathbf{y}(\mathbf{p}-\mathbf{p}')}e^{-ie\left\{a\left(\mathbf{x}+\frac{1}{2}\mathbf{y},t\right)-a\left(\mathbf{x}-\frac{1}{2}\mathbf{y},t\right)\right\}}, \qquad (3.4.15)$$

$$f^{(2)}\left(\mathbf{x},\mathbf{p};t\right)=\frac{1}{\left(2\pi\right)^3}\int d\mathbf{p}'\tilde{f}^{(2)}\left(\mathbf{x},\mathbf{p}';t\right)\int d\mathbf{y}e^{i\mathbf{y}(\mathbf{p}-\mathbf{p}')}e^{ie\left\{a\left(\mathbf{x}+\frac{1}{2}\mathbf{y},t\right)-a\left(\mathbf{x}-\frac{1}{2}\mathbf{y},t\right)\right\}},$$

$$f^{(0)}_{\alpha_1,\alpha_2}\left(\mathbf{x},\mathbf{p};t\right)=\frac{1}{\left(2\pi\right)^3}\int d\mathbf{p}'\tilde{f}^{(0)}_{\beta_1,\beta_2}\left(\mathbf{x},\mathbf{p}';t\right)\int d\mathbf{y}e^{i\mathbf{y}(\mathbf{p}-\mathbf{p}')}K^{+}_{\alpha_2\beta_2}\left(\mathbf{x}-\frac{1}{2}\mathbf{y},t\right)K_{\alpha_1\beta_1}\left(\mathbf{x}+\frac{1}{2}\mathbf{y},t\right).$$

For further calculations, it is convenient, following the methods of quantum optics (see in this connection, for example, Ref. [88]), to introduce into consideration the quantity $\Lambda(\mathbf{x}_1,\mathbf{x}_2)$,

$$a(\mathbf{x}_1,t)-a(\mathbf{x}_2,t)\equiv\Lambda(\mathbf{x}_1,\mathbf{x}_2), \qquad (3.4.16)$$

which by means of a curvilinear integral

$$\Lambda(\mathbf{x}_1,\mathbf{x}_2)\equiv\frac{1}{c}\int\limits_{\mathbf{x}_2}^{\mathbf{x}_1}A_i^{(e)}(\mathbf{r},t)\,dr_i \tag{3.4.17}$$

is associated with the vector potential of the external field $\mathbf{A}^{(e)}(\mathbf{r},t)$. The integral in (3.4.17) can be calculated along any curve connecting the points $\mathbf{x}_1,\mathbf{x}_2$. This is where the freedom in the choice of the value $a(\mathbf{x},t)$ lies, see above. For simplicity of further calculations, it is convenient to assume that the integral (3.4.17) is calculated along the straight line connecting the points $\mathbf{x}_1,\mathbf{x}_2$. The value $\Lambda(\mathbf{x}_1,\mathbf{x}_2)$ in quantum optics is called the linear Dirac-Heisenberg gauge potential or simply the Dirac-Heisenberg line, linking the coordinates $\mathbf{x}_1,\mathbf{x}_2$ with the positions of the electron and the nucleus in a hydrogen-like atom (see in this connection [88, 89]). In this paper it is also shown (this can be verified directly from (3.4.17)) that if the distance between $\mathbf{x}_1$ and $\mathbf{x}_2$ insignificantly, for example:

$$\mathbf{x}_1=\mathbf{x}+\mathbf{y}_1,\qquad \mathbf{x}_2=\mathbf{x}-\mathbf{y}_2,\qquad |\mathbf{y}_1|\ll|\mathbf{x}|,\qquad |\mathbf{y}_2|\ll|\mathbf{x}| \tag{3.4.18}$$

then the value $\Lambda(\mathbf{x}_1,\mathbf{x}_2)$ takes the form:

$$\Lambda(\mathbf{x}_1,\mathbf{x}_2)\approx\frac{1}{c}(\mathbf{y}_1-\mathbf{y}_2)\mathbf{A}^{(e)}(\mathbf{x},t). \tag{3.4.19}$$

In terms of the quantity $\Lambda(\mathbf{x}_1,\mathbf{x}_2)$ the first two formulas from (3.4.15) can be written as:

$$f^{(1)}(\mathbf{x},\mathbf{p};t)=\frac{1}{(2\pi)^3}\int d\mathbf{p}'\tilde{f}^{(1)}(\mathbf{x},\mathbf{p}';t)\int d\mathbf{y}e^{i\mathbf{y}(\mathbf{p}-\mathbf{p}')}e^{-ie\Lambda\left(\mathbf{x}+\frac{1}{2}\mathbf{y},\mathbf{x}-\frac{1}{2}\mathbf{y}\right)}, \tag{3.4.20}$$

$$f^{(2)}(\mathbf{x},\mathbf{p};t)=\frac{1}{(2\pi)^3}\int d\mathbf{p}'\tilde{f}^{(2)}(\mathbf{x},\mathbf{p}';t)\int d\mathbf{y}e^{i\mathbf{y}(\mathbf{p}-\mathbf{p}')}e^{ie\Lambda\left(\mathbf{x}+\frac{1}{2}\mathbf{y},\mathbf{x}-\frac{1}{2}\mathbf{y}\right)},$$

and the form of the third formula remains the same when changing the form of tensors $K_{\alpha\beta}$, see (3.4.6):

$$K_{\alpha_1\beta_1}\left(\mathbf{x}+\frac{1}{2}\mathbf{y},t\right)\equiv\int d\mathbf{x}\varphi_{\alpha_1}^{*}(\mathbf{z})\exp\left\{-ie\Lambda\left(\mathbf{x}+\frac{1}{2}\mathbf{y}+\frac{m_2}{M}\mathbf{z},\mathbf{x}+\frac{1}{2}\mathbf{y}-\frac{m_1}{M}\mathbf{z}\right)\right\}\varphi_{\beta_1}(\mathbf{z}), \tag{3.4.21}$$

$$K^{+}_{\alpha_2\beta_2}(\mathbf{X},t)\equiv\int d\mathbf{z}\varphi_{\alpha_2}(\mathbf{z})\exp\left\{ie\Lambda\left(\mathbf{x}-\frac{1}{2}\mathbf{y}+\frac{m_2}{M}\mathbf{z},\mathbf{x}-\frac{1}{2}\mathbf{y}-\frac{m_1}{M}\mathbf{z}\right)\right\}\varphi^{*}_{\beta_2}(\mathbf{z}).$$

In the classical limit, when the fields vary weakly at distances of the order of the de Broglie wavelength of the particle (see, for example, [3]), due to (3.4.18), (3.4.19) we have

$$\Lambda\left(\mathbf{x}+\frac{1}{2}\mathbf{y},\mathbf{x}-\frac{1}{2}\mathbf{y},t\right)\approx\frac{1}{c}\mathbf{y}\mathbf{A}^{(e)}\left(\mathbf{x},t\right), \tag{3.4.22}$$

and, as is easy to see,

$$f^{(1)}\left(\mathbf{x},\mathbf{p};t\right)\approx\tilde{f}^{(1)}\left(\mathbf{x},\mathbf{p}-\frac{e}{c}\mathbf{A}^{(e)}\left(\mathbf{x},t\right);t\right),\quad f^{(2)}\left(\mathbf{x},\mathbf{p};t\right)\approx\tilde{f}^{(2)}\left(\mathbf{x},\mathbf{p}+\frac{e}{c}\mathbf{A}^{(e)}\left(\mathbf{x},t\right);t\right). \tag{3.4.23}$$

To simplify expressions (3.4.21), along with approximation (3.4.19), we also use the point atom approximation [53]. This will greatly simplify the expressions for matrices $K_{\alpha\beta}$, $K^{+}_{\alpha\beta}$. For example, for $K_{\alpha_1\beta_1}\left(\mathbf{x}+\frac{1}{2}\mathbf{y},t\right)$ we get:

$$\begin{aligned}K_{\alpha_1\beta_1}\left(\mathbf{x}+\frac{1}{2}\mathbf{y},t\right)&=\int d\mathbf{z}\varphi^{*}_{\alpha_1}\left(\mathbf{z}\right)\exp\left\{ie\Lambda\left(\mathbf{x}+\frac{1}{2}\mathbf{y}-\frac{m_1}{M}\mathbf{z},\mathbf{x}+\frac{1}{2}\mathbf{y}+\frac{m_2}{M}\mathbf{z},t\right)\right\}\varphi_{\beta_1}\left(\mathbf{z}\right)\approx\\&\approx\int d\mathbf{z}\varphi^{*}_{\alpha_1}\left(\mathbf{z}\right)\exp\left\{-i\frac{e}{c}\mathbf{z}\mathbf{A}^{(e)}\left(\mathbf{x}+\frac{\mathbf{y}}{2},t\right)\right\}\varphi_{\beta_1}\left(\mathbf{z}\right)\approx\\&\approx\int d\mathbf{z}\varphi^{*}_{\alpha_1}\left(\mathbf{z}\right)\left\{1-i\frac{e}{c}\mathbf{z}\mathbf{A}^{(e)}\left(\mathbf{x}+\frac{\mathbf{y}}{2},t\right)\right\}\varphi_{\beta_1}\left(\mathbf{z}\right).\end{aligned} \tag{3.4.24}$$

In the classical limit, when the fields vary weakly at distances of the order of the de Broglie wavelength of the particle, from (3.4.24) we finally have:

$$K_{\alpha_1\beta_1}\left(\mathbf{x}+\frac{\mathbf{y}}{2},t\right)\approx\delta_{\alpha_1\beta_1}-i\frac{1}{c}\mathbf{d}_{\alpha_1\beta_1}\mathbf{A}^{(e)}\left(\mathbf{x},t\right)-i\frac{1}{2c}\left(\mathbf{y}\nabla\right)\mathbf{d}_{\alpha_1\beta_1}\mathbf{A}^{(e)}\left(\mathbf{x},t\right). \tag{3.4.25}$$

In deriving expression (3.4.25) from (3.4.21), we used the condition for normalizing the wave functions of the discrete spectrum of a hydrogen-like atom and introduced the concept of the tensor of dipole moments for this atom $\mathbf{d}_{\alpha\beta}$ [53]:

$$\int d\mathbf{x}\varphi^{*}_{\alpha}\left(\mathbf{x}\right)\varphi_{\beta}\left(\mathbf{x}\right)=\delta_{\alpha\beta},\qquad\mathbf{d}_{\alpha\beta}\equiv e\int d\mathbf{y}\varphi^{*}_{\alpha}\left(\mathbf{y}\right)\mathbf{y}\varphi_{\beta}\left(\mathbf{y}\right). \tag{3.4.26}$$

The use of formulas (3.4.15) - (3.4.26) allows one to obtain a rather simple expression for the gauge-invariant distribution function of neutral atoms $f^{(0)}_{\alpha;\beta}(\mathbf{x},\mathbf{p};t)$:

$$f^{(0)}_{\alpha_1,\alpha_2}(\mathbf{x},\mathbf{p};t) \approx \tilde{f}^{(0)}_{\alpha_1,\alpha_2}(\mathbf{x},\mathbf{p};t) - i\frac{1}{c}\Big[\mathbf{d},\tilde{f}^{(0)}(\mathbf{x},\mathbf{p};t)\Big]_{\alpha_1\alpha_2}\mathbf{A}^{(e)}(\mathbf{x},t) - \quad (3.4.27)$$
$$-\frac{1}{2c}\left\{\mathbf{d},\left(\frac{\partial\tilde{f}^{(0)}(\mathbf{x},\mathbf{p};t)}{\partial\mathbf{p}}\nabla\right)\right\}_{\alpha_1\alpha_2}\mathbf{A}^{(e)}(\mathbf{x},t)\cdot$$

In the last expression the notations $\big[A,B\big]_{\alpha_1\alpha_2}$, $\big\{A,B\big\}_{\alpha_1\alpha_2}$ have the traditional sense of switches and anti-switches for matrices A, B:

$$\big[A,B\big]_{\alpha_1\alpha_2} \equiv A_{\alpha_1\beta}B_{\beta\alpha_2} - B_{\alpha_1\beta}A_{\beta\alpha_2}, \quad \big\{A,B\big\}_{\alpha_1\alpha_2} \equiv A_{\alpha_1\beta}B_{\beta\alpha_2} + B_{\alpha_1\beta}A_{\beta\alpha_2}. \quad (3.4.28)$$

Thus, expressions (3.4.2) - (3.4.28) in this section make it possible to obtain kinetic equations for gauge-invariant Wigner distribution functions of particles based on kinetic equations (3.3.5), (3.3.6) for gauge-non-invariant distribution functions (3.3.7). In the obtained kinetic equations, the potentials of the external electromagnetic field $\mathbf{A}^{(e)}(\mathbf{x},t)$ и $\varphi^{(e)}(\mathbf{x},t)$ enter already in the form of combinations corresponding to the strengths of the electrical $\mathbf{E}^{(e)}(\mathbf{x},t)$ and magnetic $\mathbf{H}^{(e)}(\mathbf{x},t)$ fields, see Eq. (3.4.1).

3.5. Gauge-invariant system of kinetic equations for a low-temperature gas of hydrogen-like atoms in an external electromagnetic field

The above-mentioned procedure for deriving kinetic equations for gauge-invariant Wigner distribution functions does not contain any fundamental difficulties in its implementation. On the other hand, it presupposes a number of rather cumbersome calculations, which do not seem appropriate to give in detail within the framework of this work. To trace the characteristic techniques and methodology of these calculations, one can refer to the works [84, 85]. In this section, the final results of the above calculations will be presented in the form of a system of kinetic equations proper for a low-temperature gas of hydrogen-like atoms in an external electromagnetic field. These equations, in addition to terms taking into account the influence of the external field, also contain terms responsible for taking into account the mean or self-consistent field, the derivation of which is described in detail in [89].

Thus, the kinetic equations for the gauge-invariant distribution functions of free charged fermions of the first and second types (electrons

and the core of hydrogen-like atoms) can be represented in the following form:

$$\frac{\partial}{\partial t} f^{(1)}(\mathbf{x},\mathbf{p};t)+\frac{\partial \varepsilon^{(1)}(\mathbf{x},\mathbf{p})}{\partial \mathbf{p}}\frac{\partial f^{(1)}(\mathbf{x},\mathbf{p})}{\partial \mathbf{x}}-\frac{\partial \varepsilon^{(1)}(\mathbf{x},\mathbf{p})}{\partial \mathbf{x}}\frac{\partial f^{(1)}(\mathbf{x},\mathbf{p})}{\partial \mathbf{p}}=\mathbf{F}_L^{(1)}\frac{\partial f^{(1)}(\mathbf{x},\mathbf{p})}{\partial \mathbf{p}}, \tag{3.5.1}$$

$$\frac{\partial}{\partial t} f^{(2)}(\mathbf{x},\mathbf{p};t)+\frac{\partial \varepsilon^{(2)}(\mathbf{x},\mathbf{p})}{\partial \mathbf{p}}\frac{\partial f^{(2)}(\mathbf{x},\mathbf{p})}{\partial \mathbf{x}}-\frac{\partial \varepsilon^{(2)}(\mathbf{x},\mathbf{p})}{\partial \mathbf{x}}\frac{\partial f^{(2)}(\mathbf{x},\mathbf{p})}{\partial \mathbf{p}}=\mathbf{F}_L^{(2)}\frac{\partial f^{(2)}(\mathbf{x},\mathbf{p})}{\partial \mathbf{p}},$$

where

$$\varepsilon^{(1)}(\mathbf{x},\mathbf{p})=\varepsilon_1(\mathbf{p})-U^{(1)}(\mathbf{x},\mathbf{p};f)-U(\mathbf{x},\mathbf{p};f), \qquad \varepsilon_1(\mathbf{p})=\frac{p^2}{2m_1}, \tag{3.5.2}$$

$$\varepsilon^{(2)}(\mathbf{x},\mathbf{p})=\varepsilon_2(\mathbf{p})-U^{(2)}(\mathbf{x},\mathbf{p};f)+U(\mathbf{x},\mathbf{p};f), \qquad \varepsilon_2(\mathbf{p})=\frac{p^2}{2m_2},$$

are the Lorentz forces acting on both types of fermions are determined in the usual way:

$$\mathbf{F}_L^{(1)}\equiv e\left\{\mathbf{E}^{(e)}(\mathbf{x},t)+\frac{\mathbf{p}}{m_1 c}\times\mathbf{H}^{(e)}(\mathbf{x},t)\right\}, \qquad \mathbf{F}_L^{(2)}\equiv -e\left\{\mathbf{E}^{(e)}(\mathbf{x},t)+\frac{\mathbf{p}}{m_2 c}\times\mathbf{H}^{(e)}(\mathbf{x},t)\right\}. \tag{3.5.3}$$

In addition, the following notation was introduced in (3.5.2):

$$U^{(1)}(\mathbf{x},\mathbf{p};f)\equiv\frac{e^2}{\mathcal{V}}\sum_{\mathbf{p}'} f^{(1)}(\mathbf{x},\mathbf{p}')\nu(\mathbf{p}'-\mathbf{p}), \tag{3.5.4}$$

$$U^{(2)}(\mathbf{x},\mathbf{p};f)\equiv\frac{e^2}{\mathcal{V}}\sum_{\mathbf{p}'} f^{(2)}(\mathbf{x},\mathbf{p}')\nu(\mathbf{p}'-\mathbf{p}),$$

$$U(\mathbf{x},\mathbf{p};f)\equiv\frac{e}{\mathcal{V}}\int d\mathbf{x}'\nu(\mathbf{x}-\mathbf{x}')\left[\mathbf{d}_{\alpha_1'\alpha_3'}\sum_{\mathbf{p}_3'}\frac{\partial f^{(0)}_{\alpha_3',\alpha_1'}(\mathbf{x}',\mathbf{p}_3')}{\partial \mathbf{x}'}-e\left(\sum_{\mathbf{p}_3'} f^{(1)}(\mathbf{x}',\mathbf{p}_3')-\sum_{\mathbf{p}_3'} f^{(2)}(\mathbf{x}',\mathbf{p}_3')\right)\right],$$

while

$$\nu(\mathbf{x}-\mathbf{x}')\equiv\frac{1}{\mathcal{V}}\sum_{\mathbf{k}} e^{i\mathbf{k}(\mathbf{x}-\mathbf{x}')}\nu(\mathbf{k}). \tag{3.5.5}$$

The value $\nu(\mathbf{k})$ in Eqs. (3.5.4), (3.5.5) is still given by formula (3.2.25). When deriving equations (3.5.1) and expressions (3.5.2), (3.5.4), we used the Coulomb calibration for an external electromagnetic field

$$\operatorname{div}\mathbf{A}^{(e)}(\mathbf{x},t)=0 \tag{3.5.6}$$

and the expression for the polarization matrix $\sigma_{\alpha\beta}(\mathbf{k})$ (see (3.2.11), (3.2.13)) in the approximation of a point atom:

$$\sigma_{\alpha\beta}(\mathbf{k})\approx -i\mathbf{k}\mathbf{d}_{\alpha\beta}, \tag{3.5.7}$$

where the tensor of the atomic dipole moments is defined by formula (68).

For the gauge-invariant Wigner distribution function $f^{(0)}_{\alpha_1,\alpha_2}(\mathbf{x},\mathbf{p})$ kinetic equation has a more complex form, due also to the fact that this function of coordinates and momentum remains a single-particle density matrix in indices α_1,α_2:

$$\frac{\partial f^{(0)}_{\alpha_1,\alpha_2}(\mathbf{x},\mathbf{p})}{\partial t}+i\left[\varepsilon^{(0)}(\mathbf{x},\mathbf{p}),f^{(0)}(\mathbf{x},\mathbf{p})\right]_{\alpha_1\alpha_2}= \tag{3.5.8}$$
$$=-\frac{1}{2}\left\{\frac{\partial\varepsilon^{(0)}(\mathbf{x},\mathbf{p})}{\partial\mathbf{p}},\frac{\partial f^{(0)}(\mathbf{x},\mathbf{p})}{\partial\mathbf{x}}\right\}_{\alpha_1\alpha_2}+\frac{1}{2}\left\{\frac{\partial\varepsilon^{(0)}(\mathbf{x},\mathbf{p})}{\partial\mathbf{x}},\frac{\partial f^{(0)}(\mathbf{x},\mathbf{p})}{\partial\mathbf{p}}\right\}_{\alpha_1\alpha_2},$$

where operations like $[A,B]_{\alpha_1\alpha_2}$, $\{A,B\}_{\alpha_1\alpha_2}$ are defined by formulas (3.4.28). For the value $\varepsilon^{(0)}_{\alpha_1,\alpha_2}(\mathbf{x},\mathbf{p})$, determining the evolution of the distribution function of atoms in accordance with Eq. (3.5.8), as a result of simple but rather cumbersome calculations we arrive at the expression:

$$\varepsilon^{(0)}_{\alpha_1,\alpha_2}(\mathbf{x},\mathbf{p})=\varepsilon_{\alpha_1}(\mathbf{p})\delta_{\alpha_1\alpha_2}+U^{(0)}_{\alpha_1\alpha_2}(\mathbf{x},\mathbf{p};f)+U_{\alpha_1\alpha_2}(\mathbf{x},\mathbf{p};f)+U^{(e)}_{\alpha_1\alpha_2}(\mathbf{x},\mathbf{p};f), \tag{3.5.9}$$

where we also introduced the notation:

$$U_{\alpha_1\alpha_2}(\mathbf{x},\mathbf{p};f)=-\frac{1}{\mathcal{V}}\int d\mathbf{x}'v(\mathbf{x}-\mathbf{x}')\sum_{\mathbf{p}'}\left(\mathbf{d}\frac{\partial}{\partial\mathbf{x}'}\right)_{\alpha_1\alpha_2}\left(\mathbf{d}\frac{\partial}{\partial\mathbf{x}'}\right)_{\alpha_1'\alpha'}f^{(0)}_{\alpha',\alpha_1'}(\mathbf{x}',\mathbf{p}')- \tag{3.5.10}$$
$$-\frac{e}{\mathcal{V}}\int d\mathbf{x}'v(\mathbf{x}-\mathbf{x}')\left(\mathbf{d}\frac{\partial}{\partial\mathbf{x}'}\right)_{\alpha_1\alpha_2}\left(\sum_{\mathbf{p}'}f^{(1)}(\mathbf{x}',\mathbf{p}')-\sum_{\mathbf{p}'}f^{(2)}(\mathbf{x}',\mathbf{p}')\right),$$
$$U^{(0)}_{\alpha_1\alpha_2}(\mathbf{x},\mathbf{p})\equiv\frac{4\pi}{\mathcal{V}}\sum_{\mathbf{p}'}(\mathbf{p}'-\mathbf{p})^{-2}\left((\mathbf{p}-\mathbf{p}')\mathbf{d}\right)_{\alpha_1\alpha'}f^{(0)}_{\alpha',\alpha_1'}(\mathbf{x},\mathbf{p}')\left((\mathbf{p}'-\mathbf{p})\mathbf{d}\right)_{\alpha_1'\alpha_2},$$
$$U^{(e)}_{\alpha_1\alpha_2}(\mathbf{x},\mathbf{p};f)\equiv\left(\mathbf{E}^{(e)}(\mathbf{x},t)+\frac{\mathbf{p}}{Mc}\times\mathbf{H}^{(e)}(\mathbf{x},t)\right)\mathbf{d}_{\alpha_1\alpha_2}.$$

The system of coupled equations, expressed by formulas (3.5.1) - (3.5.10), is a solution to the problem stated in this chapter - to construct the kinetics of a low-temperature gas of hydrogen-like atoms in an external electromagnetic field, taking into account the self-consistent field, that is, in the collisionless approximation. In this regard, it is pertinent to recall that the main condition for the validity of the collisionless approximation and, therefore, equations (3.5.1), (3.5.8), is expressed by the relation (see, for example, [31] and also [84, 85, 89]):

$$\tau_0 \ll t \ll \tau_r , \tag{3.5.11}$$

where τ_0 is the chaotization time mentioned above, and τ_r is the relaxation time of the system due to collisions between particles (for more details on these characteristic times, see [3]). Relaxation time τ_r is determined precisely by the intensity of interaction $\hat{V}$, more precisely, by the collision integral, which is quadratic in the interaction, see (3.1.17). Relaxation time tends to infinity, $\tau_r \to \infty$, at $\hat{V} \to 0$ (in our work, the last relation (3.5.11) should correspond to neglect of the collision integral). In other words, the relaxation time is long in the case of a small interaction. Since the chaos time does not depend on the interaction intensity at all, condition (3.5.11) for many systems is quite realistic.

In conclusion of this section, we note that, neglecting the self-consistent field, equations (3.5.1), (3.5.8) are greatly simplified and turn into kinetic equations for the components of the system (including neutral ones) in an external electromagnetic field. However, as is easy to see, in this approximation the kinetic equations cease to be connected, that is, the components of the system evolve independently of each other.:

$$\frac{\partial}{\partial t} f^{(1)}\left(\mathbf{x},\mathbf{p};t\right) + \frac{\mathbf{p}}{m_1}\frac{\partial f^{(1)}\left(\mathbf{x},\mathbf{p};t\right)}{\partial \mathbf{x}} = e\left\{\mathbf{E}^{(e)}\left(\mathbf{x},t\right) + \frac{\mathbf{p}}{m_1 c}\times\mathbf{H}^{(e)}\left(\mathbf{x},t\right)\right\}\frac{\partial f^{(1)}\left(\mathbf{x},\mathbf{p}\right)}{\partial \mathbf{p}}, \tag{3.5.12}$$

$$\frac{\partial}{\partial t} f^{(2)}\left(\mathbf{x},\mathbf{p};t\right) + \frac{\mathbf{p}}{m_2}\frac{\partial f^{(2)}\left(\mathbf{x},\mathbf{p};t\right)}{\partial \mathbf{x}} = -e\left\{\mathbf{E}^{(e)}\left(\mathbf{x},t\right) + \frac{\mathbf{p}}{m_1 c}\times\mathbf{H}^{(e)}\left(\mathbf{x},t\right)\right\}\frac{\partial f^{(2)}\left(\mathbf{x},\mathbf{p}\right)}{\partial \mathbf{p}},$$

$$\frac{\partial f_{\alpha_1,\alpha_2}\left(\mathbf{x},\mathbf{p};t\right)}{\partial t} \approx -i\left[\varepsilon\left(\mathbf{x},\mathbf{p},t\right), f\left(\mathbf{x},\mathbf{p}\right)\right]_{\alpha_1\alpha_2} +$$

$$-\frac{1}{2}\left\{\frac{\partial\varepsilon\left(\mathbf{x},\mathbf{p};t\right)}{\partial \mathbf{p}}, \frac{\partial f\left(\mathbf{x},\mathbf{p};t\right)}{\partial \mathbf{x}}\right\}_{\alpha_1\alpha_2} + \frac{1}{2}\left\{\frac{\partial\varepsilon\left(\mathbf{x},\mathbf{p},t\right)}{\partial \mathbf{x}}, \frac{\partial f\left(\mathbf{x},\mathbf{p}\right)}{\partial \mathbf{p}}\right\}_{\alpha_1\alpha_2},$$

where

$$\varepsilon_{\alpha_1\alpha_2}\left(\mathbf{x},\mathbf{p},t\right)\equiv\varepsilon_{\alpha_1}\left(\mathbf{p}\right)\delta_{\alpha_1\alpha_2}+\left(\mathbf{E}^{(e)}\left(\mathbf{x},t\right)+\frac{\mathbf{p}}{Mc}\times\mathbf{H}^{(e)}\left(\mathbf{x},t\right)\right)\mathbf{d}_{\alpha_1\alpha_2},$$

$$\varepsilon_{\alpha}\left(\mathbf{p}\right)=\varepsilon_{\alpha}+\mathbf{p}^2/2M\,.$$

Summary and Outlook

Thus, in this chapter we have applied a microscopic approach to constructing kinetic equations (3.5.1) - (3.5.8) for all components of a weakly ionized and weakly excited gas of hydrogen-like atoms in an external electromagnetic field at low temperatures. In the absence of an external electromagnetic field, the obtained equations coincide with the kinetic equations taking into account the mean (self-consistent) field of [84, 85, 89]. On the basis of the noted equations, in these works a detailed analysis of the dispersion laws of eigenwaves, which can propagate in the system under study, was given, and their damping decrements were found. The possibility of using the obtained dispersion relations for eigenwaves in the theory of BEC photons in ultracold gases is also demonstrated. In particular, the results allow one to calculate the effective masses of photons in such media. The presence of an effective mass of a photon, as already mentioned in the Introduction (see also Refs [59 - 66]), is an indispensable condition for the realization of the BEC of photons.

Equations (3.5.1) - (3.510), as noted above, should underlie the study of effects and phenomena associated with the interaction of low-temperature gases with an external electromagnetic field. For example, these equations make it possible to study the propagation of forced waves in the systems under study, including various resonance phenomena. The latter circumstance seems to be important from the point of view of the possibility of additional pumping of photons into the medium by an external electromagnetic field (laser). The need to increase the photon density in a medium inevitably arises in the process of experimental realization of the regime with BEC of photons in it.

A separate direction of applications of the obtained equations (3.5.1) - (3.5.10) opens up if the electromagnetic field entering them is of a stochastic nature. In this connection, one should pay attention to the last of the equations (3.5.2), taking into account (3.5.3), which is simpler in comparison with (3.5.8) - (3.5.10). Due to the random nature of the external electromagnetic field, equation (3.5.2) from a mathematical point of view is an equation with a spatially inhomogeneous noise source that depends on the particle momentum. Such equations are typical for systems with active fluctuations, see Chapter II of this work. In systems of this kind, the implementation of the so-called self-propelled properties is possible. In other words, in this kind of media, structured ordered motions of particles may arise due to the accumulation and transformation of the energy of an

external stochastic field. In particular, this phenomenon is possible in the case when the structural units of the system have a head-tail asymmetry. As is easy to see from (3.5.8) - (3.5.10), (3.5.2), (3.5.3), excited atoms have such an asymmetry. In the equations, such an asymmetry lies in the presence of dipole moments of excited atoms. Thus, low-temperature weakly excited gases in an external random electromagnetic field can serve as a prototype of a physical system with active fluctuations. However, this issue requires a separate study, the results of which, unfortunately, cannot be placed within the framework of this work..

REFERENCES

1. O.Yu. Sliusarenko, A.V. Chechkin, Yu.V. Slyusarenko, The Bogolyubov-Born-Green-Kirkwood-Yvon hierarchy and Fokker-Planck equation for many-body dissipative randomly driven systems, J. Math. Phys. **56**, 043302 (2015).

2. N. Bogolyubov, *Problems of Dynamical Theory in Statistical Physic*s (Providence College, Providence, RI, 1959).

3. A.I. Akhiezer and S.V. Peletminskii, *Methods of Statistical Physics* (Pergamon, Oxford, 1981).

4. S.V. Peletminskii, Yu.V. Slyusarenko, A.I. Sokolovskii, Kinetics and hydrodynamics of long-wave fluctuations under external random force, Physica A **326,** 412 (2003).

5. N.V. Laskin, S.V. Peletminskii, V.I. Prikhod'ko, On the dynamic theory of systems in random fields, Journal of Physical Studies **1,** 6 (1998).

6. A. Chechkin, R. Metzler, J. Klafter, V. Gonchar, *Introduction to the Theory of Lévy Flights. Anomalous Transport: Foundations and Applications.* (Wiley-VCH, Weinheim, 2008).

7. A.V. Chechkin, O.Yu. Sliusarenko, Kinetic Equation for Non-Markovian Gaussian Processes in Linear Multidimensional Systems, Ukr. J. Phys. **52**, 1193 (2007).

8. O.Yu. Sliusarenko, Generalized Fokker-Planck equation and its solution for linear non-Markovian Gaussian systems, Condens. Matter Phys. **14**, 23002 (1-14) (2011).

9. S.O. Nikolayenko, Yu.V. Slyusarenko, Microscopic theory of relaxation processes in systems of particles interacting with the hydrodynamic medium, J. Math. Phys. **50**, 083305 (2009).

10. S.O. Nikolayenko, Yu.V. Slyusarenko, Theory of macroscopic fluctuations in systems of particles, interacting with hydrodynamic and gaslike media, J. Math. Phys., **51**, 113301 (2010).

11. Pierre-Henri Chavanis, Brownian particles with long- and short-range interactions, Physica A, 390, 1546 (2011).

12. M. Mayorga, L. Romero-Salazar, J.M. Rubi, Stochastic model for the dynamics of interacting Brownian particles, Physica A **307**, 297 (2002).

13. A.J. Archer and M. Rauscher, Dynamical density functional theory for interacting Brownian particles: stochastic or deterministic?, J. Phys. A: Math. Gen. **37,** 9325 (2004).

14. S. Savel'ev, F. Marchesoni, A. Taloni, and F. Nori, Diffusion of interacting Brownian particles: Jamming and anomalous diffusion, Phys. Rev. E **74**, 021119 (2006).

15. Basu, Abhik and Ramaswamy, Sriram, Perspectives on the mode-coupling approximation for the dynamics of interacting Brownian particles, Journal of Statistical Mechanics: Theory and Experiment, **11**, 11003 (2007).

16. Hui Xia, Katsuhiro Ishii, Toshiaki Iwaii, Hongjian Li, and Bingchu Yang, Dynamics of interacting Brownian particles in concentrated colloidal suspensions, Applied Optics, **47**, 1257 (2008).

17. Anita Mehta, *Granular Physics,* Cambridge University Press (Cambridge, New York, Melbourne, Madrid, Cape Town, Singapore, São Paulo, 2007).

18. J.B. Knight, H.M. Jaeger, and S.R. Nagel, Dynamics of interacting Brownian particles in concentrated colloidal suspensions, Phys. Rev. Lett., **70**, 3728 (1993).

19. Daniel C. Hong and Paul V. Quinn, Reverse Brazil Nut Problem: Competition between Percolation and Condensation, Phys. Rev. Lett. **86**, 3423 (2001).

20. T Shinbrot, Nature, Granular materials: The brazil nut effect — in reverse, 429, Issue 6990, 352 (2004).

21. D. Astumian and P. Haenggi, Brownian Motors, Phys. Today **55**, No. 11, 33 (2002).

22. P. Reimann, Brownian motors: noisy transport far from equilibrium, Phys. Rep. 361, 57 (2002).

23. F. Schweitzer, *Brownian Agents and Active Particles* (Springer, New York, 2003).

24. M. Friedrich and F. Juelicher, Chemotaxis of sperm cells, Proc. Natl. Acad. Sci. U.S.A. 104, 13256 (2007).

25. S. van Teeffelen and H. Loewen, Dynamics of a Brownian circle swimmer, Phys. Rev. E **78**, 020101 (2008).

26. D. Selmeczi et al., Cell motility as random motion: A review, Eur. Phys. J. Special Topics, **157**, 1 (2008).

27. L. Li, S.F. Nørrelykke, and E.C. Cox, Persistent Cell Motion in the Absence of External Signals: A Search Strategy for Eukaryotic Cells, PLoS ONE **3**, e2093 (2008).

28. H. Boedeker et al., Quantitative analysis of random ameboid motion, Europhys. Lett. **90**, 28005 (2010).

29. P.M. Kareiva, N. Shigesada, Analyzing insect movement as a correlated random walk, Oecologia **56**, 234 (1983).

30. N. Komin, U. Erdmann, L. Schimansky-Geier, Random walk theory applied to daphnia motion, Fluctuation Noise Lett. **4**, L151 (2004).

31. J.R. Howse, R.A.L. Jones, A.J. Ryan, T. Gough, R. Vafabakhsh, R. Golestanian, Self-Motile Colloidal Particles: From Directed Propulsion to Random Walk, Phys. Rev. Lett. **99**, 048102 (2007).

32. W.F. Paxton, K.C. Kistler, C.C. Olmeda, A. Sen, S.K. St. Angelo, Y. Cao, T.E. Mallouk, P.E. Lammert, V.H. Crespi, Catalytic Nanomotors: Autonomous Movement of Striped Nanorods, J. Amer. Chem. Soc. **126**, 13424 (2004).

33. P. Romanczuk, M. Baer, W. Ebeling, B. Lindner, and L. Schimansky-Geier, Motion of Euglena gracilis: Active fluctuations and velocity distribution, Eur. Phys. J. Special Topics **202**, 1 (2012).

34. V. Lobaskin and M. Romenskyy, Collective dynamics in systems of active Brownian particles with dissipative interactions, Phys. Rev. E 87, 052135 (2013).

35. R. Großmann, L. Schimansky-Geier and P. Romanczuk, Self-propelled particles with selective attraction–repulsion interaction: from microscopic dynamics to coarse-grained theories, New Journal of Physics **15,** 085014 (2013).

36. O. Sliusarenko and Yu. Slyusarenko, Reduced description method in the kinetic theory of Brownian motion with active fluctuations, J. Phys. A: Math. Theor. **52,** 445001 (2019).

37. A.I. Akhiezer, I.A. Akhiezer, R.V. Polovin, A.G. Sitenko and K.N. Stepanov, *Plasma Electrodynamics,* V.1. Linear Theory. Oxford-New York: Pergamon Press, 1975 (International Series of Monographs in Natural Philosophy. Vol.68).

38. A.I. Akhiezer, I.A. Akhiezer, R.V. Polovin, A.G. Sitenko and K.N. Stepanov, *Plasma Electrodynamics,* V.2. Nonlinear theory and fluctuations. Oxford-New York: Pergamon Press, 1975 (International Series of Monographs in Natural Philosophy. Vol.69).

39. Edited by Hans Wilhelmsson, *Plasma Physics: Nonlinear Theory and Experiments* (Springer Science + Business Media LLC, 1976)

40. Peter A. Sturrock, *Plasma Physics: An Introduction to the Theory of Astrophysical, Geophysical and Laboratory Plasmas* (Cambridge University Press, Cambridge, 1994).

41. T.J.M. Boyd, J.J. Sanderson, *The Physics of Plasmas* (Cambridge University Press, Cambridge, 2003).

42. B.M. Smirnov, *Physics of weakly ionized gases: (problems and solutions)* (Moscow : Mir Publishers, 1981).

43. Boris M. Smirnov, *Physics of Ionized Gases* (A Wiley-Interscience Publication, John Wiley & Sons, Inc. New York / Chichester / Weinham / Brisbane / Singapore / Toronto, 2001).

44. C.J. Pethick, H. Smith, *Bose-Einstein Condensation in Dilute Gases*, Cambridge University Press, 2002.

45. L.P. Pitaevskii, S. Stringari, *Bose-Einstein Condensation*, Clarendon Press, Oxford, 2003.

46. M.H. Anderson, J.R. Ensher, M.R. Matthews, C.E. Wieman, E.A. Cornell, Observation of Bose-Einstein Condensation in a Dilute Atomic Vapor, Science **269**, 198 (1995).

47. K.B. Davis, M.O. Mewes, M.R. Andrews, N.J. van Druten, D.S. Durfee, D.M. Kurn, W. Ketterle, Bose-Einstein Condensation in a Gas of Sodium Atoms, Phys. Rev. Lett. **75**, 3969 (1995).

48. L. Hau, S. Harris, Z. Dutton, and C. Behroozi, Light speed reduction to 17 meters per second in an ultracold atomic gas, Nature **397** (1999).

49. M. Fleischhauer, A. Imamoglu, and J.P. Marangos, Electromagnetically induced transparency: Optics in coherent media, Rev. Mod. Phys. **77**, 633 (2005).

50. Yu.V. Slyusarenko, A.G. Sotnikov, On the response of a system with bound states of particles to the perturbation by the external electromagnetic field, Condensed Matter Physics **459,** 9 (2006).

51. Y. Slyusarenko and A. Sotnikov, Green-function method in the theory of ultraslow electromagnetic waves in an ideal gas with Bose-Einstein condensates, Phys. Rev. A **78**, 053622 (2008).

52. Y. Slyusarenko and A. Sotnikov, Role of temperature effects in the phenomenon of ultraslow electromagnetic pulses in Bose-Einstein condensates of alkali-metal atoms, Phys. Rev. A **80**, 053604 (2009).

53. S.V. Peletminskii and Y.V. Slyusarenko, Second quantization method in the presence of bound states of particles, J. Math. Phys. **46**, 022301 (2005).

54. Y.V. Slyusarenko, A.G. Sotnikov, Microwaves Interaction Peculiarities with the Ideal Gas of Alkali Atoms in BEC State, J. Low Temp. Phys. 150, 618 (2008).

55. Y. Slyusarenko and A. Sotnikov, Microwaves interaction peculiarities with the ideal gas of alkali atoms in BEC state, Phys. Lett. A **373**, 1392 (2009).

56. Y.V. Slyusarenko and A.G. Sotnikov, Feasibility of using Bose-Einstein condensates for filtering optical pulses, Low Temp. Phys. **36**, 671 (2010).

57. Y. Slyusarenko and A. Sotnikov, Propagation of relativistic charged particles in ultracold atomic gases with Bose-Einstein condensates, Phys. Rev. A **83**, 023601 (2011).

58. Yu.V. Slyusarenko and A.G. Sotnikov, On the influence of the internal structure of the atom on Bose–Einstein condensation in an ideal gas of hydrogenlike atoms, Low Temp. Phys. **33**, 30 (2007).

59. J. Klaers, J. Schmitt, F. Vewinger, and M. Weitz, Nature **468,** 545 (2010).

60. J. Klaers, J. Schmitt, T. Damm, D. Dung, F. Vewinger, and M. Weitz, Proc. SPIE 8600, 86000L (2013).

61. A.-W. de Leeuw, H.T.C. Stoof, and R.A. Duine, Schwinger-Keldysh theory for Bose-Einstein condensation of photons in a dye-filled optical microcavity, Phys. Rev. A **88**, 033829 (2013).

62. D.N. Sob'yanin, Bose-Einstein condensation of light: General theory, Phys. Rev. E **88**, 022132 (2013).

63. A. Kruchkov, and Yu. Slyusarenko, Bose-Einstein condensation of photons in an ideal atomic gas, Phys. Rev. A **88**, 013615 (2013).

64. A. Kruchkov, Bose-Einstein condensation of light in a cavity, Phys. Rev. A **89**, 033862 (2014).

65. N. Boychenko, Yu. Slyusarenko, Coexistence of photonic and atomic Bose-Einstein condensates in ideal atomic gases, Condensed Matter Physics **18,** 43002 (2015).

66. J.T. Mendonça, and H. Terças, Bose-Einstein condensation of photons in a plasma, Phys. Rev. A 95, 063611 (2017).

67. Yu. L. Klimontovich, *The Kinetic Theory of Electromagnetic Processes*, (Springer-Verlag, Berlin, Heidelberg, New York, 1983).

68. Yu.L. Klimontovich, A.Yu. Shevchenko, I.P. Yakimenko, A.G. Zagorodny, Contributions to Plasma Physics, **29**, 551 (1989).

69. I Goldhirsch, S.V. Peletminskii, A.S. Peletminskii, A.I. Sokolovskii, Application of Bogolyubov's approach to the derivation of kinetic equations for dissipative systems, arXiv: 1307.3466v1. [cond-mat.stat-mach] 12 Jul. 2013.

70. L.D. Landau, E.M. Lifshitz, *Statistical physics* (Course of theoretical physics, volume 5) (Oxford, London, 1980).

71. E.A. Novikov, Functionals and the Random-force Method in Turbulence Theory, Zh. Eksp. Teor. Fiz. **47,** 1919 (1964) (Sov. Phys. JETP).

72. K. Furutsu, On the Statistical Theory of Electromagnetic Waves in a Fluctuating Medium (1), J. Res. N.B.S., **D-67**, 303 (1963).

73. S.S. Moiseev, A.V. Tur, V.V. Yanovsky, Spectra and excitation methods of turbulence in a compressible fluid, Sov. Phys. JETP **44**, 556 (1976).

74. S.Chandrasekhar, *Stokhastic Problems in Physics and Astronomy*, Reviews of Modern Physics **15**, 1 (1943).

75. J. Javier Brey, M.J. Ruiz-Montero, and D. Cubero, Homogeneous cooling state of a low-density granular flow, Phys. Rev. E **54**, 3664 (1996).

76. J. Javier Brey, M.I. Garcia de Soria, P. Maynar, and M.J. Ruiz-Montero, Energy fluctuations in the homogeneous cooling state of granular gases, Phys. Rev. E **70**, 011302 (2004).

77. I. Goldhirsch, Introduction to granular temperature, Powder Technology **182**, 130 (2008).

78. D. Serero, C. Goldenberg, S.H. Noskowicz, I. Goldhirsch, The classical granular temperature and slightly beyond, Powder Technology **182**, 257 (2008).

79. Hiizu Nakanishi, Velocity distribution of inelastic granular gas in a homogeneous cooling state, Phys. Rev. E **67,** 010301 (2003).

80. J. Weinstock, Three-Body Scattering Operator in Nonequilibrium Statistical Mechanics Phys. Rev. **132,** 470 (1963).

81. K. Kawasaki, Oppenheim I., Logarithmic Term in the Density Expansion of Transport Coefficients, Phys. Rev. A **139**, 1763 (1965).

82. G.E. Uhlenbeck, G.W. Ford, *Lectures in statistical mechanics*, (Providence Rhode Island,1963).

83. A.I. Akhiezer, V.G. Baryakhtar, and S.V. Peletminskii, *Spin waves* (Amsterdam: North Holland, 1968).

84. Yu.V. Slyusarenko, O.Yu. Sliusarenko, Kinetic theory of weakly ionized dilute gas of hydrogen-like atoms of the first principles of quantum statistics and dispersion laws of eigenwaves, J. Math. Phys. **58**, 113302 (2017).

85. A.G. Zagorodny, Yu.V. Slyusarenko, and S.N. Shulga, Kinetics of low-temperature gas of hydrogen-like atoms in an external electromagnetic field, Low Temperature Physics, **44**, (2018) 1049; doi: 10.1063/1.5055846.

86. A.S Peletminskii, S.V. Peletminskii, and Yu.V. Slyusarenko, Bose–Einstein condensation of heteronuclear bound states formed in a Fermi gas of two atomic species: a microscopic approach, J. Phys. B: At. Mol. Opt. Phys. **50,** 145301 (2017).

87. S. Fujita, *Introduction to Non-equilibrium Quantum Statistical Mechanics*, (Saunders (W.B.) Co Ltd, December 1966).

88. Wolfgang P. Schleich, *Quantum optics in Phase Space*, (WILEY-VCH, Berlin*Weinheim*New York*Chichester*Brisbane*Singapore*Toronto 2001).

89. Yu.V. Slyusarenko and O.Yu. Sliusarenko, "*Ab initio* quantum-statistical approach to kinetic theory of low-temperature dilute gases of hydrogen-like atoms," e-print arXiv:1612.02245 [cond-mat.stat-mech] (2016).

УДК 538.11
PACS number(s): 64.60.-i; 62.20.-de; 75.47.Np; 75.80.+q

CHAPTER IV

A WORLD OF STRATEGIES WITH MEMORY

V. M. Kuklin*, A. V. Priymak*, V. V. Yanovsky*, **

**V.N.Karazin Kharkiv National University, pl. Svobody, 4, 61000, Kharkiv, Ukraine*
***Institute of Single Crystals, National Academy of Sciences of Ukraine, Nauki Ave. 60, 61001 Kharkov, Ukraine*

Various scenarios of the evolution of populations of strategies with memory are considered. The strategies interact with each other in an iterated prisoner dilemma, earning evolutionary benefit points according to the pay-out matrix. The review focuses on collective characteristics such as memory, the level of aggressiveness (the share of refusals to cooperate), and the complexity of strategies. Different scenarios of evolution appear when using different selection rules for strategies intended for deletion in the corresponding generation. Cases of zeroing evolutionary advantage points after each cycle (or generation) and summing (inheriting) points of previous cycles are considered. In the first case, as a result of evolution, complex strategies with a large depth of memory dominate and are not aggressive – inclined to cooperation. The history of the evolution of a population is divided into two periods: the primitive period and the period of the developed 'community'. The primitive stage in the development of the world of strategies can be distinguished according to the following features: 1). the presence of all the most primitive strategies; 2). an increase in average aggressiveness); 3). the presence of the most aggressive strategy. In the second case, as a result of increased competition, complex strategies with a large memory depth, but aggressive ones, also win. In anomalous competition, when the most successful strategies are removed, an increase in aggressiveness is also observed for complex strategies with a large memory depth. It was empirically found that in the process of population evolution, a universal relationship between aggressiveness and points of evolutionary advantages persists, for example, a decrease in the value of points obtained with an increase in the average aggressiveness of the population is observed. Open societies, in which complex strategies with a large memory (replacing the remote losers) are injected, demonstrate greater efficiency; complex strategies with a large memory depth and less aggressive ones dominate in the emerging stationary

state. Penetration in this way into open populations of primitive strategies (with a low memory depth) leads to their dominance in a stationary state, although their average aggressiveness decreases, while around complex strategies with a greater memory depth in the population remains. The case of interaction of 50 thousand objects, each of which uses 50 strategies, is considered separately. When interacting, the losing strategy is replaced by the winning strategy. As a result, on average, subjects retain one third of strategies, and complex ones with a large memory depth dominate.

***KEYWORDS**: evolutions of populations of strategies, object with a set of strategies, prisoner dilemma, memory complexity, aggressiveness.*

***PACS numbers:** 02.50.Le, 05.10.–a, 87.23.Kg, 89.75.Fb*

SECTION 1. INTRODUCTION

A huge number of species of various living beings live on Earth. Several million species are now known. Moreover, as follows from [1], only the percentage of the total number of species is described. Among such a huge number of species, only 20 are known that have discovered social structures and social behavior. Surprisingly, these are the most thriving species. And humanity has even taken an absolutely dominant position. Other social species, such as ants, are perhaps even more successful. This is evidenced by the huge period of existence and their prevalence. It is known that the total weight of ants is approximately equal to the weight of all mankind. This raises two important questions. The first is how in the process of evolution, controlled by egoistic genes, social behavior arises that requires the manifestation of altruism and cooperation. Second, if the formation of societies is so beneficial, then why so few species have opened this way. In fact, the problem is even more complex. In some of these societies, the ultimate form of altruism is achieved, in which some individuals do not reproduce and care for the offspring of breeding individuals. For such communities, a special term has even been coined – eusociality. Research in this direction is actively developing [2].

It should be noted that similar questions should arise when creating artificial life. Understanding the nature of the emergence of cooperative behavior in different systems has been of interest to researchers for several decades.There are many approaches to creating evolution models. They can be conventionally divided into two approaches, one deterministic and the other probabilistic. An example of the first approach is a logistic mapping for population growth in discrete time. An example of a probabilistic approach is the derivation of the Hardy–Weinberg law [3], which is one of the fundamental principles of evolution during sexual reproduction. Each of these approaches is divided into continuous and discrete models. As a continuous approach, the Verhulst equation can be used to study population changes (a continuous analog of the logistic mapping). Discrete models include multi–agent systems.

After the development of game theory and its application to the description of evolution by John Maynard Smith [4], this approach became very popular. Evolutionary game theory [5] – [7] provides flexible foundations and effective methods for studying the emergence of cooperation. Among the many game models that are used to explain cooperative behavior, a special place is occupied by games, which can be viewed as a generalization of the prisoners' dilemma [8], [9], [10]. The choice of the payout matrix in this case is determined by a simple physical consideration. Cooperation always requires additional expenditure of resources in comparison with the refusal of cooperation. The tendency to save resources or efforts is manifested in the payout matrix in the fact that for each individual interaction, the individual gain in refusing to cooperate exceeds the gain in agreeing to cooperation.At every stage of the evolutionary process or generation, the population refuses to apply the least successful strategies of the previous generation.

These games serve as a paradigm that led to the discovery of the mechanism of cooperative behavior in both theory and experimental observation [11]. Since the work of Novak and May [12], evolutionary games have been extensively studied in structured populations, including on regular lattices [13–21] and complex networks [22–38]. Currently, a number of specific mechanisms have been discovered that lead to cooperation in a wide variety of systems (see, for example, [39]). Among such mechanisms, it should be noted: voluntary participation [40], punishment [41], similarity [42], heterogeneous activity [43], social diversity [44,45], dynamic connections [46], asymmetric interaction and the permutation graph [47] , migration [48–50], group favoritism [51], interactions between networks [52]. Using this approach, it is possible to find out the appearance of many different properties in evolving populations. By evolutionary populations, following Darwin, we mean a set of objects that obey the following principles. These are 1) the principle of heredity, 2) the principle of variability, and 3) natural selection.

In this review, we will analyze the impact of memory on various evolutionary scenarios. If the action of an object depends not only on the observed situation, but also on previous events, then we will assume that the object has memory. In this sense, most biological objects have memory. The main question that we will discuss in this work is how beneficial it is for the population to increase memory in the process of evolution and what consequences this leads to. The memory depth of the objects of the population determines the number of all possible strategies available in the population. An important element is the competition in the initial population of all possible strategies with upper bounded memory.

The second issue that is raised here is related to the discussion of the properties of competing strategies that lead to changes in the dominant strategies of the population in the process of evolution. Complexity is introduced and used as a characteristic of strategies. The main question boils down to: Is the complexity of strategies evolutionarily beneficial? On an intuitive level, the answers to these questions seem obvious. In modeling the interaction of strategies, a one–particle approximation was used, in which all

agents of the population professing one of the possible strategies were combined into a single cluster. Interaction took place between clusters or strategies. In other words, it is the strategies that interact. Moreover, each strategy interacts with everyone, including itself. Three types of populations are considered. Populations without memory, populations with memory depths 1 and 2.

In each case, the initial population contains all strategies with memory not exceeding the specified one. So, for example, at a memory depth of 2, all strategies with memory 2, 1, and 0 are present. As a result of numerical modeling, it is shown that increasing memory in a population is evolutionarily beneficial. Evolutionary selection winners are invariably the highest memory agents. Strategies that win in natural selection have maximum or near maximum difficulty. Along the way, it was found that in such populations the winning strategies were referred to as 'respectable' strategies inclined to cooperate. In a sense, it can be said that cooperative behavior in such cases is often established automatically. One might expect this to be a universal trend. In populations with upper–bounded memory, the competition of all possible strategies in the initial population leads to the dominance of respectable strategies in the course of evolution. A further increase in the depth of memory leads to a new problem when the number of agents in the population turns out to be less than the number of possible strategies. The consequence of this is also discussed in the conclusion of this work.

SECTION 2. STRATEGIES POPULATIONSAND THEIR EVOLUTION

Let's start by defining the population. Comes from the Latin *populus*– population, people."A population is understood as a set of individuals of a certain species, for a sufficiently long time (a large number of generations) inhabiting a certain space, within which one or another degree of panmixia is practically carried out and there are no noticeable isolation barriers, which is separated from neighbouring similar populations of individuals of a given species by this or a different degree of pressure of certain forms of isolation "[65]. In principle, the understanding of the term population is rather vague and differs in biology, medicine, sociology, ecology, demography.

In this review, a population of strategies will be understood as a subset of individuals of the population that use a strictly defined strategy of behavior. This definition simplifies the study of carrying out strategies in a population. First of all, eliminating the need to consider many of the same strategies and their interaction with many other similar strategies.

In a sense, this corresponds to the one–particle approximation in which individuals with the same strategy are considered as one object or superspecial object of the population.

The evolution of such objects is determined by the principle of heredity, the principle of variability and natural selection. By heredity we mean the transfer of a strategy to the next generation. We will not use the principle of variability of strategies at this stage of the study, having included in the initial

population all possible strategies with a certain depth of memory. In other words, there are no other strategies which they can be changed or modified, since all strategies are present in the population. Even if we allow for mutations of strategies, they will mutate into strategies available in the population.

SECTION 3. STRATEGIES INTERACTION IN THE POPULATION

The life in a population and its evolution is determined by the nature of the interaction of the strategies of the objects of the population. At the same time, three elements of interaction with whom, how and how much should be distinguished. This means three different rules. The first is how to make a choice of an "opponent" in terms of interaction. Second, what are the rules for interaction. The third is how to evaluate the results of interaction. All these rules can be divided into two classes – deterministic and random rules. In this review, we will focus on deterministic rules.

The simplest case is the pairwise interaction of strategies.There are many options for implementing this interaction. The simplest option is that each strategy interacts with everyone, including itself. This type of interaction can be carried out with a relatively small number of objects. The reason for this is the finiteness of the lifetime of a population object.

Indeed, some characteristic time is spent on the interaction of a pair of strategies and, accordingly, time will be spent on the interaction of strategies with each other. When increasing, the time can exceed the lifetime of the object.

Another way of pair interaction is when the opponent is chosen at random among the entire set of strategies, assuming they are equally probable. Another general technique that does not use randomness can be accomplished using a network of interactions. In the graph of this network, interacting strategies will be connected. It can be generalized by taking into account the interactions of distant vertices with some weight, including probabilistic. It is also possible to take into account the spatial structuring of populations [11], [13], [17], [23], [42], [59], in this case geometric structures of cooperation may arise in space [12], [60]. Another important circumstance that affects the nature of the interaction of strategies has already been noted earlier. It is the finiteness of the set of objects that make up the population. In this case, the number of strategies can significantly exceed the number of objects in society. Then interaction can occur only between a part of the strategies.

In the review, we will assume that the object does not change its strategy in the course of its life and interacts with each strategy of the population, including itself. In other words, we can say that a one–particle approximation of the interaction of strategies is considered – without taking into account the number of carriers of the strategy. The exception is the section12 in which the exchange of strategies appears. Let's move on to discussing how to interact. In accordance with the chosen rule, the two strategies interact, which in the

simplest case consists in choosing a solution to cooperate or to refuse to cooperate. The adoption of such a decision is determined by the corresponding strategy. However, with a single interaction, a strong sensitivity to the choice of the first move remains. In order to avoid such dependence, the act of interaction will consist of many moves. In other words, the interaction of strategies follows the iterated prisoners' dilemma [61].

The number of interactions of two strategies in one generation is chosen to be the same for all. Actually, the choice of a large number of interactions between the two strategies is designed to exclude the influence of the first move [64].

Let us discuss the effect of the interaction of the first move on the result. It seems natural that its influence decreases with an increase in the number of moves when the two strategies compete. Indeed, the total pay-off S_n with the number of moves n consists of two contributions – this s_0 is the number of points obtained after the first move and a set of points already using the strategy. Let the strategy, starting from the second move, gain $\overline{q}$ points on average per move. Then the total payoff is equal $S_n = s_0 + \overline{q}(n-1)$ and for large $n \gg 1$ we obtain

$$\frac{S_n}{n} = \frac{s_0 - \overline{q}}{n} + \overline{q} \qquad (1)$$

Considering that s_0 it can take on a finite value, it is easy to see that the contribution of the first move to the average value of the winnings per one move should be small. Based on the results of numerical simulation [64], it can be assumed that with an increase n, the influence of the first move disappears. For strategies with zero memory depth, this influence can be neglected even with this effect [64]. It should be expected that $n \sim 100$, for a similar reason, the influence of the first moves will be insignificant even for large memory depths.

In order to establish the result of the interaction of strategies, we define the payout matrix. Recall that the prisoner's dilemma of two players is that each player can choose between cooperation (1) or rejection (0). Depending on the opponent's strategy, the chosen player gains a_{11} if both cooperate; a_{22} – if both refuse; a_{12} – if the chosen one cooperates and the opponent refuses; and a_{21} – if the chosen one refuses and the opponent cooperates, where $a_{21} > a_{11} > a_{22} > a_{12}$ and $2a_{11} > a_{21} + a_{12}$. In the review, we use the values of the Axelrod pay-out matrix [61],

Table1

	Cooperation	Refusal
Cooperation	3,3	0,5
Refusal	5,0	1,1

Thus, the result of the interaction of strategies will be determined by this matrix. Each strategy interaction brings them a certain amount of evolutionary advantage points. These points will play an important role in preserving strategies in the future generation. We implement natural selection as follows. Let all strategies interact with each other in a circular manner in an iterated game of prisoners' dilemma. The number of interactions of two strategies in one generation is chosen to be the same for all. As a result of this competition, strategies gain points in accordance with the selected payout matrix. After all the interactions between the strategies and their accumulation of evolutionary advantage points have taken place, the losing strategy, and possibly several strategies with the minimum number of points, drop out of the next generation. Further, the points of evolutionary advantages are reset to zero and the next circle of interactions between the remaining strategies is carried out, corresponding to the formation of new generation strategies. We will discuss other options for recruiting points in more detail in the relevant sections where such changes appear.

SECTION 4. INTERACTION OF THE STRATEGIES

Strategy is the rule by which the move is made after the opponent's move, or if the strategy starts the game, then the rule by which it makes the first move. In order to list all such strategies, it is necessary to describe all the rules of reaction to the meaning of the opponent's moves. Such rules can be specified as a function or as a table. However, when designating a move from a binary alphabet $B = \{0,1\}$, the strategy can be specified in the form of a finite $-0,1$ sequence.

Indeed, let's start with the first move of the strategy if it starts the game. In this case, it is enough just to indicate its first move, for example $[0]$. If it starts the game with move 1, then it is $[1]$ also convenient to consider such a strategy as another strategy. Now we will discuss the rule of choosing a move by this strategy after a known move of the enemy. To do this, consider all the possible moves of the enemy. In our case, there are only two possibilities – the opponent can make a move of 0 or 1. It is clear that the strategy can be set by the following table

Table 2

Opponent's possible move	0	1
	⇓	⇓
Strategy response	0	0

In this table, the arrow indicates the strategy's response to the corresponding move of the rival- enemy. So the given strategy reflects the opponent's move in the strategy move. In other words, a strategy S_0 is a mapping $B \overset{S_0}{\to} B$.

It is easy to understand that if we agree on the order of recording the possible values of the opponent's moves, for example, in lexicographic order (as in the table in the top row), then to describe the rules of the strategy, it is enough to know only the bottom row or the sequence of zeros and ones. In the above case, this is a sequence 00 that can be considered as the name of this strategy, defining the rule of its actions.Since each strategy corresponds to a certain sequence of retaliatory moves, it can also be used as the name of the corresponding strategy. In this case, the name also defines the rule for the action of the strategy. It is easy to see that there are only four strategies shown in table 00 and another 01, 10, 11 strategies. Among these strategies, two are trivial. This is an extremely aggressive strategy 00 and mindlessly compromising 11. The other two are less trivial. So, for example, strategy 10 observing the opponent's move 0 will answer 1, and observing 1 in response will give 0. If we also take into account the rule of the first move, the full name of the strategy can be designated as [0] 10.Here, the first move that this strategy will execute is indicated in brackets, and the rest of the numbers determine the rule of the retaliatory move. Note that the strategies described above make a move by observing the opponent's move. In this sense, such strategies do not use data on the previous moves of the opponent and, therefore, we can assume that they have no memory. In what follows, we will assume that such strategies have a depth of memory 0 .

Thus, strategies with zero memory depth are defined by $0,1-$sequences of three elements $[x_0]x_1x_2$, where $x_0, x_1, x_2 \in B$ .Then the name of each strategy with zero memory depth is determined by a binary number with three digits. A complete description of such strategies also contains an indication of the first move of the strategy. The number of all such strategies is equal $2^3 = 8$.

SECTION 5. STRATEGIES WITH THE MEMORY

In this section, we will discuss how the strategy memory is introduced. There are several possibilities for describing strategies with memory. A convenient characteristic for such strategies is the memory depth, which determines the number of such strategies.

5.1. Memory of strategies

Let's take a look at all the strategies that use memory. Let us introduce the space of such strategies. As noted above, a strategy is a rule by which a move is determined by the known values of the opponent's moves. To classify them, we use the depth of memory. By the depth of memory we mean the number of previous moves of the opponent, which the strategy uses to make a move. The simplest strategies that do not use

memory have been described above. This means that such strategies make a move based only on the opponent's observed move.

Let us now consider all strategies with the memory of one previous move. Such strategies should take into account the opponent's two moves. Previous and observable. Then the number of possible variants of the opponent's moves increases, and the strategy must determine the retaliatory move, taking into account the previous move of the opponent. Let us again arrange all possible pairs of the opponent's moves in lexicographic order:

Table 3

Opponent's possible moves	00	01	10	11
	⇓	⇓	⇓	⇓
Strategy responses	…	…	…	…

To describe the strategy, each pair of opponent's moves must be matched 1 or 2. In other words, replace the points in the table with symbols 1or2 andthe strategy with memory about one move matches the mapping $B^2 \xrightarrow{S_1} B$. Again, with a fixed order of writing the opponent's possible moves (top row of the table), each strategy is determined by a $0,1$–sequence of 4 elements (bottom row). The name of the corresponding strategy can be selected again to match the rule of its action. Thus, the memory depth strategy names are the same as a binary number with 4 digits, or a sequence of zeros and ones of 4 characters.

A trivial aggressive strategy is called 0000. There are again as many such strategies as there are numbers from 0000 to 1111. In other words, them16. In absolutely the same way, you can define strategies with a depth of memory k . Such strategies will be defined as a signed binary number 2^{k+1}. Thus, the space of strategies with a memory depth k is $0,1$–sequences of 2^{k+1} symbols. Geometrically, this space can be represented as the vertices of a unit cube in 2^{k+1} dimensional space. So, for example, strategies with zero memory are the vertices of a unit square (see Fig. 1) in two–dimensional space, and strategies with a memory depth of 1 correspond to vertices of a unit cube in four–dimensional space.

However, the above description of depth–of–memory $k \geq 1$ strategies is not complete. The reason is that after the first move of the opponent we know only one observed value and there is no value of the previous move. Therefore, there is not enough data to apply the specified rules of the strategy. Thus, we must indicate the rule of how to make a move when the data is incomplete. For this, it is natural to use one of the memory strategies. In other words, we should indicate a strategy that does not use memory, which we will apply before information about the previous move of the enemy appears.Then the total number of strategies naturally increases and the name of the strategy changes. In the name, we must first indicate the strategy for determining the move in the absence of data on the previous move (i.e. the name of the strategy with memory depth 0) and then the name of the strategy with memory. Thus, the name (and rules) of the strategy with the memory of one previous opponent's

move looks, for example, like[01]0111. The first two digits in brackets are the name (and rules) of the strategy with memory 0, and the next four are the rules of the player's moves with the memory of one opponent's move. For convenience, strategies with less memory will be assigned to the left and enclosed in square brackets.Considering each such rule as a separate strategy, one can easily calculate the number of such strategies.

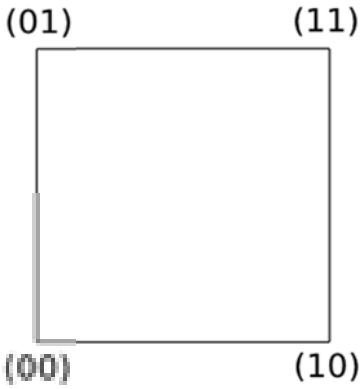

Fig. 1 A unit square on a plane with the indication of the coordinates of the vertices

Consequently, the total number of strategies with the memory of one previous opponent's move is equal $2^2 \times 2^4$. In addition, each strategy can start the game from some first move. In other words, it can start at 0 or 1. It is convenient to think of strategies that make different first moves 1or 0 as different strategies. Then the number of strategies will double $2 \times 2^2 \times 2^4 = 128$. The name of such strategies will look like, for example, [0][01]0111 this strategy will start the game from move 0. In particular, the well–known 'tit–for–tat' strategy in these designations corresponds to the strategy.It should be noted that if you know the memory depth, in this case equal $k = 1$, you do not need to use parentheses. Even if they are absent in the strategy record in the form of a definite sequence of 0.1, a rule of strategy action is unambiguously established for a given memory depth.

All strategies with the memory of the opponent's two moves, or in the general case with the memory of the opponent's moves, are listed in absolutely the same way. It is important to emphasize that the number of strategies $N_k = 2 \times 2^2 \times 2^3 \cdots 2^{2^{k+1}} = 2^{(2^{k+2}-1)}$ grows super exponentially with increasing memory length or depth k.

Let's return to the consideration of strategies with a depth of memory 1. Note that among these strategies there are strategies with zero memory depth. Indeed, if the strategy acts in the same way for different previous moves of the opponent, then it actually does not use information about the previous move or loses memory of the previous move. Accordingly, such

strategies coincide with strategies with zero memory depth. The rules of action of strategies equivalent to strategies with zero memory are defined by the following table

Table 4

Opponent's possible moves	00	01	10	11
	⇓	⇓	⇓	⇓
Strategy responses	x_1	x_2	x_1	x_2

Where x_1 and x_2 take values $\{0,1\}$. It is easy to see from the table that such strategies operate independently of the opponent's previous move. This means that strategies $x_1x_2x_1x_2$ are equivalent to zero memory strategies x_1x_2. Thus, among the strategies with the names of four–digit binary numbers, there are strategies equivalent to all strategies with no memory. So strategies $0000 \sim 00$, $0101 \sim 01$, $1010 \sim 10$ and $1111 \sim 11$. Therefore, when writing strategy names as four–digit binary numbers, all strategies with a memory depth less than or equal to 1 are present among them.

It is easy to understand that this convenient property will also be preserved when describing strategies with a greater memory depth. So the names of the depth–of–memory k strategy contain all strategies equivalent to the depth–of–memory strategies $k-1$, ... 0. This property should be taken into account when playing games between strategies. Thus, we have identified and listed all strategies with a certain finite memory depth. Therefore, further, if we talk about strategies with a depth of memory k, then we will remember that they include all strategies with a lower memory depth. These strategies include both primitive and complex strategies. Now let's discuss in more detail the concept of strategy complexity.

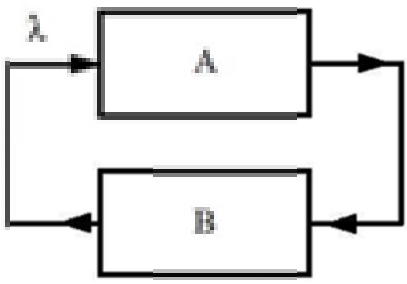

Fig. 2 The game of automata of two strategies is shown and the input symbol indicates that the strategy starts in this game

It is interesting to note that each strategy with memory can be viewed as a finite state machine [66]. For example, let us show which automaton corresponds, for example, to a strategy $A = (x_0)(x_1x_2)(x_3x_4x_5x_6)$ with a memory depth of 1, where $x_i \in B$ for $i = 0,1,2,\ldots,6$. The number of possible input signals

of such an automaton is 3. This is an empty signal λ , after which the strategy makes the first move and two game signals 0 or 1 received by the opponent's moves. The number of states of the automaton is also 3. This is the initial state q_0, waiting for the start` of the game and two states q_1, q_2.

The automaton corresponding to this strategy is determined by the following transition and exit functions

Table 5

The transition function of the automaton corresponding A

x \ q	q_0	q_1	q_2
λ	q_0	–	–
0	q_1	q_1	q_1
1	q_2	q_2	q_2

Table 6

Function of the outputs of the machine corresponding A

x \ q	q_0	q_1	q_2
λ	x_0	–	–
0	x_1	x_3	x_5
1	x_2	x_4	x_6

Dashes in the tables correspond to unrealizable situations. The symbol can be applied to the input only of the machine in the initial state. Such state machines are called partial state machines. In principle, the dashes can be filled in any way. Then the interaction or game of two strategies, for example A and B , is determined by the automata scheme, which is shown in Fig. 2. Thus, the interaction of two strategies can be viewed as the interaction of two finite state machines. From this point of view, the evolution of strategies is closely related to the evolution of finite state machines.

Note that the discussed memory strategies only react to memorized previous moves of the opponent not their own previous moves.

It is easy to remove such a restriction and build strategies that remember their previous actions and the opponent's moves. In other words, the strategy remembers a finite number of all previous moves or part of the history of the game. Such strategies were considered earlier in [53]. However, the use of such more general memory strategies is computationally intensive.

5.2. Complexity of strategies

In the previous section, it was shown that strategies are described by 0,1–sequences of a certain length or containing a certain number of members. So for the memory depth 0of such sequences 4, and for their

memory depth k there are $N_k = 2^{2^{k+1}}$ sequences, the length of the names of such strategies is 2^{k+1}. Of course, among these strategies there are strategies that are equivalent to all strategies with a smaller memory depth. The number of such strategies is also determined by their memory depth.

Thus, strategies can be characterized by the depth of memory. Another important characteristic is its complexity. On an intuitive level, it is clear that some strategies operate simply for example the 0000 strategy, others are more complex. Let's discuss ways to determine the complexity of strategies. Taking into account that strategies are described by $0,1$–sequences, let us discuss such property of $0,1$–sequences as complexity. It is an extremely deep concept that has important applications in physics and mathematics. In particular, the concept of chaos is closely related to the concept of complexity (see, for example, [55]). There are a huge number of approaches to determining the complexity, some of which can be found in the review [54]. The most natural choice of this characteristic can be considered the complexity according to Kolmogorov [56].

Let's introduce a universal way of describing a finite $0,1$–sequence using a Turing machine [57]. Indeed, for any sequence, one can associate a program under the control of which the Turing machine will print it. It is clear that there are infinitely many such programs for the chosen sequence. Therefore, following Kolmogorov, we define the concept of complexity [56]. Let the machine M print the ***zero***-one *sequence* of length n. The complexity K_M coincides with the length of the shortest program, after the execution of which the machine will print the given $0,1$–sequence $x = \left(x_1, x_2, ..., x_n\right)$

$$K_M = \begin{cases} \min \ell\left(P\right), & if\ M\left(P\right) = x \\ \infty, & if\ M\left(P\right) \neq x \end{cases},$$

Such a description of the complexity of $0,1$–sequences is the most acceptable and is used in determining, for example, finite chaotic sequences. However, here we are faced with the enormous difficulty of calculating the Kolmogorov complexity. In fact, there is no effective algorithm for calculating the Kolmogorov complexity, this problem is algorithmically unsolvable.

Therefore, we use a different approach to describing the complexity of finite $0,1$–sequences, which is based on the comparative complexity of functions, in particular, polynomials or polynomial functions. It is based on the understanding that higher degree polynomials are more complex than lower degree polynomials. Even Newton noticed that if the n–degree polynomial is differentiated n time, then we get a constant, and the derivative of it vanishes. This property is characteristic. In other words, if the n–th derivative of some function vanishes, then it is a $n-1$–degree polynomial. Thus, differentiating the polynomial gives a polynomial of lesser degree and, accordingly, less

complex than the original one. We use similar considerations following [58] to determine the complexity of finite 01–sequences. Further, we will be interested not in arbitrary 01–sequences, but in those that correspond to strategies with memory. Recall that strategies with memory depth m correspond to 01–sequences of length $n = 2^{m+1}$ and they belong to a finite set M containing $2^{2^{m+1}}$ members.

Such sequences $x = x_1 x_2 ... x_n$ can be thought of as functions that make up an integer $i \in \{1, 2, ...n\}$ value $x_i \in B$ or display $i \xrightarrow{x} x_i$. In order to use the previous considerations, it is necessary to introduce an analogue of the differentiation of such discrete functions. Taking differences is suitable as such an operation, which also goes back to Newton's idea [58].

In our case, we define the action of the difference operator $A : M \to M$ that transforms the sequence x into the sequence y

$$y = Ax$$

where the elements of the sequence $y = y_1 y_2 \dots y_n$ are determined by the differences $y_i = x_{i+1} - x_i$.

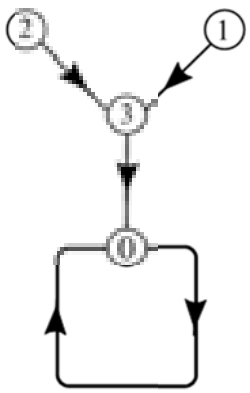

Fig. 3 A graph of strategies with zero memory. Here, for the sake of compactness, the vertices are shown by circles, inside which the strategy names are encoded in the decimal system. So the sequence 00 *is designated as 0, vertex* 01 *as 1, vertex* 10 *as 2, and finally* 11 *as 3*

Here $i = 1, 2, \dots, n$ is the item number in the sequence. When calculating the elements of a sequence y, we will use the condition that the sequence is cyclic x, counting $x_{n+1} = x_1$. In other words, we can talk about

periodic sequences of a period n. Such an operator maps a sequence x of length n to a sequence y also of length n.

$$x \xrightarrow{A} y$$

Thus, this operator maps a strategy x to a simpler strategy y. Using this property, let us compare all strategies of memory depth m with a graph positioning strategies in terms of complexity. In such a directed graph, each vertex will correspond to a certain strategy. The number of vertices of such a graph is equal to $2^{2^{m+1}}$. The edge in such a graph leaving a vertex x indicates which strategy, after applying the operator A to it, it will go and end at the corresponding vertex y. Only one edge can go out of each vertex – a consequence of the uniqueness of the "derivative".

Consider strategy graphs starting with a shallow memory depth. For sequences of length n, the graph contains 2^n vertices. Let's start with zero memory depth $m = 0$. Such strategies coincide with sequences of two elements $n = 2^{0+1}$. So the graph has 4 vertices corresponding to strategies 00, 01, 10 and 11. Applying the operator A to these strategies, we obtain the following transitions

$$00 \xrightarrow{A} 00$$
$$01 \xrightarrow{A} 11$$
$$10 \xrightarrow{A} 11$$
$$11 \xrightarrow{A} 00$$

Depicting vertices by points and connecting vertices with directed edges in accordance with the results of the operator's action A, we obtain a strategy graph with zero memory depth shown in Fig. 3. A loop or cycle going out from the top 00 and entering it arises because of the first relation.

A characteristic feature of this graph is the presence of a cycle of unit length. The length of the cycle is equal to the number of vertices included in the cycle. We will use the notation for this graph $O_1 * T_4$ in accordance with [58]. Where O_1 means a cycle of unit length, and T_4 – a binary tree with 4 vertices. It can be proved that the strategy graph will always have only one cycle O_1.

Now let us formulate the complexity as the distance of the vertices of the graph from the root of a tree or cycle [58]. The more distant the vertex is from the root of the tree, the more complicated the strategy. So 00 has zero complexity, 11 has complexity equal to 1 and two vertices (or strategies) 01 and 10 of complexity 2, they are removed from the root 00 by two edges. We will use this definition of complexity in this work.

Accordingly, among the strategies with zero memory, the simplest strategy is the most aggressive strategy 00 (see Fig. 3). She refuses any suggestions. This strategy corresponds to a constant argument function i that takes a zero value.

A more complex strategy is a mindlessly compromising strategy. This strategy is the same as a constant argument function i that takes a value of 1. "Differentiating" this function translates it into a function that takes a value of 0. Strategies 01 and 10 define linear functions. Indeed, the strategy 01 corresponds to a linear function $x(t) = (t+1) \bmod 2$, and the strategy 10 to a linear function $x(t) = t \bmod 2$. It is easy to check, for example, that the values of the function $x(t) = t+1 \bmod 2$ for integers t give a periodic sequence with period 2 and $x_1 = x(1) = 0$, $x_2 = x(2) = 1$.

Similarly, it is easy to check that the sequence 10 corresponds to the values $x(t) = t \bmod 2$ at the integer points $x_1 = x(1) = 1$, $x_2 = x(2) = 0$. This coincides with the intuitive conclusion that constant functions are simpler than linear functions.

Linear functions are a special case of polynomials of degree less p.

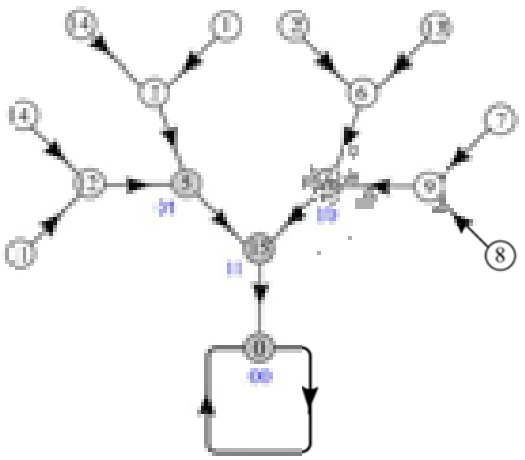

Fig.4 Graph of strategies with memory depths of 1 and 0. Strategies equivalent to strategies with zero memory depths correspond to the vertices marked in grey. The coding of strategies and, accordingly, vertices is carried out as before by recording the names of the strategies in the decimal system. Vertices are named 0000 from to 1111

Let us now turn to the strategy graph with memory depth 1. This graph is shown in Fig.4. It is easy to see that the structure of the graph is consistent $O_1 * T_{16}$. Let us discuss the location on this graph of strategies equivalent to strategies with zero memory depth. These strategies are shown in Fig. 4 with the tops shaded in grey.

The names of their equivalent zero–memory strategies are printed next to them in grey. Thus, these strategies are the simplest among strategies with a memory depth of 1. This exactly coincides with the fact that the complexity of strategies as functions i increases with distance from the root of the graph. The rest of the strategies are further away from the root and, accordingly, more complex. You can make sure that the next level of the graph corresponds to polynomials of degree 2, and the top to polynomials of degree 3. Indeed, acting on the top of the 5th level as $x^{(5)}$ an operator A, by definition, we go to the top of the 4th level $Ax^{(5)} = x^{(4)}$.

This is an obvious consequence of the structure of the tree. Similarly, the top $Ax^{(5)} = x^{(4)}$ will go down $Ax^{(4)} = x^{(3)}$ one level under the action. Repeating the action again, go to the level below $Ax^{(3)} = x^{(2)}$ and finally get $Ax^{(2)} = x^{(1)} = 0$. Combining these equalities, we get $A^4x^{(5)} = 0$. We can say that it is an attractor 0 of the movements induced by the mapping A. Then, according to Newton's proof, the top of the fifth level $x^{(5)}$ coincides with a polynomial of degree less 4.

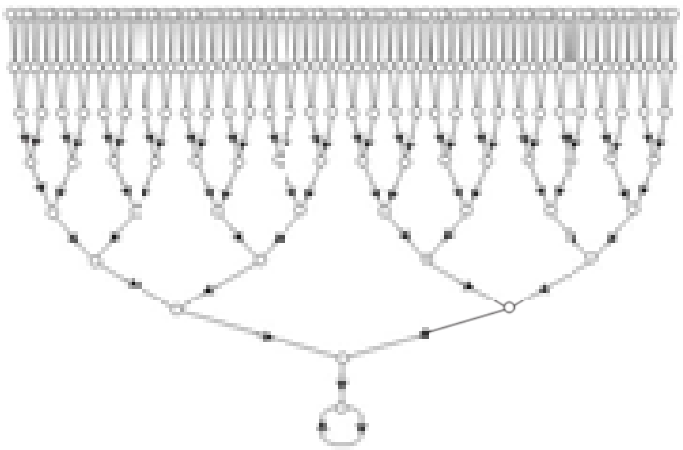

Fig.5 Strategy graph with memory depth 2. Of course, it is not possible to specify the names of the strategies in this figure

Now we will discuss the graph corresponding to strategies with memory depth m. In this case, the length of the 0,1–sequence of the defining strategy is $n = 2^{m+1}$. The total number of such strategies and, accordingly, the number of vertices in the graph. It can be proved that for $n = 2^{m+1}$, the structure of the strategy graph coincides with $O_1 * T_{2^{2^{m+1}}}$. Naturally, at the root, there are still strategies equivalent to strategies with zero memory depth, higher with a memory depth of 1, and so on up to the level

corresponding to the last level of the strategy graph with depth $m-1$, i.e. $O_1 * T_{2^{2^m}}$.

Thus, the number of strategies using exactly the memory depth m is equal $2^{2^{m+1}} - 2^{2^m} = 2^{2^m}(2^{2^m} - 1)$. As we move away from the root, the strategies become more complex and correspond to polynomials of ever higher degree. Thus, the complexity of strategies can be determined by the value of the level of the graph to which the vertex corresponding to this strategy belongs. For memory depth m, the graph contains strategies of maximum complexity $C_{max} = 2^{m+1}$. The number of such strategies in the graph is the largest and the number of strategies with a certain amount of complexity C can be easily calculated $N_C = 2^{C-1}$ for $0 < C \le C_{max}$.

As an example, in Fig. 5 we give a graph corresponding to strategies of length $n = 2^3 = 8$ ($m = 2$), which coincides with $O_1 * T_{256}$. It is difficult to indicate the names of the strategies in this figure. Maximum complexity of strategies $C_{max} = 2^{2+1} = 8$. The number of such strategies $N_8 = 2^{8-1} = 128$, strategies of complexity $C = 7$ is less and equal $N_7 = 2^{7-1} = 64$.

It is important to note that the number of possible strategies grows super exponentially with memory growth. This leads to deep computational difficulties associated with scarcity of resources when investigating the interaction of such strategies. In addition, it is interesting to note that the number of implemented strategies in finite systems is limited rather by the number of participants, and not by the number of possible strategies. In other words, in finite systems in the process of evolution, a new strategy can always appear and be used. Life is full of new ideas. This conclusion plays an important role in the numerical simulation of the interaction of a finite number of objects in the population.

5.3. Aggressive strategies

The next property of strategies, which will interest us in the future, can be called the aggressiveness of strategies. We will consider refusal to cooperate as a manifestation of aggressiveness; the more refusals a strategy makes, the more aggressive we will consider it. Thus, as a quantitative characteristic of aggressiveness, one can use the average number of refusals of a strategy from cooperation or cooperation per one move. In other words, the relative share of refusals to cooperate is the ratio of the number of refusals to the number of all strategy moves. In this case, an absolutely aggressive strategy (0) (00) will have an aggressiveness equal to 1, the rest of the strategy is the value of aggressiveness from the interval [0,1]. Of course, it is possible to introduce a definition of aggressiveness and in

a more realistic way, taking into account only refusals after the offer of cooperation as a manifestation of aggressiveness.

SECTION 6. COLLECTIVE VARIABLES DESCRIBING THE PROPERTIES OF POPULATIONS

Let's discuss a way of describing the behavior of strategies in the process of evolution.With the advent of memory and an increase in its depth, the number of strategies increases in a super exponential manner and makes it impossible and meaningless to track the behavior of each strategy. We need a rough description of a population of strategies. Therefore, it is necessary to introduce collective variables that make it possible to describe a huge number of strategies.

Let us introduce collective or coarse variables that make it possible to track certain groups of strategies, combined according to certain qualities or properties. For us, properties such as the depth of memory of strategies and the complexity of strategies will be important. Therefore, in what follows, we will use the number of strategies a_i with the i–th memory depth and the number of strategies n_i with the i–th complexity as coarse variables. So, for example, a_1 is the number of strategies with a memory depth of 1, and n_3 is the number of strategies of complexity 3. Such coarse variables make it possible to control the change in memory and the complexity of strategies of large populations of strategies during evolution.

These variables can also be given a probabilistic meaning by introducing the probability $P_i = \dfrac{a_i}{\sum a_j}$ of finding a strategy with a depth of memory i in the population and the probability $P_{ci} = \dfrac{n_i}{\sum n_j}$ of finding a strategy of complexity i. In principle, complexity allocations n_i are more fundamental than memory allocations. Knowing it is possible to recover the memory depth allocation a_i. It's really easy to understand that $a_0 = n_0 + n_1 + n_2$ as well $a_1 = n_3 + n_4$. In general $a_m = \sum_{i=2^m+1}^{2^{m+1}} n_i$ (see Section 5.2). However, for the convenience of interpretation, we will use all collective variables

SECTION 7. INTERACTION PROBLEM

Life in a population and its evolution to a certain extent is determined by the nature of the interaction of the strategies of the objects of the population. The simplest case is the pairwise interaction of strategies. There

are many options for implementing this interaction. The simplest option is that each strategy interacts with everyone, including itself. It is this kind of interaction that is considered in all sections except for section 12. This type of interaction can be implemented with a relatively small number of objects. Therefore, the review considers populations of strategies with a memory depth of no more than 2.

Using the interaction between all strategies with a finite depth of memory, let us first of all establish whether strategies with a larger memory gain an evolutionary advantage. In addition, it is interesting to study how the complexity of strategies affects the evolutionary advantages of strategies. In other words, is there a reason for the complication of social systems. Along the way, the topic of changing the aggressiveness of the population of strategies and the relationship with their effectiveness will arise.

Below we will simulate the evolution of strategies with memory. For simplicity, we will take into account the principle of variability in a simple version, assuming that all strategies with a memory depth less than or equal to are implemented in the population. Since in this case all strategies are taken into account, other strategies will not appear in the process of evolution. The principle of heredity will be to pass on winning strategies to descendants. The principle of natural selection is implemented by eliminating or eliminating losing strategies. Naturally, such a simplified version of evolution can be complicated in many ways. Some of which we will discuss later.

We implement natural selection as follows. Let all strategies interact with each other in a circular manner in an iterated game of prisoners' dilemma. The number of interactions of two strategies in one generation is chosen to be the same for all. Actually, the choice of a large number of interactions between the two strategies is designed to exclude the influence of the first move. As a result of this competition, the strategies gain points in accordance with the payoff matrix given in Section 3. After that, the losing strategy, and possibly several strategies, drop out of the next generation. The rules by which the losing strategy is determined by the points scored may be different So in Sections 8, 9, 11, the strategies that have gained the minimum number of points of evolutionary advantages are deleted, and in Section 10, the strategies that have gained the maximum number of points are removed. Further, the points of evolutionary advantages are reset to zero (except for section 9, where the variant with the accumulation of points by different generations is considered) and the next circle of interactions between the remaining strategies is carried out, which form the strategies of the new generation.

7.1. Numerical simulation technology for the interaction of strategies

The population of all strategies of a certain memory depth is considered. The number of these strategies is finite and is determined by their memory depth (see Section 5). Each strategy consists of several blocks,

for example, for a memory depth of 1, this is [0] [01] 0111, where the number in the first parenthesis determines which initial move should be made by the first subject who began interacting with a randomly chosen opponent - the second subject. The first, initial move, evokes the reaction of the opponent, who makes his move (while choosing his move according to Table 2, focusing on the second square bracket of his strategy, because he knows only one move of the partner - the first subject).

The first subject must react to the opponent's move by making a counter move - his second move. It is the second square bracket in the description of his strategy that determines how to react to the opponent's actions, in conditions when only one of his moves is known. The opponent, knowing already two moves of the first subject, must react as provided in Table. 4.

In this case, already the next four digits of the second subject's strategy determine the choice of his move on the two previous moves made by the first subject (the observed and the previous one) in full accordance with the rule described earlier (see Section 7). Each move, regardless of all others, is paid according to the pay-out matrix (see Table 1).

It is important to note that the act of interaction between the two strategies lasts for n moves. To maintain equality, the interaction of the two strategies is carried out twice. In one, one strategy makes the first move, in the second the second strategy makes the first move. As a result of interaction, strategies gain evolutionary advantage points and "remember" them.

Further, each strategy interacts in the same way with all the remaining strategies, including itself. As a result of such interactions, each strategy accumulates a certain number of points. After everyone interacts with everyone, the accumulated points of each strategy can be compared. Further, a certain rule is used that determines the losing strategies. These strategies are being removed from the next generation of strategies. The next generation of strategies with zero evolutionary advantage points (or saved points as in section 9) interact according to the rules described above. This process is repeated until a stationary set of strategies is formed.

SECTION 8. EVOLUTION OF STRATEGIES. CAUCHY PROBLEM

Consider a simple evolution of strategies in the framework of the Cauchy problem. Let at the initial moment of time we have a population of strategies with a depth of memory. In each generation, all strategies present in the population interact with each other. Each strategy meets and interacts with each strategy. When strategies interact, they receive evolutionary advantage points and accumulate them until they interact with all strategies. The strategies with the minimum number of points are removed from the population and the remaining strategies with zero evolutionary advantage points are transferred to the new generation. This

next generation of strategies is once again entering the "scramble" for points. Evolution continues until a steady state is reached, in which all the remaining strategies (possibly one) gain the same number of points.

8.1. A world without memory

Let's start by discussing the evolution of the simplest world with a memory depth of 0 or a world without memory. Let each strategy interact with another strategy once within the iterated prisoners' dilemma. The set of points is determined by the payout matrix above (see section 3) and added up over a generation. Each strategy in one game responds to the first move of the chosen opponent, and in another starts by making the first move in the game with the same opponent. In the games she starts, there are two possibilities to make the first move, which is to choose 0 or 1.A strategy that makes a specific first move is considered a separate strategy (see section 5). After thegames have been played between all such strategies, including yourself, the strategies are distributed according to the occupied places, in accordance with the points scored. The first place is occupied by the strategy with the highest amount of points. The strategy or strategies with the minimum score are excluded and not passed on to the next generation of the population. The remaining strategies are passed on to the next generation and re–enter the competition with initial zero evolutionary advantage points. These strategies can be seen as descendants of the previous generation.

In this simple world, the number of strategies is quite small ($N_0 = 8$) and it is easy to list them. So at the initial stage it contains 2 strategies of zero complexity[0]00, [1]00, two strategiies[0]11, [1]11, difficulty $C = 1$ and four strategies[0]01, [1]01 [0]10, [1]10, difficulty $C = 2$. Therefore, it is possible to trace all strategies. However, in it we will use the collective variables discussed above. In this world, all strategies have zero memory depth, and therefore variables $a_0(t)$ simply keep track of the number of strategies $a_0(t) = N_0(t)$. It is clear that when one losing strategy is removed at each stage of evolution, their number decreases linearly with time $N_0(t) = (1-t)+8$. Here $t = 1,2,...,8$ is a discrete evolutionary time. The whole time of evolution takes 8 stages (or generations) after which one strategy survives and a stationary state sets in.

Let us now turn to a discussion of the change in the complexity of society's strategies in the process of evolution. This is the main characteristic by which one can classify strategies in this world. The most detailed information about the behavior of complexity is provided by the number of strategies corresponding to the complexity at each stage of evolution. In a world with zero memory, there are strategies of complexity 0, 1 and 2. Graphs of the change over time of the number of strategies of a certain complexity are shown in Fig.6.

Note that the points are connected by lines only for clarity and the lines do not play any role. Time is discrete. On the right is the complexity of the winning strategy at the corresponding evolutionary stage. It can be seen that at the initial stage, up to the 5th generation, the most primitive strategies win or dominate. It is natural to call this period of evolution a primitive period. In the next stages, complex strategies win. This period can be called a period of development.

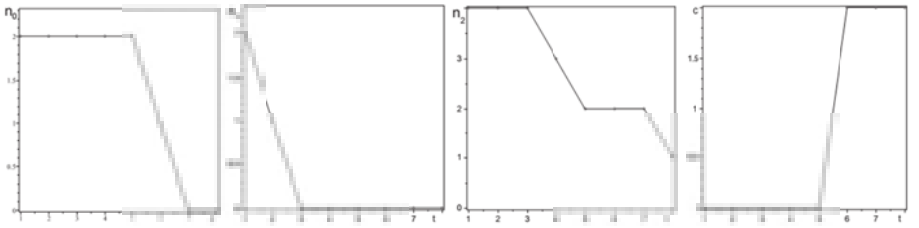

Fig. 6 On the left, change n_0 *– the number of strategies of zero complexity. To the left* n_1 *is evolution – the numbers of strategies of unit complexity and* n_2 *– complexity 2*

Where $n_0(t)$ is the number of strategies of complexity 0 at the t–th stage of evolution, $n_1(t)$ and $n_2(t)$ is the number of strategies of complexity 1 and 2, respectively, at the t–th stage of evolution. Data on their changes were obtained by numerical modeling of the evolution of a population of strategies. It can be seen from these dependencies that strategies of complexity 1 disappear already at the 3rd stage of evolution. Zero difficulty strategies disappear only at the 7th stage of evolution. Actually, this is where the evolution ends and the winning complex strategy with difficulty 2. In our case, it is a strategy $[1]01$.

Thus, the initial stage of population evolution can be characterized as a primitive period (up to stage 5 inclusive). The stage of a primitive 'society' in a world without memory lasts 62.5% the time of going to the stationary state. At these stages primitive zero–complexity strategies dominate in 'society' (see Fig. 6). The final stages correspond to a developed 'society' dominated by complex (even the most complex) strategies.

However, it should be noted that primitive strategies are present in the population even after the onset of the stage of a developed 'society'. The last primitive strategy disappears only at the 7th stage of evolution (see Fig. 6).

From the given dependences it is easy to establish not only the time of disappearance of strategies of a certain complexity, but it is possible to obtain the average value of the complexity of the entire 'society' at each stage of evolution. The average difficulty value is defined as

$$\bar{C}(t)=\frac{0\cdot n_0(t)+1\cdot n_1(t)+2\cdot n_2(t)}{n_0(t)+n_1(t)+n_2(t)}\equiv\frac{1\cdot n_1(t)+2\cdot n_2(t)}{n_0(t)+n_1(t)+n_2(t)}$$

The dependence of the average complexity of population strategies on evolution time is shown in Fig. 7.

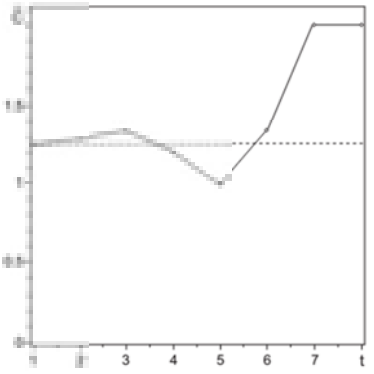

Fig.7 Change in the average value of the complexity of the population of strategies in the process of evolution. The dashed line is the initial mean of the complexity of the population

The average complexity of such a 'society' exhibits rather non–trivial behavior. At the beginning of evolution, the complexity of strategies increases slightly, but then decreases. After reaching a certain minimum value, the average difficulty begins to grow up to the maximum value. The minimum of complexity of society occurs at stage 5. In other words, there are two areas of increasing complexity (periods of development) separated by a period of decreasing complexity (period of decline).Of course, this behavior of medium complexity follows from the behavior of a number of strategies of different complexity (see Fig. 6).

Let us now consider another important characteristic of strategies. It can be conventionally called the aggressiveness of the strategy. ***By aggressiveness we mean the share of refusals of the strategy from cooperation.*** Modelling the evolution of strategies gives the change in the average aggressiveness of the population of strategies, shown in Fig. 8.

From the dependence of the aggressiveness of the population on time, it can be established that the primitive stage of development of society is also characterized by an increase in the average aggressiveness of society. At the stage of the end of the period of primitive society, its aggressiveness is maximal. Then, after the transition to a developed society, there is a monotonous decrease in the average aggressiveness of the society, and upon reaching a stationary state, the average aggressiveness is zero. In addition, the most aggressive strategy dies out at the 5th stage of evolution, the most "decent" ([1]11) at the first stage. Thus, it is possible to define the primitive era of society by the growth of aggressiveness and the primitive stage ends after reaching the maximum aggressiveness of the strategies of society. In a world without memory, this provides an equivalent definition of the primitive era of society. The third possibility of a reasonable definition of the

primitive stage is associated with the period of the presence of the most aggressive strategy in society. Its disappearance will mark the transition to a developed society.

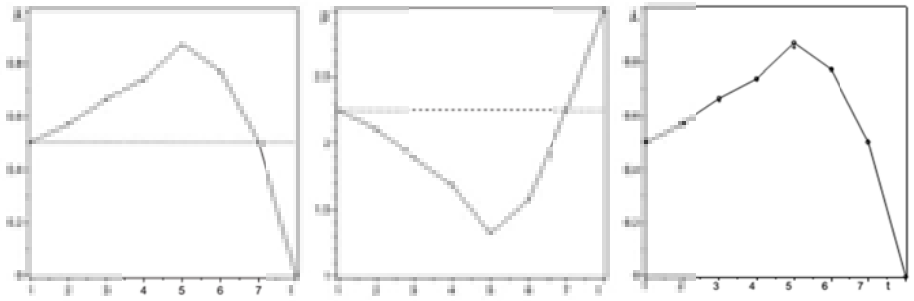

Fig. 8 On the left, the change in the average aggressiveness of 'society' over time. The dotted line coincides with the aggressiveness of a society in which all strategies are present. In this case, the aggressiveness is 0.5. In the centre is the change in the average number of points of evolutionary advantages earned by the strategy in one turn at each stage of the evolution. On the right is a comparison of the average aggressiveness obtained by numerical modelling (circles) with relation (2) (crosses)

Finally, let's move on to characterizing the set of evolutionary advantage points by strategies at different stages of evolution. This characteristic makes it possible to compare the set of points by strategies at different stages of evolution and evaluate the effectiveness of interaction. As such a value, you can use the number of points scored on one turn of the strategy on average at a certain stage of evolution. The time dependence of such a value is shown in Fig. 8. It is easy to see that with an increase in aggressiveness, the average number of points that the strategy gains decreases. The higher the aggressiveness, the lower the score. At the stage of a developed society, the received number of points begins to increase monotonically, reaching a maximum at the stationary stage. Comparing the dependences shown in Fig. 8 on the left and in the centre, it is easy to see the correlation between the behavior of these characteristics during evolution.

In a world with zero memory, there is a correlation in the behavior of average aggressiveness and average earnings per move. It can be assumed that the relationship between these characteristics is determined by the ratio

$$\overline{A}(t) = \sqrt{\lambda \cdot (\overline{P}_{max} - \overline{P}(t))} - a \qquad (1)$$

Figure 8 on the right shows a comparison of the average aggressiveness obtained by numerical modeling and with the empirical pattern given above. The scale factor was chosen on the basis of equality of these characteristics at the first stage of evolution $\lambda = 5.3/8$ and $a = 0.2$. Despite the deviation in the

region of the maximum, the graphs demonstrate good agreement in the behavior with time of these characteristics.

Such a relationship (2) establishes that a decrease in the number of points per move leads to an increase in the aggressiveness of society. Naturally, one can rewrite relation (2) by resolving it relatively $\bar{P}(t)$. Then it can be argued that an increase in aggressiveness leads to a decrease in the average number of points per strategy move according to

$$\bar{P}(t) = \bar{P}_{max} - \frac{\left(\bar{A}(t) + a\right)^2}{\lambda}$$

It's amazing how such a primitive model is similar to complex societies.

8.2. A world with a depth of memory 1

In this world, the number of all strategies increases and becomes equal to 104. It is clear that tracking each strategy, although it is still possible, does not become meaningful enough. Such detailed information is rather confusing than helping to understand the patterns of behavior of strategies. Therefore, with an increase in the depth of memory and, accordingly, the number of strategies, a collective way of describing strategies becomes extremely important. In a world with a memory depth of 1, strategies differ in complexity (0, 1, 2, 3, 4) and also in memory depth (0,1). These characteristics make it possible to classify all strategies into groups according to these properties. Thus, in this world, in addition to the characteristics of the number of strategies with a certain complexity (n_0, n_1, n_2, n_3, and n_4), one can also introduce the number of strategies of a certain memory depth. Let us denote the number of strategies with a memory depth of 0 and –the number of strategies with a memory depth of 1. These collective variables allow describing the properties of a large number of different strategies. In the course of evolution, these numbers change and provide an abbreviated description of the behavior of strategies. When modelling evolution, the evolution time in this world turned out to be equal to 100. 4 strategies remain in thestationary state.

Let's start with a discussion of evolutionary memory changes. The most complete information about this process can be obtained by observing the behavior of $a_0(t)$ and $a_1(t)$.Of course, a number of patterns are associated with the exponential difference in the number of strategies with different memory depths. So the initial number of strategies of 0–th memory depth is 8, and depth 1 is already 96. Therefore, the discreteness of the change in the number of zero–memory strategies is so noticeable in Fig.9. The behavior, although it looks like a linear function, has important differences from it. In addition, such

a significant difference in their numbers makes it not informative to compare their behavior on the same graph. Other characteristics should be used to compare their behavior.

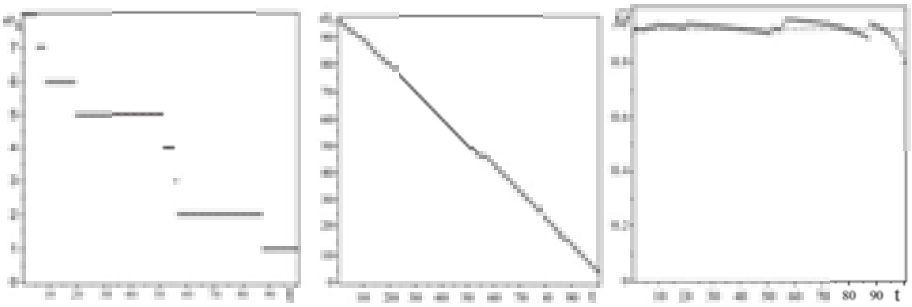

Fig. 9 On the left, the dependence of the number of strategies with zero memory depth, in the middle with a depth of 1, on time. On the right is the change in the average memory of society

Figure 9 shows that strategies with zero memory depth have been present in this world throughout the entire evolutionary time.

Functions and allow you to calculate the average depth of the memory of society, which is defined as

$$\bar{M}(t)=\frac{0\cdot a_0(t)+1\cdot a_1(t)}{a_0(t)+a_1(t)}\equiv\frac{a_1(t)}{a_0(t)+a_1(t)}$$

The averaging result is shown in Fig. 9 on the right. Based on Fig. 9, it can be seen that in the process of evolution, the average depth of the memory of a society changes insignificantly. The reason for this is associated with a small number of strategies with zero memory and with the presence of strategies with a greater memory depth even when entering a stationary state.

Additional information can be obtained by observing the properties of the winning strategy at the corresponding stage of evolution. Figure 10 shows the values of the memory depth of the winning strategies at the corresponding stages of evolution. It is easy to see that in the initial period the dominant strategies have the maximum memory depth. In this case, periods may arise when the dominant strategy has a shallow memory depth. However, this does not have a significant impact on the average memory of society. This indicates the relative paucity of strategies with low memory even at these stages.

Let's move on to the analysis of the behavior of the complexity of society. The most detailed information about the complexity of society is carried by the function $n_0(t)$, $n_1(t)$, $n_2(t)$, $n_3(t)$ and $n_4(t)$. These characteristics are shown

in Fig. 10. Let's pay attention to the initial stage, at which the most primitive strategies $n_0(t)$ are present. This period takes 55 evolutionary stages and ends after the disappearance of the most aggressive strategy 0000. Unlike strategies with zero memory, primitive strategies do not dominate in this period in this world. However, they are present in society in full force.

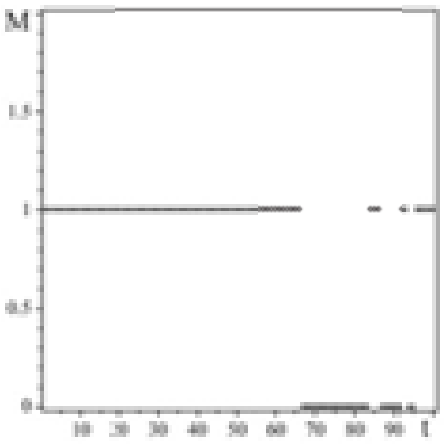

Fig. 10 The depth of memory of winning strategies at the corresponding stages of evolution

Therefore, the primitive period of the development of a society with memory is not characterized by the dominance of the most primitive strategies, but is determined by their presence. The primitive period takes the time to reach a steady state. Note that the relative duration of the primitive period decreased with increasing or, more precisely, with the advent of memory.

The first to disappear from society are strategies with complexity 1 (see Fig. 11 dependence $n_1(t)$), which include the most respectable strategy 1111, which disappears already at the 5th stage. One can only be surprised that it did not disappear at the first stage of evolution. One strategy of complexity 2, two strategies of complexity 3 and two strategies of maximum complexity 4 remain in the stationary state.

It is interesting to note that most of the most complex strategies have disappeared in the course of evolution. Despite this, it is the complex strategies that survive. In addition, it can be noted that in a world with a memory depth of 1, complex strategies dominated at all stages of evolution. This is clearly seen in Figure 12, which shows the complexity of winning strategies at each stage of the evolution of society. It is clearly seen that the most complex strategies capture primacy from the beginning of evolution and preserve it or, more precisely, share it with strategies that are close in complexity to the maximum.

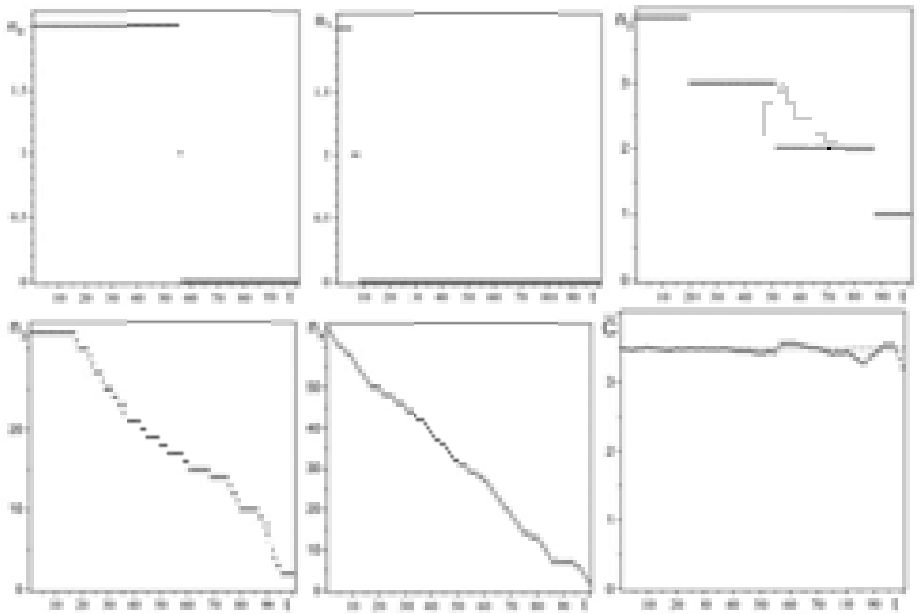

Fig. 11 The number of strategies corresponding to the complexity present in society at different times of evolution. Bottom left figure – the change over time of evolution, the average complexity of the strategies of the society. The dashed line shows the average difficulty when all strategies with a memory depth not exceeding 1 are present in society

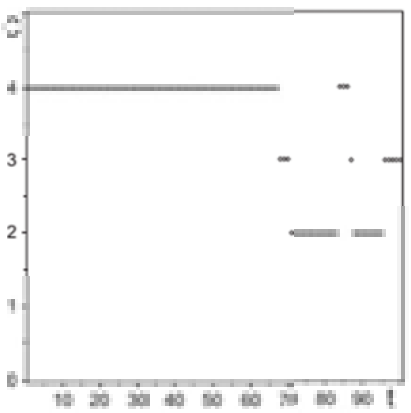

Fig. 12 The complexity of winning strategies at different stages of evolution. There is no stage of domination of primitive strategies. At all stages of evolution, the most complex strategies or those close to the maximum complexity dominate

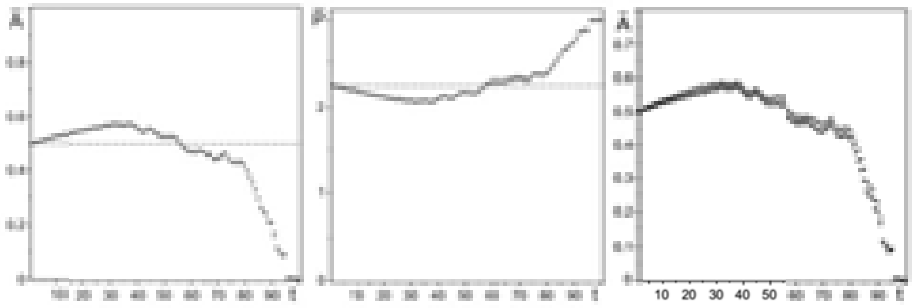

Fig.13 On the left, the change over time in the average aggressiveness of society with the depth of memory 1. In the center – the average earnings at each stage of evolution. The dotted line shows the average score for a society's turn. On the right is a comparison of the average aggressiveness –circles with the pattern (2), built according to the dependence of payments per move – crosses

Let's move on to a discussion of how the aggressiveness of strategies changes in the course of evolution. Figure 13 shows the change in the average aggressiveness of the society. It is easy to see that, as in the previous world, the average aggressiveness at the initial times increases and exceeds the average aggressiveness of a society in which all strategies are present. Then the aggressiveness decreases and reaches the average aggressiveness of a society in which all strategies are present at the stage of evolution. Further, the level of aggressiveness continues to decline, reaching a minimum upon reaching a stationary state. Qualitatively, this behavior resembles the behavior of aggressiveness and in the absence of memory. The difference lies in the shift of the maximum in the presence of memory at relatively earlier evolutionary times. Thus, the position of the maximum with a memory depth of 1 is reached at the times 37% of the evolution time, and in the absence of memory at the times 62.5% of the evolution time. Thus, if we define the primitive period after reaching the average aggressiveness of the maximum, then the stage of primitive society ends at 37, 38 stages. The stage of primitive 'society' with a memory depth of 1 is significantly shortened and is $37\% - 38\%$ of the evolution time.

Let us now consider how the set of evolutionary advantage points changes. In Fig. 13, in the center, the average number of points per strategy move is shown, calculated independently at each stage of evolution.

As in the world with zero memory, there is a correlation in the behavior of average aggressiveness and average earnings per move. If we assume that the relationship between these characteristics is determined by the relation (2), then it is possible to compare the average aggressiveness obtained by direct modeling (see Fig. 13 on the left) with the aggressiveness obtained by the average payments per move. The scale factor λ is chosen, as before, $\lambda = 5.3/8$ and $a = 0.2$, as before, so that the value at the first stage of these dependencies coincides.

The comparison shown in Fig. 13 on the left demonstrates good consistency of the obtained functions. The differences at the initial stage are insignificant and less than in the absence of memory.Of course, the pattern was obtained empirically and the mechanism of such a connection is not clear. However, good agreement between the same functions is observed at zero memory. In other words, these characteristics are not independent, and one of them depends on the other in accordance with relation (2). A reasonable assumption from which this dependence follows is the assumption that the difference $P_{max} - P$ reaches a minimum with some aggressiveness of the strategies. In the vicinity of any minimum, this dependence is quadratic.

8.3. A world with a depth of memory 2

We now turn to the analysis of patterns in the world with a depth of memory of 2. Naturally, the number of all possible strategies in this world increases and is equal to 30824. Here, a separate strategy is understood as a strategy with certain initial moves. The duration of evolution also increases and takes 256 stages. The losing strategy is removed at each stage. We will divide all strategies into 3 groups according to the depth of memory and we will monitor the change in the number of these groups. So $a_0(t)$ – the number of strategies in a society with a memory depth of 0 at the t–th stage, $a_1(t)$ – the number of strategies with a memory depth of 1 at the t–th stage, and $a_2(t)$ – the number of strategies with a memory depth of 2 at the t–th stage. When modeling the evolution of such a society, the dependence of the change in these groups over time was obtained, which are shown in Fig. 14

As expected, the discreteness of the change is most noticeable for groups with a small memory depth of 0.1 and is almost imperceptible for $a_2(t)$. The reason for this is the small number of strategies with a low memory depth.

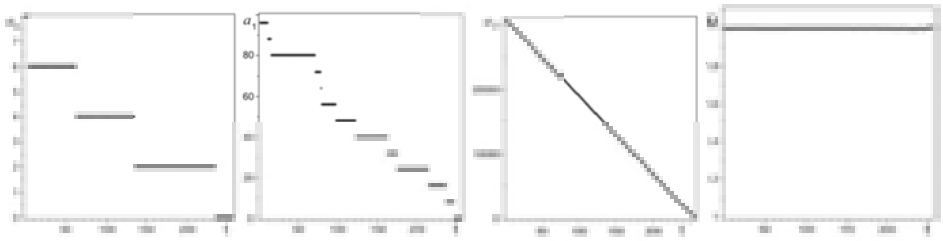

Fig.14 On the left, the change in the number of strategies with a certain depth of memory in the world with a depth of memory 2. Right figure, the change in the average depth of the memory of a society during evolution

A characteristic feature, which is clearly visible from Fig. 14, is the presence of strategies with a low memory depth throughout almost the entire time of evolution. So, with a zero memory depth, strategies disappear at stage 236, and with a memory depth of 1 at stage 249, which also takes 92% and 97% evolution time, respectively. Starting from stage 249, only strategies with the maximum memory depth participate in the evolution. In this world, memory is evolutionarily beneficial.

It should be expected that with an increase in the depth of memory, this tendency will manifest itself from earlier stages of evolution.

Using these functions, we will consider how the average memory of a society changes in the process of evolution (see Fig. 14). It is easy to see that the average depth of society's memory remains practically unchanged and is close to the maximum. At the last stages, you can notice a slight increase in the average memory depth. This is due to the disappearance at the last stages of strategies with a shallow memory depth and reaching the maximum value.

The dominance of strategies with a great depth of memory is observed in this world at all stages of evolution.

Let us turn to the behavior of the complexity of strategies over time. The numerical simulation results are shown in Fig. 15. These dependencies show that primitive strategies of low complexity disappear from society at different stages of evolution without reaching the final stages of the struggle for existence. So the first to disappear strategies of complexity 1 at stage 4 (at this stage the most "decent" strategy disappears), strategies of 0th complexity disappear at 136 stage (the last one disappears the most aggressive strategy), strategies of complexity 2 to 235, difficulty 3 to 215, difficulty 4 at 248, difficulty 5 at 216 stage. In a world with memory, the complexity of strategies is an evolutionary advantage. Evolution can be said to support and approve of the complexity of strategies.

To demonstrate this, we can cite the change in the average complexity of the strategies of the whole society in the process of evolution (see Fig. 16). It can be seen that the average complexity of strategies changes little in the course of evolution and its small oscillations at the final stages of evolution are associated with a decrease in the number of strategies in society. In this case, the disappearance of even one strategy affects the average. It can be assumed that the average value of the complexity of strategies is preserved during the evolution of society and with a greater depth of memory.

In a world with a depth of 2 memory, complex strategies dominate all stages of evolution. This is clearly seen from Figure 16, which shows the complexity of the winning strategy at each stage of evolution. It is easy to see that low complexity strategies are absent among the winners at all stages of evolution. Therefore, the primitive period of the development of society is determined by the presence of primitive strategies, and not by their domination.

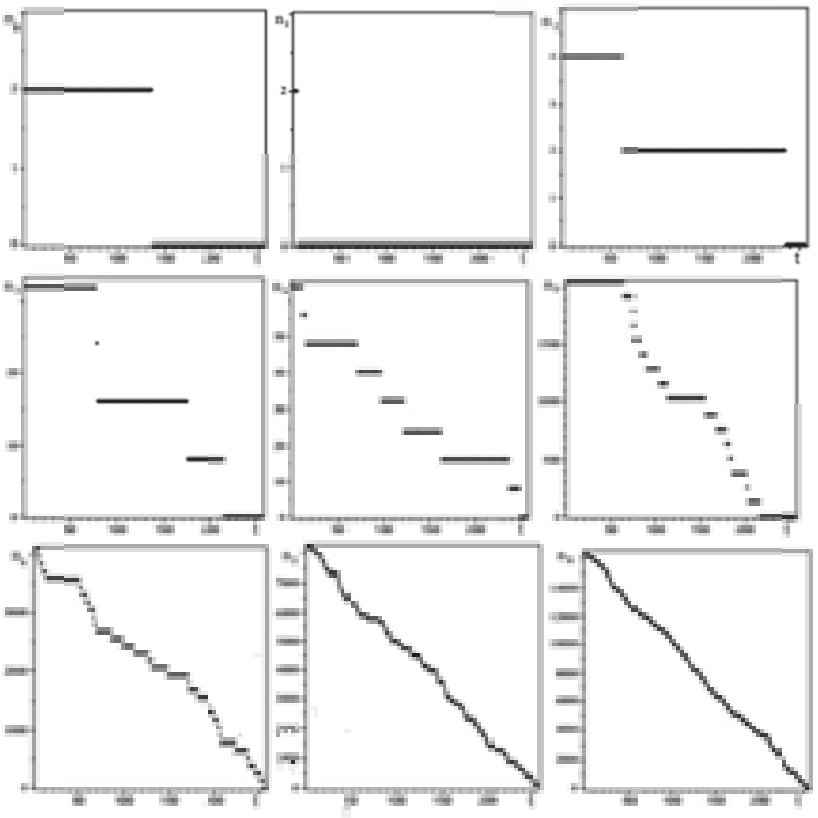

Fig. 15 Change in the number of strategies with a certain depth of memory in the world with a depth of memory 2

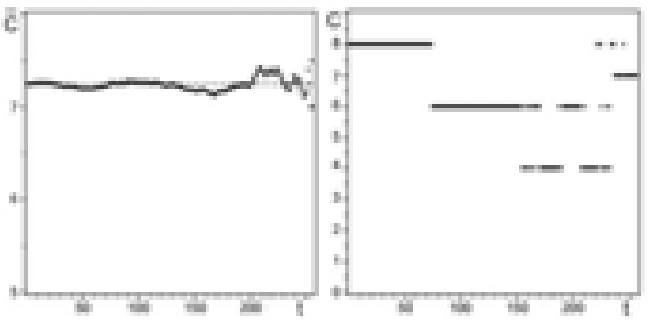

Fig.16 On the right is the behavior of the average complexity of the strategies of society. On the left is the complexity of the winner's strategy at each stage of evolution

As before, we will define the primitive period according to the increase in aggressiveness in society and the achievement of maximum value.

Figure 17 shows the average aggressiveness of the population at each stage of evolution. A characteristic dependence of average aggressiveness over time is visible. The initial primitive stage of development can be distinguished by the increase in the aggressiveness of strategies to the maximum. This period in the world with a depth of memory of 2 lasts up to $53 \div 57$ stages, and another one, close in terms of the value of aggressiveness, is achieved in $115 \div 118$ stages. Note that due to the discreteness and non–smoothness of the data, the maximum value is difficult to identify. There is a wide plateau in the data.

Therefore, we will focus on the period for which the value of the aggressiveness of the original society is reached, which takes about 188 stages. Assuming the symmetry of the maximum, we estimate the characteristic time of the primitive stage as $188 / 2 = 94$. This period takes 37% evolutionary time. Note that it ends before the most aggressive strategy disappears. The reason for the emergence of a wide plateau in the vicinity of the maximum is possibly associated with a decrease in the maximum aggressiveness value with increasing memory depth and its approach to 0.5, the average aggressiveness value of the strategist's initial population.

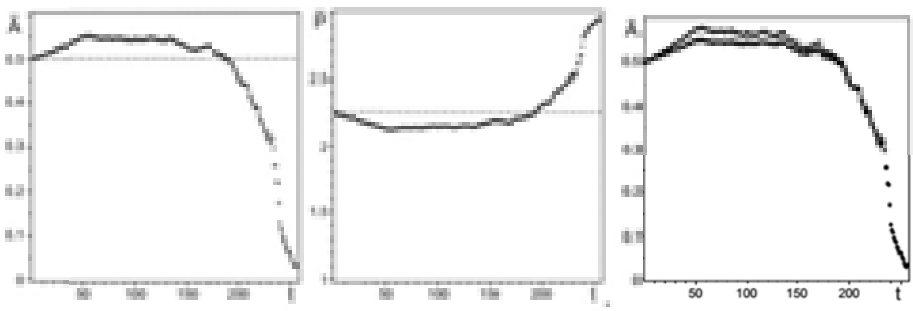

Fig. 17 On the right is the average aggressiveness of strategies at each stage of evolution. In the center is the number of points on average per one turn of the strategy. Average aggressiveness – circles and aggressiveness built according to equation (2) – crosses

We now turn to a discussion of the evolutionary advantage points obtained on average per one turn by a strategy. The general tendency of points decreasing with increasing aggressiveness persists in this world as well (see Fig. 17). The nature of the change is typical for all worlds. The differences are reduced to the relative position of the minimum evolutionary advantage points received. There is also a noticeable correlation between aggressiveness and the number of points per move.

It remains to check the feasibility of the universal connection (2) between these characteristics. Fig. 17 shows the average aggressiveness and

aggressiveness, built according to the dependence of the number of points per move. The consistency of these dependencies is clearly visible. As the memory grows, the data coincidence improves.

It is interesting to note that there is good agreement despite the fact that the same values $\overline{P}_{max} = 3$ were used in all worlds as for the coefficients $\lambda = 5.3/8$, $a = 0.2$.

In thestationary state, there are 128 strategies of memory depth $M = 2$ and complexity $C = 7$, which gain the same number of points and their average aggressiveness towards each other is close to the minimum – equal 0.03.

8.4. Comparison of worlds

Of course, we will not discuss the obvious differences in the number of strategies, times of evolution.

First of all, we note that memory and, as a consequence, complexity provides evolutionary advantages. Strategies with low memory and low complexity are dying out. The average memory and the complexity of society at a fixed memory depth of strategies change little during evolution and are close to their maximum values. Perhaps this is due to the large number of such strategies. Apparently, this is the main reason for the complication and emergence of diversity during evolution.

In all worlds, a primitive period can be distinguished during which the aggressiveness of strategies in society is growing. With increasing memory depth, the relative duration of this period decreases.

The lifetime of the most aggressive strategy in society also decreases with increasing depth of memory. So with a memory depth of 0, it takes 62.5% evolution time, in a world with memory $1 - 55\%$, and in a world with memory $2 - 53\%$.

You can see a correlation with the duration of the primitive period. In principle, you can use another definition of a primitive period, for example, according to the existence of the most aggressive strategy in it.

In all worlds, the dependence of average aggressiveness on time has a characteristic bell–shaped appearance. The differences are in the position of the maximum and its magnitude. Thus, with an increase in the depth of memory, the maximum shifts to the beginning of evolution, and its value decreases, which makes it difficult to find its position. Therefore, with increasing memory depth, its width increases.

In all worlds, aggressiveness in the process of evolution after a primitive period decreases and tends to a minimum value.

There is a universal relationship (2) between the aggressiveness of a society and the number of evolutionary advantage points obtained by the strategy on average per turn in the society.

A finite number of strategies of maximum memory depth and complexity remain in the stationary state, which gain the same number of points and their

aggressiveness towards each other and is close to the minimum. In principle, the set of the same number of points is a consequence of evolution. Otherwise, evolution continues and the strategy that scored fewer evolutionary advantage points in this generation is removed in the next generation.

Surprisingly, strategies in stationary state have zero aggressiveness towards each other. It can be assumed that without carrying out evolution, one can find sets of strategies gaining the same number of points in a circular competition with each other, and from them choose sets with zero aggressiveness. A stationary set of strategies will be a set in which strategies gain the maximum number of points per turn.

SECTION 9. EVOLUTION OF THE 'COMMUNITY' OF STRATEGIES WITH ACCUMULATION

Consider a population of all strategies whose memory is bounded from above by a certain number k .Let the first generation of these strategies interact with each other in a circular manner in an iterated game of prisoners' dilemma. The number of interactions of two strategies in one generation will be chosen equal 100 in all cases.

After that, the losing strategy, and possibly several strategies with the minimum number of points, are removed from the population. The remaining strategies form a new generation, but unlike the case considered in the previous section [67], [68], they retain the points of evolutionary advantage. The next generation is where the strategy winners are with their previous points.

Then they carry out the next circle of interactions between the remaining strategies, taking into account the accumulation of the points. According to the results of the competition, a population of next generation strategies is formed. This continues until you go to thestationary state. Consider again the evolution of communities of strategies with memory depths of 0, 1, and 2. This will allow us to compare the history of the evolution of such communities with their history in the absence of accumulation of points of evolutionary advantages [67].

9.1. The world with zero memory and accumulated points

Let's start again with a population of zero–memory strategies. There are only 8 such strategies, taking into account the first moves. The duration of evolution is determined by their number and the disappearance of 1 strategy at each stage. Therefore, the number of strategies decreases linearly with time and evolution lasts 8 stages. The most "decent" strategy [1] 11 dies out at stage 1, and the most aggressive one reaches the stationary state. This is a fairly small world of strategies in which you can follow each strategy. However, as mentioned earlier, this becomes impossible with increasing memory depth. Therefore, in this world, we use rough characteristics to describe evolution.

Considering that all the strategies of this world have zero memory depth, the main rough characteristic is the number of strategies of a certain complexity.

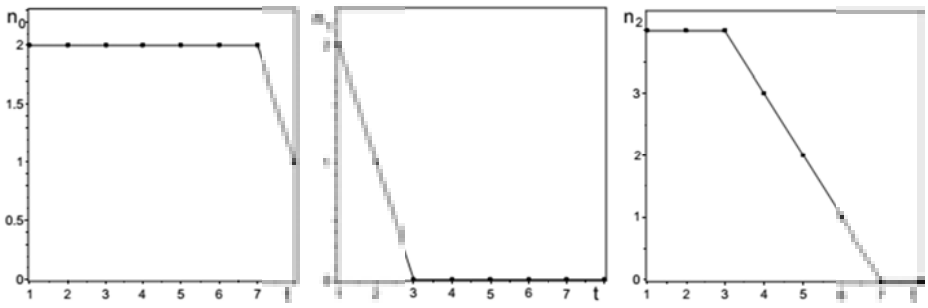

Fig. 18 Changing the number of strategies of a certain complexity. – the number of strategies of complexity 0, – the number of strategies of complexity 1, and – the number of strategies of complexity 2

Figure 18 shows the change over time of these characteristics obtained by numerical modelling of the evolution of a population of strategies.

It can be seen that strategies of complexity 1 disappear already in the third generation, and strategies of complexity 2 at stage 7. The stationary is formed by the surviving strategy of zero complexity. This strategy is extremely aggressive.

In this world with accumulation, but without memory, primitiveness and aggressiveness win, although the most difficult strategy lasted the entire time of evolution (see Fig. 18).

It should be noted that the dominant strategies that have won in every generation all had zero difficulty. Therefore, we present the complexity of losing strategies at the corresponding stage of evolution in Fig. 19. It can be seen that primitive strategies begin to compete with each other only at the 7th stage and are among the losers. At all the previous stages, strategies of greater complexity were lost.

Using the number of strategies of a certain complexity, it is possible to obtain the change over time in the average complexity of the population strategies

$$\overline{C}(t)=\frac{0\cdot n_0(t)+1\cdot n_1(t)+2\cdot n_2(t)}{n_0(t)+n_1(t)+n_2(t)}\equiv\frac{1\cdot n_1(t)+2\cdot n_2(t)}{n_0(t)+n_1(t)+n_2(t)} \qquad (2)$$

The calculation result is shown in Fig. 19. It is easy to see that the average complexity of strategies in a society with accumulation (with the transfer of accumulated points of evolutionary advantages to the next generation) monotonically decreases in the process of evolution after a small stage of increase (see Fig. 19). A small stage of growth of average complexity

coincides with the period of presence of strategies with complexity 1 in the "'community'".

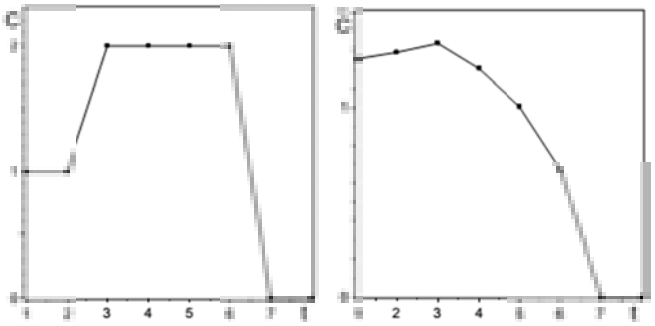

Fig. 19 On the left, the complexity of the losing strategy at the corresponding stage. On the right is the average complexity of the strategies of a society with intergenerational accumulation

The average difficulty at the 7th stage becomes zero. Only strategies of zero complexity form the stationary state. This is radically different from the change in the complexity of strategies over time in the absence of accumulation [67], [68]. In such communities of strategies, the complexity increased. In other words, in a world with zero memory depth and with the transfer of accumulated points of evolutionary advantages to the next generation, only the most primitive strategies of zero complexity survive in the process of evolution.

Thus, the stage of the 'community' of strategies – the primitive world lasts throughout evolution. At all stages in the 'community' primitive strategies of zero complexity dominate.

Let us now trace the aggressiveness of such a 'community' of strategies. By aggressiveness, as before, we mean the share of refusals of the strategy from cooperation. Modelling the evolution of strategies gives the change in the average aggressiveness of society, shown in Fig. 20. The change over time of this characteristic is fundamentally different from its behavior in the communities of strategies without accumulation. In this case, the aggressiveness of society's strategies increases monotonically over time. The stationary stateforms the most aggressive strategy.

Similarly, the behavior and the number of points of evolutionary advantages differ significantly on average for one turn of the strategy. In a 'community' with accumulation, the number of points decreases monotonically (see Fig. 20). At the same time, the universal connection (2) between the number of points of evolutionary advantages on average per one turn and average aggressiveness is also fulfilled well in this world.

It is interesting to emphasize that the values are constant $\overline{P}_{max} = 3$, $\lambda = 5.3/8$ and $a = 0.2$ the same as in [67], [68]. Figure 20 on the right shows a

comparison of these patterns. You can see a good coincidence of average aggressiveness with root dependence on $\overline{P}(t)$. This means that knowledge of one of these characteristics makes it easy to establish the value of the second.

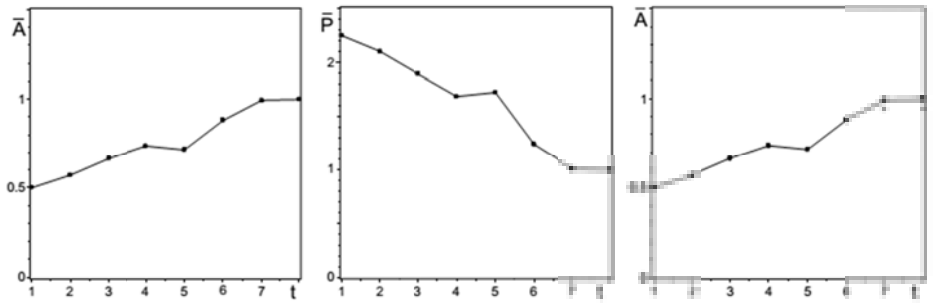

Fig. 20 On the left, the average aggressiveness of the strategies of a society with accumulation between generations. In the centre is the average number of points per strategy course in a society with accumulation between generations. On the right is a comparison of average aggressiveness (circles) with root dependence (crosses). Due to the precise overlay, some crosses are not visible

Thus, in a world without memory, the most primitive strategies ($C = 0$) dominate at all stages of evolution. In other words, the primitive period of evolution of such a 'community' of strategies takes up the entire evolutionary time. Only the most primitive and most aggressive strategy remains in thestationary state.

The universal relationship between the number of evolutionary advantage points on average per turn and the average aggressiveness remains for this world.

9.2. The world with 1 depth of memory and accumulated points

Let us now turn to the population of strategies with accumulation in the presence of memory. Let us consider the behavior of a 'community' of strategies with a depth of memory 1. The nature of the interaction of strategies and the pay-out matrix are the same as is the presence of accumulation of points of evolutionary advantages with their transfer to the next generation. Memory depth determines the number of strategies available to the 'community'. In the case $k = 1$, the number of strategies increases to 104 and, accordingly, the number of stages of population evolution or the number of generations before entering the stationary state increases.

In the presence of memory, the number of coarse or collective characteristics increases. A set of variables arises that describe the number of strategies for a particular memory. The evolution of these variables is shown in Figure 21. The notation for these variables is standard a_0– the number of

strategies with zero memory depth, a_1 – the number of strategies with a unit memory depth. The significant difference in the number of these types of strategies makes the discreteness $a_0(t)$ noticeable and is weakly manifested in more numerous strategies $a_1(t)$.

A constant plot in $a_0(t)$ means that during this time, strategies with a greater depth of memory dropped out of the 'community'. The most important difference from the previous case is that strategies with zero memory depth and, accordingly, low complexity die out at the 95th stage of evolution, which is 91% ofthe time to reach thestationary state.

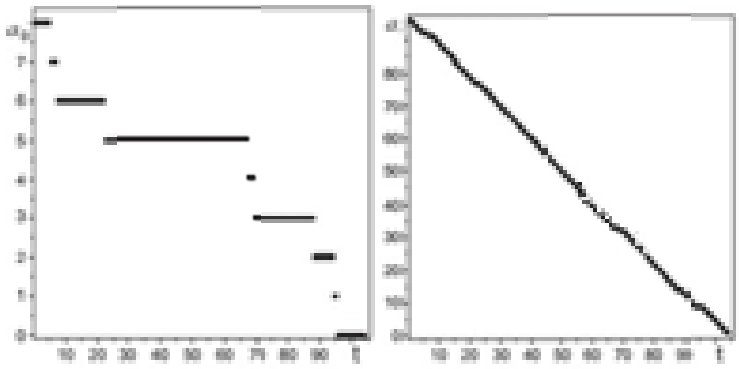

Fig.21 Change in the number of strategies of a certain memory depth. Here a_0 is the number of strategies with zero memory depth, a_1 is the number of strategies with unit memory depth

In a world with memory, primitiveness does not survive. Unlike the previous case, the primitive period of the 'community' of strategies ends. The stationary is formed by strategies with a maximum memory depth of 1 (see Fig. 21).

Therefore, the average memory depth

$$\bar{M}(t) = \frac{0 \cdot a_0(t) + 1 \cdot a_1(t)}{a_0(t) + a_1(t)}$$

practically changes slightly, being in a small vicinity of 1 and at the last stages reaches the maximum value of 1 (see Fig. 22). This is due to the paucity of disappearing primitive strategies.

Next important set of collective variables is the number of strategies of a certain complexity. Figure 23 shows the changes over time $n_0(t)$ – the number of strategies of complexity 0, $n_1(t)$ – the number of strategies of complexity 1, $n_2(t)$ – the number of strategies of complexity 2, $n_3(t)$ – the

number of strategies of complexity 3, and $n_4(t)$ – the number of strategies of complexity 4. These variables characterize the complexity of the strategies of the 'community' as a whole.

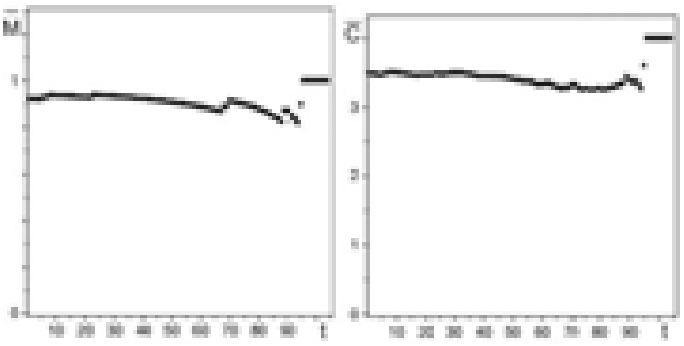

Fig. 22 On the left, the average depth of strategy memory in a society with accumulation between generations. On the right, the average complexity of the 'community' strategies have changed over time

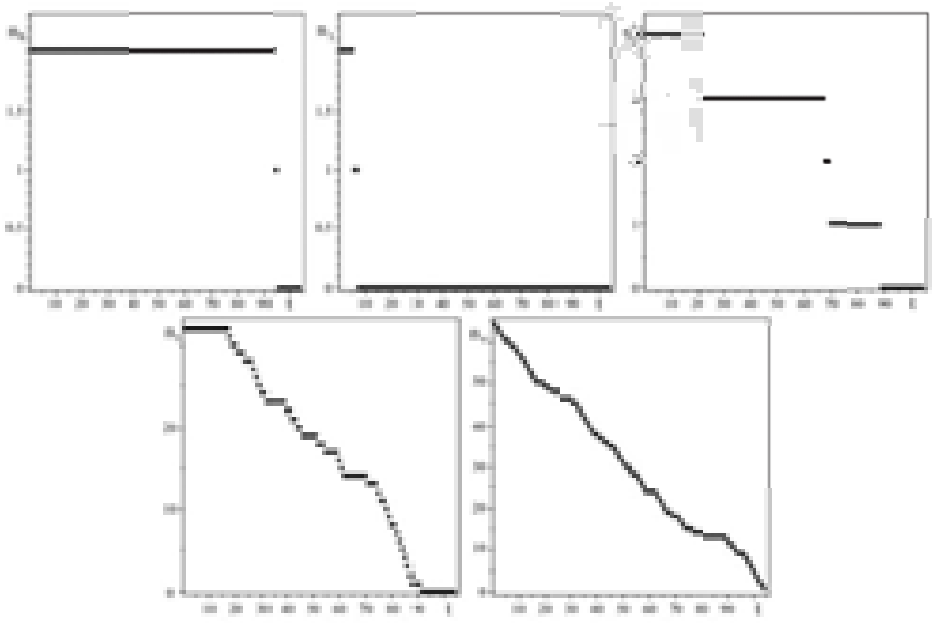

Fig. 23 Change in the number of strategies of a certain complexity over time. Here, n_0 *is the number of strategies of complexity 0,* n_1 *is the number of strategies of complexity 1,* n_3 *is the number of strategies of complexity 2, the number of strategies of complexity 3, and* n_4 *isthe number of strategies of complexity 4*

It can be seen that all primitive strategies ($C \le 2$) disappear before reaching a stationary state. So strategies of zero difficulty disappear at 95th stage, difficulty 1 at 7th stage and difficulty 2 at 88th stage. Oddly enough, the most primitive zero–complexity strategy (of the primitive strategies) disappears last at 95th stage. Only strategies of maximum complexity 4 survive to the stationary stage.

Therefore, the average complexity changes in the vicinity of the maximum value and reaches its maximum starting from the 95th stage of evolution (see Fig. 23). Thus, in the presence of memory, complexity is an evolutionarily advantageous property even in an accumulating society.

The next characteristic that interests us is the average aggressiveness of society and its change over time. Figure 24 on the left shows the results of the numerical simulation. It is easy to see that at the stage of the presence of primitive strategies in society, the average aggressiveness of society increases monotonically. Peaking at the stage preceding the disappearance of primitive strategies.

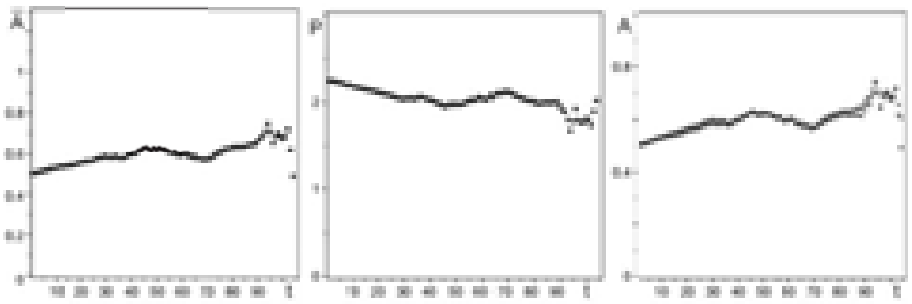

Fig. 24 On the left, the change in the average aggressiveness of "community" strategies. At the centre is the dependence of the average umber of points per strategy course in a society with accumulation between generations. On the right is a comparison of the average aggressiveness (circles) in a society with accumulation between generations with the resulting dependence according to the ratio (2) by the number of points per move (crosses)

In other words, even in a society with accumulation, the primitive period is less than the time of evolution (approximately 91% of the entire time of evolution). The aggressiveness of the winning strategies behaves differently (see Figure 25). It decreases despite the increase in average aggressiveness. Thus, in such a society, non-aggressive strategies still dominate. Figure 25 also shows the memory depth of the winning strategies and their complexity. One can see the dominance of strategies of maximum memory depth and complexity in the 'community' at all stages of evolution.

As in the previous cases, there is a correlation between the average aggressiveness and the number of points per strategy move. This can be seen by comparing the average aggressiveness in Fig. 24 on the left and the reduced change in the number of points with time in the centre of Fig. 24. It can be seen

that the average number of payments per move decreases with time over time periods where aggressiveness increases. This general pattern is observed in all cases. The relationship between these characteristics, obtained in the absence of accumulation in society, is illustrated with the same coefficients in a society with accumulation in Figure 24. The right side of Fig. 24 demonstrates good agreement even when choosing the old universal coefficients in dependence (2). Thus, the universal correlation between the aggressiveness of a society and the number of points per strategy course persists in a society with accumulation.

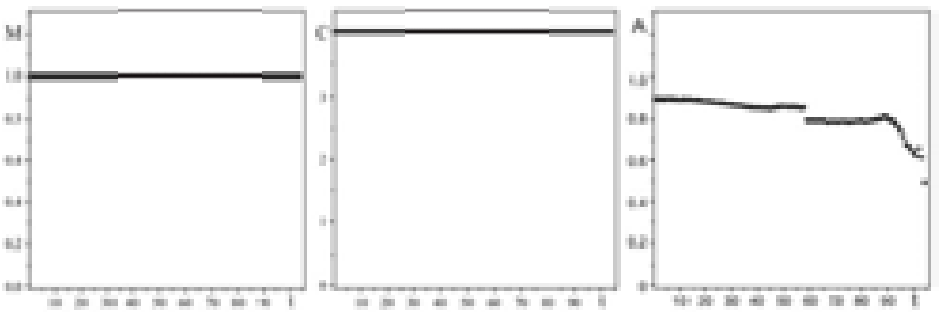

Fig. 25 On the left is the depth of memory, in the centre is the complexity of the winning strategy at the corresponding stage. On the right is the aggressiveness of the strategies that won at the corresponding stages of evolution

Let us now discuss the properties of the winning strategies at each stage of evolution. By this we mean the strategies that have gained the maximum number of evolutionary advantage points at the corresponding stage.

Figure 25 shows the dependences of the memory depth, complexity and aggressiveness of the winning strategies at the corresponding stage. It can be seen that the depth of memory and complexity of the winners is maximal at all stages of evolution. The aggressiveness of the winners decreases from the beginning of evolution, and at the final stages, this decrease occurs at a noticeably faster rate.

Thus, in the world with memory (memory depth 1), the nature of the evolution of the population of strategies with accumulation is fundamentally changing. First of all, the primitive period of the 'community'– there is no dominance of primitive strategies. Dominate at all stages of the strategy with maximum memory depth and maximum difficulty. The average memory depth, as well as the average complexity of 'community' strategies, are close to the maximum values and change little during evolution. The maximum is reached in a steady state. The average aggressiveness of the 'community' increases as long as there are primitive strategies in the 'community'. At subsequent stages, aggressiveness decreases and is minimal in thestationary state. In a world with accumulation and memory depth of 1, there remains one strategy (1)(01)0010 of complexity 4 in thestationary state.

9.3. The world with a depth of memory of 2 and with the accumulation of points between generations

Let's move on to a world with depth of memory 2 and accumulation of points. Let the previous type of interaction between strategies, the pay-out matrix, and the transfer of accumulated points to the next generation be preserved. However, the number of all possible strategies in this world increases and becomes equal to 30824. Here again, a separate strategy is understood as a strategy with certain initial moves. To significantly reduce the numerical resources and evolution time, we will delete at each stage the losing strategy (one of 256), regardless of the first moves. Then the duration of evolution takes 256 stages or generations.

In this world, as before, the main collective variables are the number of strategies with a certain depth of memory and the number of strategies of a certain complexity. Figure 26 shows the changes in the number of strategies of a certain memory depth. It can be seen that strategies with a shallow memory depth disappear in the process of evolution. So memory depths 0 disappear at stage 242, which is approximately 95% of the evolution time, memory depths 1 at stage 254 (approximately 99% of the evolution time). Only strategies with the maximum memory depth form the stationary state. The presence of a noticeable piecewise constant structure $a_0(t)$, $a_1(t)$ is associated with the relative paucity of these strategies, and at the times when their numbers are preserved, strategies of higher complexity are removed from the 'community'.

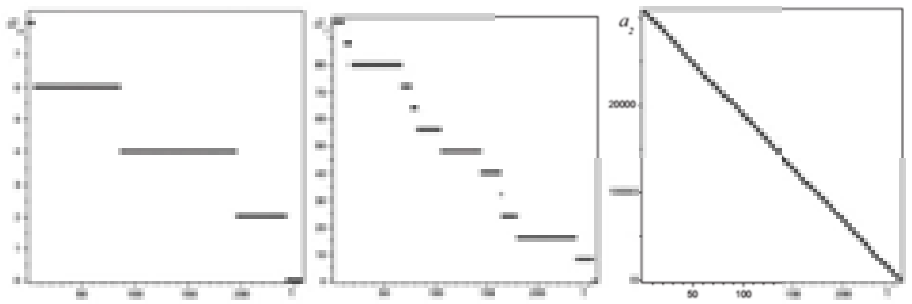

Fig. 26 Changing the number of strategies of a certain memory depth. Here a_0 is the number of strategies for memory depth 0, a_1 is the number of strategies for memory depth 1, and a_2 is the number of strategies for memory depth 2

The average depth of the "'community"' memory throughout evolution is close to the maximum, equal to 2 (see Fig. 27). This means that the depth of memory of a 'community' of strategies is determined by the initial state (in the absence of a source of strategies) and is preserved in the process of evolution. In other words, memory depth is supported by evolution. With increasing memory

depth, this property should manifest itself more clearly. The reason for this may be associated with a sharp over exponential increase in the number of strategies with a greater depth of memory.

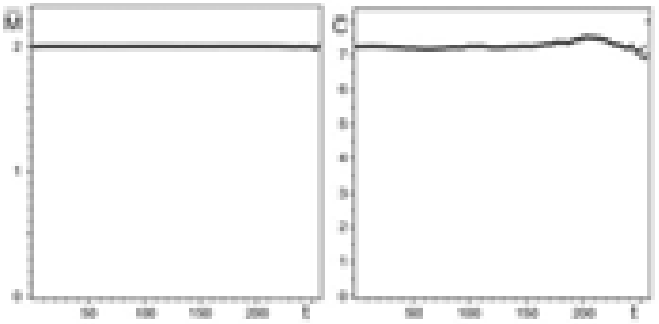

Figure 27 Change over time in the average 'community' memory depth on the left and the average complexity of the 'community' strategies on the right

This behavior of the number of strategies with different memory depths already speaks of the advantages of complex strategies.

Figure 28 shows the change in the number of strategies of varying complexity. The order of disappearance of primitive strategies is visible. The first to disappear are strategies of complexity 1. This occurs at the 5th stage of evolution; strategies of complexity 0 persist for a long time in society, which disappear at 243th stage. Strategies of difficulty 2 disappear at 196 stages, and difficulty 3.4, respectively, at 181 stages and 255 stages. Strategies 5 at 191, 6 at 255, and 7 at 249 stages. the stationary stateis formed only by strategies of maximum complexity 8

Of course, this does not mean that complex strategies are guaranteed to survive. On the contrary, the rate of extinction of the most complex strategies is the highest, but among them there are those that will survive and only among them. Therefore, the complexity of strategies is also supported by evolution.

The dependence of the average complexity of society's strategies on time is shown in Fig. 27 on the right, which is defined as

$$\overline{C}(t) = \frac{\sum_{i=0}^{2^{k+1}} i \cdot n_i}{\sum_{i=0}^{2^{k+1}} n_i},$$

here k – is the depth of memory of strategies. It is characteristic that the average complexity changes little in the course of evolution. Noticeable fluctuations in complexity are observed when approaching the stationary and, apparently, are associated with the small number of remaining strategies.

Let us now turn to the dominant strategies at the stages of evolution. By such we mean strategies that have won at a certain stage of evolution. As in the case of memory depth 1, strategies with a maximum memory depth of 2 and a maximum complexity of 8 prevailed at all stages of evolution. In this sense, the most complex strategies dominated at all stages of evolution.

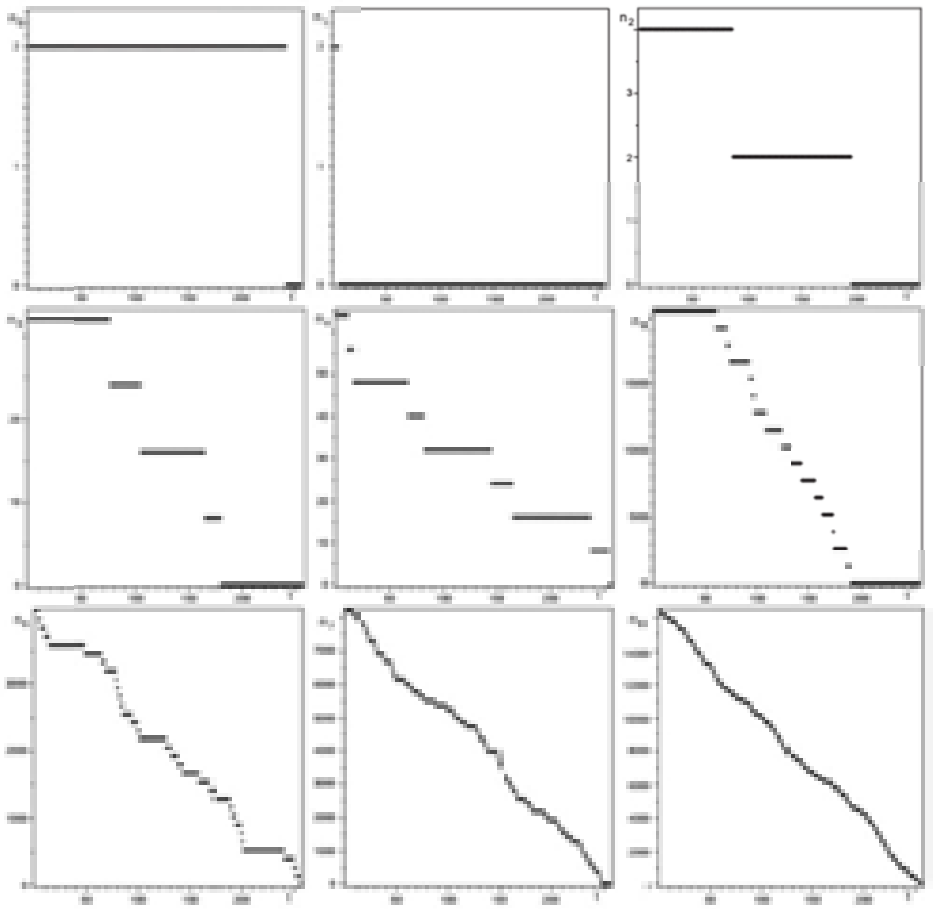

Fig. 28 Changing the number of strategies of a certain complexity. Here n_0 is the number of strategies of complexity 0, n_1 is the number of strategies of complexity 1 and n_2 is the number of strategies of complexity 2, etc

Let's move on to discussing average aggressiveness. The average aggressiveness obtained as a result of modelling such a "community" is shown in Fig. 29. It is easy to notice the monotonous increase in aggressiveness in the process of evolution. The primitive period of the development of society ends at

the 253rd stage and takes 99% ofthe entire time of going to thestationary state. In thestationary state, the aggressiveness of the strategy "'community"' decreases slightly.

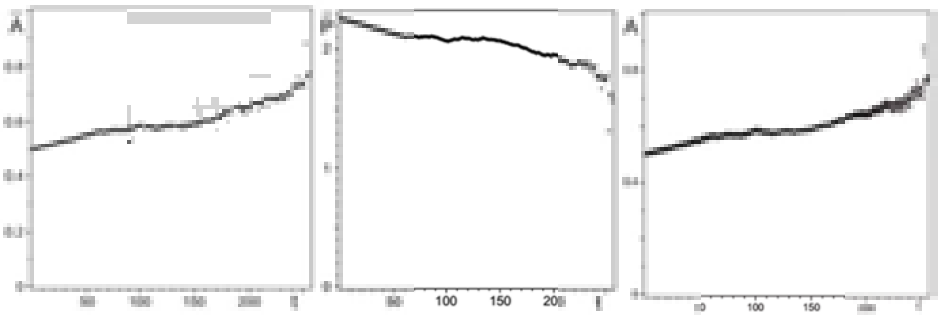

Fig. 29. On the left, the average aggressiveness of the strategy 'community' and its change over time. In the centre is the average number of society strategy points per turn. On the right is a comparison of the average aggressiveness (circles) in a society with accumulation between generations with the resulting dependence according to the ratio (2) by the number of points per move (crosses)

The correlation between the average aggressiveness and the set of the strategy points per move is preserved. The change in the average number of points per strategy move is shown in Fig. 29. It can be seen that the average number of points per move monotonically decreases with time. A quantitative comparison of the relationship between aggressiveness and points per move is shown in Figure 29 on the left. The universality of this connection covers not only worlds with different depths of memory, but also societies both without accumulation and with accumulation.

The stationary state of strategies with a memory depth of 2 and accumulation is formed by 128 strategies of maximum complexity 8. All these strategies differ only in the first strategies of a smaller memory $(x_0)(x_1x_2)(x_3x_4x_5x_6)00001000$, where $x_i \in B-$ the main or leading strategy with a memory depth of 2 is one $-`00001000$.

9.4. Comparison of worlds with accumulation

In societies with accumulation between generations, only in a world without memory, the most primitive strategies $(C = 0)$ dominate at all stages of evolution, and the most primitive and aggressive strategy (0) 00 reaches a stationary state. The average aggressiveness of the strategy 'community' increases over time. The universal connection (2) remains in this world as well.

The communities of strategies with memory and with accumulation between generations are already dominated by strategies with maximum memory depth and maximum complexity at all stages of evolution. The average values of the memory depth and complexity of the strategy "'community"'

change little over the course of evolution. The average aggressiveness of the "'community'" increases over time, and the number of Evolutionary Benefit Points earned per strategy turn decreases over time. The universal connection (2) between these quantities is preserved. the stationary stateis formed by the most complex strategies and aggressive towards each other.

SECTION 10. ALTERNATIVE EVOLUTION OF STRATEGIES WITH MEMORY

Consider a population of strategies with memory, alternative to evolution, by changing the selection rule for losing strategies. Let the strategies that have gained the maximum number of points of evolutionary advantages are removed from the population during the alternative evolution. In other words, the best strategies are removed in every generation. As before, the population at the initial stage contains all strategies with a memory depth less than or equal to 2. Since in this case all strategies are taken into account, other strategies will not appear in the process of evolution.

The principle of heredity will consist in the transmission of strategies to descendants. The principle of natural selection is realized by excluding or eliminating certain strategies. The alternative evolution removes the winning strategy in each generation. Let us consider the consequences of this method of selecting strategies in the population.

As in the previous cases, the evolution considers the pairwise interaction of strategies, in accordance with the iterated prisoners' dilemma. Moreover, each strategy interacts with everyone, including itself. In order to establish the result of the pairwise interaction of strategies, we use the payoff matrix, which coincides with the one introduced in Section 3.

We'll use collective variables again. In this section, it is convenient to use as such variables the number of strategies with a certain memory depth a_j and the number of strategies with a certain complexity a_j, where $j = 0,1,..,k$ all possible values of the memory depth run through, and i all possible values of the complexity of strategies. For example, a_0 is the number of strategies with zero memory, and n_1 is the number of strategies of complexity 1. When studying the behavior of memory and the complexity of population strategies in the process of evolution, these are quite convenient collective variables.

10.1. The world without memory

Let's start by discussing the evolution of the simplest world with a 0 memory depth. Let each strategy interact with another strategy $n = 100$ times within the iterated prisoners' dilemma. The set of points is determined by the pay-out matrix given in section 3 and is summed up. Each strategy in one game responds to the first move of the chosen opponent, and in another starts by

making the first move in the game with the same opponent. In the games she starts, there are two possibilities to make the first move, which is to choose 0 or 1. A strategy that makes a particular first move is considered a separate strategy. After the games have been played between all such strategies, including yourself, the strategies are distributed according to the occupied places in accordance with the points scored. In an alternative evolution, the strategy or strategies with the highest score are eliminated and not passed on to the next generation. The remaining strategies are passed on to the next generation and re–enter the competition with initial zero evolutionary advantage points. These strategies can be seen as descendants of the previous generation.

In this simple world, the number of strategies is quite small ($N_0 = 8$). However, we will use the collective variables discussed in Section 6. In this world, all strategies have a memory depth of 0 and therefore the variables $a_0(t)$ simply keep track of the number of strategies $a_0(t) = N_0(t)$. It is clear that when one strategy is removed at each stage of evolution, their number decreases linearly with time $N_0 = (1-t)+8$. Here $t = 1, 2, ..., 8$ is the discrete evolutionary time. With such a small number, there is no coincidence of the points scored by several strategies and is unlikely. Therefore, evolution takes 8 stages (or generations), after which one strategy survives and a stationary state sets in.

We now turn to a discussion of changes in the complexity of society's strategies. This is the main collective characteristic by which one can classify strategies in this world.

The most detailed information about the behavior of complexity is provided by the number of strategies of the corresponding complexity at each stage of evolution. In a world with zero memory, there are strategies of complexity 0, 1 and 2. Graphs of the change over time of the number of strategies of a certain complexity are shown in Fig. 30,

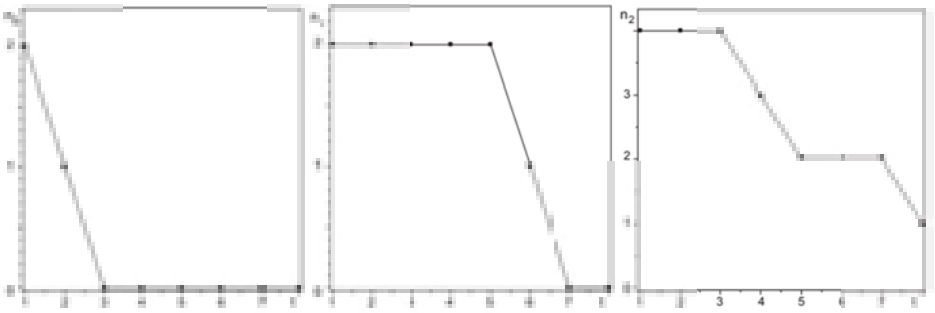

Fig. 30 Left – change n_0 – the number of strategies of zero complexity. In the middle – evolution n_1 – the number of strategies of unit complexity, on the right n_2 – complexity 2. Note that the points are connected by lines only for clarity and the lines do not play any role. Time is discrete

The given dependencies in Fig. 30 allow us to establish the disappearance time of strategies of a certain complexity. It is easy to see that despite the introduced selection rule, primitive strategies n_0 disappear already at the 3rd stage of evolution. Strategies of complexity 1 are retained in the 'community' until stage 7, and the stationary stateforms strategies of maximum complexity. In this sense, even with alternative evolution, the complexity of strategies is an evolutionarily advantageous property.

Comparing the data of the alternative evolution of Fig. 30 with the analogous data of the usual evolution of Fig. 6, it can be seen that the time dependences $n_2(t)$ coincide for both evolutions. Hence, the evolution of complex strategies over time is the same in both evolutions. The dependence $n_0(t)$ in the alternative evolution coincides with $n_1(t)$ the ordinary evolution, the analogous behavior of the $n_1(t)$ alternative one coincides with $n_0(t)$ the ordinary one.

You can also get the average value of the complexity of the entire "community" at each stage of evolution. The average difficulty value is defined as

$$\bar{C}(t) = \frac{0 \cdot n_0(t) + 1 \cdot n_1(t) + 2 \cdot n_2(t)}{n_0(t) + n_1(t) + n_2(t)} \equiv \frac{1 \cdot n_1(t) + 2 \cdot n_2(t)}{n_0(t) + n_1(t) + n_2(t)}$$

The dependence of the average complexity of population strategies on evolution time is shown in Fig. 31. The average complexity demonstrates a rather complex, oscillating behavior with reaching the maximum value in the stationary. In other words, the average complexity of the strategy 'community' increases with evolution. This means that complex strategies are profitable even in communities with alternative selection.

It is interesting to note that the nature of the dependence of the average complexity in the case of alternative evolution differs from the analogous dependence in Fig. 7 with the natural selection rule. In the alternative evolution, there are no stages at which the average complexity fell below the initial complexity of the population strategies.

In this sense, the complexity of alternative evolution increases even more.

Let us now discuss the properties of the strategies that win at different stages of 'community' evolution or the dominant strategies of the 'community'. We will monitor the complexity, aggressiveness, and the number of payments per move of winning strategies at different stages of evolution. Figure 32 shows the corresponding dependencies.

It can be seen that at the early stages of evolution (up to stage 2 inclusive), only primitive strategies with zero complexity won. Actually, this is the reason for the stronger growth in complexity and the mechanism for entering the stationary state for more complex strategies, taking into account the rule for selecting an alternative 'community'.

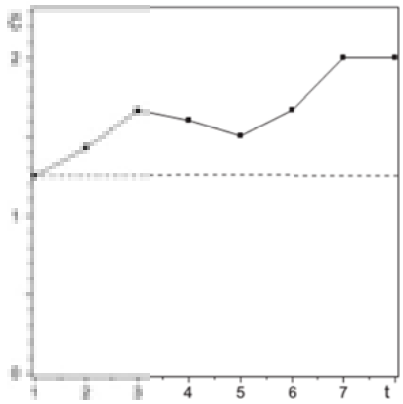

Fig.31 Changes in the average value of the complexity of the entire 'community' of strategies in the process of evolution. The dashed line is the initial average of the complexity of all 'community' strategies. This value corresponds to the average value of the complexity of the strategy 'community' in which all strategies with zero memory depth are present

Recall that in this case, the winning strategies are deleted. At the next stages, strategies of complexity 2 and 1 won. The clearly expressed stepwise nature of the change is associated with a small number of strategies with zero memory depth. The aggressiveness of the winners first falls, and then increases to the maximum value. The minimum aggressiveness correlates with the period of dominance of strategies with intermediate complexity 1. The value of the payoffs per move of winning strategies at different stages of evolution reaches a maximum at stage 3 of evolution and then decreases with time. The minimum is reached in the stationary state. Clear differences between these characteristics of winning strategies in alternative and conventional evolution can be seen by comparing them with those shown in Fig. 7.

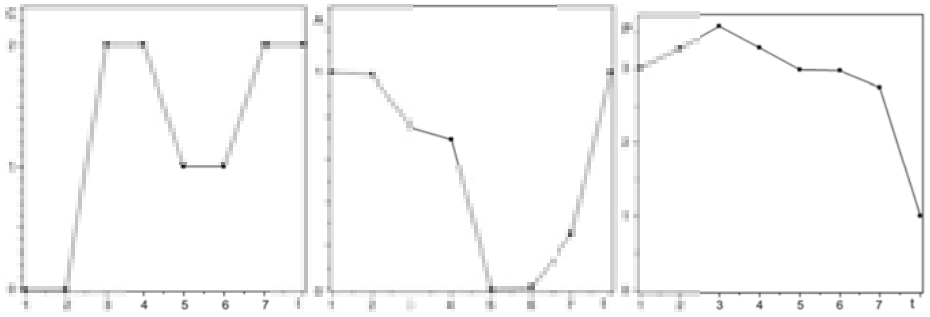

Fig. 32 On the left is the complexity of the winning strategy at the corresponding stage of evolution. At the centre is aggressiveness, winning strategies from time to time. On the right is the number of evolutionary advantage points earned by the strategy in one move of the winners at all stages of evolution

We now turn to a discussion of the change over time of the average aggressiveness and the number of payments per turn on average. These characteristics are shown in Fig. 33. It is easy to notice qualitative changes in the behavior of these characteristics during alternative evolution.

Aggressiveness, in contrast to the usual case (normal evolution), first falls, and then increases to a maximum value. Thus, the strategy 'community' becomes more aggressive in the process of alternative evolution. Similar qualitative changes are undergone by the change in the value of the number of payments per strategy course on average. In contrast to the usual case (see Fig. 8), with an alternative evolution, the value of payments reaches a maximum and then decreases. The stage of reaching the maximum payments coincides with the stage of the minimum aggressiveness of the strategy "'community"'.

Thus, with an alternative evolution, the aggressiveness of the surviving strategies increases, while the amount of payments per move decreases on average. In a world with zero memory, there is a clear correlation in the behavior of average aggressiveness and average earnings per move. It can be assumed that the relationship between these characteristics is determined by the universal relationship (2). Figure 33 on the right compares the numerically simulated average aggressiveness with the empirical pattern shown above. The scale factor was chosen from considerations of equality of these characteristics at the first stage of evolution $\overline{P}_{max} = 3$, $\lambda = 5.3/8$, and $a = 0.2$.

Despite the small deviation in the minimum region, the graphs demonstrate good agreement in the behavior of these characteristics over time. Of course, the agreement can be improved by varying the values of the constants included in relation (2). Here we have saved the values that were used in various evolution options (see previous sections). The average number of payments per strategy move depends on the average aggressiveness of the strategies according to the quadratic law

$$P_{max} - P(t) = \frac{1}{\lambda}(A(t) + a)^2 \tag{3}$$

The parameter a included in this ratio acquires a simple physical meaning. Thus, you can see that the parameter a coincides with the minimum value of the aggressiveness A_{min} of the strategy 'community' at which the maximum value of payments is reached. Therefore, it is convenient to give this ratio a clearer form

$$P(t) = P_{max} - \frac{1}{\lambda}(A(t) + A_{min})^2 \tag{4}$$

The coefficient $a = 0.2$ depends on the choice of the pay-out matrix.

Thus, the relationship (2) or (5) between these characteristics remains in the alternative evolution.

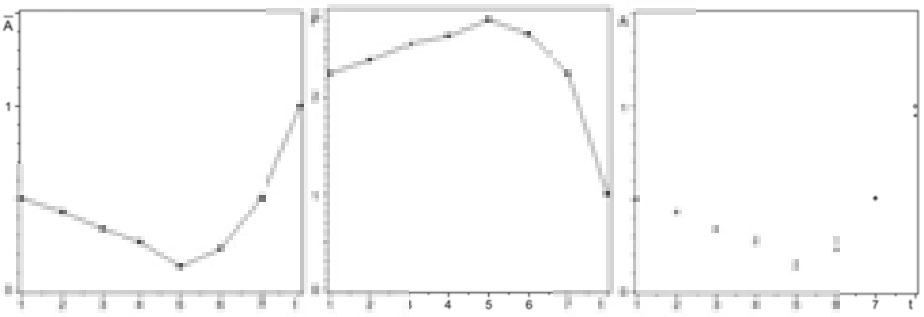

Fig. 33 On the left, the change over time in the average aggressiveness of the strategy 'community', in the centre– the average number of payments per strategy move. On the right is a comparison of the aggressiveness obtained by modelling with the aggressiveness built according to the data on the number of payments per strategy move on average (see relation (2))

10.2. A world with a depth of memory 1

Let us now consider the alternative evolution of a 'community' of strategies with a depth of memory 1. The principle of removing the winning strategies at each stage of evolution is applied in this case as well. The evolution time of this 'community' takes 97 stages, and 8 strategies remain in a stationary state (taking into account the first move). In the stationary state, they receive the same number of evolutionary benefit points. The aggressiveness of the strategies that form the stationary strategy in relation to each other is maximum and equal to 1. This is fundamentally different from the zero aggressiveness of stationary strategies under normal evolution. The names and characteristics of stationary strategies in alternative evolution are given in the table 7 below.

Table 7

strategy name	memory depth	complexity
(0)(00)0001	1	4
(0)(01)0100	1	4
(0)(00)0100	1	4
(0)(00)0111	1	4
(0)(01)0001	1	4
(0)01	0	2
(0)(01)0111	1	4
(0)(01)0011	1	3

It can be seen that the stationary strategy is formed by strategies of maximum complexity 4, only two strategies have lower complexity 3 and 2. Primitive strategies do not survive to the stationary state. This pattern also manifests itself in the depth of memory of stationary strategies – all but one have the maximum memory depth.

Thus, in the stationary state of such a 'community', only absolutely aggressive strategies with maximum memory depth and complexity are present. Only a small proportion of strategies with less memory depth and complexity, but absolutely aggressive ones, enter the stationary state.

We now turn to a description of the evolution of such a 'community' of strategies. In this world, there are already strategies with 0 (8 strategies) and 1 memory depth (96 strategies). Therefore, the number of strategies with a certain memory depth appears as a nontrivial collective variable. Figure 34 shows the results of numerical modelling of the behavior of these variables during the evolution of the 'community'. The stepped structure $a_0(t)$ is associated with a small number of such strategies and the presence of areas for their preservation is determined by the disappearance of more numerous strategies 1 of the depth of memory at these time intervals. The average 'retention' interval $a_0(t)$ is easy to estimate as $\Delta t = 97/8 \approx 12$, which is observed in Fig. 34 on the left. It can be seen that only one strategy with 0 memory depth reaches the stationary. Such a stepped structure is also present in behaviour of $a_1(t)$, but is hardly noticeable due to the large number of memory depth strategies 1.

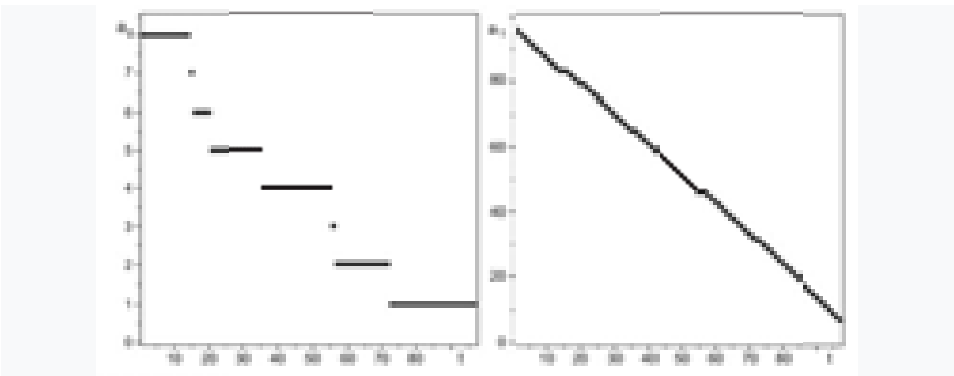

Fig. 34 On the left – change a_0 – the number of strategies with zero memory depth. On the right – evolution a_1 – the number of strategies of unit memory depth. Time is discrete

The next important collective variables are the number of strategies of a certain complexity. Figure 35 shows the time dependence of these variables obtained in the numerical simulation of evolution. The disappearance of primitive strategies is clearly visible. So strategies of

complexity 0 disappear at 16 stage of evolution (or generation), and complexity 1 at 56 stage. The time dependences $n_0(t)$ and $n_1(t)$ have a characteristic stepped structure, the nature of which is quite similar to that described above. Average interval for storing their values $\Delta t = 97/3 \approx 32$. The same structure is observed for the rest of the numbers of strategies $n_i(t)$ of a certain complexity.

The reason is not such a significant difference in their numbers in comparison with the difference in numbers $a_0(t)$ and $a_1(t)$ by an order of magnitude.

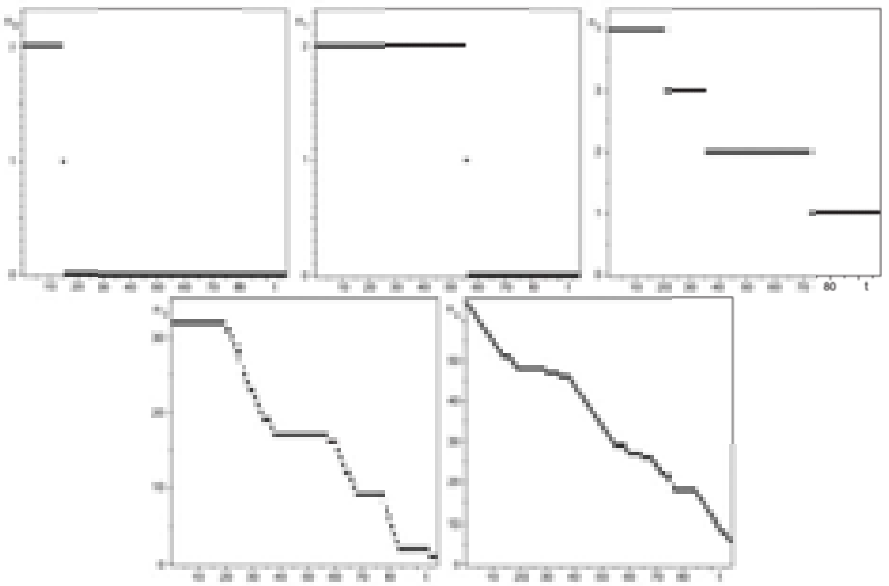

Fig. 35 Change over time n_i *– the number of strategies of i–th complexity,* $i = 0,1,2,3,4$

We now turn to a discussion of the dominant strategies in the process of 'community' evolution. As before, under the dominant strategy at a certain stage we mean the strategy that won or scored the maximum number of points at this stage. Figure 36 shows the main characteristics of strategies dominant at the stages of evolution. It can be seen that, with rare exceptions, the dominant strategies had the maximum memory depth. The proportion of time dominated by strategies with a lower memory depth is 7% ofthe entire time of evolution.

Likewise, dominant strategies are complex. The proportion of dominance of primitive strategies 0 and 1 complexity is 4% evolution time. The share of dominance of the most complex strategies is59% ofthe entire time of evolution. Let us recall that in each generation, during the alternative evolution, it was

the dominant strategies that were destroyed. Despite this, the stationary stateis forming the remaining complex strategies. The aggressiveness of dominant strategies fluctuates strongly and rather resembles a chaotic dependence. The mechanism for the appearance of such chaos is associated with the removal of the winning strategy.

Indeed, under ordinary evolution, the winning strategy retained its primacy over a certain time interval of evolution, and in the case of an alternative one, it is removed at the first victory. Therefore, the next winning strategy may have characteristics that are significantly different from the previous winner. As follows from Fig. 36 such instability is especially manifested in aggressiveness. The dependence of the number of evolutionary advantages of winning strategies behaves in a more natural way; over time, their value monotonically decreases.

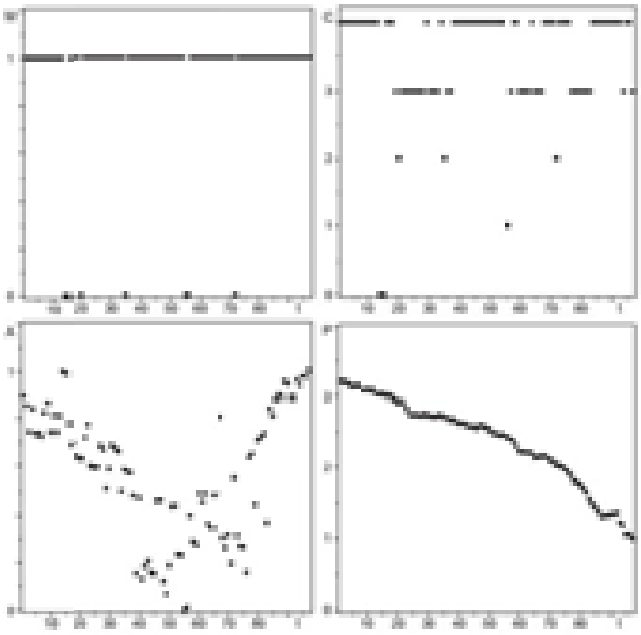

Fig. 36 At the top left is the depth of memory M , at the top right is the difficulty C , at the bottom left is aggressiveness A and at the bottom right is the number of points per move P of the winning strategy at the corresponding stage of evolution

Let us consider below the behavior of the average characteristics of a 'community' of strategies under alternative evolution. Of course, they can be obtained using the dependencies $a_i(t)$ and $n_i(t)$. Figure 37 shows the time dependences of the average characteristics of the 'community' strategies. It is easy to see that the average memory depth changes insignificantly in the course of evolution in the vicinity of the maximum value. The average complexity of the strategy "'community'" also changes slightly around the maximum value.

In other words, the average depth of memory and the complexity of 'community' strategies persists throughout the evolutionary process. The most obvious changes are undergone by the average aggressiveness of 'community' strategies and, as a consequence, the average number of payments per strategy course. The behavior of the average aggressiveness of the 'community' during alternative evolution, after reaching the minimum, begins to increase monotonically and reaches its maximum value at the stationary. Recall that in normal evolution, aggressiveness after reaching the maximum monotonically decreased, reaching the minimum value in the stationary state(see Fig. 19). The behavior of the amount of payments per strategy course is also opposite to the time change in the amount of payments under normal evolution. At the same time, the relationship (2) between the average aggressiveness and the number of payments per move remains the same. This can be seen from the lower right graph in Fig. 37.

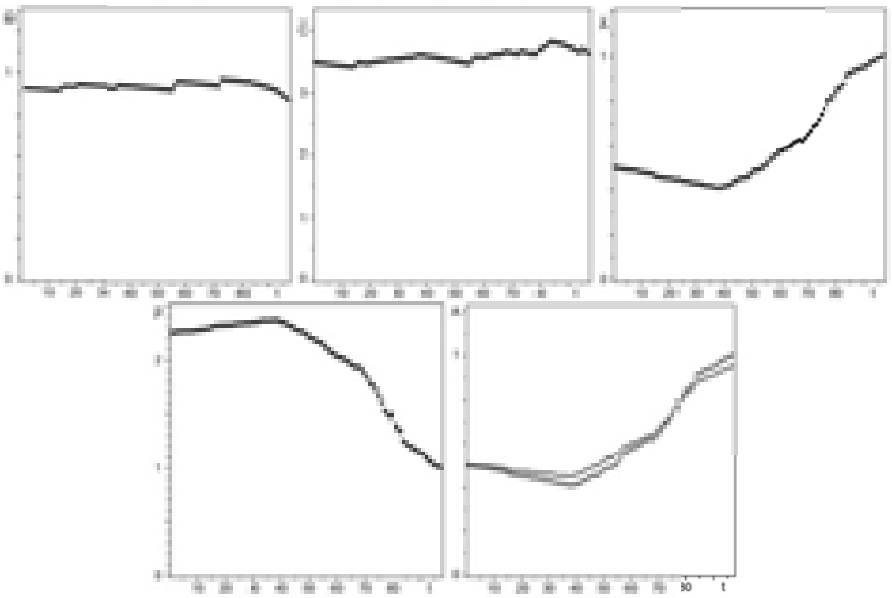

Fig. 37 On the left $\overline{C}$ *– the change in the average complexity of strategies. In the middle* $\overline{A}$ *– the evolution of the average aggressiveness of strategies, on the right* $\overline{P}$ *– the change in the number of payments per strategy course on average. Below is a comparison of the aggressiveness obtained by modeling (circles) with the aggressiveness built according to the data on the number of payments per strategy move on average (crosses) (see relation (2))*

Thus, with the alternative evolution of a 'community' of strategies with a memory depth of 1 in thestationary state, the maximum aggressiveness of the 'community' is achieved. At the same time, the memory depth and complexity of the surviving strategies are close to their maximum values.

10.3. A world with a depth of memory 2

Let us now turn to a discussion of the changes in the alternative evolution of the population of strategies with increasing memory depth. To do this, consider a 'community' of strategies with a memory depth not exceeding 2. The principle of removing the winning strategies at each stage of evolution is applied in this world as well. The pay-out matrix and the number of moves of the two strategies remain the same. Naturally, the number of all possible strategies in this world increases and equals 30824.Here again, a separate strategy is understood as a strategy with certain initial moves. To significantly reduce the numerical resources and evolution time, we will delete at each stage the losing strategy (one of 256), regardless of the first moves. Then the duration of evolution takes 256 stages. In terms of collective variables, we will divide all strategies into 3 groups according to the depth of memory and we will monitor the change in the number of these groups. So $a_0(t)$ – the number of strategies in a society with a memory depth of 0 at the t-th stage, $a_1(t)$ – the number of strategies with a memory depth of 1 at the t-th stage, and $a_2(t)$ – the number of strategies with a memory depth of 2 at the t-th stage. When modelling the evolution of such a society, the dependence of the change in the number of these groups with time was obtained, which are shown in Fig. 38.

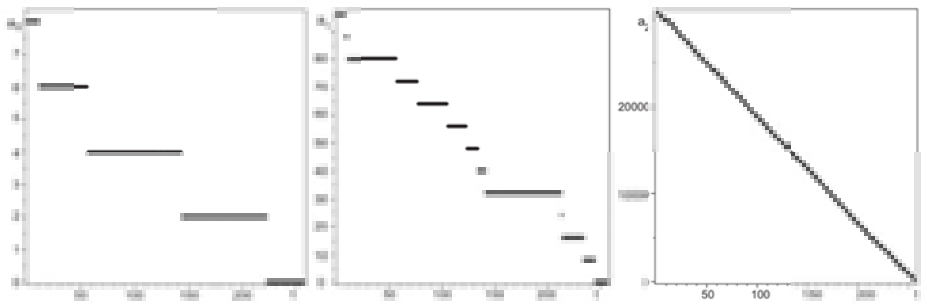

Fig. 38 Change over time a_i – the number of strategies i–th memory depth, $i = 0,1,2$

The quantities $a_0(t)$ and $a_1(t)$, as in the previous world (see Section 1), have a noticeable piecewise constant structure. As noted above, the nature of this is associated with the abundance $a_2(t)$ exceeding by several orders of magnitude $a_0(t)$ and $a_1(t)$. The main difference in the behavior of these characteristics with increasing memory depth boils down to the disappearance of all strategies in the course of evolution, except for those with the maximum memory depth. Only strategies with a maximum memory depth of 2. So strategies with a memory depth of 0 disappear at 223 stages, with a memory

depth of 1 at 245 stages of evolution. The number of strategies in the stationary stateis 128.

The next quantities, the change of which during evolution is important to monitor, are the number of strategies of a certain complexity $n_i(t)$. In that world $i = 0,1,2,3,4$. The numerical simulation results are shown in Fig. 39. These dependencies demonstrate that primitive strategies of low complexity disappear from the 'community' at the early stages of evolution, without reaching the final stages of the struggle for existence. So, the first to disappear are strategies of complexity 0 – at stage 12, strategies of 1st complexity disappear at 144th stage, strategies of complexity 2 – at 223, difficulty 3 – at 214, difficulty 4 – at 245, difficulty 5 – at 220 stage and 6 – at 254 stage. At the final stage, only complex strategies (difficulty 7 and 8) compete. The maximum difficulty strategy disappears at stage 256. the stationary stateis formed only by strategies of complexity 7.

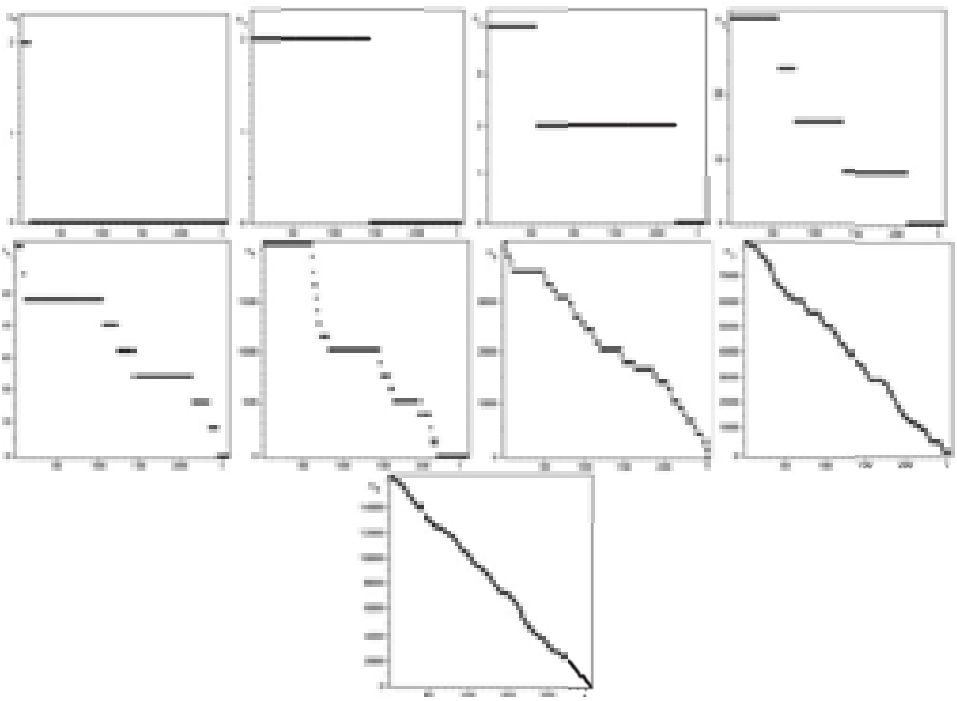

Fig. 39 Change over time n_i *– the number of strategies of* i*-th complexity,* $i = 0,1,2,3,4$

Thus, qualitatively, the behavior of the number of strategies of a certain complexity corresponds to the behavior of these characteristics in the previous world. The differences are quantitative.

Let's move on to discussing the dominant strategies of this world. Figure 40 shows the main characteristics of dominant strategies at each stage of

evolution. As in the previous case, the main share of dominance falls on strategies with the maximum memory depth and maximum complexity. The obvious reason for this is the large number of such strategies and the removal of the winner at each stage. In addition, the aggressiveness of the winning strategies remains highly sensitive to the removal of the winning strategies. The rest of the dependencies differ only quantitatively, maintaining the typical nature of changes over time.

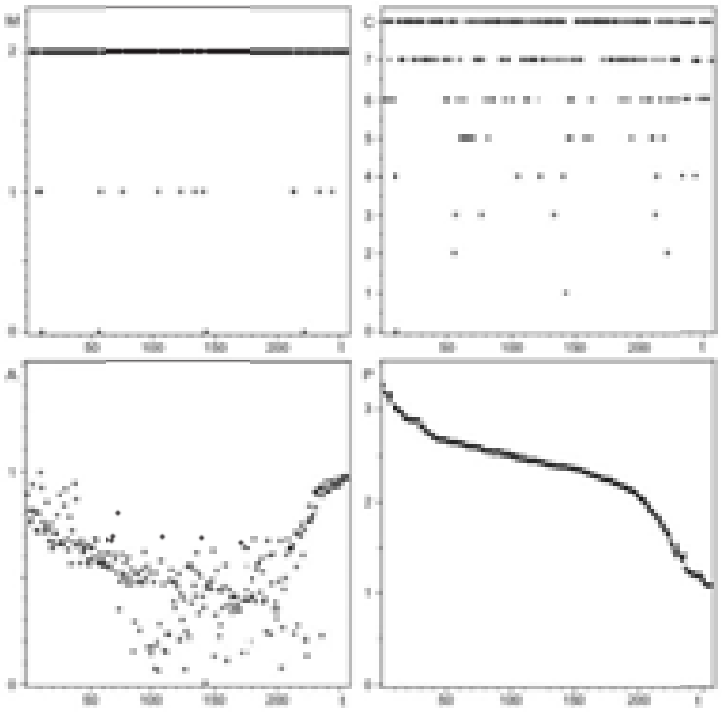

Fig. 40 At the top left is the depth of memory M , at the top right is the difficulty C , at the bottom left is aggressiveness A and on the right at the bottom is the number of points per move P of the winning strategy at the corresponding stage of evolution

Using collective variables, you can get the average characteristics of the 'community' of strategies and study their change over time. Figure 41 shows the changes over time in average difficulty, aggressiveness, and payoffs per turn. The average value of the memory depth remains close to 2 throughout evolution and is not given because of the simplicity of behavior. The average complexity remains at the level of the average for all strategies with a memory depth not exceeding 2.

Small fluctuations are observed, as usual, with a decrease in the number of 'community' strategies near thestationary state. After reaching the minimum, the average aggressiveness begins to increase and reaches its

maximum in thestationary state. The stationary stateis formed by strategies that are aggressive towards each other. This change is opposite to the behavior of the average aggressiveness of strategies during normal evolution (see Fig. 23). The same qualitative change is undergone by the average number of payments per strategy course. At the same time, the connection between these characteristics remains the same (see relation (2) and (5)).

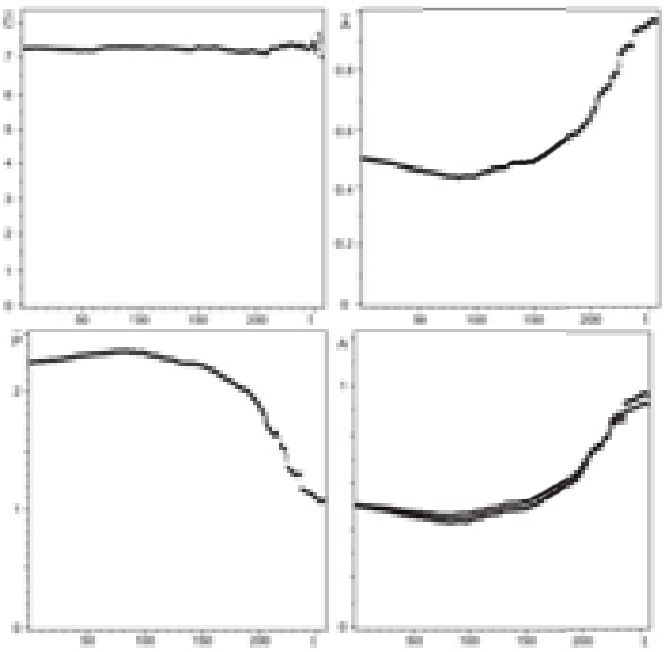

Fig. 41 Left – change in the average complexity of strategies $\overline{C}$ *. In the middle – the evolution of the average aggressiveness of strategies* $\overline{A}$ *, on the right – the change in the number of payments per strategy course on average* $\overline{P}$ *. Below is a comparison of the aggressiveness obtained by modelling (circles) with the aggressiveness built according to the data on the number of payments per strategy move on average (crosses) (see relation (2))*

The main difference between the alternative evolution and the usual one is the increase in the average aggressiveness of the strategy 'community' after reaching a minimum. the stationary stateis formed by the most aggressive strategies towards each other. A 'community' of 'spiders in a bank' is formed.

At the same time, the depth of memory and the complexity of strategies are evolutionarily advantageous properties. The universal relationship between the average aggressiveness and the number of payments per strategy course remains on average in the case of alternative evolution.

SECTION 11. EVOLUTION OF COMMUNITIES OF STRATEGIES IN THE PRESENCE OF SOURCES

Consider the evolution of a population of strategies in the presence of sources and sinks of strategies. At each stage of evolution, the losing strategy is removed from the population and is not passed on to the next generation. Instead of the disappeared strategy, a new strategy is thrown into the population. In other words, a non-equilibrium situation with the sources and sinks of strategies is modelled. In a certain sense, a strongly nonequilibrium state far from thermodynamic equilibrium is modelled in this way. This state is close in meaning to turbulent states with fluxes along the spectrum [69]. As before, we will be interested in two main characteristics of strategies – the depth of memory and complexity of strategies and the corresponding characteristics of the population of strategies. Therefore, we will use the collective variables proposed earlier [6] for a rough description of populations.

Accordingly, there are several options for choosing the properties of the source of strategies for the population of strategies.The emerging non-equilibrium populations can be classified according to the depth of memory of the initial 'community' and according to the depth of memory of the source of strategies. In other words, randomly dropped strategies may have a memory depth greater or less than the memory depth of strategies presents in the population. It is clear that such sources should influence the evolution of the population of strategies in different ways. The role of the flow of strategies is played by the removal of the losing strategy after the competition between the strategies of the population.

Let us consider the evolution of a population of strategies in the presence of sources of strategies with different memory depths. The source of strategies models the variability of strategies, for example, as a result of mutations. In this case, the properties of the initial 'community' strategies may differ significantly from the properties of the strategies thrown in by the source. Two fundamentally different cases are important. First, throw–in strategies can have a greater depth of memory than the population. In this case, more complex strategies are thrown in. Second, throw–in strategies may have a lower memory depth than population strategies. In this case, more primitive strategies are thrown into the population. The properties of population evolution in these cases are of primary interest. Let's start with the case when the memory depth of the thrown strategies is greater than the memory depth of the population at the initial stage of evolution.

11.1 The 'community' of zero and unit memory strategies and a source of 2 memory depth strategies

Let the initial state of the population of strategies be formed by all strategies with a depth of memory $k \le 1$. The number of such strategies is

104. The evolution is carried out with the pay-out matrix used earlier. Each strategy competes with every other strategy in society (including itself) 100 times. This is consistent with the iterated prisoners' dilemma. The increase in the number of competitions with each other no longer affects the distribution of places as a result of competitions (see [5]). All evolutionary advantage points won by the strategy are added up at this stage.

After all the meetings have been held, the losing strategy (with the lowest amount of points) is removed and is not allowed to the next stage of evolution. A strategy with a memory depth of 2 is thrown into the remaining 'community' at random. All the remaining strategies and thrown in again enter the competition with initial zero points of evolutionary advantage. These strategies can be seen as descendants of the previous generation with a mutating new strategy. Then the process is repeated to the stationary state.

In the case under consideration, in the numerical simulation, the stationary is reached at the 2590 stage of evolution. Of course, the time to go to the stationary state in different implementations may differ due to the use of random throw–in strategies. The typical time for stationary stateis of the order of several thousand generations. There are 104 strategies in the stationary state, taking into account the differences in the first move. All these strategies have zero aggressiveness towards each other and gain the same number of points (31200.0) at the stationary stage of evolution. This property, in a sense, coincides with the evolution of communities of strategies even in the absence of sources of strategies (see [5]).

In addition, as shown by numerical modelling, the stationary state is formed by strategies with a greater memory depth and maximum or close to it complexity. Figure 42 shows the number of strategies versus memory depth and stationary state complexity.

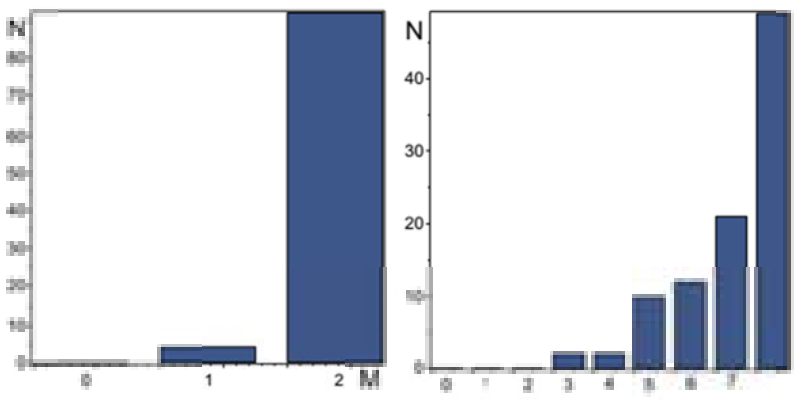

Fig. 42 Histograms of the number of strategies N *in the stationary statewith a certain memory depth* M *on the left and the number of strategies of a certain complexity* C *on the right*

It is easy to see that in the stationary state, most of the strategies have the maximum memory depth and maximum complexity. A small part of the strategies 4.8% have a memory depth less than the maximum and those remaining in the stationary state 45.2% have a complexity less than the maximum. At the same time, primitive strategies with complexity 0, 1 are completely absent in the stationary state. In other words, the society is captured by complex strategies with maximum memory depth.

Let us now discuss how the entrance to the stationary state takes place. The main characteristics of interest should be related to the depth of memory and the complexity of the strategies. Keeping track of all strategies is pointless due to the large number of possible strategies. Therefore, we use collective variables – the number of strategies with a certain depth of memory and the number of strategies of a certain complexity (see [6]). These variables contain the most detailed information about the behavior of the depth of memory and the complexity in the 'society' of strategies during evolution. Numerical simulation of evolution makes it possible to determine the change in the number of strategies with a certain depth of memory. The behavior of these characteristics is shown in Fig. 43.

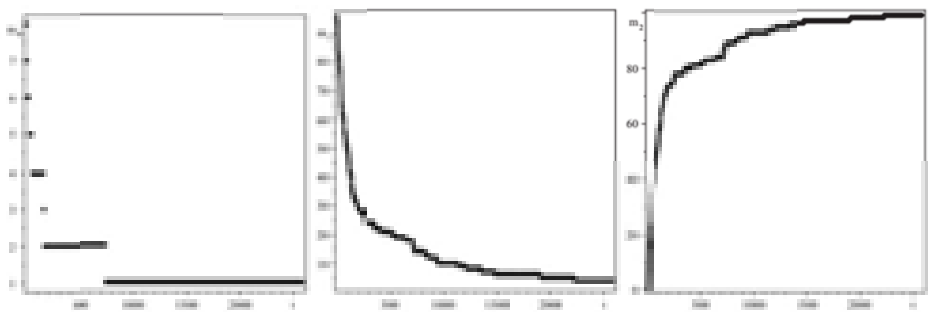

Fig. 43 Change over time in the number of strategies in society with a memory depth of 0 (left), 1 (centre) and 2 (right)

The monotonic decrease in the number of strategies with a memory depth of 0 (left curve) and with a memory depth of 1 (central curve) in Fig. 43 is clearly visible. One strategy with zero memory depth survives to the stationary state (this is strategy (1) 01) and 4 with memory depth 1 (in this implementation, these are strategies (1) (11) 0111, (1) (01) 0111, (1) (11) 0011 and (1) (01) 0011). Only the number of strategies with a memory depth of 2 (right curve) increases monotonically. This information allows you to calculate the average memory depth of the population.

Another important information already about the complexity of 'community' strategies is the number of strategies of a certain complexity. Their evolutionary behavior is shown in Fig. 44. Actually, given that each memory depth contains 3 levels of complexity, this allows us to understand in more detail what strategies are used to regulate each value of the memory depth.

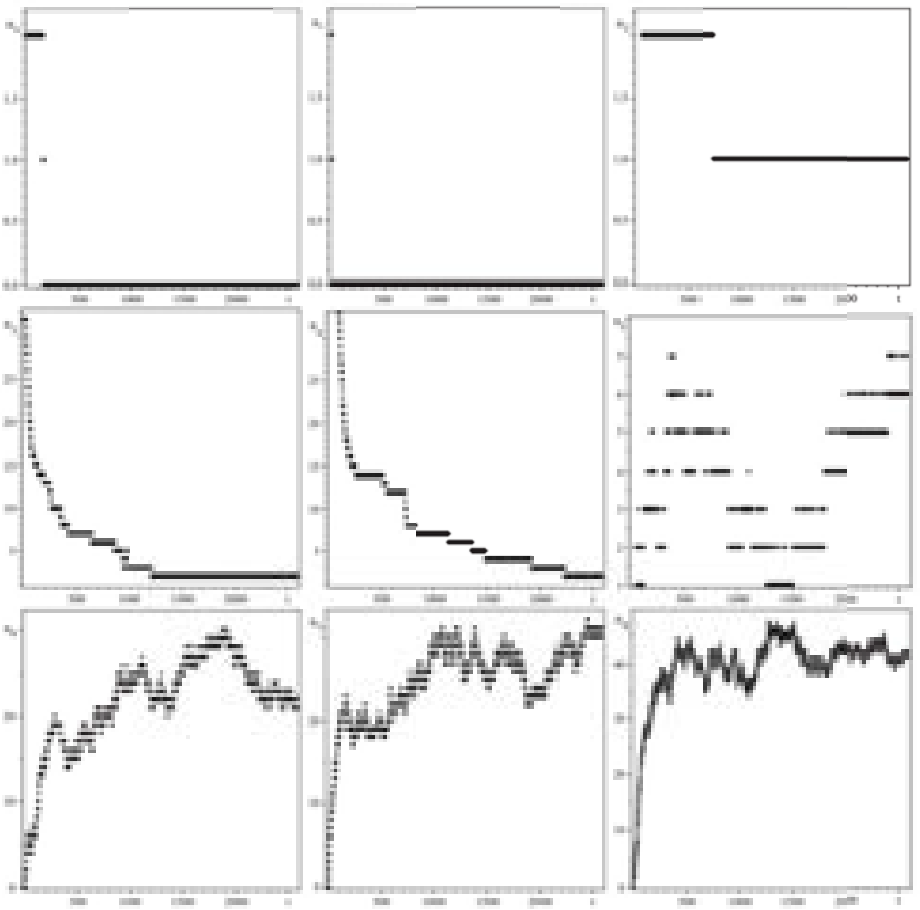

Fig. 44 Change over time in the number of strategies of the society with complexity 0 ($n_0(t)$) and with the complexity i of graphics $n_i(t)$, respectively $i = 1, 2...8$. The strategies of the upper series of complexity form strategies with a zero memory depth, the middle one with a memory depth of 1, and the lower strategy of a memory depth of 2

It can be seen that the number of strategies of low complexity (0, 1, 2, 3, 4) decreases with time, and only the number of strategies with complexity 6,7 and 8 increases. The number of strategies of boundary complexity 5 oscillates with increasing approach to the station. Primitive strategies of complexity 0 and 1 do not survive to a stationary state.

Only one strategy of difficulty 2 – (1) 01 ("tit for tat") survives to the stationary state, two strategies of difficulty 3 – (1) (11) 0011, (1) (01) 0011 and two difficulty 4 – (1) (11) 0111, (1) (01) 0111.

We now turn to a discussion of the average characteristics of 'community' strategies. Let's start with the behavior of the average memory depth of a

'community' over time. The average value of the memory depth is easy to determine by the known $m_i(t)$ as

$$\overline{M} = \frac{0 \cdot m_0(t) + 1 \cdot m_1(t) + 2 \cdot m_2(t)}{m_0(t) + m_1(t) + m_2(t)}$$

The result of calculating the change in the average memory depth of the strategy 'community' is shown in Fig. 45.

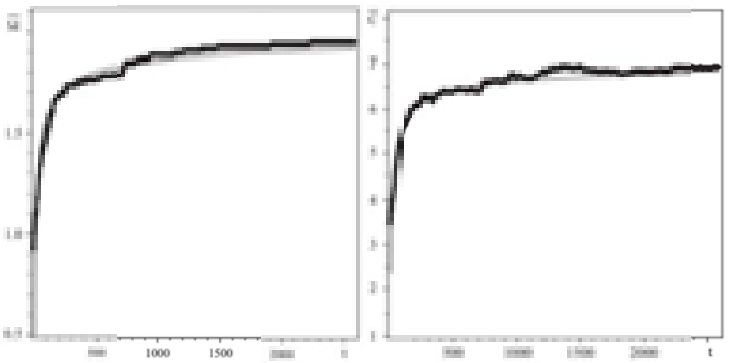

Fig. 45 On the left, the change in the average depth of society's memory over time (points) and the empirical curve $\bar{M} = 2 - \frac{2}{\sqrt{\frac{t}{5}+1}}$ *– a line. These dependencies show good agreement. On the right, the change in the average complexity of society's strategies over time is a thin curve corresponding to the root law of stationary state* $\bar{C} = 7.1 - \frac{5}{\sqrt{t/9+1}}$. *Good agreement between these dependences is seen*

It is easy to see that the average memory depth increases with time and reaches the maximum possible value close to 2 ($\bar{M} \approx 1.9$) in the stationary state.

It is possible that if the observation time is increased by an order of magnitude, then the maximum value of 2 will be reached. The character of reaching the stationary state has a power–law character close to, the coincidence of the dependences can even be improved by choosing constants. It should be noted that this relationship can be considered as a consequence of a kind of integral of motion $(M_{max} - M)^2 (Dt + 1) = const$. Statistical interpretation of this relationship leads to a quantity $\Delta r = \frac{1}{M_{max} - M}$ that performs normal Brownian motion with a diffusion coefficient D.

The calculation of the average complexity of a 'community' of strategies is also easy to perform using the number of strategies of a certain complexity $n_i(t)$ according to

$$\overline{C}(t) = \frac{\sum_{i=0}^{8} i n_i(t)}{\sum_{i=0}^{8} n_i}$$

The result of calculating the average complexity of the strategies is shown in Fig. 45. It can be seen that the average complexity increases monotonically, reaching asymptotically a plateau corresponding to the average complexity $\overline{C} \approx 7.1$. This is a fairly close value to the maximum possible complexity 8. Analysing these data, one can notice a satisfactory coincidence of the relaxation law of average complexity to the phenomenological root law (see Fig. 45)

$$\overline{C}(t) = 7.1 - \frac{5}{\sqrt{t/9+1}}$$

It should be noted that random throwing in strategies gives relatively small fluctuations in average memory depth and average complexity.

Another important characteristic of the population is the aggressiveness of strategies. By aggressiveness, as before, we mean the share of refusals of the strategy from cooperation. Below we restrict ourselves to a description of the behavior of the average aggressiveness of the population of strategies. The result of numerical simulation with the calculation of the average aggressiveness is shown in Fig. 46.

It can be seen that the average aggressiveness of society's strategies decreases over time (see Fig. 46). An exception is the short initial section, where an increase in aggressiveness is observed. Its value is close to the period of the disappearance of primitive strategies.

Data on the behavior of aggressiveness indicate a pronounced decline in the average aggressiveness of the society. It is important to note that the stationary state is formed by strategies that do not show aggressiveness towards each other. In the stationary state, the aggressiveness of the strategies is zero.

Perhaps this can be formulated as some kind of evolutionary principle for the selection of strategies. Thus, dividing the strategies of the population into classes of strategies with zero aggressiveness between the strategies within the class, one can establish contenders for survival in the process of evolution. The nature of the decline in aggressiveness, which can be established from numerical data, is not sufficiently pronounced, and is apparently close to linear.

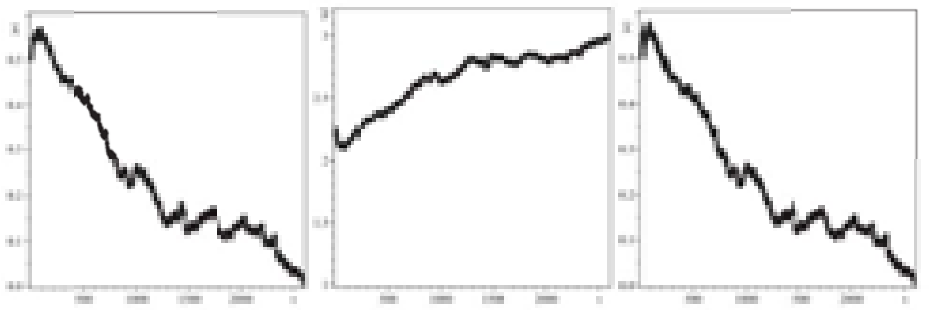

Fig. 46 On the left, the change in the average aggressiveness of society's strategies over time. In the center is the change over time in the number of points per turn of the strategy of the society on average. On the right is a comparison of the average aggressiveness obtained by numerical modelling (squares) with relation (2) (crosses). A slight difference can be seen only in the maximum, in the rest there is an overlap of points

Finally, let's move on to a discussion of how strategies set evolutionary advantage points at different stages of evolution. This characteristic makes it possible to compare the effectiveness of the interaction of strategies at different stages of evolution.

As such a characteristic, you can use the number of points scored in one turn of the strategy on average at a certain stage of evolution. The number of evolutionary advantage points gained by the strategy on average per turn increases with time (see Fig. 46). In other words, the interaction of strategies becomes more and more beneficial in the process of evolution.

Let's pay attention to the very short initial stage of points reduction per move. The correlation between the average aggressiveness of society and the number of points per strategy move becomes, at first glance, less noticeable than in evolution without a source of new strategies.

The universal connection between aggressiveness and the number of points scored on one turn of the strategy (2) remains in the presence of sources. The result of comparing the regularity (2) with the same choice of constants is shown in Fig. 46. The values of the constants in all cases are chosen the same $\overline{P}_{max} = 3$, $\lambda = 5.3/8$, and $a = 0.2$. Differences are difficult to notice due to the almost complete coincidence of the points. In other words, the universal law (2) is fulfilled not only in the statement of the Cauchy problem, but also in nonequilibrium cases with a source of strategies. At the end of this section, we will discuss the dominant strategies at each stage of evolution. By dominant strategies we mean winning strategies in each generation. Of course, the names or rules of the strategies are too detailed and not very informative. We will be interested in such properties of winning strategies as memory depth and complexity. Figure 47 shows the depth of memory and the complexity of winning strategies at all stages of evolution.

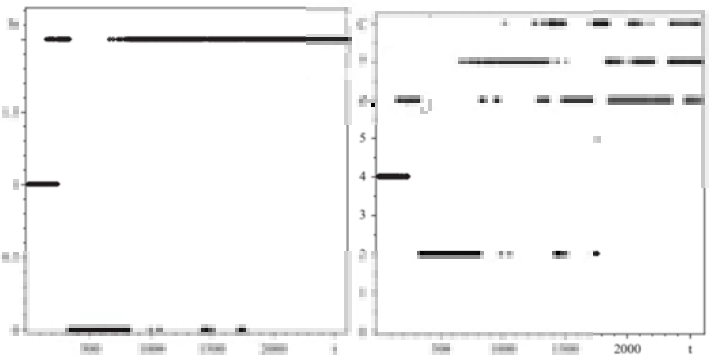

Fig. 47 On the left is the depth of memory of winning strategies at the corresponding stage of evolution. The right shows the complexity of the winning strategies at the corresponding stage of evolution

It is easy to see that as the 'community' evolves, deep–memory strategies and complex strategies begin to dominate it. However, at the initial stage of evolution, there were periods of dominance of strategies without memory and low complexity 2. Single stages of dominance of such strategies occur up to 1771 generations, which is 68% of the entire time of going to the stationary state.

It should be expected that in other communities of strategies with a greater depth of memory, the dominance of primitive strategies can be observed at significant periods of evolution.

11.2. 'Community' of strategies with unit memory and source of strategies with depth of 2 memory

Let us now turn to the 'community' of strategies, from which primitive strategies without memory are excluded and there is a source of strategies with a depth of memory 2. At the initial stage, the 'community' contains all strategies with a single memory. In principle, this is a fairly close situation to the one considered above, and the main interest is the influence of primitive strategies on the evolution of communities.

Each strategy enters into competition with every other strategy of society (including itself) 100 times as in the previous case. Evolution is carried out according to the same rules that were described in detail above. The evolutionary process continues until stationary state.

Thus, the main difference from the previous case is the absence of strategies with zero memory depth throughout evolution.

In the case under consideration, the stationary is reached at the 2656 stage of evolution a little later than in the presence of strategies with zero memory depth in the 'community'. There are 96 strategies in the stationary state, taking into account the differences in the first move.

All these strategies have zero aggressiveness towards each other and gain the same number of points (28800.0) at the stationary stage of evolution.

At the stationary stage, strategies with greater depth of memory and complex ones survive. Fig. 48 shows the number of strategies in the stationary state depending on the depth of memory and complexity.

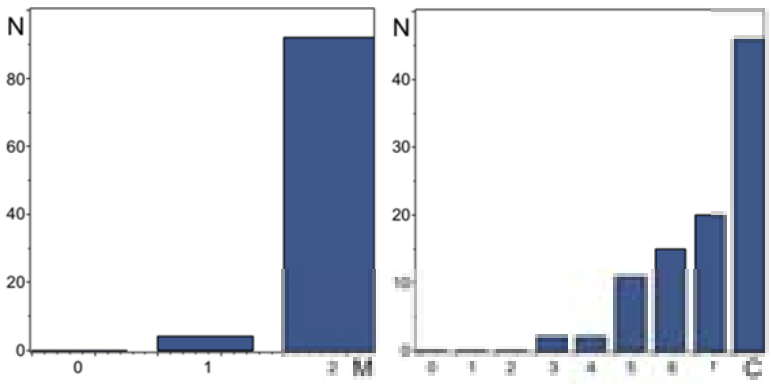

Fig. 48 The number of strategies N in the stationary state with a certain memory depth M on the left and the number of strategies of a certain complexity C on the right

It is easy to see that in the stationary state, most of the strategies have the maximum memory depth and maximum complexity. It contains only 4 strategies with 1 memory depth, a pair of which has complexity 3 (these are strategies (1) (01) 0011 and (1) (11) 0011), and the second pair (1) (01) 0111 and (1) (11) 0111 – complexity 4. A small part of the strategies have a memory depth less than the maximum and those remaining in the stationary state have a complexity less than the maximum. At the same time, primitive strategies with complexity 0, 1, 2 are completely absent in the stationary state. In other words, the population is captured by complex strategies with maximum depth of memory.

Let us now discuss going to the stationary state. Let's start with the evolution of the number of strategies with different memory depths. In the case under consideration, the number of strategies with zero memory depth is equal to zero in the formulation of the problem. Therefore, Fig. 49 shows the time dependences of the number of strategies only with a memory depth of $1-m_1(t)$ and with a memory depth of $2-m_2(t)$.

It is easy to see that the number of strategies $m_1(t)$ decreases over time, while the number $m_2(t)$ increases. It is interesting to note the absence of significant fluctuations in their numbers, despite the presence of a random source of strategy. The behavior of these quantities is quite close to their behavior in the previous case.

Let's move on to the behavior of the complexity of strategies. Figure 50 shows the number of strategies with a certain difficulty. There are no strategies with difficulty 0,1,2 in the 'community' and their number is zero.

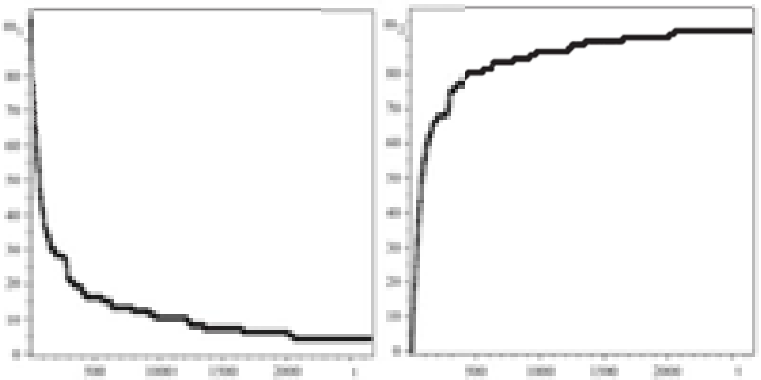

Fig. 49 Change over time in the number of strategies of society with a depth of memory 1 (left) and 2 (right)

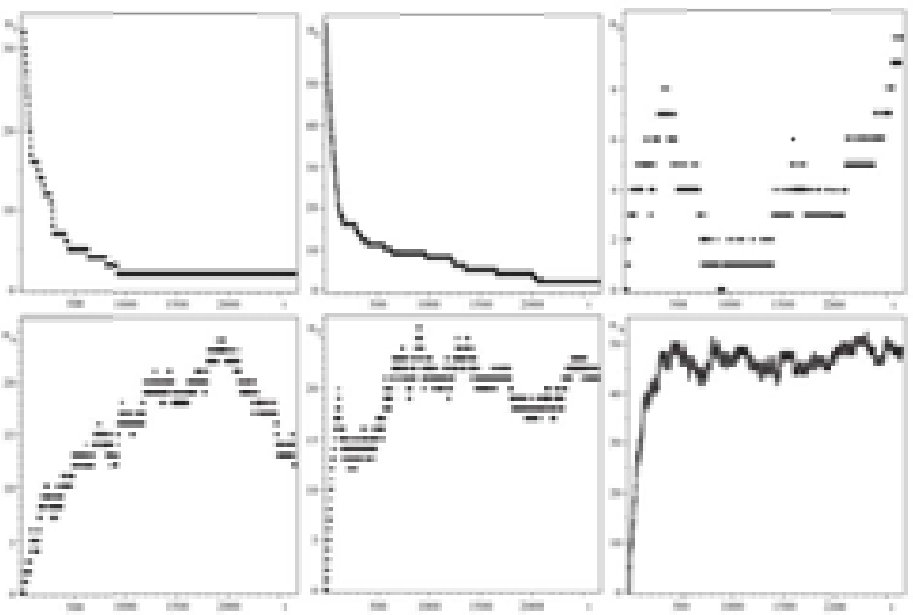

Fig. 50 Change over time in the number of strategies of society with complexity 3 ($n_3(t)$) and with complexity i*, graphs* $n_i(t)$*, respectively* $i = 4...8$

As in the previous case, the number of strategies with difficulty below 5 decreases, and above it increases with noticeable oscillations. The number of complexity 5 is boundary, separating qualitatively different modes. Oscillations in the number are, naturally, most noticeable in the case of a small number of strategies. In these cases, random throwing in strategies has a significant impact. Therefore, the relative amplitude of fluctuations $n_8(t)$ is less than $n_7(t)$ and $n_6(t)$. The maximum amplitude of oscillations is reached at the value of the boundary abundance $n_5(t)$. The amplitude of the corresponding oscillations of the order of $\sqrt{n_i(t)}$ where $i = 5,6,...,8$. With increasing numbers, the relative amplitude decreases $\sim \frac{1}{\sqrt{n_i(t)}}$ in accordance with the usual statistical laws.

The dependencies obtained above make it easy to establish the change in the average memory depth and average complexity of 'community' strategies over time. So the dependence of the average memory on time is shown in Fig. 51. There is a monotonic increase in the average memory depth with the approach to a stationary value close to 2. It is interesting to note that the previously discovered root law of reaching the stationary state is in good agreement with this case as well. This can be seen by comparing the behavior of the average memory depth, which is obtained by numerical simulation with the analytical dependence

$$\bar{M} = 2 - \frac{2}{\sqrt{\frac{t}{5}+1}}$$

It can be noted that good agreement of these dependences is an additional argument for the statement that with increasing time, the average memory will tend to the value of 2.

The result of modelling the behavior of the average complexity of 'community' strategies is shown in Fig. 51. The same figure shows the analytical dependence of the behavior of medium complexity, which is in good agreement with the results of modelling the evolution of 'community' strategies with 0 and 1 memory depths (see Section 11.1). In the case under consideration, the same curve shows good agreement with the simulation data. In other words, the entrance to the stationary state in this case also occurs according to the root law

$$\bar{C} = 7.2 - \frac{5}{\sqrt{t/9+1}}$$

and the stationary state is formed by complex strategies close to maximum complexity.

Let us now turn to the average aggressiveness of society. Its change over time is shown in Fig. 52. The nature of the change in the average aggressiveness persists in this case as well. Average aggressiveness decreases over time. the stationary state is formed by strategies that have zero aggressiveness towards each other.

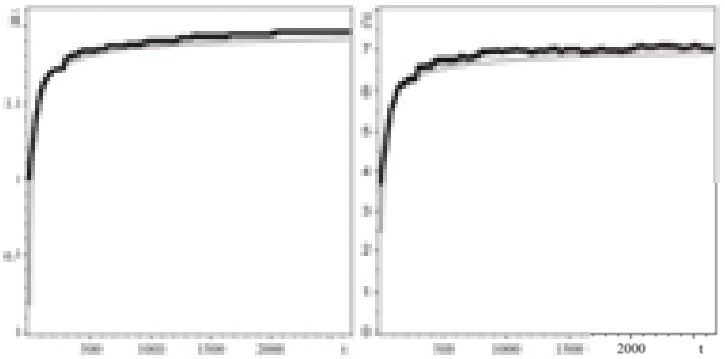

Fig. 51 On the left, the change in the average depth of society's memory over time (points) and the empirical curve $\overline{M} = 2 - \frac{2}{\sqrt{\frac{t}{5}+1}}$ *is a line. These dependencies are in good agreement. On the right, the change in the average complexity of society's strategies over time is a thin curve corresponding to the root law of exit to the stationary state* $\overline{C} = 7.2 - \frac{5}{\sqrt{t/9+1}}$ *. Good agreement between these dependences is seen*

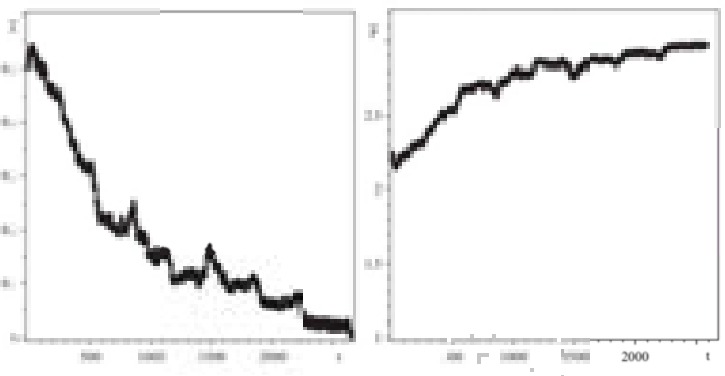

Fig. 52 On the left, the change in the average aggressiveness of society's strategies over time. On the right, the change over time in the number of points per turn of the strategy of the society on average

In accordance with the universal relationship (2), the average number of evolutionary advantage points should be expected to increase over time. Figure 52 on the right shows the time dependence of the average number of evolutionary advantage points per strategy turn. The data are in good agreement with the empirical relationship (2).

Thus, all dependencies are qualitatively preserved, and the resulting differences are reduced to small quantitative changes.

Consequently, in the process of evolution, society is captured by complex strategies with great complexity and maximum depth of memory. All stationary strategies have zero aggressiveness towards each other. Moreover, these patterns are true for all societies, when strategies of greater complexity are thrown in than were initially present in society.

The case of a society with a memory depth of 0 is considered, and strategies with a memory depth of 1 and separately with a memory depth of 2 are thrown in. The patterns of behavior of the population strategies described above are retained in these cases as well.

Therefore, let us consider the case when strategies of a smaller depth of memory are thrown in than they were initially in society.

11.3. 'Community' of strategies with unit memory and source of strategies with memory depth 0

The selection rules and pay-out matrix for evolution modelling remain the same. The typical time to reach the stationary states 583 stages. 96 strategies remain in the stationary state(this is taking into account the differences in the first move or the number of strategy carriers). The distribution of strategies by memory depth and complexity is shown in Fig. 53

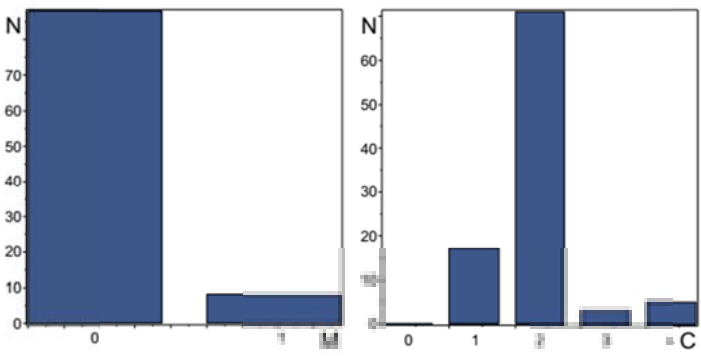

Fig. 53 The number of strategies N in the stationary state with a certain memory depth M on the left and the number of strategies of a certain complexity C on the right

It can be seen that the distribution of strategies by memory depth and complexity changes qualitatively in comparison with the previous cases. The maximum number of strategies with zero memory, but with a unit memory depth, strategies are present in the stationary state. The number of complexity also has significant differences. First of all, there is a maximum number at the complexity of strategies 2. Note that this value of complexity corresponds to the maximum complexity among the strategies to be thrown in. Actually, these strategies also dominate in the stationary state.

It can be assumed that the maximum number in the problems with the throw–in of strategies is achieved on the throw–in strategies with the maximum complexity. This rule is fulfilled in all considered cases. Primitive strategies of complexity 0 disappear from the stationary state as in the previous cases. A small number of the most complex strategies (5.2%) survive (see Fig. 53) despite a large numerical advantage and the throw–in of primitive strategies. Approximately the same number of strategies with maximum memory (8.3%) remain in the stationary state. In other words, even in such an unfavourable situation, the complexity of the strategy allows one to survive and penetrate into the stationary state of the population. All stationary strategies have 0 aggressiveness towards each other. Each stationary state strategy scores the same 28,800 evolutionary advantage points.

The rule of zero aggressiveness is fulfilled in all the cases considered, both in the absence of a source and in the presence of a source of new strategies. The exception is alternative evolution and cumulative populations.

Let's move on to the evolution of strategies over time. The extinction period of the most aggressive strategy (0) 0000 takes 319 stages and is the time it takes 54.7% to enter the stationary state. The change in the distribution of the number of strategies by memory depth is shown in Fig. 54. The qualitative difference from the previous cases consists in an increase in the number of strategies with zero memory depth and a decrease in the number of strategies with a greater memory depth.

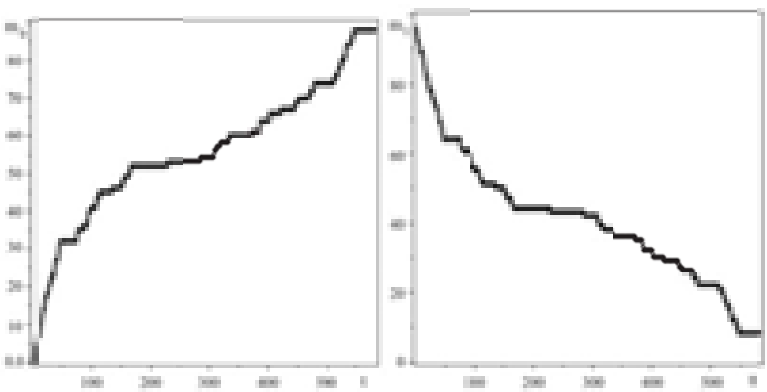

Fig.54 Changes in the number of strategies over time with a memory depth of 0 is shown on the left, and with a 1st depth on the right

The nature of the dependences of the number of strategies of a certain complexity is rather nontrivial (see Fig. 55). It can be seen that at the initial stage the number of strategies with zero complexity increased, but rather quickly their number decreased to zero and such strategies did not enter the stationary mode. There were no strategies with difficulty 1 at the initial stages, but their numbers began to increase starting from about half of the time they entered the stationary state. The number of strategies with complexity 2 monotonically increased throughout the entire evolutionary time. Strategies of higher complexity decreased their numbers throughout the entire time of admission to the stationary state. However, their number reaches the final non-zero value in the stationary state.

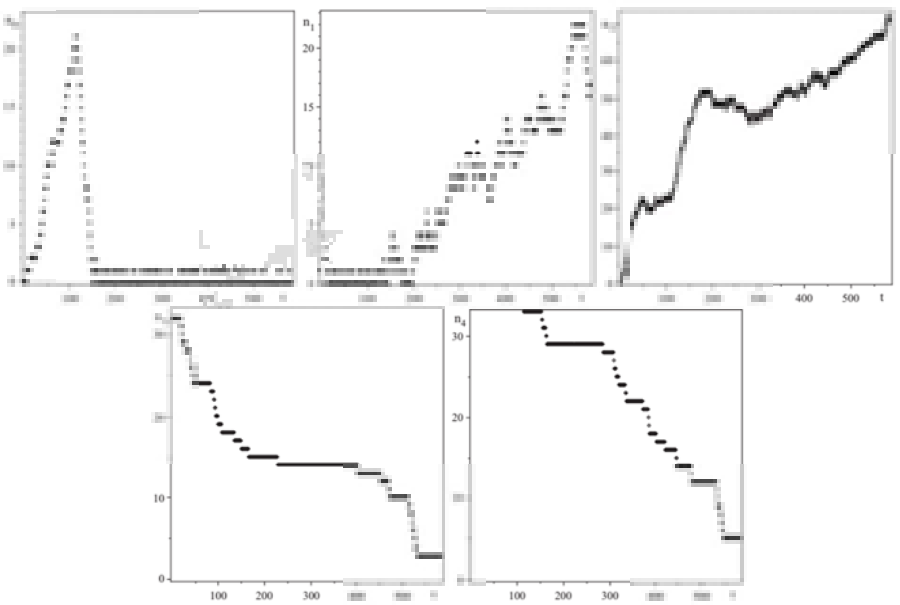

Fig. 55 Shows the change over time in the number of strategies with a certain complexity in society at different stages of evolution. Difficulty 0 – $n_0(t)$ *, difficulty 1 –* $n_1(t)$ *, difficulty 2 –* $n_2(t)$ *, difficulty 3 –* $n_3(t)$ *and difficulty 4 –* $n_4(t)$

The change in the average depth of a society's memory over time is easy to derive from addictions $m_0(t)$, $m_1(t)$. The average depth of memory of society over time is shown in Fig. 56

One can see a characteristic decline over time to a low level of memory depth, equal to in the stationary state. The average complexity of society's strategies is shown in Figure 56. There is a noticeable decrease in the average complexity of strategies. The stationary level of complexity is slightly higher than 2. The fluctuations of this and the previously given dependencies are associated with a random throw–in of strategies of complexity 0.1 and 2.

The change in the average aggressiveness of strategies is shown in Fig. 57.

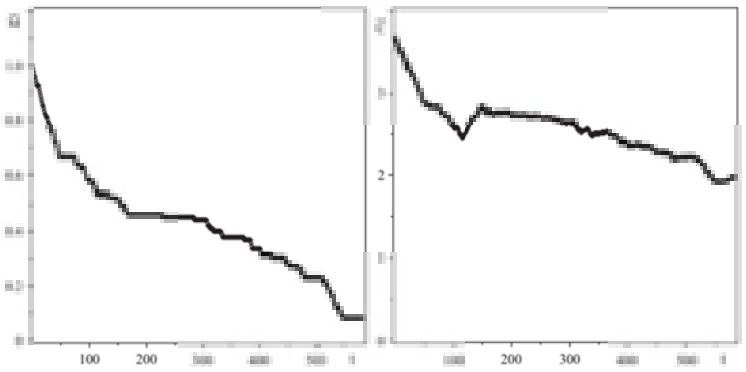

Fig. 56 On the left is the average depth of the memory of society from time to time. On the right is the average complexity in society at different stages of evolution

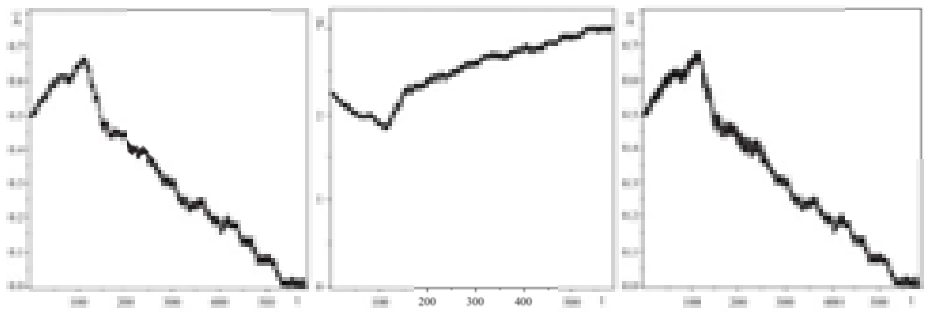

Fig. 57 On the right is the average aggressiveness of society at different stages of evolution. In the centre is the average number of points per strategy turn at different stages of evolution. On the left is a comparison of the average aggressiveness with the aggressiveness built according to relation (2) according to the data on the number of points per move of the average strategy (crosses). A good match of the dependencies is seen

It is interesting to note that the change in the aggressiveness of society is qualitatively preserved, as in the evolution of society without a source of new strategies. This dependence has a maximum at the initial stages of evolution and a monotonic (possibly linear) decrease to 0 before reaching the stationary state.

Based on this dependence, one can distinguish a primitive stage in the development of society with an increase in aggressiveness. The position of this maximum correlates well with the observed dip in the average complexity of strategies (compare with Fig. 57).

Let us now present the dependence of the evolutionary advantage points obtained on average by the strategy per one move in Fig. 57. There is a qualitative relationship between the number of points and aggressiveness. With an increase in aggressiveness, the number of points decreases, and with a decrease in aggressiveness, the number of points increases. The strategy receives the maximum number of points in the stationary state with zero aggressiveness towards each other.

It is interesting to note that the universal relationship (2) between aggressiveness and the number of points per strategy move holds well in this case as well. Comparison of the average aggressiveness with that built according to relation (2) is shown in Fig. 57.

Let us now discuss the dominance of strategies in the evolutionary process. Figure 58 shows the memory depth of the winning strategies on the left and the complexity of the winning strategies on the right. The dominance of strategies with maximum memory depth is interspersed with periods of dominance of strategies with zero memory depth. When approaching thestationary state, strategies with the maximum possible memory depth dominate. Similarly, the dominance of strategies with maximum complexity occurs with the presence of periods of dominance of strategies of lower complexity. However, there are no periods of dominance of strategies of minimum complexity 0, and the only case of dominance of a strategy of complexity 1 at the last stage is rather an exception to the rule.

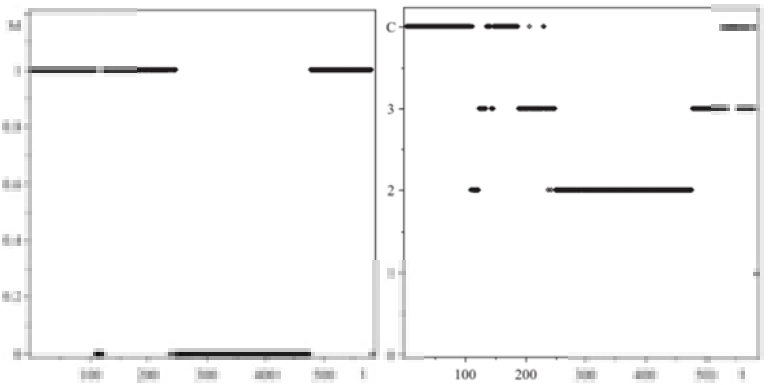

Fig. 58 On the left is the depth of memory of the winning strategy, on the right is the complexity of the winning strategy at the corresponding stage of evolution. Thus, the strategy 'community' is dominated by complex strategies

In the presence of sources and sinks of strategies, complex strategies are present in the stationary state as well as strategies with the maximum memory depth. Zero–memory strategies die out before stationary state. In this sense, the depth of memory and the complexity of strategies are evolutionarily beneficial properties. The maximum number of strategies in

problems with a source is achieved at the maximum complexity of the strategies being thrown in.

In all cases, the aggressiveness of the strategies decreases and reaches zero at the stationary stage. Perhaps this universal property can be used as a basic principle for the selection of strategies in evolution and in more complex communities. There is a universal relationship (2) between aggressiveness and the number of points per strategy move. The higher the aggressiveness, the lower the evolutionary advantage points per strategy turn.

SECTION 12. THE EVOLUTION OF MEMES

Prior to this section, different cases of evolution of individual strategies were considered. In this section, we will consider the evolution of individuals, each of which has a finite set of strategies with memory [71].

In this case, it is naturally necessary to change the rules of meeting strategies, interaction and their selection. In a population, all individuals at each stage of evolution are randomly divided into pairs of individuals that interact. All strategies of one individual interact with the strategies of another individual, also randomly dividing into opposing pairs. These pairs of strategies compete according to the iterated prisoners' dilemma. The pay-out matrix remains the same as in previous cases. The winning strategy in a pair struggle of strategies replaces the losing strategy of the corresponding individual. In other words, there is an exchange of strategies between individuals with the removal of losing strategies.

After the interaction of all pairs of individuals in accordance with the described rules, the next stage of evolution begins. Again, all individuals are randomly divided into pairs that interact. In a certain abstract sense, it resembles the evolution of ideas or memes in different societies. Evolution stops when the population enters a stationary state. In the course of evolution, we will monitor the properties of the strategies of the population and all individuals included in the population.

Let us now discuss the choice of the initial distribution of strategies over individuals of the population. The total number of strategies with a memory depth of 2 is distributed among individuals. The process of distributing strategies among individuals can be carried out in different ways. Below we will implement two ways of distributing strategies. In the second method, we will choose strategies for an individual or a carrier, assuming their uniform distribution over the memory depth. In other words, all strategies are divided according to the memory depth into three sets, and it is assumed that the choice from each such set is equally probable when forming the initial distribution of the strategies of an individual.

Another feature of the considered population of individuals is the emergence of collective variables to describe individuals, and not just the population of strategies.

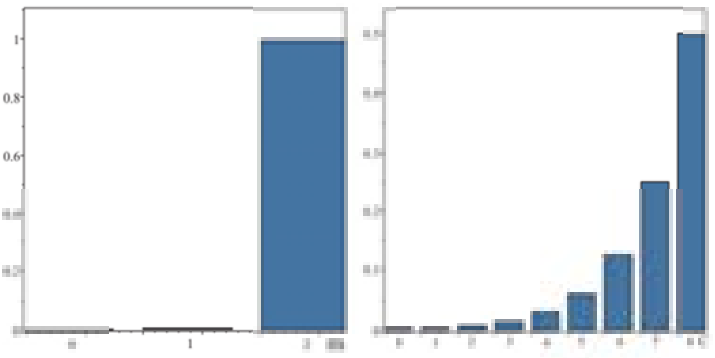

Fig. 59 The share of strategies of a certain memory depth – on the left, and the share of strategies of different complexity – on the right in the middle individual at the beginning of evolution. The same histogram determines the probability of finding in an individual a strategy of a certain depth of memory (left) and complexity (right) at the initial stage of evolution

Thus, each individual has a distribution of strategies in terms of memory and complexity, and the entire individual can show quite a certain aggressiveness. Therefore, the characteristics of the individual appear, such as the distribution of the strategies of the individual by the depth of memory and by the complexity. These distributions determine the average depth of memory, the complexity i of an individual and its average aggressiveness.

$$\langle M\rangle_i = \sum_{j=1}^{N_i} \frac{M_{ij}}{N_i}, \langle C\rangle_i = \sum_{j=1}^{N_i} \frac{C_{ij}}{N_i}, \langle A\rangle_i = \sum_{j=1}^{N_i} \frac{a_{ij}}{N_i}$$

Here $\langle M\rangle_i$, $\langle C\rangle_i$, $\langle A\rangle_i$ respectively, average memory, average complexity, average aggressiveness of an individual, N_i number of strategies in an individual, M_{ij} depth of strategy memory j in an individual i, $C_{ij} - j$ strategy complexity in an individual i, $a_{ij} - j$ strategy aggressiveness in an individual i.

These local characteristics can be used to track changes in the properties of individuals in the population during evolution. In addition, global characteristics of the population appear, such as the average values of memory, complexity and aggressiveness of individuals of the entire population.

$$\overline{M} = \sum_{i=1}^{S} \frac{\langle M\rangle_i}{S}, \overline{C} = \sum_{i=1}^{S} \frac{\langle C\rangle_i}{S}, \overline{A} = \sum_{i=1}^{S} \frac{\langle A\rangle_i}{S}$$

Here S is the number of individuals in the population. These characteristics are calculated by averaging over all individuals in the

population and determine the typical characteristics of an individual in the population. Another useful characteristic determines the diversity of strategies in a population – this is the number of different strategies in a population, which we will call generating strategies. The generative strategies of a population are understood as the number of different strategies present in the population at some stage of evolution. Accordingly, as characteristics of the generating strategies of the population, we use

$$\langle M\rangle = \sum_{i=1}^{N}\frac{M_i}{N}, \langle C\rangle = \sum_{i=1}^{N}\frac{C_i}{N}, \langle A\rangle = \sum_{i=1}^{N}\frac{a_i}{N}$$

Here N is the number of generating strategies of the population, and $\langle M\rangle$, $\langle C\rangle$ и $\langle A\rangle$ accordingly, the average memory, complexity and aggressiveness of the generating strategy.

12.1. Evolution of individuals with an initial uniform distribution of strategies

Consider a population of 50,000 individuals, each with 50 strategies. The ratio between these values is chosen so that all strategies with a memory not exceeding 2 are present among the individuals of the population. The choice of these strategies is carried out in an equiprobable manner from the set of all strategies with a memory depth of no more than 2.).

In this case, in individuals of the population, strategies with memory 2 dominate in accordance with the largest number of such strategies in the initial set of strategies (32640) and a significantly smaller number of strategies with a memory depth of 1 (120 strategies) and a very small number of strategies with a zero memory depth (8 strategies). The initial distribution of strategies by individuals is shown in Fig. 59 and inherits the distribution properties of all strategies. The overwhelming number of strategies with a memory of depth 2 and maximum complexity, characteristic of the initial distribution of strategies in an individual in Fig. 59, is a consequence of the selected rule for selecting strategies for an individual. Further, when calculating the characteristic properties of individuals, averaging was carried out over 10 realizations of the initial state and their evolution. Thus, the initial distribution of individual strategies in terms of memory depth and complexity is shown in Fig. 59.

Let us discuss the initial distribution of aggressiveness, which is formed in individuals of the population with such an initial distribution of strategies. To do this, we will carry out the interaction of individuals at the first step of evolution, which will allow us to determine the initial aggressiveness of individuals in the population. At the first stage of evolution, all individuals are randomly divided into pairs of individuals that interact.

All the strategies of one individual interact with the strategies of another, also randomly dividing into opposing pairs of strategies, in accordance

with the iterated prisoner's dilemma. The number of moves was chosen equal to 100 (see the rationale for this choice [64]). In this case, the strategies compete twice, in one meeting one strategy makes the first move, and another strategy starts the second. This way of competing between the two strategies negates the importance of the first move. The pay-out matrix [61,64,67] to identify the winning strategy is chosen as on table1.

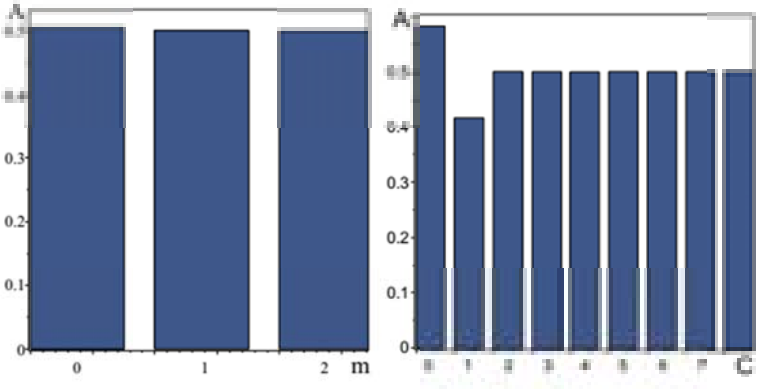

Fig. 60 The initial distribution of the aggression of individuals of the population by memory (left) and by complexity (right), calculated at the first step of evolution

The winning strategy, or the one with the highest number of points, replaces the losing strategy of the corresponding individual in a pair struggle of strategies.

According to the results of the competition, the aggressiveness shown by the individual (or the relative number of refusals to cooperate) at the first stage of evolution is determined. This is actually the initial aggressiveness of individuals. Fig. 60 shows the distribution of the initial aggressiveness of individuals of the population in terms of memory and complexity. It is easy to see that the average aggressiveness of individuals in the population is close 0.5. At the same time, strategies with different memory depths show approximately the same aggressiveness.

The aggressiveness of strategies with zero complexity is maximum, and aggressiveness of complexity 1of strategies is minimum value, strategies of greater complexity have the same aggressiveness (see Fig. 60). Thus, the aggressiveness of primitive strategies with memory depth 0 and complexity 0 is maximal.

Further evolution makes it possible to establish characteristic changes in the basic characteristics of individuals with the time of evolution.

First of all, the number of strategies for each individual decreases. Figure 61 shows the average decrease in the number of strategies in a single individual. In the process of evolution, after the stage of exponential decline in the number, its approach to a stationary value is observed. With such a

ratio of individuals and their strategies, the stationary is achieved at the average. Thus, individuals form a stationary set of strategies with certain properties.

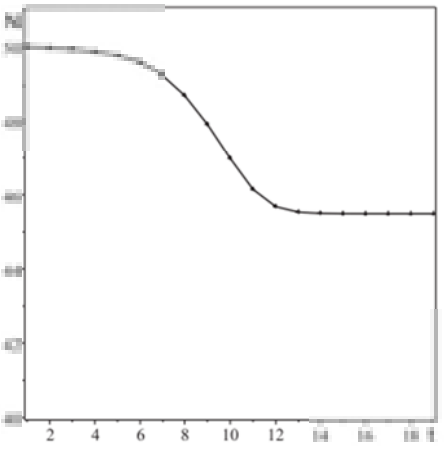

Fig.61 Change in the number of strategies on average in an individual of the population with the time of evolution

Let us consider how the distribution of strategies in terms of the memory depth of an individual changes over time. Figure 62 shows the changes in the distribution of strategies of an individual by memory in the process of evolution. As a convenient characteristic for this, we use the probability of finding a strategy in an individual with a depth of memory $m = 0,1,2$ respectively. The probability of detecting strategies with a memory depth of 0 and 1 in an individual increased to 10 and 9 steps, respectively, at the same time the probability of strategies with a memory depth of 2 decreased insignificantly and stabilized at a significant level (Fig. 62).

It is clearly seen that the probability of detecting strategies of maximum memory depth in an individual throughout evolution remains high.

Note that the probability of detecting strategies with minimal memory 0 and 1 did not decrease over time, but even increased. So for memory 0 the probability of detecting it increased by an order of magnitude, and for memory 1 – 3 times, while remaining at a low level.

The composition of the strategies of an individual also undergoes qualitative changes in terms of complexity. Let us consider the change in the probability of finding a strategy of a certain complexity in an individual in the process of evolution. Figure 63 shows the probabilities of finding strategies of a certain complexity in an individual at the corresponding stages of evolution.

A rather varied behavior of these probabilities is noticeable. Each probability of corresponding difficulty follows three different types of behavior: decreasing, increasing, and oscillating. These probabilities go to certain stationary levels. At the end of evolution, the most complex strategies with

complexity 6 ($P_{c6} \approx 0.12$), 7 ($P_{c7} \approx 0.25$), 8 ($P_{c8} \approx 0.5$)are most likely, and their changes over time are negligible.

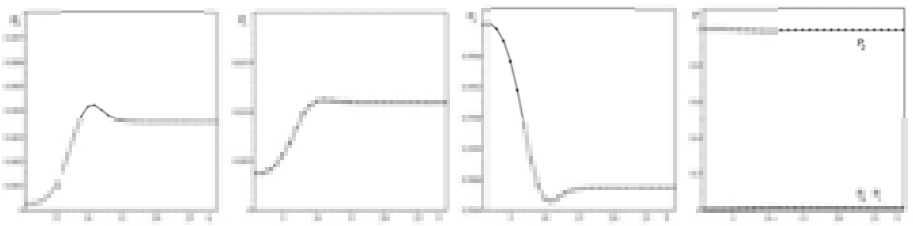

Fig. 62 Shows the time variation of the detection probability in an individual of a strategy with a memory depth of 0 – P_0, with a memory depth of 1 – P_1 and with a memory depth of 2 – P_2. Right – these dependencies are shown at the same scale. It can be seen that the changes in the initial probabilities are relatively insignificant

Roughly speaking, they easily maintain their high numbers and the likelihood of their presence in the individual. Strategies of complexity 1, which disappeared from the population after the 12th step of evolution, exhibit significantly different behavior. Note that these strategies were the least aggressive among all strategies. It can be noted that the probability of detecting strategies with memory depth 0 increases due to the increasing probabilities of strategies of complexity 0 and 2. It is interesting to note that although the probability of detecting the most primitive strategies with zero memory and complexity increases by $4 \div 5$ times, it remains low $P_{c0} \approx 0.02$. The increase in strategies with zero memory occurs mainly due to the increase in primitive strategies.

The most common is the behavior of the probabilities to detect the most complex strategies P_{c6}, P_{c7} P_{c8}, which practically retain their initial value. The reason for this is their overwhelming number and small number of low–complexity strategies, which does not allow them to significantly influence strategies of high complexity. The probabilities P_{c5}, P_{c4} of detecting, undergo noticeable changes. By the nature of their behavior, over time, it is noticeable that strategies of complexity 5 and 4 are competing for their presence in an individual, influencing each other. Strategies of lower complexity have little impact on their fight. Thus, in an individual in a stationary state, strategies of maximum memory depth and complexity close to maximum have a dominant probability. Despite this, the most primitive strategies did not disappear and even increased their likelihood of being present in an individual while remaining at a low level.

More obvious tendencies are manifested by the change in the aggressiveness of individuals in the population. The average aggressiveness of individuals of the population tends to the maximum possible aggressiveness equal to 1. The distribution of aggressiveness by the depth of memory is shown

in Fig.64. It can be seen that strategies with zero memory show the greatest aggressiveness at all times of evolution, and strategies with memory depth 1 show the least aggressiveness. After the 10th stage of evolution, the difference in their aggressiveness disappears, coinciding with the behavior of average aggressiveness (see Fig. 64). The stratification of aggressiveness by difficulty also indicates a typical increase in aggressiveness and striving for maximum value. The exception is strategies of complexity 1, as the least aggressive strategies that disappear from the population after stage 12.

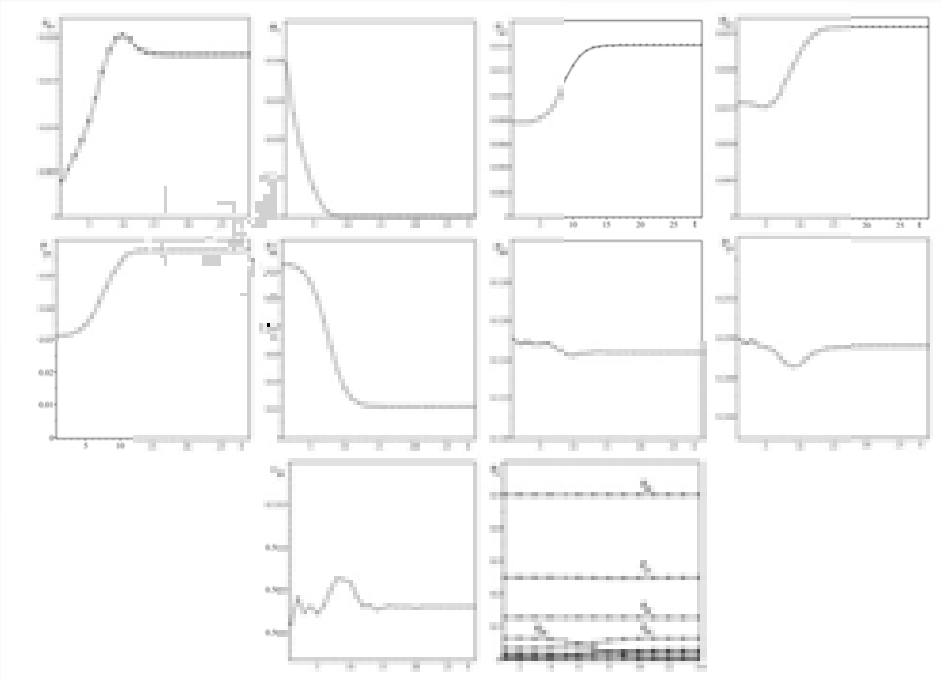

Fig. 63 Shows the time variation of the detection probability for an individual with a strategies with a complexity of 0.1, ..., 8, which are designated P_{c0}, P_{c1}, ... , P_{c8} ... P_{c0}, P_{c1}, ... , P_{c8}, *respectively. A typical decrease in probabilities is observed only for strategies of complexity 1 and 5. The last figure shows these dependencies on the same scale*

Thus, the aggressiveness of population strategies, regardless of the depth of memory and the complexity of strategies, grows with evolution and reaches a maximum value in the stationary state. The stationary set of strategies of an individual is made up of the most aggressive strategies in relation to the strategies of other individuals.

The stationary distribution of strategies is formed by strategies of maximum memory depth and complexity. The variety of strategies present in the population is significantly reduced. The number of generating

strategies in the stationary state decreased by 97.7% relative to the initial one, while the number of strategies of an individual decreased by 9% only. It should be noted that in the process of evolution, no strategy was able to spread to all individuals. The maximum presence of one strategy in individuals was on average 21%, which differed from the initial number by no more than 0.4%. It should be noted that an increase in the number of individuals does not affect the characteristic behavior of their strategies. All trends of changes in individuals are retained as well as stationary values. Apparently, this is due to the presence of all forming strategies in individuals in the initial population; therefore, a further increase in the population size does not lead to significant changes.

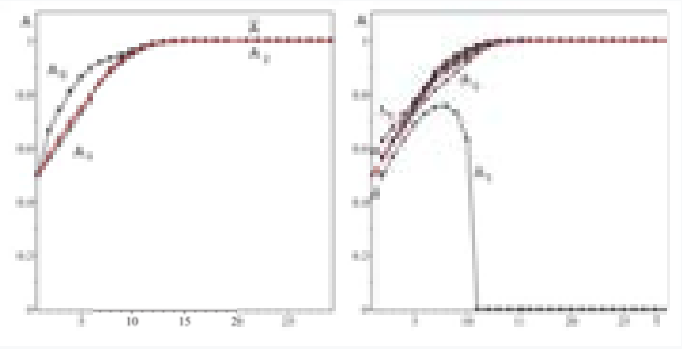

Fig. 64 Average aggressiveness of an individual of a population with evolutionary time. On the left, in the depth of memory, where $\overline{A}$ it corresponds to the average aggressiveness of the population, A_0, A_1, A_2 to the aggressiveness of strategies with a memory depth of 0, 1, 2. On the right, in terms of complexity, where $\overline{A}$ it corresponds to the average complexity of the population, and $A_0, A_1, ..., A_8$ to the aggressiveness of strategies with the complexity from 0 to 8

12.2. Evolution of individuals with an initial uniform distribution of strategies on memory

Let us now consider the evolution of a population with a different initial distribution of strategies among individuals. We will form the initial distribution of the strategies of an individual by choosing equally probable strategies of different memory depths from the generating strategies. ...

In other words, all generating strategies are divided into three classes, each with its own memory depth, and the choice is made equally likely from these classes. All characteristics will be averaged over ten different realizations or experiments with the same initial parameters. In this section, the number of carriers or individuals is 50,000, and the number of strategies for each is 24. With this choice, each individual has an equal

number of strategies of different memory depths (Fig. 65) at the beginning of evolution. The main difference from the previous case is the equal proportion of strategies with memory 0.1 and 2 for each individual in the initial population.

As a result, the initial distribution of the complexity of strategies in a typical individual has a non–monotonic dependence as shown in Fig. 65 on the right. There is a reduced initial number of complex strategies with $C = 6,7,8$ and an increased number of strategies with $C = 2,4$ (see Fig. 65). However, although the ratio of the share of strategies of complexity 2 (maximum) to the share of strategies of complexity 5 (minimum) reaches 10, on the whole, all the difficulties for an individual are presented more evenly than in the previous case.

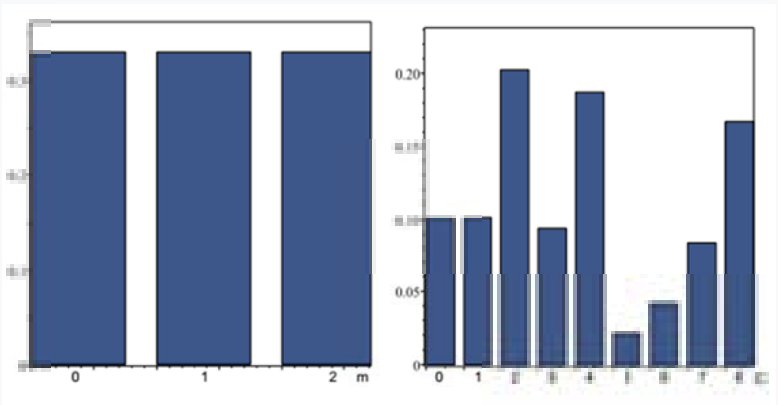

Fig. 65 Initial distribution of strategies in the average individual in the population in terms of memory depth (left) and complexity (right)

To clarify the aggressiveness of the strategies of the population, we will carry out the first stage of the evolution of strategies and determine the initial value of their aggressiveness. Fig. 66 shows the results of modelling and the dependence of aggressiveness on the depth of memory and the complexity of population strategies.

First of all, we note that, despite the significantly different distribution of strategies among individuals, the initial distribution of aggressiveness in terms of memory depth and complexity remains the same. At the same time, the tendency for an increased average aggressiveness of strategies of 0 complexity and a decreased aggressiveness of strategies of complexity 1 even intensified due to an increase in the number of these strategies.

Let us now consider how the evolution of such an initial population affects the number of strategies of an individual and their memory depth. Fig. 67 shows the change in the number of strategies on average for an individual – on the left. The change in the number of strategies in an individual is of a universal nature, demonstrating a decrease in their number in the course

of evolution. To control the change in the memory depth of an individual, we use the probability of detecting a strategy of a certain memory depth in an individual, which are shown in Fig. 67 on the right.

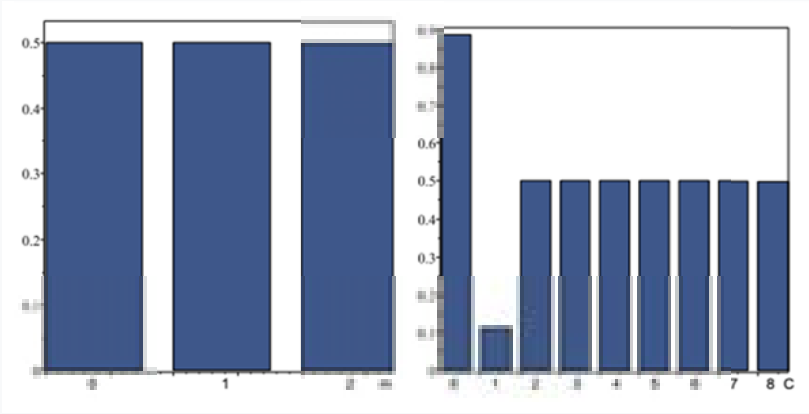

Fig. 66 Histogram defining the distribution of the initial aggressiveness of the strategies of an individual in the population by the depth of memory (left) and complexity (right)

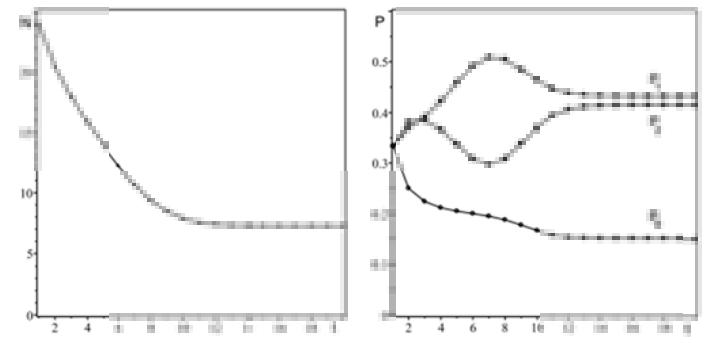

Fig. 67 Change in the total number of strategies in an average carrier (left) and the probability of detecting the presence of a strategy with a certain memory depth (right), where P_0 – the probability of detecting a strategy with memory depth 0, P_1 – memory depth 1, P_2 – depth memory 2

At the initial stage, these probabilities are equal. During evolution, the probability of detecting strategies with zero memory depth drops to a certain stationary level $P_{s0} \approx 0.15$. The probability of detecting strategies with a memory depth of 1 increases to a certain maximum value and then falls to a stationary value $P_{s1} \approx 0.43$. In contrast to the previous case, strategies with memory depth 1 dominate in the stationary state. It is more difficult to change the probability of detecting the strategy of memory depth 2. Two stages of

growth of this probability are observed, separated by a segment of its decline, and reaching a stationary value $P_{s2} \approx 0.41$.

It is interesting to note that the minimum value of the probability P_2 is reached at the stage of reaching the maximum value of the probability P_1. In other words, it is these components that compete with each other for their presence in an individual. Thus, in the stationary state, strategies with a memory depth of 1, 2 dominate with a significant presence of strategies with a zero memory depth. The stationary values for this distribution are radically different from the corresponding values found in the previous section. The nature of these probabilities has also changed dramatically. Now, in the process of evolution, the probability P_0 does not increase, but the probabilities P_1, P_2 also exceed their initial level. Thus, the capture of an individual by the strategies of memory depths 1 and 2 is observed.

For a more detailed analysis of the behavior of the strategies of an individual, let us consider how the complexity of an individual and the complexity of strategies with a certain memory evolve. Fig. 68 shows the average complexity of an individual in the population and the change in the complexity components of strategies that have a certain memory depth. It is easy to see that the complexity of the average individual has two areas of increase, separated by a stage of decrease in complexity. The time period of decline in the complexity of an individual can be called a period of decline or a primitive period of evolution.

Periods of increasing complexity can be called periods of development. The first period of development lasted 2 stages of evolution (or 9% of evolution time), the period of decline took 4 stages (or 18% of evolution time) and the last one lasted until reaching the stationary after 22 stages of evolution (or 72% of evolution time). These periods correlate with the behavior of strategies with a certain depth of memory. For example, the probability of detecting a strategy of memory depth 2 in an individual correlates with a change in the complexity of the individual's strategies (see Fig. 67). The reason for this is related to the greater complexity of the strategies contained in the class of strategies with a memory depth of 2.

It should be noted that the average complexity of an individual is significantly lower than in the previously considered case. This is due to the large number of strategies with zero and one memory depth in an individual and a low initial complexity of individual strategies. In the process of evolution, complex strategies dominate and therefore the stationary level of complexity ($\overline{C}_s \approx 4.3$) of strategies of an individual exceeds the initial ($\overline{C}|_{t=0} \approx 3.8$).

A more detailed behavior of the complexity of strategies in an individual, on average, can be obtained by plotting the dependence of the number or probability of the presence of a strategy, of a certain complexity, on the evolutionary time. The change in the number of strategies in an individual in terms of complexity is rather complex, depending on the magnitude of the complexity (Fig. 68).

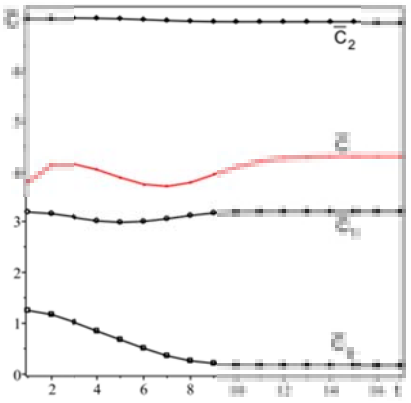

Fig. 68 Evolution of the average complexity of an individual in the population $\overline{C}$ *(red curve) and in terms of memory depth (*$\overline{C}_0$ *– the complexity of strategies of an individual with a memory depth of 0,* $\overline{C}_1$ *– with a memory depth of 1,* $\overline{C}_2$ *– with a memory depth of 2)*

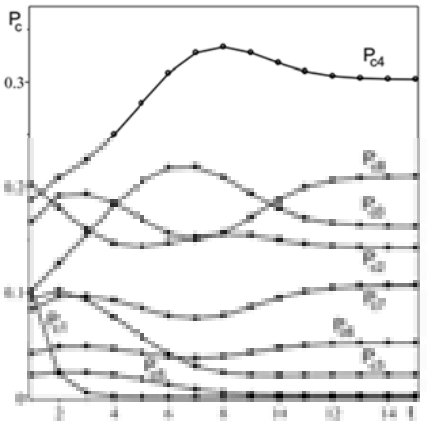

Fig.69 Probabilities of finding strategies of a certain complexity in the average individual of the population (P_0, P_1 ... P_8 *correspond to complexity 0..8, respectively)*

So strategies of complexity 0, 4, 6, 7, 8 in the process of evolution increased the likelihood of their presence in an individual. The most primitive strategies of zero complexity even came out third in terms of probability after strategies of complexity 4 (maximum value) and complexity 8. The probabilities of strategies of complexity 1, 2, 3, and 5 decreased their presence in individuals of the population. Strategies of complexity 1, as the most non–aggressive ones, have completely disappeared from the population.

Let's move on to the evolution of an individual's aggressiveness in a population. In Fig. 70, you can see that the strategies of memory depth 0 were more aggressive, and depth 1 less during evolution. In terms of complexity, strategies of complexity 0 are distinguished as the most aggressive. Strategies of complexity 1, as the most non–aggressive ones, disappear from the population after the 12th step of evolution. Difficulty 8 strategies are less aggressive than other strategies, exceeding the aggressiveness of only difficulty 1 strategies.

In the previous type of distribution, strategies of complexity 1 also disappeared from the population, and all the others tend to the maximum possible value of aggressiveness, which indicates the universality of these patterns. Also, with the previous distribution, the aggressiveness of the strategies of complexity 0 was the greatest. The average aggressiveness of an individual is determined by the aggressiveness of the strategies of memory depth 2 and complexity 8, as can be seen from Fig. 70.

Thus, the stationary state is formed in this case by the most aggressive individuals, whose strategies have the greatest complexity and depth of memory. The presence of strategies of zero memory depth in the stationary state increased in comparison with the initial one by about 2 times.

Moreover, it is the primitive strategies of zero complexity that have survived, while less aggressive strategies of complexity 1 have disappeared from the population. Complex strategies ($C = 6, 7, 8$) increased their presence in individuals of the population as well as complexity $C = 4$. Reduced their presence strategy complexity $C = 1, 2, 3, 5$.

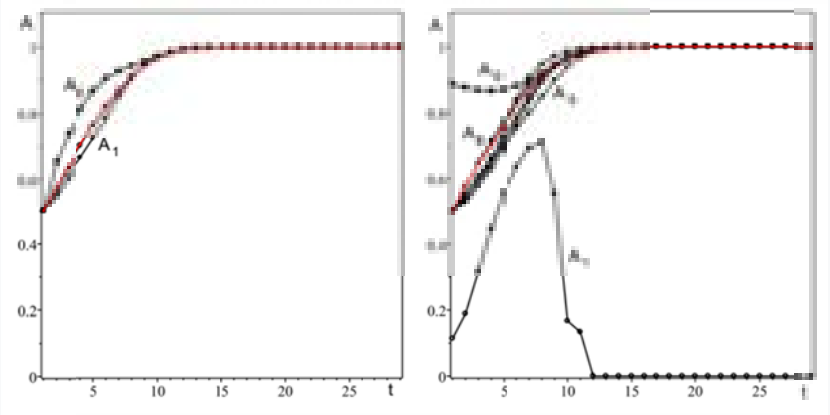

Fig. 70 Aggressiveness of a population in terms of memory depth (left), in terms of complexity (right), where A – average aggressiveness (red curve), A_0, A_1, A_2 –aggressiveness for memory depth from 0 to 2, $A_0, A_1, ..., A_8$ – aggressiveness for complexity from 0 to 8

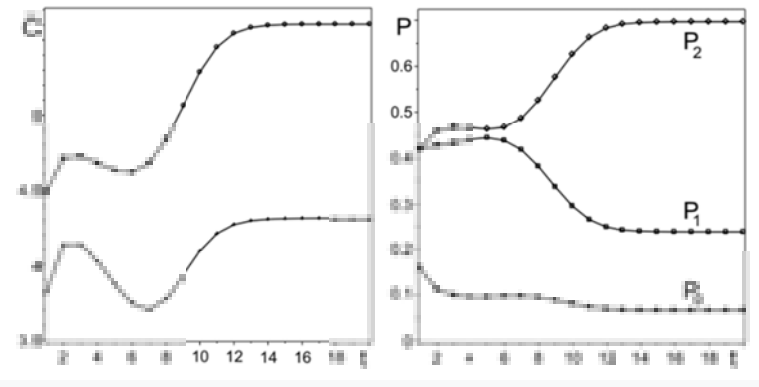

Fig. 71 On the left, the change in the average complexity of an individual with an initial number of strategies of 24 (crosses) and an average complexity of an individual with an initial number of strategies of 50 (circles). On the right, the probability of detecting a strategy of a certain memory depth in an individual with an initial number of strategies of 50

Let us now discuss the effect of an increase in the number of strategies in an individual while maintaining the initial distribution of strategies with equal probabilities in memory depth. Naturally, this will lead to an increase in the average complexity of the strategies of an individual, due to an increase in the number of strategies of maximum complexity.

Therefore, the stationary value of the average complexity of the strategies of an individual will also increase. The dependence of its changes over time with the presence of two periods of growth and one period of decline will remain (see Fig. 71). The probabilities of discovering strategies of a certain depth of memory in an individual are subject to more radical changes. For example, when choosing the initial number of strategies in an individual – 50 at all evolutionary times, the probability of finding a strategy of memory depth 2 in it exceeds the probability of finding a strategy of memory depth 1 as shown in Fig. 71. The corresponding dependence for the initial number of strategies in individual 24 is shown in Fig. 67

Thus, the tendency for the dominance of strategies of maximum memory and complexity in an individual only increases with an increase in the number of its strategies.

12.3. Comparison of the evolution of populations with different initial distributions of strategies on individuals

Thus, evolution, with such an exchange of strategies, supports individuals with the most aggressive strategies with the maximum memory depth and great complexity.

The stationary set of strategies of an individual consists mainly of such strategies with a certain share of the most primitive strategies.

The number of strategies of the average individual decreases with the evolution time, reaching a certain stationary value, which depends on the initial distribution of strategies.

The variety of strategies with evolution decreases more significantly; in the stationary state it remains 6% original, forming strategies. Strategies of complexity 1, as the least aggressive ones, even disappear from the population.

Complex behavior and periods of growth and decline in complexity appear with a significant initial share of strategies of low complexity and low memory, otherwise these strategies do not affect the nature of evolution, being suppressed at early times by more complex strategies with a large memory depth.

SECTION 13. CONCLUSION

From the analysis of the models discussed in the review, one can try to draw conclusions that go beyond the formal description. First of all,

Section 8 discusses the evolution of the population of strategies, from which those that gain the minimum number of points during the cycle of interaction with all participants are excluded.

In each cycle of interaction, each strategy interacts once with all the others, including itself. After gaining points–advantages, strategies–outsiders are removed, they are abandoned. These outsiders correspond to the unsuccessful survival behavior of their owners – the objects of the population. By the beginning of the next cycle, all the accumulated points of the surviving strategies are reset to zero. In the conditions of selection of the strategies that are most effective in terms of the number of points scored and the exclusion of strategies with a minimum set of points, the following tendencies appear. The average complexity of strategies, as well as the average memory depth, practically does not change during evolution.

The history of the evolution of the population is divided into two periods, the primitive period and the period of the developed "'community"'. The primitive stage in the development of the world of strategies can be distinguished by the following features: 1) the presence of all the most primitive strategies n0; 2) an increase in average aggressiveness (dominance of refusals from friendly behavior); 3). The presence of the most aggressive strategy. With an increase in average aggressiveness, the value of the set of points (advantages) decreases and vice versa, and there is a universal relationship between these values.

Despite the typical behavior of averages, initially aggressive strategies and then strategies with low complexity, less than average, may turn out to be the winners at different points in time. Average aggressiveness first grows, then, after overcoming the primitive stage of the world's development, it rapidly decreases. Incidentally, an increase in the memory depth of population strategies decreases the relative duration of the primitive stage of development and increases the proportion of complex strategies. In the resulting stationary state, strategies are not aggressive and achieve equal advantages. A somewhat unexpected result is that, despite the greater reward for aggressiveness (that is, despite the encouragement of non–cooperation), friendly and non–aggressive strategies gain the largest number of advantage points.

Section 9 considers the case of a population of strategies with the accumulation of advantages between generations (when strategies do not zero their points between cycles). In a world with zero memory, despite the long existence of a complex strategy, the most primitive and aggressive strategies win. Their history consists only of the primitive period

Despite the increased survivability of aggressive and primitive strategies in the case of nonzero memory, they nevertheless disappear in the process of evolution. At the same time, the dominance of primitive strategies is not observed, and complex strategies dominate at all stages. The average aggressiveness of such populations monotonically increases in the course of evolution. The rate of scoring decreases during periods of growth of average aggressiveness. That is, in this case, the inverse relationship between changes in average aggressiveness and changes in the rate of scoring remains.

The most complex strategies with the greatest possible memory dominate, but their aggressiveness is also great. the stationary state is formed by strategies of maximum complexity. Complexity and memory are evolutionarily advantageous in this case. While allowing strategies to maintain previously gained advantages, the system encourages aggressiveness. An important consequence of the accumulation of advantages in inheritance is a noticeable increase in aggressiveness.

The considered scenarios of evolution can be called democratic, they are based on natural competition of strategies, both without the accumulation of advantages, and taking into account the inheritance of advantages, in more aggressive societies can be rejected.

The alternative of this aggressive world discussed in Section 10 can be manifested in the fact that after each cycle of interaction of strategies, the most successful ones, who have gained the highest number of points, are removed. This variant of evolution is imposed, that is, some force intervened in evolutionary selection, preventing the use of the most successful and successful scenarios of behavior. This power overwhelms all opportunities for quick gains. Even with zero memory, primitive strategies quickly gain points, which are removed and the average complexity grows.

Average aggressiveness reaches a minimum, then increases rapidly, the value of the acquired points behaves exactly the opposite. Aggressiveness and scoring rate for winning strategies behave approximately the same. In the case of nonzero memory, primitive strategies also quickly disappear, dominated by very aggressive strategies with the greatest memory and complexity. Average aggressiveness also reaches a minimum and grows, and the rate of scoring tends to reverse. That is, as in previous cases, complex strategies with a large memory remain evolutionarily advantageous, but they are characterized by significant aggressiveness.

It is interesting that in general, the set of points–advantages in the ensemble decreases.

Let us discuss (see Section 11) the evolution of strategies in an open society or in a highly disequilibrium population. Now let another strategy be introduced into their population instead of the losing strategy (which scored the minimum points per cycle). In this case, we can talk about the presence of a source and a sink of strategies. Let us first discuss the case where new strategies are more complex and have more memory. If strategies with a memory depth of 2 are thrown into the generality of strategies with unit and zero memory instead of losers, then in a steady state they will dominate.

At the same time, the average aggressiveness drops significantly, and the rate of gaining points – advantages, on the contrary, grows. The average complexity and average memory depth are also growing. The steady state is reached after a certain time amounting to the order of several thousand generations or cycles. The number of strategies remains constant, they are not aggressive and they achieve equal advantages. If we exclude strategies with zero memory at the initial moment, the evolution of the system occurs without

noticeable fluctuations (appearing in the presence of strategies with zero memory).

Empirical analytical dependences of the average parameters of the strategy system are obtained. The question naturally arises: What happens if all the strategies to be thrown in are more primitive than the previous ones? If strategies with zero memory are thrown into the "'community'" of strategies with unit memory according to the scenario described above, then non–aggressive and most complex strategies with zero memory remain in the stationary resulting state and less than ten percent of the strategies that are most complex and have maximum memory with equal advantages achieved.

Despite the strong dominance of relatively complex zero–memory strategies, a small proportion of more complex strategies with more memory are able to survive in these conditions.

Section 12 discusses a more complex case of evolution of a population of subject individuals (50 thousand), each of which uses a set of strategies. When these individuals communicate randomly, their strategies interact in such a way that the strategy that loses in a pair struggle is removed from the set, and the winning strategy takes its place. Each cycle includes communication of all pairs of subjects of individuals, who thus exchange strategies that perform the functions of ideas or memes.

Each subject at the beginning of evolution is endowed with a certain finite number of strategies (50), randomly choosing them from a set of all similar ones, achieving a uniform distribution of the pool of strategies in memory. It is important that now the subjects – individuals have new characteristics – the average values of memory, complexity and aggressiveness of the sets of strategies assigned to them. Since the number of strategies with memory 2 is more than two orders of magnitude greater than the number of strategies with memory 1, it is clear that out of fifty strategies of each subject, almost all have memory 2.

At the same time, it is clear that the average complexity of strategies in this environment is the same as the complexity of the full set of strategies with memory 2 practically does not change, and the most complex ones survive in the stationary state. The average memory of strategies is practically equal to 2. Aggressiveness grows and reaches its maximum value in a steady state. With a random choice of strategies for each subject, the most interesting is the nature of the distribution of strategies. The maximum presence of one strategy in the stationary resulting state of the 'community' did not exceed. The number of different strategies decreases by more than 15 times, and the number of strategies for an individual subject has decreased on average by.

If the initial set of strategies for each subject contains the same shares of strategies with different memory, this will make the distribution of strategies in terms of complexity very different. The average difficulty does not change much, but for individual subjects the behavior of complexity is very whimsical. On average, the subject retains strategies, the total number of strategies decreases by almost 18 times, the average aggressiveness increases and is maximal in the steady state. Thus, in all cases, the depth of memory and the

complexity of strategies are evolutionarily advantageous properties. The complexity should increase in the course of evolution, this determines the direction of time. Aggressiveness and the received number of points of evolutionary advantages change over time in accordance with each other in accordance with the empirical universal law.

REFERENCES

[1]Kenneth J. Locey and Jay T. Lennon PNAS May 24, 2016 113 (21) 5970–5975; first published May 2, 2016; https://doi.org/10.1073/pnas.1521291113

[2]Nowak, Martin A., Corina E. Tarnita, Wilson O. Edward, The evolution of eusociality?, Nature. Vol/466, P.1057—1062, 2010.

[3] Li C. C., First course in population genetics, California, 1975.

[4] J. Maynard Smith, Mathematical ideas in biology, Cambridge, University press, 1968.

[5] J.W.Weibull, Evolutionary Game Theory. MIT Press, Cambridge, MA (1993).

[6] M.A.Nowak, Evolutionary Dynamics. Cambridge, MA (2006).

[7] J.C.Claussen, Discrete stochastic processes, replicator and Fokker–Planck equations of coevolutionary dynamics in finite and infinite populations, Banach Center Publications 80: 17–31 (2008).

[8]A.Traulsen, J.C.Claussen, C.Hauert, Coevolutionary dynamics: From finite to infinite populations, Phys. Rev. Lett. 95, 238701 (2005)

[9]M.A.Nowak, R.M.May, The spatial dilemmas of evolution, Int. J. Bifurcation Chaos Appl. Sci. Eng. 3, 35 (1993).

[10]M.A.Nowak, K. Sigmund, A strategy of win–stay, lose–shift that outperforms tit–for–tat in Prisoner's Dilemma, Nature 364, 56 (1993).

[11]H.Brandt, C.Hauert, K.Sigmund, Proc. R. Soc. Lond.B 270, 1099 (2003).

[12]M.A.Nowak, R.M.May, Evolutionary games and spatial chaos, Nature, 359, 826 – 829 (29 October 1992)

[13] G.Szab'o, C.Hauert, Phase transitions and volunteering in spatial public goods games, Phys. Rev. Lett, 89, 118101 (2002)

[14] M.Perc, Chaos promotes cooperation in the spatial prisoner's dilemma game, Europhys. Lett., 75 (6), pp.841–846, (2006)

[15] M.Perc, A.Szolnoki, G.Szab'o, Restricted connections among distinguished players support cooperation, Phys. Rev. E 78, 066101(6), (2008)

[16] S.K.Baek, B.J.Kim, Intelligent tit–for–tat in the iterated prisoner's dilemma game, Phys.Rev.E, 78, 011125, (2008)

[17]A.Szolnoki, M.Perc, Reward and cooperation in the spatial public goods game, EPL 92 38003 (2010)

[18]A.Szolnoki, M.Perc, Impact of critical mass on the evolution of cooperation in spatial public goods games, Phys.Rev.E 81, 057101, (2010)

[19] A.Szolnoki, M.Perc, Group–size effects on the evolution of cooperation in the spatial public goods game, Phys. Rev.E 84, 047102(4), (2011)

[20]Y.Liu, X.Chen, L.Wang, B.Li, W.Zhang, H.Wang, 2011 EPL 94 60002

[21] A.Szolnoki, M.Perc, Conditional strategies and the evolution of cooperation in spatial public goods games, Phys.Rev.E 85, 026104(7), (2012)

[22] G.Szab'o, G.F'ath, Evolutionary games on graphs. Phys Rep 446: 97–216 (2007).

[23] H.Ohtsuki, C.Hauert, E.Lieberman, M.A.Nowak, A simple rule for the evolution of cooperation on graphs and social networks, Nature 441 502, (2006)

[24] F.C.Santos, J.M.Pacheco, Scale–Free Networks Provide a Unifying Framework for the Emergence of Cooperation, Phys.Rev.Lett. 95 098104, (2005)

[25] S.Assenza, J.G'omez–Garde'nes, V.Latora, Enhancement of cooperation in highly clustered scale–free networks, Phys.Rev.E 78, 017101, (2008)

[26]X.Chen, F.Fu, L.Wang, Interaction stochasticity supports cooperation in spatial Prisoner's dilemma, Phys.Rev.E 78, 051120, (2008)

[27] Perc M, Evolution of cooperation on scale–free networks subject to error and attack, New J. Phys. 11 033027 (2009)

[28] F.Fu, L.Wang, M.A.Nowak, C.Hauert, Evolutionary dynamics on graphs: Efficient method for weak selection, Phys. Rev. E 79 046707, (2009)

[29] W.X.Wang, R.Yang, Y.C.Lai, Cascade of elimination and emergence of pure cooperation in coevolutionary games on networks, Phys. Rev. E 81 035102(R) (2010)

[30]W.X. Wang, J.Ren, G.Chen, B.H.Wang, Memory–based snowdrift game on networks, Phys.Rev.E 74 056113 (2006).

[31] C.L.Tang, W.X.Wang, X.Wu, B.H.Wang, Effects of average degree on cooperation in networked evolutionary game, Eur. Phys. J. B 53, 411–415 (2006).

[32] J.Ren, W.X.Wang, F.Qi, Randomness enhances cooperation: A resonance—type phenomenon in evolutionary game, Phys.Rev.E 75 045101(R) (2007).

[33] W.X.Wang, J.Lu, G.Chen, P.M.Hui, Phase transition and hysteresis loop in structured games with global updating, Phys. Rev. E 77 046109 (2008).

[34] W.B.Du, X.B.Cao, M.B.Hu, W.X.Wang, Asymmetric cost in snowdrift game on scale–free networks, EPL 87 60004 (2009).

[35] Rong Z, Yang H X and Wang W X, Feedback reciprocity mechanism promotes the cooperation of highly clustered scale–free networks, Phys. Rev. E 82 047101 (2010)

[36] J.Poncela, J.Gomez–Gardens, Y.Moreno, Cooperation in Scale–free networks with limited associative capacities. Phys.Rev. E 83, 057101 (2011)

[37] J.G'omez–Garde'nes, M.Romance, R.Criado, D.Vilone, A.S'anche, Evolutionary games defined at the network mesoscale: The public goods game, Chaos 21 016113 (2011)

[38] H.X.Yang, Z.X.Wu, W.B.Du, Evolutionary games on scale–free networks with tunable degree distribution, EPL 99 10006, (2012)

[39]M.A.Nowak, R.Highfield, Super Cooperators: Altruism, Evolution, and Why We Need Each Other to Succeed, Free Press, 2012.

[40] G.Szab'o, C.Hauert, Evolutionary prisoner's dilemma games with voluntary participation, Phys. Rev. E 66, 062903 (2002)

[41] C.Hauert, A.Traulsen, H.Brandt, M.A.Nowak, K.Sigmund, Via freedom to coercion: The emergence of costly punishment, 2007 Science 316 1905

[42] A.Traulsen, J.C.Claussen, Similarity based cooperation and spatial segregation, 2004 Phys. Rev. E 70 046128

[43] A.Szolnoki, G.Szab'o, Cooperation enhanced by inhomogeneous activity of teaching for evolutionary prisoner's dilemma games, EPL 77 30004 (2007)

[44] M.Perc, A.Szolnoki, Social diversity and promotion of cooperation in the spatial prisoner's dilemma game, Phys. Rev. E 77 011904, (2008)

[45] H.X.Yang, W.X.Wang, Z.X.Wu, Y.C.Lai, B.H.Wang, Diversity–optimized cooperation on complex networks, Phys. Rev. E 79, 056107 (2009)

[46] J.M.Pacheco, A.Traulsen, M.A.Nowak, Coevolution of strategy and structure in complex networks with dynamical linking, Phys. Rev. Lett. 97 258103 (2006)

[47] H.Ohtsuki, M.A.Nowak, J.M.Pacheco, Breaking the symmetry between interaction and replacement in evolutionary dynamics on graphs, Phys. Rev. Lett. 98 108106 (2007)

[48] S.Meloni, A.Buscarino, L.Fortuna, M.Frasca, J.G'omez–Garde'nes, V.Latora, Y.Moreno, Effects of mobility in a population of prisoner's dilemma players, Phys. Rev. E 79, 067101 (2009)

[49] L.L.Jiang, W.X.Wang, Y.C.Lai, B.H.Wang, Role of adaptive migration in promoting cooperation in spatial games, Phys. Rev. E 81, 036108 (2010)

[50] F.Fu, M.A.Nowak, Global migration can lead to stronger spatial selection than local migration, J. Stat. Phys. 151 637 (2013).

[51] F.Fu, C.E.Tarnita, N.A.Christakis, L.Wang, D.G.Rand, M.A.Nowak, Evolution of in–group favoritism, Sci. Rep. 2 460 (2012)

[52] Z.Wang, A.Szolnoki, M.Perc, Optimal interdependence between networks for the evolution of cooperation, Sci. Rep. 3 2470, (2013)

[53]Kristian Lindgren, Evolutionary Phenomena in Simple Dynamics, Conference: Artificial Life IIAt: Santa Fe, USA, January p.295–312, 1991.

[54]Seth Lloyd, Measures of Complexity a non—exhaustive list, IEEE Control Systems Magazine, Vol. 21, Issue: 4, p.7–8, 2001

[55] AN Kolmogorov, Three approaches to the definition of the concept of "amount of information", Problems of information transmission. - v. 1, No.1, p. 3-11, 1965.(in Russian).

[56] AN Kolmogorov, On the logical foundations of information theory and probability theory, Problems of information transmission, 3, pp. 3–7, 1969 (in Russian).

[55]A.M.Turing, On Computable Numbers with an Application to the Entscheidungsproblem, Proc. Lond. Math. Soc. (ser.2), 42, p.230–265, 1936/37.

[58] VI Arnold, Experimental observation of mathematical facts, Moscow, MTsNMO, 2006, 120 p.(in Russian).

[56]E. Lieberman, C. Hauert, M. A. Nowak, Evolutionary dynamics on graphs, Nature (London) 433, 312 (2005).

[57] HauertC., DoebeliM. Spatial structure often inhibits the evolution of cooperation in the snowdrift game, Nature (London) 428, 643 (2004).

[58]AxelrodR. The evolution of cooperation, Basic Books, New York (1984).

[62] MoninA.S., YaglomA.M. Statistical hydromechanics. The mechanics of turbulence. Volume 1, M., Nauka, 1965, 640s.(in Russian).

[59]HartleyR.V.L., Transmission of information, Bell Syst.Techn.J. 1928, July, 535.

[64] KuklinV.M., PriymakA.V., YanovskiyV.V. The influence of memory on the evolution of populations, Bulletin of Karazin'sKharkiv National University series. "Mathematical Models. Information technologies. Automated control systems "v.29, pp.41–66, 201(in Russian).

[65] Timofeev-Ressovsky N.V., Yablokov A.V., Glotov N.V. Essay on the theory of population, Institute of Developmental Biology of the USSR Academy of Sciences, Moscow, Nauka, 1973, 280 p.(in Russian).

[66] GlushkovB. M. Abstract theory of automata, UMN, 1961, volume 16, issue 5 (101), 3–62.(in Russian).

[67] YanovskyV.V., PriymakA.V., KuklinV.M. Evolution of Strategies Communities, (in press).

[68] YanovskyV.V., PriymakA.V., Evolution of strategies communities in the presence of sources, (in print).

[69] BBKadomtsev, VMKantorovich, Theory of turbulence in hydrodynamics and plasma, Izv.Uzov, Radiofizika, vol. 17, no. 4, p. 511-540, 1974

[70] KuklinV.M., AVPriymakA.V., YanovskyV.V. The influence of memory on the evolution of populations, Bulletin of Karazin'Kharkiv National University .series "Mathematical Models. Information technologies. Automated control systems "v.29, p.41-66, 2016

[60]ShatskyK.V., YanovskyV.V. Evolution of memes, Bulletin of Karazin'Kharkiv National University .series "Mathematical Models. Information technologies. Automated control systems "v.49, p.83–97, 2021.(in Russian).

[72] R. Dawkins, The Selfish Gene, M., Mir, 1993, 318 pp.(in Russian).

[61]D.Dennett, C.Danvin's Dangerous Idea: Evolutionand the Meanings of Life, Simon and Schuster, 1995, .

[62]H.Plotkin, Danvin Machines and the Nature of Knowledge, Harvard University Press, 1993,

УДК 538.945, 537.9
PACS number: 74.72.–h, 74.78.Fk, 74.50.+r, 52.35.Mw

CHAPTER V

FINE STRUCTURE OF THE LOCAL ALFVEN RESONANCES IN CYLINDRICAL PLASMAS WITH AXIAL PERIODIC INHOMOGENEITY

I. O. Girka

V. N. Karazin Kharkiv National University, 4 Svobody Sq., Kharkiv, 61022, Ukraine

Local Alfven resonance iswell-known to manifest itself in cylindrical plasma with radially nonuniform particle density and uniform axial external static magnetic field via rapid increase of electromagnetic field amplitude when approaching the resonant radius. First, Physics of the phenomenon is explained in the present review. Plasma axial periodic nonuniformity is shown to be usual feature of the modern plasma devices. Satellite local Alfven resonances are shown to arise in axially periodically nonuniform plasma both in general and resonant cases. Resonant case takes place if the wave length is twice as large as plasma axial period. Conditions are derived under which fine structure of the satellite Alfven resonance is determined just by plasma axial periodic nonuniformity.

Keywords: *plasma axial periodic nonuniformity, Alfven resonance, satellite Alfven resonance, wave packet.*

PACS numbers: *02.30.Gp, 52.35.-g, 94.20.-y*

SECTION 1. INTRODUCTION

The overview is written on the base of theoretical research carried out at the Department of General and Applied Physics of V. N. Karazin Kharkiv National University in collaboration with physicists from the Institute for Plasma Physics of National Science Centre "Kharkiv Institute of Physics and Technology" during more than twenty years.

Electromagnetic waves propagating with the frequency of the order of ion cyclotron frequency in the magnetoactive plasma are the matter of intense scientific research. This is explained by the wide practical application of these waves.

Theoretical and experimental studies of propagation, damping, excitation and conversion of fast magnetosonic waves (FMSWs) and Alfven waves (AWs) are intensively carried out for about eighty years. First of all, this is associated with numerous applications of the results of this research to the problem of controlled nuclear fusion, chain of problems in geophysics and astrophysics. FMSWs and AWs are the powerful tool for plasma production and heating in toroidal traps (tokamaks and stellarators) [1–3]. Radiofrequency (RF) heating provides ion temperatures of about 15÷20 keV in modern tokamaks. Along with neutral beam injection (NBI), ion cyclotron, low-hybrid and electron cyclotron heating, magnetohydrodynamic (MHD) waves are planned to be used as the main method for plasma heating in the future fusion reactor. FMSWs and AWs can be used for production of current drive [4]. Solving the problem of current drive maintenance due to plasma loading with RF power would provide designing the stationary tokamak and fusion reactor-tokamak on its base. Production of current drive can be also applied in stellarators – with the goal to control the profile of the rotational transform and achievement, on account of this, better MHD stability of plasmas.

Simplicity of tokamak design, which makes it possible to construct the devices of larger and larger dimensions, improvement of experiment technique, application of powerful sources for additional heating provided the plasma production with the parameters close to fusion ones. At the same time, new obstacles have arisen at the stage of designing the reactor based on tokamak concept. First, these are the disruptive instability (it causes danger for the reactor first wall), nonstationarity (it influences on the duration of the operating life of the constructive materials) and smallness of the aspect ratio (ratio of the large radius to the small one), which cause complicated technological problems [5].

If these problems are such, that they are too difficult to overcome, then one can consider the stellarator concept, for which the abovementioned dangers do not portend. In contrast to a tokamak, in which the rotational transform of the magnetic field force lines is caused by the electric current, flowing through the plasma, in a stellarator, it is caused by current-carrying conductors which are external in respect to the plasma. For plasma confinement in stellarators, one does not need to arrange any electric current through the plasma. That is why a stellarator is a stationary trap. The problem of plasma production and heating is separated from the problem of its confinement. The idea of stellarator was supposed by Lyman Spitzer in 1951 [6]. It is popular in many countries. In particular, stellarator concept is intensively developed nowadays in Germany and Japan.

After their prediction by Hannes Alfven in 1942 [7] AWs appeared to play an important role in different plasma phenomena. AWs were observed for the first time in an experiment at the end of fifties in XX century (see, e.g., [8]).

Detailed theoretical studies of MHD oscillations of plasma cylinder were initiated in 1950-1970 with applying simplifying assumptions, in particular, about the homogeneity of axial static magnetic field (see., e.g., [9–13] and references therein), due to their possible application in fusion problems. At the same time, solution of such a problem with account for complicated shape of external static magnetic field of real geometry on the base of analytic or even numerical methods is very difficult and impossible problem so far. This initiates numerous novel analytic and numerical studies of different aspects of MHD wave propagation in inhomogeneous plasmas of fusion traps.

Weak periodic spatial inhomogeneity of external static magnetic field $\vec{B}_0$ can significantly affect on the properties of MHD waves. At the first glance, this influence can be considered as obvious one. Indeed, e.g., it is well-known from the solid state physics [14], that periodic «potential» (similar to the plasma inhomogeneity, caused by periodic spatial inhomogeneity of external static magnetic field) gives rise to gaps in the spectrum, known as forbidden energetic zones. However, thorough study of $\vec{B}_0$ periodic inhomogeneity role discovers a number of new physical phenomena. To demonstrate the intensity of studying the influence of $\vec{B}_0$ periodic spatial inhomogeneity (elliptical shape of poloidal cross-section of magnetic surfaces, helical and toroidal inhomogeneity, and $\vec{B}_0$ axial periodic inhomogeneity) on the properties of RF waves only some examples of such investigations are given below. For example, existence of eigen Alfven modes, initiated by elliptical shape of plasma poloidal cross-sections, so-called EAMs, was demonstrated in [15]. These Alfven modes have their own macrostructure, they propagate in plasmas with uniform particle density and have a lot of common features with eigen Alfven modes, initiated by plasma toroidicity. In the next paper [16], the same authors have demonstrated the possibility to excite these modes by energetic alpha particles due to transit resonance. The influence of plasma toroidicity and elliptical shape of plasma column cross-sections on the eigen frequencies and eigen modes of MHD waves was studied in [17]. Gaps in Alfven continuum, caused by the toroidicity, were studied in [18, 19]. Existence of eigen Alfven modes initiated by the toroidicity in plasmas with shear and with the frequencies inside the respective gaps was foreseen in the same paper and was observed experimentally later on.

Two experimental observations were emphasized within the paper [20] by Wendelstein 7-X team. Firstly, independent of magnetic configuration and heating scenario, broadband fluctuations were measured around the frequency of 180 kHz. The nature of these fluctuations is possibly associated with ellipticity-induced Alfvén eigenmodes in the outer regions of the plasma. The latter was inferred by studying corresponding theoretically predicted Alfvén continua calculated with the 3D-MHD continuum code CONTI. Secondly, fast collapses of plasma current and energy, which occurred during recent operational phases at W7-X, showed a clear magnetic signature. Short time scale Alfvénic bursts were revealed, which were induced during these sawtooth-like collapses.

Fast-particle driven Alfvén Eigenmodes were observed in low-collisionality discharges with off-axis neutral beam injection (NBI), electron cyclotron resonance heating (ECRH) and a reduced toroidal magnetic field in the TCV tokamak [21]. During NBI and ECRH, toroidicity induced Alfvén Eigenmodes (TAEs) appeared in frequency bands close to 200 kHz and energetic-particle-induced geodesic acoustic modes (EGAMs) were observed at about 40 and 80 kHz. When turning off ECRH in the experiment, those beam-driven modes disappeared. In contrast, coherent fluctuations close to the frequency of the beam-driven TAEs were present throughout the experiment. The modes were even observed during ohmic plasma conditions, which clearly demonstrated that they were not caused by fast particles and suggested an alternative drive, such as turbulence.

The discrete Alfvén Eigenmode spectrum below the TAE frequency was studied for hybrid and sawtooth scenarios in tokamaks whereby the full coupling between the Alfvén and slow magnetosonic waves was taken into account [22]. It was found that the number of modes below the TAE gap was the highest for weakly reversed profiles of safety factor q while the number of modes increased with pressure. The frequency behaviour of the modes below the TAE gap was studied for a reversed shear q-profile in which $q_{\min}$ was varied and it was found that Alfvén-Slow Eigenmodes frequencies increased and/or decreased as a function of $q_{\min}$ thereby emerging from and/or disappearing into the continuum.

Plasma production and heating in fusion devices have initiated intensive studying the electromagnetic wave conversion and absorption in the vicinity of the local Alfven resonance (AR) [1–3, 23]. Local AR in the case of plasma traps with uniform external static magnetic field $\vec{B}_0$ is intensively studied for more than fifty five years [24–28]. Interest to this phenomenon is explained, first of all, by its application to effective plasma production and heating in fusion traps. It was demonstrated in the mentioned papers, that in approach of the cold plasma, solutions of Maxwell's equations for the fields of electromagnetic waves have a singularity at the certain radius of the plasma column. If to replace this simple approach by the models which take into account the particle thermal motion, finite electron inertia, weak nonlinearity or dissipations, then the conversion of these waves into small-scale oscillations and their absorption can change significantly. During the plasma heating by RF waves, the most RF power is absorbed in the vicinity of the local AR.

Detailed overview of theoretical studies of AR was given in [23]. In particular, anteriority of the Kharkiv physicists in studying the fine structure of AR was recognised there. Such appreciation of Soviet scientists, generally speaking, was not typical for foreign colleagues. AR is effectively used for plasma production and heating on stellarators «Uragan» at National Science Centre «Kharkiv Institute of Physics and Technology». This allowed plasma production with particle density up to 10^{13} cm^(-3) and temperature of electrons and ions of about several hundreds of electron-Volt. Such plasma production made it possible to study a number of physical phenomena, which took place

during Alfven heating. Heat and particle transport, including neutral particles, during the RF heating using AR was studied experimentally and theoretically in [29]. In [30], AWs absorption caused by parametric ion cyclotron instability was explained theoretically, profiles of energy absorption were calculated, and plasma particles and heat transport in «Uragan-3 M» were studied on this base.

At the same time, position of AR is well-known to move to the plasma periphery with increase in plasma column density and dimensions. This reduces the efficiency of Alfven method of plasma heating in fusion traps, since it causes the heating of plasma periphery, rather than its core, which, in its turn, intensifies undesirable plasma-surface interaction. To avoid plasma periphery heating and heat core plasma layers, one can apply the waves with large magnitude of longitudinal wavenumber k_z, for which the local AR is situated in the plasma core. But this is difficult due to wide barrier of nontransparency at the plasma periphery for such waves. One way more to avoid the energy losses at the plasma periphery is to apply the waves with the low frequency and small k_z, for which local AR is also situated in the plasma core. But in this case, one needs the antenna with large length in axial direction. All these unfavourable circumstances make it difficult to use Alfven method of plasma heating in large traps and initiate the search of new physical ways to increase its efficiency.

RF power, absorbed in the vicinity of AR in the case of linear radial density profile, is inversely proportional to the density gradient [24]. This is the reason, for which the case, if the density radial profile reaches its extremum in the vicinity of AR, is of a special interest [31–34].

Despite of a large number of papers, devoted to AR, an interest to it and its application in the sphere of fusion continues to initiate new research. In particular, sufficiently detailed analysis of applicability of MHD equations to the case of AR can be found, e.g., in the paper [35]. Conversion of fast waves excited by an antenna into slow waves at the fusion plasma periphery was studied in [36]. It is shown in framework of two-dimensional numerical simulation in [37] that direct electron heating, investigated with the help of radiometry of electron cyclotron emission, was caused by the local AR in the plasma of TCABR tokamak. Observed profiles of energy absorption also were in a good agreement with scatterometric measurements of the particle density fluctuations, caused by the action of electromagnetic waves in the vicinity of the local ARs. In [38], a compact four-contour antenna was proposed to provide the wave radiation with large longitudinal wavenumbers $k_{||}$. The main objective of the study was to suppress the heating of the plasma periphery in the vicinity of AR, which took place in the result of unavoidable excitation of the waves with small $k_{||}$. It was shown that special choice of the heating regime could reject the periphery heating to the acceptable level, and the most part of the electromagnetic power would absorb in the plasma core of medium-size torsatron «Uragan-2M». Absorption of the wave energy in cold magnetized plasma with two ion species was studied in [39]. The energy absorption was shown to take place in that part of space, which can be considered as analogue to the local AR. In the case of slanting wave incidence, if the wave frequency

was much smaller than plasma frequency approximate resonance was shown to take place in the spectrum of wavenumber projections on the perpendicular to the external static magnetic field. This resonance was possible to consider as analogue to AR in ordinary electron-ion plasma.

Despite the author is not a specialist in the field of ionosphere geophysics, it is impossible to ignore here a tremendous number of papers, devoted to studying AR and its application in the mentioned sphere of physics. Detailed overview to the AW properties in cosmic and laboratory plasmas is given in [40]. Influence of the finite Larmor radius, electron inertia, and finite wave frequency on the properties of these waves was demonstrated in the linear (in the respect of the wave amplitude) approach. Detailed discussion of the properties of inertial and kinetic AW was provided. Experimental data, obtained on the space vehicles Freja, Fast, etc., were generalized. Laboratory experiments on AWs, which were of the most interest to physics of ionosphere, were overviewed.

Since the magnetosphere was recently assumed to be better modelled in some cases by a waveguide than a cavity, the authors of [41] analysed numerically the linear MHD theory of the waves in a uniform waveguide with a small plasma beta. AR was shown to arise under the condition, if the wave frequencies coincide with the eigen frequencies of fast axially symmetric waveguide modes.

The data on observing the flashes in the solar corona from the X-ray telescope, placed on the Japan satellite Yohkoh, were analysed in [42]. Scaling of the heating velocity due to AW resonant absorption was determined in numerical way. The scaling was shown to agree well with the heating velocity, calculated on the base of observation data.

Solution to kinetic and MHD wave equations with full account for the finite ion Larmor radius, and resonant interaction wave-particle for electrons and ions, which modelled the dissipations, was derived in [43]. Propagation of ultra low-frequency waves of large amplitude of compressional type from the magnetic sheath to the magnetopause under the conditions of the presence of large gradients in the density, pressure, and magnetic field was also described there. The research was initiated by experimental observation of the respective MHD activity.

Experimental data on Fourier analysis were given in [44], which demonstrated the presence of a number of standing waves in the range of Alfven frequency. The dependence of the wave frequency on the external static magnetic field was measured for three local ARs.

Statistic processing of spectral resonance structures of AR in ionosphere was reported in [45]. The structures were observed in the frequency range 0.1÷5.0 Hz since 2000 till 2002 on the station Karimshyno (Kamchatka, Russian Federation) with the help of ordinary three-component induction magnetometer. To single out the data about just AR, the dynamics of three-component spectrum, and polarization spectrum were analysed.

Spatial structure of ultra low-frequency electromagnetic waves with zero azimuthal wavenumber in one-dimensionally inhomogeneous plasma was

studied in [46] with account for finite magnitude of ion cyclotron frequency. These waves can propagate in the magnetosphere of Earth or in the magnetosphere of the Mercury planet. Wave field amplitudes were shown to rapidly increase at the certain magnetic surfaces, which was analogous to AR in one-fluid MHD theory.

The method of simplified selected asymptotic expansions, developed for nonlinear slow resonant waves, was applied in [47] for the description of nonlinear phenomena within the Alfven dissipative layer. Wave dynamics in the vicinity of AR (with isotropic and anisotropic dissipation) was shown to be described with high accuracy in framework of linear theory.

The present overview is arranged in the following manner. Section 2 is devoted to presenting the theory of the local Alfven resonance in one-dimensionally inhomogeneous plasmas. The case of monotonous plasma particle density inhomogeneity is considered. Exception is the subsection 2.8, wherein the peculiarities of AR fine structure and electromagnetic power absorption within it are studied under the condition of quadratic dependence of the plasma particle density on the radial coordinate in vicinity of AR. It is demonstrated, how the numerous real specific features of the laboratory plasma influence on the structure of AR. These features are as follows: weak collisions between the plasma particles, nonzero azimuthal wavenumber, $k_y \neq 0$, finite electron inertia, finite Larmor radius, striction nonlinearity, and kinetic ion cyclotron turbulence. It is shown in details, how the characteristic width of AR, characteristic magnitude of the wave electric field parallel to the density gradient, as well as the density of the electromagnetic power absorption can be derived analytically.

Specific features of AR fine structure in external static magnetic field with axial periodic inhomogeneity (bumpy magnetic field) are studied in the Section 3. Such an inhomogeneity of $\vec{B}_0$ is inherent in both tokamaks and stellarators. Electromagnetic waves are shown to propagate in the form of wave packets in the bumpy magnetic field which can cause initiation of additional, so-called satellite ARs (SARs).The fine structure of the main AR is studied in the case, if it is determined just by inhomogeneity of $\vec{B}_0$, including the resonant case in which axial period of the main wave harmonic is twice as large as axial period of the bumpy magnetic field. Besides, the fine structure of a SAR is determined in the case of moderate inhomogeneity, in which the fine structure is determined just by the inhomogeneity rather than other weak phenomena.

Conclusions contain the brief results of the research presented in the overview. Their scientific and methodological significance is outlined as well.

The overview would be of interest for undergraduate and PhD students, who are specialized in the sphere of plasma physics and electrodynamics, as well as to those scientists who deal with the problems of controlled nuclear fusion, physics (geophysics) of the terrestrial space, and theoretical physics.

SECTION 2. LOCAL ALFVEN RESONANCE IN PLASMAS WITH ONE-DIMENSIONAL INHOMOGENEITY

Main features of arising of the local Alfven resonance (AR) are presented in this Section with applying the model of one-dimensionally monotonously inhomogeneous plasma. Cold plasma with weak collisions is assumed to fill the spatial layer $0 \le x \le L$ in Cartesian coordinates. The plasma electrodynamic properties are described by the permittivity tensor

$$\hat{\varepsilon} = \begin{pmatrix} \varepsilon_1 & i\varepsilon_2 & 0 \\ -i\varepsilon_2 & \varepsilon_1 & 0 \\ 0 & 0 & \varepsilon_3 \end{pmatrix}, \tag{2.1}$$

which components can be written in the hydrodynamic approach as follows [12, 48, 49]:

$$\varepsilon_1 = 1 - \sum_\alpha \frac{\omega_{p\alpha}^2}{\omega^2 - \omega_{c\alpha}^2},\ \varepsilon_2 = -\sum_\alpha \frac{\omega_{p\alpha}^2 \omega_{c\alpha}}{\omega(\omega^2 - \omega_{c\alpha}^2)},\ \varepsilon_3 = 1 - \sum_\alpha \frac{\omega_{p\alpha}^2}{\omega^2}. \tag{2.2}$$

The plasma is assumed to be infinite and uniform in the directions y and z. For definiteness, external static magnetic field is assumed to be uniform (in this Section only) and parallel to the z axis. Plasma inhomogeneity is determined by the particle density, which is assumed to monotonously increase in x direction (see, e. g., Fig. 2.8.4, where an example of the radial plasma particle density profile is presented in the case of linear dependence on the radial coordinate).

Spatial distributions of electromagnetic wave fields are derived from the Maxwell's equations:

$$rot\vec{B} = \frac{1}{c}\frac{\partial \vec{D}}{\partial t}, \qquad rot\vec{E} = \frac{-1}{c}\frac{\partial \vec{B}}{\partial t}, \tag{2.3}$$

applying the concept of Fourier series. In particular, for axial component of the wave magnetic field the series reads as:

$$B_z(x,y,z) = \sum_{k_z=-\infty}^{+\infty} \sum_{k_y=-\infty}^{+\infty} B_z(x)\, exp\left(ik_z z + ik_y y - i\omega t\right). \tag{2.4}$$

Taking into account the form of the tensor (2.1), the Maxwell's equations can be written in terms of electric field $\vec{E}$ and magnetic flux density $\vec{B}$, which is equal to the magnetic field strength $\vec{H}$:

$$\begin{cases} \frac{\partial B_z}{\partial y} - \frac{\partial B_y}{\partial z} = \frac{-i\omega}{c}\left(\varepsilon_1 E_x + i\varepsilon_2 E_y\right), \\ \frac{\partial B_x}{\partial z} - \frac{\partial B_z}{\partial x} = \frac{-i\omega}{c}\left(\varepsilon_1 E_y - i\varepsilon_2 E_x\right), \\ \frac{\partial B_y}{\partial x} - \frac{\partial B_x}{\partial y} = \frac{-i\omega}{c}\varepsilon_3 E_z, \end{cases} \qquad \begin{cases} \frac{\partial E_z}{\partial y} - \frac{\partial E_y}{\partial z} = \frac{i\omega}{c} B_x, \\ \frac{\partial E_x}{\partial z} - \frac{\partial E_z}{\partial x} = \frac{i\omega}{c} B_y, \\ \frac{\partial E_y}{\partial x} - \frac{\partial E_x}{\partial y} = \frac{i\omega}{c} B_z. \end{cases} \tag{2.5}$$

After substituting the expression (2.4) to the Maxwell's equations (2.5) the set of six equations can be derived for one spatial harmonic:

$$\begin{cases} ik_y B_z - ik_z B_y = \frac{-i\omega}{c}\left(\varepsilon_1 E_x + i\varepsilon_2 E_y\right), \\ ik_z B_x - \frac{\partial B_z}{\partial x} = \frac{-i\omega}{c}\left(\varepsilon_1 E_y - i\varepsilon_2 E_x\right), \\ \frac{\partial B_y}{\partial x} - ik_y B_x = \frac{-i\omega}{c}\varepsilon_3 E_z, \end{cases} \qquad \begin{cases} ik_y E_z - ik_z E_y = \frac{i\omega}{c} B_x, \\ ik_z E_x - \frac{\partial E_z}{\partial x} = \frac{i\omega}{c} B_y, \\ \frac{\partial E_y}{\partial x} - ik_y E_x = \frac{i\omega}{c} B_z. \end{cases} \quad (2.6)$$

One can also get use of the fact that absolute value of the component ε_3 of the plasma permittivity tensor is much larger than $\varepsilon_{1,2}$: $|\varepsilon_3| >> |\varepsilon_{1,2}|$, in the range of ion cyclotron frequency, $\omega \sim \omega_{ci}$. Then the third equation in the first subset gives, that longitudinal wave electric field E_z is negligibly small as compared to B_x and B_y, and respectively, with all the wave field components, $E_z \to 0$. This makes it possible to neglect this physical observable below. If to get use of the expressions (2.2) for ε_i, then it appears that the ratio $|\varepsilon_3| / |\varepsilon_{1,2}| \sim m_e/m_i$. That is why neglecting the longitudinal electric field is referred sometimes as neglecting the electron inertia.

Below, the main features of AR are determined. To do this, a harmonic with zero magnitude of the transverse wavenumber is chosen, $k_y=0$ (the results to be derived will be generalized afterwards on the case $k_y \neq 0$):

$$\begin{cases} -ik_z B_y = \frac{-i\omega}{c}\left(\varepsilon_1 E_x + i\varepsilon_2 E_y\right), \\ ik_z B_x - \frac{\partial B_z}{\partial x} = \frac{-i\omega}{c}\left(\varepsilon_1 E_y - i\varepsilon_2 E_x\right), \end{cases} \qquad \begin{cases} -ik_z E_y = \frac{i\omega}{c} B_x, \\ ik_z E_x = \frac{i\omega}{c} B_y, \\ \frac{\partial E_y}{\partial x} = \frac{i\omega}{c} B_z. \end{cases} \quad (2.7)$$

The set of eqs. (2.7) is studied in the following manner. First, the observables B_x and B_y are derived from the first and second equations of the second subset in terms of E_x and E_y. Second, the observables B_x and B_y are substituted into the first subset. Third, E_x and E_y are expressed in terms of longitudinal wave magnetic field B_z:

$$\begin{cases} E_x = \frac{-c}{\omega N_\perp^2}\mu \frac{\partial B_z}{\partial x}, \\ E_y = \frac{-ic}{\omega N_\perp^2}\frac{\partial B_z}{\partial x}. \end{cases} \quad (2.8)$$

In (2.8), the following notations are applied: $\mu = \varepsilon_2 / \left(\varepsilon_1 - N_z^2\right)$, $N_\perp^2 = \left(\varepsilon_1 - N_z^2\right)\left(1 - \mu^2\right)$, $N_z = ck_z/\omega$ is the longitudinal refractive index. Then the expression for E_y is to be substituted into the last equation in (2.7), and the differential equation for the field B_z is derived:

$$\frac{\partial}{\partial x}\left(\frac{1}{k_\perp^2}\frac{\partial B_z}{\partial x}\right) + B_z = 0, \tag{2.9}$$

here $k_\perp^2 = (\omega/c)^2 N_\perp^2$.

The plasma particle density profile is assumed to contain the point $x=x_A$ inside the layer $0 \le x \le L$, in which

$$\varepsilon_1 = N_z^2. \tag{2.10}$$

This point is called as that of the local Alfven resonance. Rapid increase of the wave field amplitudes and electromagnetic power absorption take place in the vicinity of this point, as it is shown below.

Axial wave magnetic field slowly (logarithmically) varies in the vicinity of AR. To confirm this the plasma particle density is assumed to vary linearly in the vicinity of AR:

$$\varepsilon_1 = N_z^2 + \frac{d\varepsilon_1}{dx}(x - x_A). \tag{2.11}$$

Since $k_\perp^2 \propto (x - x_A)^{-1}$ in the vicinity of AR, then to analyze the dependence $B_z(x)$ in the vicinity of AR the eq. (2.9) is suitable to be rewritten in the following schematic form:

$$\frac{d}{d\rho}\rho\frac{dB_z}{d\rho} + B_z = 0. \tag{2.12}$$

If to assume that one of the linearly independent solutions of the eq. (2.12) weakly depends on x, $B_z \approx B_{z0}$, then one can replace the second term in the eq. (1.12) by the constant B_{z0}:

$$\frac{d}{d\rho}\rho\frac{dB_z}{d\rho} + B_{z0} = 0. \tag{2.13}$$

Then the eq. (2.13) can be integrated as follows:

$$\rho\frac{dB_z}{d\rho} = -\int B_{z_0} d\rho + C; \Rightarrow \quad \frac{dB_z}{d\rho} = \frac{-\int B_{z_0} d\rho + C}{\rho}; \quad \Rightarrow$$
$$B_z = B_{z_0} + \int \frac{C - \int B_{z_0} d\rho}{\rho} d\rho \propto ln(\varepsilon_1 - N_z^2). \tag{2.14}$$

As it follows from the eq. (2.13), the second linearly independent solution of eq. (2.12) varies logarithmically in the vicinity of AR. Analysis of eq. (2.8) shows that E_y is almost of constant magnitude in the vicinity of AR, and $E_x \propto(\varepsilon_1 - N_z^2)^{-1}$. Keeping in mind eq. (2.7), one can conclude that B_x weakly varies in the vicinity of AR, and B_y also has the singularity, $B_y \propto (\varepsilon_1 - N_z^2)^{-1}$.

It is the rapid increase of the wave magnetic field B_y in the vicinity of AR that makes it possible to apply magnetic probes for experimental study

of AR [50, 51]. Authors of the paper [50] studied the spatial position of AR exciting the axially symmetric AWs by Stix coils. Maximum magnitude of azimuthal magnetic field was observed in the vicinity of AR, which position depended on the wave frequency and wavelength. Position of AR was experimentally determined in [51] from measuring the wave poloidal magnetic field in the tokamak Tokapole II. The radial position agreed well with the calculations made on the base of MHD theory.

To conclude, spatial dependence of the wave field components can be generalized in the following manner:

$$E_x,\, B_y \propto (\varepsilon_1 - N_z^2)^{-1},\, B_x, B_z \propto ln|\varepsilon_1 - N_z^2|,\, E_y \approx Const. \qquad (2.15)$$

The field E_x has the most pronounced singularity among the electric fields. Just this electric field determines the field structure in the vicinity of the resonance. It is spatial distribution of the field E_x which is to be investigated in the present overview and is called as fine structure of AR.

Account for nonzero transverse wavenumber $k_y \neq 0$ weakly affect the field spatial distribution (2.15). As it is shown below, logarithmic dependence of the wave field component E_y on the coordinate arises in the vicinity of AR in this case. The other wave field components keep the same dependences (2.15) on the coordinate under taking into account $k_y \neq 0$ as they are in the symmetric case, $k_y = 0$.

2.1. AR fine structure and the power density absorption within it in presence of weak collisions between the plasma particles

The magnitude of electromagnetic power absorbed by the plasma in the vicinity of AR is studied in this subsection. The absorption is assumed for simplicity to take place in the result of the collisions between the plasma particles. In other words, the presence of the small imaginary term in the components of the permittivity tensor is taken into account. The account removes nonphysical singularity of the wave fields (2.15). Properly speaking, the presence of the dissipative phenomena is enough to account in the component ε_1 only:

$$\varepsilon_1 \to Re(\varepsilon_1) + i\varepsilon_1^{(c)}. \qquad (2.1.1)$$

Details are ignored here: it does not mind, which collisions and why cause arise of imaginary part of the plasma permittivity tensor. This question was studied in details in [52]:

$$\varepsilon_1^{(c)} = \sum_{a,b} \frac{\omega_{pa}^2 \nu_{ab}}{\omega(\omega^2 - \omega_{ca}^2)} \left(\frac{\omega^2 + \omega_{ca}^2}{\omega^2 - \omega_{ca}^2} - \frac{e_b m_a}{e_a m_b} \frac{\omega^2 + \omega_{ca}\omega_{cb}}{\omega^2 - \omega_{cb}^2} \right). \qquad (2.1.2)$$

The summation in (2.1.2) is carried out over all the plasma species, e_α is the charge of the particles of the specie α, the collision frequency

$$\nu_{ab}=\frac{4(2\pi)^{\frac{1}{2}}e_a^2e_b^2n_bL}{3(m_aT^3)^{\frac{1}{2}}}\left(\frac{m_b}{m_a+m_b}\right)^{\frac{1}{2}}, \tag{2.1.3}$$

L is Coulomb logarithm.

The magnitude of the electromagnetic power P_r, absorbed by the unit surface of the plasma layer in the vicinity of AR, is determined by the work, carried out by the wave electric fields over the RF currents in the plasma, caused by the wave propagation through the plasma:

$$P_r = 0.5\,Re\left\{\int\left(\vec{j}^*,\vec{E}\right)dx\right\}. \tag{2.1.4}$$

As it is shown above, the main contribution to the scalar product $\left(\vec{j}^*,\vec{E}\right)$ is done by just x-component of the wave electric field, that is why:

$$P_r \approx 0.5\,Re\{\int {j_x}^* E_x dx\}. \tag{2.1.5}$$

It is appropriate to remind that RF electric currents are linked with the wave electric field via permittivity tensor:

$$j_x \approx \frac{\omega}{4\pi i}(\varepsilon_1 - 1)E_x. \tag{2.1.6}$$

Qualitative relation $E_x \propto (\varepsilon_1 - N_z^2)^{-1}$ can be replaced by the precise one:

$$E_x = -\frac{A}{\varepsilon_1 - N_z^2}. \tag{2.1.7}$$

Physical sense of the constant A can be easily understood from analysis of the first and fourth equations in the set (2.7):

$$\begin{cases} -ik_zB_y = \frac{-i\omega}{c}\left(\varepsilon_1E_x + i\varepsilon_2E_y\right), \\ ik_zE_x = \frac{i\omega}{c}B_y. \end{cases} \tag{2.1.8}$$

After substituting the wave magnetic field B_y from the second equation (2.1.8) to the first one, one derives the constant A:

$$A = -E_x(\varepsilon_1 - N_z^2) = i\varepsilon_2E_y. \tag{2.1.9}$$

That is, the constant A is determined as the product of the second component of the permittivity tensor and the wave electric field E_y in the point of AR.

Now, one can calculate the absorbed electromagnetic power density P_r:

$$P_r = 0.5\,Re\int_{x_A-\Delta x}^{x_A+\Delta x} j_x{}^* E_x d = 0.5\,Re\int \frac{\omega}{-4\pi i}(\varepsilon_1^* - 1)E_x^* E_x dx = \quad (2.1.10)$$
$$= \int \frac{\omega}{8\pi} Im\varepsilon_1^* |E_x|^2 dx = \frac{\omega}{8\pi}|A|^2 \int \frac{Im\,\varepsilon_1 dx}{\left(\varepsilon_1 - N_z^2\right)^2 + (Im\,\varepsilon_1)^2} = \frac{\omega}{8}|A|^2 \left|\frac{d\varepsilon_1}{dx}\right|^{-1}.$$

Doing this the properties of the Dirac delta-function are applied [53]:

$$\delta(x) = \frac{1}{\pi}\frac{\Delta}{x^2+\Delta^2}. \quad (2.1.11)$$

In the case, if the dissipative processes are the main mechanism of electromagnetic energy absorption, then the characteristic width of AR is determined just by these processes. Characteristic spatial scale of varying the component ε_1 can be introduced as follows:

$$\frac{d\varepsilon_1}{dx} \sim \frac{Re\,\varepsilon_1}{a^*}. \quad (2.1.12)$$

Then the characteristic width of AR Δx_c, determined by the collisions, can be estimated in terms of a^*:

$$\Delta x_c \sim a^* \varepsilon_1^{(c)} / N_z^2. \quad (2.1.13)$$

Account for the presence of the collisions between the plasma particles results, as it was mentioned above, in removal of nonphysical singularity of the wave fields in the vicinity of AR (see Fig. 2.1.1). Dashed curve in Fig. 2.1.1 is put to compare the wave field spatial distribution with asymptote $E_x \propto (x - x_A)^{-1}$. The dependence $\mathrm{Re}(E_x)$ is calculated in arbitrary units. Maximum absolute magnitude of the wave electric field is not more infinite in the vicinity of AR, it is equal

$$E_x = 0.5A/\varepsilon_1^{(c)}. \quad (2.1.14)$$

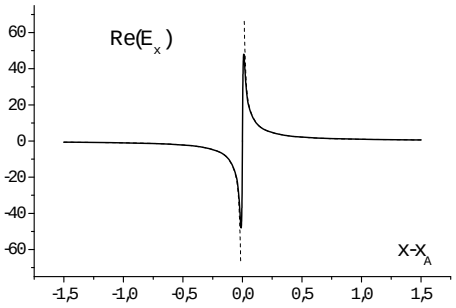

Fig. 2.1.1. Fine structure of AR when determined by the collisions (solid curve), $\nu_{ab}/\omega = 10^{-4}$

Thus, the present overview deals with the problem of diffraction rather than that of eigen functions and eigen values. The question is which part of electromagnetic energy passes through the region of AR and which part is transferred to the plasma particles, that is which part of energy is absorbed in the vicinity of AR. The wave frequency ω is considered to be defined by the generator, wavenumbers k_y and k_z are defined by the antenna shape and phasing.

2.2. Account for the nonzero wavenumber $k_y \neq 0$

If the electromagnetic wave propagates with the nonzero transverse wavenumber, $k_y \neq 0$, the relation (2.7) between the wave magnetic fields B_x and B_y with the electric fields does not change as compared to the case of the zero transverse wavenumber considered above:

$$\begin{cases} -N_z E_y = B_x, \\ N_z E_x = B_y. \end{cases} \tag{2.2.1}$$

However, the expressions of the wave electric fields in terms of the wave longitudinal magnetic field is somewhat more complicated (compare with (2.8)):

$$\begin{cases} E_x = \frac{-c}{\omega\, N_\perp^2}\left(k_y B_z + \mu \frac{\partial B_z}{\partial x}\right), \\ E_y = \frac{-ic}{\omega\, N_\perp^2}\left(k_y \mu B_z + \frac{\partial B_z}{\partial x}\right). \end{cases} \tag{2.2.2}$$

The form of the differential equation for the wave longitudinal magnetic field also becomes more complicated (compare with (2.9)):

$$\frac{\partial}{\partial x}\left(\frac{1}{k_\perp^2}\frac{\partial B_z}{\partial x}\right) + \left[1 - \frac{k_y^2}{k_\perp^2} + k_y \frac{\partial}{\partial x}\left(\frac{\mu}{k_\perp^2}\right)\right] B_z = 0. \tag{2.2.3}$$

However, this does not change the character of the wave field dependence on the coordinate x in the vicinity of AR, except of the field E_y. As one can see from eq. (2.2.2), the term, proportional to k_y, depends on x in the same way, as the field B_z. Thus, those harmonics of the field E_y, which propagate with $k_y \neq 0$, have a logarithmic singularity in the vicinity of AR (compare with (2.15)):

$$E_y \propto ln|\varepsilon_1 - N_z^2|. \tag{2.2.4}$$

In this case the wave field E_x, all the same, remains to be the most increasing one in the vicinity of AR. That is why account for the nonzero k_y weakly changes the explicit expression for the electromagnetic power P_r, absorbed in the vicinity of AR. One has to keep in mind only, that the

constant A, which takes part in the expression (2.1.9), has the other sense in this case. The sense is as follows. After substituting the expression (2.2.1) for the wave field B_y into the first equation from the set (2.7) one derives, that for the waves with $k_y \neq 0$

$$A = -E_x(\varepsilon_1 - N_z^2) = i\varepsilon_2 E_y + B_z c k_y/\omega. \qquad (2.2.5)$$

The circumstance, that the combination (2.2.5) slowly (even without the logarithmic singularity) varies in the vicinity of AR, can be helpful for calculating the spatial distribution of electromagnetic wave fields in the vicinity of AR. It also makes the reason to treat the combination as the pumping wave.

2.3. Account for the finite electron inertia

Up to now, longitudinal (in respect of external static magnetic field) wave electric field was assumed to be negligibly small. This was justified by the smallness of the electron inertia as compared to the ion inertia. Nevertheless, the analysis of the third equation from the set (2.6) clearly shows that the field E_z is even more singular than E_x:

$$E_z = \frac{ic}{\omega\varepsilon_3}\left(\frac{\partial B_y}{\partial x} - ik_y B_x\right) \approx \frac{ic}{\omega\varepsilon_3}\frac{\partial}{\partial x}(N_z E_x) \propto (\varepsilon_1 - N_z^2)^{-2}. \qquad (2.3.1)$$

One can conclude from the second subset in eq. (2.6), that account for the electron finite inertia causes the most influence on the spatial distribution of the wave magnetic field B_y (compare with (2.2.1)), rather than B_x:

$$B_y = N_z E_x - \frac{c^2}{\omega^2\varepsilon_3} N_z \frac{\partial^2 E_x}{\partial x^2}. \qquad (2.3.2)$$

This changes the structure of the equation for the wave electric field (compare with (2.2.1)):

$$N_z^2 \frac{c^2}{\omega^2\varepsilon_3}\frac{\partial^2 E_x}{\partial x^2} + (\varepsilon_1 - N_z^2) E_x = -A. \qquad (2.3.3)$$

Dimensionless variable is convenient to be introduced here

$$\zeta = k(x - x_A),\ k^3 = -\frac{\omega^2\varepsilon_3}{N_z^2 c^2}\frac{d\varepsilon_1}{dx}. \qquad (2.3.4)$$

Equation (2.3.3) changes to the following form in terms of this variable

$$\frac{\partial^2 E_x}{\partial \zeta^2} - \zeta E_x = -\frac{1}{\pi}\left(-A\pi k \left(\frac{d\varepsilon_1}{dx}\right)^{-1}\right). \qquad (2.3.5)$$

The smallness of the factor nearby the second derivative in eq. (2.3.3) means the smallness of the spatial scale (along x) of varying the wave electric field E_x in the vicinity of AR, $ka^*>>1$. The width of AR Δx_m, caused by finite electron inertia, can be estimated as follows (compare with (2.1.13)):

$$\Delta x_m \sim a^* \left(\frac{m_e}{m_i a^{*2} k_z^2}\right)^{\frac{1}{3}}. \qquad (2.3.6)$$

In (2.3.6), the expression (2.2) for the permittivity tensor component ε_3 is applied.

Equation (2.3.5) has the structure of inhomogeneous Airy equation [54]. Its solution has the following form

$$E_x = \left(-A\pi k \left(\frac{d\varepsilon_1}{dx}\right)^{-1}\right)[Gi(\zeta) - iAi(\zeta)]. \qquad (2.3.7)$$

This solution satisfies the following boundary conditions. It is finite in the vicinity of AR; it describes the conversion of MHD waves into the small-scale waves, which carry the energy out of the AR region; it damps in the result of taking into account the weak dissipation in the component ε_1 of the permittivity tensor. The properties of the function $[Gi(\zeta) - iAi(\zeta)]$, which describes the radial dependence of the wave electric field, were studied in detail in [24].

The solution (2.3.7) has the following asymptote for the large magnitudes of the argument, $\zeta \to -\infty$

$$[Gi(\zeta) + iAi(\zeta)] \approx \frac{1}{\pi\zeta} + \frac{1}{\sqrt[4]{\pi^2|\zeta|}} exp\left\{-i\left[\frac{2}{3}(-\zeta)^{\frac{3}{2}} + \frac{\pi}{4}\right]\right\}. \qquad (2.3.8)$$

The representation (2.3.8) makes it possible to assume that the small-scale ion cyclotron wave (the second term in (2.3.8)) rapidly damps with going away from AR point in the close vicinity of the AR point due to the Landau damping. In the case of weak damping of the small-scale wave, the asymptote (2.3.8) should match up the solution of eq. (2.3.3), which is found by WKB method and which corresponds to the waves carrying the energy away from the conversion point either to the plasma core or to the plasma periphery. Small-scale waves are assumed to be completely absorbed during one passage. This means that the phenomena are neglected which can take place in the case of very weak damping, in particular, arising of the global resonances with high magnitude of the radial number.

If the weak collisions are taken into account in eq. (2.3.3), $\varepsilon_1 \to \varepsilon_1 + i\nu^*/\omega$, then the argument of the functions $Gi(\zeta)$ and $Ai(\zeta)$ becomes a complex number with a small imaginary part, $\zeta \to \zeta + i\frac{\nu^* k}{\omega}\left(\frac{d\varepsilon_1}{dx}\right)^{-1}$. Then the argument of the exponent in the asymptote (2.3.8) gets the real term, proportional to ν^*:

$$-i\left[\frac{2}{3}(-\zeta)^{\frac{3}{2}}+\frac{\pi}{4}\right]\rightarrow -i\left[\frac{2}{3}\left(-\zeta-\frac{i\nu^{*}k}{\omega}\left(\frac{d\varepsilon_1}{dx}\right)^{-1}\right)^{\frac{3}{2}}+\frac{\pi}{4}\right]\rightarrow$$
$$\rightarrow -i\left[\frac{2}{3}(-\zeta)^{\frac{3}{2}}\left(1-\frac{i\nu^{*}k}{(-\zeta)\omega}\left(\frac{d\varepsilon_1}{dx}\right)^{-1}\right)^{\frac{3}{2}}+\frac{\pi}{4}\right]\rightarrow$$
$$\rightarrow -i\left[\frac{2}{3}(-\zeta)^{\frac{3}{2}}+\frac{\pi}{4}\right]-i\frac{2}{3}(-\zeta)^{\frac{3}{2}}\frac{3}{2}\frac{i\nu^{*}k}{(-\zeta)\omega}\left(\frac{d\varepsilon_1}{dx}\right)^{-1}\rightarrow$$
$$\rightarrow -i\left[\frac{2}{3}(-\zeta)^{\frac{3}{2}}+\frac{\pi}{4}\right]-(-\zeta)^{\frac{1}{2}}\frac{\nu^{*}k}{\omega}\left(\frac{d\varepsilon_1}{dx}\right)^{-1}. \qquad (2.3.9)$$

Since k and the derivative $(d\varepsilon_1/dx)$ are of the same sign, then the presence of the real term, proportional to the effective collision frequency ν^*, does cause the exponential reduction of the second term in the asymptote (2.3.8) with going away from the AR point (if $(-\zeta)\rightarrow+\infty$). This is the reason to choose the sign «–» in the square brackets in (2.3.7).

The electric field increases in the vicinity of AR. However, it does not increase infinitely. Its characteristic magnitude (compare with (2.1.14)) can be derived by the order of magnitude from eq. (2.3.7):

$$E_x \sim A\frac{\pi}{N_z^2}\left(\frac{m_i}{m_e}k_z^2 a^{*2}\right)^{\frac{1}{3}}. \qquad (2.3.10)$$

Doing this, one gets advantage from the fact that the functions $Gi(\zeta)$ and $Ai(\zeta)$ are the values of the order of a unit in the vicinity of the zero.

Physical mechanism of electromagnetic wave damping appears not to influence on the magnitude of the electromagnetic power density, absorbed in the vicinity of AR. To tell the truth, this statement is right only in the framework of the assumption, that AR width is small. Absorption of electromagnetic power in the vicinity of AR (averaged on the wave temporal period) is determined by the variation of the Poynting vector

$$\vec{S}=\frac{c}{8\pi}Re\left[\vec{E}^{*},\vec{B}\right], \qquad (2.3.11)$$

after passing the AR point $x=x_A$. In the considered here case, the electromagnetic power propagates along the x axis. That is why one can calculate just x component S_x:

$$S_x=\frac{c}{8\pi}\mathrm{Re}\,(E_y^{*}B_z-E_z^{*}B_y). \qquad (2.3.12)$$

Since the magnitude of the longitudinal component of the wave electric filed E_z is neglected due to the smallness of the electron inertia,

$$S_x\approx\frac{c}{8\pi}\mathrm{Re}\,(E_y^{*}B_z). \qquad (2.3.13)$$

The field E_y, as it is shown above, weakly varies in the vicinity of AR, that is why

$$\Delta S_x \approx \frac{c}{8\pi}\mathrm{Re}\,(E_y^* \Delta B_z). \qquad (2.3.14)$$

Variation of the longitudinal wave magnetic field ΔB_z in the result of passing the AR can be determined from the eq. (1.8):

$$\Delta B_z \approx \int_{x_A-\Delta x}^{x_A+\Delta x} \frac{\omega}{c}\varepsilon_2 E_x dx \approx \frac{\omega}{c}\varepsilon_2 \int_{x_A-\Delta x}^{x_A+\Delta x} E_x dx. \qquad (2.3.15)$$

The presence of the weak dissipation can be taken into account by the presence of the small imaginary part (2.1.1) in the component ε_1 of the permittivity tensor. During integrating in (2.3.15) the expression (2.1.7) for the component E_x of the wave electric field is applied:

$$\int_{x_A-\Delta x}^{x_A+\Delta x} E_x dx = \int_{x_A-\Delta x}^{x_A+\Delta x} \frac{-A}{\frac{d\varepsilon_1}{dx}(x-x_A)+i\frac{\nu^*}{\omega}} dx. \qquad (2.3.16)$$

In the case of plasma particle density increasing with the coordinate x the derivative $d\varepsilon_1/dx>0$. And residual point (the point in which the denominator is equal to zero) is situated in the complex plane a little bit below the real axis,

$$x = x_A - i\frac{\nu^*}{\omega\frac{d\varepsilon_1}{dx}}. \qquad (2.3.17)$$

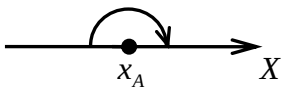

Fig. 2.3.1. The rule for passing the residual point in the integral (2.3.16)

That is why the integration in (2.3.16) can be carried out along the upper semi-circumference in the complex plane (see Fig. 2.3.1):

$$\int_{x_A-\Delta x}^{x_A+\Delta x} E_x dx = \frac{-A}{\frac{d\varepsilon_1}{dx}} \int_{x_A-\Delta x}^{x_A+\Delta x} \frac{dz}{z-z_A} = \frac{-A}{\frac{d\varepsilon_1}{dx}} i(-\pi). \qquad (2.3.18)$$

The expression (2.3.7) for definition of the wave electric field E_x as well as the Airy function properties [54] make it possible to carry out precise integration:

$$\int_{-\infty}^{0} Ai(\zeta)d\zeta = \frac{2}{3}, \qquad \int_{0}^{+\infty} Ai(\zeta)d\zeta = \frac{1}{3}. \qquad (2.3.19)$$

Then

$$\int_{x_A-\Delta x}^{x_A+\Delta x} E_x dx \approx \int_{-\infty}^{+\infty} \frac{iA\pi k}{\frac{d\varepsilon_1}{dx}} Ai(\zeta)dx = \frac{iA\pi}{\frac{d\varepsilon_1}{dx}} \int_{-\infty}^{+\infty} Ai(\zeta)d\zeta = \frac{iA\pi}{\frac{d\varepsilon_1}{dx}}. \qquad (2.3.20)$$

As one can see, calculating the electromagnetic power absorption with the assumption that it is determined by the finite electron inertia (expression (2.3.20)) provides the same result as with the assumption that the absorption is determined by the weak collisions between the plasma particles (2.3.18).

If the dissipations and the electron inertia are neglected, then the fields E_y and B_z are shifted in phase by $\pi/2$. One can see this, in particular, from the eq. (2.2.2). If the weak phenomena mentioned above are taken into account then the electromagnetic power density, absorbed in the vicinity of AR, can be calculated from eq. (2.3.14). In this case one has to take into account the relation (2.1.7) between the field E_y and the constant A along with the result (2.3.20):

$$\Delta S_x \approx \frac{c}{8\pi}\mathrm{Re}\,(E_y^{*}\Delta B_z)=\frac{c}{8\pi}\mathrm{Re}\left(\left(\frac{A}{i\varepsilon_2}\right)^{*}\frac{\omega\varepsilon_2}{c}\frac{iA\pi}{\frac{d\varepsilon_1}{dx}}\right)= 0{,}125\omega|A|^2(d\varepsilon_1/dx)^{-1}. \quad (2.3.21)$$

This result precisely coincides with the calculations (2.1.10) of the electromagnetic energy density, carried out with the help of the Dirac delta-function.

2.4. Account for the finite larmor radius

In the calculations presented above, the plasma was assumed to be cold. In other words, the radius of the plasma particle gyration along the Larmor orbits was neglected. Account for the nonzero radius of the gyration in the external static magnetic field results in changing of the form of the component ε_3 of the permittivity tensor as compared to the expression (2.2), which was derived in MHD approach [52]:

$$\varepsilon_3=\frac{\omega_{pe}^2}{k_z^2 v_{Te}^2}\left[1+i\sqrt{\pi}Z_e W(Z_e)\right], \text{ where } Z_e=\frac{\omega}{\sqrt{2}|k_z|v_{Te}}. \quad (2.4.1)$$

The function $W(Z_e)$ reads as

$$W(\xi)=exp(-\xi^2)\left[1+\frac{2i}{\pi}\int_0^{\xi} exp(t^2)\,dt\right]. \quad (2.4.2)$$

For the long wavelength waves ($k_z\to 0$, $Z_e\to\infty$) Landau damping can appear to be weak, then the asymptote of the expression (2.4.1) gives

$$\varepsilon_3 \approx -\frac{\omega_{pe}^2}{\omega^2}+i\sqrt{\pi}Z_e\, exp(-Z_e^2). \quad (2.4.3)$$

In this case, one has to apply the definition of ε_3 with account for the collisions (compare with (2.2)):

$$\varepsilon_3=-\frac{\omega_{pe}^2}{\omega(\omega+i\nu_{ei})}. \quad (2.4.4)$$

Account for the finite Larmor radius influences also the component ε_1 of the permittivity tensor:

$$\varepsilon_1 \to \varepsilon_1 + \varepsilon_T \frac{c^2}{\omega^2} \frac{d^2}{dx^2}, \tag{2.4.5}$$

here [52]

$$\varepsilon_T = \sum_i \frac{3\omega^2 \omega_{pi}^2(x) v_{Ti}^2(x)}{c^2(\omega^2 - \omega_{ci}^2)(\omega^2 - 4\omega_{ci}^2)}. \tag{2.4.6}$$

In this case, the equation for the wave electric field E_x can be written as follows (compare with (2.3.3)):

$$\left(\varepsilon_T + \frac{N_z^2}{\varepsilon_3}\right) \frac{c^2}{\omega^2} \frac{\partial^2 E_x}{\partial x^2} + (\varepsilon_1 - N_z^2) E_x = -A. \tag{2.4.7}$$

Its solution can be written in the form (2.3.7) with

$$k^3 = -\frac{\omega^2}{c^2\left(\varepsilon_T + \frac{N_z^2}{\varepsilon_3}\right)} \frac{d\varepsilon_1}{dx}. \tag{2.4.8}$$

The wavenumber is determined now by the order of magnitude as follows

$$k \sim \left(\rho_{Li}^2 a^* \right)^{-\frac{1}{3}}, \tag{2.4.9}$$

here ρ_{Li} is the Larmor radius of plasma ions which is assumed to be small: $\rho_{Li} << a^*$. This results in the smallness of the wavelength (characteristic spatial scale along the x coordinate) of the wave electric field E_x in the vicinity of AR, $ka^* >> 1$.

The width of AR Δx_T, caused by the finite Larmor radius (nonzero plasma temperature), can be estimated by the order of magnitude from eq. (2.4.9) as follows (compare with (2.1.13) and (2.3.6)):

$$\Delta x_T \sim a^* (\rho_{Li}/a^*)^{\frac{2}{3}}. \tag{2.4.10}$$

Characteristic magnitude of the wave electric field E_x in the vicinity of AR can be estimated analogously. One derives it basing on the estimation (2.4.9) for k and taking into account that the functions $Gi(\zeta)$ and $Ai(\zeta)$ are the values of the order of a unit in the vicinity of zero. Then the characteristic magnitude of E_x appears to be:

$$E_x \sim A \frac{\pi}{N_z^2} \left(\frac{a^*}{\rho_{Li}}\right)^{\frac{2}{3}}. \tag{2.4.11}$$

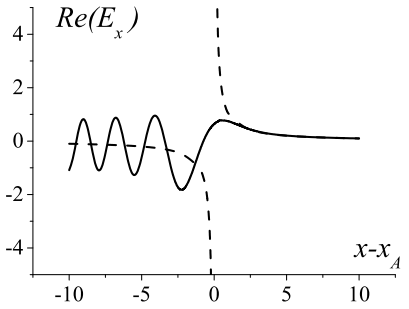

Fig. 2.4.1. Fine structure of AR with account for finite ion Larmor radius (solid curve), $\rho_{Li}/a^*=10^{-5}$

The fine structure of AR in the case, if it is determined just by the finite ion Larmor radius, is shown in the Fig. 2.4.1. Dashed curve, as earlier, shows the dependence $E_x \propto (x-x_A)^{-1}$ just for a comparison.

2.5. On the possibility to neglect the larmor radius in the viccinity of AR

Application of the cold plasma permittivity tensor (2.1) – (2.2) is justified, if the assumption is true, that Larmor radius is small as compared with the wavelength, $k_{x,y,z}\rho_{Li} \ll 1$. As it was already mentioned above, $\varepsilon_1 \to N_z^2$ in the vicinity of AR (2.10). This causes that transverse refractive index squared $N_\perp^2$ (see notations to eq. (2.8)) is also singular, $N_\perp^2 \propto (\varepsilon_1 - N_z^2)^{-1}$. This can cause infinite increase of k_x (or, which is the same, reduction of the wavelength $2\pi/k_x$), which would mean violation of the mentioned above assumption about the smallness of Larmor radius.

In the following, it is analysed [55], which type are the waves, excited in the vicinity of AR (2.10), of. This can be done on the base of analysing the solution of the eq. (2.2.3) obtained in the framework of WKB approach. In this case, the dependence of the wave fields on x coordinate is assumed to be as follows: $B_z \propto exp(i\int k_x dx)$. The small terms, determined by the account for the small Larmor radius and the electron inertia, cause the most influence on the first term of the eq. (2.2.3):

$$\left[1-\frac{k_y^2}{k_\perp^2}+k_y\frac{\partial}{\partial x}\left(\frac{\mu}{k_\perp^2}\right)\right]B_z+\frac{\partial}{\partial x}\left(\frac{\varepsilon_1-N_z^2+\left(\varepsilon_T+\frac{N_z^2}{\varepsilon_3}\right)\frac{c^2}{\omega^2}\frac{\partial^2}{\partial x^2}}{k_\perp^2(\varepsilon_1-N_z^2)}\frac{\partial B_z}{\partial x}\right)=0. \qquad (2.5.1)$$

WKB approach also assumes, that the plasma parameters vary weakly at the wavelength: $k_x a^* \gg 1$. This makes it possible to neglect the terms, proportional to the plasma particle density gradient dn/dx. Then eq.

(2.5.1) transforms into the quadratic equation for the refractive index squared $N_x^2=c^2k_x^2/\omega^2$ with the following solution:

$$N_{x\pm}^2=\frac{\varepsilon_3(\varepsilon_1-N_z^2)}{2(\varepsilon_T\varepsilon_3+N_z^2)}\left[1\pm\sqrt{1-4\left(N_\perp^2-\frac{c^2k_y^2}{\omega^2}\right)\frac{\varepsilon_T\varepsilon_3+N_z^2}{\varepsilon_3(\varepsilon_1-N_z^2)}}\right]. \qquad (2.5.2)$$

The dependence $N_\perp^2(x)$ (in other words, the cold limit) is shown in Figs. 2.5.1, and 2.5.2 by dashed curves. The dependence $N_x^2(x)$ which takes into account both finite Larmor radius and electron inertia has the form which is demonstrated in Figs. 2.5.1, and 2.5.2 by the solid curves.

If the plasma ion temperature is small, $\beta_i\equiv 4\pi T_i n/B_0^2<<m_e/m_i$, then the conversion of MHD wave in the vicinity of AR is determined by the electron inertia. In this case (see Fig. 2.5.1), the considered MHD wave is incident on AR from the side of dense plasma (from right to left). If the MHD wave approaches to the resonant point $x=x_A$ at the distance of the order of $\frac{a^*}{N_z^2}\left(\frac{m_e}{m_i}\right)^{\frac{1}{2}}$, then its refractive index squared N_{x-}^2 rapidly increases in absolute value and in the point, where the derivative dN_{x-}^2/dx turns to infinity, N_{x-}^2 reaches the magnitude of the order of $(m_i/m_e)^{\frac{1}{2}}$. In the neighbourhood of the resonant point x_A with the width of $\frac{a^*}{N_z^2}\left(\frac{m_e}{m_i}\right)^{\frac{1}{2}}$ (by the order of magnitude) MHD wave transforms into the small-scale ion cyclotron wave, which propagates to the periphery with $N_{x+}^2\approx\frac{\omega_{pi}^4}{N_z^2\omega_{ci}^4}\frac{m_i}{m_e}$. Refractive index squared of the large-scale MHD wave is shown in Figs. 2.5.1 and 2.5.2 by thicker curves and is figured by «1». The refractive index squared of the small-scale wave is larger (the wavelength $\lambda_x=2\pi c/(\omega N_x)$: the larger is N_x, the smaller is the wavelength, and the smaller is the scale of the wave) than N_x^2 of the large-scale wave. The refractive index squared of the small-scale wave is demonstrated in Figs. 2.5.1 and 2.5.2 by thinner curves and figured by «2».

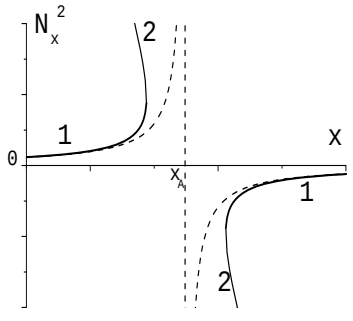

Fig. 2.5.1. Refractive index squared vs x coordinate

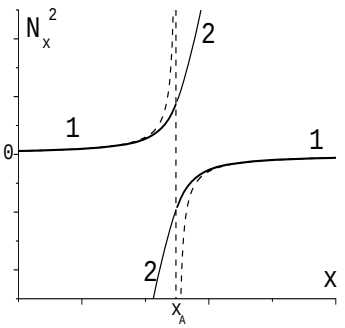

Fig. 2.5.2. Refractive index squared vs x coordinate

If the ions are not very cold ($\beta_i >> m_e/m_i$) in the vicinity of AR (2.10), then the conversion of MHD waves is determined by the finite ion Larmor radius. In this case, the width of the conversion region appears to be equal by the order of magnitude to $a^* \upsilon_{Ti}/(N_z^2 c)$. The refractive index squared N_{x+}^2 becomes equal to (c/υ_{Ti}) by the order of magnitude in the neighbourhood of the resonant point, and characteristic parameter

$$k_{x\pm}^2 \rho_{Li}^2|_{x_A} = \frac{\upsilon_{Ti}^2 \omega^2}{c^2 \omega_{ci}^2} \left(\frac{\varepsilon_2^2}{\varepsilon_T}\right)^{\frac{1}{2}} \sim \frac{\upsilon_{Ti}}{c} << 1. \qquad (2.5.3)$$

Strong inequality (2.5.3) justifies applicability of the plasma permittivity tensor (2.2), (2.4.1) and (2.4.6) for the plasma description in the vicinity of AR. If herewith the frequency of MHD wave satisfies the condition $\varepsilon_T < -N_z^2 (Re\varepsilon_3)^{-1}$, then the small-scale ion cyclotron wave propagates from the conversion region to the plasma periphery (from right to left) with $k_{x+}^2 \approx \rho_{Li}^{-2}$ (see Fig. 2.5.1). If the frequency of MHD wave is such that $\varepsilon_T > -N_z^2 (Re\varepsilon_3)^{-1}$, then the small-scale ion cyclotron wave, propagating away from the conversion region into the plasma core, can transform into more small-scale wave with $k_{x+}\rho_{Li} > 1$ (see Fig. 2.5.2).

The case of the «narrow layer» [56] is considered in the present overview. That is the wavelength of the large-scale MHD wave is assumed to be much larger than the characteristic scale of plasma parameters variation,

$$a^* << max(1/k_y, c/\omega, 1/k_z). \qquad (2.5.4)$$

This inequality is opposite to the condition of applicability of WKB approach. That is why the dependences $N_x^2(x)$ shown in Figs. 2.5.1, and 2.5.2 can serve only as a qualitative illustration of the wave conversion in the vicinity of the resonant point (2.10).

2.6. Influence of the striction nonlinearity

If the pumping wave is sufficiently powerful, then the influence of nonlinear phenomena on the MHD wave field distribution in the direct neighbourhood of AR can appear to be significant. The influence of the striction nonlinearity is studied in the present subsection. It is the main nonlinear phenomenon in the case of fast wave processes (if the wave phase velocity $\upsilon_{ph} >> \upsilon_{Ti}$). Nonlinearity on the second harmonic prevails for the slow wave processes [57], $\upsilon_{ph} < \upsilon_{Ti}$. The striction changes the plasma particle density, $n(r) \rightarrow n_{NL}$,

$$n_{NL} = n(r) \cdot exp(-U^{\sim}/T). \qquad (2.6.1)$$

Potential energy of the plasma particles [58] in the field of the pumping wave reads as: $U^{\sim}=U^{(0)}$, where

$$U^{(0)} = \sum_{\alpha} \frac{e_{\alpha}^2 n_{\alpha}\left[|E_x|^2+|E_y|^2+i(\omega_{c\alpha}/\omega)\left(E_x^* E_y - E_x E_y^*\right)\right]}{4m_{\alpha} n_e\left(\omega^2-\omega_{c\alpha}^2\right)}. \quad (2.6.2)$$

Due to the assumption of the striction weakness, $U^{\sim}<<T$, it is enough to account for the replacement $n(r)\to n_{NL}$ in eq. (2.2.3) only in the factor $\varepsilon_1 - N_z^2$, which is small in the vicinity of AR,

$$\varepsilon_1 - N_z^2 \to (\partial\varepsilon_1/\partial x)_{x_A}(x - x_A) + (\varepsilon_1 - 1)(-U^{\sim}/T) + O\left(U^{\sim 2}/T^2\right). \quad (2.6.3)$$

The striction nonlinearity can determine the AR fine structure (spatial distribution of the wave fields in the vicinity of AR), if the following inequality is valid,

$$|(\varepsilon_1 - 1)(U^{\sim}/T)| > |N_z^2/(a^* k)|. \quad (2.6.4)$$

After simplifying the condition (2.6.4) becomes the condition on the amplitude of the pumping wave A,

$$A^2 >> E_0^2 N_z^2 (\rho_{Li}/a^*)^{4/3}. \quad (2.6.5)$$

Here

$$\frac{1}{E_0^2} = -\sum_{\alpha} \frac{e_{\alpha}^2 n_{\alpha}}{4m_{\alpha} n_e T\left(\omega^2-\omega_{c\alpha}^2\right)}. \quad (2.6.6)$$

Spatial distribution of RF waves in the vicinity of AR under the condition (2.6.4) (see Fig. 2.6.1, and 2.6.2) was studied numerically in [59]. Figures 2.6.1 and 2.6.2 show the comparison of AR fine structure in linear approach (solid curve figured by «1») (in other words, the amplitude of the pumping wave in the case, if the structure is determined by the finite Larmor radius) with the AR fine structure in the nonlinear case (dash-dotted curve figured by «2»). The following parameters of the deuterium plasma were chosen for the calculations: plasma particle density in the point of AR $n(r_A)$=2,53×10^{13} cm^{-3}, ion temperature T=0,2 keV, axial external static magnetic field B_{0z}=1,1 T, longitudinal wavenumber k_z=0,2 cm^{-1}, frequency of the generator ω=0,8 ω_{ci}, characteristic scale, at which the plasma particle density varies, a^*=2 m. The observable E_0, which is defined by eq. (2.6.6), is equal E_0 =1,3 kV/cm. Under these conditions, the striction nonlinearity results in forming of strongly nonlinear kinetic Alfven wave in the vicinity of AR. Two ordinate scales are applied in Figs. 2.6.1 and 2.6.2 for the linear and nonlinear waves. The scale for the linear wave is present on the left ordinate axis, and that for the nonlinear wave – on the right axis.

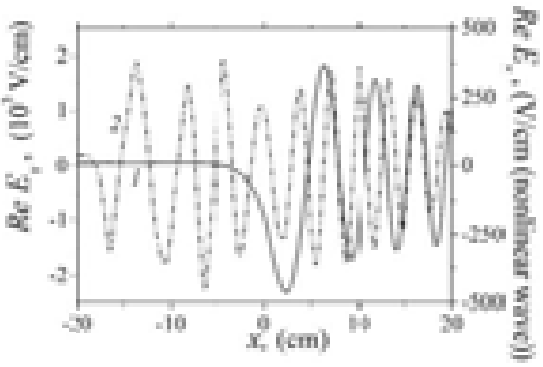

Fig. 2.6.1. Spatial distribution of the real part of the electric field component in the case of linear (solid curve) and nonlinear (dash-dotted curve) waves

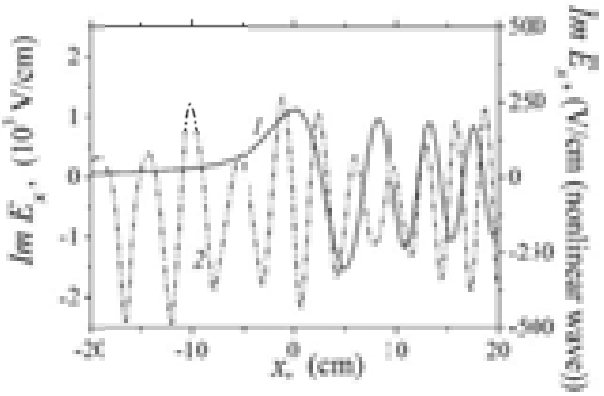

Fig. 2.6.2. Spatial distribution of imaginary part of the electric field component in the case of linear (solid curve) and nonlinear (dash-dotted curve) waves

2.7. Influence of the kinetic ion cyclotron turbulence

Reverse influence of the plasma kinetic parametric ion cyclotron instabilities on the pumping waves is studied in this subsection. Ions scatter on the turbulent oscillations at the nonlinear stage of the cyclotron oscillation growth. This provides the reason to consider the scattering as collisions with a perfect effective collision frequency [60]. Turbulent absorption of MHD waves can be taken into account by replacement of the frequency of the plasma particle collisions by the effective frequency of their collisions with the turbulent fluctuations,

$$\varepsilon_1^{(c)} \to \varepsilon_{1eff} = \frac{16\pi n T_i}{B_0^2}\left(\frac{c|E|}{v_{Ti}B_0}\right)^3\left(\frac{c}{v_{Ti}}\right)^2\left(1+\frac{k_z^2c^2}{\omega_{pi}^2}\right). \quad (2.7.1)$$

The electromagnetic power W^T, absorbed by the unit of the plasma layer surface in the vicinity of AR due to effective dissipation – ion cyclotron turbulence – is equal by the order of magnitude

$$W^T \sim \omega \Delta x_{NL} \varepsilon_{1eff} |E_x|^2/(8\pi) \propto |E_x|^8. \quad (2.7.2)$$

Here

$$\Delta x_{NL} \sim a^* \varepsilon_{1eff}/N_z^2 \quad (2.7.3)$$

is the width of the plasma layer, wherein the turbulence is significant.

Characteristic magnitude of the wave electric field amplitude in the vicinity of AR can be estimated from eq. (2.7.1) and (2.1.14)

$$E_x \sim \left(A\frac{B_0^3 v_{Ti}^3}{c^3 N_z^2}\right)^{\frac{1}{4}}. \quad (2.7.4)$$

One can see from estimations (2.7.2), (2.7.3) and (2.7.4), that the power W^T depends overall on the pumping wave amplitude quadratically, $W^T \propto A^2$.

SECTION 3. LOCAL ALFVEN RESONANCE IN PLASMAS WITH TWO-DIMENSIONAL INHOMOGENEITY

External static magnetic field $\vec{B}_0$ is often bumpy one in laboratory plasma. The term «bumpy» means that the field has weak axial inhomogeneity. This takes place in adiabatic traps with the bumpy magnetic field [64, 65], in particular, in tokamaks, where the inhomogeneity is caused by the discreteness of the coils of the toroidal magnetic field. It also took place in toroidal systems with the bumpy magnetic field like ELMO BUMPY TORUS [66, 67]. So-called «mirror» inhomogeneity [68] was planned to prevail in the confining magnetic field of the Helias modular stellarator. If one replaces the flow coordinates, suggested in [68] for presenting the Helias reactor magnetic field, by cylindrical coordinates, then this representation of the «mirror» inhomogeneity coincides with the representation of the bumpy magnetic field, which is considered in the present overview. In this sense the undertaken consideration can be applied for studying the AR fine structure in Helias configuration.

The theory of MHD wave propagation in the plasma column, which is placed into the external static magnetic field with the weak axial inhomogeneity, was presented in [69–72]. Electromagnetic perturbations propagate in the bumpy external static magnetic field in the form of the wave packet. Generally speaking, infinite number of satellite harmonics is present in the wave packet along with the main harmonic. The research, carried out in

[69], has demonstrated, that the multimodality of MHD waves, caused by the external static magnetic field inhomogeneity, results in general case in the shift of the eigen frequency of MHD waves. The latter shift is the small value of the second order in the small parameter of the inhomogeneity. Eigen plasma oscillations, caused by so-called «mirror» inhomogeneity of the confining magnetic field of the modular stellarator Helias, which spatial distribution is analogous to the bumpy magnetic field, was foreseen in [73–76].

In the present section, the influence of the axial inhomogeneity of the external static magnetic field, wherein the plasma column is placed, on the conversion and absorption of MHD waves is studied. The presence of additional resonant regions (so-called satellite ARs) is shown to be possible in the traps with the bumpy magnetic field along with conventional AR. Rapid growth of the amplitudes of small satellite harmonics of MHD waves and their conversion into small-scale kinetic waves take place within these SARs. The magnitude of the RF power, absorbed in the vicinity of these additional resonances, is determined.

The fine structure of the local SARs is determined, in particular, under the condition, that the influence of the external static magnetic field inhomogeneity on the structure is stronger than those of the plasma particle collisions, ion thermal motion and electron inertia. These conditions can be realized in the peripheral plasma, where the inhomogeneity is stronger and the plasma is colder.

The main general principles of the considered in the present section model of the cylindrical plasma, placed into the bumpy magnetic field, are as follows.

In the case of weak inhomogeneity ($/\varepsilon_m/<<1$), the radial and axial components of the external static magnetic field $\vec{B}_0 = B_{0r}\vec{e}_r + B_{0z}\vec{e}_z$ (in cylindrical coordinates) are as follows, respectively (see Fig. 3.1.):

$$B_{0r}=B_0(\varepsilon'_m/k_m)\sin(k_b z), \qquad B_{0z}=B_0[1+\varepsilon_m(r)\cos(k_b z)], \tag{3.1}$$

here $\varepsilon_m' \equiv d\varepsilon_m/dr$, $k_b=2\pi/L$, L is the axial period of inhomogeneity. The parameter of inhomogeneity ε_m is usually the small value, $/\varepsilon_m/<<1$, in modern fusion devices. For example, in the plasma edge of the tokamak ASDEX-U, Germany, it reaches the magnitude of $\sim 5\cdot 10^{-2}$ [70, 77]. In Helias configuration [73–76], the «mirror» inhomogeneity is planned to be more significant, $\varepsilon_m \sim 0.13$.

It is opportunely to note that eq. (2.1) doesn't automatically provide the fundamental equation $div\vec{B}_0=0$. After substituting the definitions (3.1) to the fundamental equation, one obtains the relation, which determines the dependence of the small parameter ε_m on the radial coordinate r. The relation has the form of the Bessel equation. Solution of the latter equation makes it possible to conclude, that ε_m is proportional to the Bessel modified function of the zeroth order. This means, that ε_m can be considered as a constant, if the axial period of the inhomogeneity is large as compared with

the small radius of the device chamber. Otherwise, if the axial period of the inhomogeneity is small, the observable ε_m decreases approximately exponentially with going away from the plasma boundary. In this case, the inhomogeneity of the external static magnetic field is significant in the narrow layer with the width k_b^{-1} nearby the metal wall.

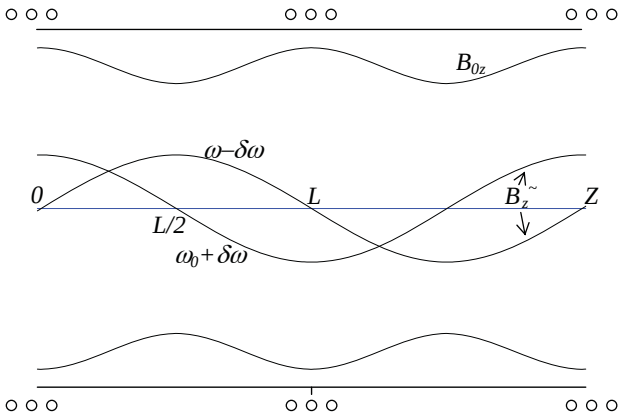

Fig. 3.1. Schematic of the dependence of the absolute value of the external static magnetic field and spatial distribution of eigen MHD waves on the axial coordinate in the case of the bumpy magnetic field (3.1)

Magnetic force lines are well-known to be parallel to the external static magnetic field $\vec{B}_0$ in every point. Vector form of this condition reads as

$$[\vec{B}_0, d\vec{r}] = 0, \tag{3.2}$$

which results in the following equation for the force lines in cylindrical coordinates,

$$\frac{dr}{B_{0r}} = \frac{dz}{B_{0z}}. \tag{3.3}$$

The equation for the magnetic surface can be derived in the result of integrating the eq. (3.3) after substituting the explicit expressions (3.1) for B_{0r} and B_{0z} to it,

$$r - r_0 = -\frac{cos(k_b z)}{r} \int_0^r r \varepsilon_m dr + O(\varepsilon_m^2). \tag{3.4}$$

Taking into account the properties of $\varepsilon_m(r)$ as a Bessel modified function one can rewrite the eq. (3.4) in more convenient form,

$$r_0 = r - cos(k_b z)\ (1 - 0.5\varepsilon_m\, cos(k_b z))\ \varepsilon'_m / k_b^2 + O(\varepsilon_m^3). \tag{3.5}$$

In this section, the main principles of the theory of the conversion and absorption of MHD waves with the frequency $\omega << \omega_{ce}, \omega_{pe}$ in the plasma cylinder placed into the bumpy magnetic field are presented. Studying this problem is of interest mostly due to its application to the problem of plasma heating with these waves in the plasma traps with the bumpy magnetic field. The case of the plasma with the low pressure is under the consideration. In this case, one can neglect the electron inertia during studying the fast magnetosonic and Alfven branches of MHD waves. In such a plasma, equilibrium plasma particle density $n(r,z)$ can be introduced as a function of one variable, that is the «number» of the magnetic surface, $n(r,z) = n(r_0)$. The external static magnetic field inhomogeneity is considered to be weak one. This makes it possible to apply the method of successive approximations for solving the Maxwell's equations.

The components $\varepsilon_{1,2}$ of the cold plasma permittivity tensor, which determine the MHD wave propagation, connect the components of the vector of the wave electric displacement field $\vec{D}$ with the vector of the wave electric field $\vec{E}$ as follows:

$$D_r + \gamma D_z = \varepsilon_1(1+\gamma^2)E_r + i\varepsilon_2\sqrt{1+\gamma^2}\,E_\vartheta, \tag{3.6}$$

$$D_\vartheta = \varepsilon_1 E_\vartheta - i\varepsilon_2\sqrt{1+\gamma^2}\;E_r, \tag{3.7}$$

here $\gamma = B_{0r}/B_{0z}$. The components ε_1 and ε_2 of the cold plasma permittivity tensor are determined as follows under assumption of neglecting the collisions between the plasma particle,

$$\varepsilon_1 = 1 - \sum_i \omega_{pi}^2(r_0)/\left(\omega^2 - \omega_{ci}^2\right), \quad \varepsilon_2 = -\sum_i \omega_{pi}^2(r_0)\omega/\left[\left(\omega^2 - \omega_{ci}^2\right)\omega_{ci}\right]. \tag{3.8}$$

The following expressions for $\varepsilon_{1,2}$ with accuracy up to the small terms of the first order in ε_m are applied below:

$$\varepsilon_{1,2}(r,z) = \varepsilon_{1,2}^{(0)}(r) + \varepsilon_{1,2}^{(1)}(r)\,cos(k_b z) + O(\gamma^2), \tag{3.9}$$

here $\left|\varepsilon_{1,2}^{(1)}\right| \sim \left|\varepsilon_m \varepsilon_{1,2}^{(0)}\right|$. In absence of the axial inhomogeneity ($\varepsilon_m = 0$), the components $\varepsilon_{1,2}$ read as

$$\varepsilon_1^{(0)} = 1 + \frac{\omega_{pi}^2(r)}{\omega_{ci}^{(0)2} - \omega^2}, \tag{3.10}$$

$$\varepsilon_2^{(0)}(r) = \frac{\omega_{pi}^2(r)\omega}{\omega_{ci}^{(0)}(\omega_{ci}^{(0)2} - \omega^2)}, \tag{3.11}$$

here $\omega_{ci}^{(0)}=\omega_{ci}(B_0)$ is calculated in the zeroth approach, that is under the condition of neglecting the axial inhomogeneity of external static magnetic field, $\omega_{ci}^{(0)} = eB_0/(m_i c)$, and $N_A(r)=\omega_{pi}(r)/\omega_{ci}^{(0)}$ is Alfven refractive index.

The corrections $\varepsilon_{1,2}^{(1)}$ of the first order read as:

$$\varepsilon_1^{(1)}(r) = \left(\frac{\partial\omega_{pi}^2}{\partial r}\right)_{|\varepsilon_m=0} \frac{\varepsilon_m'}{k_m^2}\sum\left(\omega^2-\omega_{ci}^{(0)2}\right)^{-1} - 2\varepsilon_m\sum_i \frac{\omega_{pi}^2(r)\omega_{ci}^{(0)2}}{\left(\omega^2-\omega_{ci}^{(0)2}\right)^2}, \quad (3.12)$$

$$\varepsilon_2^{(1)}(r) = \left(\frac{\partial\, ln\left(\omega_{pi}^2\right)}{\partial r}\right)_{|\varepsilon_m=0} \frac{\varepsilon_m'}{k_m^2}\varepsilon_2^{(0)} - \varepsilon_m\sum_i \frac{\omega_{pi}^2(r)\omega\left(3\omega_{ci}^{(0)2}-\omega^2\right)}{\omega_{ci}^{(0)}\left(\omega^2-\omega_{ci}^{(0)2}\right)^2}. \quad (3.13)$$

To solve the problem the following orthonormal set of coordinate vectors $(\vec{e}_1,\vec{e}_2,\vec{e}_2)$, connected with the force lines of $\vec{B}_0$ is convenient to introduce. The first vector is perpendicular to the magnetic surfaces, $\vec{e}_1=\nabla r_0/|\nabla r_0|$. The second vector coincides with the azimuthal unit vector in cylindrical coordinates, $\vec{e}_2 = \vec{e}_\vartheta$. The third vector is parallel to the magnetic force lines, $\vec{e}_3=\vec{B}_0/|\vec{B}_0|$. Application of the conditions of the smallness of the axial inhomogeneity and electron inertia ($|\varepsilon_3|\to\infty$) during solving the Maxwell's equations results in equality to zero of the wave longitudinal electric field in entire plasma volume: $E_3\equiv(B_{0z}E_z + B_{0r}E_r)/|B_0|\to 0$. The latter condition forms the connection between the wave radial and axial electric fields, which in turn makes it possible to write down the following simplified set of Maxwell's equations in cylindrical coordinates:

$$\frac{im}{r}\frac{B_{0r}}{B_{0z}}E_r - \frac{\partial E_\vartheta}{\partial z} = \frac{i\omega}{c}B_r, \quad (3.14)$$

$$\frac{\partial E_r}{\partial z} - \frac{\partial}{\partial r}\left(\frac{B_{0r}}{B_{0z}}E_r\right) = \frac{i\omega}{c}B_\vartheta, \quad (3.15)$$

$$\frac{1}{r}\frac{\partial}{\partial r}(rE_\vartheta) - \frac{im}{r}E_r = \frac{i\omega}{c}B_z, \quad (3.16)$$

$$B_{0z}\left(imB_z - r\frac{\partial B_\vartheta}{\partial z}\right) + B_{0r}\left(\frac{\partial}{\partial r}(rB_\vartheta) - imB_r\right) = \frac{\omega\, r}{ic}(\varepsilon_1 B_{0z}E_r + i\varepsilon_2|B_0|E_\vartheta), \quad (3.17)$$

$$\frac{\partial B_r}{\partial z} - \frac{\partial B_z}{\partial r} = \frac{\omega}{ic}\left(\varepsilon_1 E_\vartheta - i\varepsilon_2\frac{B_{0z}}{|B_0|}E_r\right). \quad (3.18)$$

The set of eqs. (3.14)-(3.18) is valid under the condition of neglecting the plasma particle collisions, electron inertia, and finite ion Larmor radius.

3.1. Additional plasma heating in the vicinity of satellite alfven resonances in the traps with the bumpy magnetic field

The possibility of RF power absorption in the vicinity the satellite ARs (SARs) is considered in the present subsection [78-81]. Rapid growth of the amplitudes of the electromagnetic wave satellite harmonics and their conversion into the small-scale waves take place in the vicinity of SARs. In the bumpy external static magnetic field (3.1), MHD waves propagate in the form of the wave packet. In particular, the radial component of the MHD wave electric field propagates in the following form:

$$E_r = [E_r^{(0)}(r) + E_r^{(+)}(r)\exp(ik_b z) + E_r^{(-)}(r)\exp(-ik_b z)]\exp[i(k_z z + m\vartheta - \omega t)]. \quad (3.1.1)$$

In (3.1.1), two the nearest satellite harmonics $\propto exp[i(k_z \pm k_b)z]$ are taken into account along with the main harmonic $\propto exp[i(k_z z)]$. The amplitudes of the satellite harmonics are assumed to be small values everywhere, except of the regions of the local resonances [69],

$$|E_r^{(\pm)}| \sim \varepsilon_m |E_r^{(0)}|. \quad (3.1.2)$$

In the representation (3.1.1), m is azimuthal wave index, k_z is axial wavenumber of MHD waves in the zeroth approach (in the case of forced oscillations, the magnitude of k_z is determined by antenna). Representation of the other components of MHD wave magnetic and electric fields are similar to (3.1.1).

It is shown in the present subsection, that two additional resonances, $r = r_A^{(\pm)}$, within which

$$\varepsilon_1^{(0)}(r) = (N_z \pm N_b)^2, \quad (3.1.3)$$

can exist in the traps with the bumpy magnetic field with weak inhomogeneity ($|\varepsilon_m| \ll 1$) along with the main AR, $r = r_A^{(0)}$, within which the condition (2.10) takes place. Here $N_z = ck_z/\omega$ is longitudinal refractive index, $N_b \equiv ck_b/\omega$. It is natural to call these resonances as satellite Alfven resonances (SARs). RF power absorption in the vicinity of SARs and the damping rate of MHD waves caused by this absorption are the small values of the second order in the parameter ε_m. Nevertheless, some situations exist in which the considered phenomenon can be significant for the plasma heating.

Amplitudes of satellite harmonics of the MHD wave electric and magnetic fields increase in the vicinity of SARs. And conversion of these oscillations into small-scale waves takes place there. This phenomenon is observed for both Alfven waves with the frequency $\omega < \omega_{ci}$ (if $(N_z \pm N_b)^2 > 1$)

and fast magnetosonic waves with the frequency $\omega > \omega_{ci}$ (if $(N_z \pm N_b)^2 < 1$) – in a rarefied plasma.

Since the values $\mu^{(\pm)} = \varepsilon_2/(\varepsilon_1 - (N_z \pm N_b)^2)$, $k_\pm^2 = (\omega/c)^2(\varepsilon_1 - (N_z \pm N_b)^2)\left(1 - \mu^{(\pm)^2}\right)$ are singular: $\mu_\pm$, $k_\pm^2 \propto [\varepsilon_1^{(0)} - (N_z \pm N_b)^2]^{-1}$ in the vicinity of SARs, then the amplitudes of satellite harmonics also have the singularities of the following forms there:

$$E_r^{(\pm)}, B_\vartheta^{(\pm)} \propto (\varepsilon_1 - (N_z \pm N_b)^2)^{-1}, E_z^{(\pm)} \propto (\varepsilon_1 - (N_z \pm N_b)^2)^{-2},$$
$$E_\vartheta^{(\pm)}, B_r^{(\pm)}, B_z^{(\pm)} \propto ln|\varepsilon_1 - (N_z \pm N_b)^2|. \quad (3.1.4)$$

In the vicinity of SARs (3.1.3), the amplitudes of satellite harmonics $E_r^{(\pm)}$ describe joint propagation of MHD waves and small-scale waves. The amplitudes are determined with account for the electron inertia, finite ion Larmor radius, and collisions between the plasma particles from the following equation (compare with eq. (2.4.7)):

$$\left(\varepsilon_T + \frac{N_z^2}{\varepsilon_3}\right)\frac{c^2}{\omega^2}\frac{\partial^2 E_r^{(\pm)}}{\partial r^2} + \left(\varepsilon_1 + i\varepsilon^{(c)} - (N_z \pm N_b)^2\right)E_r^{(\pm)} = -A^{(\pm)}. \quad (3.1.5)$$

In eq. (3.1.5), the following notations are introduced by analogy with eq. (2.2.5)

$$-A^{(\pm)} \equiv -i\varepsilon_2^{(0)} E_\vartheta^{(\pm)} - \frac{cm}{\omega r} B_z^{(\pm)} - 0.5\varepsilon_1^{(1)} E_r^{(0)} - 0.5i\varepsilon_2^{(1)} E_\vartheta^{(0)}. \quad (3.1.6)$$

Here, the term $\varepsilon_1^{(c)}$ provides account for the plasma particle collisions [52], it is given in the subsection 2.1 in eq. (2.1.2). The term ε_T in (3.1.5) accounts for the finite ion Larmor radius [49], it is defined in the subsection 2.4 in eq. (2.4.6). The electron inertia is taken into account in (3.1.5) in the component ε_3 of the permittivity tensor, its form is given in the subsection 2.4 in eqs. (2.4.1)–(2.4.4).

To solve eq. (3.1.5) one can get use of the fact, that the combination $A^{(\pm)}$ varies weakly and can be considered as a constant in the vicinity of SAR points (3.1.3). It should be underlined that the combination $\left[\frac{cm}{r\omega} B_z^{(\pm)} + i\varepsilon_2^{(0)} E_\vartheta^{(\pm)}\right]$, which is the part of (3.1.6), slowly varies in the vicinity of $r_A^{(\pm)}$, despite the dependences $B_z^{(\pm)}(r)$ and $E_\vartheta^{(\pm)}(r)$ have singularities within the point $r_A^{(\pm)}$, (compare with [24, 55, 63]).

Variation of the plasma parameters in the vicinity of SAR point is assumed to be weak. This makes it possible to apply the magnitudes of the right hand side of eq. (3.1.5) as well as such physical observables as ε_T, ε_3, and $\varepsilon_1^{(c)}$ in the point $r = r_A^{(\pm)}$ during solving the equation. The solution of eq. (3.1.5) reads as (compare with (2.3.7)):

$$E_r^{(\pm)} = -A^{(\pm)}\pi k_1 \left(\frac{d\varepsilon_1}{dx}\right)^{-1} u_0(\xi), \tag{3.1.7}$$

here

$$u_0(\xi)=[Gi(\zeta) - iAi(\zeta)],$$

$$\xi = k_1\left(r - r_A^{(\pm)}\right) - i\eta, \quad \eta = -k_1\varepsilon_1^{(c)}\left(\frac{\partial\varepsilon_1^{(0)}}{\partial r}\right)^{-1}\Big|r_A^{(\pm)},$$

$$k_1=\left(-\frac{\omega^2\partial\varepsilon_1^{(0)}}{c^2\partial r}\,\frac{\varepsilon_3}{\varepsilon_T\varepsilon_3+\varepsilon_1^{(0)}}\right)^{1/3}\Big|r_A^{(\pm)} = |k_1|\,exp(\,i\psi). \tag{3.1.8}$$

Basing on the asymptote (2.3.8) of the solution (3.1.7) of the eq. (3.1.5) for $Re\xi\to-\infty$, one can assume that small-scale kinetic wave (the second term in eq. (2.3.8)) strongly damps in the vicinity of the resonant point due to collisions or Landau mechanism when going away from the SAR point. If the damping is weak, then the asymptote (2.3.8) should match up the solution of eq. (3.1.5), which is derived in the WKB approach and corresponds to the waves, which carry the energy away from the conversion point of SAR either into the plasma core or to the periphery. In this case, the reflected wave is assumed to be absent. In other words, these small-scale waves are assumed to absorb during one passage along the plasma column radius. This makes it possible to avoid studying numerous phenomena, resulting from weak damping, as well as formation of the global resonances with high magnitude of the radial wavenumber in this case.

It is appropriate to remind, that eq. (3.1.5) describes joint propagation of Alfven waves (or FMSWs) and small-scale waves in the vicinity of SAR points $r=r_A^{(\pm)}$.

Now one can analyze the SAR fine structure, applying the research, presented in Section 2. Namely, if the collisions prevail, then SAR width is determined by the expression (2.1.13),

$$\Delta r_c \sim a^*\varepsilon_1^{(c)}/(N_z \pm N_b)^2, \tag{3.1.9}$$

and characteristic magnitude of satellite harmonic, which grows within SAR, can be estimated as follows (compare with (2.1.14)):

$$E_r^{(\pm)} = 0.5A^{(\pm)}/\varepsilon_1^{(c)}. \tag{3.1.10}$$

If the fine structure of SAR is determined by the electron finite inertia, then SAR width is determined by eq. (2.3.6),

$$\Delta r_m \sim a^*\left(\frac{m_e}{m_i a^{*2}(k_z \pm k_b)^2}\right)^{\frac{1}{3}}. \tag{3.1.11}$$

And characteristic magnitude of the satellite harmonic amplitude in the vicinity of SAR can be estimated as follows (compare with (2.3.10)):

$$E_r^{(\pm)} \sim A^{(\pm)} \frac{\pi}{(N_z \pm N_b)^2} \left(\frac{m_i}{m_e} k_z^2 a^{*2}\right)^{\frac{1}{3}}. \quad (3.1.12)$$

In the case if SAR fine structure is determined by finite ion Larmor radius, characteristic SAR width is determined by eq. (2.4.10),

$$\Delta r_T \sim a^* (\rho_{Li}/a^*)^{\frac{2}{3}}. \quad (3.1.13)$$

And characteristic magnitude of amplitude of satellite harmonic of the wave electric field in the vicinity of SAR can be estimated as follows (compare with (2.4.11)):

$$E_r^{(\pm)} \sim A^{(\pm)} \frac{\pi}{(N_z \pm N_b)^2} \left(\frac{a^*}{\rho_{Li}}\right)^{\frac{2}{3}}. \quad (3.1.14)$$

In the following, the magnitude of electromagnetic power, absorbed in the vicinity of SAR point at the unit length of the plasma column, is calculated. It consists of the work done by the wave field satellite harmonics over the radial RF currents $j_r \propto exp[i(k_z \pm k_b)z + im\vartheta - i\omega t)]$,

$$P_r^{(\pm)} = \pi r^{(\pm)} Re \int j_r^* E_r^{(\pm)} dr = \frac{\pi \omega r_A^{(\pm)}}{4} \frac{\partial \varepsilon_1^{(0)}}{\partial r}^{-1}_{\Big| r_A^{(\pm)}} \left|A^{(\pm)}\right|^2, \quad (3.1.15)$$

and the work over axial RF currents,

$$P_z^{(\pm)} = \pi r_A^{(\pm)} Re \int j_Z^* E_z^{(\pm)} dr =$$
$$= \left(\left| \frac{d\varepsilon_1^{(0)}}{dr} \right|^{-1} \frac{r \varepsilon_1^{(0)} Im(\varepsilon_3^*)}{\left| \varepsilon_T \varepsilon_3^2 + \varepsilon_1^{(0)} \varepsilon_3 \right|} \right)_{r = r_A^{(\pm)}} \frac{\omega}{4} |k_1| \left|A^{(\pm)}\right|^2 \int_{-\infty}^{+\infty} \left| \frac{\partial u_0}{\partial \xi} \right|^2 d\, r. \quad (3.1.16)$$

Well-known expressions [63] for the power $P^{(0)}$, which is absorbed in the vicinity of the main AR (2.10), can be obtained from (3.1.15) and (3.1.16), if to replace $r_A^{(\pm)} \to r_A$, $(N_z \pm N_b) \to N_z$, $E_\vartheta^{(\pm)} \to E_\vartheta^{(0)}$, $B^{(\pm)} \to B^{(0)}$, and $A^{(\pm)} \to A$. During calculating the RF power absorption within SAR (3.1.3) one has to keep in mind that the satellite harmonic $\propto exp[i(-k_z \mp k_b)z]$, excited my MHD wave with axial wavenumber $-k_z$, is resonantly absorbed along with the satellite harmonic $\propto exp[i(k_z \pm k_b)z]$, excited by MHD wave with the axial wavenumber k_z.

It is in place to remind, that the contribution $P_z^{(\pm)}$ to the plasma heating is not small, if $Im\varepsilon_3 > Re\varepsilon_3$:

$$\frac{P_z^{(\pm)}}{P_r^{(\pm)}} \sim \left| \frac{\varepsilon_1}{\varepsilon_1 + \varepsilon_T \varepsilon_3} \right| \frac{Im\, \varepsilon_3}{|\varepsilon_3|}. \quad (3.1.17)$$

RF power absorption in the vicinity of SAR (3.1.3) causes growth of the satellite harmonic amplitude $E_r^{(\pm)}$ within the SAR point, while the amplitude in other regions decreases $\propto exp(-\gamma t)$ [82]. Expression for the damping rate γ of MHD waves, caused by the plasma heating in the vicinity of SAR, is presented in [78].

The results, obtained in the present subsection can be summarized as follows. Additional (as compared with the ordinary AR (2.10)) absorption of electromagnetic energy of MHD waves is shown in the present subsection to take place in SAR regions (3.1.3) in the plasma with radially inhomogeneous plasma particle density, which is placed into the bumpy magnetic field. The magnitude of the RF power absorption in the vicinity of these additional resonances is determined by the expressions (3.1.15) and (3.1.16). The magnitude of the RF power (3.1.15) and (3.1.16), absorbed by the plasma, is proportional to the small parameter of inhomogeneity squared and usually is small as compared with the power, absorbed within the main AR. However, in some cases, given below, power absorption in the regions of SARs appears to be more significant than within the main AR. These cases are as follows.

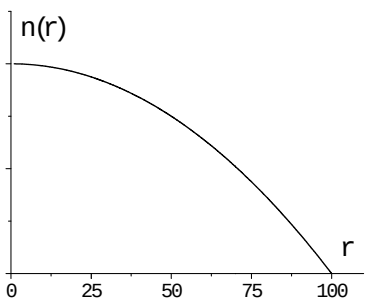

Fig. 3.1.1. Model quadratic radial profile of the plasma particle density

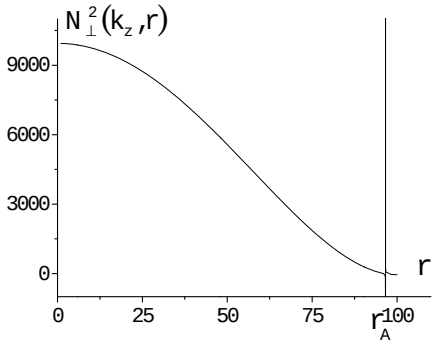

Fig. 3.1.2. Radial dependence of the perpendicular refractive index squared of the main harmonic

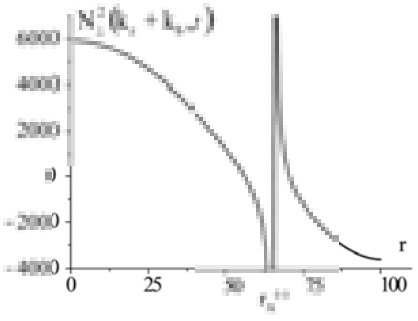

Fig. 3.1.3. Radial dependence of the perpendicular refractive index squared of the satellite harmonic

The first case. If the magnitude of k_z is sufficiently small, and the plasma particle density is sufficiently large, then the main resonance $r=r_A$ is situated at the plasma periphery. The shift of the resonant point $r=r_A$ to the plasma periphery is accompanied by the increase of the plasma particle density gradient, and the RF power, absorbed in the vicinity of the main resonance, decreases, $P^{(0)} \propto (\varepsilon_2^{(0)})^2 (\partial \varepsilon_1^{(0)}/\partial r)^{-1}$. In the case of sufficiently large magnitudes of k_b, SARs $r=r_A^{(\pm)}$ can be situated in the plasma core (see Figs. 3.1.1–3.1.3). Radial coordinate in cm is used as the abscissa axis in these figures. The model density radial profile is shown in Fig. 3.1.1, for which the curves in the following two figures are calculated. This model profile is quadratic, $n(r)=n(0)(1-r^2/a^2)$.

The radial dependence of the perpendicular refractive index squared $N_\perp^2(k_z,r)$ of the main harmonic is presented in Fig. 3.1.2. The parameters of the plasma-wave system are chosen in such a way that the local AR (the point, where $N_\perp^2(k_z,r)$ is singular) is situated at the plasma periphery.

The radial dependence of the perpendicular refractive index squared $N_\perp^2(k_z+k_b,r)$ of the satellite harmonic is shown in Fig. 3.1.3. The parameters of the plasma-wave system are chosen such that $k_b=2k_z$. As the result, the satellite AR (the point, where $N_\perp^2(k_z+k_b,r)$ is singular) appears to be situated much more far from the plasma periphery, than the main AR. The ratio $P_r^{(\pm)}/P_r^{(0)}$ is equal by the order of magnitude (see eq. (3.1.15))

$$P_r^{(\pm)}/P_r^{(0)} \sim [n(r_A^{(\pm)})/n(r_A)]\ [(k_z \pm k_b)/k_z]^2 \,|\, E_\varphi^{(\pm)}/\, E_\varphi^{(0)} \,|^2. \qquad (3.1.18)$$

One can see from eq. (3.1.18), that $P_r^{(\pm)}$ can be larger than $P_r^{(0)}$, if k_b is sufficiently large as compared with k_z, and the plasma particle density $n(r^{(0)})$ is small as compared with $n(r^{(\pm)})$. Doing this one has to keep in mind that the electromagnetic field can have a narrow barrier of nontransparency at the plasma periphery [13] due to small k_z and hence better penetrate into the plasma core, where the field corresponds to the fast magnetosonic wave in the region of sufficiently high plasma particle density, $\left(\omega_{pi}^2/[\omega_{ci}(\omega+\omega_{ci})] > N_z^2\right)$. This fast magnetosonic wave linearly interact in the bumpy external static magnetic field [1] with Alfven wave with axial wavenumber $(k_z \pm k_b)$ and hence is resonantly absorbed in the vicinity of the SAR points $r_A^{(\pm)}$.

Electromagnetic wave $B_z^{(0)}$ can be eigen one (with a weak damping) for the considered plasma waveguide (plasma resonator, in the case of plasma torus – plasma cylinder with identified ends). In this case the satellite harmonics $B_z^{(\pm)}$ also increase resonantly, and the power, which is absorbed in the vicinity of the AR point, $r=r_A$, increases, as well as those, absorbed in the SAR points, $r=r_A^{(\pm)}$.

The satellite harmonic power absorption within the points $r=r_A^{(\pm)}$ can also be enhanced in the case, if the wave with the longitudinal wavenumber $(k_z \pm k_b)$ is eigen one for the waveguide. In this case, two first terms in (3.1.6) $\left(iE_\vartheta^{(\pm)} + \frac{c(m\mp l)}{\omega\, r\varepsilon_2^{(0)}} B^{(\pm)}\right)\Big|_{r=r_A^{(\pm)}}$ increase resonantly.

The second case. The main AR is absent in principle in the plasma of small density, $N_z^2>\varepsilon_1^{(0)}$. In this case, the SAR $r=r_A^{(\pm)}$, can be present and provide absorption of the pumping wave. The power absorption in this resonance can be also be enhanced in the case, if the satellite harmonic is the eigen mode of the waveguide.

The third case. FMSWs with axial wavenumber $|k_z|>\omega/c$ and the frequency $\omega>\omega_{ci}$ do not have the main resonance (2.10) in contrast to AWs. (Conversion and resonant absorption of the FMSWs with $|k_z|>\omega/c$ and the frequency $\omega>\omega_{ci}$ in peripheral plasma was studied in [55, 83].) If herewith $|k_z-k_b|<\omega/c$, then for such FMSWs, SAR (2.1.3) comes into being in the plasma column. Since $\omega_{pi}^2>\omega_{ci}^2$ in the core of the fusion plasma, then this SAR point $r=r_A^{(-)}$ is situated at plasma column periphery. On the one hand, the plasma particle density $n(r_A^{(-)})$ and the axial wavenumber squared $(k_z-k_b)^2$ of the harmonic, which are the cofactors in the expression (3.1.18), are not large in this case. On the other hand, the deviation of the magnetic surface shape from the straight cylinder is the most pronounced just at the plasma periphery (the parameter of inhomogeneity ε_m increases with increasing of the radius). Moreover, the amplitude of the pumping wave is usually the largest just near the plasma interface. That is why the SAR, studied in the present subsection, can make a significant contribution to the undesirable plasma periphery heating in a fusion device with the bumpy magnetic field.

3.2. Influence of axial periodic inhomogeneity of the external static magnetic field on the fine structure and alfven heating of cylindric plasma nearby the main AR

In the present subsection, the fine structure of the main local AR and RF power absorption in cylindrical plasma placed into external static magnetic field with a moderate inhomogeneity is studied [84]. Confining magnetic field $\vec{B}_0 = B_{0r}\vec{e}_r + B_{0\vartheta}\vec{e}_\vartheta + B_{0z}\vec{e}_z$ (in cylindrical coordinates) is modeled in such a way that its radial and axial components are determined by eqs. (3.1), and azimuthal component $B_{0\vartheta}(r) \ll B_0$ describes the rotational transform, caused by the axial electric current in the tokamak plasma or the currents in the modular coils of stellarators.

In the bumpy magnetic field, electromagnetic perturbations propagate in the form of wave packet, in which, generally speaking, infinite number of satellite harmonics is present along with the main harmonic. In the present subsection, the influence of the moderate inhomogeneity of the confining magnetic field on the conversion and absorption of AW in the vicinity of AR is studied for the main harmonic. It is shown that the contribution of the magnetic field inhomogeneity into the determining the fine structure of AR can be of the same order as those caused by the plasma particle collisions, finite ion Larmor radius, and the electron inertia.

The problem is formulated as follows. During studying the Alfven and fast magnetosonic branches of MHD oscillations in the plasma with a small gas kinetic pressure, one can neglect the electron inertia everywhere, except of the narrow region of the local AR. Application of the conditions of smallness of the magnetic field inhomogeneity and smallness of the electron inertia ($/\varepsilon_3/\to\infty$) during solving the Maxwell's equations results in equality to zero of the longitudinal wave electric field, $E_3=(B_{0r}E_r+B_{0\vartheta}E_\vartheta+ B_{0z}E_z)/\left|\vec{B}_0\right| \to 0$, in entire plasma volume. Derived in such a way relation between the components of the wave electric field makes it possible to write down the simplified set of Maxwell's equations in cylindrical coordinates (3.14)–(3.18) under the condition of neglecting the collisions between the plasma particles, electron inertia and ion thermal motion.

To solve the set of equations (3.14)–(3.18), one needs the expressions (3.8) –(3.13) for the components $\varepsilon_{1,2}$ of the plasma permittivity tensor with account for the small terms of the first order of smallness in respect of the parameter ε_m.

Basing on the spatial dependence (3.9) of the components of the plasma permittivity tensor, the solution of the set of equations (3.14)–(3.18) is found for the radial component of the MHD wave electric field in the following form:

$$E^{\sim}{}_r = \left[E_z^{(0)}(r) + E_r^{(+1)}(r)e^{ik_b z} + E_r^{(-1)}(r)e^{-ik_b z}\right] exp\, i\,(k_z z + m\vartheta - \omega t). \tag{3.2.1}$$

The packet (3.2.1) along with the main harmonic $\propto exp(ik_z z)$ contains also two the nearest satellite harmonics $\propto exp[i(k_z \pm k_b)z)]$. Representation of the other components of MHD wave magnetic and electric fields in the form of series is analogous to eq. (3.2.1).

In the following, the main equation of this problem is derived. Application of the expression (3.9) for the plasma permittivity tensor and the condition of vanishing of the wave longitudinal electric field E_3 make it possible to derive the following set of coupled equations for the amplitudes of the main $E_r^{(0)}$ and satellite $E_r^{(\pm 1)}$ harmonics of the radial component of the wave electric field from the Maxwell's equations:

$$\begin{aligned}
&\left[\left(\varepsilon_1^{(0)} - N_z^2 - 2N_z N_\vartheta B_{0\vartheta}/B_0\right)E_r^{(0)} - A\right]+\\
&+\frac{c^2\delta^2}{2\omega^2}\frac{d^2E_r^{(0)}}{dr^2} + 0.5\varepsilon_1^{(1)}E_r^{(+1)} + \frac{c^2 k_b \delta}{2\omega^2}\frac{dE_r^{(+1)}}{dr}+\\
&+\frac{c^2}{\omega^2}\delta(k_z - k_b)\frac{dE_r^{(+1)}}{dr} + \frac{c^2 k_b \delta}{2\omega^2}\frac{dE_r^{(-1)}}{dr} +\\
&+0.5\varepsilon_1^{(1)}E_r^{(-1)} - \frac{c^2}{\omega^2}\delta(k_z + k_b)\frac{dE_r^{(-1)}}{dr} = 0,
\end{aligned} \tag{3.2.2}$$

$$-\frac{c^2}{2\omega^2}\delta(\pm 2k_z + k_b)\frac{dE_r^{(0)}}{dr} + (N_z \pm N_b)^2 E_r^{(\pm 1)} - \frac{c^2\delta^2}{2\omega^2}\frac{d^2E_r^{(\pm 1)}}{dr^2} -$$
$$- N_z^2 E_r^{(\pm 1)} + \frac{c^2\delta^2}{4\omega^2}\frac{dE_r^{(\mp 1)}}{dr} = 0. \qquad (3.2.3)$$

Here $N_\vartheta = cm/(\omega r)$ is azimuthal refractive index, the small parameter $\delta = \varepsilon_m'/k_b$ originates from account for the small radial component of the confining magnetic field (3.1).

In the following, the dependence of the small parameter δ on the spatial period of inhomogeneity L is discussed. At first sight, the dependence can look as direct proportionality, since δ contains the factor $1/k_m \sim L$. But besides, δ is proportional to the derivative $d\varepsilon_m/dr$ in respect of radius from the amplitude of modulation of the axial component of the external static magnetic field, and ε_m in turn is proportional to the Bessel function of the zeroth order. Thus, the dependence of the small parameter on the spatial period of the inhomogeneity is proportional to the modified Bessel function of the first order $I_1(k_m r)$.

The approach of the narrow layer [24] is applied to derive the set of equations (3.2.2), (3.2.3). This approach means weak variation of the wave fields in the vicinity of AR in both axial and azimuthal directions and can be expressed as the following inequalities

$$\left|dB_z^{(0)}/dr\right| >> \left|k_{z\,max}^{(0)} B_z^{(0)}\right|, \quad k\,max(m/r, k_z, k_m, \omega/c)_{max}. \qquad (3.2.4)$$

This approach foresees also weak variation of the plasma particle density in radial direction.

It is in place to remind that the azimuthal component of the wave magnetic field varies in the radial direction in the vicinity of AR as rapidly, as E_r does (see eq. (2.15)). Radial dependence of the other components of the wave electric and magnetic fields in the vicinity of AR is weaker, namely:

$$B_r, B_z, E_\vartheta \propto ln\left(\varepsilon_1^{(0)} - N_z - \frac{2N_z N_\vartheta B_{0\vartheta}}{B_0}\right),$$
$$E_r, B_\vartheta \propto \left(\varepsilon_1^{(0)} - N_z^2 - 2N_z N_\vartheta B_{0\vartheta}/B_0\right)^{-1}. \qquad (3.2.5)$$

It is taken into account here, that in presence of azimuthal static magnetic field $B_{0\vartheta}$ the position of AR is determined as follows:

$$\varepsilon_1^{(0)} = N_z^2 + 2N_z N_\vartheta B_{0\vartheta}/B_0, \qquad (3.2.6)$$

It is appropriate to remind that the combination $A = \left(-i\varepsilon_2^{(0)} E_\vartheta^{(0)} - N_\vartheta B_z^{(0)}\right)_{|r=r_A}$ in the square brackets in eq. (3.2.2) weakly varies in the vicinity of the local resonance [24, 55, 63], despite of the fact that the fields $B_z^{(0)}$ and $E_\vartheta^{(0)}$ have a logarithmic singularity there in the cold approach.

Account for the azimuthal component of the external static magnetic field changes the amplitude of the main harmonic by the small term of the order of $(B_{0\vartheta}/B_0)$ [85]. Influence of the axial inhomogeneity of the confining magnetic field on the amplitude of the main harmonic out of the main AR neighbourhood manifests in the second order of smallness in respect of the small parameter of inhomogeneity ε_m. The amplitudes of the satellite harmonics are smaller by the order than that of the main harmonic [69],

$$E_r^{(\pm 1)} \sim \varepsilon_m E_r^{(0)}. \tag{3.2.7}$$

Since the amplitude of the main harmonic, as well as the amplitudes of the satellite harmonics resonantly increase in the vicinity of AR, then the relation (3.2.7) cannot be applied for analysis of the set of equations (3.2.2), (3.2.3) in the vicinity of the local AR (3.2.6). The following consideration shows, that the relation (3.2.7) does stop to be true within the AR.

The set (3.2.2), (3.2.3) can be reduced to the following differential equation of the sixth order for the amplitude of the main harmonic $E_r^{(0)}$:

$$\begin{aligned}
&\frac{3}{16}\frac{c^4}{\omega^4}\delta^4\frac{d^4}{dr^4}\left[\left(\varepsilon_1^{(0)} - N_z^2 - 2N_zN_\vartheta B_{0\vartheta}/B_0\right)E_r^{(0)} + A\right] - \\
&-\frac{c^2}{\omega^2}\delta^2 N_b^2\frac{d^2}{dr^2}\left[\left(\varepsilon_1^{(0)} - N_z^2 - 2N_zN_\vartheta B_{0\vartheta}/B_0\right)E_r^{(0)} + A\right] + \\
&+N_b^2\left(N_b^2 - 4N_z^2\right)\left[\left(\varepsilon_1^{(0)} - N_z^2 - 2N_zN_\vartheta B_{0\vartheta}/B_0\right)E_r^{(0)} + A\right] + \\
&+\frac{3}{32}\frac{c^6}{\omega^6}\delta^6\frac{d^6}{dr^6}E_r^{(0)}{}_{|(6,6)} - \frac{1}{8}\frac{c^4}{\omega^4}\delta^4\left(N_b^2 + 4N_z^2\right)\frac{d^4}{dr^4}E_r^{(0)}{}_{|(4,4)} - \\
&-\frac{3}{8}\frac{c^3}{\omega^3}\delta^3 N_b\varepsilon_1^{(1)}\frac{d^3}{dr^3}E_r^{(0)}{}_{|(4,3)} + \\
&+\frac{1}{2}\frac{c}{\omega}\delta N_b\varepsilon_1^{(1)}\left(N_b^2 - 4N_z^2\right)\frac{d}{dr}E_r^{(0)}{}_{|(2,1)} = 0.
\end{aligned} \tag{3.2.8}$$

Two subscripts are assigned to each of the last four terms in this equation. Their sense is explained below for the last term as an example. The subscripts (2,1) show that **quadratic** in respect of the small parameter coefficient stays nearby the **first** derivative in this term. Analysis of the relations between the order of smallness of the coefficient and the order of the respective derivative makes it possible to simplify eq. (3.2.8) to the following form:

$$\begin{aligned}
&-\frac{1}{8}\frac{c^4}{\omega^4}\delta^4\left(N_b^2 - 4N_z^2\right)\frac{d^4}{dr^4}E_r^{(0)} + \\
&+N_b^2\left(N_b^2 - 4N_z^2\right)\left[\left(\varepsilon_1^{(0)} - N_z^2 - 2N_zN_\vartheta B_{0\vartheta}/B_0\right)E_r^{(0)} + A\right] = 0.
\end{aligned} \tag{3.2.9}$$

After solving eq. (3.2.9) one can analyse the precision, with which the equation corresponds to eq. (3.2.8).

Solution of eq. (3.2.9) is found by the Laplace method,

$$E_r^{(0)} = (a^* k_1 / N_z^2) A u_0[k_1(r - r_A)], \quad (3.2.10)$$

here

$$u_0(\xi) = \int_0^\infty exp[i(t\xi + t^5/5)]\ dt,$$

$$k_1 = \left(\frac{c^4\delta^4 a^*}{8\omega^4 N_b^2 N_z^2}\frac{N_b^2+4N_z^2}{N_b^2-4N_z^2}\right)^{-1/5} \sim [k_z^2 k_b^2/(\delta^4 a^*)]^{1/5} \propto \delta^{-4/5}, \quad (3.2.11)$$

$a^* = \left|d\ ln\left|\varepsilon_1^{(0)}\right|/dr\right|^{-1}_{|r_A}$ is characteristic radial scale, at which the plasma particle density varies. The solution satisfies the following boundary conditions: it is finite both in the point of AR and with going away from it; it describes the conversion of the electromagnetic wave into small-scale wave, which carries the energy from the resonant point; it damps in the case of account for weak dissipation in expression for $\varepsilon_1^{(0)}$. The plot of the function $u_0(\xi)$ is shown in Fig. 3.2.1 (the real part is shown by the solid curve, and imaginary – by the dashed curve).

In the case if axial wave length is twice as long as the spatial period of inhomogeneity, $2k_z=k_m$, the coefficient nearby the second term in eq. (3.2.9) becomes equal to zero, and hence our solution loses sense. In this case two main harmonics, coupled into one wave packet by the inhomogeneity of the external static magnetic field, have their AR in the same point. The influence of the inhomogeneity of the external static magnetic field on the AR finite structure in this resonant case was studied in [86] and is described in the next subsection.

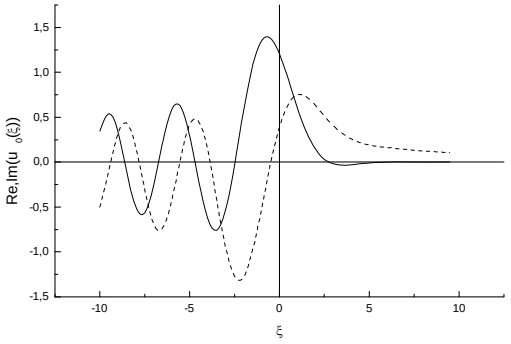

Fig. 3.2.1. Dependence of the real (solid curve) and imaginary (dashed curve) parts of the function $u_0(\xi)$

The characteristic width of AR

$$\Delta r = |k_1|^{-1} \sim [k_z^2 k_b^2/(\delta^4 a^*)]^{-1/5} \propto \delta^{4/5} \quad (3.2.12)$$

is equal by the order of magnitude to the width of AR in the mentioned above resonant case and by $\delta^{-2/15}$ times smaller than the width of SAR, studied in [87] and described in the subsection 2.4 for the case, if the

structure of SAR is determined by the inhomogeneity of external static magnetic field. Respectively, characteristic magnitude of the amplitude $E_r^{(0)}$ of the main harmonic of the radial component of the wave electric field within the local AR can be estimated from eqs. (3.2.10) and (3.2.11) by the order of magnitude,

$$E_r^{(0)} \sim ak_1 A/N_z^2 \sim \left(\frac{\omega^4 a^4 N_b^2}{\delta^4 N_z^8 c^4}\right)^{\frac{1}{5}} A. \qquad (3.2.13)$$

The wave electric field in the resonant point $E_r^{(0)}(r_A)$ is of the order of ambipolar electric field $\sim T/ea^*$, if the pumping wave is of the following order

$$E_\vartheta \sim \frac{m_i \rho_{Li}^2 \omega^3{}_{ci}}{e\omega a^2}\left(\frac{a\delta^4}{k_b^2 k_z^2}\right)^{\frac{1}{5}}. \qquad (3.2.14)$$

Under this condition one can neglect nonlinear phenomena in the vicinity of AR.

At the beginning of analyzing the set of equations (3.2.2), (3.2.3), the relation (3.2.7) was assumed to deny in the vicinity of AR. The following simplified expressions for the amplitudes of the satellite harmonics can be derived from eq. (3.2.3) with accuracy of $\delta^{2/5}$,

$$E_r^{(\pm 1)} = -(\varepsilon'/2k_b^2)\, dE_r^{(0)}/dr,\ E_r^{(\pm 2)} = -(\varepsilon'/4k_b^2)\, dE_r^{(\pm 1)}/dr \ldots \qquad (3.2.15)$$

That is the amplitude of n-th satellite harmonic is by the order of $\delta^{-n/5}$ times smaller than that of the main harmonic,

$$E_r^{(\pm 1)} \sim \frac{k_1 \delta}{k_b} E_r^{(0)} \sim \left(\frac{\omega^3 a^3}{\delta^3 c^3 N_b N_z^6}\right)^{\frac{1}{5}} A. \qquad (3.2.16)$$

Amplitudes of the satellite harmonics remain smaller than that of the main harmonic, despite of the fact that they increase in the vicinity of AR rapidly than the amplitude of the main harmonic. However, their smallness as compared with the amplitude of the main harmonic is not so pronounced in the vicinity of AR as out of the AR region.

It is the place to estimate the precision of transition from eq. (3.2.8) to simplified eq. (3.2.9). The largest term among the neglected ones, $-\frac{c^2}{\omega^2}\delta^2 N_b^2 \frac{d^2}{dr^2}\left[\left(\varepsilon_1^{(0)} - N_z^2 - 2N_z N_\vartheta B_{0\vartheta}/B_0\right)E_r^{(0)} + A\right]$, is small value of the order of $\sim\delta^{2/5}$ as compared with the third kept term in (3.2.9). The first term in (3.2.8) is the small value of the order of $\delta^{4/5}$. The terms, to which the subscripts (i,j) are assigned, can be estimated as compared with the kept term with the subscripts (4,4), as small values of the order of $\delta^{(i-4\cdot 0.8(j-4))}$.

Among the amplitudes of the main harmonics, just axial component of the wave electric field increases the most rapidly in the vicinity of AR as compared with the magnitude, typical for it outside the AR:

$$E_z \approx \frac{ic}{\omega\varepsilon_3}\frac{\partial B_\vartheta}{\partial r} = \frac{ic}{\omega\varepsilon_3} N_z \frac{\partial E_r}{\partial r} \sim \frac{k_z a}{N_z^2}\rho_{Li}^2 \left(\frac{k_z^2 k_b^2}{\delta^4 a}\right)^{\frac{2}{5}} A. \qquad (3.2.17)$$

However, this component remains much smaller than the wave radial component $E_r^{(0)}$, and influence of E_z on the plasma particle transition from trapped states to passing ones can be neglected in linear (in respect of the wave amplitude) approach.

In the following, the conditions are found under which finite structure of the local AR is determined by the inhomogeneity of the external static magnetic field rather than the electron inertia, finite ion Larmor radius $\rho_{Li}=v_{Ti}/\omega_{ci}$ or the plasma particle collisions. These weak phenomena can be taken into account in eq. (3.2.9) analogously to that how it was done in the case of uniform axial external static magnetic field [24, 55, 63] with the following replacement:

$$\varepsilon_1^{(0)} - N_z^2 \to \varepsilon_1^{(0)} - N_z^2 + i\varepsilon_1^{(c)} + \left(\varepsilon_T + \frac{\varepsilon_1^{(0)}}{\varepsilon_3}\right)\frac{c^2}{\omega^2}\frac{\partial^2}{\partial r^2}. \qquad (3.2.18)$$

Varying the plasma parameters in the vicinity of AR is assumed to be weak, that is why one can apply the magnitudes of the physical observables ε_T, ε_3, $\varepsilon_1^{(c)}$, $\varepsilon_{1,2}^{(0,1)}$, and $\varepsilon_1^{(2)}$ in the resonant point $r=r_A$. Here the term $(i\varepsilon_1^{(c)})$ is presented in the subsection 2.1 by eq. (2.1.2), it accounts for the collisions between the plasma particles [52]. The coefficient ε_T in eq. (3.2.18) is given in the subsection 2.4 (see eq. (2.4.6)), it provides account for the finite ion Larmor radius [49]. The electron inertia is also taken into account in (3.2.18) via the component ε_3 of the plasma permittivity tensor. One can apply the expressions (2.4.1)–(2.4.4) for ε_3, which are presented in the subsection 2.4.

The conditions, under which the influence of weak axial periodic inhomogeneity of $\vec{B}_0$ on the fine structure of the main AR is stronger than that of the other weak phenomena, can be derived from analysis of eq. (3.2.18). In particular, the influence of $\vec{B}_0$ inhomogeneity is stronger than that of the finite ion Larmor radius, if

$$\delta^{12/5} >> (\rho_{Li}/a)^2 (k_z k_b a^2)^{6/5}. \qquad (3.2.19)$$

This condition can be satisfied in the peripheral plasma, where the inhomogeneity of the external static magnetic field is more significant, and the plasma is colder, than in the plasma core. The condition (3.2.19) can be realized under lower temperatures than analogous condition for the case of satellite AR [87]. The inequality (3.2.19) can be treated as follows. The radial deviation $r-r_A$ of the magnetic surface (3.4) from the cylinder with average radius is larger than the characteristic width $(\rho_{Li}^2 a)^{1/3}$ of AR, which is known for the case of uniform external static axial magnetic field [1]. Under the condition (3.2.19) the width of the resonant region Δr is larger

than in the case of the uniform external static axial magnetic field, $\Delta r \sim k_1^{-1} >> (\rho_{Li}^2 a)^{1/3}$.

In the following, the magnitude of the small parameter of inhomogeneity is estimated, for which the influence of the inhomogeneity cannot be neglected in studying the conversion of AWs in the vicinity of the local AR in traps with Helias parameters [68]. Influence of the inhomogeneity is of the same order as that of finite ion Larmor radius (see (3.2.19)), if axial wavenumber is sufficiently small, $k_z^{6/5} << 10^{-2}$ (here k_z is in centimeters), that is for quite real for modern fusion devices magnitudes of k_z.

Now, the electromagnetic power, which is absorbed at the unit length of the plasma column in the vicinity of AR, is to be calculated. The power consists of the work of the wave electric field over the radial RF currents, $P_r = 0.5\, Re\{\int j_r^* E_r 2\pi r dr\}$, and the work over axial RF currents, $P_z = 0.5\, Re\{\int j_z^* E_z 2\pi r dr\}$; here

$$P_r = \frac{r\omega}{4}\left|\frac{d\varepsilon_1}{dr}\right|^{-1} |A|^2{}_{|r=r_A} \int_{-\infty}^{+\infty} Im(u_0(x))\, dx, \tag{3.2.20}$$

$$P_z = \frac{r\omega k_1^3 a^2}{4|\varepsilon_3|^2 k_b{}^2} Im(\varepsilon_3)_{|r=r_A} |A|^2 \int_{-\infty}^{+\infty} |u_0'(x)|^2 dx. \tag{3.2.21}$$

If to replace the function u_0 in eq. (3.2.20) by Airy function, then the expression coincides with that for the power, which is absorbed in the vicinity of AR in the case, if its structure is determined by finite ion Larmor radius or finite electron inertia (see, e.g., [24, 55]). The integral from the imaginary part of u_0 in the right-hand part of eq. (3.2.20) appears to be equal precisely to π as it is in the case of integrating the imaginary part of Airy function. This means that RF power, which is absorbed in the vicinity of AR due to the work over the radial RF currents, does not depend on the type of small-scale wave (kinetic or caused by the inhomogeneity), into which large-scale electromagnetic wave transforms in the vicinity of AR.

As it was noted in [78], the contribution of RF power P_z cannot be neglected as compared with P_r, if $Im\,(\varepsilon_3) \geq Re(\varepsilon_3)$. The expression (3.2.21) coincides with analogous expression for RF power, which is absorbed in the vicinity of AR due to the work of RF fields over axial RF currents in the case, if the fine structure of AR is determined by finite ion Larmor radius or finite electron inertia, with replacement of the function u_0 by Airy function with the argument $[k_1(r-r_A)]$, multiplied by the small factor $(k_1/k_T)^3$. The following notations are applied here

$$k_T^3 = -\frac{\omega^2}{c^2}\frac{\partial \varepsilon_1}{\partial r}\frac{\varepsilon_3}{\varepsilon_T \varepsilon_3 + N_z^2}. \tag{3.2.22}$$

Considering the asymptote of the function u_0, one can conclude that $|u'_0(\xi)|^2 \propto (-\xi)^{1/4}$ for $Re(\xi) \to -\infty$, and hence, the integral $\int_{-\infty}^{+\infty} |u_0'(x)|^2 dx$ in the expression (3.2.21) diverges. This divergence can be removed by taking into

account the dissipative phenomena: plasma particle collisions or Landau damping (i.e. $Im(\varepsilon_3)$). If the dissipative phenomena are so strong that the relation $Im(\varepsilon_3)\sim Re(\varepsilon_3)$ is valid, then the respective integral from the derivative of the Airy function squared can be estimated as a value of the order of a unit. The damping rate in the considered here case can be estimated from eq. (3.2.9) with account for the replacement (3.2.18):

$$Im(k_1)\sim k_1^4/(2k_T^3). \tag{3.2.23}$$

Then the integrand in eq. (3.2.21) decreases proportionally to $exp[2\,Im(k_1)(r-r_A)]$ along the negative semi axis of integration, and the integral can be estimated by the order of magnitude as k_T^3/k_1^3. This affirms that RF power, which is absorbed in the vicinity of AR due to the work over axial RF currents, also does not depend on the type of the small-scale wave, into which the large-scale electromagnetic wave transforms in the vicinity of AR, at least, by the order of magnitude.

Finally, the results obtained in the present subsection are to be discussed. The fine structure of the local AR and RF power resonant absorption in the case of uniform axial external static magnetic field is determined by the plasma particle collisions, finite ion Larmor radius, and electron inertia. It is shown in the present subsection that in cylindrical plasma, placed into external static magnetic field with axial periodic inhomogeneity, fine structure of the local AR can essentially depend on the degree of the inhomogeneity. The conditions, under which the influence of the studied phenomenon is determinative, are realized, e.g., in modular stellarators of the Wendelstein series, Germany.

The influence of the confining magnetic field inhomogeneity on the AR fine structure causes also the shift of AR point from the axis of the plasma cylinder by the small distance δr ($r_A \to r_A+\delta r$),

$$\delta r = -\varepsilon_1^{(2)}\left(\partial\varepsilon_1^{(0)}/\partial r\right)^{-1}_{r=r_A}. \tag{3.2.24}$$

In (3.2.24), the small correction of the second order $\varepsilon_1^{(2)}$ is equal

$$\varepsilon_1^{(2)} = \frac{\partial\varepsilon_1}{\partial n}\frac{\partial^2 n}{\partial r^2}_{|\varepsilon_m=0}\frac{{\varepsilon_m'}^2}{4k_b^4} + \frac{\partial\varepsilon_1}{\partial n}\frac{\partial n}{\partial r}_{|\varepsilon_m=0}\frac{\varepsilon_m'\varepsilon_m}{4k_b^2} + \frac{\partial\varepsilon_1}{\partial B}_{|\varepsilon_m=0}\frac{B_0{\varepsilon_m'}^2}{4k_b^2} + \\ + \frac{\partial^2\varepsilon_1}{\partial B^2}_{|\varepsilon_m=0}\left(\frac{B_0\varepsilon_m}{2}\right)^2 - \frac{\partial^2\varepsilon_1}{\partial B\partial n}\frac{\partial n}{\partial r}_{|\varepsilon_m=0}\frac{B_0\varepsilon_m\varepsilon_m'}{2k_b^2}. \tag{3.2.25}$$

One cannot conclude from the form of $\varepsilon_1^{(2)}$ what is the sign of δr. However, e.g., if the AR region is situated in the plasma core ($r\sim 0.5a_p$, where a_p is the plasma column radius) with the parabolic profile of the plasma particle density, $n(r)=n(0)(1-r^2/a_p^2)$, and the parameter of inhomogeneity weakly varies in the plasma volume, $|r\varepsilon'| << |\varepsilon|$, then the

resonant point r_A shifts from the axis due to $\vec{B}_0$ inhomogeneity at the distance of the order of $\delta r \sim \varepsilon^2 a_p$.

The conditions are determined (e.g., (3.2.19)), under which the influence of the external magnetic field inhomogeneity on the AR fine structure is stronger, than that of other weak phenomena (dissipations, finite ion Larmor radius, electron inertia). These conditions can be realized in the peripheral plasma, where the inhomogeneity is stronger, and the plasma is colder.

RF field spatial distribution is determined from the simplified eq. (3.2.9). It is valid with accuracy up to small terms of the order of $\varepsilon_m^{2/5}$.

One can see from eq. (3.2.15), that the amplitudes of satellite harmonics increase in the vicinity of AR more rapidly than the amplitude of the main harmonic, and almost symmetrically: $E_r^{(+1)} \approx E_r^{(-1)}$, $E_r^{(+2)} \approx E_r^{(-2)}$... The amplitudes of satellite harmonics remain small values of the order of $\varepsilon_m^{1/5}$ in the vicinity of AR as compared with the amplitude of the main harmonic. Their reversed influence on the distribution of the main harmonic $E_r^{(0)}(r)$ removes the singularity of the solutions of Maxwell's equations, which takes place in the vicinity of AR in the cold approach in axial uniform external static magnetic field. This significantly distinguishes the axial spatially periodic inhomogeneity of the external static magnetic field from, e.g., toroidal inhomogeneity, which influence results in the small change of the shape of the surface, where the singularity takes place [88, 89].

Some conclusions can be made from the comparison of the obtained results with those presented in Section 2 of the monograph [90], where the influence of inhomogeneity of helical external static magnetic field on the AR fine structure was studied. These two magnetic configurations differ from each other in principle: they cannot be obtained from each other in any limiting case. However, the results of these two studies make it possible to make the following main common conclusion. It is the modulation of just radial component of the confining magnetic field, which determines the spatial distribution of RF wave fields in the vicinity of AR under respective conditions, like inequalities (3.2.19). In this respect the conclusions, presented in this overview, contradict with the conclusions of [91], wherein similar problem about AW propagation in the magnetic field of a single adiabatic trap was considered. Analytical estimations carried out there, as well as numerical calculations demonstrated that two-dimensional inhomogeneity of the system does not remove the field singularities within AR. The indicated contradiction is explained by application in [91] of the dispersion relation, derived in the approach of geometrical optics (!), which is inapplicable within AR.

RF power, which is absorbed within AR due to electromagnetic wave conversion into small-scale waves, caused by the $\vec{B}_0$ inhomogeneity, following by their absorption due to the plasma particle collisions and Landau mechanism, is calculated in the present subsection. Its magnitude coincides with that of RF power, which is absorbed within AR both in the case if the absorption is determined by the collisions and if it is caused by the conversion of electromagnetic wave into small-scale kinetic AW.

The local resonance (3.2.6) can take place for both AWs and FMSWs with $\omega<\omega_{ci}$ (if $k_z^2>\omega^2/c^2$), and FMSWs with $\omega>\omega_{ci}$ (if $k_z^2<\omega^2/c^2$) in rarefied plasma. The conversion and absorption of FMSWs with $\omega>\omega_{ci}$ and $k_z^2<\omega^2/c^2$ in the region of the local resonance (3.2.6) at the periphery of cylindrical plasma in the case of uniform axial external static magnetic field was studied in [55, 83].

3.3. Resonant influence of periodic axial inhomogeneity of external static magnetic field on the fine structure of the local alfven resonance

The present subsection is devoted to studying the fine structure of AR for electromagnetic waves with the resonant magnitude of axial wavenumber k_z of the main harmonic [86, 87],

$$k_b=\pm 2k_z. \tag{3.3.1}$$

In other words, the electromagnetic waves are considered, which axial wavelength of the main harmonic is twice as large as axial period L of the inhomogeneity of the external static magnetic field (3.1). The condition (3.3.1) can be satisfied in tokamaks with even number N of the toroidal magnetic field coils. This is the case in TCV, Switzerland ($N=16$); LCT-1, USA ($N=100$); Ignitor, Italy ($N=24$); JET, Euratom ($N=8$) etc. This resonant condition causes a weak coupling between the harmonics with opposite magnitudes of axial wavenumber in the case, if the coupling is determined by axial periodic inhomogeneity of external static magnetic field (3.1). That is why both main harmonics, coupled into one wave packet by the magnetic field inhomogeneity, have their AR in one point.

Since the waves with the axial wavenumbers, different from those determined by the resonant condition (3.3.1), are out of scope in the present subsection (this is already done in the previous subsection), the significance of the results of the present study for the problem of the plasma heating, when usually wide spectrum of axial wavenumbers is observed, can seem to be low one ex facte. However, RF power, excited by an antenna, usually is loaded just into the waves with axial wavenumbers of the order of $2\pi/L_z$. In turn axial dimension L_z of the antenna usually is restricted by the distance between two flanges, which is approximately equal to the spatial period of inhomogeneity L. That is why RF power absorption within AR, which corresponds to the electromagnetic waves with resonant magnitude (3.3.1) of axial wavenumber of the main harmonic, can be essential one.

The AR fine structure is determined in the present subsection for the resonant case (3.3.1). The conditions are derived, under which the AR fine structure is determined by just weak plasma spatial periodic inhomogeneity rather than other weak phenomena. The main difference in physical essence of the present consideration from the previous studies (e.g., [19], where the toroidal inhomogeneity of the external static magnetic field was considered)

consists in the fact, that external static magnetic field contains nonzero periodic radial component, $B_{0r} \neq 0$.

First of all, one has to derive the main equation of the present problem. Assumption about the smallness of the inhomogeneity makes it possible to write down the components $\varepsilon_{1,2}$ of the permittivity tensor in the form of Fourier series (3.9) with account for the small terms of the first order in ε_m only. Neglection of the electron inertia, $|\varepsilon_3| \to \infty$, makes it possible to simplify the set of Maxwell's equations to the form (3.14)–(3.18). During deriving the set (3.14)–(3.18), the plasma particle collisions and finite ion Larmor radius ρ_{Li} are also neglected.

Basing on the problem symmetry, in particular, applying the symmetry of expressions (3.9), and keeping in mind the resonant condition (3.3.1), the solution of the Maxwell's equations (3.14)–(3.18) should be found in the following form:

$$E_r = \left\{E_r^{(+1)}(r)e^{ik_z z} + E_r^{(-1)}(r)e^{-ik_z z} + \right.$$
$$\left. + E_r^{(+3)}(r)e^{i3k_z z} + E_r^{(-3)}(r)e^{-i3k_z z}\right\} \times exp[i(m\vartheta - \omega t)]. \qquad (3.3.2)$$

Presentation in the form of Fourier series for the other components of the wave magnetic and electric fields is similar to (3.3.2). The amplitudes $E_r^{(\pm 3)}$ of the satellite harmonics are well-known to be small values,

$$E_r^{(\pm 3)} \sim \left|\varepsilon_m E_r^{(\pm 1)}\right|, \qquad (3.3.3)$$

everywhere in the plasma column, except of the AR region. Note, that the assumption is not made in advance, that the amplitudes $E_r^{(\pm 3)}$ of the satellite harmonics are small also in the AR region. In other words, one does not presuppose here in advance, that the relation (3.3.3) is true within the AR. The results of the present study confirm that this relation is not valid there.

To solve the problem the method of the narrow layer [24] is applied. It foresees weak variation of the plasma particle density and external static magnetic field in radial direction in AR region. Weak variation of the fields in other directions, rather than radial is also assumed,

$$(\partial E_r/\partial r) >> k|E_r|_{max},\ k\ max(m/r_A, k_z, \omega/c)_{max}. \qquad (3.3.4)$$

After substituting the expressions (3.3.2) for MHD wave fields and (3.9) for the components of the plasma permittivity tensor into Maxwell's equations (3.14)–(3.18) the terms, proportional to $exp(\pm ik_z z)$ and $exp(\pm i3k_z z)$ are singled out. No attention is paid to the order of these terms in respect of ε_m so far. The equations for the radial component of the wave electric field are known to be the most convenient for studying the AR fine structure.

That is why the consideration can be limited to the following closed set of four equations, derived from eqs. (3.14)–(3.18),

$$B_{\vartheta}^{(\pm 1)} = \pm N_z E_r^{(\pm 1)} \pm \frac{c\varepsilon_m'}{2\omega k_b}\frac{\partial}{\partial\, r}\left(E_r^{(\mp 1)} - E_r^{(\pm 3)}\right), \tag{3.3.5}$$

$$B_{\vartheta}^{(\pm 3)} = \pm 3N_z E_r^{(\pm 3)} \pm \frac{c\varepsilon_m'}{2\omega k_b}\frac{\partial}{\partial\, r}E_r^{(\pm 1)}, \tag{3.3.6}$$

$$\left(\varepsilon_1^{(0)} - N_z^2\right)E_r^{(\pm 1)} + \frac{\boldsymbol{\varepsilon_1^{(1)}}}{\mathbf{2}}\left(\boldsymbol{E_r^{(\mp 1)}} + \boldsymbol{E_r^{(\pm 3)}}\right) + \left(i\varepsilon_2^{(0)}E_{\vartheta}^{(\pm 1)} + \frac{cm}{\omega r}B_z^{(\pm 1)}\right) =$$
$$= \pm \boldsymbol{N_z}\left(\boldsymbol{B_{\vartheta}^{(\pm 1)}} \mp \boldsymbol{N_z E_r^{(\pm 1)}}\right) \pm \frac{\boldsymbol{c\varepsilon_m'}}{\boldsymbol{2\omega k_b}}\frac{\boldsymbol{\partial}}{\boldsymbol{\partial\, r}}\left(\boldsymbol{B_{\vartheta}^{(\mp 1)}} - \boldsymbol{B_{\vartheta}^{(\pm 3)}}\right), \tag{3.3.7}$$

$$\left[-8N_z^2 + \left(\frac{c\varepsilon_m'}{2\omega k_b}\right)^2 \frac{\partial^2}{\partial\, r^2}\right]E_r^{(\pm 3)} = \frac{c^2\varepsilon_m'}{\omega^2}\frac{\partial\, E_r^{(\pm 1)}}{\partial\, r} + \left(\frac{c\varepsilon_m'}{2\omega k_b}\right)^2 \frac{\partial^2 E_r^{(\mp 1)}}{\partial\, r^2}. \tag{3.3.8}$$

The combination $\left(i\varepsilon_2^{(0)}E_{\vartheta}^{(\pm 1)} + \frac{cm}{\omega r}B_z^{(\pm 1)}\right) = A^{(\pm)}$ in the left-hand side of (3.3.7) appears to vary weakly in the vicinity of AR, despite both fields $E_{\vartheta}^{(\pm 1)}$ and $B_z^{(\pm 1)}$ are singular (3.2.5) n the vicinity of AR in the cold approach. This is the reason to consider the combination as a constant, associated with the pumping wave. To derive the wanted equation for $E_r^{(\pm 1)}$, one has to substitute eqs. (3.3.5), (3.3.6), and (3.3.8) into the eq. (3.3.7). Those terms in (3.3.7) are marked in bold, which differ this equation from the analogous one in the case of uniform axial external static magnetic field. They are these terms which determine the peculiarities of the AR structure. It is important to underline, that the right-hand side of eq. (3.3.7) does not contain precisely any terms of the first, second and third order in the respect of the parameter ε_m.

To simplify the following consideration, the second term $\propto \partial^2/\partial r^2$ in square brackets in the left-hand side in (3.3.8) is assumed to be small as compared with N_z^2. Then the following equation can be derived for the amplitudes $E_r^{(\pm 1)}$ of the main harmonics of the MHD wave:

$$\left(\varepsilon_1^{(0)} - N_z^2 - \frac{\varepsilon_1^{(1)}\varepsilon_m'}{4k_b^2}\frac{\partial}{\partial\, r} + \frac{{\varepsilon_m'}^4 c^2}{32k_b^6\omega^2}\frac{\partial^4}{\partial\, r^4}\right)E_r^{(\pm 1)} + \frac{\varepsilon_1^{(1)}}{2}\left[E_r^{(\mp 1)} - \frac{1}{8}\left(\frac{\varepsilon_m'}{k_b^2}\right)^2 \frac{\partial^2 E_r^{(\mp 1)}}{\partial \cdot r^2}\right] = -A^{(\pm)}. \tag{3.3.9}$$

The following analysis of eq. (3.3.9) shows that one can neglect the term, which contains the first derivative, as compared with the term, proportional to the fourth derivative. One can neglect the second term in the square brackets in eq. (3.3.8) with the same accuracy. In the result of these simplifications, the main equation gets the final form to be studied,

$$\left(\varepsilon_1^{(0)} - N_z^2 + \frac{{\varepsilon_m'}^4 c^2}{32k_b^6\omega^2}\frac{\partial^4}{\partial\, r^4}\right)E_r^{(\pm 1)} + \frac{\varepsilon_1^{(1)}}{2}E_r^{(\mp 1)} = -A^{(\pm)}. \tag{3.3.10}$$

To analyse the influence of this term on the properties of MHD wave, it is convenient to rewrite the set of equations (3.3.10) in the following form:

$$\hat{Q}E_r^{(+1)} = -0{,}5\varepsilon_1^{(1)}E_r^{(-1)},\ \ \hat{Q}E_r^{(-1)} = -0{,}5\varepsilon_1^{(1)}E_r^{(+1)}, \qquad (3.3.11)$$

where the differential operator of the fourth order $\hat{Q}$ is determined as follows:

$$\hat{Q}E_r^{(\pm 1)} \equiv \left(\varepsilon_1^{(0)} - N_z^2 + \frac{{\varepsilon_m'}^4 c^2}{32k_b^6\omega^2}\frac{\partial^4}{\partial r^4}\right)E_r^{(\pm 1)} - A^{(\pm)}. \qquad (3.3.12)$$

Account for the inhomogeneity of the external static magnetic field results in introduction of two new terms in the main eq. (3.3.10) as compared with the case of uniform axial magnetic field. The first among these two terms contains the amplitude $E_r^{(\mp 1)}$ of the other main harmonic with the opposite sign of axial wavenumber. The rise of this term is caused by the weak axial periodic inhomogeneity of the longitudinal component B_{0z} of the static magnetic field (3.1).

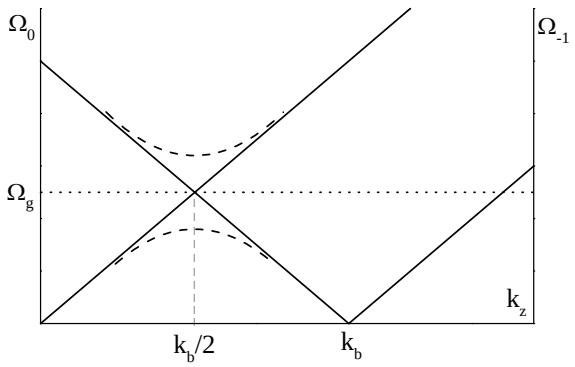

Fig. 3.3.1. Schematic description of the dependence of the resonant Alfven frequency on the axial wavenumber. Solid curves correspond to the case of uniform magnetic field. Dashed curves demonstrate rise of the gap in Alfven continuum, caused by the inhomogeneity of the external static magnetic field. Dotted curve corresponds to the frequency of a generator

Eigen values of $\hat{Q}$ can be derived from eq. (3.3.11):

$$Q^2 = \left(0{,}5\varepsilon_1^{(1)}\right)^2 > 0. \qquad (3.3.13)$$

Positiveness of Q^2 should be stressed due its special significance. This fact has the following sense. The dependence $\Omega_0(k_z) = |k_z\upsilon_A|$ should be introduced, in which the magnitude of Alfven velocity $\upsilon_A = c\omega_{ci}/\omega_{pi}(r)$ is assumed to be fixed one. Here Ω_0 is the frequency of the local AR (in other

words, if an antenna excites electromagnetic waves with the frequency Ω_0, then AR is situated in the point $r=r_A$ for the harmonic with axial wavenumber k_z in uniform axial external static magnetic field). The dependence $\Omega_{-1}(k_z)= /(k_z-k_b)\ \upsilon_A/$ for the same fixed magnitude of Alfven velocity should be introduced as well: if the antenna radiates RF power at the frequency Ω_{-1}, then AR is observed in the point $r=r_A$ for the harmonic with axial wavenumber (k_z-k_b) (see Fig. 3.3.1) in the uniform external static magnetic field. These two curves intersect for the resonant magnitude (3.3.1) of axial wavenumber. In other words, if electromagnetic power is generated with the frequency $\Omega_g=\Omega_0(k_b/2)=\Omega_{-1}(k_b/2)$, which corresponds to the intersection of these curves, then both harmonics have their local ARs in the point $r=r_A$. Then in the inhomogeneous external static magnetic field (3.1) the gap appears in Alfven continuum, $\Omega^2=\Omega_0^2(0.5\ k_b)\ (1+\Delta_b)$, with

$$\Delta_b = \pm\frac{1}{\omega_0^2}\left[\frac{\partial\left(\varepsilon_1^{(0)}-N_z^2\right)}{\partial\left(\omega^2\right)}\right]^{-1}\frac{\varepsilon_1^{(1)}}{2}. \qquad (3.3.14)$$

In other words, neither harmonic with axial wavenumber k_z, nor the harmonic with (k_z-k_b) have their local AR in the point $r=r_A$, if the antenna functions at the frequency Ω_g in the case of inhomogeneous external static magnetic field.

It is natural to compare the gap with the other, which is caused by the toroidicity and is known to be described by the following dependence: $\Omega^2=\Omega_0^2\ (1+\Delta_t)$. The halfwidth of the gap Δ_t reads as:

$$\Delta_t = \pm\frac{1}{\omega_0^2}\left[\frac{\partial\left(\varepsilon_1^{(0)}-N_z^2\right)}{\partial(\omega^2)}\right]^{-1}\frac{\varepsilon_t}{\sqrt{2}}, \qquad (3.3.15)$$

here

$$\varepsilon_t = \frac{\omega_{pi}^2}{\omega_{ci}^{2(0)}-\omega^2}\frac{\partial\ ln\ n}{\partial r}\left|\Delta-\frac{r}{R}\frac{2\omega_{pi}^2\omega_{ci}^{2(0)}}{\left(\omega_{ci}^{2(0)}-\omega^2\right)^2}-\frac{2r}{R}N_z^2\right.. \qquad (3.3.16)$$

The comparison mentioned above reduces to analysis of the relation between the parameter of inhomogeneity and the parameter of toroidicity r/R (R is large radius of the torus). The last parameter is usually larger in toroidal traps. However, the $\vec{B}_0$ inhomogeneity can provide appearance of the gap in Alfven continuum in Low Curvature Tokamak and straight magnetic traps.

The gaps in Alfven continuum, caused by toroidicity, were studied in [18, 19]. Eigen Alfven modes, caused by toroidicity, with the frequencies inside the respective gaps were foreseen in [19] and were then observed experimentally.

The general form of the expression (3.3.14) agrees good with the conclusions of A. Yelfimov [18]. He has demonstrated, that the width of the

gap in Alfven continuum, caused by toroidicity, is proportional to the amplitude of modulation $\varepsilon_1^{(1)}$ of the component ε_1 of the permittivity tensor.

The second term, which differs the main eq. (3.3.10) from analogous in the case of uniform external axial static magnetic field, is proportional to the fourth derivative. It is associated with the radial component B_{0r} of external static magnetic field (3.1). This term is a little bit larger by the order of magnitude, than the first one, which influence is studied above.

If radial profile of the plasma particle density is linear one in the AR region,

$$\left(\varepsilon_1^{(0)} - N_z^2\right) = \partial\varepsilon_1^{(0)}/\partial r\,|r_A(r - r_A), \tag{3.3.17}$$

then the analytical solution of eq. (3.3.10) can be obtained by Laplace method in the following form:

$$E_r^{(\pm 1)} = (ak_1/N_A^2)A^{(\pm)}u_0[k_1(r - r_A)], \tag{3.3.18}$$

$$u_o(\xi) = \int_0^\infty exp[i(t\xi + t^5/5)]\,dt,\ \ k_1 = \left(\varepsilon_m'^{\,4}a/8k_b^8\right)^{-1/5}. \tag{3.3.19}$$

The dependence of the function $u_0(\xi)$ is presented in Fig. 3.2.1 and analysed in the subsection 3.2.

The characteristic width of AR

$$\Delta r = k_1^{-1}\left(\varepsilon_m'^{\,4}a/8k_b^8\right)^{1/5}, \tag{3.3.20}$$

in the case, studied in the present subsection, has the same order of magnitude, as the width of AR in nonresonant case (see (3.2.12)).

Characteristic magnitude of the amplitude $E_r^{(\pm 1)}$ of the main harmonic of the radial component of the MHD wave electric field within the AR can be estimated from eqs. (3.3.10) and (3.3.19) by the order of magnitude as follows:

$$E_r^{(\pm 1)} \sim k_1 a\, A^{(\pm)}/N_z^2. \tag{3.3.21}$$

This expression has the same order of magnitude as in a nonresonant case (3.2.16).

During the present study the assumption, that the amplitudes $E_r^{(\pm 3)}$ of satellite harmonics are small as compared with $E_r^{(\pm 1)}$, was not applied still. Now, the characteristic magnitude of $E_r^{(\pm 3)}$ in the vicinity of AR can be estimated by the order of magnitude, basing on the eq. (3.3.8), as follows:

$$E_r^{(\pm 3)} \sim (\varepsilon_m/k_b a)^{1/5}E_r^{(\pm 1)} \sim A^{(\pm)}\,(k_b a/\varepsilon_m)^{3/5}/N_z^2. \tag{3.3.22}$$

The comparison of expressions (3.3.3) and (3.3.22) shows, that the amplitudes $E_r^{(\pm 3)}$ of satellite harmonics increase with approaching to the AR region even more rapidly than the amplitudes $E_r^{(\pm 1)}$ of the main harmonics. The amplitudes $E_r^{(\pm 3)}$ remain smaller than those of $E_r^{(\pm 1)}$ within the AR region, but the difference in the order of magnitude between the $E_r^{(\pm 1)}$ and $E_r^{(\pm 3)}$ is not so pronounced within the AR region as outside of it.

All mentioned above makes it possible to estimate, that the transform of eq. (3.3.7) into eq. (3.3.9) and eq. (3.3.9) into (3.3.10) is valid with accuracy of $\left(\varepsilon_m/(ak_b)\right)^{2/5} << 1$.

In the following, the conditions are derived, under which the structure of the local AR in the resonant case (3.3.1) is determined just by the weak axial periodic inhomogeneity of $\vec{B}_0$, rather than finite electron inertia, ion Larmor radius or collisions. These weak phenomena can be taken into account in eq. (3.3.10) by applying the replacements (3.2.18).

Analysis of the main eq. (3.3.10) with account for the replacement (3.2.18) shows, in particular, that the influence of the $\vec{B}_0$ inhomogeneity on the AR structure is more significant, than the influence of finite ion Larmor radius and electron inertia, if the following inequality is valid:

$$\varepsilon_m{}^{12/5} >> (k_b a)^{12/5}(\rho_{Li}/a)^2. \qquad (3.3.23)$$

This condition can be realized in the peripheral plasma, where $\vec{B}_0$ inhomogeneity is the most significant and the plasma is colder, than in the plasma core. The condition (3.3.23) can be commented as follows. Radial deviation $r-r_A$ of the magnetic surface (3.5) from the cylinder with average radius is larger than the characteristic width $(\rho_{Li}{}^2 a)^{1/3}$ of AR region, which is well-known in the case of uniform external static axial magnetic field.

It is in place to make the conclusions. The results of theoretical studying the AR fine structure in cylindrical plasma, placed into the bumpy magnetic field (3.1), are exposed in the present subsection for the waves with resonant magnitude (3.3.1) of axial wavenumber. Spatial distribution of electromagnetic fields in the vicinity of AR is determined and analysed with account for the axial periodic inhomogeneity of external static magnetic field, electron inertia, ion Larmor radius and collisions.

Axial periodic inhomogeneity of external static magnetic field is identified to cause the coupling of spatial harmonics of electromagnetic waves with opposite magnitudes of axial wavenumbers. In particular, in the bumpy magnetic field with the period of inhomogeneity L, electromagnetic waves with the resonant magnitudes $k_z=\pm\pi/L$ of axial wavenumber belong to the same packet (see eq. (3.3.2)), in which two the nearest satellite harmonics with axial wavenumbers $k_z=\pm 3\pi/L$ are taken into account in the present subsection.

The condition (3.3.23) is also derived in the present subsection. Under the condition the spatial distribution of electromagnetic wave fields with the resonant values of axial wavenumber in the vicinity of AR is determined just by

the modulation of the radial component of the external static magnetic field, rather than by electron inertia and finite ion Larmor radius. The inequality (3.3.23) can be realized in cold peripheral plasma, wherein the inhomogeneity of the external static magnetic field is the most pronounced. And exactly there the region of the local AR is displaced in the result of the plasma particle density increase, which is observed during the plasma production in fusion devices. The characteristic width (3.3.20) of AR region is larger in this case than in uniform external static axial magnetic field ceteris paribus.

Note, that the versions of designing the Helias reactor [92] with four or five modules were considered in due time. If it is manufactured with four modules, then the present study of the resonant influence of the mirror inhomogeneity of the external static magnetic field on the AR structure is actual also for the Helias project.

The presentation (3.1) of the external static magnetic field in the form of a single harmonic $\propto sin(k_b z)$ is very simplified. Actually, the spatial spectrum of the external static magnetic field is wide one and contains also the harmonics $\propto sin(j k_b z)$, $j=2,3,4\ldots$ Consequently, axial periodic inhomogeneity of $\vec{B}_0$ causes resonant influence on the local AR structure for the electromagnetic waves with axial wavenumber $k_z=j\pi/L$. However, these phenomena can be significant only if the conditions, similar to the inequalities (3.3.23), are valid.

Amplitudes of satellite harmonics increase with approaching to the AR point even more rapidly, than the amplitudes of the main harmonic. This causes removing the singularities of solutions to Maxwell's equations for the fields of electromagnetic waves, which are known to take place under the condition of neglecting the plasma particle collisions, electron inertia and ion thermal motion in the case of uniform external static axial magnetic field, by axial periodic inhomogeneity of the magnetic field. Characteristic magnitude (3.3.21) of the wave radial electric field is smaller than in uniform external static axial magnetic field under the condition (3.3.23).

Axial periodic inhomogeneity of external static magnetic field is shown to be the reason of arising the gap in Alfven continuum.

Satellite AR (in which vicinity both wave satellite harmonics (3.3.2) with amplitudes $E_r^{(\pm 3)}$ transform into small-scale kinetic waves) is situated deeper in the plasma, where the plasma particle density is nine times larger, than in the main AR (just this situation is shown in Figs. 3.1.1–3.1.3). Then one can expect, that additional plasma heating within the satellite ARs for electromagnetic waves, which main harmonic is characterized by axial wave length $2L$, can be significant [78].

3.4. Fine structure of satellite alfven resonance in cold plasma in the moderate bumpy magnetic field

First of all, it is important to identify the specific object of the research carried out in the present subsection. The possibility of additional plasma heating in SARs, where the condition (3.1.3) is valid, was proved in

the subsection 3.1. Radial deviation of the magnetic surface from the cylinder of radius $r_A^{(\pm)}$ was assumed there to be smaller than the characteristic width $\Delta r_T = (\rho_{Li}^2 a *)^{1/3}$ of AR region, which is well-known in the case of uniform external static axial magnetic field [24]. Appearance of SARs is manifested in the rapid increase of amplitudes of the satellite harmonics in the vicinity of the resonant points $r = r_A^{(\pm)}$ (3.1.3). Spatial distribution of electromagnetic wave fields within SARs [87], which is studied in the present subsection, generalises the results, obtained in the subsection 3.1 on the case, in which the radial deviation of the magnetic surface is larger than Δr_T and spatial distribution of RF wave fields is determined just by axial periodic inhomogeneity of the bumpy magnetic field.

To derive the main equations of the problem, one has, first of all, to choose appropriate frame of reference. Cylindrical coordinates do not suit, since all the nine components of the plasma permittivity tensor are nonzero ones in the case of the cold plasma placed into the bumpy magnetic field (3.1). In contrast to cylindrical coordinates, the plasma permittivity tensor has the simplest form in the coordinates associated with the force lines of external static magnetic field. The electron inertia is known to be negligibly weak for Alfven and fast magnetosonic branches of MHD waves. Neglecting the electron inertia for MHD waves, $|\varepsilon_3| \to \infty$, is equivalent to the fact that longitudinal component of the wave electric field is equal to zero everywhere in plasma. Basing on this circumstance, one can write down the set (3.14)–(3.18) of Maxwell's equations with applying the relations (3.6) and (3.7) between the vector of the wave electric displacement field $\vec{D}$ and the vector of the wave electric field $\vec{E}$. Assumption about the smallness of the axial periodic inhomogeneity of the external static magnetic field makes it possible to write down the expressions for the components $\varepsilon_{1,2}$ in the form of Fourier series (3.9), keeping the terms of the first order of smallness in the parameter ε_m only.

The symmetry of the problem (in particular, the form of the expressions (3.9) for the components of the tensor ε_{ik}) provides the reason to search the solution of Maxwell's equations for the radial component of the wave electric field in the form of the wave packet:

$$E_r = [E_r^{(0)}(r) + E_r^{(+1)}(r)\exp(ik_b z) + E_r^{(+2)}(r)\exp(2ik_b z)] \times \\ \times \exp[i(k_z z + m\vartheta - \omega t)]. \qquad (3.4.1)$$

Along with the first satellite harmonic $\propto \exp[i(k_z + k_b)z]$, which amplitude is singular in the SAR point (3.1.3) in the case of the cold plasma, one takes into account the main $\propto \exp(ik_z z)$ and the second satellite $\propto \exp[i(k_z + 2k_b)z]$ harmonics. The latter two harmonics are those with which the first satellite harmonic is coupled the most strongly by axial periodic inhomogeneity of the bumpy magnetic field (3.1).

Representations of the other components of the wave magnetic and electric fields in the form of Fourier series are similar to eq. (3.4.1). Such an

approach to solving the Maxwell's equations is usually called as Floquet-Bloch method (see, e.g., [93]).

In approaching along the radius to the SAR region, amplitudes of satellite harmonics of the electromagnetic wave fields diverge in the case of the cold plasma as follows,

$$E_r^{(+1)}, B_\vartheta^{(+1)} \propto (\varepsilon_1^{(0)} - (N_z+N_b)^2)^{-1},\ E_\vartheta^{(+1)}, B_r^{(+1)}, B_z^{(+1)} \propto \ln / \varepsilon_1^{(0)} - (N_z+N_b)^2 /. \tag{3.4.2}$$

Applying the method presented in [24], one can use the approach of «narrow layer». The latter foresees the weak variation of the plasma particle density and external static magnetic field in radial direction in the vicinity of SAR. Weak variation (3.3.4) of the fields in all the directions, except of the radial is also assumed.

Amplitudes of the first satellite harmonics are known to be smaller than those of the main harmonics by the order of ε_m^{-1} everywhere in the plasma column, except of the SAR vicinity [93]. However, this relation is not assumed in advance to be applicable also in the vicinity of SAR. After substituting the expressions (3.4.1) for the wave fields and (3.8) – for the components of the permittivity tensor into Maxwell's equations (3.14)–(3.18), the terms are singled out in these equations, which are proportional to the Fourier factors $\propto exp[i(k_z+k_b)z]$, $\propto exp(ik_z z)$ and $\propto exp[i(k_z+2k_b)z]$ without paying attention to the order of these terms in respect of ε_m. Since the equation for the radial component of the wave electric field is the most convenient for studying the fine structure of SAR, then it is sufficient to present here only the following set of coupled equations for the amplitudes of the main and two satellite harmonics, which can be derived from the set (3.14)–(3.18),

$$N_b(2N_z+N_b)E_r^{(0)} + i\varepsilon_2^{(0)}E_\vartheta^{(0)} + N_\vartheta B_z^{(0)} = (2N_z+N_b)\frac{c\varepsilon_m'}{2\omega k_b}\frac{dE_r^{(+1)}}{dr} + \left(\frac{c\varepsilon_m'}{2\omega k_b}\right)^2 \frac{d^2E_r^{(+2)}}{dr^2}, \tag{3.4.3}$$

$$[\varepsilon_1^{(0)} - (N_z+N_b)^2 + \lambda(d^2/dr^2)]E_r^{(+1)} = A^{(+)},$$
$$\lambda = -(N_z+0.5N_b)c\varepsilon_m{}^2/(2\omega k_b{}^3), \tag{3.4.4}$$

$$E_r^{(+2)} = (\varepsilon_m'/(2k_m{}^2))dE_r^{(+1)}/dr. \tag{3.4.5}$$

Despite of the fact that the fields $E_\vartheta^{(+1)}$ and $B_z^{(+1)}$ have singularities (3.4.2) in the vicinity of SAR in the cold approach, the right-hand side of eq. (3.4.4) varies weakly in the vicinity of SAR,

$$A^{(+)} = (-i\varepsilon_2^{(0)}E_\vartheta^{(+1)} - N_\vartheta B_z^{(+1)})\Big|r_A^{(+)}. \tag{3.4.6}$$

This is the reason to consider the combination (3.4.6) as a constant, which is associated with the pumping wave. The combination $A^{(+)}$ can be

calculated, applying the solutions of Maxwell's equations out of the SAR region. These solutions can be obtained numerically for arbitrary plasma particle density (see, e.g., [13, 49]). The right-hand side of eq. (3.4.4) can be estimated by the order of magnitude as follows: $A^{(+)} \sim \varepsilon_m \varepsilon_2^{(0)} E_\vartheta^{(0)}$. Weak variation of the combination (3.4.6) in the vicinity of SAR is analogous to well-known issue in the case of uniform external static axial magnetic field (see, e.g., [24, 55]). This weak variation results from the fact, that those singular terms, which cause the singularities (3.4.2) for the wave poloidal electric and axial magnetic fields, cancel, if they are taken in the combination (3.4.6).

Transfer from the Maxwell's equations (3.14)–(3.18) to the set (3.4.3)–(3.4.6) can seem to be very complicated. That is why the procedure of the transfer is explained in detail below. The procedure is convenient to divide into seven steps.

The first step. The difference between the absolute value of the confining magnetic field $/\vec{B}_0/$ and that of uniform external static magnetic field B_0, $/\vec{B}_0/ = B_0(1+O(\varepsilon_m^2))$ is neglected. In particular, this note is important to apply to the eq. (3.17).

The second step. The term in eq. (3.17), which is proportional to B_r, is neglected since it is smaller by the order of magnitude, than the terms, which are proportional to B_z and E_ϑ. The last two terms are kept without any change, since their combination (3.4.6) weakly varies in the vicinity of SAR. To confirm this, one can consider eqs. (3.16) and (3.18), and single out therein the terms, proportional to the Fourier factors $exp[i(k_z+k_b)z]$:

$$\frac{c}{\omega}\frac{d}{dr}B_z^{(+1)} = \varepsilon_2^{(0)} E_r^{(+1)} + i[(N_z+N_b)B_r^{(+1)} + \varepsilon_1^{(0)} E_\vartheta^{(+1)}] + \\ + \{0.5\varepsilon_2^{(1)}(E_r^{(0)}+E_r^{(+2)}) + 0.5i\varepsilon_1^{(1)}(E_\vartheta^{(0)}+E_\vartheta^{(+2)})\}, \qquad (3.4.7)$$

$$id(rE_\vartheta^{(+1)})/dr = -mE_r^{(+1)} - [\omega r B_z^{(+1)}/c]. \qquad (3.4.8)$$

The terms in figure brackets in eq. (3.4.7) are neglected since they are small values of the order of $\varepsilon_m^{4/3}/(a^* k_b)^{1/3}$. The term in the left-hand side and the first term in the right-hand side of (3.4.7) and (3.4.8) have the singularity of the highest order, namely, they are proportional to $(\varepsilon_1^{(0)} - (N_z+N_b)^2)^{-1}$. Those terms, which are placed in square brackets in eqs. (3.4.7) and (3.4.8), have singularities of lower order: they are proportional to $ln/\varepsilon_1^{(0)} - (N_z+N_b)^2/$. After integrating these equations in respect of radial coordinate, the eq. (3.4.8) should be multiplied by $\varepsilon_2^{(0)}/r$, and eq. (3.4.7) – by m/r. After adding of these equations, the combination $i\varepsilon_2^{(0)} E_\vartheta^{(+1)} + cmB_z^{(+1)}/(r\omega)$ turns in the left-hand side. The most dangerous terms in the right-hand side of the equation, which are proportional to $E_r^{(+1)}$, cancel. The terms of the next order of smallness in the right-hand side do not cause rapid variation of this combination.

The third step. The field B_ϑ from eq. (3.12) should be substituted to eq. (3.14),

$$i\varepsilon_2 E_\vartheta + N_\vartheta B_z = (1+\varepsilon_m \cos(k_b z))\left(-\varepsilon_1 E_r - \frac{c^2}{\omega^2}\frac{\partial^2 E_r}{\partial z^2}\right) + \{(1+\varepsilon_m \cos(k_b z))$$
$$(-1)\frac{c^2}{\omega^2}\frac{\partial^2}{\partial z \partial r}\left[\frac{\varepsilon'_m}{k_b}\frac{\sin(k_b z)}{1+\varepsilon_m \cos(k_b z)} E_r\right]\} -$$
$$-\frac{\varepsilon'_m}{k_b}\sin(k_b z)\frac{c^2}{\omega^2}\frac{\partial^2}{\partial z \partial r} E_r - \frac{\varepsilon'_m}{k_b}\sin(k_b z)\frac{c^2}{\omega^2}\frac{\partial^2}{\partial r^2}\left[\frac{\varepsilon'_m}{k_b}\frac{\sin(k_b z)}{1+\varepsilon_m \cos(k_b z)} E_r\right], \quad (3.4.9)$$

here $N_\vartheta = cm/(\omega r_s^{(\pm)})$ is azimuthal refractive index.

The fourth step. Application of the method of «narrow layer» makes it possible to consider eq. (3.4.9) as equation with constant coefficients. After calculating the partial derivative $\partial/\partial z$ in the term, marked by figure brackets in the right-hand side of eq. (3.4.9), one derives the following

$$i\varepsilon_2 E_\vartheta + N_\vartheta B_\vartheta = -(1+\varepsilon_m \cos(k_b z))\left(\varepsilon_1 E_r + \right.$$
$$\left. + \frac{c^2}{\omega^2}\frac{\partial^2 E_r}{\partial z^2}\right) - (0.5\varepsilon_m + \cos(k_b z) - 0.5\varepsilon_m \cos(2k_b z))\frac{c^2}{\omega^2}\varepsilon'_m \frac{\partial E_r}{\partial r} -$$
$$-2\frac{\varepsilon'_m}{k_b}\sin(k_b z)\frac{c^2}{\omega^2}\frac{\partial^2}{\partial z \partial r} E_r - \frac{\varepsilon'^2_m}{k_b^2}\frac{c^2}{\omega^2}\ (0.5 - 0.25\varepsilon_m \cos(k_b z) - 0.5\cos(2k_b z))\frac{\partial^2}{\partial r^2} E_r. \quad (3.4.10)$$

The fifth step. The terms proportional to $\exp\{i[k_z z + m\vartheta - \omega t]\}$ are singled out in eq. (3.4.10),

$$i\varepsilon_2^{(0)} E_\vartheta^{(0)}{}_{(0,0)} + N_\vartheta B_z^{(0)}{}_{(0,0)} = -\varepsilon_1^{(0)} E_r^{(0)}{}_{(0,0)} + N_z^2 E_r^{(0)}{}_{(0,0)} - 0.5\varepsilon_1^{(1)} E_r^{(+1)}{}_{(2,-1)} -$$
$$-0.5\varepsilon_m \varepsilon_1^{(0)} E_r^{(+1)}{}_{(2,-1)} - 0.5\varepsilon_m \varepsilon_1^{(1)} E_r^{(0)}{}_{(2,0)} +$$
$$+0.5\varepsilon_m (N_z + N_b)^2 E_r^{(+1)}{}_{(2,-1)} - 0.5\varepsilon_m \varepsilon'_m \frac{c^2}{\omega^2}\frac{\partial E_r^{(0)}}{\partial r}_{(2,0)} - \quad (3.4.11)$$
$$-0.5\varepsilon'_m \frac{c^2}{\omega^2}\frac{\partial E_r^{(+1)}}{\partial r}_{(2,-2)} + 0.25\varepsilon_m \varepsilon'_m \frac{c^2}{\omega^2}\frac{\partial E_r^{(+2)}}{\partial r}_{(4,-3)} + \frac{\varepsilon'_m}{k_b}\frac{c^2}{\omega^2}(k_z + k_b)\frac{\partial E_r^{(+1)}}{\partial r}_{(2,-2)}$$
$$\mathbf{-0.5\frac{\varepsilon'^2_m}{k_b^2}\frac{c^2}{\omega^2}\frac{\partial^2 E_r^{(0)}}{\partial r^2}_{(2,0)}} + 0.125\varepsilon_m \frac{\varepsilon'^2_m}{k_b^2}\frac{c^2}{\omega^2}\frac{\partial^2 E_r^{(+1)}}{\partial r^2}_{(4,-3)} + \mathbf{0.25\frac{\varepsilon'^2_m}{k_b^2}\frac{c^2}{\omega^2}\frac{\partial^2 E_r^{(+2)}}{\partial r^2}_{(4,-4)}}.$$

Two subscripts are assigned to each term in eq. (3.4.11). The first subscript indicates the order of the term in respect of the small parameter ε_m. The second subscript corresponds to the degree of the term singularity in the vicinity of SAR. This assignment of subscripts is relevantly to explain taking as example those terms, which are marked in bold in eq. (3.4.11). The first term $-0.5\frac{\varepsilon'^2_m}{k_b^2}\frac{c^2}{\omega^2}\frac{\partial^2 E_r^{(0)}}{\partial r^2}_{(2,0)}$ is proportional to ε'^2_m, that is why it is assigned the first subscript «2». It is shown below that satellite harmonics weakly influence on radial dependence of the field $E_r^{(0)}$. That is why «0» is assigned as the second subscript to this term. The factor ε'^2_m introduces two units to the first subscript of the term $0.25\frac{\varepsilon'^2_m}{k_b^2}\frac{c^2}{\omega^2}\frac{\partial^2 E_r^{(+2)}}{\partial r^2}_{(4,-4)}$. Two units more

originate from the second satellite harmonic $E_r^{(+2)}$ of the wave radial electric field which is a part of the term. The field $E_r^{(+1)}$ diverges (see eq. (3.4.2)) as $(\varepsilon_1^{(0)}-(N_z+N_b)^2)^{-1}$. Then the field $E_r^{(+2)}$ diverges (see (3.4.5)) as $(\varepsilon_1^{(0)}-(N_z+N_b)^2)^{-2}$ and its second derivative $\partial^2 E_r^{(+2)}/\partial r^2$ is proportional to $(\varepsilon_1^{(0)}-(N_z+N_b)^2)^{-4}$. This is the reason to assign the second subscript «– 4» to this term in eq. (3.4.11).

Along with the terms of zeroth order in ε_m in eq. (3.4.11), which do not diverge (their subscripts are (0,0)), the most dangerous terms (with the subscripts (2,–2) and (4,–4)) are also kept in eq. (3.4.11). At the same time, e.g., the terms with the subscripts (4,–3) are neglected. The term (4,–4) is kept. It is smaller by two orders in ε_m, but it is respectively more singular (by two orders). The term with the subscripts (4,–3) has, on the contrary, the same order of smallness in ε_m, as the term with the subscripts (4,–4), but it is less singular, which makes it possible to neglect it. Finally, the selection rule can be formulated as follows. The term with the subscripts (i,j) is neglected as compared with the term with the subscripts (k,l), if $i+2j/3>k+2l/3$. The origin of the factor 2/3 nearby j and l is explained by the dependence of the radial short wavenumber $k_s\sim\partial/\partial r\propto\varepsilon_m^{-2/3}$ to be derived in the present subsection. For example, the term $0.125\varepsilon_m\frac{\varepsilon_m'^2}{k_b^2}\frac{c^2}{\omega^2}\frac{\partial^2 E_r^{(+1)}}{\partial r^2}_{(4,-3)}$ is neglected with accuracy $(\varepsilon_m^2 a^* k_b)^{1/3}\ll 1$.

The sixth step. The terms $\propto exp\{i[(k_z+2k_b)z+m\vartheta-\omega t]\}$ are singled out in eq. (3.4.10),

$$i\varepsilon_2^{(0)}E_\vartheta^{(+2)}{}_{(2,0)}+N_\vartheta B_z^{(+2)}{}_{(2,0)}=-\varepsilon_1^{(0)}E_r^{(+2)}{}_{(2,-2)}+(N_z+2N_b)^2E_r^{(+2)}{}_{(2,-2)}-$$
$$-0.5\varepsilon_1^{(1)}E_r^{(+1)}{}_{(2,-1)}-0.5\varepsilon_m\varepsilon_1^{(0)}E_r^{(+1)}{}_{(2,-1)}-0.5\varepsilon_m\varepsilon_1^{(1)}E_r^{(+2)}{}_{(4,-2)}-$$
$$-0.5\varepsilon_m\varepsilon_1^{(1)}E_r^{(0)}{}_{(2,0)}+ \qquad (3.4.12)$$
$$0.5\varepsilon_m(N_z+N_b)^2E_r^{(+1)}{}_{(2,-1)}-0.5\varepsilon_m\varepsilon'_m\frac{c^2}{\omega^2}\frac{\partial E_r^{(+2)}}{\partial r}_{(4,-3)}-0.5\varepsilon'_m\frac{c^2}{\omega^2}\frac{\partial E_r^{(+1)}}{\partial r}_{(2,-2)}$$
$$+0.25\varepsilon_m\varepsilon'_m\frac{c^2}{\omega^2}\frac{\partial E_r^{(0)}}{\partial r}_{(2,0)}-\frac{\varepsilon'_m}{k_b}\frac{c^2}{\omega^2}(k_z+k_b)\frac{\partial E_r^{(+1)}}{\partial r}_{(2,-2)}-0.25\frac{\varepsilon_m'^2}{k_b^2}\frac{c^2}{\omega^2}\frac{\partial^2 E_r^{(0)}}{\partial r^2}_{(2,0)}+$$
$$0.125\varepsilon_m\frac{\varepsilon_m'^2}{k_b^2}\frac{c^2}{\omega^2}\frac{\partial^2 E_r^{(+1)}}{\partial r^2}_{(4,-3)}-0.5\frac{\varepsilon_m'^2}{k_b^2}\frac{c^2}{\omega^2}\frac{\partial^2 E_r^{(+2)}}{\partial r^2}_{(4,-4)}.$$

The most dangerous terms are kept in eq. (3.4.12) with the subscripts (2,–2),

$$0=-\varepsilon_1^{(0)}E_r^{(+2)}{}_{(2,-2)}+(N_z+2N_b)^2E_r^{(+2)}{}_{(2,-2)}-$$
$$-0.5\varepsilon'_m\frac{c^2}{\omega^2}\frac{\partial E_r^{(+1)}}{\partial r}_{(2,-2)}-\frac{\varepsilon'_m}{k_b}\frac{c^2}{\omega^2}(k_z+k_b)\frac{\partial E_r^{(+1)}}{\partial r}_{(2,-2)}. \qquad (3.4.13)$$

The terms with the subscripts (4,–4) are neglected with accuracy $(\varepsilon_m/(a^*k_b))^{2/3}\ll 1$. Taking into account the identity

$$\frac{1}{2}+\frac{k_z+k_m}{k_m}=\frac{2k_z+3k_m}{2k_m}, \tag{3.4.14}$$

and the approximate equality

$$(N_z+2N_b)^2-\varepsilon_1^{(0)}(r_s^{(+)})\approx(2N_z+3N_b)N_b, \tag{3.4.15}$$

the eq. (3.4.5) is derived from eq. (3.4.13).

The seventh step. The terms $\propto exp\{i[(k_z+k_b)z+m\vartheta-\omega t]\}$ are singled out in eq. (3.4.10),

$$\begin{aligned}
&i\varepsilon_2^{(0)}E_\vartheta^{(+1)}{}_{(1,0)}+N_\vartheta B_z^{(+1)}{}_{(1,0)}=-\varepsilon_1^{(0)}E_r^{(+1)}{}_{(1,-1)}-0.5\varepsilon_1^{(1)}E_r^{(0)}{}_{(1,0)}\\
&-0.5\varepsilon_1^{(1)}E_r^{(+2)}{}_{(3,-2)}+\\
&+(N_z+N_b)^2E_r^{(+1)}{}_{(1,-1)}-0.5\varepsilon_m\varepsilon_1^{(0)}E_r^{(0)}{}_{(1,0)}-0.5\varepsilon_m\varepsilon_1^{(0)}E_r^{(+2)}{}_{(3,-2)}-\\
&0.5\varepsilon_m\varepsilon_1^{(1)}E_r^{(+1)}{}_{(3,-1)}+\\
&+0.5\varepsilon_m N_z^2E_r^{(0)}{}_{(1,0)}+0.5\varepsilon_m(N_z+2N_b)^2E_r^{(+2)}{}_{(3,-1)}-0.5\varepsilon_m\varepsilon'_m\frac{c^2}{\omega^2}\frac{\partial E_r^{(+1)}}{\partial r}_{(3,-2)}-\\
&-0.5\varepsilon'_m\frac{c^2}{\omega^2}\frac{\partial E_r^{(0)}}{\partial r}_{(1,0)}-\\
&-0.5\varepsilon'_m\frac{c^2}{\omega^2}\frac{\partial E_r^{(+2)}}{\partial r}_{(3,-3)}-\frac{\varepsilon'_m}{k_b}\frac{c^2}{\omega^2}k_z\frac{\partial E_r^{(0)}}{\partial r}_{(1,0)}+\frac{\varepsilon'_m}{k_b}\frac{c^2}{\omega^2}(k_z+2k_b)\frac{\partial E_r^{(+2)}}{\partial r}_{(3,-3)}-\\
&-0.5\frac{\varepsilon'^2_m}{k_b^2}\frac{c^2}{\omega^2}\frac{\partial^2E_r^{(+1)}}{\partial r^2}_{(3,-3)}+\\
&+0.125\varepsilon_m\frac{\varepsilon'^2_m}{k_b^2}\frac{c^2}{\omega^2}\left(\frac{\partial^2E_r^{(0)}}{\partial r^2}_{(3,0)}+\frac{\partial^2E_r^{(+2)}}{\partial r^2}_{(5,-3)}\right).
\end{aligned} \tag{3.4.16}$$

To derive the wanted eq. (3.4.4) the terms with subscripts (1,–1) and (3,–3) are kept, as well as two terms in the left-hand side of eq. (3.4.16) which aggregate to the combination (3.4.6). For example, the term with the subscripts (3,–2) are neglected with accuracy $(\varepsilon_m^2a^*k_b)^{1/3}<<1$.

The eqs. (3.4.3)–(3.4.5) are to be solved in the case, if the SAR fine structure is determined just by the periodic axial inhomogeneity of $\vec{B}_0$, rather than other weak phenomena. In other words, collisions between the plasma particles, electron inertia and finite ion Larmor radius are neglected in the present subsection. The radial profile of the plasma particle density is assumed to be linear one in the vicinity of SAR,

$$\varepsilon_1^{(0)}-(N_z+N_b)^2=\left(d\varepsilon_1^{(0)}/dr\right)\Big|_{r_s^{(+)}}(r-r_s^{(+)}). \tag{3.4.17}$$

The solution of the inhomogeneous Airy equation (3.4.4), which amplitude decreases with going away from SAR and which carries out the wave energy from the SAR, reads as

$$E_r^{(+1)}=-ik_sa^*(N_z+N_b)^{-2}A^{(+)}v(k_s(r-r_s^{(+)})), \tag{3.4.18}$$

here

$$v(\xi)=s\int_0^\infty exp[is(t\xi + t^3/3)]\,dt, \quad k_s=((-1/\lambda)d\varepsilon_1^{(0)}/dr)^{1/3}\Big|r_s^{(+)}=/k_s/e^{i\varphi}. \tag{3.4.19}$$

The direction, in which the small-scale wave propagates, is determined by the parameter s,

$$s=sign[d\varepsilon_1^{(0)}/dr)\Big|r_s^{(+)}\,Re(k_s)]. \tag{3.4.20}$$

As it was noted in [59], absolute value of the inhomogeneous Airy function $v(\xi)$ has its maximum at $\xi_m\approx -1.8$ rather than at $\xi=0$.

Characteristic width δr of SAR region (3.1.3) can be estimated from eq. (3.4.19) as follows:

$$\delta\, r=(\varepsilon_1^{(0)}/(a^*\lambda))^{-1/3}\sim a^*(\varepsilon_m/(k_b a^*))^{2/3}<<a^*. \tag{3.4.21}$$

If the inequality (3.4.21) is valid, then the method of narrow layer is applicable (see inequalities (3.2.4)). Analysis of eq. (3.4.21) makes the reason to conclude, that the width $\delta\, r$ of SAR region is larger than that of the main AR ceteris paribus.

The characteristic magnitude of the amplitude $E_r^{(\pm 1)}$ of satellite harmonics of radial wave field in the vicinity of SAR can be estimated by the order of magnitude basing on eqs. (3.4.4) and (3.4.21) as follows,

$$E_r^{(\pm 1)}\sim A^{(\pm)}(k_b a^*)^{2/3}/[(N_z+N_b)^2\varepsilon_m^{2/3}]. \tag{3.4.22}$$

The estimation (3.4.22) shows that the amplitudes of the satellite harmonics are smaller than that of the main harmonic even in the vicinity of SAR. That is why they weakly influence on its spatial dependence in this region. The radial dependence $E_r^{(0)}(r)$ can be determined with neglecting the amplitudes $E_r^{(\pm 1,\pm 2)}$ of satellite harmonics even in the vicinity of SAR, since the rigth hand side of eq. (3.4.3) is equal by the order of magnitude to $(\varepsilon_m/(k_b a^*))^{2/3}N_z^2E_r^{(0)}$. This circumstance is applied above to explain the fifth step in the transfer from the set of eqs. (3.14)–(3.18) to (3.4.3)–(3.4.5).

The amplitude $E_r^{(+2)}$ of the second satellite harmonic is known to be the small value out of the SAR region, $E_r^{(+2)}\sim\varepsilon_m E_r^{(+1)}\sim\varepsilon_m^2E_r^{(0)}$ [69]. When approaching to the SAR region the amplitude $E_r^{(+2)}$ increases more rapidly than $E_r^{(+1)}$, namely, $E_r^{(+2)}\propto[\varepsilon_1^{(0)}-(N_z+N_b)^2]^{-2}$. This causes limitation of increase of the first harmonic amplitude. Amplitudes of the satellite harmonics are larger within the SAR region than out of it. One can estimate by the order of magnitude, that $E_r^{(+2)}\sim\varepsilon_m^{1/3}E_r^{(+1)}\sim\varepsilon_m^{2/3}E_r^{(0)}$. Nevertheless, they remain smaller than that of the main harmonic. The significance of this result is explained by the following issue. Before carrying out this detailed analysis, it was natural to expect that the amplitude $E_r^{(+1)}$ of the satellite

harmonic can be larger in the vicinity of SAR than that of the main harmonic, $E_r^{(0)}$. Then one could expect, that the nonlinearity in the respect of the wave amplitude plays a significant role within SAR and/or turbulent absorption of RF power of the satellite harmonic under the condition of linear (in the respect of the wave amplitude) propagation of the main harmonic takes place. However, the results of the presented detailed analysis prove, that even in the vicinity of SAR, the amplitude $E_r^{(+1)}$ of the satellite harmonic remains smaller, than the amplitude $E_r^{(0)}$ of the main harmonic. In other words, the present research proves that the mentioned phenomena are impossible.

The amplitude $E_\vartheta^{(+1)}(r)$ of the first satellite harmonic of the wave azimuthal electric field can be shown to have the logarithmic singularity (3.4.2) when approaching to SAR, $/r-r_s^{(\pm)}/>k_s^{-1}$. This singularity is the weakest, that is why the amplitude $E_\vartheta^{(+1)}$ remains the same by the order of magnitude within the SAR region as out of it, $E_\vartheta^{(+1)}\sim\varepsilon_m E_\vartheta^{(0)}$. Such radial dependence of $E_\vartheta^{(+1)}(r)$ within SAR is similar to that of $E_\vartheta^{(0)}(r)$ within AR.

To make the obtained analytical results more visual, the eq. (3.4.4) should be replaced by the equivalent one:

$$\varepsilon_m^2 y^{(1)}{}'' - x y^{(1)} = \varepsilon_m \,. \tag{3.4.23}$$

The distribution $y^{(1)}(x)$ of the amplitude of the satellite harmonic within SAR is shown in Fig. 3.4.1. The magnitude of the small parameter is chosen to be $\varepsilon_m=0.1$. To analyse the curve $y^{(1)}(x)$ in Fig. 3.4.1 it is appropriate to apply the estimations (3.4.21) and (3.4.22).

The characteristic magnitude of the function $y^{(1)}$ can be estimated from the eq. (3.4.22). It is equal by the order of magnitude $y^{(1)}\sim 0.1^{1/3}=0.464$. The characteristic width of the resonance δx in Fig. 3.4.1 is given by the expression (3.4.21). Its magnitude is equal, $\delta x\sim 0.1^{2/3}=0.215$. These estimations are in good agreement with the behavior of the curve, presented in Fig. 3.4.1.

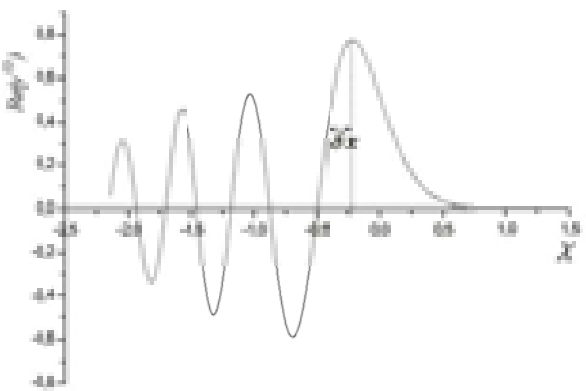

Fig. 3.4.1. Modelling the radial dependence of the amplitude $E_r^{(+1)}(r)$ of the first satellite harmonic in the vicinity of SAR based on the solution to the eq. (3.4.23)

The conditions, under which the fine structure of the local satellite AR is determined just by the weak periodic axial inhomogeneity of $\vec{B}_0$, rather than electron inertia, ion Larmor radius or the plasma particle collisions, are found below. These weak phenomena can be taken into account by the aid of the following replacement in the eq. (3.4.4):

$$\varepsilon_1^{(0)}-(N_z+N_b)^2\rightarrow\varepsilon_1^{(0)}-(N_z+N_b)^2+\sigma. \qquad (3.4.24)$$

The term σ in eq. (3.4.24) reads as:

$$\sigma=i\varepsilon_1^{(c)}+(\varepsilon_T+c^2(N_z+N_b)^2/(\omega^2\varepsilon_3))(d^2/dr^2). \qquad (3.4.25)$$

Electron inertia, ion Larmor radius and the particle collisions are taken into account in the eq. (3.4.24) via the term σ analogously to the case of uniform external static axial magnetic field, presented in [24, 55, 63]. Being in the framework of the method of the narrow layer, the magnitudes of the observables ε_T, ε_3 and $\varepsilon_1^{(c)}$ in the point of SAR are applied here. The term $(i\varepsilon_1^{(c)})$ is presented in the subsection 2.1 in eq. (2.1.2). It takes into account the collisions between the plasma particles [52]. The coefficient ε_T in eq. (3.4.25) is given in the subsection 2.4 (see eq. (2.4.6)). It accounts for the finite ion Larmor radius [49]. Electron inertia is also taken into account in (3.4.25) via the component ε_3 of the plasma permittivity tensor. One can apply the definitions (2.4.1)–(2.4.4) of ε_3, provided in the subsection 2.4 with the replacement $k_z\rightarrow k_z+k_b$.

The influence of the weak periodic inhomogeneity of $\vec{B}_0$ on the fine SAR structure is more important, than that of finite ion Larmor radius and electron inertia, if the following inequality is valid,

$$\varepsilon_m^2>>(k_m a^*)^2(\rho_{Li}/r_s^{(\pm)})^2((N_z\pm N_b)/N_b). \qquad (3.4.26)$$

The condition can be realized in the peripheral plasma, where the periodic axial inhomogeneity of $\vec{B}_0$ is more pronounced, and the plasma is colder, than in the core. The inequality (3.4.26) can be realized even for higher ion temperature, than the similar condition (3.2.19), which takes place in the case of the main AR. The magnitude of the small parameter ε_m is estimated below, under which one cannot neglect the influence of the periodic axial inhomogeneity of the external static magnetic field during studying the conversion of RF waves within SAR in the devices with the parameters, typical for the planned Helias reactor [92] ($\rho_{Li}/a^*=1/30$, $a^*/R=0.1$, here R is the large radius of plasma torus, $\varepsilon_m\sim0.13$, $N=4$). The inequality (3.4.26) becomes as follows, $k_zR<<380$. Hereby, the condition (3.4.26) will be absolutely feasible for such type reactors.

The condition (3.4.26) can be treated as follows. The radial deviation $r-r_s^{(\pm)}$ of the magnetic surface (3.5) from the cylinder with average radius

$r_s^{(\pm)}$ is larger than the characteristic width Δr_T of the SAR region, known for the case of uniform external static axial magnetic field.

The results obtained in the present subsection can be summarized as follows. The influence of the moderate periodic axial inhomogeneity of the bumpy magnetic field $\vec{B}_0$ on the spatial distribution of RF fields in the vicinity of satellite Alfven resonance in plasma with radially inhomogeneous density is analytically studied in the present subsection.

The periodic axial inhomogeneity of the bumpy magnetic field causes the coupling of separate spatial harmonics of electromagnetic field. The amplitude of the second satellite harmonic is negligibly small outside of the SAR region of the first harmonic. However, it increases when approaching in radial direction to the SAR region even more rapidly than that of the first harmonic. It is this increase which removes the singularities of electromagnetic fields of the first satellite harmonic, which takes place under the condition of neglecting the collisions between the plasma particles, electron inertia and ion thermal motion.

The condition (3.4.26) is derived, under which the modulation of the radial component of the external static axial magnetic field influences on the SAR structure stronger, than plasma particle collisions, finite ion Larmor radius and electron inertia. The condition (3.4.26) can be realized in the plasma periphery of large fusion devices, where the deviation of the magnetic surfaces from the circular cylinder is larger and the plasma is colder, than in the core. The region of the local AR is known to move there while the plasma particle density increases, which takes place during plasma production in fusion devices. In particular, the inequality (3.4.26) is valid for the planned parameters of Helias reactor [92]. Ceteris paribus, the modulation of $\vec{B}_0$ can be a little bit smaller within the SAR region to satisfy the inequality (3.4.26) as compared with the modulation of $\vec{B}_0$ within the main local AR, which is necessary to satisfy the inequality (3.2.19).

One can conclude from the research, that the characteristic magnitude (3.4.22) of the radial electric field of the electromagnetic field is smaller, than in the case of uniform external static axial magnetic field, under the condition (3.4.26).

The characteristic width of SAR is larger under the condition (3.4.26), than in uniform external static axial magnetic field ceteris paribus. Radial distribution of RF fields in the vicinity of AR is rather difficult to measure because of the small width of the regions. SARs are more attractive from this point of view – they can be recommended for experimental study since SARs are wider (see (3.4.21)) than the main AR (see (3.2.12)). However, one has to keep in mind, that the characteristic magnitude of the amplitude of the satellite harmonic of the RF wave field is smaller than that of the main harmonic even within SAR.

Since the fine structure of SAR (3.1.3) is studied in the subsection 3.1 for the case of very weakly modulated external static axial magnetic field (when the inequality opposite to (3.4.26) is valid), then the present research generalises the analysis made in 3.1 to the case, if the influence of the

inhomogeneity of the external static magnetic field is comparable with or even stronger, than that of finite ion Larmor radius and electron inertia.

It is periodic inhomogeneity of radial component B_{0r} of the confining magnetic field (rather than weak axial periodic inhomogeneity of axial component B_{0z}) which influences the spatial distribution of the wave RF fields in the vicinity of AR. This circumstance is associated with the fact, that it is radial refractive index, which is singular within SAR in the approach of cold magnetic hydrodynamics.

It should be noted, that the form (3.1) of the confining magnetic field, which contains only one spatial harmonic $\propto sin(k_b z)$, is very simplified. In the reality, the spectrum of the confining magnetic field is rather wide and contains also the harmonic $\propto sin(jk_b z)$, $j=2,3,4...$ Account for the other harmonics of $\vec{B}_0$, which are proportional to $sin(jk_b z)$, gives rise to the next SARs, where $\varepsilon_1^{(0)}=(N_z \pm jN_b)^2$. Analysis of these SARs is not carried out here, since it does not contain anything new in physics as compared with already presented in this subsection.

SECTION 4. CONCLUDING REMARKS

Hannes Olof Gösta Alfvén published his paper [7] about eighty years ago. The date can be considered as that of discovery of Alfven waves. Since that, physics of plasma and controlled fusion has successfully developed both in theory and practical realisation. Nevertheless, the topic of Alfven oscillations is not exhausted. Complicated geometry of the external static magnetic field in fusion traps gives wide possibilities to scientists for searching new branches of Alfven oscilaltions.

Twenty-three years had passed after Alfven discovery before V. V. Dolgopolov and K. N. Stepanov described the fine structure and absorption of MHD waves in the vicinity of the local Alfven resonance [24]. In the paper, the authors had given ground for plasma Alfven heating. Fifty-five years had passed since then. However, the topic is not exhausted. Moreover, been started in the interest of controlled fusion, it is now widely applied also in geophysics of terrestrial space.

The present overview presents fundamentals of Alfven resonance (AR) theory. The theory is generalised with account for special features of periodic spatial inhomogeneity of external static magnetic field of fusion traps, in particular, tokamaks. The most results presented in the second section of the overview are obtained in original papers, written by the author under supervision of Professor K. N. Stepanov and in coauthorship with the colleagues. Fine structures of AR for the main and satellite harmonics are determined. The magnitude of RF power, absorbed in the vicinity of AR, is calculated. The specific features of AR, which are caused by nonmonotonous character of the spatial distributions of the plasma parameters, are established. Novelty of the obtained results is confirmed by the priority in publishing the scientific papers. Their credibility is determined by application of adequate

methods of solving the problems and their reporting at numerous international conferences. The presented results can be applied for planning and explaining the experiments on plasma heating in fusion devices, as well as geophysical experiments.

The main new results, presented in the overview, are as follows. The influence, caused by spatial periodic plasma inhomogeneity, on conversion and absorption of MHD waves is determined here. First of all, the spatial plasma periodic inhomogeneity causes the coupling of spatial harmonics of electromagnetic wave fields. In other words, the waves propagate in such plasma in the form of wave packets.

The possibility of existence, along with AR for the main harmonic, of additional resonance regions (SAR) in the plasma, which is periodically inhomogeneous in the direction of external magnetic field, is established. Rapid increase of the amplitudes of small satellite harmonics of MHD waves and their conversion into small-scale waves takes place within these SARs. The conditions, under which the additional plasma heating in the vicinity of SARs can be significant, are determined.

Singularities of the solutions to Maxwell's equations for the fields of electromagnetic waves, which take place in the case of cold plasma in uniform axial magnetic field, are shown to be suppressed in peripheral plasma of fusion devices by spatial periodic inhomogeneity of external static magnetic field. Herewith, it is shown that the fine structure of the main and satellite ARs can be determined by the modulation δ of the radial component of external static magnetic field (rather than ion thermal motion or finite electron inertia). It should be underlined that RF power absorption in the vicinity of these resonances does not depend on the mechanism of absorption. The characteristic width of the main AR by the order of magnitude reads as

$$\Delta r_T = (\rho_{Li}^2 a^*)^{1/3} \to \Delta r_\delta \sim [\delta^4 a^*/(k_z^2 k_b^2)]^{1/5} \propto \delta^{4/5} . \qquad (4.1)$$

The magnitude of RF power, absorbed within AR in the case if minimum (maximum) is observed on the plasma particle density radial profile, is found to be by $(a^*/\rho_{Li})^{1/2}$ times larger as compared with the case of linear density profile. The increase is explained by the increase of characteristic magnitudes of both the AR width by the factor of $(a^*/\rho_{Li})^{1/6}$ and amplitudes of Alfven wave fields within AR by the factor of $(a^*/\rho_{Li})^{2/15}$. Here a^* is characteristic radial scale of the density inhomogeneity, and ρ_{Li} is ion Larmor radius.

The author considers as a pleasant duty to express sincere gratitude to the corresponding member of the NAS of Ukraine K. M. Stepanov, who taught the plasma theory to the students of the School of Physics and Technology of V. N. Karazin Kharkiv National University (including the author of the present overview) in 1965-2011. Professor K. Stepanov was the supervisor of the author when the latter started studying the influence of spatial periodic plasma inhomogeneity on the properties of MHD waves, prepared the thesis of Candidate of Sciences. Many problems, which solutions are presented in the monograph, were solved either in co-authorship with Professor K. Stepanov or

in the result of discussions with him. The author is also very thankful to Professor Ye. D. Volkov, who was official opponent at the defense of the thesis of Doctor of Sciences by the author, and proposed the idea of writing the present overview. The author is also grateful to other co-authors of the papers, which form the basis for the monograph, e.g., to docent M. R. Belyaev, who taught higher mathematics to the students (including the author of the present overview) of the School in 1971-2009. Docent M. Belyaev proved numerically the coincideness of electromagnetic power absorption in the vicinity of AR in two cases: if AR fine structure is determined by ion thermal motion and by axial periodic inhomogeneity of external static magnetic field. Doctor S. V. Kasilov designed the numerical code, which was used for verification of analytical results of studying the MHD wave absorption within AR, if minimum (maximum) is observed on the radial profile of the plasma particle density. Doctor P. K. Kovtun improved application of local frame of references for solving the Maxwell's equations. Professor V. I. Lapshin taught the author of the overview to study influences of striction nonlinearity and ion cyclotron turbulence on electromagnetic power absorption in the vicinity of SARs in the devices with the bumpy magnetic field.

REFERENCES

[1] Longinov A. V. Radio-frequency plasma heating in tokamaks in the ion-cyclotron frequency range / Longinov A. V. & Stepanov K. N. // In: High-Frequency Plasma Heating, ed. A.G. Litvak, New York: AIP, 1992. – Pp. 93–237.

[2] Yelfimov A. G. Plasma Alfven heating and current drive generation / A. G. Yelfimov, A. G. Kirov, V. P. Sidorov // Radiofrequency plasma heating. Gorkii : IAP AS USSR, 1983. - P. 211-252 (in Russian).

[3] Golant V. E. Radiofrequency methods of plasma heating in toroidal fusion devices / V. E. Golant, V. I. Fedorov. - M. : Energoatomizdat, 1986. - 197 p. (in Russian).

[4] Kolesnichenko Ya. I. generation of noninduction current in a tokamak / Ya. I. Kolesnichenko, V. V. Parail, G. V. pereverzev // Problems of plasma theory. Issue 17. - M. : Energoatmizdat, 1989. - P. 3-156 (in Russian).

[5] Kadomtsev B. B. Essay on the prehistory and development of the main directions of thermonuclear research / B. B. Kadomtsev, S. A. Smirnov // Questions of the history of natural science and technology. - 1981. - V. 1. - P. 35-46 (in Russian).

[6] Spitzer L. The stellarator concept // Phys. Fluids. – 1958. – Vol. 1, no. 1. – Pp. 253–264.

[7] Alfven H. Existence of electromagnetic – hydrodynamic waves // Nature. – 1942. – Vol. 150, no. 3805. – Pp. 405–406.

[8] Allen T. K. Experimental generation of plasma Alfven waves / T. K. Allen, W. R. Baker, R. V. Pyle, J. M. Wilcox // Phys. Rev. Lett. – 1959. – Vol. 2, no. 9. – Pp. 383–384.

[9] Paoloni F. J. Boundary effects on m=0,±1 Alfven waves in a cylindrical, collisionless plasma // Phys. Fluids. – 1975. – Vol. 18, no. 6. – Pp. 640–644.

[10] Equipe TFR, presented Cano R. Experiments on magnetosonic wave excitation in toroidal plasma // 3rd Symposium on plasma heating in toroidal devices. Varenna, Italy, Sep.6-17 (lectures and contributed papers).– 1976.– Pp. 43–49.

[11] Messiaen A. M. Coupling of RF energy in toroidal devices by means of magnetoacoustic resonances / A. M. Messiaen, R. R. Weynants, V. P. Bhatnagar et al. // Proc. of the Joint Varenna-Grenoble International Symposium on heating in toroidal plasmas. Grenoble, July 3–7. – 1978. – Vol. 2. – Pp.229–240.

[12] Stix T.H. Waves in plasmas/ T. H. Stix. – New York : American Institute of Physics (AIP), 1992. – 579 p.

[13] Longinov A. V. Fast magnetosonic wave excitation in large tokamak plasmas / A. V. Longinov, K. N. Stepanov, V. A. Tsurikov // Proceedings of 7-th International Conference on Plasma Physics and Controlled Nuclear Fusion Research. Innsbuck, 1978. Nuclear Fusion Supplement. – 1979. – Vol. 2. – Pp. 583–605.

[14] Kittel C. Introduction to Solid State Physics. Chapter 7: Energy Bands. – John Wiley &Sons, Inc., 1992. – P. 175.

[15] Betti R. Ellipticity induced Alfven eigenmodes / R. Betti, J. P. Freidberg // Phys. Fluids B. – 1991. – Vol. 3, no. 8. – Pp. 1865–1870.

[16]. Betti R. Stability of Alfven gap modes in burning plasmas / R. Betti, J. P. Freidberg // Phys. Fluids B. – 1992. – Vol. 4, no. 6. – Pp. 1465–1474.

[17] Girka I. A. Effect of toroidicity and ellipticity of plasma column on the spectra of MHD waves / I. A. Girka, K. N. Stepanov // Ukrainian Journal of Physics. - 1991. - V. 36, No. 7. - P. 1051-1058 (in Russian).

[18] Yelfimov A. G. Effect of plasma toroidicity on the local Alfven resonance // plasma Physics Reports. - 1988. - V. 14, No. 7. - P. 835 -839 (in Russian).

[19] Cheng C. Z. Low – n shear Alfven spectra in axisymmetric toroidal plasmas / C. Z. Cheng, M. S. Chance // Phys. Fluids. – 1986. – Vol. 29, no. 11. – Pp. 3695–3701.

[20] Rahbarnia K. Alfvénic fluctuations measured by in-vessel Mirnov coils at the Wendelstein 7-X stellarator / K. Rahbarnia, H. Thomsen, J. Schilling et al. // PPCF. – 2020. – Vol. 63, no. 1. – 015005.

[21] Geiger B. Observation of Alfvén Eigenmodes driven by off-axis neutral beam injection in the TCV tokamak / B. Geiger, A. N. Karpushov, P. Lauber et al. // PPCF. – 2020. – Vol. 62, no. 9, 095017.

[22] Kramer G. J. Simulation of the eigenmode spectrum below the Toroidicity-induced Alfvén eigenmode gap generated by the coupling of Alfvén and slow-magnetosonic waves in tokamaks / G. J. Kramer, C. Z. Cheng, M. Podestà, R. Nazikian // PPCF. – 2020. – Vol. 62, no. 7, 075012.

[23] Vaclavik J. Theory of plasma heating by low frequency waves: magnetic pumping and Alfven resonance heating / J. Vaclavik, K. Appert // NF. –1991. – Vol. 31, no. 10. – Pp. 1945–1997.

[24] Dolgopolov V. V. Cerenkov absorption of Alfvén waves and of fast magneto-acoustic waves in an inhomogeneous plasma/ V.V. Dolgopolov, K.N. Stepanov // Nuclear Fusion. - 1965. - T. 5, № 4. - P. 276-278. https://iopscience.iop.org/article/10.1088/0029-5515/5/4/003/pdf

[25] Uberoi C. Alfven waves in inhomogeneous magnetic fields // Phys. Fluids. – 1972. – Vol. 15. – Pp. 1673–1675.

[26] Tataronis J. Decay of MHD Waves by Phase Mixing. I. The Sheet-Pinch in Plane Geometry / J. Tataronis, W. Grossman // Zeitschrift fuer Physik. – 1973. – Vol. 261. – P. 203–216.

[27] Tataronis J. Decay of MHD Waves by Phase Mixing. II. The Theta-Pinch in Cylindrical Geometry / J. Tataronis, W. Grossman // Zeitschrift fuer Physik. – 1973. – Vol. 261. – Pp. 217–236.

[28] Chen L. Plasma heating by spatial resonance of Alfven wave / L. Chen, A. Hasegawa // Phys. Fluids. – 1974. – Vol. 17, no. 7. – Pp. 1399–1403.

[29] Volkov E. D. Confinement of RF heated plasma in the Uragan – 3M torsatron / E. D. Volkov, I. Yu. Adamov, A. V. Arsen'ev et al. // 14th Intern. Conf. on Plasma Physics and Controlled Nuclear Fusion Research. Wuerzburg. – 1992. – Vol. 2. – Pp. 679–688.

[30] Besedin N. T. Numerical simulation of particle and energy transport in Uragan – 3M torsatron / N. T. Besedin, S. V. Kasilov, I. M. Pankratov et al. // IAEA Technical Committee Meeting on "Stellarators and other helical confinement systems". Garching, Germany. – 1993. – P. 277–281.

[31] Lapshin V. I. Singularities of the local MHD – resonances in solar chromosphere plasma / V. I. Lapshin, K. N. Stepanov, E. A. Fedutenko // Proceedings of the Joint Varenna-Abastumani International School & Workshop on Plasma Astrophysics. Varenna, Italy. – 1988. – ESA SP-285, Vol. 1. – Pp. 111–114.

[32] Girka I. O. Enhancement of RF power absorption within the local Alfven resonance when the density profile differs from the linear one (maximum or inflection point) / I. O. Girka, S. V. Kasilov, V. I. Lapshin, K. N. Stepanov // Problems of Atomic Science and Technology. Series: Plasma Physics. NSC "Kharkov Institute of Physics & Technology". Kharkov – 1999. – no. 1, 2. – Pp. 148–150.

[33] Mahajan S. M. Kinetic theory of shear Alfven waves // Phys. Fluids. – 1984. – Vol. 27, no. 9. – Pp. 2238–2247.

[34] Girka I. O. Small scale Alfven waves in the region of maximum (minimum) at the density radial profile between two local Alfven resonances / I. O. Girka, P. P. Rutkevich // Вісник Харківського національного університету ім. В.Н. Каразіна. Серія фізична "Ядра, частинки, поля". – 2001. – № 529, випуск 3. – С. 43–46.

[35] Bellan P. M. Alfven resonance reconsidered: Exact equations for wave propagation across a cold inhomogeneous plasma // PoP. – 1994. – Vol. 1, no. 11. – Pp. 3523–3541.

[36] Moiseenko V. E. A fast wave antenna for ICRF plasma heating // Transactions of Fusion Technology. – 2001. – Vol. 39. – Pp. 65–72.

[37] Elfimov A. G. Results of Localized Alfv´en Wave Heating in TCABR / A. G. Elfimov, E. A. Lerche, R. M. O. Galv˜ao, L. F. Ruchko, A. M. M. Fonseca, R. P. da Silva, V. Bellintani // Brazilian Journal of Physics. – 2004. – Vol. 34, no. 4B. – Pp. 1707–1714.

[38] Moiseenko V. E. Alfvén resonance heating in Uragan-2M torsatron / V. E. Moiseenko, Ye. D. Volkov, V. I. Tereshin, Yu. S. Stadnik // Plasma Physics Reports. – 2009. – Vol. 35, no. 10. – Pp. 828–833.

[39] Cramer N. F. The Alfvén resonance in pair plasmas // PoP. – 2010. – Vol. 17, Issue 2. – Paper 022103 (6 pp).

[40] Stasiewicz K. Small scale Alfvenic structure in the aurora / K. Stasiewicz, P. Bellan, C. Chaston, C. Kletzing, R. Lysak, J. Maggs, O. Pokhotelov, C. Seyler, P. Shukla, L. Stenflo, A. Streltsov, J.-E. Wahlund // Space Science Reviews. – 2000. – Vol. 92. – Pp. 423–533.

[41] Rickard G. J. Alfven resonance excitation and fast wave propagation in magnetospheric waveguides / G. J. Rickard, A. N. Wright // Journal of Geophysical Research. – 1994. – Vol. 99, no. A7. – Pp. 13,455–13,464.

[42] Ofman L. Signatures of Global Mode Alfvén Resonance Heating in Coronal Loops / L. Ofman, J. M. Davila, T. Shimizu // The Astrophysical Journal. – 1996. – Vol. 459. – Pp. L39–L42.

[43] Johnson J. R. Kinetic Alfven waves and plasma transport at the magnetopause / J. R. Johnson, C. Z. Cheng // Geophysical Research Letters. – 1997. – Vol. 24, no. 11. – Pp. 1423–1426.

[44] Mitchell C. Laboratory observation of Alfv´en resonance/ C. Mitchell, S. Vincena, J. Maggs, W. Gekelman // Geophysical Research Letters. – 2001. – Vol. 28, no. 5. – Pp. 923–926.

[45] Molchanov O. A. Ionospheric Alfven resonance at middle latitudes: results of observations at Kamchatka / O. A. Molchanov, A. Yu. Schekotov, E. Fedorov, M. Hayakawa // Physics and Chemistry of the Earth, Parts A/B/C. – 2004. – Vol. 29, Issues 4–9. – Pp. 649–655.

[46] Klimushkin D. Yu. Axisymmetric Alfv´en resonances in a multi-component plasma at finite ion gyrofrequency / D. Yu. Klimushkin, P. N. Mager, K.-H. Glassmeier // Annales Geophysicae. – 2006. – Vol. 24. – Pp. 1077–1084.

[47] Clack C. T. M. On the validity of nonlinear Alfven resonance in space plasma / C. T. M. Clack, I. Ballai, M. S. Ruderman // Astronomy & Astrophysics. – 2009. – Vol. 494. – Pp. 317–327.

[48] Alexandrov A. F. Principles of plasma electrodynamics / A. F. Alexandrov , L. S. Bogdankevich, A. A. Rukhadze // Berlin: Springer-Verlag, 1984. – 490 p.

[49] Akhiezer A. I. Plasma electrodynamics. Vol. 1. Linear theory / A. I. Akhiezer, I. A. Akhiezer, R. V. Polovin, A. G. Sitenko, K.N. Stepanov // Oxford: Pergamon Press, 1975. – 431 p.

[50] Tsushima A. Observation of spatial Alfven resonance / A. Tsushima, Y. Amagishi, M. Inutake // Phys. Letters A. – 1982. –Vol. 88, no. 9. – Pp. 457–460.

[51] Witherspoon F. D. Experimental Observation of the Shear Alfvén Resonance in a Tokamak / F. D. Witherspoon, S. C. Prager, J. C. Sprott // Phys. Rev. Lett. – 1984. – Vol. 53. – Pp. 1559–1562.

[52] Akhiezer A. I. Theory of damping of magnetohydrodynamic waves in a high-temperature plasma/ A.I. Akhiezer, V.I. Lapshin, K.N. Stepanov// Sov. Phys. -JETP. - 1976. - V. 43, No 1. - P. 42-47.

[53] Korn G. A. Mathematical Handbook for Scientists and Engineers / G. A. Korn, T. M. Korn. - Mineola, New York: Dover Publication Ink, 2013. - 1152 p.

[54] Abramovitz M. Handbook of Mathematical Functions with Formulas, Graphs and Mathematical Tables / M. Abramovitz, I. A. Stegun// Nat. Bureau of Standards, Applied Math. Series 55, 1964. – Pp. 771–802.

[55] Girka I. A. Absorption and conversion of long wavelength FMSWs in the region of local resonance in plasma periphery / I. A. Girka, K. N. Stepanov // Ukrainian Journal of Physics. - 1990. - V. 35, No. 11. - P. 1680-1688 (in Russian).

[56] Stepanov K. N. Effect of plasma resonance on surface wave propagation in nonuniform plasma // Soviet physics. Technical physics. - 1965. - V. 35, No. 6. - P. 1002-1014 (in Russian).

[57] Davydova T. A. Modulation instability and arising of solitons under ion-ion resonance // Plasma Physics Reports. - 1990. - V. 16, No. 8 - P. 907-915 (in Russian).

[58] Klima R. The drifts and hydrodynamics of particles in a field with a high – frequency component // Czechoslovak Journal of Physics. – 1968. – Vol. B18. – Pp. 1280–1291.

[59] Lapshin V. I. Excitation of nonlinear kinetic wave in the vicinity of local Alfven resonance / V. I. Lapshin, K. N. Stepanov, V. O. Shtrasser // Plasma Physics Reports. - 1992. - V. 18, No. 5. - P. 660-663 (in Russian).

[60] Silin V. P. parametric influence of high power radiation on plasma / M. : Nauka, 1973. - 288 p.

[61] Girka I. O. Enhancement of RF power absorption within the local Alfven resonance when the density profile differs from the linear one (maximum or inflection point) / I. O. Girka, S. V. Kasilov, V. I. Lapshin, K. N. Stepanov // 6 Ukrainian Conference and School on Plasma Physics and Controlled Fusion, as a section of Conference "Physics in Ukraine". Alushta (Crimea, Ukraine). Book of Abstracts. Published by NSC KIPT. Kharkov. – 1998. – P. 84.

[62] Voloshko A. Yu. Radiofrequency plasma heating in a toroidal trap / A. Yu. Voloshko, V. S. Voitsenya, A. V. Longinov, G. A. Miroshnichenko, G. Ya. Nizhnik, S. I. Solodovchenko // JETP Letters. - 1972. - V. 16, No. 2. - P. 80-83 (in Russian).

[63] Grekov G. L. Excitation of axially nonsymmetrical waves in plasma in presence of local Alfven resonance / D. L. Grekov, K. N. Stepanov, J. A. Tataronis // Plasma Physics Reports. - 1981. - V. 7, No. 4. - P. 752-763 (in Russian).

[64] Kadomtsev B. B. Magnetic traps with bumpy magnetic field // Plasma physics and the problem of controlled thermonuclear reactions. - M. : Publishing house of AS of USSR, 1958. - V. 3. - P. 285 -299 (in Russian).

[65] Ryutov D. D. Open-ended traps/ D. D. Ryutov // Soviet Physics Uspekhi. - 1988, V. 31, No. 4. - P. 300-327.

[66] Baity F. W. Plasma properties and ion heating in EBT-S and hot electron rings at TRW / F. W. Baity, L. A. Berry, L. Bighel et al. // Proceedings of 9th Conference on Plasma Physics and Controlled Nuclear Fusion Research, Baltimore, September 1 – 8, 1982. – 1983. – Vol. 2. – Pp. 185–196.

[67] Fujiwara M. Experimental and numerical studies on plasma confinement in Nagoya Bumpy Torus (NBT) / M. Fujiwara, R. Kamimura, M. Hosokawa et al. // Ibid. – Pp. 197–207.

[68] Beidler C. D. Helias reactor studies / C. D. Beidler, G. Grieger, E. Harmeyer et al. // Preprint MPIPP 2/330. – October 1995. – 21 p.

[69] Girka I. A. Plasma MHD oscillations in bumpy magnetic field / I. A. Girka, K. N. Stepanov // Ukrainian Journal of Physics. - 1992. - V. 37, No. 1. - P. 69 -75 (in Russian).

[70] Girka I. O. How ripples of the Steady Magnetic Field in Tokamaks Influence Propagation, Conversion and Absorption of Alfven and Fast Magnetosonic Waves // Preprint of Max-Planck-Institut fuer Plasmaphysik, 85748 Garching bei Muenchen, FRG. IPP 4/274. – 1996. – 15 p.

[71] Girka I. A. MHD oscillations of plasma torus with elliptical cross-section in bumpy magnetic field / I. A. Girka // Abstracts of the conference "Interaction of electromagnetic radiation with plasma", Dushanbe. - 1991. - P. 146 (in Russian).

[72] Girka I. A. Effect of the periodic axial plasma inhomogeneity on propagation, conversion and absorption of Alfven and fast magnetosonic waves in fusion devices / I. A. Girka, V. I. Lapshin, K. N. Stepanov // International Symposium Plasma '97, «Research and Applications of Plasmas». Invited Papers. – Opole, Poland. – 1997. – Vol. 2. – Pp. 19–26.

[73] Kolesnichenko Ya. I. Alfven continuum and high – frequency eigenmodes in optimized stellarators / Ya. I. Kolesnichenko, V. V. Lutsenko, H. Wobig et al. // PoP. – 2001. – Vol. 8, no. 2. – Pp. 491–509.

[74] Kolesnichenko Ya. I. Alfven eigenmodes in Helias configurations (Part 1) / Ya. I. Kolesnichenko, V. V. Lutsenko, H. Wobig et al. // Preprint MPIPP 3/261. – May 2000. – 65 p.

[75] Kolesnichenko Ya. I. Alfven continuum in stellarators: general analysis and specific examples / Ya. I. Kolesnichenko, H. Wobig, Yu. V. Yakovenko // International Workshop «Innovative concepts and theory of stellaartors». Abstracts. – Kyiv, Ukraine. – 2001. – p. 7.

[76] Kolesnichenko Ya. I. Alfven continuum in stellarators: general analysis and specific examples / Ya. I. Kolesnichenko, H. Wobig, Yu. V. Yakovenko, J. Kisslinger // Scientific Papers of the Institute for Nuclear Research. – 2001. – no. 4. – P. 69–75.

[77] Noterdaeme J.-M. Ion cyclotron resonance frequency heating on ASDEX Upgrade: an overview // Problems of Atomic Science and Technology. – Series: Plasma Physics, no. 1, 2. – Pp. 65–69.

[78] Girka I.O. Plasma Heating near Satellite Alfven Resonances in Confinement Systems with a Ripple Magnetic Field / I. O. Girka, V. I. Lapshin, K. N. Stepanov // Plasma Physics Reports. – 1994. - vol. 20, No. 11. - Pp. 916-922.

[79] Girka I. A. Turbulent plasma heating in satellite Alfven resonances in devices with bumpy magnetic field / I. A. Girka, V. I. Lapshin // Progress in Astronautics and Aeronautics. Progress in Fluid Flow Research: Turbulence and Applied MHD. – 1998. – Vol. 182, no. 63. – Pp. 887–897.

[80] Girka I. O. Alfven wave heating of plasma in devices with bumpy magnetic field / I. O. Girka, V. I. Lapshin, K. N. Stepanov // Contributed Papers. 20th EPS Conference on Controlled Fusion and Plasma Physics. – Lisboa, Portugal. – 1993. – Part 3. – Pp. III-877–III-880.

[81] Girka I. A. Turbulent plasma heating in satellite Alfven resonances in devices with bumpy magnetic field / I. A. Girka, V. I. Lapshin // Abstracts. The Eighth Beer-Sheva International Seminar on MHD-Flows and Turbulence. – Jerusalem, Israel. – 1996. – P. 70.

[82] Dolgopolov V. V. Character of collisionless damping of electromagnetic waves in the region of cold plasma strong inhomogeneity / V. V. Dolgopolov, A. Ya. Omelchenko // Journal of Experimental and Theoretical Physics. - 1970. - V. 58, No 4. - P. 1384-1389 (in Russian).

[83] Sugihara R. Resonance absorption of ICRF waves in edge plasma / R. Sugihara, K. Yamanaka // NF. – 1988. – Vol. 28, no. 12. – Pp. 2161–2169.

[84] Belyaev N.R. Effect of the Periodic Ripple in an Axial Confining Magnetic Field on the Alfven Heating of a Cylindrical Plasma / N. R. Belyaev, I. O. Girka, V. T. Gritsyna // Plasma Physics Reports. – 2003. - Vol. 29, No. 5. – Pp. 399-406.

[85] Girka I. A. Effect of azimuthal magnetic field on the spectra of magnetosonic oscilaltions of a plasma cylinder / I. A. Girka, K. N. Stepanov // Reports of AS of UkrSSR. Series A. - 1990. - No. 3. - P. 66-71 (in Russian).

[86] Girka I. O. Resonant influence of steady magnetic field ripples on the structure of the local Alfven resonance // Contributions to Plasma Physics. – 2001. – Vol. 41, no. 1. – Pp. 33–44.

[87] Girka I. O. Fine structure of the local Alfven resonances in cold plasma placed in bumpy magnetic field // Contributions to Plasma Physics. – 2002. – Vol. 42, no. 5. – Pp. 476–497.

[88] Moiseenko V. E. Local Alfven resonance in axisymmetric toroidal systems // Plasma Physics Reports. - 1986. - V. 2, No. 11. - P. 1376-1378 (in Russian).

[89] Dolgopolov V. V. Local Alfven resonance in toroidal plasma / V. V. Dolgopolov, A. V. Kryukov, S. S. Romanov // Ukrainian Journal of Physics. - 1986. - V. 31, No. 2. - P. 210-217 (in Russian).

[90] Fine structure of local Alfven resonance in periodically inhomogeneous plasma of fusion traps : monograph / I. O. Girka. - Kharkiv : V. N. Karazin Kharkiv national University, 2012. - 179 p. (in Ukrainian).

[91] Timofeev A. V. Plasma Alfven heating in open traps // Plasma Physics Reports. - 1988. - V.14, No. 10. - P. 1266 -1269 (in Russian).

[92] Beidler C. D. Stochastic diffusion of energetic ions in optimized stellarators / C. D. Beidler, Ya. I. Kolesnichenko, V. S. Marchenko et al. // PoP. –2001. – Vol. 8, no. 6. – Pp. 2731–2737.

[93] Karpov S.Yu. Propagation and transformation of electromagnetic waves in one- dimensional periodic structures / S. Yu. Karpov, S. N. Stolyarov // Physics- Uspekhi. – 1993 – Vol. 36, No. 1. – Pp. 1-22.

[94] Longinov A. V. Studying the electromagnetic field distribution in plasma cylinder under excitation of fast magnetosonic wave in the range of ion cyclotron frequency / A. V. Longinov, V. A. Tsurikov // Plasma Physics Reports. - 1990. - V. 16, No. 1. - P. 39-45 (in Russian).

LIST OF ABBREVIATIONS

NF – Nuclear Fusion
Phys. Fluids – Physics of Fluids
Phys. Rev. Lett. – Physical Review Letters
PoP – Physics of Plasmas
PPCF – Plasma Physics and Controlled Fusion

УДК 53.01
PACS numbers: 05.40.-a, 05.45.-a, 52.25.Gj , 52.35.Mw

CHAPTER VI

ELECTROMAGNETIC WAVES IN ARTIFICIAL COMPOSITE MEDIA: A REVIEW

V. I. Fesenko*, D. M. Vavriv*

**Institute of Radio Astronomy, National Academy of Sciences of Ukraine, Mystetstv Str. 4, 61002, Kharkiv, Ukraine*

The electromagnetic waves interaction with composite media attract great attention of researches for many decades due to its relevance to problems in condensed matter physics, optics, photonics, plasmonics, and chemistry. During last two decades, metamaterials and photonic crystals have been in the top of research due to their unprecedented possibilities to manipulate the electromagnetic parameters of both materials and electromagnetic waves. The review is devoted to different types of artificial composite media, their classification, discussion of their unique characteristics and ways of control of their dispersion. Comprehensive review of the electromagnetic properties of periodic and aperiodic planar Bragg reflectors (that is, photonic crystals) and planar Bragg reflective waveguides is carried out. The dispersion features of Bragg reflective waveguides with both periodic and aperiodic arrangements of layers in their claddings are discussed and methods of their control are presented. It was found that an aperiodic configuration of cladding of Bragg reflection waveguide could give rise to exceptionally strong mode selection and tuning the polarization-discrimination effects. On the other hand, artificial media called metamaterials (and especially, hyperbolic metamaterials) created using subwavelength resonant building blocks, are also useful for both controlling light propagation and dispersion management. They can be easily made by alternating dielectric and metal layers or by embedding arrays of parallel metallic rods in a dielectric matrix. This review discusses a particular example of hyperbolic metamaterial, represented by a superlattice consisting of ferrite and semiconductor layers, which is influenced by an external static magnetic field. Within the framework of the effective medium theory, such an artificial structure can be reduced to a homogenized medium, which is described the effective permittivity and permeability tensors. Due to the

components of both tensors show significant sensitivity to the external magnetic field, these artificial structures can exhibit the great variety of high-frequency properties. For instance, it is observed that in the case when specific conditions related to the superlattice's constitutive parameters and filling factor are satisfied, the regions of existence of the bulk and surface polaritons can totally overlap. Besides, it is found out that in an extremely anisotropic medium, the dispersion characteristics of extraordinary bulk waves exhibit a number of unusual behaviors, including atypical topological transitions of isofrequency surfaces. The conditions for appearance of mono-hyperbolic, bi-hyperbolic, tri-hyperbolic and tetra-hyperbolic-like forms of isofrequency surfaces are also discussed.

KEYWORDS: *photonic crystals, metamaterials, superlattices, dispersion characteristics, hyperbolic dispersion.*

PACS numbers: *42.25.Bs, 42.70.Qs, 68.65.Cb, 78.67.Pt*

SECTION 1. INTRODUCTION

In recent years, the special attention has been paid to artificial composite media due to their specific electrodynamic, electro-optical, magneto-optical, polarization, resonance and dynamic characteristics (see, a comprehensive review on theory, methods for fabricating and applications of artificial media in Refs . [1–9]). Artificial composite structures can be characterized by anisotropy (or gyrotropy) of their material parameters, optical activity, significant spatial inhomogeneity, material and structural dispersion, as a result, they exhibit specific electromagnetic characteristics, which cannot be obtained using conventional natural materials.

Despite the significant scientific results obtained since the first half of the last century (see, for example, Refs. [10–15]), in the last years, renewing interest to such media is observed due to the rapid progress in the technologies for their manufacturing and the appearance of new opportunities for experimental investigation of their characteristics. The impetus for the resumption of research in this area was papers of Eli Yablonovitch, John Sajeev and John Pendry. In 1987, Eli Yablonovitch [16] and John Sajeev [17] published the papers, which introduced the term "***photonic crystals***", substantiated the concept of the photonic band-gap (PBG) for the electromagnetic waves in superlattices, and noted that within the spectral region of the complete PBG the spontaneous emission is impossible. In this content we should note that the idea of the analogy of PBG for photons in the photonic crystals spectrum and the energy gap (that is, an energy range in a solid where no electronic states can exist) for electrons in the crystal was firstly proposed by V.P. Bykov in 1972 [18]. In turn, in 1999, John Pendry with colleagues identified a practical way to obtain left-handed materials [19], firstly proposed by V. G. Veselago in 1967 [20] (in this regard, it should be noted that historically, the possibility of obtaining negative refractive index, was firstly analyzed by L. I. Mandelstam in 1945 [21]). Later then, several types of composite media that can be used as ***metamaterials*** were proposed and theoretically investigated [22]. Such

composite structures were formed by a periodic array of thin conductive wires or metal split ring resonators. Theoretical analysis of composites formed by periodically located thin wires has shown that they are characterized the negative value of permittivity in the frequency range close to the plasma frequency [22]. While a design with periodically located split ring resonators demonstrated negative value of magnetic permeability [23]. Experimental papers soon appeared, which confirmed the obtained theoretical results [23, 24]. The metamaterials were firstly obtained in 2000 by the research teams led by David Smith and Richard Shelby of the University of San Diego. At that, Smith experimentally shown the left-handed material which is characterized by simultaneously negative permittivity and permeability at microwave frequencies [23]. Whereas Shelby [24] demonstrated the possibility of arising narrow frequency band with negative refraction index, when left-handed material with unit cell based on the split ring resonator and thin copper wire has been used [24].

It should be especially noted that in the late 60's and early 70's of last century, a group of scientists led by V. G. Veselago made a number of unsuccessful attempts to obtain left-handed materials. In particular, the attempt to obtain an exotic mixture of electric and magnetic charges whose properties were considered in Ref. [25], and the attempt to create a material with a negative refractive index based on a magnetic semiconductor $CdCr_2Se_4$, but this attempts were unsuccessful due to existing technological difficulties. These failures, as well as the lack of known natural left-handed materials led to the fact that the topic of metamaterials remained out of the attention of scientists for more than three decades.

In this brief review, we concentrate our attention on the one-dimensional photonics crystals and metamaterials (including hyperbolic metamaterials) associated with dispersion control, including their theory, constructing methods and possible applications. This paper organized as follow: in section 2, we give short classification of natural and artificial media. Sections 3 and 4 present some ways to the dispersion control in the photonic crystals and metamaterials, respectively. Finally, some conclusions are given in section 5.

SECTION 2. CLASSIFICATION OF NATURAL AND ARTIFICIAL MEDIA

2.1 Classification based on material properties

It is known that an electromagnetic response of a bulk medium depends on the dispersion characteristics of its permeability $\mu(\omega)$ and permittivity $\varepsilon(\omega)$. Using these two fundamental characteristics we can divide natural materials into four large classes:

– Class I with $(\mu > 0) \wedge (\varepsilon > 0)$ comprises most of dielectric materials;

– Class II, with $(\mu > 0) \wedge (\varepsilon < 0)$, corresponds to plasma, metals and doped semiconductors below their plasma frequency ω_p;

– Class III, with $(\mu < 0) \wedge (\varepsilon < 0)$ corresponds to doped magnetic semiconductors in close vicinity of their plasma ω_p and ferromagnetic ω_s resonance frequencies (at that characteristic resonant frequencies should be closely spaced within the same frequency band and $\omega_p > \omega_s$). Here, we should note, that such materials were obtained quite recently (see, for instance, Ref. [26] where possibility of obtaining negative refractive index using $In_{2-x}Cr_xO_3$ magnetic-semiconductor is demonstrated) and usually this group is referred as not accessible to natural materials (see, the review in Ref. [27]));

– Class IV with $(\mu < 0) \wedge (\varepsilon > 0)$ includes gyromagnetic media (i.e., ferrites) in close proximity to ω_s.

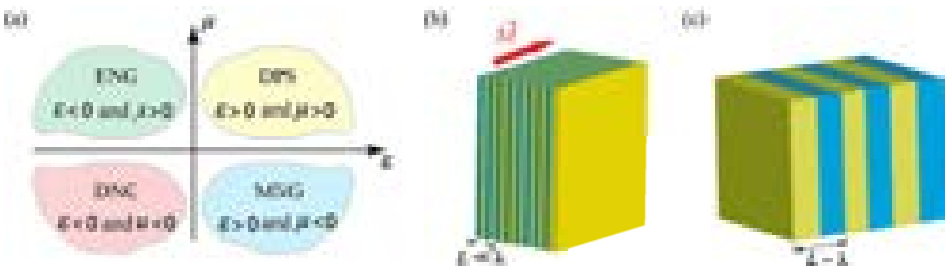

Figure 1. (a) Definition of materials classes according to their material properties. (b, c) Schematic representation of some types of one dimensional artificial periodic structures: (b) metamaterials and (c) photonic crystals

The materials of Classes II-IV are usually called as epsilon-negative (ENG), mu-negative (MNG) and double-negative (DNG) media. While Class I corresponds to double-positive (DPS) media. For clarity, the schematic representation of such materials classifications are presented in Fig. 1(a).

2.2 Classification based on a structural size

According to another classification, all material media can be divided into four main categories depending on their structural size (here, we follow the classification proposed in Ref. [28]).

In order of increasing size scale they are:

– Ordinary materials;
– Mixtures;
– Metamaterials (usually correspond to Classes II-IV);
– Photonic crystals.

Ordinary materials are formed at the molecular level. They are the most common and used as structural elements for the following three categories. In turn, mixtures are a certain combination of conventional materials [29]. They are usually intended to creation of dielectrics with moderate dielectric constant $\varepsilon = 6 \div 20$ [28].

Despite the prevalence of such materials and the simplicity of their manufacturing, their inherent dispersion characteristics are determined by the molecular and atomic structure of the material, which significantly complicates, and sometimes makes it impossible, to manage them [29]. This limitation stimulates the search and implementation of alternative material media and composite structures that can provide flexible control of the dispersion characteristics of electromagnetic waves in a given spectral range.

The term "dispersion" is commonly used for any situation in which the electromagnetic characteristics of the medium change, which leads to a change in the conditions of propagation of electromagnetic waves in this medium compared to free space. There are various types of dispersion, including material, structural, chromatic, spatial, and polarization, which are the most interesting in terms of controlling the dispersion behaviors of electromagnetic waves in the artificial media, such as metamaterials (including metasurfaces) and photonic crystals. It is conditioned by the complex spatial design of such composite media and the variety of materials used as their structural elements.

Metamaterials are artificial composite media (usually periodic, with a period L much shorter than the wavelength λ in the medium, i.e., $L \ll \lambda$ as shown in Fig. 1(b)) formed on the basis of resonant elements, so that their electrodynamic properties are caused not by diffraction phenomena, but are determined by the resonant characteristics of their individual subwavelength elements [4, 27, 28]. This property distinguishes them from another class of artificial periodic structures (in particular structures that exhibit refractive index periodicity), that are called photonic crystals for which the condition $L \sim \lambda$ is satisfied (see, for clarity, Fig. 1(c)), i.e., the lattice spacing is large enough to diffract waves [3, 6].

The spectral and dispersion properties of metamaterials and photonic crystals depend on both the material and geometric parameters of their individual structural elements (that is, layers, rods, wires, rings, etc.) and even more on how they are arranged into a single structure [3, 6, 7, 9, 27, 28]. Namely, they are determined by the simultaneous influence of both material and structural dispersion. This makes it possible to effectively control the spectral and dispersion characteristics of artificial composite media in a wide frequency range.

In following sections, we briefly discuss one-dimensional artificial media such as photonic crystals and metamaterials, their unique characteristics, and ways to control of their dispersion

SECTION 3. ONE-DIMENSIONAL LAYERED STRUCTURES

3.1 Photonic crystals. Spectral behaviors

Photonic crystals are novel class of optical media represents by artificial structures with spatially periodic properties. Their optical properties are similar to the electronic properties of solids (crystals), which provides their

name. Namely, with a certain ratio of geometric and material parameters of the structural elements of photonic crystals, in their spectrum there is a so-called photonic band gap, for which, in the ideal case, propagation of electromagnetic waves is completely inhibited. That is, when an electromagnetic wave with frequency inside the PBG incidents the photonic crystal, it appears to be totally reflected (see, Fig. 2(a)).

From a physical point of view, the formation of PBG occurs due to the destructive interference of waves at the structural boundaries of photonic crystals [6, 7]. Depending on the type of photonic crystals (one-dimensional, two-dimensional or three-dimensional) photonic band-gap can be either partial or complete. Complete PBG occurs in the case of three-dimensional photonic crystals, when radiation incident on the structure from any direction is completely reflected in the opposite direction.

In the case of introducing defects to the strictly periodic structure, within the PBG, high-quality resonant transmission peaks are formed due to the significant localization of the electromagnetic field in structural defects (so-called defect modes) [7], as shown in Fig. 2(b). Thus radiation within defect frequencies can propagate inside the structure. The number of defect modes and their spectral position depend on both the number of defects in the periodic lattice and their spatial location. Consequently, the desired transformation of the spectral response of photonic crystals can be achieved by combining defects of different types (materials, thicknesses and their position in the structure), which allows to effectively control optical and dispersion characteristics of photonic crystals [6, 7, 30]. We should note that, in disordered media, such a process is called Anderson localization of light.

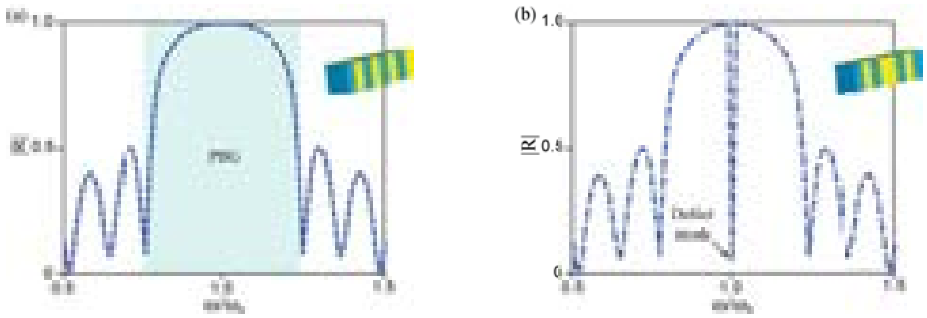

Figure 2. Typical reflectance spectra of (a) strictly periodic structure and (b) photonic crystal with a single defect layer. Shaded region corresponds to the PBG. ω_0 is the central frequency which corresponds to the Bragg wavelength λ_{Br}

Spatial modulation of the refractive index of photonic crystals leads to the appearance of some unusual and practically important effects. In particular, the group and phase velocities of light is significantly reduced (more than an order of magnitude) at the PBG edges compared to their magnitudes outside the PBG. Thus, the photonic-crystal devices are very attractive for generating

slow light [31]. In addition, a significant decrease in the group velocity of wave packets at the PBG edges leads to a significant increase in the photon density of states within the structure, such effect is particularly desirable for applications where nonlinear optical transformations are required [32].

The most common example of the one-dimensional photonic crystal is the Bragg reflector, as shown in Fig. 1(c). At that, usually a quarter-wave design of the reflector is used, in which optical thicknesses of layers correspond to one quarter of the chosen wavelength. Despite the simplicity of the structure, due to its specific dispersion characteristics, this artificial medium is widely used in different devices from microwave to optical ranges such as mirrors of vertical cavity surface emitting lasers (VCSEL) [33], periodic and aperiodic layered claddings of optical waveguides [34–37], chromatic dispersion compensators [38], omnidirectional reflectors [39, 40], CWDM demultiplexers, and etc.

3.2 Dispersion characteristics of Bragg reflection waveguides

Of considerable practical interest is the use of the Bragg reflectors in the area of integrated optics, in particular in the design of planar waveguides (so-called, Bragg reflection waveguides). It is known, that conventional three-layer planar waveguides usually act as connecting nodes (paths) in integrated optical circuits, while Bragg reflection waveguides, due to their specific spectral and dispersion characteristics, are directly used in the construction of active and passive integrated optical devices [42–45]. In particular, devices that combine characteristics of waveguides and Bragg reflectors can be used as polarization splitter or combiner [42], high-efficiency all-optical diodes [43], adaptive dispersion compensators [44], accelerators [45], and etc.

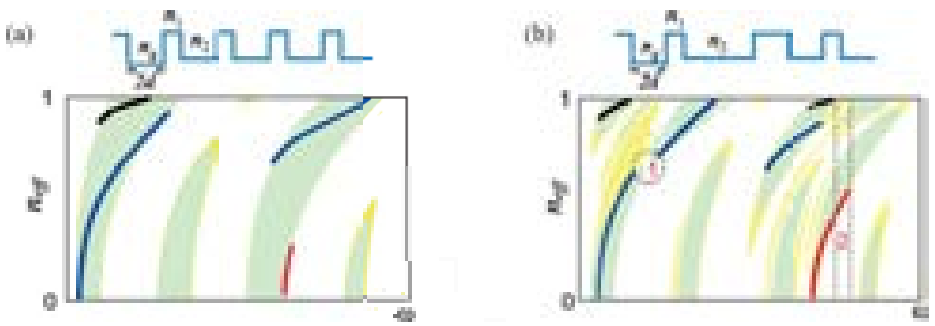

Figure 3. Typical band diagrams (the colored regions correspond to PBGs with level of reflection $|R| > 0.9$) and dispersion curves (the case of TE waves is considered) in the Bragg reflection waveguides with (a) periodic and (b) aperiodic cladding (see, for instance, [34 – 37]). The dispersion curves of the different colors correspond to guided modes with different mode index: $m = 0$ (blue), $m = 1$ (red) and $m = -1$ (black). Here, $d_g = 2d$ is thickness of the guiding layer, n_1, n_2 and n_g are refractive indices of the constitutive layers of the cladding and the guiding layer, respectively

An ordinary Bragg reflection waveguide consists of a low-index guiding layer sandwiched between two identical Bragg reflectors [41], and its distinctive characteristics is conditioned by a multilayered configuration of composite cladding. For clarity, the refractive index profile in the cross-section of waveguide is presented in the insert of Fig. 3(a). Due to the existence of PBGs in the spectra of the multilayered cladding, light is confined within the low-index core with a refractive index below the effective refractive index of the cladding (that is, $n_g < n_2 < n_1$; the core is usually considered to be an air gap with $n_g = 1.0$ [41, 46]). This method of localization of guided modes in the waveguide core has a number of significant advantages over the method of the total internal reflection inside a high index core, which is inherent in standard (three-layer) optical waveguides [47]. In particular, due to the fact that electromagnetic radiation is mostly propagates in the air layer both the power losses and the influence of nonlinear effects on the waves propagation can be significantly reduced.

In a one-dimensional case, the transfer matrix formalism is widely used to solve the problem. As a result, the dispersion characteristics of TM and TE modes of the Bragg reflection waveguides can be obtained from following equation [36, 37]:

$$1 - R^2 \exp\left[4ik_0 d_g \left(n_g^2 - n_{eff}^2\right)^{1/2}\right] = 0, \qquad (1)$$

where $n_{eff} = \beta / k_0$ is the effective mode index, β is the longitudinal propagation constant, $k_0 = \omega / c$ is the wave number in free space, R is the reflection coefficient of the cladding, $d_g = 2d$ and n_g are thickness and refractive index of the core layer, respectively.

As typical examples in Figs. 3(a) and 3(b), we demonstrate the band diagrams and dispersion curves that were calculated using Eq. (1) for Bragg waveguides with periodic and aperiodic configurations of claddings (with finite number of the constitutive layers), respectively.

Even in the simplest symmetric configuration of planar Bragg reflection waveguide, a number of unique dispersion characteristics, which cannot be obtained in a conventional planar waveguides can be observed, as shown in Fig. 3(a). In particular, it can be noted [37, 41, 48, 49]: each guided mode has several cutoff frequencies, it allows to design waveguides which support only higher-order modes, instead of the fundamental one (see, Region 2 in Fig. 3(b)); there is a possibility of suppression of unwanted mode in the required frequency ranges by shrinking PBG into point (see, Region 1 in Fig. 3(b)); the appearance of a special class of modes with a negative mode index ($m = -1$) is possible in waveguide structure which core layer is thin enough.

On the other hand, the dispersion characteristics of the Bragg waveguide can be significantly modified by selecting specific designs of its cladding, on today, the following optimization methods have been proposed: the use of asymmetric claddings based on two different Bragg reflectors with different spectral characteristics [34, 35]; introducing defect layer into Bragg reflectors

[50]; layers chirping in the cladding [50, 51], and placing matching layers between the core and layered cladding [52]. Besides, authors of this review have recently proposed another, more effective method of optimizing both the dispersion and spectral characteristics of Bragg reflection waveguide, which is based on the using aperiodic layered claddings in the waveguide design [36, 37]. It was shown that in the aperiodic configuration, the dispersion curves have more cutoff points for each mode than those of periodic one [36, 37]. It means that Bragg reflection waveguides with aperiodic cladding are easier to be optimized than that ones with periodic cladding to support propagation of desired modes only. Thus, it could give rise to exceptionally strong mode selection and tuning the polarization-discrimination effects, and can be used in the integrated optic devices that are designed for mode selection, adaptive dispersion compensation, frequency and polarization filtering

As most of the characteristics of the planar Bragg waveguides are similar to those of the cylindrical Bragg fibers, we argue that obtained results are also applicable for the prediction of optical features of the latter ones.

Not only the problem of passive control of the dispersion characteristics of electromagnetic waves interacting with media is important, but even more, the task of active control of them. To solve this problem in the design of photonic crystals (and devices based on their basis) usually use active media, such as ferrites, semiconductors or graphene. Such media can change their properties under external influence (for example, when the temperature changes or under the action of electric and magnetic fields), which provides additional opportunities to control a wide range of their characteristics (including dispersion) and significantly expand their functional potential, see for example [53, 54]. In particular, the possibility of effective control of the spectral characteristics of a magneto-photonic crystal by changing the magnitude of the external magnetic field was experimentally demonstrated in [53], and it was proposed to use such a structure as a polarizing element. In addition, the characteristics of a planar waveguide formed on the basis of a half-wave magneto-optical layer located between two isotropic Bragg reflectors were investigated in Ref. [54]. The authors of this paper indicated the possibility of excitation of hybrid plasmon waves localized in a layered claddings, which leads to additional resonances in optical spectra and enhancement of magneto-optical effects. In turn, the polarization filtration of TE and TM modes in a planar waveguide based on a magneto-optical layer placed on a dielectric substrate and combined with a one-dimensional photonic crystal is considered in [55, 56]. In addition, active structures are used to create distributed feedback lasers [57], optical amplifiers [58], and many other integrated optics devices.

SECTION 4. METAMATERIALS

4.1 Multilayer metamaterial structures. Effective medium theory

In modern devices of photonics and plasmonics, composite artificial media (that is, metamaterials and metasurfaces) based on subwavelength

structural elements are often used as active media [59]. A particular example of such metamaterials is a superlattice consists of ferrite and semiconductor layers, which is influenced by an external static magnetic field $\vec{M}$, as shown in Fig. 1(b).

Given the fact that metamaterials are composed by subwavelength elements (i.e., all characteristics dimensions of structure are much smaller than the wavelength in the corresponding parts of the structure) they can be described in the framework of the effective medium theory. From the physical point of view, this theory allows to replace an artificial composite medium by its equivalent continuous (homogenized) medium, which can be described by the tensors of relative effective permittivity $\hat{\varepsilon}_{eff}$ and relative effective permeability $\hat{\mu}_{eff}$. Due to the resonant characteristics inherent in the individual elements (building blocks) of metamaterials, their effective material parameters demonstrate a significant dispersion, and can be characterized by the presence of frequency ranges with negative values of effective permittivity as well as permeability. For clarity, typical dispersion characteristics of the tensor components of relative effective permeability $\hat{\mu}_{eff}$ and relative effective permittivity $\hat{\varepsilon}_{eff}$ for a biaxial bigyrotropic medium are presented in Fig. 4(a) and Fig. 4(b), respectively.

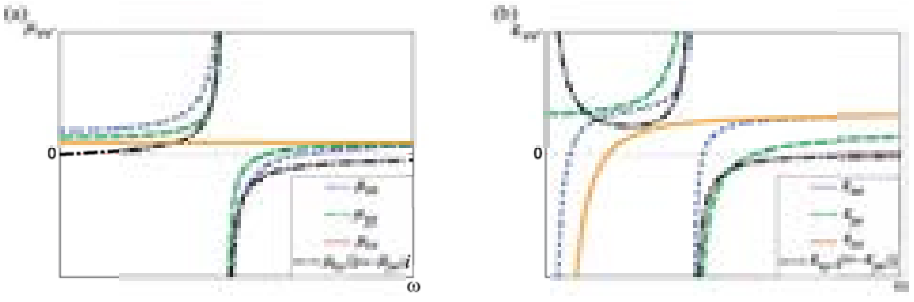

Figure 4. Typical dispersion curves of the tensor components of (a) relative effective permeability $\hat{\mu}_{eff}$ and (b) relative effective permittivity $\hat{\varepsilon}_{eff}$ for a biaxial bigyrotropic crystal [60]. Here v, v' iterates over x, y and z

Building blocks (i.e., layers) with different physical properties, such as dielectrics, semiconductors [61] and ferrites [62], are usually using in the formation of superlattices. In the presence of an external static magnetic field, the electrodynamic characteristics of such a gyroelectromagnetic medium are determined by two tensors: the tensor of the effective permittivity $\hat{\varepsilon}_{eff}$ and effective permeability $\hat{\mu}_{eff}$. As a result, the dispersion characteristics of electromagnetic waves propagating in such a medium are determined by different combinations of components of these tensors. Due to the components of both tensors show significant sensitivity to the external magnetic field, these artificial structures can exhibit the great variety of high-frequency properties [63]. Thus, studying dispersion characteristics of bulk and surface

electromagnetic waves in such metamaterials, and in particular the dispersion characteristics of surface polaritons at the interface of the layered metamaterial/free medium is very important task.

Surface polaritons are a special type of electromagnetic waves propagating along the interface between two media, which are characterized by different signs of material parameters (e.g., permittivity and permeability). In particular, this situation is typical for a metal/dielectric interface [64]. It is known, that surface waves are strongly localized at the interface and penetrate into the surrounding media over a distance approximately equal to the wavelength in the corresponding material [64, 65]. This significant localization of the electromagnetic field in a small spatial volume beyond the diffraction limit leads to a significant increase in the interaction of the electromagnetic field with matter (medium) and makes attractive the using surface waves in a wide range of practical applications: from microwave and optical devices to solar cells [66 – 68]. Moreover, the study of the dispersion characteristics of surface waves has significant potential in terms of solid state physics, because their nature can provide detailed information about the quality of the interface and the material parameters (such as permittivity and permeability) of media located on both sides of the interface [68]. High sensitivity to the electromagnetic properties of the medium allows the use of surface waves in the sensing applications, in particular in sensors of chemical and biological substances [67]. Thus, the study of the dispersion characteristics of surface waves is essential task for both physics of surfaces and physical optics; in the latter case, these activities have led to the formation of a new direction of research: plasmonics [59, 65, 68].

Nowadays, plasmonics is a field that is developing extremely fast and is characterized by a variety of possible practical applications, for many of which the ability to control the propagation of surface waves is a crucial characteristic. In particular, in recent decades, significant efforts have been made to implement active components (which can be reconfigured) for integrated plasmonic systems, such as switches, active couplers, modulators, etc. [69]. In this regard, the search for effective ways of controlling the characteristics of the propagation of plasmon-polaritons due to the influence of external factors is an extremely important task.

To date, it has been proposed to use nonlinear, thermo-optical and electro-optical effects in plasmonic devices to control the propagation of plasmon-polaritons [70 – 72]. In such devices, the control of the dispersion characteristics of the electromagnetic waves occurs by changing the dielectric constant of the medium by applying an external electric field or by adjusting the temperature of the material. At the same time, the use of an external magnetic field as a driving agent to control the distribution of polaritons is more promising, because such external influences can change both the permeability of ferrites and the permittivity of metals and semiconductors. It should be noted that the uniqueness of this control mechanism is that the dispersion characteristics of polaritons depend not only on the magnitude of the applied external magnetic field, but also on its direction. For example, the external

magnetic field creates additional dispersion branches in the spectra of surface magnetic plasmon-polaritons what leads to the possibility of obtaining a multi-band propagation, which may be accompanied by non-reciprocal effects [62 – 64, 73 – 78]. Thus, the combination of plasmon and magnetic functionality opens a wide prospect of creating new active devices, which are characterized by additional degrees of freedom to control the dispersion characteristics of plasmon-polaritons. Such systems have already found a number of practical applications in integrated photonics and telecommunication systems (see, for example, [68] and references therein).

In this context, using superlattices consisting of layers of different materials, alternating with each other according to a given law, which are able to provide combined plasmonic and magnetic functionality, instead of traditional plasmons systems, where a metal-dielectric interface is assumed, has a significant practical potential [66]. In particular, this is because the superlattices show a number of exotic electronic and optical properties unattainable for homogeneous (bulk) media, due to the presence of additional periodic potential with the period, which exceeds the lattice constant [75]. An external static magnetic field applied to the superlattice leads to the appearance of so-called magneto-plasmon-polariton excitations [64]. The properties of magnetic polaritons in superlattices of different types under the action of an external static magnetic field have been studied by many teams over the past few decades (in particular, see [62, 63, 73–78]). It should be noted that the problem was usually considered within two separate approximations, namely, results were obtained for gyroelectric media with magneto-plasmons [61, 75] and gyromagnetic media with magnons [62, 74, 76, 77], which are characterized by either a permittivity or permeability tensor having non-zero off-diagonal elements. The application of this approach is generally justified due to the fact that the resonant frequencies of the magnetic permeability of magnetic materials are usually in the microwave range, while the characteristic dielectric permeability frequencies of semiconductors are usually in the infrared range of the electromagnetic wave spectrum.

At the same time, it is obvious that the combination of magnetic and semiconductor materials into a single gyroelectromagnetic superlattice, in which both the permeability and permittivity are tensors, provides additional opportunities in controlling dispersion characteristics of surface waves using an external magnetic field what is unattainable in separate both gyromagnetic and gyroelectric media [78–85]. Obviously, it is possible to create heterostructures in which the characteristic resonant frequencies of semiconductor and magnetic materials may be different, but closely spaced within the same frequency range. As an example, we can mention the heterostructures proposed in [60, 78, 81–85], which show a gyroelectromagnetic effect in the range from GHz to tens of THz, in a result the electromagnetic waves in such superlattices demonstrate some unusual properties. For instance, extraordinary dispersion features of both bulk and surface electromagnetic waves in finely stratified magnetic-semiconductor superlattice which is influenced by an external static magnetic field in the both polar and Voigt geometries have been recently reported in

papers [60, 78, 86]. Namely, it was observed that in case when specific conditions related to the superlattice's material and geometric parameters are satisfied, the regions of existence of the bulk and surface polaritons overlap (for clarity, see, Figs. 3, 4 in Ref. 78 and Fig.4 in Ref. 86). Such peculiarities can give great advantages when providing excitation of surface polaritons via nonlinear coupling [78].

An effective way to analyze the dispersion of electromagnetic waves in composite artificial media is to study their isofrequency surfaces (so-called Fresnel surfaces) [87, 88]. This is especially true for hyperbolic metamaterials, which have been the subject of intensive study due to their inherent specific dispersion characteristics unattainable in ordinary natural media (a detailed review of the general theory and applications of hyperbolic materials is given in Refs. [89–100]).

To date, hyperbolic materials have been implemented in devices operating in the microwave, terahertz, and optical ranges, and a variety of their specific properties have been demonstrated, such as: negative refraction [90], significant enhancement of spontaneous emission [91], subwavelength imaging [93], subwavelength focusing [94], signal routing [95], and many others.

4.2 Hyperbolic metamaterials

Hyperbolic dispersion is inherent to the so-called extremely anisotropic media, which are also known as indefinite media [96–100]. In such media, at least the magnetic or dielectric constant is a tensor quantity:

$$\hat{\eta} = \left[\eta_{xx}, 0,0;\ 0, \eta_{yy}, 0;\ 0,0, \eta_{zz}\right], \quad (\eta = \varepsilon,\ \mu), \tag{2}$$

and one of the diagonal (that is, principal) components of the tensor $\hat{\eta}$ (real part) differ in sign from other diagonal components. The medium is called a hyperbolic uniaxial crystal or a hyperbolic biaxial crystal, when the tensor's principal components η_{ii} $(i = x, y, z)$ satisfy the next conditions:

- $\eta_{xx} < 0 < \eta_{yy} = \eta_{zz}$ – hyperbolic uniaxial crystal;
- $\eta_{xx} < 0 < \eta_{yy} < \eta_{zz}$ – hyperbolic biaxial crystal.

In such media, topological transitions of the isofrequency surface occur when the real part of one of the components of the dielectric or magnetic permeability tensor changes its sign to the opposite (see, for example, Fig. 4).

As a rule, the hyperbolic dispersion is observed in nonmagnetic metamaterials, which are characterized by an indefinite permittivity tensor, while their permeability is a scalar quantity ($\mu_{xx} = \mu_{yy} = \mu_{zz} = 1$). The negative value of the permittivity is a common property of metals in the spectral range near their plasmon resonance frequency, thus hyperbolic metamaterials usually include metal components. In this case, the metamaterials are designed either in the form of a superlattice, which combines metal and dielectric layers [101–103] or in the form of an array of

conductive rods immersed into a dielectric medium [104–107]. Besides, hyperbolic metamaterials can be obtained using media with an indefinite permeability tensor and such property was at first demonstrated for metamaterials composed on the basis of metallic slit-ring resonators [19].

Hyperbolic dispersion is also inherent for some natural media that exhibit gyroelectric (that is, plasma or semiconductors) or gyromagnetic (that is, ferrites) properties when they are under the influence of an external static magnetic field [108–112]. In the case when such media are magnetized to saturation, they become extremely anisotropic in some frequency band near plasmon or ferromagnetic resonances [113–115]. This results in a hyperbolic shape of the isofrequency surfaces for extraordinary waves, while the isofrequency surface of ordinary waves remains unchanged and has a form of closed ellipsoid.

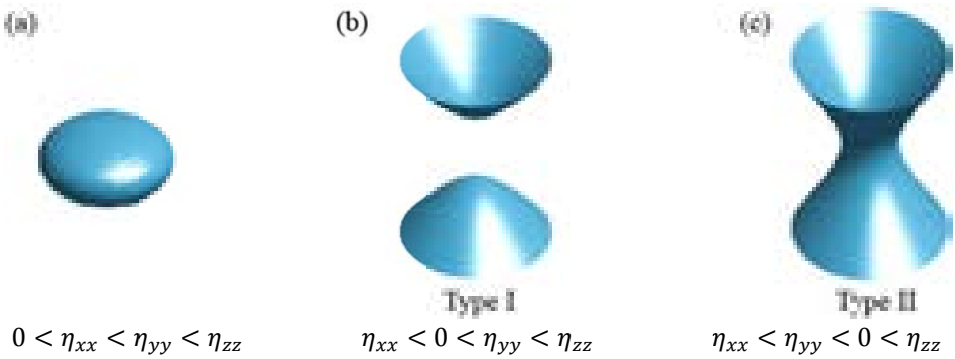

Figure 5. Typical topologies of the isofrequency surfaces of the electromagnetic waves in an extremely anisotropic medium [78]: (a) closed ellipsoid; (b) hyperboloid type I; (c) hyperboloid type II

4.3 Topological transitions of the isofrequency surfaces

In the general case of a biaxial gyroelectric or gyromagnetic medium there are topological transitions of the isofrequency surface for the extraordinary waves from a closed ellipsoid with $\eta_{xx} < \eta_{yy} < \eta_{zz}$ to the open asymmetric/symmetric hyperboloid type I with $\eta_{xx} < 0 < \eta_{yy} < \eta_{zz}$ or asymmetric/symmetric hyperboloid type II with $\eta_{xx} < \eta_{yy} < 0 < \eta_{zz}$ are possible [88, 116], see, for clarity Fig. 5.

At the same time, it was recently demonstrated [78 – 86], that the semiconductor and magnetic materials combined into a unified gyroelectromagnetic superlattice with tensor like forms of both permittivity and permeability give additional opportunities for manipulation of the dispersion of bulk as well as surface waves. In the long-wavelength limit, such a finely stratified structure can be equivalently represented by homogenized medium in which all principal components of both constitutive tensors are different (that

is, $\eta_{xx} \neq \eta_{yy} \neq \eta_{zz}$) and their off-diagonal components are non-zero values (that is, $\eta_{xy} = -\eta_{yx} \neq 0$). Such a situation is corresponds to the case of biaxial bigyrotropic crystal. Two axes of anisotropy are due to simultaneous effect of both the influencing external static magnetic field and the periodicity of the structure. The simultaneous presence of two axes of anisotropy as well as gyrotropy leads to some specific distortions of the isofrequency surface of the extraordinary bulk waves. In particular, in such a homogenized medium the topological transition from a closed ellipsoid to open type I and type II hyperboloids as well as a bi- and terta-hyperboloids are observed [116, 117] (for additional information, see, Fig. 2 in Ref. [116] and Fig. 3 in Ref. [117], as well as Fig. 6 in this paper).

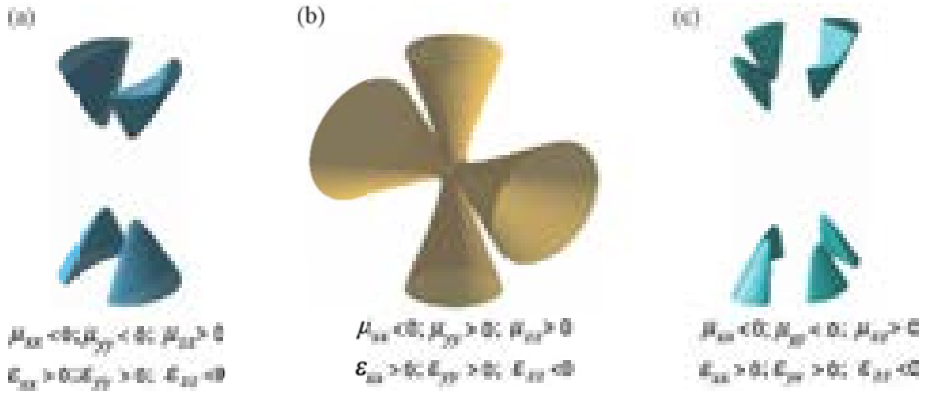

Figure 6. Topological forms of the isofrequency surfaces related to the extraordinary waves propagating trough biaxial gyroelectromagnetic medium [117]: (a, b) bi-hyperbolics (c) tetra-hyperbolic

The complete taxonomy of isofrequency surfaces that can be realized in uniaxial anisotropic and biaxial bianisotropic optical materials, includes following (for obtaining extra information, see, Refs. [80, 116 – 120]):

- Tetra-hyperbolic (Fig. 6 (c));
- Tri-hyperbolic (see, Fig. 3(a) in Ref. [80]);
- Bi-hyperbolic (Figs. 6(a, b));
- Mono-hyperbolic (Figs. 5(b, c));
- Non-hyperbolic (that is, closed ellipsoid or toroid; Fig. 5(a)).

The most important property of hyperbolic metamaterials is related to behavior of electromagnetic waves with large values of the wavevector (so-called, high-k waves). In a vacuum, such waves are evanescent and decay exponentially. However, in lossless hyperbolic media, the high-k waves can propagate without attenuation due to the open form of the isofrequency surface.

The ability of hyperbolic materials to maintain high-k waves leads to some unusual effects, including, a significant enhancement of spontaneous emission [91, 121], infinite density of states [92], the ability to control the direction of wave propagation [95, 122], the photonic spin Hall effect

[123, 124], abnormal scattering [125], subwavelength focusing [126], and many others. These properties are of considerable practical interest and make hyperbolic materials promising media for use in devices of micro- and nano-electronics, photonics and plasmonics, which in turn requires the development of new effective methods for their analysis.

SECTION 5. CONCLUSIONS

One dimensional photonic crystals and metamaterials exhibit many extraordinary properties such as, negative-refraction, slow light, abnormal scattering, and subwavelength focusing phenomena. In the last two decades, they have been widely studied with implementations based on different artificial and natural media. Especially, the great interest has been attracted to the hyperbolic metamaterials due to unusual nature of the isofrequency surface of electromagnetic waves propagating through such structures. The fascinating characteristics of hyperbolic metamaterials is associated with hyperbolic dispersion. Due to the extraordinary properties of photonic crystals and hyperbolic metamaterials, it can be expected that many new photonics and plasmonics devices will soon be developed on their basis.

REFERENCES

[1] Quevedo-Teruel, O., Chen, H., Díaz-Rubio, A., Gok, G., Grbic, A., Minatti, G., ... & Zheludev, N. I. (2019). Roadmap on metasurfaces. Journal of Optics, 21(7), 073002.

[2] Kuznetsov, A. I., Miroshnichenko, A. E., Brongersma, M. L., Kivshar, Y. S., & Luk'yanchuk, B. (2016). Optically resonant dielectric nanostructures. Science, 354 (6314).

[3] Johnson, S. G., & Joannopoulos, J. D. (2001). Photonic crystals: the road from theory to practice. Springer Science & Business Media.

[4] Serebryannikov A. E., Colak E., Petrov A., Usik P.V., Ozbay E. (2016). Multifrequency spatial filtering: A general property of two-dimensional photonic crystals, Photonics and Nanostructures - Fundamentals and Applications, 18, 1–9.

[5] Khizhnyak, N.A., Ryazantseva, N.V., Yachin, V.V. (2021). The scattering of electromagnetic waves by a periodic magnetodielectric layer Journal of Electromagnetic Waves and Applications, 10(5), 731–739.

[6] Joannopoulos J. Photonic crystals: molding the flow of light / J. Joannopoulos, R. Meade, J. Winn – Princeton: Princeton University, 1995. 137 p.

[7] Sakoda K. Optical properties of photonic crystals / K. Sakoda. – Berlin: Springer, 2001. – 223

[8] Lyubchanskii, I. L., Dadoenkova, N. N., Lyubchanskii, M. I., Shapovalov, E. A., & Rasing, T. (2003). Magnetic photonic crystals. Journal of Physics D: Applied Physics, 36(18), R277.

[9] Brener, I., Liu, S., Staude, I., Valentine, J., & Holloway, C. (Eds.). (2019). Dielectric Metamaterials: Fundamentals, Designs and Applications. Woodhead Publishing.

[10] Brown, J. Artificial dielectrics having refractive indices less than unity. Proceedings of the IEE Part IV: Institution Monographs. 1953. vol. 100 , 5, 51 – 62.

[11] W. Rotman. Plasma simulation by artificial dielectrics and parallel-plate media, IEEE Trans. Antennas Propag. 1962. vol. 10, 82-95 .

[12] Rytov S.M. Electromagnetism of finely stratified media. JEPT, 1956. vol.2, 5, 606-615.

[13] Yeh, P., Yariv, A., & Hong, C. S. (1977). Electromagnetic propagation in periodic stratified media. I. General theory. JOSA, 67(4), 423-438.

[14] Yariv, A., & Yeh, P. (1977). Electromagnetic propagation in periodic stratified media. II. Birefringence, phase matching, and x-ray lasers. JOSA, 67(4), 438-447.

[15] Bulgakov, A. A. (1985). Surface acoustic oscillations in a periodically layered medium. Solid State Communications, 55(10), 869-872.

[16] Yablonovitch, E. (1987). Inhibited spontaneous emission in solid-state physics and electronics. Physical Review Letters, 58(20), 2059.

[17] John, S. (1987). Strong localization of photons in certain disordered dielectric superlattices. Physical Review Letters, 58(23), 2486.

[18] Bykov V.P. Excited molecules in a medium with negative dielectric constant. JETP. 1972. vol. 62: 505.

[19] Pendry, J. B., Holden, A. J., Robbins, D. J., & Stewart, W. J. (1999). Magnetism from conductors and enhanced nonlinear phenomena. IEEE Transactions on Microwave Theory and Techniques, 47(11), 2075-2084.

[20] Veselago V.G. The electrodynamics of substances with simultaneously negative values of ε and μ. Sov. Phys. Usp. 1968. Vol. 10, 509.

[21] Mandelstam, L. I. (1945). Group velocity in a crystal lattice. Zhurnal Eksperimental'noi I Teoreticheskoi Fiziki, 15(9), 475 – 478.

[22] Pendry, J. B. (2000). Negative refraction makes a perfect lens. Physical Review Letters, 85(18), 3966.

[23] Smith, D. R., Padilla, W. J., Vier, D. C., Nemat-Nasser, S. C., & Schultz, S. (2000). Composite medium with simultaneously negative permeability and permittivity. Physical Review Letters, 84(18), 4184.

[24] Shelby, R. A., Smith, D. R., & Schultz, S. (2001). Experimental verification of a negative index of refraction. Science, 292(5514), 77-79.

[25] Minakov, A.A., Vinogradova, G.I., Golant, K.M., Makhotkin, V.E., Veselago, V.G. (1977). Effect of doping on the exchange interactions in the magnetic semiconductor CdCr2Se4.Sov Phys Solid State, 1977. vol. 19 (7), 1214–1215

[26] Kussow, A. G., & Akyurtlu, A. (2008). Negative refraction index in the magnetic semiconductor $In_{2-x}Cr_xO_3$: Theoretical analysis. Physical Review B, 78(20), 205202.

[27] Xiao, S., Wang, T., Liu, T., Zhou, C., Jiang, X., & Zhang, J. (2020). Active metamaterials and metadevices: a review. Journal of Physics D: Applied Physics, 53(50), 503002.

[28] Rumpf, R. C. (2015). Engineering the dispersion and anisotropy of periodic electromagnetic structures. In Solid State Physics (Vol. 66, pp. 213-300). Academic Press.

[29] Sihvola, A. (2000). Mixing rules with complex dielectric coefficients. Subsurface Sensing Technologies and Applications, 1(4), 393-415.

[30] Fesenko, V. I. (2014). Aperiodic birefringent photonic structures based on Kolakoski sequence. Waves in Random and Complex Media, 24(2), 174-190.

[31] Gersen, H., Karle, T. J., Engelen, R. J. P., Bogaerts, W., Korterik, J. P., Van Hulst, N. F., ... & Kuipers, L. (2005). Real-space observation of ultraslow light in photonic crystal waveguides. Physical Review Letters, 94(7), 073903.

[32] Scalora, M., Bloemer, M. J., Manka, A. S., Dowling, J. P., Bowden, C. M., Viswanathan, R., & Haus, J. W. (1997). Pulsed second-harmonic generation in nonlinear, one-dimensional, periodic structures. Physical Review A, 56(4), 3166.

[33] Lysak, V. V., Safonov, I. M., Song, Y. M., Sukhoivanov, I. A., & Lee, Y. T. (2008). High speed intracavity-contacted vertical cavity surface emitting lasers with separated quantum wells. Optical and Quantum Electronics, 40(14-15), 1219-1225.

[34] Li, J., & Chiang, K. S. (2008). Light guidance in a photonic bandgap slab waveguide consisting of two different Bragg reflectors. Optics Communications, 281(23), 5797-5803.

[35] Li, Y., Xi, Y., Li, X., & Huang, W. P. (2009). A single-mode laser based on asymmetric Bragg reflection waveguides. Optics Express, 17(13), 11179-11186.

[36] Fesenko, V. I., & Tuz, V. R. (2016). Dispersion blue-shift in an aperiodic Bragg reflection waveguide. Optics Communications, 365, 225-230.

[37] Fesenko, V. I., Tuz, V. R., Shulika, O. V., & Sukhoivanov, I. A. (2016). Dispersion properties of Kolakoski-cladding hollow-core nanophotonic Bragg waveguide. Nanophotonics, 5(4), 556-564.

[38] Yakushev, S. O., Shulika, O. V., Petrov, S. I., & Sukhoivanov, I. A. (2008). Chirp compression with single chirped mirrors and its assembly. Microelectronics Journal, 39(3-4), 690-695.

[39] Fink, Y., Winn, J. N., Fan, S., Chen, C., Michel, J., Joannopoulos, J. D., & Thomas, E. L. (1998). A dielectric omnidirectional reflector. Science, 282(5394), 1679-1682.

[40] Fesenko, V. I. (2015). Omnidirectional reflection from generalized Kolakoski multilayers. Progress In Electromagnetics Research, 41, 33-41.

[41] Yeh, P., & Yariv, A. (1976). Bragg reflection waveguides. Optics Communications, 19(3), 427-430

[42] Simova, E., & Golub, I. (2003). Polarization splitter/combiner in high index contrast Bragg reflector waveguides. Optics Express, 11(25), 3425-3430..

[43] Liu, B., Liu, Y. F., Li, S. J., & He, X. D. (2016). High efficiency all-optical diode based on photonic crystal waveguide. Optics Communications, 368, 7-11.

[44] Sakurai, Y., Matsutani, A., & Koyama, F. (2006). Tunable stop-band hollow waveguide Bragg reflectors with tapered air core for adaptive dispersion-compensation. Applied Physics Letters, 88(12), 121103.

[45] Mizrahi, A., & Schächter, L. (2004). Optical Bragg accelerators. Physical Review E, 70(1), 016505.

[46] Fox, A. J. (1974). The grating guide – a component for integrated optics. Proceedings of the IEEE, 62(5), 644-645.

[47] Snyder, A. W., & Love, J. (2012). Optical waveguide theory. Springer Science & Business Media.

[48] West, B. R., & Helmy, A. S. (2006). Properties of the quarter-wave Bragg reflection waveguide: theory. JOSA B, 23(6), 1207-1220.

[49] Li, J., & Chiang, K. S. (2007). Guided modes of one-dimensional photonic bandgap waveguides. JOSA B, 24(8), 1942-1950.

[50] Nistad, B., Haakestad, M. W., & Skaar, J. (2006). Dispersion properties of planar Bragg waveguides. Optics Communications, 265(1), 153-160.

[51] Pal, B. P., Ghosh, S., Varshney, R. K., Dasgupta, S., & Ghatak, A. (2007). Loss and dispersion tailoring in 1D photonics band gap Bragg reflection waveguides: finite chirped claddings as a design tool. Optical and Quantum Electronics, 39(12-13), 983-993.

[52] Abolghasem, P., & Helmy, A. S. (2009). Matching layers in Bragg reflection waveguides for enhanced nonlinear interaction. IEEE Journal of Quantum Electronics, 45(6), 646-653.

[53] Eliseeva, S. V., Fedorova, I. V., & Sementsov, D. I. (2017). Modification of the transmission spectrum of the" semiconductor-dielectric" photonic crystal in an external magnetic field. Advanced Electromagnetics, 6(4), 83-89.

[54] Namdar A., Abdi-Ghaleh R., amshidi-Ghaleh K., (2013). nfluence of arrangement order ratio on the magneto-optical properties of one-dimensional microcavity structures, Applied Optics, 52, 2564-2569.

[55] Khokhlov, N. E., Prokopov, A. R., Shaposhnikov, A. N., Berzhansky, V. N., Kozhaev, M. A., Andreev, S. N., ... & Belotelov, V. I. (2015). Photonic crystals w ith plasmonic patterns: novel type of the heterostructures for enhanced magneto-optical activity. Journal of Physics D: Applied Physics, 48(9), 095001.

[56] Dadoenkova, N. N., Panyaev, I. S., Sannikov, D. G., Dadoenkova, Y. S., Rozhleys, I. A., Krawczyk, M., & Lyubchanskii, I. L. (2016). Complex waveguide based on a magneto-optic layer and a dielectric photonic crystal. Superlattices and Microstructures, 100, 45-56.

[57] Bonal, V., Quintana, J. A., Villalvilla, J. M., Boj, P. G., & Díaz-García, M. A. (2019). Controlling the emission properties of solution-processed organic distributed feedback lasers through resonator design. Scientific Reports, 9(1), 1-10.

[58] Yeatman E.M. (2004) Planar Waveguide Optical Amplifiers. In: Aegerter M.A., Mennig M. (eds) Sol-Gel Technologies for Glass Producers and Users. Springer, Boston, MA.

[59] Zayats, A. V., & Maier, S. (Eds.). (2013). Active plasmonics and tuneable plasmonic metamaterials (Vol. 8). John Wiley & Sons.

[60] Tuz, V. R., Fedorin, I. V., & Fesenko, V. I. (2018). Modal phenomena of surface and bulk polaritons in magnetic-semiconductor superlattices. Surface Waves, 99-125.

[61] Wallis, R. F., Brion, J. J., Burstein, E., & Hartstein, A. (1974). Theory of surface polaritons in anisotropic dielectric media with application to surface magnetoplasmons in semiconductors. Physical Review B, 9(8), 3424.

[62] Camley, R. E., & Mills, D. L. (1982). Surface polaritons on uniaxial antiferromagnets. Physical Review B, 26(3), 1280.

[63] Kaganov, M. I., Pustyl'nik, N. B., & Shalaeva, T. I. (1997). Magnons, magnetic polaritons, magnetostatic waves. Physics-Uspekhi, 40(2), 181.

[64] Agranovich, V. M., & Ginzburg, V. (2013). Crystal optics with spatial dispersion, and excitons (Vol. 42). Springer Science & Business Media.

[65] Ozbay, E. (2006). Plasmonics: merging photonics and electronics at nanoscale dimensions. Science, 311(5758), 189-193.

[66] Armelles, G., Cebollada, A., García–Martín, A., & González, M. U. (2013). Magnetoplasmonics: combining magnetic and plasmonic functionalities. Advanced Optical Materials, 1(1), 10-35.

[67] Anker, J. N., Hall, W. P., Lyandres, O., Shah, N. C., Zhao, J., & Van Duyne, R. P. (2010). Biosensing with plasmonic nanosensors. In Nanoscience and Technology: A Collection of Reviews from Nature Journals (pp. 308-319).

[68] Stockman, M. I., Kneipp, K., Bozhevolnyi, S. I., Saha, S., Dutta, A., Ndukaife, J., ... & Boltasseva, A. (2018). Roadmap on plasmonics. Journal of Optics, 20(4), 043001.

[69] Jun, Y. C. (2012). Electrically-driven active plasmonic devices. Plasmonics-Principles and Applications. InTech: Rijeka, 383-400.

[70] Dicken, M. J., Sweatlock, L. A., Pacifici, D., Lezec, H. J., Bhattacharya, K., & Atwater, H. A. (2008). Electrooptic modulation in thin film barium titanate plasmonic interferometers. Nano letters, 8(11), 4048-4052.

[71] Min, C., Wang, P., Jiao, X., Deng, Y., & Ming, H. (2007). Beam manipulating by metallic nano-optic lens containing nonlinear media. Optics Express, 15(15), 9541-9546.

[72] Hu, B., Zhang, Y., & Wang, Q. J. (2015). Surface magneto plasmons and their applications in the infrared frequencies. Nanophotonics, 1(open-issue), 383-396.

[73] Abraha, K., Smith, S. R. P., & Tilley, D. R. (1995). Surface polaritons and attenuated total reflection spectra of layered antiferromagnets in the Faraday configuration. Journal of Physics: Condensed Matter, 7(32), 6423.

[74] Elmzughi, F. G., Constantinou, N. C., & Tilley, D. R. (1995). Theory of electromagnetic modes of a magnetic superlattice in a transverse magnetic field: An effective-medium approach. Physical Review B, 51(17), 11515.

[75] Kushwaha, M. S. (2001). Plasmons and magnetoplasmons in semiconductor heterostructures. Surface Science Reports, 41(1-8), 1-416.

[76] Abraha, K., & Tilley, D. R. (1995). The theory of far-infrared optics of layered antiferromagnets. Journal of Physics: Condensed Matter, 7(14), 2717.

[77] Bulgakov, A. A., Girich, A. A., Khodzitsky, M. K., Shramkova, O. V., & Tarapov, S. I. (2009). Transmission of electromagnetic waves in a magnetic fine-stratified structure. JOSA B, 26(12), B156-B160.

[78] Fesenko, V. I., Fedorin, I. V., & Tuz, V. R. (2016). Dispersion regions overlapping for bulk and surface polaritons in a magnetic-semiconductor superlattice. Optics letters, 41(9), 2093-2096.

[79] Han, N., Liu, J., Gao, Y., Zhou, K., & Liu, S. (2020). Topologically Protected and Highly Localized Surface Waves in Gyro–Electromagnetic Metamaterials. Annalen der Physik, 532(8), 2000022.

[80] Durach, M., Williamson, R., Laballe, M., & Mulkey, T. (2020). Tri-and tetrahyperbolic isofrequency topologies complete classification of bianisotropic materials. Applied Sciences, 10(3), 763.

[81] Datta, S., Furdyna, J. K., & Gunshor, R. L. (1985). Diluted magnetic semiconductor superlattices and heterostructures. Superlattices and Microstructures, 1(4), 327-334.

[82] Munekata, H., Zaslavsky, A., Fumagalli, P., & Gambino, R. J. (1993). Preparation of (In, Mn) As/(Ga, Al) Sb magnetic semiconductor heterostructures and their ferromagnetic characteristics. Applied Physics Letters, 63(21), 2929-2931.

[83] Koshihara, S. Y., Oiwa, A., Hirasawa, M., Katsumoto, S., Iye, Y., Urano, C., ... & Munekata, H. (1997). Ferromagnetic order induced by photogenerated carriers in magnetic III-V semiconductor heterostructures of (In, Mn) As/GaSb. Physical Review Letters, 78(24), 4617.

[84] Ta, J. X., Song, Y. L., & Wang, X. Z. (2012). Magneto-phonon polaritons in two-dimension antiferromagnetic/ion-crystalic photonic crystals. Photonics and Nanostructures-Fundamentals and Applications, 10(1), 1-8.

[85] Jungwirth, T., Sinova, J., Mašek, J., Kučera, J., & MacDonald, A. H. (2006). Theory of ferromagnetic (III, Mn) V semiconductors. Reviews of Modern Physics, 78(3), 809.

[86] Tuz, V. R., Fesenko, V. I., Fedorin, I. V., Sun, H. B., & Han, W. (2017). Coexistence of bulk and surface polaritons in a magnetic-semiconductor superlattice influenced by a transverse magnetic field. Journal of Applied Physics, 121(10), 103102.

[87] Landau L. D. and Lifshitz E. M. (1960). Electrodynamics of Continuous Media (Volume 8 of A Course of Theoretical Physics), Pergamon, Oxford.

[88] Felsen L. B. and Marcuvitz N. (1994). Radiation and Scattering of Waves. IEEE-Wiley, New York.

[89] Ferrari, L., Wu, C., Lepage, D., Zhang, X., & Liu, Z. (2015). Hyperbolic metamaterials and their applications. Progress in Quantum Electronics, 40, 1-40.

[90] Cortes, C. L., Newman, W., Molesky, S., & Jacob, Z. (2012). Quantum nanophotonics using hyperbolic metamaterials. Journal of Optics, 14(6), 063001.

[91] Poddubny, A. N., Belov, P. A., & Kivshar, Y. S. (2013). Purcell effect in wire metamaterials. Physical Review B, 87(3), 035136.

[92] Jacob, Z., Smolyaninov, I. I., & Narimanov, E. E. (2012). Broadband Purcell effect: Radiative decay engineering with metamaterials. Applied Physics Letters, 100(18), 181105.

[93] Liu, Z., Lee, H., Xiong, Y., Sun, C., & Zhang, X. (2007). Far-field optical hyperlens magnifying sub-diffraction-limited objects. Science, 315(5819), 1686-1686.

[94] Smith, D. R., Schurig, D., Mock, J. J., Kolinko, P., & Rye, P. (2004). Partial focusing of radiation by a slab of indefinite media. Applied Physics Letters, 84(13), 2244-2246.

[95] Kapitanova, P. V., Ginzburg, P., Rodríguez-Fortuño, F. J., Filonov, D. S., Voroshilov, P. M., Belov, P. A., ... & Zayats, A. V. (2014). Photonic spin Hall effect in hyperbolic metamaterials for polarization-controlled routing of subwavelength modes. Nature Communications, 5(1), 1-8.

[96] Smith, D. R., & Schurig, D. (2003). Electromagnetic wave propagation in media with indefinite permittivity and permeability tensors. Physical Review Letters, 90(7), 077405.

[97] Shekhar, P., Atkinson, J., & Jacob, Z. (2014). Hyperbolic metamaterials: fundamentals and applications. Nano Convergence, 1(1), 14.

[98] Davidovich, M. V. (2019). Hyperbolic metamaterials: production, properties, applications, and prospects. Physics-Uspekhi, 62(12), 1173.

[99] Takayama, O., & Lavrinenko, A. V. (2019). Optics with hyperbolic materials. JOSA B, 36(8), F38-F48.

[100] Guo, Z., Jiang, H., & Chen, H. (2020). Hyperbolic metamaterials: From dispersion manipulation to applications. Journal of Applied Physics, 127(7), 071101.

[101] Schilling, J. (2006). Uniaxial metallo-dielectric metamaterials with scalar positive permeability. Physical Review E, 74(4), 046618.

[102] Zhukovsky, S. V., Kidwai, O., & Sipe, J. E. (2013). Physical nature of volume plasmon polaritons in hyperbolic metamaterials. Optics Express, 21(12), 14982-14987.

[103] Poddubny, A., Iorsh, I., Belov, P., & Kivshar, Y. (2013). Hyperbolic metamaterials. Nature Photonics, 7(12), 948-957.

[104] Simovski, C. R., Belov, P. A., Atrashchenko, A. V., & Kivshar, Y. S. (2012). Wire metamaterials: physics and applications. Advanced Materials, 24(31), 4229-4248.

[105] Sun, J., Zeng, J., & Litchinitser, N. M. (2013). Twisting light with hyperbolic metamaterials. Optics Express, 21(12), 14975-14981.

[106] Mirmoosa, M. S., Kosulnikov, S. Y., & Simovski, C. R. (2015). Unbounded spatial spectrum of propagating waves in a polaritonic wire medium. Physical Review B, 92(7), 075139.

[107] Mirmoosa, M. S., Kosulnikov, S. Y., & Simovski, C. R. (2016). Magnetic hyperbolic metamaterial of high-index nanowires. Physical Review B, 94(7), 075138.

[108] Li, W., Liu, Z., Zhang, X., & Jiang, X. (2012). Switchable hyperbolic metamaterials with magnetic control. Applied Physics Letters, 100(16), 161108.

[109] Macêdo, R. (2017). Tunable hyperbolic media: Magnon-polaritons in canted antiferromagnets. In Solid State Physics (Vol. 68, pp. 91-155). Academic Press.

[110] Kolmychek, I. A., Pomozov, A. R., Leontiev, A. P., Napolskii, K. S., & Murzina, T. V. (2018). Magneto-optical effects in hyperbolic metamaterials. Optics Letters, 43(16), 3917-3920.

[111] Pomozov, A. R., Kolmychek, I. A., Gan'shina, E. A., Volkova, O. Y., Leont'ev, A. P., Napol'skii, K. S., & Murzina, T. V. (2018). Optical effects in magnetic hyperbolic metamaterials. Physics of the Solid State, 60(11), 2264-2268.

[112] Fedorin, I. V. (2018). Electrodynamic properties of a hypercrystal with ferrite and semiconductor layers in an external magnetic field. Superlattices and Microstructures, 113, 337-345.

[113] Lan, C., Bi, K., Zhou, J., & Li, B. (2015). Experimental demonstration of hyperbolic property in conventional material—Ferrite. Applied Physics Letters, 107(21), 211112.

[114] Lokk, E. G. (2017). Isofrequency surfaces and dependences of electromagnetic waves in infinite ferromagnetic space. Journal of Communications Technology and Electronics, 62(3), 251-259.

[115] Akhiezer, A. I., Akhiezer, I. A., & Polovin, R. V. (2017). Plasma Electrodynamics: Linear Theory (Vol. 68). Elsevier, Chap. 5.

[116] Fesenko, V. I., & Tuz, V. R. (2019). Lossless and loss-induced topological transitions of isofrequency surfaces in a biaxial gyroelectromagnetic medium. Physical Review B, 99(9), 094404.

[117] Tuz, V. R., & Fesenko, V. I. (2020). Magnetically induced topological transitions of hyperbolic dispersion in biaxial gyrotropic media. Journal of Applied Physics, 128(1), 013107.

[118] Ballantine, K. E., Donegan, J. F., & Eastham, P. R. (2014). Conical diffraction and the dispersion surface of hyperbolic metamaterials. Physical Review A, 90(1), 013803.

[119] Depine, R. A., Inchaussandague, M. E., & Lakhtakia, A. (2006). Classification of dispersion equations for homogeneous, dielectric-magnetic, uniaxial materials. JOSA A, 23(4), 949-955.

[120] Durach, M. (2020). Tetra-hyperbolic and tri-hyperbolic optical phases in anisotropic metamaterials without magnetoelectric coupling due to hybridization of plasmonic and magnetic Bloch high-k polaritons. Optics Communications, 476, 126349.

[121] Sreekanth, K. V., Biaglow, T., & Strangi, G. (2013). Directional spontaneous emission enhancement in hyperbolic metamaterials. Journal of Applied Physics, 114(13), 134306.

[122] High, A. A., Devlin, R. C., Dibos, A., Polking, M., Wild, D. S., Perczel, J., ... & Park, H. (2015). Visible-frequency hyperbolic metasurface. Nature, 522(7555), 192-196.

[123] Tang, T., Li, C., & Luo, L. (2016). Enhanced spin Hall effect of tunneling light in hyperbolic metamaterial waveguide. Scientific Reports, 6, 30762.

[124] Takayama, O., Sukham, J., Malureanu, R., Lavrinenko, A. V., & Puentes, G. (2018). Photonic spin Hall effect in hyperbolic metamaterials at visible wavelengths. Optics Letters, 43(19), 4602-4605.

[125] Shen, H., Lu, D., VanSaders, B., Kan, J. J., Xu, H., Fullerton, E. E., & Liu, Z. (2015). Anomalously weak scattering in metal-semiconductor multilayer hyperbolic metamaterials. Physical Review X, 5(2), 021021.

[126] Novitsky, A., Repän, T., Zhukovsky, S. V., & Lavrinenko, A. V. (2018). Subwavelength hyperlens resolution with perfect contrast function. Annalen der Physik, 530(3), 1700300.

Buts V.A., Zagorodny A.G. Features of the dynamics of charged particles in electromagnetic fields// Problems of theoretical physics. Scientific works. Issue 5 / Yu. O. Averkov, V. A. Buts, V. I. Fesenko, I. O. Girka, V. M. Kuklin, A. V. Priymak, Yu. V. Prokopenko, O.Yu. Slyusarenko, Yu.V. Slyusarenko, D. M. Vavriv, V. M. Yakovenko, V. V. Yanovsky, A.G. Zagorodny; under the general edited by A.G. Zagorodny, N. F. Shulga, ed. no. 5. V. A. Buts - Kh.: V. N. Karazin Kharkiv National University, 2023. 488 p. (Series "Problems of Theoretical and Mathematical Physics. Scientific Works").

Annotation

This review describes some important features of the interaction of charged particles with electromagnetic waves. Both regular regimes and chaotic regimes of such interaction are described. The mechanisms of the transition of the regular motion of particles (and waves) to stochastic regimes are described. The role of additive and multiplicative fluctuations on the dynamics of individual particles and on their collective dynamics is described. It is shown that in many regimes the chaotic dynamics is such that the highest moments turn out to be much larger than the lowest moments. Such regimes must be described by kinetic equations, in which the role of higher moments is significantly reflected. Note that the Einstein-Fokker-Planck equations contain only the first two moments. The equations that take into account the higher moments are formulated in the review. Particular attention in this review is paid to resonances. In particular, the review describes new cyclotron resonances. The conditions of these new resonances differ from the known ones in that they substantially take into account the influence of the field strength of the wave with which the particles interact. The dynamics of particles under the conditions of these new resonances is described. New resonances in the interaction of charged particles with waves in vacuum are also described. The presence of such resonances leads to practically unlimited acceleration of charged particles by fields of electromagnetic waves (lasers) in a vacuum. The review also discusses and describes new mechanisms for the emergence of regimes with dynamic chaos. In particular, when waves are excited by an electron beam in a constant magnetic field, regimes with dynamic chaos arise as a result of a rapid, qualitative and periodic change in the form of the phase portrait. Regimes with dynamic chaos under the conditions of new cyclotron resonances arise as a result of the passage of phase trajectories through regions in which the uniqueness theorem is violated. Such regimes can arise even in systems with one degree of freedom.

Keywords: Cyclotron resonances, new cyclotron resonances, dynamic chaos, additive and multiplicative fluctuations, beam-plasma interaction, acceleration, synchronization.

PACS numbers: 05.45.Ac ; 05.45.Xt; 41.75.Jv; 52.25.Gj; 52.35.Mw; 52.50.Sw.

Abstract

It is known that in plasma physics there are two main fundamental processes. It is a wave-particle interaction process and a wave-wave interaction process. In this review, we describe some new results concerning wave-particle interactions. Both

regular regimes of such interaction and chaotic regimes are considered. The main features of cyclotron resonances are described, and the conditions for the appearance of new cyclotron resonances and resonances in the interaction of charged particles with waves in vacuum are described. The overview is divided into seven sections. The authors tried to describe the review material in such a way that practically each of them was independent. ***The first section*** describes the features of nonlinear cyclotron resonances. The widths of these resonances and the distances between these resonances are found. Using the Chirikov criterion, the conditions for the emergence of regimes with chaotic particle dynamics are outlined. It is noted that this criterion in some cases may give incorrect results. The reasons for this violation of the criteria are discussed. ***In the second section***, the results of the influence on the dynamics of charged particles of additive and multiplicative fluctuations at cyclotron resonances are described. It is shown that in the presence of additive fluctuations, the dynamics of particles at autoresonance is anomalously sensitive to the presence of such fluctuations. It is shown that such sensitivity can lead to superdiffusion of particles in space of energy. The presence of multiplicative fluctuations affects particle dynamics in an even more radical way. In the presence of such fluctuations, the so-called fluctuation instability develops. It is shown that in regimes with stochastic dynamics the higher moments can increase exponentially. Moreover, the increments of the higher moments turn out to be larger than the increments of the lower moments. Attention is drawn to the fact that such regimes cannot be described by equations of the Einstein-Fokker-Planck type (only the first two moments are taken into account in these equations). An equation is given, in which the role of higher moments is taken into account. ***The third section*** describes the features of new cyclotron resonances. Note that the known conditions for the occurrence of cyclotron resonances contain only the dispersion property of the wave (frequency and wave vector), as well as only the strength of the external magnetic field. In addition to these characteristics, new cyclotron resonances contain the magnitude of the strength of the electromagnetic wave with which the particles interact. Note that if at known cyclotron resonances the dynamics of particles was mainly determined by the equation of a mathematical pendulum, then the dynamics of particles under conditions of new cyclotron resonances is mainly determined by the Adler equation. A new mechanism for the emergence of regimes with dynamic chaos is described. Such regimes can arise even in systems with one degree of freedom. In this case, in the phase space, the trajectory of the particles passes through the point at which the uniqueness theorem is violated. The mechanism of the occurrence of chaos in this case resembles the process of throwing a dice with an unlimited number of sides. Such dynamics was called piecewise homogeneous deterministic dynamics. In the previous sections, the dynamics of isolated particles was mainly determined. ***In the fourth section***, the influence of spatial and temporal fluctuations on the collective dynamics of particles is considered. In particular, the plasma-beam instability was considered. It is shown that the presence of such fluctuations significantly limits the spatial and temporal intervals in which regular modes of excitation of oscillations in plasma-beam interaction can be realized. ***In the fifth section***, the role of collective processes in the emergence of regimes with chaotic dynamics is also studied. In this section, we consider the dynamics of electron beam particles in an external magnetic field under conditions close to those of autoresonance. The well-known one-particle criteria do not allow one to be realized in such a model of regimes with dynamic chaos. However, numerical studies show that such regimes arise. The reason for the emergence of these modes has been clarified. This reason is the periodic qualitative change in the shape of the phase portraits. Conventional models that describe the interactions of charged particles with fields of

electromagnetic waves are usually limited to the model of one regular electromagnetic wave. In reality, particles always interact with some packet of electromagnetic waves. The question arises: When can the model of one regular electromagnetic wave be used? The answer to this question is contained ***in the sixth section.*** It is shown that if the phase and group velocities of an electromagnetic wave are close to each other, then the model of one regular electromagnetic wave is quite acceptable. If these velocities differ significantly (as for longitudinal waves in plasma), the dynamics of particle in the packet can be radically different from the dynamics in one regular wave. In such package, regimes with dynamic chaos can develop. ***The seventh section*** is devoted to the description of new resonances that arise when waves interact with charged particles in a vacuum. It should be noted that the appearance of these new resonances is somewhat unusual. This unusualness is due to the fact that rigorous solutions were known about the dynamics of particles in the field of an electromagnetic wave in a vacuum. There were no resonances in such solutions. The presence of such solutions, in a sense, was a kind of brake on the search for resonances. It turned out that these exact solutions do not describe all possible particle dynamics. Other resonant solutions were found. An analogy was found between new resonances in vacuum and the appearance of cyclotron resonances (with the exception of autoresonances). The analogy is that both resonances arise only when the electromagnetic wave (with which the particles interact) has a nonzero transverse component of the wave vector.

Keywords: Cyclotron resonances, new cyclotron resonances, dynamic chaos, additive and multiplicative fluctuations, beam-plasma interaction, acceleration, synchronization.

PACS numbers: 05.45.Ac ; 05.45.Xt; 41.75.Jv; 52.25.Gj; 52.35.Mw; 52.50.Sw

Буц В.О., Загородній А.Г. Особливості динаміки заряджених частинок в електромагнітних полях

Анотація

В обзорі описані деякі важливі особливості взаємодії заряджених частинок з електромагнітними хвилями. Описані як регулярні режими, так і хаотичні режими такої взаємодії. Описані механізми переходу регулярного руху частинок (і хвиль) до стохастичних режимів. Описана роль адитивних та мультиплікативних флуктуацій на динаміку як окремих частинок та на їх колективну динаміку. Показано, що в багатьох режимах хаотична динаміка така, що вищі моменти являються значно більшими, ніж нижчі моменти. Такі режими необхідно описувати кінетичними рівняннями, в яких суттєво відображена роль вищих моментів. Відмітимо, що рівняння Ейнштейна-Фоккера-Планка мають тільки два перших моменти. Рівняння, які враховують вищі моменти, сформульовані в обзорі. Особлива увага в обзорі приділена на резонанси. Зокрема, в обзорі описані нові циклотронні резонанси. Умови цих нових резонансів відрізняються від відомих тим, що в них суттєво враховується вплив напруженості поля хвилі, з якою взаємодіють частинки. Описана динаміка частинок в умовах цих нових резонансів. Описані також нові резонанси при взаємодії заряджених частинок з хвилями в вакуумі. Наявність таких резонансів призводить практично до необмеженого прискорення заряджених частинок полями електромагнітних хвиль (лазерів) в вакуумі.. В обзорі також обговорюються та описані нові механізми виникнення режимів з динамічним хаосом. Зокрема, при збудженні коливань електронним пучком в постійному магнітному полі режим з динамічним хаосом виникають в результаті швидкої, якісної та періодичної зміни виду фазового портрету. Режим з динамічним хаосом

в умовах цих циклотронних резонансах виникає в разі проходження фазових траєкторій через області, в яких порушується теорема єдності. Такі режими можуть виникати навіть в системах з одним ступенем свободи.

Ключеві слова: Циклотронні резонанси, нові циклотронні резонанси, динамічний хаос, адділтівні та мультіплікатівні флуктуації, пучково-плазмова взаємодія, прискорення, синхронізація.

PACS numbers: 05.45.Ac ; 05.45.Xt; 41.75.Jv; 52.25.Gj; 52.35.Mw; 52.50.Sw.

Реферат

Відомо, що у фізиці плазми виділяють два основних фундаментальних процеси. Це процес взаємодії типу хвиля-частинка і процес взаємодії типу хвиля-хвиля. У цьому огляді описані деякі нові результати, які стосуються взаємодії типу хвиля-частинка. Розглянуто як регулярні режими такої взаємодії, так і хаотичні режими. Описано основні особливості циклотронних резонансів, а також описані умови появи нових циклотронних резонансів і резонансів при взаємодії заряджених частинок з хвилями в вакуумі. Огляд розділений на сім розділів. Автори потурбувались описати матеріал огляду таким чином, щоб практично кожен розділ був незалежним. ***У першому розділі*** описані особливості нелінійних циклотронних резонансів. Знайдено ширини цих резонансів і відстані між цими резонансами. Використовуючи критерій Чирикова, виписані умови виникнення режимів з хаотичною динамікою частинок. Відзначено, що цей критерій в деяких випадках може давати неправильні результати. Обговорюються причини такого порушення критеріїв. ***У другому розділі*** описані результати впливу на динаміку заряджених частинок адитивних і мультиплікативних флуктуацій при циклотронних резонансах. Показано, що при наявності адитивних флуктуацій динаміка частинок при авторезонансі виявляється аномально чутливою до наявності таких флуктуацій. Показано, що така чутливість може призводити до супердифузії частинок в просторі енергією. Наявність мультиплікативних флуктуацій впливає на динаміку частинок ще більше радикальним чином. При наявності таких флуктуацій розвивається, так звана, флуктаційна нестійкість. Показано, що в режимах зі стохастичною динамікою вищі моменти можуть зростати за експоненціальним законом. Причому, інкременти вищих моментів виявляються більшими, ніж інкременти нижчих моментів. Звертається увага на те, що такі режими не можуть бути описані рівняннями типу Ейнштейна-Фоккера-Планка (в цих рівняннях враховується тільки два перших моменти). Наведено рівняння, в якому врахована роль вищих моментів. ***У третьому розділі*** описані особливості нових циклотронних резонансів. Відзначимо, що відомі умови виникнення циклотронних резонансів містять тільки дисперсійну властивість хвилі (частота і хвильовий вектор), а також тільки напруженість зовнішнього магнітного поля. Нові циклотронні резонанси крім цих характеристик містять величину напруженості електромагнітної хвилі, з якою взаємодіють частинки. Відзначимо, що якщо при відомих циклотронних резонансах динаміка частинок, в основному, визначалася рівнянням математичного маятника, то динаміка частинок, в основному, визначається рівнянням Адлера. Описано новий механізм виникнення режимів з динамічним хаосом. Такі режими можуть виникати навіть у системах з одним ступенем свободи. При цьому у фазовому просторі траєкторія частинок проходить через точку, в якій порушується теорема єдиності. Механізм виникнення хаосу при цьому нагадує процес кидання гральної кістки з необмеженим числом сторін. Така динаміка була названа кусочно-однорідною детерміністичною динамікою.У попередніх розділах, в основному, визначалася динаміка ізольованих частинок. ***У четвертому розділі*** розглянуто вплив просторових і часових флуктуацій на колективну динаміку частинок. Зокрема, розглянута

плазмово-пучкова нестійкість. Показано, що наявність таких флуктуацій істотно обмежує просторовий і тимчасовий інтервали, завдяки яких можна реалізувати регулярні режими збудження коливань при плазмово-пучкових взаємодіях.

У п'ятому розділі також вивчена роль колективних процесів при виникненні режимів з хаотичною динамікою. У цьому розділі розглянуто динаміку частинок електронного пучка в зовнішньому магнітному полі в умовах, близьких до умов авторезонансу. Відомі одночасткові критерії не дозволяють реалізуватися в такій моделі режимів з динамічним хаосом. Однак чисельні дослідження показують, що такі режими виникають. З'ясована причина виникнення цих режимів. Цією причиною є періодична якісна зміна форми фазових портретів. Звичні моделі, які описують взаємодії заряджених частинок з полями електромагнітних хвиль, зазвичай обмежуються моделлю однієї регулярної електромагнітної хвилі. Насправді частки завжди взаємодіють з деяким пакетом електромагнітних хвиль. Виникає питання: Коли може бути використана модель однієї регулярної електромагнітної хвилі? Відповідь на це питання міститься ***в шостому розділі.*** Показано, що якщо фазова і групова швидкості електромагнітної хвилі близькі один до одного, то модель однієї регулярної електромагнітної хвилі є цілком прийнятною. Якщо ж ці швидкості істотно відрізняються (як для поздовжніх хвиль в плазмі), динаміка в пакеті може бути радикально відмінною від динаміки в одній хвилі. В такому пакеті можуть розвиватися режими з динамічним хаосом. ***Сьомий розділ*** присвячений опису нових резонансів, які виникають при взаємодії хвиль із зарядженими частинками в вакуумі. Слід зазначити на деяку незвичайність виникнення цих нових резонансів. Ця незвичайність пов'язана з тим, що були відомі строгі рішення про динаміку частинок в полі електромагнітної хвилі в вакуумі. У таких рішеннях відсутні резонанси. Наявність таких рішень, в якомусь сенсі, було якимось чином для відшукання резонансів. Виявилося, що ці точні рішення не описують всієї можливої динаміки частинок. Були знайдені інші резонансні рішення. Була виявлена аналогія між новими резонансами в вакуумі і виникненням циклотронних резонансів (за винятком авторезонансу). Аналогія полягає в тому, що ті і інші резонанси виникають тільки в тому випадку, коли електромагнітна хвиля (з якою взаємодіють частинки) має відмінну від нуля поперечну компоненту хвильового вектора.

Ключеві слова: Циклотронні резонанси, нові циклотронні резонанси, динамічний хаос, аддітівні та мультіплікатівні флуктуації, пучково-плазмова взаємодія, прискорення, синхронізація.

PACS numbers: 05.45.Ac ; 05.45.Xt; 41.75.Jv; 52.25.Gj; 52.35.Mw; 52.50.Sw

Averkov Yu. O. Prokopenko Yu. V., and. Yakovenko V. M. Excitation of electromagnetic radiation during the interaction of charged particles with dielectric and plasma-like solid media // Problems of theoretical physics. Scientific works. Issue 5 / Yu. O. Averkov, V. A. Buts, V. I. Fesenko, I. O. Girka, V. M. Kuklin, A. V. Priymak, Yu. V. Prokopenko, O.Yu. Slyusarenko, Yu.V. Slyusarenko, D. M. Vavriv, V. M. Yakovenko, V. V. Yanovsky, A.G. Zagorodny; under the general edited by A.G. Zagorodny, N. F. Shulga, ed. no. 5. V. A. Buts - Kh.: V. N. Karazin Kharkiv National University, 2023. 488 p. (Series "Problems of Theoretical and Mathematical Physics. Scientific Works").

Annotation

The features of the processes of interaction of charged particles and flows of charged particles with dielectric and solid-state dispersive plasma-like media are presented. The dispersion characteristics of oblique surface plasma eigenwaves in a structure with a two-dimensional plasma layer lying on the surface of a three-dimensional plasma half-space are analyzed. It is shown that from the analysis of the expression for the spectral density of the electron energy losses on the excitation of these waves, it is possible to establish the type of the dispersion law of charge carriers in a two-dimensional electron gas at the interface between the media. The results of a theoretical study of beam instability during the motion of a nonrelativistic thin tubular electron beam over a solid cylinder made of artificial material are presented. The possibility of occurrence of absolute instability in the frequency range where the metamaterial exhibits left-handed properties is shown. The effect of nonlinear stabilization of such a beam as it moves along the surface of a solid-state cylinder made of a dielectric as well as a plasma-like media is theoretically investigated. It is established, in particular, that in the electrostatic approximation, when the beam moves along a plasma-like cylinder, the nonlinear stabilization of the growth of the wave amplitude occurs due to the effect of self-trapping of the beam electrons by the field of the electrostatic wave of the beam itself.

Keywords: surface magnetoplasmons, two-dimensional plasma layer, tubular electron beam, solid-state cylinder, eigenmodes, dispersive metamaterial, left-handed media, absolute beam instability, Cherenkov resonance, anomalous Doppler effect, nonlinear stabilization, self-trapping.

PACS numbers: 03.50.-z, 52.40.-w, 52.59.-f, 85.45.-w

Abstract

This chapter considers the problems of excitations of surface and bulk-surface (waveguide) electromagnetic waves by both individual charged particles and flows of nonrelativistic charged particles moving along dielectric or plasma-like media (including metamaterials), and also studies the problems of nonlinear stabilization of emerging instabilities.Thus, in the electrostatic approximation, the energy losses of an electron for the excitation of surface magnetoplasmons, which moves in vacuum parallel to a constant magnetic field along the flat boundary of a solid-state plasma-like medium, are calculated. It is assumed that there is a two-dimensional conducting layer at this boundary, in which the dispersion law of charge carriers can be both quadratic (two-dimensional Drude electron gas) and

linear (two-dimensional gas of Dirac massless fermions). Excitation of surface magnetoplasmons occurs due to the fulfillment of the Vavilov-Cherenkov resonance condition. The dispersion characteristics of oblique surface plasma eigenwaves in the absence of the charged particle are investigated in detail. The expression for the spectral density of the electron energy losses due to the excitation of surface plasmons is obtained and its numerical analysis is performed. It has been shown that the dependences of the maxima of the spectral density on the electron density in the two-dimensional plasma are in qualitative agreement with similar dependences for the Fermi energies in the two-dimensional conducting layer with the corresponding dispersion law of electrons. This means that the position of the maximum of the angular distribution of the intensity of excited surface plasmons can indicate the qualitative character of the dispersion law of electrons in the two-dimensional plasma. The interaction of a nonrelativistic tubular charged particle beam with a cylindrical dispersive metamaterial is investigated. The dispersion equation for the spectra of the eigenmodes of the metamaterial and the spectra of the coupled modes of the system are obtained and numerically analyzed. The case where this metamaterial have negative permittivity and negative permeability simultaneously over a certain frequency range, i.e. it behaves like a left-handed metamaterial, is investigated in detail. The possibility of the occurrence of absolute instability is demonstrated, expressions for the growth rates of such instability are obtained, and the dependences of the rates on the values of the azimuthal and radial mode indices of the excited waves are investigated. The instability is shown to be caused by Cherenkov or anomalous Doppler effects depending on the radial distance between the cylinder and the beam. The obtained results suggest applications of left-handed metamaterials as delaying media for the generation of bulk-surface waves and eliminate the need for creating artificial feedbacks in slow-wave structures. The nonlinear stages of stabilization of beam instability are investigated by the method of macroparticles for the cases of propagation of a nonrelativistic tubular electron beam over plasma-like (e.g., semiconductor) as well as dielectric solid-state cylinders. It has been assumed that the beam electrons satisfy the Vavilov-Cherenkov resonance condition. In the case where the electron collision frequency in the cylinder plasma is much higher than the frequencies of plasma eigenwaves (or oscillations), expressions for the increments of the emerging resistive instability are obtained in the electrostatic approximation. It is shown that the growth of the wave amplitude is stabilized nonlinearly due to the self-trapping of the beam electrons by the field of the electrostatic wave excited in the beam itself. For the case of propagation of a tubular beam over a dielectric cylinder, the excitation of azimuthally symmetric bulk-surface (waveguide) electromagnetic waves of the electric type is considered. It has been established that the method of slowly varying amplitudes and phases ceases to be applicable for waves with radial mode index greater than a certain “critical” value, for which the characteristic period of oscillations of the field amplitudes at the nonlinear stage of instability becomes comparable with the period of fast oscillations of the excited wave. The analysis of slowly varying field amplitudes as a function of time has shown that, as the radial mode index increases, the instability saturation time and the maximum values and the period of amplitude oscillations at the nonlinear instability saturation stage decrease. The polarization of the excited waves has been studied.

Keywords: surface magnetoplasmons, two-dimensional plasma layer, tubular electron beam, solid-state cylinder, eigenmodes, dispersive metamaterial, left-handed media, absolute beam instability, Cherenkov resonance, anomalous Doppler effect, nonlinear stabilization, self-trapping.

PACS numbers: 03.50.-z, 52.40.-w, 52.59.-f, 85.45.-w

Аверков Ю. О., Прокопенко Ю. В. і. Яковенко В. М. Збудження електромагнітного випромінювання при взаємодії заряджених частинок з діелектричними та плазмоподібними твердими середовищами

Анотація

Представлені особливості процесів взаємодії заряджених часток та потоків заряджених часток з діелектричними та твердотілими диспергувальними плазмоподібними середовищами.

Аналітично досліджено дисперсійні характеристики власних (косих) поверхневих плазмових хвиль у структурі з двовимірним плазмовим шаром, що лежить на поверхні тривимірного плазмового напівпростору. Показано, що з аналізу виразу для спектральної щільності втрат енергії електрона на збудження цих хвиль можна встановити тип закону дисперсії носіїв заряду у двомірному електронному газі на межі розділу середовищ. Наведено результати теоретичного дослідження пучкової нестійкості під час руху нерелятивістського тонкого трубчастого електронного пучка над твердотілим циліндром, виготовленим зі штучного матеріалу. Показано можливість виникнення абсолютної нестійкості в області частот, де метаматеріал демонструє лівосторонні властивості. Теоретично досліджено ефект нелінійної стабілізації нестійкості такого пучка при його русі вздовж поверхні твердотільного діелектричного та плазмоподібного циліндрів. Встановлено, зокрема, що в електростатичному наближенні під час руху пучка вздовж плазмоподібного циліндра нелінійна стабілізація зростання амплітуди хвилі здійснюється за рахунок ефекту самозахоплення електронів пучка полем електростатичної хвилі самого пучка.

Ключові слова: поверхневі магнітоплазмони, двомірний електронний газ, трубчастий електронний пучок, твердотільний циліндр, власні моди, диспергувальний метаматеріал, лівобічне середовище, абсолютна нестійкість, черенковський резонанс, аномальний ефект Доплера, нелінійна стабілізація, самозахоплення.

PACS numbers: 03.50.-z, 52.40.-w, 52.59.-f, 85.45.-w

Реферат

У цьому розділі розглянуто задачі збудження поверхневих і об'ємно-поверхневих (хвилевідних) електромагнітних хвиль як окремими зарядженими частинками, так і потоками нерелятивістських заряджених часток, що рухаються уздовж діелектричних і плазмоподібних (в тому числі штучних) середовищ, а також вивчені питання нелінійної стабілізації виникаючих нестікостей. Так, в електростатичному наближенні розраховані втрати енергії електрона на збудження поверхневих магнітоплазмонів, який рухається у вакуумі паралельно постійному магнітному полю уздовж плоскої межі твердотільного плазмоподібного середовища. Передбачається, що на цій межі знаходиться двовимірний провідний шар, закон дисперсії носіїв заряду в якому може бути як квадратичним (двовимірний друдевський електронний газ), так і лінійним (двовимірний газ діраковських безмасових ферміонів). Збудження поверхневих магнітоплазмонів відбувається завдяки виконанню умови резонансу Вавилова-Черенкова. Детально досліджені дисперсійні характеристики власних (косих) поверхневих магнітоплазмових хвиль в відсутність зарядженої частинки. Отримано вираз для спектральної щільності втрат енергії електрона на збудження поверхневих магнітоплазмонів і виконаний його чисельний аналіз. Встановлено, що якісна поведінка залежностей максимумів спектральної щільності від концентрації електронів в 2D-плазмі узгоджується з поведінкою аналогічних залежностей для енергій Фермі в 2D-плазмі з відповідним законом дисперсії електронів. Це означає, що по положенню максимуму кутового розподілу інтенсивності збуджених поверхневих магнітоплазмонів можна вказати якісний характер закону дисперсії електронів в 2D-плазмі. Досліджено взаємодію нерелятивістського трубчастого пучка заряджених часток з диспергуючим мета-

матеріалом циліндричної форми. Отримано і чисельно проаналізовано дисперсійне рівняння для спектрів власних мод метаматериала і спектрів зв'язаних мод системи. Детально досліджено випадок, коли метаматериал характеризується негативною діелектричної та магнітної проникностями, тобто, коли він демонструє лівобічні властивості. Продемонстровано можливість виникнення абсолютної нестійкості, отримані вирази для інкрементів такої нестійкості і досліджена їх залежність від значень азимутального і радіального модового індексів збуджуваних хвиль. Показано, що причиною нестійкості може бути як ефект Вавилова-Черенкова, так і аномальний ефект Доплера в залежності від радіальної відстані між циліндром і пучком. Отримані результати дозволяють зробити висновок про те, що лівобічний метаматериал може бути використаний в якості уповільнюючого середовища в генераторах електромагнітного випромінювання без необхідності забезпечення додаткового зворотного зв'язку в системі, як в лампі зворотної хвилі. Нелінійні етапи стабілізації пучкової нестійкості досліджені методом макрочасток для випадків поширення нерелятивістського трубчастого електронного пучка над плазмоподібним (наприклад, напівпровідниковим) і діелектричним твердотільними циліндрами. Передбачалося, що електрони пучка задовольняють умові резонансу Вавилова-Черенкова. Для випадку, коли частота зіткнень електронів плазми циліндра набагато перевищує частоти власних плазмових хвиль (коливань), в електростатичному наближенні отримано вирази для інкрементів виникає резистивної нестійкості. Показано, що нелінійна стабілізація зростання амплітуди хвилі здійснюється за рахунок ефекту самозахоплення електронів пучка полем електростатичної хвилі самого пучка. Для випадку поширення трубчастого пучка над діелектричним циліндром розглянуто збудження азимутально-симетричних об'ємно-поверхневих (хвилевідних) електромагнітних хвиль електричного типу. Встановлено, що використаний метод повільно змінних у часі амплітуд і фаз перестає бути придатним для хвиль із значеннями радіального модового індексу, які перевищують деяке «критичне» значення, для якого характерний «період» осциляцій амплітуд полів на нелінійної стадії нестійкості стає сумірним із періодом «швидких» осциляцій порушуваної хвилі. Показано, що зі збільшенням радіального модового індексу хвилі час насичення нестійкості, максимальні значення і «період» осциляцій амплітуд на нелінійної стадії насичення нестійкості зменшуються. Вивчено питання про поляризацію порушуваних хвиль.

Ключові слова: поверхневі магнітоплазмони, двомірний електронний газ, трубчастий електронний пучок, твердотільний циліндр, власні моди, диспергувальний метаматеріал, лівобічне середовище, абсолютна нестійкість, черенковський резонанс, аномальний ефект Доплера, нелінійна стабілізація, самозахоплення.

PACS numbers: 03.50.-z, 52.40.-w, 52.59.-f, 85.45.-w

Slyusarenko O.Yu. , Yu.V. Slyusarenko Yu.V , Zagorodny A.G. The reduced description method in the kinetic theory of complex systems of identical particles // Problems of theoretical physics. Scientific works. Issue 5 / Yu. O. Averkov, V. A. Buts, V. I. Fesenko, I. O. Girka, V. M. Kuklin, A. V. Priymak, Yu. V. Prokopenko, O.Yu. Slyusarenko, Yu.V. Slyusarenko, D. M. Vavriv, V. M. Yakovenko, V. V. Yanovsky, A.G. Zagorodny; under the general edited by A.G. Zagorodny, N. F. Shulga, ed. no. 5. V. A. Buts - Kh.: V. N. Karazin Kharkiv National University, 2023. 488 p. (Series "Problems of Theoretical and Mathematical Physics. Scientific Works").

Annotation

Microscopic approaches to the description of non-equilibrium processes in complex systems of identical particles, in particular, at the kinetic stage of evolution, have been developed. In this work, the term “complex” unites some selected systems of many identical constituent particles with a complex internal structure. The internal structure of particles is reflected in the peculiarities of their interaction, both among themselves and with an external field acting on the medium. Such systems are nonlinear, open (regarding the presence of an external field), demonstrating the emergence of self-organization and new properties in the process of evolution. As an example of such systems, we consider dissipative media (media with internal friction between structural units) under the influence of an external random field, active media (in this case, the dissipative media, the structural units of which are influenced by an external stochastic field, the action of which depends on the velocity of the structural unit), low-temperature gases of hydrogen-like atoms in an external electromagnetic field. The systems are specially selected in such a way as to cover the cases of both classical and quantum complex systems. For systems of this kind, recipes have been proposed for constructing microscopic approaches to describing their evolution, in particular, its kinetic stages. The approaches are constructed in such a way that the noted internal structure of the structural units of the system does not affect the possibilities of considering these composite particles as point objects. The motivation for the research is, first of all, the fact that consistent microscopic approaches to the description of evolutionary processes in these systems are currently either completely absent or insufficiently developed. The development of microscopic approaches is based on the generalization of the Bogolyubov - Peletminsky reduced description method to the case of the listed complex systems of identical particles. The procedure for constructing microscopic approaches to describing the evolution of dissipative systems (including those with active fluctuations) demonstrates the possibility of dynamically substantiating the kinetic theory of dissipative systems of identical particles in an external stochastic field. Within the framework of the developed approaches, a procedure is proposed for deriving kinetic equations for all the systems mentioned in the case of weak interaction between particles and a low intensity of the external field. A number of particular solutions of the obtained equations are analyzed, in particular, with the aim of further applications of the developed theory.

Keywords: complex systems, dissipative media, active fluctuations, low-temperature gases of hydrogen-like atoms, evolutionary processes, stochastic field,

Furutsu-Novikov formula, chains of BBGKY equations, reduced description method, kinetic equations, self-propelled properties of dissipative systems.

PACS numbers: 05.20.-y; 05.20.Dd; 05.10.Gg; 05.40.-a; 05.40.Jc; 45.70.-n; 47.70 Nd

Abstract

Microscopic approaches have been developed to describe non-equilibrium processes in complex systems of identical particles, in particular, at the kinetic stage of evolution. In this work, the term "complex" unites some selected systems of many identical constituent particles with a complex internal structure. The internal structure of particles is reflected in the peculiarities of their interaction, both among themselves and with an external field acting on the environment. Such systems are nonlinear, open (due to the external field), demonstrating the emergence of self-organization and new properties within the process of evolution. As examples of such systems, we consider dissipative media (media with internal friction between structural units) under the influence of an external random field, active media (in this case, dissipative media, the structural units of which are influenced by an external stochastic field, the action of which depends on the velocity of the structural unit), low-temperature gases of hydrogen-like atoms in an external electromagnetic field. The systems are specially selected in such a way as to cover the cases of both classical and quantum complex systems. For systems of this kind, recipes have been proposed for constructing microscopic approaches to describing their evolution, in particular, its kinetic stages. The approaches are constructed in such a way that the noted internal structure of the structural units of the system does not affect the possibilities of considering these composite particles as point objects. The motivation for the research is, first of all, the fact that consistent microscopic approaches to the description of evolutionary processes in the systems mentioned are either completely absent or insufficiently developed. The development of microscopic approaches is based on the generalization of the Bogolyubov - Peletminskii abbreviated description method to the case of the listed complex systems of identical particles. Within the framework of the developed microscopic approach, a formalism is proposed for deriving kinetic equations for many-particle dissipative systems (including those with active fluctuations) in an external random field. The Liouville equation is derived from the Hamilton equations generalized to the case of many-particle dissipative systems in a stochastic field. A method is constructed for averaging such a Liouville equation over the external random force. The method is based on a generalization of the Furutsu-Novikov formula for the case of non-Gaussian noise, as well as the presence of nonlinear friction (dissipative interaction), the local nature of the action of an external random field with active correlations. An infinite chain of equations is written for many-particle distribution functions averaged over external noise. Such a chain is a generalization of the well-known BBGKY chain to the case of dissipative systems in a stochastic field. A regular procedure for breaking this chain is proposed in the case of weak interaction between particles and a weak stochastic field intensity. It is shown that, within the framework of the developed microscopic approach, it is possible to construct a kinetic theory of active particles both in the case of two-dimensional and three-dimensional systems. Closed kinetic equations are obtained for the one-particle distribution function. It is shown that in this approximation the kinetic equation has the form of the Fokker-Planck equation, generalized to the case of non-Gaussian noise or the local nature of the action of an external random field with active correlations. Some special cases are determined in which the derived kinetic equations have solutions that coincide with the results known for systems of active particles from earlier works of other authors. It is also shown that one of the consequences of the local nature of active fluctuations is the

manifestation of self-propelling properties of systems of active particles, even in the case of only linear friction. The parameters of such a self-propelled motion are self-consistently expressed through the internal characteristics of a many-particle system - the density of the number of particles in the system, the parameters of the dissipative function, and the characteristics of the external action - pair correlation functions of a stochastic field with active fluctuations. Within the framework of the developed approach, a consistent construction of the kinetic theory of low-temperature dilute gases of hydrogen-like atoms in an external electromagnetic field is demonstrated. The approach is based on the formulations of the second quantization method in the presence of bound states of particles. A hydrogen-like alkali metal atom is considered as a bound state of two types of charged fermions. A system of kinetic equations is obtained for the Wigner distribution functions of free fermions of both types (electrons and cores) and their bound states - hydrogen-like atoms, taking into account the effect of external and self-consistent (mean) fields on the system. The derived equations of motion for the Wigner distribution functions should serve as a basis for analyzing nonequilibrium effects and phenomena associated with the action of an external electromagnetic field (including a stochastic one) on low-temperature gases of alkali metals. For example, these equations make it possible to study the propagation of forced waves in the systems under study, including various resonance phenomena. The latter circumstance seems to be important from the point of view of the possibility of additional pumping of photons into the medium by an external electromagnetic field (laser). The need to increase the photon density in a medium inevitably arises in the process of experimental realization of the regime with a Bose-Einstein condensate of photons in it. A separate line of application of the obtained equations opens up if the electromagnetic field entering them is of a stochastic nature. Due to the random nature of the external electromagnetic field, the noted equation from a mathematical point of view is an equation with a spatially inhomogeneous noise source that depends on the particle momentum. Such equations are typical for the systems with active fluctuations mentioned above, in which the self-propelling properties are possible. In particular, this phenomenon is possible when the structural units of the system have a head-to-tail asymmetry. Excited atoms with a dipole moment exhibit such asymmetry. Thus, low-temperature weakly excited gases in an external random electromagnetic field can serve as a prototype for a physical system with active fluctuations.

Keywords: complex systems, dissipative media, active fluctuations, low-temperature gases of hydrogen-like atoms, evolutionary processes, stochastic field, Furutsu-Novikov formula, chains of BBGKY equations, reduced description method, kinetic equations, self-propelled properties of dissipative systems.

PACS numbers: 05.20.-y; 05.20.Dd; 05.10.Gg; 05.40.-a; 05.40.Jc; 45.70.-n; 47.70 Nd

Слюсаренко О.Ю., Слюсаренко Ю.В., Загородній А.Г. Метод скороченого опису в кінетичній теорії складних систем тотожних частинок

Анотація

Розроблено мікроскопічні підходи до опису нерівноважних процесів у складних системах тотожних частинок, зокрема, на кінетичному етапі еволюції. У даній роботі термін «складні» об'єднує деякі обрані системи багатьох тотожних частинок зі складною внутрішньою структурою. Внутрішня структура частинок відображується на особливостях їх взаємодії, як між собою, так і з зовнішнім полем, що діє на середовище. Такі системи є нелінійними, відкритими (наявність зовнішнього поля!) і такими, що демонструють появу самоорганізації в процесі еволюції,

а також інших нових властивостей. Як приклади таких систем розглядаються дисипативні середовища (середовища з внутрішнім тертям між структурними одиницями) під дією зовнішнього випадкового поля, активні середовища (у даному випадку – дисипативні середовища, структурні одиниці яких підпадають під вплив зовнішнього стохастичного поля, дія якого залежить від швидкості структурної одиниці), низькотемпературні гази водневоподібних атомів у зовнішньому електромагнітному полі. Системи спеціально підібрані таким чином, щоб охопити розглядом випадки як класичних, так і квантових складних систем. Для подібного роду систем запропоновано рецепти побудови мікроскопічних підходів до опису їх еволюції, зокрема, кінетичного її етапу. Підходи будуються таким чином, щоби зазначена внутрішня структура частинок не позначалася на можливостях розгляду цих складних структурних одиниць як точкових об'єктів. Мотивацією досліджень у першу чергу були ті обставини, що послідовні мікроскопічні підходи до опису еволюційних процесів у зазначених системах до теперішнього часу або повністю відсутні, або розвинені в недостатній мірі.

В основі розвитку мікроскопічних підходів лежить узагальнення на випадок перелічених складних систем тотожних частинок методу скороченого опису Боголюбова - Пелетминського. Процедура побудови мікроскопічних підходів до опису еволюції дисипативних систем (у тому числі, і з активними флуктуаціями) демонструє можливість динамічного обґрунтування кінетичної теорії дисипативних систем тотожних частинок у зовнішньому стохастичному полі. У рамках розвинутих підходів запропоновано процедури виведення кінетичних рівнянь для всіх зазначених систем у випадку слабкої взаємодії між частинками та малої інтенсивності зовнішнього поля. Проаналізовано низку часткових розв'язків здобутих рівнянь, зокрема, з метою подальших застосувань розвинутої теорії.

Ключові слова: складні системи, дисипативні середовища, активні флуктуації, низькотемпературні гази водневоподібних атомів, еволюційні процеси, стохастичне поле, формула Фуруцу-Новікова, ланцюжки рівнянь ББГІК, метод скороченого опису, кінетичні рівняння, «самохідні» властивості дисипативних систем.

PACS numbers: 05.20.-y; 05.20.Dd; 05.10.Gg; 05.40.-a; 05.40.Jc; 45.70.-n; 47.70 Nd

Реферат

Розроблено мікроскопічні підходи до опису нерівноважних процесів в складних системах тотожних частинок, зокрема, на кінетичному етапі еволюції. У даній роботі термін «складні» об'єднує деякі вибрані системи багатьох тотожних складових частинок зі складною внутрішньою структурою. Внутрішня структура частинок відбивається на особливостях їх взаємодії, як між собою, так і з зовнішнім полем, яке впливає на середовище. Такі системи є нелінійними, відкритими (наявність зовнішнього поля!), та демонструють появу в процесі еволюції самоорганізації та нових властивостей. Розглядаються приклади таких систем: дисипативні середовища (середовища з внутрішнім тертям між структурними одиницями) під впливом зовнішнього випадкового поля, активні середовища (в даному випадку - дисипативні середовища, структурні одиниці яких підпадають під вплив зовнішнього стохастичного поля, дія якого залежить від швидкості структурної одиниці), низькотемпературні гази водневоподібних атомів у зовнішньому електромагнітному полі. Системи спеціально підібрані таким чином, щоб охопити розглядом випадки як класичних, так і квантових складних систем. Для подібного роду систем запропоновані рецепти побудови мікроскопічних підходів до опису їх еволюції, зокрема, кінетичних її етапів. Підходи будуються таким чином, щоб зазначена

внутрішня конструкція структурних одиниць системи не позначалася на можливостях розгляду цих складових частинок як точкових об'єктів. Мотивацією досліджень у першу чергу є та обставина, що послідовні мікроскопічні підходи до опису еволюційних процесів у згаданих системах в даний час або повністю відсутні, або розвинені в недостатній мірі. В основі розвитку мікроскопічних підходів лежить узагальнення на випадок перерахованих складних систем тотожних частинок методу скороченого опису Боголюбова - Пелетминського. У рамках розвиненого мікроскопічного підходу запропоновано формалізм виведення кінетичних рівнянь для багаточастинкових дисипативних систем (у тому числі, з активними флуктуаціями) в зовнішньому випадковому полі. Отримано рівняння Ліувілля виходячи з рівнянь Гамільтона, узагальнених на випадок багаточастинкових дисипативних систем у стохастичному полі. Побудовано метод усереднення такого рівняння Ліувілля за зовнішньою випадковою силою. В основу методу закладено узагальнення формули Фуруцу-Новікова на випадок негаусових шумів, а також наявності нелінійного тертя (дисипативної взаємодії), локального характеру впливу зовнішнього випадкового поля з активними кореляціями. Виписано нескінченний ланцюжок рівнянь для багаточастинкових функцій розподілу, усереднених за зовнішнім шумом. Такий ланцюжок є узагальненням відомого ланцюжка ББГКІ на випадок дисипативних систем у стохастичному полі. Запропоновано регулярну процедуру обриву цього ланцюжка в разі слабкої взаємодії між частинками та слабкої інтенсивності стохастичного поля. Показано, що в рамках розвиненого мікроскопічного підходу можлива побудова кінетичної теорії активних частинок як у випадку двовимірних, так і тривимірних систем. Отримано замкнуті кінетичні рівняння для одночастинкової функції розподілу. Показано, що в цьому наближенні кінетичне рівняння має вигляд рівняння Фоккера-Планка, узагальнене на випадок негаусових шумів або локального характеру впливу зовнішнього випадкового поля з активними кореляціями. Визначено деякі окремі випадки, в яких виведені кінетичні рівняння мають розв'язок, що збігається з результатами, відомими для систем активних частинок з більш ранніх робіт інших авторів. Показано також, що одним із наслідків локального характеру активних флуктуацій є прояв самохідних властивостей («self-propelling»), характерних для систем активних частинок, навіть у випадку тільки лінійного тертя. Параметри такого самохідного руху самоузгодженим чином виражаються через внутрішні характеристики багаточасткових систем - густину числа частинок в системі, параметри дисипативної функції, і характеристики зовнішнього впливу - парні кореляційні функції стохастичного поля з активними флуктуаціями. В рамках розвиненого підходу продемонстровано послідовну побудову кінетичної теорії низькотемпературних розріджених газів водневоподібних атомів у зовнішньому електромагнітному полі. Підхід базується на формулюваннях методу вторинного квантування при наявності зв'язаних станів частинок. Як приклад зв'язаного стану двох сортів заряджених ферміонів розглянуто водневоподібний атом лужного металу. Отримано систему кінетичних рівнянь для вігнерівських функцій розподілу вільних ферміонів обох сортів (електронів і кістяків) та їх зв'язаних станів - водневоподібних атомів з урахуванням впливу на систему зовнішнього і самоузгодженого (середнього) полів. Виведені рівняння руху для вігнерівських функцій розподілу повинні служити основою для аналізу нерівноважних ефектів і явищ, пов'язаних із впливом зовнішнього електромагнітного поля (в тому числі, й стохастичного) на низькотемпературні гази лужних металів. Наприклад, ці рівняння дають можливість вивчати поширення вимушених хвиль у досліджуваних системах, включаючи різні резонансні явища. Остання обставина є важливою з точки зору можливості додаткового накачування фотонів в середовище зовнішнім електромагнітним полем (лазером). Необхідність

збільшення густини фотонів у середовищі неминуче виникає в процесі експериментальної реалізації режиму з бозе-ейнштейнівським конденсатом фотонів у ній. Окремий напрямок застосування отриманих рівнянь відкривається в тому випадку, якщо електромагнітне поле, що входить до них, носить стохастичний характер. Через випадковий характер зовнішнього електромагнітного поля зазначені рівняння з математичної точки зору є рівняннями з просторово-неоднорідним джерелом шуму, що залежать від імпульсу частинки. Такі рівняння типові для згаданих вище систем з активними флуктуаціями, в яких можлива реалізація самохідних властивостей. Зокрема, таке явище можливе у випадку, коли структурні одиниці системи мають асиметрію «голова - хвіст». Збуджені атоми, що мають дипольний момент, мають і таку асиметрію. Таким чином, низькотемпературні слабко збуджені гази в зовнішньому випадковому електромагнітному полі можуть служити прототипом фізичної системи з активними флуктуаціями.

Ключові слова: складні системи, дисипативні середовища, активні флуктуації, низькотемпературні гази водневоподібних атомів, еволюційні процеси, стохастичне поле, формула Фуруцу-Новікова, ланцюжки рівнянь ББГКІ, метод скороченого опису, кінетичні рівняння, «самохідні» властивості дисипативних систем.

PACS numbers: 05.20.-y; 05.20.Dd; 05.10.Gg; 05.40.-a; 05.40.Jc; 45.70.-n; 47.70 Nd

Kuklin V. M., Priymak A. V., Yanovsky V. V. A world of strategies with memory // Problems of theoretical physics. Scientific works. Issue 5 / Yu. O. Averkov, V. A. Buts, V. I. Fesenko, I. O. Girka, V. M. Kuklin, A. V. Priymak, Yu. V. Prokopenko, O.Yu. Slyusarenko, Yu.V. Slyusarenko, D. M. Vavriv, V. M. Yakovenko, V. V. Yanovsky, A.G.Zagorodny; under the general edited by A.G. Zagorodny, N. F. Shulga, ed. no. 5. V. A. Buts - Kh.: V. N. Karazin Kharkiv National University, 2023. 488 p. (Series "Problems of Theoretical and Mathematical Physics. Scientific Works").

Annotation

Various scenarios of the evolution of populations of strategies with memory are considered. The strategies interact with each other in an iterated prisoner dilemma, earning evolutionary benefit points according to the pay-out matrix. The review focuses on collective characteristics such as memory, the level of aggressiveness (the share of refusals to cooperate), and the complexity of strategies. Different scenarios of evolution appear when using different selection rules for strategies intended for deletion in the corresponding generation. Cases of zeroing evolutionary advantage points after each cycle (or generation) and summing (inheriting) points of previous cycles are considered. In the first case, as a result of evolution, complex strategies with a large depth of memory dominate and are not aggressive – inclined to cooperation. The history of the evolution of a population is divided into two periods: the primitive period and the period of the developed 'community'. The primitive stage in the development of the world of strategies can be distinguished according to the following features: 1). the presence of all the most primitive strategies; 2). an increase in average aggressiveness); 3). the presence of the most aggressive strategy. In the second case, as a result of increased competition, complex strategies with a large memory depth, but aggressive ones, also win. In anomalous competition, when the most successful strategies are removed, an increase in aggressiveness is also observed for complex strategies with a large memory depth. It was empirically found that in the process of population evolution, a universal relationship between aggressiveness and points of evolutionary advantages persists, for example, a decrease in the value of points obtained with an increase in the average aggressiveness of the population is observed. Open societies, in which complex strategies with a large memory (replacing the remote losers) are injected, demonstrate greater efficiency; complex strategies with a large memory depth and less aggressive ones dominate in the emerging stationary state. Penetration in this way into open populations of primitive strategies (with a low memory depth) leads to their dominance in a stationary state, although their average aggressiveness decreases, while around complex strategies with a greater memory depth in the population remains. The case of interaction of 50 thousand objects, each of which uses 50 strategies, is considered separately. When interacting, the losing strategy is replaced by the winning strategy. As a result, on average, subjects retain one third of strategies, and complex ones with a large memory depth dominate.

Keywords: evolutions of populations of strategies, object with a set of strategies, prisoner dilemma, memory complexity, aggressiveness.

PACS numbers: 02.50.Le, 05.10.−a, 87.23.Kg, 89.75.Fb

Abstract

Various scenarios of the evolution of populations of strategies with memory are considered. The strategies interact with each other in an iterated prisoner dilemma, earning evolutionary benefit points according to the pay-out matrix. The review focuses on collective characteristics such as memory, the level of aggressiveness (the share of refusals to cooperate), and the complexity of strategies. Different scenarios of evolution appear when using different selection rules for strategies intended for deletion in the corresponding generation. Cases of zeroing evolutionary advantage points after each cycle (or generation) and summing (inheriting) points of previous cycles are considered. In the first case, as a result of evolution, complex strategies with a large depth of memory dominate and are not aggressive – inclined to cooperation. The history of the evolution of a population is divided into two periods: the primitive period and the period of the developed 'community'. The primitive stage in the development of the world of strategies can be distinguished according to the following features: 1). the presence of all the most primitive strategies; 2). an increase in average aggressiveness); 3). the presence of the most aggressive strategy. With an increase in average aggressiveness, the value of the set of points (advantages) decreases and vice versa, and there is a universal relationship between these values. Despite the typical behavior of averages, initially aggressive strategies and then strategies with low complexity, less than average, may turn out to be the winners at different points in time. Average aggressiveness first grows, then, after overcoming the primitive stage of the world's development, it rapidly decreases. Incidentally, an increase in the memory depth of population strategies decreases the relative duration of the primitive stage of development and increases the proportion of complex strategies. In the resulting stationary state, strategies are not aggressive and achieve equal advantages. In the second case, as a result of increased competition, complex strategies with a large memory depth, but aggressive ones, also win. The stationary state is formed by strategies of maximum complexity. Complexity and memory are evolutionarily advantageous in this case. While allowing strategies to maintain previously gained advantages, the system encourages aggressiveness. An important consequence of the accumulation of advantages in inheritance is a noticeable increase in aggressiveness. In anomalous competition, when the most successful strategies are removed, an increase in aggressiveness is also observed for complex strategies with a large memory depth. It was empirically found that in the process of population evolution, a universal relationship between aggressiveness and points of evolutionary advantages persists, for example, a decrease in the value of points obtained with an increase in the average aggressiveness of the population is observed. Average aggressiveness also reaches a minimum and grows, and the rate of scoring tends to reverse. That is, as in previous cases, complex strategies with a large memory remain evolutionarily advantageous, but they are characterized by significant aggressiveness. Open societies, in which complex strategies with a large memory (replacing the remote losers) are injected, demonstrate greater efficiency; complex strategies with a large memory depth and less aggressive ones dominate in the emerging stationary state. Penetration in this way into open populations of primitive strategies (with a low memory depth) leads to their dominance in a stationary state, although their average aggressiveness decreases, while around complex strategies with a greater memory depth in the population remains. The case of interaction of 50 thousand objects, each of which uses 50 strategies, is considered separately. When interacting, the losing strategy is replaced by the winning strategy. As a result, on average, subjects retain one third of strategies, and complex ones with a large memory depth

dominate. Thus, in all cases, the depth of memory and the complexity of strategies are evolutionarily advantageous properties. The complexity should increase in the course of evolution, this determines the direction of time. Aggressiveness and the received number of points of evolutionary advantages change over time in accordance with each other in accordance with the empirical universal law.

Keywords: evolutions of populations of strategies, object with a set of strategies, prisoner dilemma, strategy memory, complexity, aggressiveness.

PACS numbers: 02.50.Le, 05.10.−a, 87.23.Kg, 89.75.Fb

Куклін В. М., Приймак О. В., Яновский В. В. Світ стратегій з пам'яттю

Анотація

Розглянуто різні сценарії еволюції популяцій стратегій з пам'яттю. Стратегії взаємодіють один з одним в рамках ітерованої дилеми ув'язнених, отримуючи бали еволюційних переваг відповідно до матриці виплат. В огляді основну увагу приділено колективним характеристикам таким як пам'ять, рівень агресивності (частка відмов від співробітництва), складність стратегій. Різні сценарії еволюції з'являються при використанні різних правил відбору стратегій, призначених для видалення в відповідному поколінні. Розглянуто випадки обнулення балів еволюційних переваг після кожного циклу (або покоління) і підсумовування (успадкування) балів попередніх циклів. У першому випадку в результаті еволюції домінують складні стратегії з великою глибиною пам'яті і не агресивні - схильні до співпраці. Історія еволюції популяції ділиться на два періоди: примітивний період і період розвиненого суспільства. Примітивний етап розвитку світу стратегій можна виділити за такими ознаками: 1). наявності всіх найпримітивніших стратегій; 2) зростання середньої агресивності); 3). присутністю самої агресивної стратегії. У другому випадку в результаті посилення конкуренції виграють також складні стратегії з великою глибиною пам'яті, але агресивні. При аномальної конкуренції, коли видаляються найбільш успішні стратегії, спостерігається також зростання агресивності для складних стратегій з великою глибиною пам'яті. Емпірично виявлено, що в процесі еволюції популяції зберігається універсальна залежність між агресивністю і балами еволюційних переваг так, наприклад, спостерігається зниження величини одержуваних балів при зростанні середньої агресивності популяції. Відкриті суспільства, в якіх відбувається ін'єкція складних стратегій з великою пам'яттю (замінюють віддалених-хто програв) демонструють більшу ефективність, у стаціонарі домінують складні стратегії, з великою глибиною пам'яті і менш агресивні. Проникнення подібним чином у відкриті популяції примітивних стратегій (з малою глибиною пам'яті) призводить до їх домінування в стаціонарному стані, хоча їх середня агресивність падає, при цьому близько 10% складних стратегій із більшою кількістю пам'яті в популяції зберігається. Окремо розглянуто випадок взаємодії 50 тис. об'єктів, кожен з яких використовує 50 стратегій. При взаємодії стратегія, яка програла, замінюється стратегією-переможцем. В результаті в середньому суб'єкти зберігають третину стратегій, причому домінують складні, з великою глибиною пам'яті.

Ключові слова: Еволюції популяцій стратегії, об'єктів з набором стратегій, дилема ув'язненого, пам'ять, складність, агресивність стратегій.

PACS numbers: 02.50.Le, 05.10.−a, 87.23.Kg, 89.75.Fb.

Реферат

Розглянуто різні сценарії еволюції популяцій стратегій з пам'яттю. Стратегії взаємодіють одна з одною в повторюваної проблеми ув'язненого, заробляючи бали еволюційної вигоди відповідно до матриці виплат. В огляді розглядаються такі

колективні характеристики, як пам'ять, рівень агресивності (частка відмов від співробітництва) і складність стратегій. Різні сценарії еволюції виникають при використанні різних правил вибору стратегій, призначених для видалення в відповідному поколінні. Розглянуто випадки обнулення балів еволюційної переваги після кожного циклу (або покоління) і підсумовування (успадкування) балів попередніх циклів. У першому випадку в результаті еволюції переважають складні стратегії з великою глибиною пам'яті, неагресивні - схильні до співпраці. Історія еволюції популяції ділиться на два періоди: первісний період і період розвиненого «спільноти». Первісний етап розвитку світу стратегій можна виділити за такими ознаками: 1). наявність всіх найпримітивніших стратегій; 2). підвищення середньої агресивності); 3). наявність найбільш агресивної стратегії. Зі збільшенням середньої агресивності значення набору балів (переваг) зменшується і навпаки, і між цими значеннями існує універсальна взаємозв'язок. Незважаючи на типову поведінку середніх значень, спочатку агресивні стратегії, а потім стратегії з низькою складністю, нижчу за середню, можуть виявитися переможцями в різні моменти часу. Середня агресивність спочатку наростає, а потім, подолавши примітивну стадію розвитку світу, швидко знижується. Між іншим, збільшення глибини пам'яті популяційних стратегій зменшує відносну тривалість примітивної стадії розвитку і збільшує частку складних стратегій. В кінцевому стаціонарному стані стратегії не є агресивними і дають рівні переваги. У другому випадку в результаті загострення конкуренції також виграють складні стратегії з великою глибиною пам'яті, але агресивні. Стаціонарний стан формується стратегіями максимальної складності. В цьому випадку еволюційно вигідні складність і пам'ять. Дозволяючи стратегіям зберігати раніше досягнуті переваги, система заохочує агресивність. Важливе наслідок накопичення переваг у спадок - помітне підвищення агресивності. При аномальної конкуренції, коли видаляються найбільш успішні стратегії, спостерігається зростання агресивності і для складних стратегій з великою глибиною пам'яті. Емпірично встановлено, що в процесі еволюції популяції зберігається універсальний взаємозв'язок між агресивністю і балами еволюційної переваги, наприклад, спостерігається зниження значення балів, отриманих при збільшенні середньої агресивності популяції. Середня агресивність теж доходить до мінімуму і зростає, а показник набраних очок має тенденцію до зворотного. Тобто, як і в попередніх випадках, складні стратегії з великою пам'яттю залишаються еволюційно вигідними, але для них характерна значна агресивність. Відкриті суспільства, в які вводяться складні стратегії з великою пам'яттю (замінюють віддалених тих, хто програв), демонструють більшу ефективність. У стаціонарному стані переважають складні стратегії з великою глибиною пам'яті і менш агресивні. Проникнення в такий спосіб у відкриті популяції примітивних стратегій (з малою глибиною пам'яті) призводить до їх домінування в стаціонарному стані, хоча їх середня агресивність знижується, але 10% складних стратегій із більшим значенням пам'яті в популяції залишається. Окремо розглядається випадок взаємодії 50 тисяч об'єктів, кожен з яких використовує 50 стратегій. При взаємодії програшна стратегія замінюється виграшною. В результаті в середньому у об'єктів зберігається третина стратегій, а переважають складні з великою глибиною пам'яті. Таким чином, у всіх випадках глибина пам'яті і складність стратегій є еволюційно вигідними властивостями. Складність повинна збільшуватися в ході еволюції, це визначає напрямок часу. Агресивність і отримана кількість балів еволюційної переваги змінюються з часом відповідно до емпіричного універсального закону.

Ключові слова: Еволюції популяцій стратегії, об'єктів з набором стратегій, дилема ув'язненого, пам'ять, складність, агресивність стратегій.

PACS numbers: 02.50.Le, 05.10.−a, 87.23.Kg, 89.75.Fb

Girka I. O. Fine structure of the local Alfven resonances in cylindrical plasmas with naxial periodic inhomogeneity // Problems of theoretical physics. Scientific works. Issue 5 / Yu. O. Averkov, V. A. Buts, V. I. Fesenko, I. O. Girka, V. M. Kuklin, A. V. Priymak, Yu. V. Prokopenko, O.Yu. Slyusarenko, Yu.V. Slyusarenko, D. M. Vavriv, V. M. Yakovenko, V. V. Yanovsky, A.G. Zagorodny; under the general edited by A.G. Zagorodny, N. F. Shulga, ed. no. 5. V. A. Buts - Kh.: V. N. Karazin Kharkiv National University, 2023. 488 p. (Series "Problems of Theoretical and Mathematical Physics. Scientific Works").

Annotation

Local Alfven resonance id well-known to manifest itself in cylindrical plasma with radially nonuniform particle density and uniform axial external static magnetic field via rapid increase of electromagnetic field amplitude when approaching the resonant radius. First, Physics of the phenomenon is explained in the present review. Plasma axial periodic nonuniformity is shown to be usual feature of the modern plasma devices. Satellite local Alfven resonances are shown to arise in axially periodically nonuniform plasma both in general and resonant cases. Resonant case takes place if the wave length is twice as large as plasma axial period. Conditions are derived under which fine structure of the satellite Alfven resonance is determined just by plasma axial periodic nonuniformity.

Keywords: plasma axial periodic nonuniformity, Alfven resonance, satellite Alfven resonance, wave packet.

PACS numbers: 02.30.Gp, 52.35.-g, 94.20.-y

Abstract

The present review is based on the theoretical research carried out at the Department of General and Applied Physics of Kharkiv University in collaboration with scientists of Institute of Plasma Physics, National Science Center "Kharkiv Institute of Physics and Technology".

Electromagnetic waves with the frequency in the range of ion cyclotron frequency, in particular, Fast Magnetosonic Waves (FMSWs) and Alfven Waves (AWs), - in magnetoactive plasmas are the subject of extensive research. This is associated, first of all, with numerous applications of the results of these studies in solving the problem of controlled nuclear fusion, geophysics and astrophysics. FMSWs and AWs are effective tool for plasma production and heating in toroidal magnetic traps (tokamaks and stellarators). Along with neutral injection, ion cyclotron heating, low-hybrid heating and electron cyclotron heating, magnetohydrodynamic waves (MHD waves) are planned to be used as the main method of plasma heating in future fusion reactor. FMSWs and AWs can be used also for current drive production. Solving the problem of maintenance of current drive during plasma loading by RF power would provide creation of the stationary tokamak and thermonuclear tokamak-reactor on this base. Production of current drive could be applied also in stellarators – for controlling the profile of rotational transform and achieving on this base better plasma MHD stability.

Plasma production and heating in fusion devices initiated intense research of electromagnetic wave conversion and absorption in the vicinity of Alfven resonance (AR).

Interest to this phenomenon is caused mostly by its application for efficient plasma production and heating in fusion traps. In approach of the cold plasma, solutions of Maxwell's equations for electromagnetic wave fields have singularities at the definite radius of plasma cylinder. If to replace this approach by the models which take into account the thermal motion of the particles, finite electron inertia, weak nonlinearity or dissipations, then conversion of these waves into small-scale oscillations and their absorption can significantly change.

During plasma heating by RF fields, most of RF power is absorbed in the vicinity of the local AR. Enhancement of plasma column density and radius causes motion of AR to the plasma periphery. This decreases the efficiency of Alfven method of plasma heating in fusion devices since results in heating of peripheral plasma rather than its central part, which in turn increases undesired plasma-wall interaction. To avoid the heating of peripheral plasma and heat just plasma depth one can apply the waves with large magnitude of longitudinal wavenumber k_z, for which the region of the local AR is placed in the plasma depth. However, this is complicated because of wide barrier of nontransparency at the plasma edge for these waves. The other way to avoid the energy losses at the plasma periphery is application of the waves with low frequency and small k_z, for which the region of the local AR is also situated in the plasma depth. However, in this case one needs the antenna which is long in axial direction. All these unfavorable circumstances make it difficult to utilize Alfven method of plasma heating in large traps and initiate the search for new physical ways of its efficiency enhancement.

Weak periodic axial nonuniformity of plasma can significantly affect on the AR fine structure and result in arising the satellite ARs. The present review is devoted to Physics of AR and peculiarities of mathematical methods, which are effective for solving these problems of plasma electrodynamics.

Keywords: plasma axial periodic nonuniformity, Alfven resonance, satellite Alfven resonance, wave packet.

PACS numbers: 02.30.Gp, 52.35.-g, 94.20.-y

Гірка І.О. Тонка структура локальних альфвенових резонансів в циліндричній плазмі з аксіальною періодичною неоднорідністю

Анотація

Як відомо, локальний альфвенів резонанс проявляється в циліндричній плазмі з радіально неоднорідною густиною частинок і однорідним аксіальним зовнішнім сталим магнітним полем у термінах різкого зростання амплітуд електромагнітного поля при наближенні до резонансного радіусу. Спочатку, в цьому огляді пояснюється фізика явища. Показано, що аксіальна періодична неоднорідність плазми є звичайною ознакою сучасних плазмових пристроїв. Показано, що сателітні локальні альфвенові резонанси виникають у аксіально періодично неоднорідній плазмі як у загальному, так і в резонансному випадку. Резонансний випадок має місце, якщо довжина хвилі вдвічі більша за аксіальний період плазми. Виведені умови, за яких тонка структура сателітного альвенового резонансу визначається саме аксіальною періодичною неоднорідністю плазми.

Ключові слова: аксіальна періодична неоднорідність плазми, альфвенів резонанс, сателітний альфвенів резонанс, хвильовий пакет.

PACS numbers: 02.30.Gp, 52.35.-g, 94.20.-y

Реферат

Цей огляд написано за результатами теоретичних досліджень, що виконувалися на кафедрі загальної та прикладної фізики Харківського університету

у співавторстві з ученими Інституту фізики плазми Національного наукового центру «Харківський фізико-технічний інститут».

Електромагнітні хвилі з частотою порядку іонної циклотронної, а саме, швидкі магнітозвукові хвилі (ШМЗХ) і альфвенові хвилі (АХ), - у магнітоактивній плазмі є предметом інтенсивних наукових досліджень. Насамперед, це пов'язано з численними застосуваннями здобутків цих досліджень у вирішенні проблеми керованого термоядерного синтезу (КТС), низки задач геофізики та астрофізики. ШМЗХ і АХ є потужнім засобом створення і нагрівання плазми в тороїдних магнітних уловлювачах (токамаках і стелларатарах). Поряд з інжекцією нейтралів, іонним циклотронним, нижньогибридним і електронним циклотронним нагріванням магнітогідродинамічні хвилі (МГДХ) передбачається використовувати як основний метод нагрівання плазми в майбутньому термоядерному реакторі. ШМЗХ і АХ можуть бути також використані для створення струмів захоплення. Розв'язання задачі підтримання струму захоплення при введенні до плазми ВЧ потужності допоможе створенню стаціонарного токамака і на його основі термоядерного реактора-токамака. Створення струмів захоплення може бути використаним також і в стелларатарах – з метою керування профілем обертального перетворення і досягнення, за рахунок цього, кращої МГД стійкості плазми.

Створення і нагрівання плазми в пристроях КТС ініціювали інтенсивні дослідження процесів конверсії і поглинання електромагнітних хвиль поблизу альфвенового резонансу (АР). Інтерес до цього явища обумовлений, головним чином, його застосуванням для ефективного створення і нагрівання плазми в термоядерних пастках. У наближенні холодної плазми розв'язки рівнянь Максвелла для полів електромагнітної хвилі мають сингулярність на певному радіусі плазмового циліндра. Якщо це наближення замінити на моделі, які враховують тепловий рух частинок, скінченну інерцію електронів, слабку нелінійність або дисипації, то конверсія цих хвиль у дрібномасштабні коливання та їхнє поглинання можуть значно змінитися.

При нагріванні плазми ВЧ полями, більшість ВЧ потужності поглинається в околі локального АР. При збільшенні густини та розмірів плазмового шнура області АР зміщаються на його периферію. Це знижує ефективність альфвенового метода нагрівання плазми в пастках КТС, оскільки призводить до нагрівання периферійної плазми, а не її центральної частини, що, в свою чергу, підсилює небажану взаємодію плазми зі стінкою. Аби уникнути нагрівання периферійної плазми і гріти глибинні шари плазми, можна застосовувати хвилі із великим значенням поздовжнього хвильового числа k_z, для яких область локального АР розташована в глибині плазми. Але це є складним через широкий бар'єр непрозорості на краю плазми для таких хвиль. Іншим способом уникнути втрат енергії на периферії плазми є застосування хвиль із низькою частотою і малим k_z, для яких область локального АР також знаходиться в глибині плазми. Але для цього потрібна довга в аксіальному напрямку антена. Всі ці несприятливі обставини ускладнюють використання альфвенового методу нагрівання плазми у великих пастках та ініціюють пошук нових фізичних шляхів підвищення його ефективності.

Слабка періодична аксіальна неоднорідність плазми може істотно впливати на тонку структуру АР, спричиняти виникнення сателітних АР. Фізиці та особливостям математичних методів, які є ефективними для розв'язання таких задач плазмової електродинаміки, присвячено цей огляд.

Ключові слова: аксіальна періодична неоднорідність плазми, альфвенів резонанс, сателітний альфвенів резонанс, хвильовий пакет.

PACS numbers: 02.30.Gp, 52.35.-g, 94.20.-y

Fesenko V. I., Vavriv D. M. Electromagnetic waves in artificial composite media: a review // Problems of theoretical physics. Scientific works. Issue 5 / Yu. O. Averkov, V. A. Buts, V. I. Fesenko, I. O. Girka, V. M. Kuklin, A. V. Priymak, Yu. V. Prokopenko, O.Yu. Slyusarenko, Yu.V. Slyusarenko, D. M. Vavriv, V. M. Yakovenko, V. V. Yanovsky, A.G. Zagorodny; under the general edited by A.G. Zagorodny, N. F. Shulga, ed. no. 5. V. A. Buts - Kh.: V. N. Karazin Kharkiv National University, 2023. 488 p. (Series "Problems of Theoretical and Mathematical Physics. Scientific Works").

Annotation

The electromagnetic waves interaction with composite media attract great attention of researches for many decades due to its relevance to problems in condensed matter physics, optics, photonics, plasmonics, and chemistry. During last two decades, metamaterials and photonic crystals have been in the top of research due to their unprecedented possibilities to manipulate the electromagnetic parameters of both materials and electromagnetic waves. The review is devoted to different types of artificial composite media, their classification, discussion of their unique characteristics and ways of control of their dispersion. Comprehensive review of the electromagnetic properties of periodic and aperiodic planar Bragg reflectors (that is, photonic crystals) and planar Bragg reflective waveguides is carried out. The dispersion features of Bragg reflective waveguides with both periodic and aperiodic arrangements of layers in their claddings are discussed and methods of their control are presented. It was found that an aperiodic configuration of cladding of Bragg reflection waveguide could give rise to exceptionally strong mode selection and tuning the polarization-discrimination effects. On the other hand, artificial media called metamaterials (and especially, hyperbolic metamaterials) created using subwavelength resonant building blocks, are also useful for both controlling light propagation and dispersion management. They can be easily made by alternating dielectric and metal layers or by embedding arrays of parallel metallic rods in a dielectric matrix. This review discusses a particular example of hyperbolic metamaterial, represented by a superlattice consisting of ferrite and semiconductor layers, which is influenced by an external static magnetic field. Within the framework of the effective medium theory, such an artificial structure can be reduced to a homogenized medium, which is described the effective permittivity and permeability tensors. Due to the components of both tensors show significant sensitivity to the external magnetic field, these artificial structures can exhibit the great variety of high-frequency properties. For instance, it is observed that in the case when specific conditions related to the superlattice's constitutive parameters and filling factor are satisfied, the regions of existence of the bulk and surface polaritons can totally overlap. Besides, it is found out that in an extremely anisotropic medium, the dispersion characteristics of extraordinary bulk waves exhibit a number of unusual behaviors, including atypical topological transitions of isofrequency surfaces. The conditions for appearance of mono-hyperbolic, bi-hyperbolic, tri-hyperbolic and tetra-hyperbolic-like forms of isofrequency surfaces are also discussed.

Keywords: photonic crystals, metamaterials, superlattices, dispersion characteristics, hyperbolic dispersion.

PACS numbers: 42.25.Bs, 42.70.Qs, 68.65.Cb, 78.67.Pt

Abstract

The electromagnetic waves interaction with composite media attract great attention of researches for many decades due to its relevance to problems in condensed matter physics, optics, photonics, plasmonics, and chemistry. During last two decades, metamaterials and photonic crystals have been in the top of research due to their unprecedented possibilities to manipulate the electromagnetic parameters of both materials and electromagnetic waves. Regardless of the type and method of realization of artificial composite materials, the solution of the problem of the propagation of electromagnetic waves in them is reduced to the study of dispersion characteristics. The dispersion characteristic is a key parameter that determines the characteristics and features of the use of such materials. Thus, the problem of the dispersion management is vital for any practical applications. Photonic crystals and metamaterials provide unprecedented opportunities for flexible control of the characteristics (in particular, dispersion) of the propagation of electromagnetic waves. The dispersion characteristics of such artificial media are determined not so much by the material and geometric parameters of their structural elements (that is, layers, rods, rings, etc.), but more by how these elements are arranged in a single composite structure.

The review is devoted to different types of artificial composite media, their classification, discussion of their unique characteristics and ways of control of their dispersion. Comprehensive review of the electromagnetic properties of periodic and aperiodic planar Bragg reflectors (that is, photonic crystals) and planar Bragg reflective waveguides is carried out. The dispersion features of Bragg reflective waveguides with both periodic and aperiodic arrangements of layers in their claddings are discussed and methods of their control are presented. It was found that an aperiodic configuration of cladding of Bragg reflection waveguide could give rise to exceptionally strong mode selection and tuning the polarization-discrimination effects, and can be used in the integrated optic devices that are designed for mode selection, adaptive dispersion compensation, frequency and polarization filtering.

On the other hand, artificial media called metamaterials (and especially, hyperbolic metamaterials) created using subwavelength resonant building blocks, are also useful for both controlling light propagation and dispersion management. They can be easily made by alternating dielectric and metal layers or by embedding arrays of parallel metallic rods in a dielectric matrix. This review discusses a particular example of hyperbolic metamaterial, represented by a superlattice consisting of ferrite and semiconductor layers, which is influenced by an external static magnetic field. Within the framework of the effective medium theory, such an artificial structure can be reduced to a homogenized medium, which is described the effective permittivity and permeability tensors. Due to the components of both tensors show significant sensitivity to the external magnetic field, these artificial structures can exhibit the great variety of high-frequency properties. For instance, it is observed that in the case when specific conditions related to the superlattice's constitutive parameters and filling factor are satisfied, the regions of existence of the bulk and surface polaritons can totally overlap. Besides, it is found out that in an extremely anisotropic medium, the dispersion characteristics of extraordinary bulk waves exhibit a number of unusual behaviors, including atypical topological transitions of isofrequency surfaces. The conditions for appearance of mono-hyperbolic, bi-hyperbolic, tri-hyperbolic and tetra-hyperbolic-like forms of isofrequency surfaces are also discussed. Today, there are a number of practical applications for which the unique dispersion properties of hyperbolic media are not only desirable but also critical to achieve the required functionality of modern plasmonics and optoelectronics devices. For instance, in practical applications which are related to broadband

enhancement of the density of states, subwavelength imaging and focusing, negative refraction, heat transport and acoustics.

The artificial structures considered in this review are important for both theoretical and applied physics, with the purpose to design highly efficient devices for photonics, microelectronics, optoelectronics, and plasmonics, and for deepening fundamental knowledge about the interaction of electromagnetic waves with artificial composite media.

Keywords: photonic crystals, metamaterials, superlattices, dispersion characteristics, hyperbolic dispersion.

PACS numbers: 42.25.Bs, 42.70.Qs, 68.65.Cb, 78.67.Pt

Фесенко В. І., Ваврів Д. М. Електромагнітні хвилі в штучних композитних середовищах: огляд

Анотація

Взаємодія електромагнітних хвиль зі штучними композитними середовищами знаходиться в центрі уваги дослідників на протязі багатьох років завдяки наявності широкого спектру можливих практичних застосувань, зокрема, в областях оптики, фотоніки, плазмоніки та хімії. Протягом останніх двох десятиліть, метаматеріали та фотонні кристали, були предметом інтенсивних досліджень, що обумовлено безпрецедентними можливостями, які вони надають для маніпулювання як параметрами матеріальних середовищ, так і властивостями електромагнітних хвиль, що поширюються в них. В даній оглядовій статті розглянуто різні типи штучних композитних середовищ, їх унікальні характеристики та способи контролю їх дисперсійних характеристик. Проведено огляд електродинамічних властивостей періодичних та аперіодичних планарних брегівських відбивачів (фотонних кристалів) та планарних хвилеводів створених на їх базі. Детально обговорено дисперсійні характеристики планарних брегівських хвилеводів з періодичним та аперіодичним розташуванням шарів в їх оболонках, та представлено методи їх контролю. Зокрема виявлено, що аперіодична конфігурація оболонки хвилеводу дозволяє проводити більш гнучку селекцію мод, що в свою чергу відкриває більше можливостей в керуванні поляризаційно-залежними ефектами. З іншого боку, штучні середовища створені з використанням субхвильових резонансних елементів (тобто метаматеріали, і особливо, гіперболічні метаматеріали), також привабливі з точки зору контролю поширення електромагнітних хвиль. У даній роботі розглядається окремий випадок гіперболічного метаматеріалу, який представлено надрешіткою створеною на базі феритового та напівпровідникового шарів, на яку впливає зовнішнє статичне магнітне поле. В рамках теорії ефективного середовища така штучна структура була зведена до гомогенізованого середовища, що описується ефективними тензорами діелектричної та магнітної проникностей. Завдяки тому, що компоненти обох тензорів демонструють значну чутливість до зовнішнього магнітного поля, такі штучні структури можуть проявляти значне розмаїття високочастотних властивостей. Зокрема, продемонстровано, що шляхом відповідного вибору матеріальних і геометричних параметрів надрешітки можна отримати таку її конфігурацію, в якій регіони існування поверхневих та об'ємних поляритонів частково, або повністю, перекриваються. Крім того, виявлено, що в надзвичайно анізотропному середовищі дисперсійні характеристики незвичайних об'ємних хвиль демонструють низку нетипових властивостей, включаючи нетипові топологічні переходи ізочастотних поверхонь. Обговорено умови виникнення моно-гіперболічних, бі-гіперболічних, три-гіперболічних та тетра-гіперболічних форм ізочастотних поверхонь.

Ключові слова: фотонні кристали, метаматеріали, надрешітки, дисперсійні характеристики, гіперболічна дисперсія.

PACS numbers: 42.25.Bs, 42.70.Qs, 68.65.Cb, 78.67.Pt

Реферат

Взаємодія електромагнітних хвиль зі штучними композитними середовищами знаходиться в центрі уваги дослідників на протязі багатьох років завдяки наявності широкого спектру можливих практичних застосувань, зокрема, в областях оптики, фотоніки, плазмоніки та хімії. Протягом останніх двох десятиліть, метаматеріали та фотонні кристали, були предметом інтенсивних досліджень, що обумовлено безпрецедентними можливостями, які вони надають для маніпулювання як параметрами матеріальних середовищ, так і властивостями електромагнітних хвиль, що поширюються в них. Незалежно від типу та способу реалізації штучних композитних матеріалів, розв'язок електродинамічної задачі про поширення в них електромагнітних хвиль зводиться до вивчення дисперсійних характеристик. Дисперсійна характеристика є ключовим параметром, що визначає характеристики та особливості використання таких матеріалів. Таким чином, задача контролю та управління дисперсією має суттєве прикладне значення. Фотонні кристали та метаматеріали забезпечують безпрецедентні можливості для гнучкого контролю характеристик (і зокрема, дисперсійних) поширення електромагнітних хвиль. Дисперсійні характеристики таких штучних середовищ зумовлюються не стільки матеріальними та геометричними параметрами їх структурних елементів (наприклад, шарів, стрижнів, кілець та ін.), але, в більшій мірі, від того, яким чином ці елементи скомпоновано в єдину композитну структуру.

В даній оглядовій статті розглянуто різні типи штучних композитних середовищ, їх унікальні характеристики та способи контролю їх дисперсійних характеристик. Проведено огляд електродинамічних властивостей періодичних та аперіодичних планарних брегівських відбивачів (фотонних кристалів) та планарних хвилеводів створених на їх базі. Детально обговорено дисперсійні характеристики планарних брегівських хвилеводів з періодичним та аперіодичним розташуванням шарів в їх оболонках, та представлено методи їх контролю. Зокрема виявлено, що аперіодична конфігурація оболонки хвилеводу дозволяє проводити більш гнучку селекцію мод, що в свою чергу відкриває більше можливостей в керуванні поляризаційно-залежними ефектами, та може бути використано на практиці в пристроях інтегральної оптики які призначені для селекції мод, адаптивної компенсації дисперсії, частотної та поляризаційної фільтрації.

З іншого боку, штучні середовища створені з використанням субхвильових резонансних елементів (тобто метаматеріали, і особливо, гіперболічні метаматеріали), також привабливі з точки зору контролю поширення електромагнітних хвиль. Такі штучні середовища, зокрема, можуть бути отримані або шляхом поєднання діелектричних та металічних шарів в єдину надрешітку або шляхом розташування масиву паралельних металевих стрижнів в діелектричній матриці. У даній роботі розглядається окремий випадок гіперболічного метаматеріалу, який представлено надрешіткою створеною на базі феритового та напівпровідникового шарів, на яку впливає зовнішнє статичне магнітне поле. В рамках теорії ефективного середовища така штучна структура була зведена до гомогенізованого середовища, що описується ефективними тензорами діелектричної та магнітної проникностей. Завдяки тому, що компоненти обох тензорів демонструють значну чутливість до зовнішнього магнітного поля, такі штучні структури можуть проявляти значне розмаїття високочастотних властивостей. Зокрема, продемонстровано, що шляхом відповідного вибору матеріальних і геометричних параметрів

надрешітки можна отримати таку її конфігурацію, в якій регіони існування поверхневих та об'ємних поляритонів частково, або повністю, перекриваються. Крім того, виявлено, що в надзвичайно анізотропному середовищі дисперсійні характеристики незвичайних об'ємних хвиль демонструють низку нетипових властивостей, включаючи нетипові топологічні переходи ізочастотних поверхонь. Обговорено умови виникнення моно-гіперболічних, бі-гіперболічних, три-гіперболічних та тетра-гіперболічних форм ізочастотних поверхонь.

Розглянуті в даній оглядовій статті штучні структури є важливими як для теоретичної, так і для прикладної фізики, з точки зору створення високоефективних пристроїв для фотоніки, мікроелектроніки, оптоелектроніки та плазмоніки, а також для поглиблення фундаментальних знань про особливості взаємодії електромагнітних хвиль зі штучними композитними середовищами.

Ключові слова: фотонні кристали, метаматеріали, надрешітки, дисперсійні характеристики, гіперболічна дисперсія.

PACS numbers: 42.25.Bs, 42.70.Qs, 68.65.Cb, 78.67.Pt

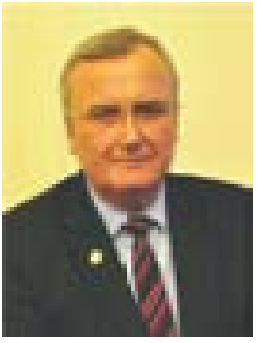

Zagorodny Anatoly Hlibovych *– Doctor of Physical and Mathematical Sciences, Professor, Academician of the National Academy of Sciences of Ukraine, President of the National Academy of Sciences of Ukraine, full member of T.G. Shevchenko Scientific Society, Director of M.M. Bogolyubov's Institute for Theoretical Physics (Kyiv)*

Averkov Yurij Olegovich *– PhD, Doctor of physical and mathematical sciences, Head of the Department of Solid-State Radiophysics of O. Ya. Usikov Institute for Radiophysics and Electronics of the NAS of Ukraine (Kharkiv), Professor of V. N. Karazin's Kharkiv National University*

Buts Vyacheslav Aleksandrovich *– PhD, Doctor of Physical and Mathematical Sciences, Professor, Head of laboratory of National Science Center "Kharkov Institute of Physics and Technology", Kharkov, Ukraine; Professor of V.N. Karazin's Kharkiv National University.*

Fesenko Volodymyr Ivanovitch *– PhD, Doctor of Physical and Mathematical Sciences, Associate Professor, Senior researcher of Institute of Radio Astronomy of the National Academy of Sciences of Ukraine.*

Girka Igor Oleksandrovych *– PhD, Doctor of Physical and Mathematical Sciences, Professor, Corresponding member of NASU, Dean of the School of Physics and Technology, V. N. Karazin's Kharkiv National University.*

Kuklin Volodymyr Michailovich *– PhD, Doctor of Physical and Mathematical Sciences, Professor, Head of AI department of V.N. Karazin's Kharkiv Natioinal University*

Prymak Aleksey Victorovich *– PhD, Assistant Professor of AI department of V.N. Karazin's Kharkiv Natioinal University.*

Prokopenko Yurij Volodymyrovich *– PhD, Doctor of physical and mathematical sciences, Leading Researcher of O. Ya. Usikov Institute for Radiophysics and Electronics of the NAS of Ukraine (Kharkiv), Professor of Kharkiv National University of Radio Electronics.*

Slyusarenko Oleksii Yuriyovych *– PhD, Senior Researcher, Senior Research Fellow of O.I. Akhiezer Institute for Theoretical Physics of NSC KIPT.*

Slyusarenko Yurii Viktorovych *– PhD, Doctor of Physical and Mathematical Sciences, Professor, Academician of the National Academy of Sciences of Ukraine, Head of the Department of O.I. Akhiezer Institute for Theoretical Physics of NSC KIPT, Professor of V.N. Karazin's Kharkiv National University.*

Vavriv Dmytro Mikhailovich *– PhD, Doctor of Physical and Mathematical Sciences, Professor, Deputy director of the Institute of Radio Astronomy of the National Academy of Sciences of Ukraine, Corresponding Member of the National Academy of Sciences of Ukraine, Honored Worker of Science and Technology of Ukraine.*

Yakovenko Volodymyr Mefodievich *– PhD, Doctor of physical and mathematical sciences, Professor, Academician of the National Academy of Sciences of Ukraine, Honorary Director of O. Ya. Usikov's Institute for Radiophysics and Electronics of the NAS of Ukraine, Professor of V. N. Karazin's Kharkiv National University.*

Yanovsky Volodymytr Volodymyrovich *– PhD, Doctor of physical and mathematical sciences, Head of department of Institute of Single Crystals, National Academy of Sciences of Ukraine, professor of AI department of V. N. Karazin's Kharkiv Natioinal University.*

Наукове видання

Загородній Анатолій Глібович
Аверков Юрій Олегович
Буц В'ячеслав Олександрович
Фесенко Володимир Іванович
Гірка Ігор Олександрович
Куклін Володимир Михайлович
Приймак Олексій Вікторович
Прокопенко Юрій Володимирович
Слюсаренко Олексій Юрійович
Слюсаренко Юрій Вікторович
Ваврів Дмитро Михайлович
Яковенко Володимир Мефодійович
Яновський Володимир Володимирович

ПРОБЛЕМИ ТЕОРЕТИЧНОЇ ФІЗИКИ

Збірник наукових праць

Випуск 5

PROBLEMS OF THEORETICAL PHYSICS

Scientific works

Issue 5

(Англ. мовою)

Науковий редактор випуску № 5 проф. В. О. Буц

Серія «Проблеми теоретичної і математичної фізики»

За загальною редакцією
академіка А. Г. Загороднього,
академіка М. Ф. Шульги

Коректор *О. В. Анцибора*
Комп'ютерне верстання *О. С. Чистякова*
Макет обкладинки *І. М. Дончик*

Формат 70×100/16. Ум. друк. арк. 24,9. Наклад 300 пр. Зам. № 130/22.

Видавець і виготовлювач
Харківський національний університет імені В. Н. Каразіна,
61022, м. Харків, майдан Свободи, 4.
Свідоцтво суб'єкта видавничої справи ДК № 3367 від 13.01.2009

Видавництво ХНУ імені В. Н. Каразіна